

# **DETECTION OF PERIODONTAL BACTERIA IN ATHEROSCLEROTIC PLAQUE**

by

Robin John Moll MSc BSc (Hons)

A thesis submitted in partial fulfilment of the requirements for the degree of  
Doctor of Philosophy at the University of Central Lancashire

School of Dentistry

University of Central Lancashire

Preston

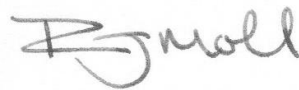
Dec 2016

# STUDENT DECLARATION FORM

I declare that while registered as a candidate for the research degree, I have not been a registered candidate or enrolled student for another award of the University or other academic or professional institution

I declare that no material contained in the thesis has been used in any other submission for an academic award and is solely my own work

**Signature of Candidate:**



---

**Type of Award: Doctorate**

---

**School: School of Dentistry**

---

## Abstract

Atherosclerosis is an inflammatory vascular disease caused by a variety of environmental and genetic factors. Forming during the first decade of life, atherosclerosis develops over time to form complicated intimal lesions known as atherosclerotic plaque. The developing plaque affects the normal function of the vascular endothelium, inducing acute inflammatory responses which harden vessels leading to vascular stenosis. This study aims to examine the role infection plays in the pathogenesis of atherosclerosis through the molecular identification of latent bacterial species present in atherosclerotic plaque tissue from the carotid artery. Initial immunohistological examination of the atherosclerotic plaque tissue revealed widespread localisation of the bacterial cell wall constituent peptidoglycan (PGN). Anti-PGN was localised most prominently within regions of plaque tissue comprising foam cell-like cells, within elastin tissue and around lipid pools. Targeted PCR amplification of the 16S rRNA gene permitted identification of a diverse collection of 16S rDNA sequences within atherosclerotic plaque samples. Overall 13 out of 21 (61.9%) plaques contained bacterial 16S rDNA relating to periodontal (*P. gingivalis* and *T. forsythia*), oral (*Streptococcus sanguinis* and *Streptococcus mitis*), and respiratory (*Klebsiella pneumoniae* and *Mycobacterium tuberculosis*) and commensal (*Propionibacterium acnes* and *Staphylococcus epidermidis*) species. Viable growth of was established through culturing atherosclerotic plaque tissue in a developed bacterial culture medium. Of the 100 isolates recovered *P. acnes* (91%) was most frequently detected, followed by *Lactobacillus spp.* (3%), *S. epidermidis* (3%), *S. mitis* (3%) and *S. sanguinis* (1%). Direct 16S rDNA screening and tissue culturing demonstrated a complete absence of bacteria in the healthy left internal thoracic artery (LITA) control tissue. Challenge of THP-1 cells with a *P. acnes* isolate recovered from atherosclerotic plaque, resulted in significant temporal up-regulation the major cholesterologenic transcription factor, *SREBP2* and its two target transcripts, LDLR and HMGR. Similarly, the cholesterol transporter gene ABCA1 was highly expressed in *P. acnes*-infected THP-1 cells in addition to inflammatory cytokines/chemokines TNF $\alpha$ , IL-1 $\beta$ , CCL3 (MIP-1 $\alpha$ ), cell adhesion molecule ICAM-1. Anti-apoptotic gene BCL2A1 showed the greatest increase in mRNA compared to all tested genes. Expression of the same panel of genes direct in atherosclerotic plaque tissue resulted in similar expression patterns. Taken together, these studies indicate a potential role for infection in the development of atherosclerotic plaque, particularly through mediation of cholesterologenic genes, which may potentiate lipid-loading and foam cell formation in macrophages.

## Table of Contents

Abstract.....	i
Table of Contents.....	ii
List of Tables and Figures.....	vii
List of abbreviations .....	xvii
Acknowledgements.....	xix
Dedication.....	xx
<b>1.0</b> Main Introduction.....	21
1.1 Epidemiology of cardiovascular disease.....	22
1.2 Anatomy of the artery .....	23
1.2.1 The common carotid artery and greater vasculature of the neck and head.....	26
1.3 Atherosclerosis and the carotid artery .....	26
1.3.1 Complications of carotid atherosclerosis .....	27
1.3.2 Clinical symptoms arising from ruptured or thrombosed plaques in the carotid artery .....	28
1.3.3 Surgical intervention .....	28
1.3.4 Atherogenesis .....	29
1.4 Risk factors associated with the development of atherosclerosis.....	33
1.4.1 Non-modifiable risk factors.....	33
1.4.2 Modifiable risk factors .....	34
1.4.3 Infection as a risk factor for the development of atherosclerosis .....	36
1.5 Periodontal disease.....	37
1.5.1 Periodontal bacteria.....	38
1.5.2 Periodontitis and Atherosclerosis .....	40
1.6 Genes expressed in atherosclerotic plaque tissue .....	46
1.6.1 SREBP2 and transcripts LDLR and HMGR.....	46
1.6.2 3-hydroxy-3-methylglutaryl coenzyme A reductase (HMGR) .....	48
1.5.3 ATP-binding cassette, sub-family A 1 (ABCA1) .....	50
1.5.4 Tumour necrosis factor (TNF) $\alpha$ .....	50
1.5.5 Interleukin 1 (IL-1) $\beta$ .....	52
1.5.6 B Cell Lymphoma-2 protein A1 .....	53
1.6 Inflammation and cholesterol homeostasis.....	56
1.7 <i>Propionibacterium acnes</i> .....	58
1.7.1 <i>P. acnes</i> virulence.....	58
1.7.2 <i>P. acnes</i> role in disease and detection in atherosclerotic plaque.....	59
<b>2.0</b> Materials & Methods.....	60

2.1	Human tissue procurement.....	61
2.1.1	Ethical clearance & study cohort.....	61
2.1.2	Tissue collection & sample processing.....	61
2.2	Histological & immunological examination of atherosclerotic plaque & left internal thoracic artery tissue .....	63
2.2.1	Tissue fixation, demineralisation and paraffin embedding .....	63
2.2.2	Hematoxylin & eosin staining (HE) .....	63
2.2.3	Masson's Trichrome Staining (MTC).....	64
2.2.4	Bacterial peptidoglycan monoclonal antibody staining .....	64
2.2.5	Antibody and chromagen optimisation .....	65
2.3	Anaerobic Bacterial cultures .....	65
2.3.1	Maintenance of periodontal red complex bacteria .....	65
2.3.2	Development and optimisation of a bacteriological liquid growth medium.....	68
2.3.3	Isolating viable anaerobic bacteria from human CAP tissue.....	72
2.3.4	Archiving viable isolates .....	73
2.4	Identification of bacterial DNA extracted directly from CAP tissue and cultured anaerobic bacteria .....	74
2.4.1	DNA extraction from CAP and LITA tissue.....	74
2.4.2	DNA extraction from bacterial cultures .....	74
2.4.3	Polymerase Chain Reaction .....	75
2.4.4	Agarose gel electrophoresis.....	76
2.4.5	TOPO® 16S rDNA Cloning.....	78
2.4.6	Colony screening .....	79
2.4.7	Mini-prep isolation of plasmid DNA.....	79
2.4.8	Sequencing of the vector insert.....	80
2.5	Gene expression analysis of atherosclerotic plaque tissue.....	81
2.5.1	Oligonucleotide primer design & optimisation.....	81
2.5.2	RNA extraction from atherosclerotic plaque tissue .....	82
2.5.3	Optimisation of Reverse-transcription Polymerase Chain Reaction (RT-PCR) reagents .....	83
2.5.4	RT-PCR of CAP and LITA specimens .....	84
2.5.5	Quantitative real-time PCR (qPCR) .....	85
2.5.6	Gene expression data analysis for atherosclerotic plaque tissue - $\Delta\Delta C_T$ .....	87
2.6	Infection of a human monocyte cell line with <i>P. acnes</i> , <i>in-vitro</i> .....	88
2.6.1	THP-1 cell culture .....	88
2.6.2	Normal growth characteristics for THP-1 cell line .....	89
2.6.3	THP-1 challenge with <i>Escherichia coli</i> LPS .....	91

2.6.4	THP-1 challenge with <i>P. acnes</i> .....	91
2.6.5	Gene expression data analysis for <i>P. acnes</i> -infected THP-1 .....	92
2.7	Statistical testing .....	92
2.7.1	Power calculations for population sample size .....	92
2.7.2	Statistical analysis of bacterial growth in media supplemented with different concentrations of growth reagent supplements .....	93
2.7.3	Statistical analysis of gene expression in atherosclerotic plaque tissue .....	94
2.7.4	Statistical analysis of <i>P. acnes</i> -infected THP-1 gene expression .....	94
<b>3.0</b>	<b>Examination of Carotid Atherosclerotic Plaque &amp; Left Internal Thoracic Artery Tissue through Histopathological &amp; Immunohistochemical Analysis .....</b>	<b>95</b>
3.1	Introduction .....	96
3.2	Chapter aims .....	104
3.3	Method overview .....	104
3.4	Results.....	105
3.4.1	Power calculations for population sample size .....	105
3.4.2	Histopathology of plaques from the carotid artery .....	106
3.4.3	Localisation of bacterial PGN .....	114
3.5	Discussion .....	120
3.5.1	Immune cell infiltration .....	120
3.5.2	Intra-plaque vessels .....	121
3.5.3	Intraplaque haemorrhage .....	122
3.5.4	Calcified plaques .....	124
3.5.5	PGN localisation.....	125
3.6	Conclusion .....	127
<b>4.0</b>	<b>Evaluation of the Role 16S rDNA PCR in the Detection of Bacterial DNA in Human Internal Carotid Artery Atherosclerotic Plaques .....</b>	<b>130</b>
4.1	Introduction.....	131
4.2	Aims.....	136
4.3	Methods overview .....	137
4.4	Results.....	138
4.4.1	Bacterial DNA amplification using species-specific primer sets .....	139
4.4.2	Bacterial DNA amplification using genus-specific primer sets .....	143
4.5	Discussion .....	153
4.6	Conclusion .....	160
<b>5.0</b>	<b>Development of a Culture Medium to Support the Growth of Red Complex Bacteria ..</b>	<b>162</b>
5.1	Introduction.....	163
5.2	Aims and method overview.....	165

5.3	Results.....	166
5.3.1	Growth characteristics of red complex bacteria.....	166
5.3.2	Growth of red complex bacteria in alternative media .....	174
5.3.3	Development & optimisation of a Tryptic Soy base medium for the growth of periodontal bacteria .....	176
5.3.4	Isolation of viable bacteria species present in CAP tissue. ....	190
5.4	Discussion .....	193
<b>6.0</b>	<b>A Study of Gene Expression in Human Internal Carotid Atherosclerotic Plaques .....</b>	<b>201</b>
6.1	Introduction.....	202
6.2	Chapter aims .....	208
6.3	Method overview .....	208
6.4	Results.....	208
6.5	Discussion .....	214
6.5.1	Sterol Regulatory Binding Protein.....	214
6.5.2	3-hydroxy-3-methylglutaryl coenzyme A reductase (HMGR) .....	215
6.5.3	ATP-binding cassette, sub-family A (ABC1), member 1 .....	217
6.5.4	Low density Lipoprotein Receptor .....	218
6.5.5	Chemokine (C-C motif) Ligand 3 (CCL3) .....	218
6.5.6	Chemokine (C-C motif) Ligand 2 (CCL2) .....	219
6.5.7	Intracellular Adhesion Molecule 1 (ICAM-1) .....	220
6.5.8	Tumor Necrosis Factor-alpha (TNF- $\alpha$ ).....	221
6.5.9	Interleukin 1-beta (IL-1 $\beta$ ).....	222
6.5.9.1	BCL2-related protein A1 (BCL2A1).....	223
6.6	Conclusion .....	224
<b>7.0</b>	<b>The Effect of Propionibacterium acnes on a Human Monocytic Cell Line <i>in vitro</i> .....</b>	<b>227</b>
7.1	Introduction.....	228
7.2	Aims.....	231
7.3	Method .....	231
7.2	Results.....	232
7.2.1	THP-1 growth characteristics .....	232
7.2.2	Oligonucleotide optimisation.....	234
7.2.3	RT-PCR reagent optimisation.....	240
7.2.4	THP-1 gene expression response to <i>Escherichia coli</i> lipopolysaccharide.....	241
7.2.5	Measuring optimal multiplicity of infection (MOI) for monocyte cell line infection with <i>Propionibacterium acnes</i> .....	252
7.2.6	THP-1 cells challenged with <i>Propionibacterium acnes</i> : an <i>in vitro</i> model of infection.....	253

7.3	Discussion .....	260
7.4	Conclusion .....	270
<b>8.0</b>	<b>General Discussion .....</b>	<b>272</b>
8.1	Bacteria present in atherosclerotic plaque tissue .....	274
8.1.1	Periodontopathic bacteria .....	274
8.1.2	<i>Streptococcus</i> spp.....	276
8.1.3	<i>Propionibacterium acnes</i> .....	277
8.1.4	<i>Lactobacillus</i> spp.....	278
8.1.5	<i>Mycobacterium tuberculosis</i> .....	278
8.2	Potential routes of translocation to the Carotid artery .....	279
8.2.1	Oral bacteraemia.....	279
8.2.2	Macrophage internalisation and translocation .....	279
8.2.3	Leaky gut and intestinal bacteraemia.....	280
8.3	THP-1 gene expression .....	280
8.3.1	Expression of cholesterol homeostatic gene in <i>P. acnes</i> -infected THP-1 cells ...	280
8.3.2	Expression of cytokines/chemokines in <i>P. acnes</i> -infected THP-1 cells.....	286
8.4	Conclusion .....	289
<b>9.0</b>	<b>References .....</b>	<b>291</b>
<b>10.0</b>	<b>Appendices .....</b>	<b>327</b>
	Appendix A. Brain heart infusion (BHI).....	327
	Appendix B. Tryptic Soy Broth (TSB) .....	328
	Appendix C. Tryptone-Yeast extract-Gelatine-Volatile Fatty Acid-Serum (TYGVS).....	329
	Appendix D. Final developed growth medium to support the growth of all RCB.....	330

## List of Tables and Figures

### Chapter 1 - Figures

**Figure 1.0:** The vasculature of the human body.

**Figure 1.02:** Layers of the artery.

**Figure 1.03:** The arterial circulation of the head and neck.

**Figure 1.04:** Carotid endarterectomy procedure.

**Figure 1.05:** Leukocytes recruitment and extravasation of the endothelium.

**Figure 1.06:** Regulation of SREBP transcription factor for the up-regulation of cholesterologenic genes.

### Chapter 2 – Figures

**Figure 2.01:** CAP and LITA tissue processing.

### Chapter 2 - Tables

**Table 2.01:** Alternative growth media used in stage 1 to culture test bacteria species/strains.

**Table 2.02:** Individual VFA concentrations used as part of a solution to test bacteria growth in culture medium.

**Table 2.03:** Media supplements selected for stage 2 of bacterial growth medium development.

**Table 2.04:** Progressive development of bacterial growth medium.

**Table 2.05:** Primer sequences for 16S rDNA amplification.

**Table 2.06:** Thermo cycling conditions for 16S rDNA primer sets and  $\beta$ -globin

**Table 2.07:** Oligonucleotide primers designed for real-time PCR

**Table 2.08:** Thermal-cycler parameters for gene expression assays using SYBR® Select.

### Chapter 3 - Figures

- Figure 3.01:** Atherosclerotic plaque formation.
- Figure 3.02:** A-C six-piece stitched image of atherosclerotic plaque tissue from the internal carotid artery from a 72 year old male.
- Figure 3.03:** Cholesterol clefts formation in atherosclerotic plaque tissue.
- Figure 3.04:** Large accumulation of foam cell-like structures within and around a sizable lipid pool.
- Figure 3.05:** Large CAP tissue sections stained with MTC and captured at X4 magnification then manually stitched together.
- Figure 3.06:** Shows the varied formation of intraplaque vessels.
- Figure 3.07:** Large region is characteristic of calcium mineralisation.
- Figure 3.08:** Shows the immune cell activity at the shoulders of the plaque tissue.
- Figure 3.09:** Frequency of plaques (n = 20) that contained common histopathological features of atherosclerotic disease.
- Figure 3.10:** Representative sections of LITA tissue stained with HE
- Figure 3.11:** Bar graph to show the presence and degree of PGN localisation in CAP specimens was expressed as a percentage of total number of samples (n = 20).
- Figure 3.12:** Anti-PGN staining around a large lipid pool
- Figure 3.13:** Anti-PGN staining shows PGN localisation between fibrous tissue around a large lipid pool with necrotic core.
- Figure 3.14:** Anti-PGN staining in fibrous collagen-like tissue
- Figure 2.15:** anti-PGN staining within cholesterol region of plaque accompanied by cholesterol clefts.

### Chapter 3 - Tables

- Table 3.01** Power calculations to establish require population number (*n*) to minimise margin of error.

**Table 3.02:** Histological features observed within formalin fixed paraffin embedded CAP specimens.

#### Chapter 4: Figures

**Figure 4.01:** Flow diagram that details the materials & methods (including section numbers) used in this chapter of work to identify bacterial 16S rDNA sequences present in human internal atherosclerotic plaques.

**Figure 4.02:** Gel electropherogram shows amplification of the internal control, HBG.

**Figure 4.03:** Agarose gel electropherograms (2%) for the detection of *P. acnes* 16S rDNA in CAP tissue.

**Figure 4.04:** Agarose gel electropherograms (2%) for the detection of *P. gingivalis* 16S rDNA in CAP tissue and LITA tissue specimens (C & D).

**Figure 4.05:** Agarose gel electropherograms (2%) for the detection of *T. forsythia* 16S rDNA in CAP tissue (A & B) and LITA tissue specimens (C & D).

**Figure 4.06:** Agarose gel electropherograms (2%) for the detection of *T. denticola* 16S rDNA.

**Figure 4.07:** Agarose gel electropherograms (2%) for the detection of *Streptococcus* spp 16S rDNA in CAP samples (A & B) and LITA control samples (C & D).

**Figure 4.08:** Agarose gel electropherograms (2%) for the detection of *Lactobacillus* spp.

**Figure 4.09:** PCR amplification of Bacteroidetes 16S rDNA. Each gel represents one tissue sample from one patient. CAP specimen was divided into manageable sample sizes for DNA extraction (e.g. 8 sub-samples for CAP sample #7 (B)).

**Figure 4.10:** PCR amplification of 16S rDNA using universal (d88/E94) primers for targeting most bacteria. Each gel represents on tissue sample from one patient.

**Figure 4.11:** Chemically competent *E. coli* (DH5 $\alpha$ ) transfected with TOPO<sup>®</sup> pCR<sup>®</sup>2.1 vector on selective LB agar in the presence of (X-gal).

**Figure 4.12:** PCR colony screen analysis of a crude colony cell suspension using M13 primers to confirm the presence of a cloned DNA insert.

**Figure 4.13:** Data output from chimera detection software Pintail v 1.1. Data relates to a sequence identified as *P. acnes* SK137 using universal primers compared to the reference sequence for the same strain in the NCBI-BLASTn taxID:2 database.

#### Chapter 4: Tables

**Table 4.01:** A basic table plot showing the samples that exhibited amplifiable bacterial 16S rDNA.

**Table 4.02:** List of the bacterial taxa identified using universal, phyla (Bacteroidetes) and genus (*Streptococcus*) specific primer sets.

#### Chapter 5: Figures

**Figure 5.01:** *T. forsythia* colonies on blood agar.

**Figure 5.02:** Growth curve representing the growth of *T. forsythia* in TSB liquid medium

**Figure 5.03:** Shows the linear relationship between number (cfu/ml) vs OD<sub>600</sub> during exponential growth of *T. forsythia*.

**Figure 5.04:** *P. gingivalis* 11834 grows on blood agar.

**Figure 5.05:** Growth curve representing the growth of *P. gingivalis* 11834 in BHI liquid medium.

**Figure 5.06:** Shows the linear relationship between bacteria cell number (cfu/ml) vs OD<sub>600</sub> during exponential growth of *P. gingivalis* 11834.

**Figure 5.07:** *P. gingivalis* W50 colonies on blood agar.

**Figure 5.08:** Growth curve representing the growth of *P. gingivalis* W50 in BHI liquid medium.

**Figure 5.09:** Shows the linear relationship between number (cfu/ml) vs OD<sub>600</sub> during exponential growth of *P. gingivalis* W50.

**Figure 5.10:** *T. denticola* colonies on semi-solid TYGVS medium.

**Figure 5.11:** Growth curve representing the growth of *T. denticola* in TYGVS medium

- Figure 5.12:** Shows the linear relationship between number (cfu/ml) vs OD<sub>600</sub> during exponential growth of *T. denticola*.
- Figure 5.13:** Shows the mean OD<sub>600</sub> values of RCB cultured in TSB medium. Each line represents the mean OD<sub>600</sub> values calculated from three technical replicate cultures of each species.
- Figure 5.14:** Shows the mean OD<sub>600</sub> values of RCB cultured in BHI broth. Each line represents the mean OD<sub>600</sub> values calculated from three technical replicate cultures of each species.
- Figure 5.15:** Shows the mean OD<sub>600</sub> values of RCB cultured in TYGVS medium. Each line represents the mean OD<sub>600</sub> values calculated from three technical replicate cultures of each species.
- Figure 5.16:** Growth curves of *T. denticola* in TYGVS medium following the individual removal of each inorganic salt.
- Figure 5.17:** Bar chart shows the mean (n = 3) culture turbidity readings (OD<sub>600</sub>) for *T. forsythia* (Tf), *P. gingivalis* (11843 & W50) and *T. denticola* (Td) growth incubated in a 'base' medium supplemented with 0.25, 0.5, 0.75 or 1 mg/ml (NH<sub>4</sub>)<sub>2</sub>SO<sub>4</sub>.
- Figure 5.18:** Growth curve for all species in medium A.
- Figure 5.19:** Bar graph shows the mean culture turbidity readings (OD<sub>600</sub>) for *T. forsythia* (Tf), *P. gingivalis* (11843 & W50) and *T. denticola* (Td) when incubated in base medium supplemented with conc. gradient of K<sub>2</sub>HPO<sub>4</sub> compared to control medium (without K<sub>2</sub>HPO<sub>4</sub>).
- Figure 5.20:** Shows growth curves for each test species incubated in medium B
- Figure 5.21:** Bar chart shows the mean (n = 3) culture turbidity readings (OD<sub>600</sub>) for *T. forsythia* (Tf), *P. gingivalis* (11843 & W50) & *T. denticola* (Td) when incubated in medium B supplemented with a conc gradient of NaCl<sub>2</sub> or without NaCl<sub>2</sub> (control).

- Figure 5.22:** Shows growth curves for all test species incubated in TSB medium containing all preceding optimum supplement concentrations, including 1 mg/ml NaCl<sub>2</sub>,
- Figure 5.23:** Bar chart shows the mean (n = 3) culture turbidity readings (OD<sub>600</sub> for *T. forsythia* (Tf), *P. gingivalis* (11843 & W50) and *T. denticola* (Td) ) in late-log, early-plateau growth phase when incubated in 'medium C' supplemented with 4, 6, 8 or 10% volatile fatty acid (VFA) solution or medium without VFA (control).
- Figure 5.24:** Shows growth curves for all test species incubated in TSB medium containing all preceding optimum supplement concentrations, including 6% VFA solution, (medium D; table 5.03).
- Figure 5.25:** Bar chart shows the culture turbidity readings (OD<sub>600</sub>) for *T. forsythia* (Tf), *P. gingivalis* (11843 & W50) and *T. denticola* (Td) during late-log, early-plateau growth phase when incubated in medium D supplemented with 12, 12.5, 13 and 13.5 µg/ml thiamine pyrophosphate (TPP) or medium without TPP (control).
- Figure 5.26:** Growth curves for all test species incubated in TSB medium with all preceding optimum supplement concentrations, including 12.5 µg/ml TPP, (medium E; table 5.03).
- Figure 5.27:** Bar chart shows the mean (n = 3) culture turbidity readings (OD<sub>600</sub>) for *T. forsythia* (Tf), *P. gingivalis* (11843 & W50) and *T. denticola* (Td) ) in late-log, early-plateau growth phase when incubated in media E supplemented with 225, 250, 275 or 300 µg/ml sodium pyruvate (SP).
- Figure 5.28:** Growth curves for all test species incubated in TSB medium with all preceding optimum supplement concentrations, including 250 µg/ml SP, (medium F; table 5.03).
- Figure 5.26:** Bar chart shows the mean (n = 3) culture turbidity readings (OD<sub>600</sub>) for *T. forsythia* (Tf), *P. gingivalis* (11843 & W50) and *T. denticola* (Td)) when incubated in medium F supplemented with 5, 10 and 15% rabbit serum (RS).

**Figure 5.27:** Line graphs for mean growth curve of all test species, *T. forsythia*, *P. gingivalis* (11843 & W50) and *T. denticola* in TSB medium G containing all optimum media supplements, including 10% RS.

**Figure 5.28:** Growth curves for all test species incubated in TSB medium with all preceding optimum supplement concentrations, including 250 µg/ml SP, (medium F; table 5.03).

**Figure 5.29:** Bar chart shows the mean (n = 3) culture turbidity readings (OD<sub>600</sub>) for *T. forsythia* (Tf), *P. gingivalis* (11843 & W50) and *T. denticola* (Td) when incubated in medium F supplemented with 5, 10 and 15% rabbit serum (RS).

**Figure 5.30:** Line graphs for mean growth curve of all test species, *T. forsythia*, *P. gingivalis* (11843 & W50) and *T. denticola* in TSB medium G containing all optimum media supplements, including 10% RS

**Figure 5.31:** Multiple colonies incubated on blood agar anaerobically (A, B, C & D) using liquid cultures derived from human CAP tissue homogenates.

**Figure 5.32:** Fresh colonies of *Propionibacterium acnes* picked from mixed blood agar plates derived from atherosclerotic plaque.

**Figure 5.33:** Fresh blood agar plates containing pure colonies picked and inoculated from mixed plates containing atherosclerotic cultures.

#### Chapter 5: Tables

**Table 5.01:** Shows the number of doublings occurring during the 192 h culture time, growth rate, population doubling time and the cells/ml conversion for 1 optical density unit for *T. forsythia*, *P. gingivalis* (W50 & 11834) and *T. denticola*.

**Table 5.02:** Taken from section 2.3.2 materials & method. Medium supplements for stage 2 of the medium development.

**Table 5.03:** Shows the sequential development of experimental TSB medium supplements.

## Chapter 6: Figures

**Figure 6.01:** *Cholesterol Uptake/Efflux.*

**Figure 6.02:** Mevalonate pathway and isoprenoid synthesis.

**Figure 6.03:** Shows boxplot graphs for fold change expression of *HMGR* (A), *SCAP* (B), *SREBP2* (C), *ABCA1* (D) and *CCL3* (E) in plaque (n = 15) vs LITA (n = 7) tissue.

**Figure 6.03:** *Continued.* Shows boxplot graphs for the gene expression fold change of *CCL2* (G), *ICAM1* (H), *TNF $\alpha$*  (I), *IL1 $\beta$*  (J) and *BCL2A1* (K) in plaque (n = 15) vs LITA (n = 7) tissue.

## Chapter 6: Tables

**Table 6.01:** Gene expression results for CAP expression relative to LITA and normalised to RPL27A.

## Chapter 7: Figures

**Figure 7.01:** Basal growth curve and population doubling calculations for THP-1 cells

**Figure 7.02:** Line graph of mean THP-1 cell exponential growth (24-72 h).

**Figure 7.03:** Optimum amplification efficiency for the endogenous control gene *RPL27A*.

**Figure 7.04:** Efficiency comparison example. C<sub>T</sub> values were determined for *HMGR* and housekeeping gene *ACTB* (A) and *RPL27A* (B) using cDNA extracted and reverse transcribed from LPS infected THP-1 cells.

**Figure 7.05:** Dissociation curves from melt curve analysis.

**Figure 7.06:** Agarose gel electropherogram for PCR amplification of *MYD88* cDNA shows the amplification of two discrete PCR products (~140 bp) in the same reaction with *MYD88* primers.

**Figure 7.07:** Temporal expression of THP-1 gene *HMGR* in response to *E. coli* LPS.

**Figure 7.08:** Temporal expression of THP-1 gene *SCAP* in response to *E. coli* LPS.

**Figure 7.09:** Temporal expression of THP-1 gene *SREBP2* in response to *E. coli* LPS.

- Figure 7.10:** Temporal expression of THP-1 gene *LDLR* in response to *E. coli* LPS.
- Figure 7.11:** Temporal expression of THP-1 gene *CCL3* in response to *E. coli* LPS.
- Figure 7.12:** Temporal expression of THP-1 gene *CCL2* in response to *E. coli* LPS.
- Figure 7.13:** Temporal expression of THP-1 gene *ICAM-1* in response to *E. coli* LPS.
- Figure 7.14:** Temporal expression of THP-1 gene *TNF $\alpha$*  in response to *E. coli* LPS.
- Figure 7.15:** Temporal expression of THP-1 gene *IL-1 $\beta$*  in response to *E. coli* LPS.
- Figure 7.16:** Temporal expression of THP-1 gene *TLR2* in response to *E. coli* LPS.
- Figure 7.17:** Temporal expression of THP-1 gene *NF- $\kappa$ B* in response to *E. coli* LPS.
- Figure 7.18:** Temporal expression of THP-1 gene *BCL2A1* in response to *E. coli* LPS.
- Figure 7.19:** Fold change gene expression of 6 THP-1 cell target genes when exposed to three different MOI of *P. acnes* (MOI 25, 50 & 100; figures A-C, respectively).
- Figure 7.20:** Gene expression fold change for *HMGr* following challenge of THP-1 monocyte cell line with *P. acnes* at an MOI OF 25 (blue boxes).
- Figure 7.21:** Gene expression fold change for *SCAP* following challenge of THP-1 monocyte cell line with *P. acnes* at an MOI of 25 (blue boxes).
- Figure 7.22:** Gene expression fold change for *SREBP2* following challenge of THP-1 monocyte cell line with *P. acnes* at an MOI of 25 (blue boxes).
- Figure 7.23:** Gene expression fold change for *LDLr* following challenge of THP-1 monocyte cell line with *P. acnes* at an MOI of 25 (blue boxes).
- Figure 7.24:** Gene expression fold change for *ABCA1* following challenge of THP-1 monocyte cell line with *P. acnes* at an MOI of 25 (blue boxes).
- Figure 7.25:** Gene expression fold change for *CCL3* following challenge of THP-1 monocyte cell line with *P. acnes* at an MOI of 25 (blue boxes).
- Figure 7.27:** Gene expression fold change for *ICAM-1* following challenge of THP-1 monocyte cell line with *P. acnes* at an MOI of 25 (blue boxes).
- Figure 7.28:** Gene expression fold change for *TNF $\alpha$*  following challenge of THP-1 monocyte cell line with *P. acnes* at an MOI of 25 (blue boxes).

**Figure 7.29:** Gene expression fold change for *IL1 $\beta$*  following challenge of THP-1 monocyte cell line with *P. acnes* at an MOI of 25 (blue boxes).

**Figure 7.30:** Gene expression fold change for *NF- $\kappa$ B* following challenge of THP-1 monocyte cell line with *P. acnes* at an MOI of 25 (blue boxes).

**Figure 7.31:** THP-1 monocyte expression fold change of *BCL2A1* following challenge with *P. acnes* at an MOI of 25 (blue boxes).

#### Chapter 7: Tables

**Table 7.01:** Primer optimisation to amplification efficiency of primer over three primer concentrations 0.2  $\mu$ M, 0.1  $\mu$ M and 0.05  $\mu$ M

**Table 7.02:** Amplification efficiencies and dynamic ranges for different combinations of reverse transcriptase and MgCl<sub>2</sub>. Grey shaded area indicates the reagents composition chosen for reverse transcription that provided the optimum reaction efficiency and range.

**Table 7.03:** Gene expression fold change values for THP-1 cells exposed to three concentrations of *E. coli* LPS over 20 hours.

**Table 7.04:** Gene expression fold change values for THP-1 cells challenged with a *P. acnes* MOI of 20. Fold change was calculated using the comparative C<sub>T</sub> ( $\Delta\Delta$ C<sub>T</sub>) method.

#### Chapter 8: Figures

**Figure 8.01:** Flow schematic of the hypothetical mechanisms that give rise to transient bacteraemia of the species detected in CAP samples studied in the present investigation.

## List of abbreviations

ABCA1	ATP-binding cassette transporter A1
ACAT1	Acetyl-CoA Acetyltransferase 1
ACEH	acid cholesterol ester hydrolase
ACS	acute coronary syndrome
AP	Atherosclerotic plaque
ApoB	Apolipoprotein B
ApoE	Apolipoprotein E
Bak	Bcl-2 homologous antagonist/killer
Bax	Bcl-2 associated X-protein
BCL2A1	B Cell Lymphoma-2 protein A1
BHI	Brain heart infusion
Bid	BH3 interacting-domain death agonist
CAM	Cell adhesion molecule
Camp	cyclic adenosine monophosphate
CAP	Carotid atherosclerotic plaque
CCA	Common carotid artery
CCL2	C-C motif ligand 2
CCL3	C-C motif ligand 3
CCL5	C-C motif ligand 5
CCR2	C-C motif receptor 2
CD36	Cluster of differentiation 36
CD60	Cluster of differentiation 60
CE	Cholesterol ester
CHD	Coronary heart disease
CSF-1	Colony stimulating factor
CVD	Cardiovascular disease
CXCL1	Chemokine (C-X-C motif) ligand 1
EC	Endothelial cells
ED	Endothelial dysfunction
EGF	Endothelial growth factor
ER	Endoplasmic reticulum
FHS	Framingham Heart Study
H&E	Haematoxylin & Eosin
HDL	High density lipoprotein
HMG-CoA	3-hydroxymethylglutaryl-coenzyme A
HMGR	3-hydroxy-3-methylglutaryl coenzyme A reductase
HUVEC	Human umbilical vascular endothelial cells
ICAM1	Intracellular adhesion molecule 1
IFN- $\gamma$	Interferon- gamma
IHC	Immunohistochemistry
IL1-ra	Interleukin 1 receptor agonist
IL1 $\beta$	Interleukin 1 beta
IL-6	Interleukin 6
IPH	Intraplaque haemorrhage
IPV	Intraplaque vessels
I $\kappa$ B $\beta$	I $\kappa$ B kinase- $\beta$
LDL	Low density lipoprotein
LDLR	Low density lipoprotein receptor
LITA	Left internal thoracic artery (mammary artery)

LPS	Lipopolysaccharide
LTA	Lipoteichoic acid
M-CSF	Macrophage colony stimulating factor
MIF	Macrophage inhibitory factor
MMP	Matrix metalloproteinase
MOI	Multiplicity of infection
MTC	Masson's trichrome
MyD88	Myeloid differentiation primary response gene 88
NADPH	Nicotinamide adenine dinucleotide phosphate
NCEH1	Neutral cholesterol ester hydrolase 1
NF- $\kappa$ B	Nuclear factor kappa-light-chain-enhancer of activated B cells
NICE	National Institute for Care and Excellence
NLRP3	Nacht, LLR and PYD domains-containing protein 3
NO	Nitric oxide
OD <sub>600</sub>	Optical density at wavelength of 600 nanometers
oxLDL	Oxidised LDL
PAF	Platelet activating factor
PCAM-1	Platelet endothelial cell adhesion molecule 1
PCR	Polymerase chain reaction
PGN	Peptidoglycan
PGSL	P-selectin glycoprotein ligand 1
PMA	Phorbol 12-myristate 13-acetate
qPCR	Quantitative real-time PCR
RAN $\kappa$ L	Receptor activator of ligand factor kappa-B ligand
RBC	Red blood cells
RCB	Red complex bacteria
RCT	Revers cholesterol transport
ROS	Reactive oxygen species
SMC	Smooth muscle cells
SR-A1	Scavenger receptor A1
SRE-1	Sterol regulatory element 1
SREBP2	Sterol regulatory binding protein 2
SSD	Sterol sensing domain
TIA	Transient ischemic attack
TNF $\alpha$	Tumor necrosis factor alpha
TPP	Thiamine triphosphate
TSB	Tryptic soy broth
TYGVS	Trypticase Yeast Glucose Volatile fatty acid Serum
UC	Unesterified cholesterol
VEGF- $\beta$ 1	Vascular endothelial growth factor beta 1
VLDL	Very low density lipoprotein
VSMC	Vascular smooth muscle cells

## Acknowledgements

I wish to thank the School of Medicine and Dentistry for allowing me the chance to fulfil one of my life's goals to research within such a welcoming and experienced school. A very special thanks to Professor Crean, who through his commitments to fund all aspect of my project has made it possible for me to complete novel research in such a fascinating field of study. I also wish to thank all members of the Oral and Dental Sciences Research Group, particularly Dr Paola Dey and Neil Cook who organised skills workshops, lectures and conferences; all of which allowed me to develop both personally and professionally.

I would like to thank both Dr Graham Stafford (School of Dentistry, Sheffield University) and Dr David Dymock (School of Oral and Dental Sciences, Bristol University) who kindly provided me with viable bacterial strains of *Porphyromonas gingivalis* W50/11834 and *Treponema denticola* ATCC 35405, respectively. Without these kind donations, the medium development section of my research may not have been possible. Also, I owe a debt of gratitude to Dr Jelena Gavrilovic (School of Biological Sciences, University of East Anglia) who kindly provided the human monocytic cell line, THP-1. A large chapter of my work was conducted with these cells so I am extremely grateful for her kind donation. I also wish to thank Augustine Tang MD and Vittorio Perricone MD and their surgical staff who provided the tissue for this project.

But I owe the greatest debt of gratitude to Dr Peter Robinson who has been an endless support to me over the last 4 years. Dr Robinson has not only been a wealth of scientific knowledge and research experience but also helped me on a personal level at many points throughout the project.

To all of you I wish to say a huge thank you.



# **MAIN INTRODUCTION**

## 1.1 Epidemiology of cardiovascular disease

Cardiovascular disease (CVD) refers to any abnormal condition characterised by the dysfunction of the heart or blood vessels. It includes diseases such as coronary heart disease (CHD), hypertension and cerebrovascular disease. CVD is the primary cause of death in modern industrialised countries. According to the World Health Organisation (WHO) in 2012, an estimated 17.5 million people died worldwide from CVD, which represents 31% of all deaths; more than all communicable, maternal, neonatal and nutritional disorders combined and double the number of death caused by all cancer (Luengo-Fernández et al. 2006). CVD is still the leading cause of death in Europe today accounting for over 4 million deaths per year. A wide geographical variation in CVD mortality rates exists throughout Europe; Denmark and Norway have among the lowest rates of age-adjusted CVD mortality, which are similar to France, Portugal, the Netherlands and Spain (Nichols et al. 2013). The very highest rates of CVD mortality are found within the Eastern European countries, such as the Russian Federation and Belarus for men and Uzbekistan and Kyrgyzstan for women (Nichols et al. 2013). In Europe, CVD mortality caused 51% of deaths among women and 42% among men in the last year of data, compared with 19 and 23%, respectively, for all cancers combined (Nichols et al. 2014). The situation does seem to be improving somewhat in the United Kingdom; where CVD was found to be the second greatest cause of death at 28% of all deaths after cancer at 29%. However CHD by itself is still the leading cause of death in the UK in 2012 (Townsend et al. 2014). Nearly 41,000 deaths were the result of stroke in the UK, which resulted in a disproportionate mortality rate among females (9%) compared to males (6%) (Townsend et al. 2014). Though overall, men have a greater rate of CVD mortality compared to women, at 29% vs 28%, respectively.

As well as the human cost, both CVD and CHD have major economic consequences for the UK. A study by the *BHF* established that £6.8 billion was spent on treating CVD within the NHS in England between 2012/13; with secondary care accounting for £4,373 million (67%) of these costs and primary care costs were £1,925 million (21%) (Townsend et al. 2014). Though, when additional factors are considered, such as lost productivity, informal healthcare and welfare costs, the figure is more closer to £123 billion (Leal et al. 2006). When considering both the human and economic cost of CVD, any research that focus on understanding the etiological factors that initiate and/or progress CVD, would have great benefit from a clinical and economic perspective.

## 1.2 Anatomy of the artery

The arterial system is a system of blood distribution that originates in the left ventricle and is designed to carry oxygenated blood from the heart to the tissues. Anatomically, it consists of contractile and elastic membranous ducts classified according to size into arteries, (larger diameter) and arterioles (smaller diameter), which will later give rise to blood capillaries (tiny vessels specialized in gaseous exchange between blood and tissues) (figure 1.01). Large arteries have very elastic walls to withstand high pressures. The artery proper is made up of a number of functional discrete layers. The innermost layer is the Tunica intima (commonly referred to as the intima), which is in direct contact with the flow of blood. The intima consists of the endothelium (a type of epithelium) made up of ~60 trillion endothelial cells (EC) and is the largest organ in the body. The subendothelium layer of the intima consists of connective tissue. The middle layer of the artery is known as the Tunica media (or just media), which consists mainly of smooth muscle cells (SMC) and elastic tissue. Between the intima and media is the internal elastic lamina. The outermost layer of the artery is the Tunica adventitia, which mostly comprise collagen, however between the media and the adventitia, is the external elastic lamina. A network of tiny capillary-like vessels known as the vasa vasorum that originates in the adventitia (vasa vasorum externa). The vasa vasorum functions as a blood supply and nourishes the outer vessel layers. Arterioles are smaller vessels that distribute blood to all the organs and branch inside them. As the arterial wall contains a large amount of smooth muscle, arterioles are also known as “muscular arteries”; for identical reasons, larger arteries have been termed “elastic arteries”. Arterioles are also referred to as resistance vessels since, due to their small diameter; they are the primary site of peripheral resistance to blood flow. The last arteriole branching just before a capillary is known as precapillary arteriole.

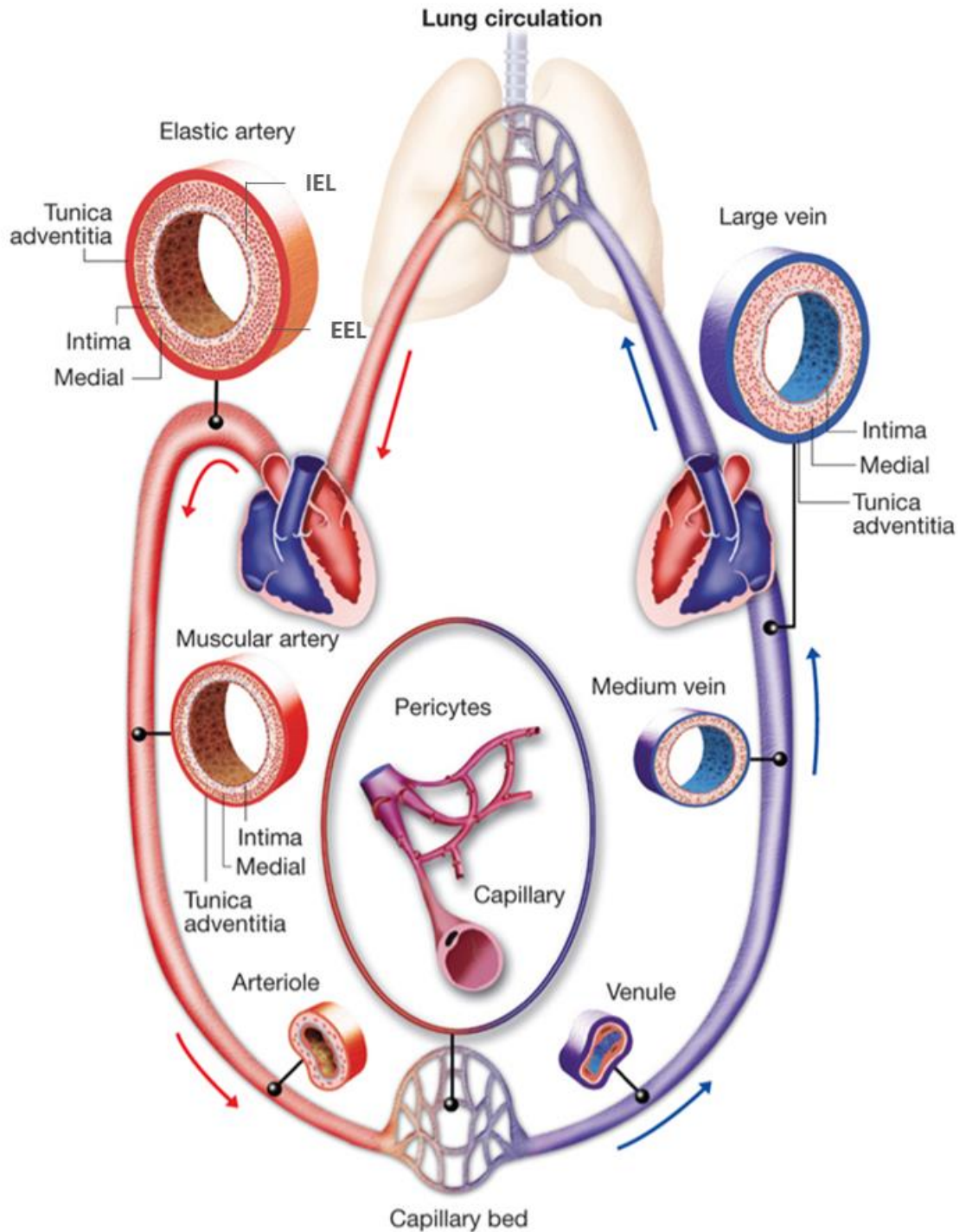


**Figure 1.0:** The vasculature of the human body. The vascular system is divided into two main types of vessels: arteries, which carry blood from the heart to the tissues; and veins, which collect blood from peripheral tissues and return it to the heart. There are two large circuits of blood circulation: systemic circulation and pulmonary circulation. In systemic (greater) circulation oxygen-rich blood is distributed throughout the body and returns to the heart as desaturated blood. Conversely, in pulmonary (lesser) circulation, unoxygenated blood flows from the heart to the lungs, where it is oxygenated to return to the heart. Blood pumped by the left ventricle travels to peripheral tissues through the aorta. The aorta is responsible for supplying the head, the neck and the rest of the body. Thanks to a partial pressure gradient of gases, when the blood reaches the capillaries, it delivers oxygen to the tissues and picks up carbon dioxide. Desaturated blood from tissue capillaries is collected by the systemic veins that enter the right atrium via the superior vena cava and the inferior vena cava.

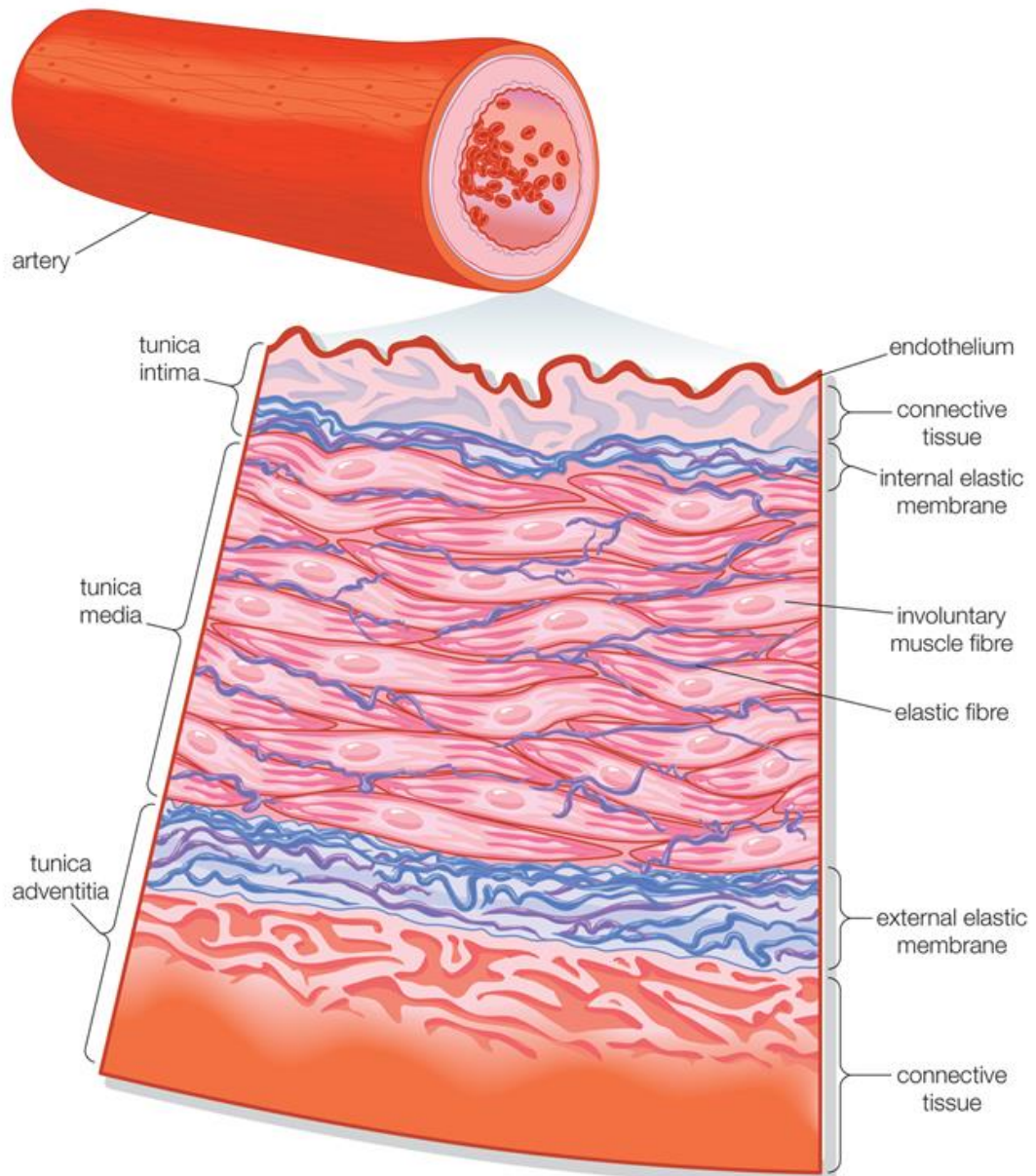


**Figure 1.02:** Layers of the artery. Includes the innermost layer, the tunica intima consisting of the endothelium connective tissue. The middle, fibrous muscular layer, the tunica media, is separated from the intima by the internal elastic membrane. The tunica media comprises smooth muscle cells and elastin and is separated from the outermost layer of connective tissue, the tunica adventitia by the external elastic membrane.

### 1.2.1 The common carotid artery and greater vasculature of the neck and head

Blood is pumped from the heart to the ascending aorta. Blood then passes through the aortic arch and into the brachiocephalic trunk and into the left and right common carotid artery (CCA) that run laterally up either side of the neck (figure 1.03a). A bifurcation in the CCA provides blood flow into the external carotid artery that supplies the face through the mandibular, facial, temporal and occipital artery. The internal carotid artery commences at the bifurcation of the CCA and runs perpendicularly upwards, in front of the transverse processes of the three upper cervical vertebrae, to the carotid foramen in the petrous portion of the temporal bone. The internal carotid artery passes through the carotid canal, curves upwards by the anterior clinoid process, where it pierces the dura mater and divides into its terminal branches (Williams et al. 1995). The internal carotid artery that provides oxygenated blood directly to the vasculature of the brain. The internal carotid artery anastomoses with the middle and anterior cerebral artery and together with the vertebral artery form the cerebral circuit or rather, the circle of Willis.

### 1.3 Atherosclerosis and the carotid artery

Atherosclerosis is the pathology that underlies cardiovascular disease CVD. It is a major progressive form of CVD that produces a focal, inflammatory fibro-proliferative response within the artery wall. These factors can result in hyperlipidaemia and increased permeability of endothelial cells, which allows infiltration of lipoproteins and other plasma constituents into the intimal layer of arteries. This invokes an inflammatory response, resulting in hardening of the vessels caused mainly by the subendothelial accumulation of necrotic foam cells (monocyte derived macrophages) to form occlusive fibrolipidic lesions, known as atheroma.

One of the main vessels affected by atherosclerosis is the common carotid artery and its two branches (external and internal). The most frequent locations for CCA atherosclerosis are the carotid bifurcation, the internal carotid artery and the external carotid artery (De Syo et al. 2005) (figure 1.03b). In the internal carotid arteries atheromatous plaques are characterized by being particularly fragile, ulcerated, with superimposed thrombosis (Golledge et al. 2000). Apparently, atheromatous plaques in these arteries present a thinner fibrous layer which facilitates ulceration, rupture and secondary thrombosis. A carotid bruit detected on systematic physical examination is a sign of atheromatosis. When

stenosis is greater, clinical signs may appear such as transient loss of sight (amaurosis fugax) or disorders related to sensitivity or muscle strength in the limbs or the face on the opposite side of the artery involved.

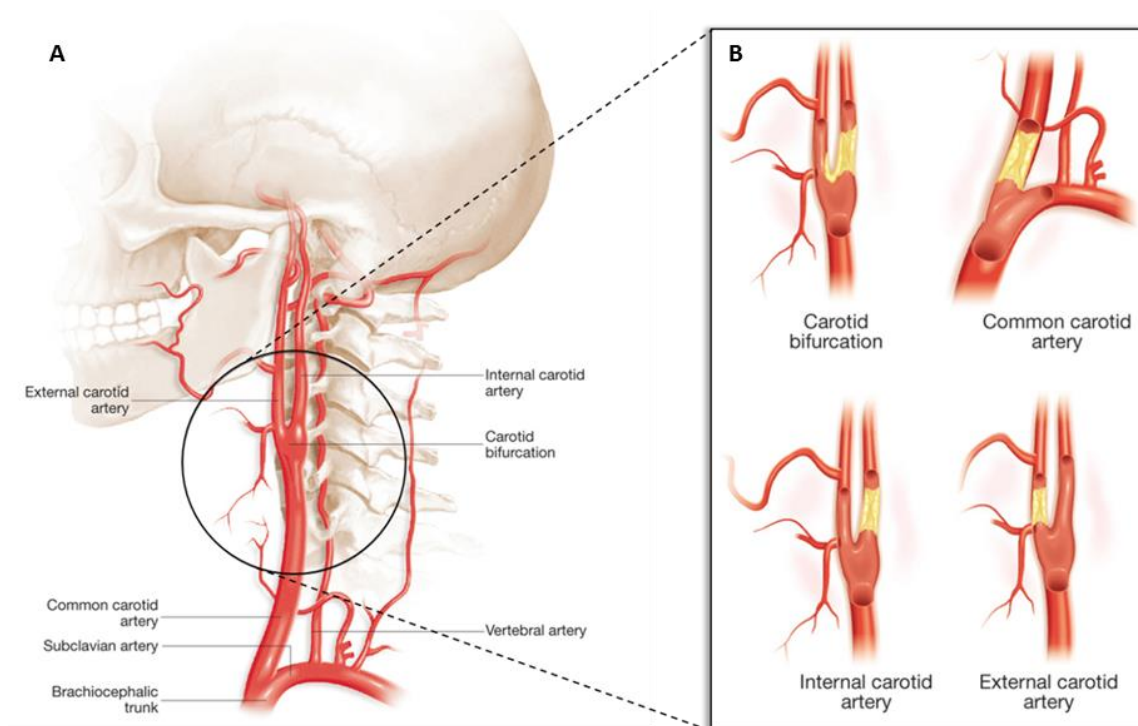


**Figure 1.03:** The arterial circulation of the head and neck shows the carotid artery and the surrounding vasculature and the orientation to the skull (A). Four general distributions of atherosclerotic plaque are typically observed in the carotid artery (B). The plaques that form across the carotid bifurcation are most frequently encountered.

### 1.3.1 Complications of carotid atherosclerosis

Atherosclerotic plaques that develop within the carotid artery can erode overtime resulting in a structural weakening of the lesion leading to plaque fragmentation or rupture at the plaque surface. The local breakdown of the plaque tissue produces emboli that travel in the bloodstream to narrow vessels within the brain where they can cause occlusive ischemic events, such as stroke (Takaya et al. 2005). Ischemia resulting from sudden changes in plaque stability can either be temporary, known as a transient ischemic attack (TIA) or present as permanent stenosis, caused by a focal plaque thrombus or large embolus, termed thromboembolic stroke. Further occlusive complications can arise following small plaque ruptures, such as thromboses at rupture sites caused by red blood

cells (RBC) responses. RBC form aggregates with platelets at the site of the rupture in an attempt to heal the plaque injury. In an already occluded vessel, thrombi can cause further localised vessel occlusion, or can break free, settling at a bifurcation or a narrow vessel of the brain resulting in thromboembolic stroke.

### 1.3.2 Clinical symptoms arising from ruptured or thrombosed plaques in the carotid artery

The clinical presentation of ischemic stroke is characterized by the sudden onset of neurological symptoms caused when a particular neurological vascular territory is affected. For example, lesions located within the lateral aspect of the cerebral hemisphere (territory of the middle cerebral artery) will present with the following signs and symptoms: hemiparesis, hemihypesthesia, motor aphasia, central aphasia, apraxia and hemianopia (Ferro & Fonseca 2014). If located in the midbrain (territory of the posterior cerebral artery) ipsilateral paralysis of the third cranial nerve and contralateral hemiplegia may result (Ferro & Fonseca 2014). If the medulla oblongata (vertebral and posterior inferior cerebellar artery) is affected, such an event is most commonly accompanied by hemiplegia, altered contralateral proprioceptive sensitivity, ipsilateral hypoglossal paralysis and a lateral syndrome that includes hypaesthesia, nystagmus, ataxia and ipsilateral paralysis of the 9<sup>th</sup>, 10<sup>th</sup> and 11<sup>th</sup> cranial nerves, with contralateral thermalgia (Ferro & Fonseca 2014).

### 1.3.3 Surgical intervention

According to the National Institute for Health and Care Excellence (NICE) carotid arteries that present with 50 - 70% stenosis require surgical intervention to reduce the prognoses of further symptomatology. A surgical procedure known as carotid endarterectomy is frequently performed when patient satisfies the correct criteria (figure 1.04). Carotid endarterectomy involves dissecting through the tissues of the neck to expose the occluded vessel. The internal, external and CCA are clamped up and downstream of the occlusion, which temporarily stems the flow of blood to the brain, allowing clear access to the occluded site. Clamping the artery also minimises the risk of stray plaque fragments entering the brain during the procedure. The artery is then dissected longitudinally at the occluded site and the atheroma striped from the artery wall.

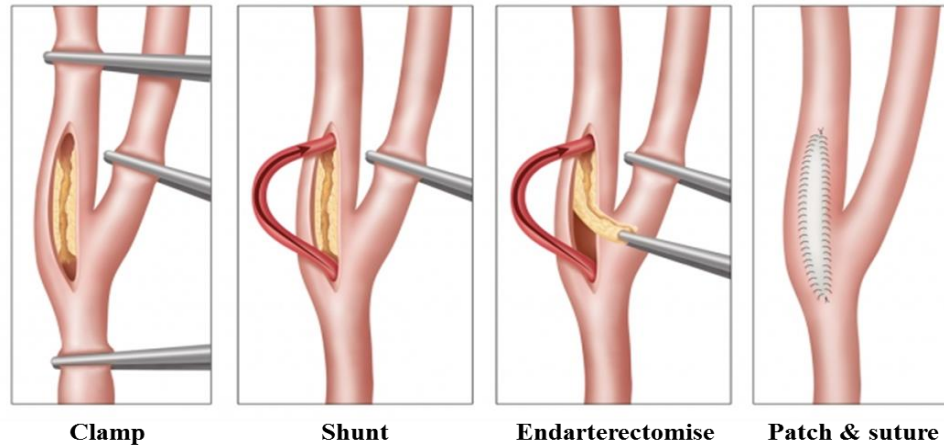


**Figure 1.04:** Carotid endarterectomy procedure involves dissecting through the tissues of the neck to expose the vasculature of the neck. The internal, external and CCA are clamped up and downstream of the occluded atherosclerotic vessel, which temporarily stems the flow of blood to the brain, allowing clear access to the occluded site. Occasional shunting of the blood flow provides a circulation during lengthy procedures. The artery is then dissected longitudinally at the occluded site and then the atheroma removed from the artery wall. A patch is sutured over the surgical incision widening the artery lumen to prevent re-stenosis.

#### 1.3.4 Atherogenesis

Atherosclerotic plaque formation encompasses a series of highly specific cellular and molecular responses during a process of chronic inflammation. The theory supporting that this process occurs as a response to injury proposes that endothelial dysfunction (ED) is the first step in atherogenesis. ED commonly arises at vascular regions where a disruption in blood flow dynamics occurs due to bifurcation or curvature of vessels, which produces an increase or reduction in shear stress leading to a loss of endothelial ability to modulate normal cellular processes. At vascular sites affected by ED the initial phase of atherogenesis is characterized by a chain of events that starts with one or more of the following pathways: high levels of circulating low density lipoprotein (LDL) (Ross et al. 1977), free radicals such as reactive oxygen species (ROS) (Szocs 2004), genetic variations (Bonetti 2002; Jones & Hingorani 2005) and shear stress in areas of turbulent blood flow (Chatzizisis et al. 2007) or inflammatory signals such as cytokines (Ait-Oufella et al. 2011).

As a macromolecule, LDL can transigrate through the permeable endothelium and accumulates in the intimal layer of the artery where it becomes oxidised by ROS. Oxidised (ox)LDL is highly toxic to the surrounding tissue and therefore promotes an inflammatory response in local vascular smooth muscle cells (VSMC) (Kiyani et al. 2014) and further promoted ED (Valente et al. 2014). Two of the pro-inflammatory cytokines stimulated by

oxLDL are interleukin (IL)-1 $\beta$  and tumour necrosis factor (TNF) $\alpha$  that both activate the endothelium to up-regulate cell adhesion molecules (CAMs), intracellular adhesion molecule (ICAM)-1 and vascular cell adhesion molecule (VCAM)-1 as well as selectins P and E-selectin (Falk 2006). Both CAMs act by signalling for the recruitment of circulating leukocytes and lymphocytes. Monocyte recruitment to the vascular site of injury is facilitated by monocyte chemoattract protein (MCP)-1 also known as C-C motif ligand (CCL)2, which forms a concentration gradient that is strongest at its source. Monocytes sense CCL2 secretion by a receptor expressed on its plasma membrane called C-C motif receptor (CCR)2, which acts by guiding the monocyte toward CCL2, thereby bringing the monocyte in contact with the endothelium (Shi & Pamer 2011). Monocytes tether P- and E-selectin of the activated endothelium and commence a rolling motion across the surface of the endothelium due to the high velocity of the arterial blood circulation and the weak affinity between endothelial P- and E-selectin and their monocyte ligands, P-selectin Glycoprotein Ligand (PGSL)-1 and the sialylated Lewis X (sLe<sup>x</sup>) antigen, respectively (Mestas & Ley 2008). Endothelial cells also express platelet activating factor (PAF) that when interacting with monocyte PAF receptor activates monocyte integrins such as Lymphocyte function-associated antigen (LFA)-1 which forms a strong interaction with its endothelial expressed ligand ICAM-1, which immobilises the rolling monocyte at the site of inflammation (Marlin & Springer 1987). Additional signalling events cause the profound reorganisation of the cytoskeletal structure of the monocyte, resulting in the spreading of one edge of the monocyte (Middleton et al. 2002). The leading edge of the monocyte inserts itself between endothelial cells in a process involving further CAM activation (PCAM-1) that function to aid monocyte extravasation and migration into the intimal space (Woodfin et al. 2007). Figure 1.05 highlights the recruitment of monocytes to the activated endothelium and the

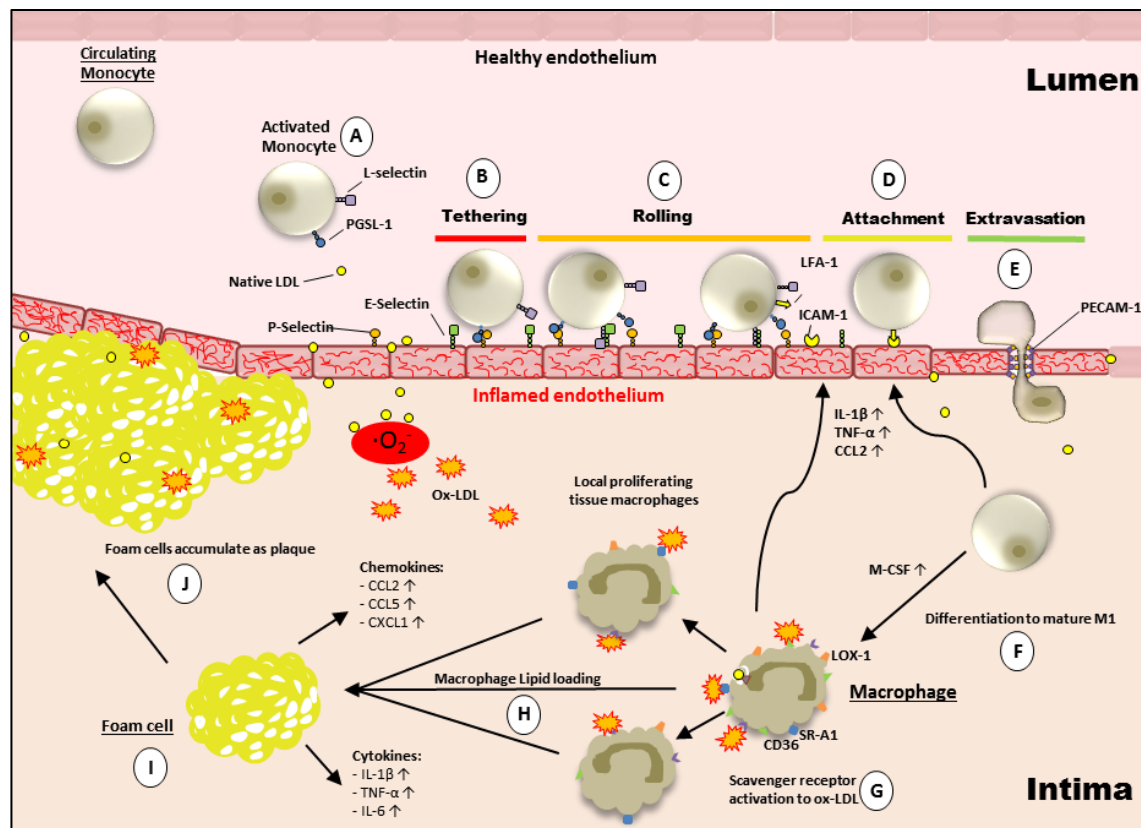


**Figure 1.05:** Leukocytes recruitment and extravasation of the endothelium. Shows the innate immune responses that progress the development of an atherosclerotic lesion. At vascular regions prone to atherosclerosis due changes in blood flow dynamics and shear stress, circulating monocyte subsets are activated in response to vascular inflammation, expressing PGSL-1 and L-selectin in response to the expression of endothelial P and E-selectin, respectively (A). The monocytes are tethered to the endothelium via selectin interaction which rapidly decelerates the monocytes as it exits the velocity of the blood flow (B). Because selectins only bond with weak affinity monocytes begin to roll on the surface of the endothelium (C). At the site of injury ICAM-1 is expressed which binds with high affinity to monocyte-expressed lymphocytes function-associated antigen (LFA)-1, attaching the monocyte to the endothelium surface (D). The cytoskeleton of the monocyte is reorganised in such a way that the monocyte spreads out over the endothelium surface permitting transmigration of the monocytes via the aid of platelet endothelial cell adhesion molecule (PECAM)-1 (a protein found at the endothelial cell intercellular junction) that assists leukocyte diapedesis into the sub-endothelium space (E). Once residing in the intima monocytes undergo differentiation to tissue macrophages mediated by macrophage colony stimulating factor (M-CSF), which simultaneously involves the release of pro-inflammatory cytokines (TNF- $\alpha$ , IL-1 $\beta$  and CCL2) that act on the endothelium to elicit further leukocytes recruitment and chemotaxis (F). Monocyte-derived macrophages express scavenger receptors at the surface of their plasma membrane and undergo rapid proliferation (G). Macrophages avidly take up native and modified (for example, oxidized) low-density lipoprotein (LDL) via macropinocytosis or scavenger receptor-mediated pathways (including via scavenger receptor A1 (SR-A1) and CD36) (H), which results in the formation of the foam cells. These foam cells secrete pro-inflammatory cytokines (including interleukin-1 (IL-1), IL-6, and tumour necrosis factor (TNF)) and chemokines (such as CC-chemokine ligand 2 (CCL2), CCL5 and CXC-chemokine ligand 1 (CXCL1)) (I). The accumulation of foam cells are a hallmark of the atherosclerotic plaque (J). Figure adapted from (Moore et al. 2013)

When residing in the intimal space, monocyte differentiation to tissue macrophage development is mostly influenced by colony stimulating factor (CSF)-1 (also known as macrophage-colony stimulating factor M-CSF), produced by stromal cells within the blood and in tissues (Hamilton 2008). During differentiation monocyte-derived

macrophages up-regulate the expression of a host of membrane surface receptors known as scavenger receptors in response to a number of stimuli including CCL2 (Tabata et al. 2003). Macrophages expressing scavenger receptors then seek out and phagocytise large amounts of oxLDL relentlessly. This excessive internalisation of oxLDL leads to the development of macrophage foam cells; grossly over-sized lipid-loaded macrophages that have an appearance of foam due to the lipid droplets that form in their cytosol. In addition, scavenger receptor binding of oxLDL and foam cell formation induces further macrophage expression of chemotactic M-CSF, MIF and up-regulation of proinflammatory cytokines, such as TNF $\alpha$  and IL-1 $\beta$ , IL-12 and IL-18 (Autieri 2012). Foam cells internalise vast amounts of oxLDL cholesterol they become immobile, unable to egress, thereby accumulating in the atherosclerotic lesion where they become necrotic. Foam cell apoptosis results in the release of stored reactive lipids and toxic debris, which collectively form the lipid core; a distinctive hallmark of atheroma formation (Hegyri et al. 1996). The deposition of increasing excess reactive lipoprotein and apoptotic cellular debris becomes completely overwhelming as efferocytosis and phagocytosis becomes defective (Thorp & Tabas 2009). As further inflammatory signalling is induced in an effort to clear the accumulating reactive lipid the entire process thereby continues in a perpetual negative cycle of LDL entry to the subendothelium, LDL oxidation, cell activation and leukocyte recruitment, monocyte differentiation, foam cell formation and necrosis until a large lipid core develops with extensive necrosis. These processes represent the central paradigm of atherogenesis.

While the innate immune response is potent and plays the greater role, an adaptive response also exists within the atherosclerotic lesion. For example, IL-12 and IL-18 stimulate T-cell differentiation from naive to Th1- and Th2-cells, respectively (Nakanishi et al. 2001). While Th1 cells further potentiate the inflammatory response through secreting proinflammatory cytokines that promote leukocyte activation and proliferation in the lesion, Th2 cells work to inhibit the effects of these responses by promoting anti-inflammatory factors (Packard et al. 2009). When plaques become advanced, cytokines (i.e. IL-1 $\beta$ , IL-6 and TNF- $\alpha$ ), extracellular matrix components (e.g. collagen I, V and VIII) and growth factors (e.g. epidermal growth factor (EGF) vascular endothelial growth factor- $\beta$ 1 (VEGF- $\beta$ 1), basic fibroblast growth factor (bFGF) and platelet derived growth factor (PDGF), stimulate smooth muscle cells (SMC) proliferation and migration through the atherosclerotic lesion to the surface *tunica intima* (Rudijanto). This response is one of healing; in an attempt to cover the atherosclerotic plaque and highly thrombogenic

contents of the lipid core SMC act in paracrine manner to produce a layer of collagen and fibrin over the plaque. This feature is known as the fibrous cap and although it represents an attempt to protect the lesion it can result in plaque rupture. SMC also transdifferentiate to macrophage-like cells that actively scavenge and load themselves on modified LDL in the plaque and develop into foam cells. In a recent immunohistochemical study to identify macrophages and foam cells in atherosclerotic plaque, it was noted that as much as 40% of foam cells expression CD60 (a macrophage specific marker) originated as SMC (Allahverdian et al. 2014). As SMC can essentially transdifferentiate into macrophage-like cells that lose many of their classic SMC markers, these cells facilitate multiple roles, each of which progress plaque development.

#### 1.4 Risk factors associated with the development of atherosclerosis

The term “risk factor” is widely used to describe any attribute, characteristic or exposure of an individual that have been shown in epidemiological studies, autopsy studies, metabolic studies, and genetic studies to increase the likelihood of developing a disease. Risk factors can be categorised as personal, lifestyle, biochemical or physiological characteristics that are either modifiable or not. The vast majority of risk factors involving the development of CVD are modifiable and are well advertised. In 1948 a critical study known as the Framingham Heart Study (FHS) was initiated in the USA and provided the first major open access data relating to >5000 participants. Prior to this study, little was known about the relative risk of genetic and environmental factors in the development and progression of CVD. Over 1000 studies have resulted from the FHS to identify major CVD risk factors, such as high blood pressure, high serum cholesterol, diabetes, smoking, obesity and physical inactivity (Kannel et al. 1961; Cornfield 1962; Kannel et al. 1965; Kannel & McGee 1979; Hubert et al. 1983; Freund et al. 1993; Sherman et al. 1994).

##### 1.4.1 Non-modifiable risk factors

###### 1.4.1.1 Age

Age is one of the non-modifiable cardiovascular risk factors together with sex and genetic factors. Cardiovascular risk is directly related with age, partly due to “aging” of the cardiovascular system itself, but also due to increased prevalence of other risk factors such as hypertension, diabetes, obesity, sedentary lifestyle, etc. All the cardiovascular risk

scoring tables based on the prediction model of the Framingham Heart Study include age as one of the factors to take into account (Wilson et al. 1998).

#### 1.4.1.2 Genetic mutations – familial

It is not completely clear whether the correlation between a family history of heart disease and increased cardiovascular risk is only attributable to genetic factors or is a consequence of habits and lifestyle inherited from parents. However, certain genetic defects have been linked with increased cardiovascular risk, e.g. polymorphism of the fibrinogen beta-chain gene (Iacoviello et al. 2001) or genotypes expressed as homozygous and heterozygous forms of familial hypercholesterolemia (Hobbs et al. 1992). Hypercholesterolemia results from mutation in the gene that encodes apolipoprotein (apo)B or (apoE) specific LDL receptor that is inherited as the heterozygous genotype or as the much rarer (1 in 1 million births) homozygous genotype; inherited in an autosomal dominant pattern (Rader et al. 2003; Soutar & Naoumova 2007). Most primary disorders associated with atherogenic dyslipidemias have an unknown molecular base and are classified as “polygenic” (Kathiresan et al. 2009).

#### 1.4.1.3 Congenital defects

The presence of congenital diseases of the homocysteine metabolism (with homozygous genotype) and very high serum homocysteine levels are positively correlated with premature atherosclerosis; these patients may have a myocardial infarction during the second decade of life. Homocysteine is toxic to endothelium: it has a prothrombotic effect, promotes collagen formation and reduces NO availability. In certain cases, patients suffer from moderate hyperhomocysteinemia; this disorder is positively correlated with risk for cardiovascular disease although not as closely as with the so-called major risk factors (Yang et al. 2005).

### 1.4.2 Modifiable risk factors

#### 1.4.2.1 Affluent diet

Epidemiological studies carried out all over the world and in large population groups have determined that consumption of the typical affluent cholesterol-rich diet of industrialized countries is closely related to the prevalence of atherosclerosis (Wilson et al. 1998). A cholesterol-rich diet is characterized by excess saturated fat and cholesterol; the two key

nutrients for developing dyslipidemia, as well as animal protein, refined sugars and sodium chloride, very low intake of vegetal fibres and a high total caloric value. This kind of diet is not only associated with atherosclerosis and its related conditions (coronary heart disease, cerebrovascular disease, peripheral vascular disease, among others) but also to other conditions which sometimes coexist thus increasing the cardiovascular risk; examples of these are hypertension, type 2 diabetes and obesity (Wilson et al. 1998).

#### 1.4.2.2 Plasma LDL cholesterol levels

Prolonged intake of a cholesterol-rich diet increases plasma levels of LDL cholesterol. It is currently accepted that elevated plasma LDL concentrations are major risk factors for developing CHD. This correlation has been well identified in epidemiologic/observational studies of important cohorts that have been prospectively followed (Anon 2002; Grundy et al. 2004). Evidence shows a continuous positive relation between risk for CHD and plasma LDL-cholesterol levels, and there is no defined “threshold” below which lower concentrations are associated with lower risk (Siri-Tarino et al. 2010). These studies suggest that the cardiovascular risk increases by 2% every 1% increase in total cholesterol. In addition, the predictive value of HDL cholesterol levels as a risk factor inversely correlated with cardiovascular disease has been extensively confirmed (Castelli 1986; Assmann et al. 1996; Curb et al. 2004; Mahdy Ali et al. 2012; Nomikos et al. 2015). Recent data has evidenced that triglyceride values above 2 g/l entail a high risk for CHD and suggest that target values are below 1 g/l. Lipoprotein(a) is an independent risk factor for CHD. A relative risk for myocardial infarction 1.75 times higher if Lipoprotein(a) levels are over or equal to 300 mg/l has been reported (Schaefer 2002; Schmitz & Orsó 2015). Obese individuals have a three-fold higher risk to develop CHD as compared to subjects with a normal body mass index (BMI) (Poirier et al. 2006).

#### 1.4.2.3 Hypertension

High blood pressure is directly related to the risk of cerebrovascular accident and myocardial infarction. Although hypertension is often associated to obesity and insulin resistance, the risk posed by hypertension enhances the risk presented by any of the other cardiovascular risk factors. The higher the blood pressure levels, the higher the risk of cardiovascular disease (Mann et al. 2011). A physiological and pathogenic observation reveals three hypertension-related disorders causing vascular damage: pulsatile blood flow, endothelial cell dysfunction, and vascular smooth muscle hypertrophy. High systolic

pressure is known to be the main causal agent for these disorders; it entails a greater risk than high diastolic pressure (Mann et al. 2011).

#### 1.4.2.4 Smoking tobacco

Several studies have conclusively shown that smoking accelerates arteriosclerosis and atherosclerosis, increasing the risk for coronary artery disease, cerebrovascular disease and peripheral vascular disease (Howard et al. 1998). The smoking habit raises LDL and triglyceride levels and reduces HDL levels; also, it promotes endothelial hypoxia as it raises blood levels of carbon monoxide. Furthermore, nicotine and other tobacco derivatives are toxic to endothelium and may cause its dysfunction. In addition, it promotes arterial vasoconstriction. In addition, cigarette smoking increases platelet reactivity and aggregation, and plasma fibrinogen concentration, which results in higher blood viscosity. These negative effects of tobacco are directly related to the number of cigarettes smoked per day. Furthermore, passive smokers are at an increased risk for CHD (Benowitz & Gourlay 1997).

#### 1.4.2.5 Type 2 diabetes

Coronary artery disease accounts for almost 75% of deaths in diabetic individuals (Sowers et al. 2001). Although hyperglycemia is associated with small vessel disorders, insulin resistance promotes by itself, the development of atherosclerosis even before it manifests clinically as diabetes (Aronson & Rayfield 2002). Diabetic patients show a marked impairment of the vascular smooth muscle and endothelial functions, as well as an increased leukocyte adhesion to the vascular endothelium, which plays a critical role in atherogenesis (Sowers et al. 2001). The triad hypertriglyceridemia plus HDL cholesterol reduction plus increase in small and dense LDL particles promotes the development of atherosclerosis; some authors term it “atherogenic dyslipidemia” (Manjunath et al. 2013).

### 1.4.3 Infection as a risk factor for the development of atherosclerosis

Further to the aforementioned “traditional risk factors”, such as plasma LDL level, smoking, cholesterol-rich diet and physical inactivity, other potential sources of risk are now associated with the initiation and progression of atherosclerosis. One such factor that has been demonstrated to be associated with the development of various forms of CVD is infection (Shah 2001). A link between infection and atherosclerosis was first proposed over a century ago by Sir William Osler (1908). Even though the association was mostly

rejected at the time, a renewed interest in the role infection plays in the pathogenesis was revisited some 70 years later by germ free chickens developing atherosclerotic lesions following infection with avian herpes (Fabricant et al. 1978). Current opinion is that increased incidence of CVD is probably the result of a high prevalence of both traditional risk factors and infectious agents (Campbell & Rosenfeld 2015). A large number of infectious agents have been linked with an increased risk of CVD. These include, *C. pneumoniae*, *Helicobacter pylori*, influenza A virus, cytomegalovirus, and human immunodeficiency virus (Madjid et al. 2004; Simanek et al. 2011; Joshi et al. 2013; Sharma & Aggarwal 2015).

#### 1.4.3.1 Direct and indirect inflammation

These infectious agents drive inflammation in two ways, either via direct infection of artery wall where they activate an innate immune response by the vessel cells and/or via systemic raising of inflammatory markers such as acute phase reactants and cytokines from distant sites of the body (Rosenfeld & Campbell 2011; Campbell & Rosenfeld 2015). In order to demonstrate a pathogenic response, the initial criteria for Koch's postulate should be observed, in that there should be evidence of the presence of the agent within the atherosclerotic plaque but not within normal blood vessels. Better still, evidence that the pathogen has infected plaque/artery cells and isolation of the viable organism from cells suggesting active inflammation. The isolated strain must accelerate atherosclerosis when used to challenge in vivo models of atherosclerosis. The infectious agent may also induce inflammation from non-vascular sites such as the lungs (*C. pneumoniae*) and the oral cavity (*P. gingivalis*) (Rosenfeld 2013). Sites of infection can cause a systemic rise in inflammatory cytokines and other secreted factors, such as acute phase reactants that are secreted by the liver, circulate in the bloodstream and activate the endothelium at atheroprone regions of the vasculature (Ebersole 2003; Loos 2005). This can exacerbate the inflammatory milieu already active within the atherosclerotic plaque and further progress atherogenesis (Rosenfeld 2013).

### 1.5 Periodontal disease

Periodontitis is a highly destructive form of periodontal disease that affects the soft and hard tissues of the periodontium as opposed to gingivitis that only affects the gingival tissue. It is a chronic inflammatory disease caused by a multitude of factors, of which

specific oral pathogens and the host immune system play predominant roles. Endo and exotoxins produced by periodontal bacteria in subgingival dental plaque induce pathways that mediate a complex set of inflammatory reactions (Cekici et al. 2014). Periodontitis is characterised by inflamed bleeding gums, which recede from the tooth forming deep pockets at the gingival sulcus. Periodontal pockets become difficult to clean, forming reservoirs for food debris and periodontal bacteria driving infections deeper into the periodontium. Chronic periodontal infections result in progressive erosion of alveolar bone and subsequent detachment of periodontal ligaments that eventually leads to tooth loss (Cekici et al. 2014). One of the mediators of bone resorption is IL-12 that differentiates T-cells to TH1-cells producing IFN- $\gamma$ , the IL-12-IFN- $\gamma$  pathway can induce bone resorption by production of proinflammatory cytokines, such as TNF- $\alpha$  and IL-1 $\beta$ , which leads to the activation of osteoclasts (Queiroz-Junior et al. 2010). Receptor activator of NF- $\kappa$ B ligand (RANKL) and osteoprotegerin (OPG), a decoy receptor of RANKL are both implicated in osteoclast differentiation and activation, and therefore strong mediators of alveolar bone destruction (Queiroz-Junior et al. 2010).

### 1.5.1 Periodontal bacteria

There is estimated to be in excess of 600 prevalent taxa at the species level present within the average healthy human oral cavity, with distinct subsets predominating at different habitats (Aas et al. 2005). Many bacterial species co-exist in an aggregate, wherein bacteria adhere to other bacteria and to the pellicle surface of the tooth. This tight polymicrobial network is known as a dental biofilm, or more commonly as dental plaque (Jakubovics 2010). While large numbers of different bacteria co-exist in dental plaque, it is recognised that many beneficial species in biofilms. It is not the entire bacterial load that attenuates progression from healthy gingivae to periodontal disease, but rather the presence of a minority of pathogenic strains that trigger pathology in susceptible individuals (Marsh 2006). According to phylogenetic studies using the bacterial genetic marker 16S rRNA, only few Gram negative bacteria species were typically recognised as “periodontopathic” and therefore implicated in the initiation and progression of periodontitis, namely, *Aggregatibacter actinomycetemcomitans*, *Porphyromonas gingivalis*, *Tannerella forsythia*, *Treponema denticola*, *Prevotella intermedia*, *Prevotella nigrescens*, *Campylobacter rectus*, *Fusobacterium nucleatum*, *Streptococcus mutans* and *Eikenella corrodens* (Ashimoto et al. 1996; Paster et al. 2001; Haffajee et al. 2008; Heller et al. 2012). Later, it was discovered that genera of Gram positive species were the most

predominant bacteria detected in subgingival plaque, including *Propionibacterium*, *Peptostreptococcus* and *Filifactor* (Kumar et al. 2005). Amongst the eleven Gram negative putative periodontal bacteria, *P. gingivalis*, *T. forsythia* and *T. denticola* are more frequently detected in sub-gingival dental plaque (Heller et al. 2012). This occurrence is suggested to be a consequence of bacterial affinity to form complexes in subgingival plaque (Socransky et al. 1998). Known as ‘red complex bacteria’ (RCB), this triad of gram-negative anaerobic bacteria is present in healthy individuals (Haffajee et al. 2008), although in much lower numbers compared with individuals with active moderate to severe forms of chronic periodontitis (Wara-Aswapati et al. 2009).

However, these earlier studies did not provide a comprehensive view of bacterial communities associated with periodontitis. 16S rRNA gene amplification and next generation sequencing (NGS) has resulted in a major advance in our understanding of the polymicrobial composition of periodontal plaque and provides a much more complete picture of the structures of the microbiome in periodontitis and health (Griffen et al. 2012; Abusleme et al. 2013; Szafranski et al. 2015). Using 454 sequencing of 16S rRNA genes, Griffen et al. (2012) compared subgingival bacterial communities from 29 periodontally healthy controls and 29 subjects with chronic periodontitis. The authors generated over 1.3 million sequences that were identified through BLAST reference searches and were mapped to 16 phyla, 106 genera and 596 species (Griffen et al. 2012). By assessment at each phylogenetic level and genetic distance and principal coordinate analysis, Griffen et al. (2012) found that 123 species were more predominant in disease and 53 in health. Typically Spirochetes, Synergistetes and Bacteroidetes were frequently detected in disease, whereas Proteobacteria were in higher numbers in healthy subjects (Griffen et al. 2012). Using the same experimental design Abusleme et al. (2013) found that presence of bleeding was not associated with microbial diversity in subgingival plaque, though bleeding sites were associated with greater total bacterial load. In contrast, there was a large difference in microbial diversity and load bacterial communities between health and periodontitis (Abusleme et al. 2013). Periodontitis communities showed higher proportions of Spirochetes, Firmicutes and Chloroflexi, whereas Actinobacteria, particularly *Actinomyces* spp. were more prevalent in healthy tissue. However, *Actinomyces* spp. load were unchanged in both health and periodontitis (Abusleme et al. 2013). Other researchers have investigated subgingival plaque tissue for potential biomarkers that may be present using NGS methods of the V1-V2 and V5-V6 hypervariable regions of 16S rRNA gene (Szafranski et al. 2015). The authors generated

sequences for 523 operational taxonomic units (OTUs) for V1-V2 and 432 from the V5-V6 regions. Of these 80 biomarkers of periodontitis and 17 of health were identified. The study demonstrated that these biomarkers could be used as a diagnostic tool when 10 biomarkers for periodontitis were used, 15 of 17 samples were correctly diagnosed for the disease (Szafranski et al. 2015).

### 1.5.2 Periodontitis and Atherosclerosis

As previously noted, infection is proposed as a risk factor in the development atherosclerosis. A major hallmark of periodontitis is the presence of many of the aforementioned putative periodontal pathogens in dental biofilms (both supra- and sub-gingival) that characterise the periodontal pathological process. Many of these putative strains have been associated CVD (Trevisan & Dorn 2010). However, even after nearly three decades of broad study in this field there is extensive variability of the strength of associations, in part, due to the variation in markers used to investigate periodontitis (Beltrán-Aguilar et al. 2012). These include: oral bacteria or antibodies to oral bacteria, salivary flow, self-reported periodontal status, tooth loss, or one of many scoring indices that measure a variation of physical characteristics such as, probing depth, bleeding on probing and attachment loss.

#### 1.5.2.1 Presence of periodontal bacteria in carotid atherosclerotic plaque tissue

Many studies have identified periodontal bacteria in atherosclerotic plaque from various affected arteries using immunohistochemistry (IHC) or PCR. These include *P. gingivalis*, *T. forsythia*, *P. intermedia*, *A. actinomycetemcomitans*, *F. nucleatum*, *C. rectus*. To date thirteen previous studies have attempted to detect periodontal bacteria in carotid atherosclerotic plaque (CAP) samples (Chiu 1999; Haraszthy & Zambon 2000; Cairo et al. 2004; Fiehn & Larsen 2005; Ford et al. 2006; Padilla et al. 2006; Aimetti et al. 2007; Romano et al. 2007; Aquino et al. 2011; Figuero et al. 2011; Armingohar et al. 2014; S. Morita et al. 2014; Rangé et al. 2014). Of these, seven studies have managed to detect DNA from periodontal bacteria (Chiu 1999; Haraszthy & Zambon 2000; Fiehn & Larsen 2005; Ford et al. 2006; Padilla et al. 2006; Figuero et al. 2011; Armingohar et al. 2014), but the remaining four did not (Cairo et al. 2004; Aimetti et al. 2007; Romano et al. 2007; Aquino et al. 2011). Studies that yielded positive results in CAP samples, *T. denticola* DNA was completely absent; whereas 5 out of 7 studies detected *P. gingivalis* and 2 out

of 7 were positive for *T. forsythia*. Interestingly, two of the studies that successfully identified periodontal bacterial DNA in CAP samples did not test the periodontal status of patients (Haraszthy & Zambon 2000; Fiehn & Larsen 2005). Though only Haraszthy & Zambon (2000) showed high detection rates for most of their targets including for *P. gingivalis* (13/50) and *T. forsythia* (30/50), Fiehn & Larsen (2005) did not. Thus, historical oral infection or possibly randomly selected patients with active periodontal infection at the time of the may explain these high detection rate.

Historical infection building over time may also account for findings by Kozarov et al. (2006), who showed the highest percentage detection of all studies for DNA from eight periodontal species in carotid plaque tissue. The author compared detection rates in two groups (young and elderly). Five of eight periodontitis-associated pathogens were detected in both groups. For the elderly group *P. gingivalis* was detected the most (88.8%); markedly higher than that reported for the younger group (18.3%), which may be due to historical buildup of pathogens over time. These findings were also in agreement with other studies testing age as a factor for the severity of infectious agents in atherosclerotic plaque (Haraszthy & Zambon 2000; Pucar et al. 2007). However Kozarov et al. (2006) examined plaque from a mix of affected arteries within the same study, making it difficult to specifically summarise these results for carotid. Percentage of *P. gingivalis* in the elderly group was comparable to those reported by Figuero et al. (2011) (78.5%), although Figuero et al. (2011) reported detection of less species compared to Kazarov (2006), the overall percentages for each of the species reported by Figuero (2011) were higher.

Ford et al. (2006) investigated the presence of periodontal bacteria using specific antibodies for their detection in CAP tissue from individuals with periodontitis. Five different periodontal bacteria including *P. gingivalis* (52%) and *T. forsythia* (34%) were frequently detected in CAP tissue and 76% of samples contained more than one species. In contrast, Padilla et al. (2006) examined the presence of periodontal bacteria in both subgingival plaque and CAP samples using PCR. Although DNA from a number of species were detected in subgingival plaque tissue, including *P. gingivalis*, *A. actinomycetemecomitans* and *P. intermedia*, only *A. actinomycetemecomitans* was detected in CAP tissue. Similarly, Armingohar et al. 2014, reported a very high load and mean diversity of previously undetected bacterial 16S rDNA sequences in CAP tissue. Interestingly though, while 70% of subgingival plaque specimens from patients with chronic periodontitis showed presence of RCB DNA, only *P. gingivalis* was

detected in one vascular biopsy (Armingohar et al. 2014). Moreover, the authors showed a large number of oral and non-orally derived bacterial 16S rDNA sequences in CAP samples that were not detected in subgingival plaque tissue. Therefore, species that are typically considered to have a commensal relationship with the host, can potentially act as opportunistic pathogens by gaining entry to the blood stream and invading plaque tissue where they may contribute to inflammatory milieu. A recent study examining the presence of *P. gingivalis* in carotid (n 31) and coronary (n 32) artery plaques of patients with periodontal disease demonstrated that five times as many carotids plaques were positive for *P. gingivalis* (15 compared to 3); despite greater percentages of *P. gingivalis* in the periodontal pockets of coronary (87.5%) compared to carotid patients (61.3%). Because both arteries were processed in the same way, this study raises the question of whether certain periodontal bacteria have an affinity for particular vascular beds or if the perhaps their time in transit through the blood is determined by their size, morphology or motility.

Typically then, there is massive variation in the detection rates between different studied of the carotid artery plaque samples. All bar one of these studies used PCR for detection so it is likely the variation is due to the different DNA extraction methods or PCR methods used between studies. DNA extraction is a critical part in the experimental design for bacterial DNA detection investigations, because, if the method is sub-optimal then many organisms may not be adequately lysed and subsequently discarded. When it is expected that bacterial DNA is likely to be present at low copy number quantities any loss could be devastating.

#### 1.5.2.2 Periodontal bacteria present in other arteries

In studies with a similar experimental design where different atherosclerotic arteries have been investigated, such as coronary, aorta or femoral for the presence of periodontal bacterial DNA, the same degree of variation in detection rates are observed between studies (Kozarov et al. 2006; Mahendra et al. 2010; Nakano et al. 2011). Both Gaetti-Jardim (2009) and Ishihara et al. (2004) reported detection of 5 of 8 periodontitis-associated pathogens in coronary plaques, however percentages seen by Gaetti-Jardim (2009) for each species were mostly twice that observed by Ishihara (2004).

Unlike the carotid artery, which has not yet been shown to yield *T. denticola*, atherosclerotic plaque from aorta and coronary samples have (Nakano et al. 2006;

Ohki et al. 2012). There are over 50 individual investigations assessing the dissemination of oral bacteria into the blood following various categories of endodontic treatment; however, there has not yet been data describing the dissemination of oral Spirochetes from the mouth in experimental human odontogenic bacteraemias (Parahitiyawa et al. 2009). Spirochetes are abundant in the oral cavity, in healthy and diseased oral tissue, the absence of *T. denticola* DNA in the carotid but not coronary or aorta may reflect its size compared to other coccobacillus species for the RCB.

### 1.5.2.3 Viable bacteria present in carotid plaque tissue

Previous attempts to isolate and identify bacterial species present in atherosclerotic plaque have generally been unsuccessful, possibly due to the presence of unculturable species or bacteria numbers too low to culture (Fiehn & Larsen 2005). Hence, bacteria have been isolated from carotid plaque in a viable form just to a much lesser extent. *C. pneumoniae* was among the first species to be isolated from the carotid artery in an early study (Jackson et al. 1997). However this study was only conducted on plaque from one carotid vessel. Kozarov et al. (2005) rightly proposed that 16S rDNA detection or *in situ* detection of bacteria in the walls of the artery or the atherosclerotic plaque does not prove the presence of live bacteria, which are able to invade cells and induce inflammation. Therefore they developed an assay to confirm the invasive capability of *P. gingivalis* and *A. actinomycetemcomitans*. Through co-incubation of homogenates of atherosclerotic plaque from the carotid artery with the endothelial cell line ECV-304, Kozarov et al. (2005) observed *P. gingivalis* and *A. actinomycetemcomitans* inside ECV-304 cells. This study provided the first evidence that periodontal bacteria present with atherosclerotic plaque tissue were viable, because only live cells would have the ability to invade endothelial cells.

Rafferty et al. (2011) took a similar approach to the previous study by using the monocyte cell line THP-1 in the recovery of unculturable species present in carotid and femoral atherosclerotic plaques. Viability of isolated species was then confirmed through lysis of THP-1 cells and subsequent growth of bacteria on solid microbiological medium. To determine whether recovered species were intracellular, medium was flooded with antibiotic so that only bacteria within THP-1 cells would survive. Along with *P. gingivalis*, 872 isolates were recovered using this method, such as *Propionibacterium acnes*, *Staphylococcus epidermidis* and *Streptococcus infantis*. It was reported that the recovery

rate using THP-1 cells was 5.6-times greater than incubating plaque homogenates in just medium alone. Viability was confirmed by treating. This study not only highlights the presence of diverse viable species in carotid plaque tissue but also details one of the mechanisms hypothesised to contribute to bacteria entering the plaque tissue. The so called “Trojan horse” model. Bacteria are phagocytised by macrophages, which then respond to inflammatory signals from the endothelium delivering their bacterial cargo once they become necrotic through lipid-loading. Interestingly, Rafferty et al. (2011) recovered a high frequency of viable *P. acnes* which has since been showed to be able to survive for up to two weeks inside THP-1, which may explain its high frequency (Fischer et al. 2013).

#### 1.5.2.4 *In vitro* evidence

*P. gingivalis* is the most studied periodontal pathogen due its key role in the initiation and progression of periodontitis (Mysak et al. 2014). *P. gingivalis* virulence factors are well characterised, comprising fimbriae, Arg- and Lys-gingipain cysteine proteinases (Holt & Kesavalu 1999), proteolytic enzymes, lipopolysaccharides (LPS), hemagglutinins (Bélanger et al. 2012) and outer membrane vesicles (Veith et al. 2014). *P. gingivalis* and the cariogenic *Streptococcus sanguis* express virulence factors called collagen-like platelet aggregation associated proteins that induce platelet activation *in vitro* and *in vivo* (Herzberg et al. 1996; 1998; Lourbakos et al. 2001). Platelets bind to activated endothelium and hence considered atheroprogenic. Certain fimbriated strains of *P. gingivalis* such as 381 are able to adhere to and invade epithelial and endothelial cells (Lamont *et al*, 1995; Deshpande *et al*, 1998a; Dorn *et al*, 1999). Evidence which supports a role for fimbriae in host cell invasion shows that a *P. gingivalis* 381 mutant lacking the major fimbriae protein, cannot invade these cell types due to its inability to adhere (Enersen et al. 2013). *In vitro* adhesion experiments have shown that challenge of human umbilical vein endothelial cells (HUVEC) with *P. gingivalis* 381 induces endothelial cell surface expression of VCAM-1, ICAM-1 and P-selectin (Khlghatian et al. 2002). Roth et al. (2007), demonstrated expression of chemokines MCP-1, IL-6 and IL-8 in HUVEC challenged with *P. gingivalis* 381. These inflammatory modulators are implicated in the adhesion, chemotaxis and diapedesis of leukocytes to the vascular tissue that contributes to atherosclerotic lesions.

#### 1.5.2.5 *In vivo* evidence

Li et al. (2002) examined inflammatory responses in ApoE<sup>+/-</sup> mice following intravenous inoculation with *P. gingivalis*. Infected mice were fed either normal or high fat chow and compared with noninoculated littermates. The authors reported a 9-fold increase of atherosclerotic plaque in the aortic arch of mice fed on normal chow compared to noninoculated littermates. Infected mice fed on high fat diet showed a 2-fold increase in aortic plaque compared to noninoculated littermates fed on the same diet. These findings demonstrate that *P. gingivalis* bacteraemia exacerbates inflammatory responses in artery tissue that leads to an increase in plaque formation. Furthermore, plaque development was evident in both groups of infected mice fed on high fat or normal chow; demonstrating lesion development is not exclusively attributed to high blood cholesterol level but to a greater extent implicating *P. gingivalis* bacteraemia as a main factor in lesion development. Lalla et al. (2003) investigated inflammatory responses of mice homozygous for ApoE<sup>-/-</sup> following oral inoculations of *P. gingivalis*. Mice infected with *P. gingivalis* developed symptoms of periodontitis, such as alveolar bone loss as well as elevated serum IgG levels compared to non-infected mice. Development of early atherosclerotic lesions was also reported for mice that developed periodontal infections compared to non-infected mice. These results demonstrate the pathogenesis of *P. gingivalis* to initiate oral infection, its ability to invade epithelial cells and enter the blood stream causing an increase in circulating inflammatory proteins that could accelerate atherogenesis. In addition, Lalla et al. (2003) established the presence of *P. gingivalis* DNA and upregulation of VCAM-1 in aortic artery tissue of infected mice. These findings demonstrate the capability of *P. gingivalis* to upregulate endothelial adhesion molecules implicated in recruitment of circulating monocytes are known to advance lesion development. Björkbacka et al. (2004), demonstrated the significance of endothelial Toll-like receptors TLR-2 and TLR-4 in the development of atherosclerosis in double knockout mice MyD88/ApoE mice. MyD88 is termed the 'universal adapter' protein as it is utilised by all except one TLR. TLRs are membrane bound pattern recognition receptors that play a key role in the adaptive immune system by recognising molecules broadly shared by pathogens known as pathogen associated molecular pattern (PAMP), which are distinguishable from host cells. TLR/MyD88/PAMP complex results in intracellular cascade that results in activation of transcription factors such as nuclear factor kappa-light-chain-enhancer of activated B cells (NF-κB) controlling the transcription of DNA for the production of cytokines. MyD88/ApoE mice challenged with *P. gingivalis* showed 64% decrease in atherosclerotic

plaque compared to hyperlipidemic ApoE mice. The reduced number of macrophage foam cells in the lesions of the MyD88/ApoE mice suggested that MyD88 has a crucial role in macrophage lipid uptake (Bjorkbacka et al. 2004). Building on this, Gibson et al. (2004) demonstrated that only fimbriated *P. gingivalis* accelerates atherosclerotic plaque. The authors found that after oral inoculation, bacteraemia of both fimbriated and non-fimbriated *P. gingivalis* ensued in ApoE mice, however only fimbriated *P. gingivalis* provoked up-regulation of innate immune receptors TLR-2 and 4 (Gibson et al, 2004). Observations by Gibson et al, (2004) supports earlier *in vitro* finding (Lamont et al. 1995; Deshpande et al. 1998) and demonstrates that due to its invasive ability, fimbriated *P. gingivalis* has the greatest pathogenic potential to cause infection at distant sites and accelerate lesion development.

Some of the latest research shows us that *P. gingivalis* is able to manipulate the immune system by synergising with C5a (fragment of complement protein C5) to increase cyclic adenosine monophosphate (cAMP) concentrations, resulting in suppression of macrophage immune function and enhanced pathogen survival *in vitro* and *in vivo*; essentially turning the macrophage from a destroyer to a carrier (Wang et al. 2010). The microbe can then use the macrophages to transport it to other bodily niches.

## 1.6 Genes expressed in atherosclerotic plaque tissue

### 1.6.1 SREBP2 and transcripts LDLR and HMGCR

The American biochemists and 1985 Nobel Prize winners, Mike Brown and Joseph Goldstein, showed that cellular cholesterol content is regulated by two parallel mechanisms. When the content of unesterified cholesterol in cells increases the expression of the LDL-receptor (LDLR) protein decreases. In addition, the key enzymes of cholesterol biosynthesis (hydroxymethylglutaryl (HMG)-CoA synthase, HMG-CoA reductase, squalene synthase, farnesyl diphosphate synthase; are repressed. Thus, any further increase in cellular cholesterol is minimised. Alternatively, if intracellular levels of unesterified cholesterol are depleted, these pathways are activated (figure 1.06). The genes encoding for these proteins contain an upstream sequence known as the sterol regulatory element (SRE)-1 (Kim et al. 1995). The transcription factor responsible for binding to SRE-1 DNA sequence TCACNCCAC to activate expression of each gene, is part of a larger protein complex known as sterol regulatory binding protein (SREBP) (Eberlé et al. 2004). SREBP belong to the basic-helix-loop-helix leucine zipper class of membrane bound transcription

factors which is normally localised in the endoplasmic reticulum (ER) (Sakai 1995). SREBP precursors are maintained in the ER membrane and closely associated with (SREBP)-cleavage activating protein (SCAP) which contains a sterol sensing domain (SSD) to actively monitor sterol levels in the cytosol. SCAP itself interacts with insulin induced gene (Insig) which sequesters the SREBP/SCAP complex in the ER when SCAP senses that sterol levels are high. Sterols directly interact with the SSD of SCAP and modulate SCAP conformation.

In cholesterol-depleted cells, SREBP binds to SCAP which senses the diminished cholesterol levels and disrupts its interaction with Insig allowing SCAP to be sorted into COPII-coated transport vesicles (Sun et al. 2005). SCAP then transports SREBP in the COPII vesicle from the ER to the Golgi apparatus where the N-terminal transcriptionally active domain, nuclear SREBP (nSREBP), is proteolytically cleaved from the SREBP/SCAP complex by site 1 (S1P) and site 2 (S2P) proteases, thus enabling its translocation through the nuclear envelope (Duncan 1997; Espenshade et al. 1999). In the nucleus nSREBP binds with the necessary SRE sequence in the promoter of the target gene (Horton et al. 2002).

Three members of the SREBP family have been described in several mammalian species: SREBP1a and 1c produced from a single gene (*SREBP1*) located on human chromosome 17p11.2 (Hua et al. 1995) and SREBP2 from a separate gene (*SREBP2*) located on human chromosome 22q13 (Miserez et al. 1997). SREBP2 is the isoform responsible for regulating cholesterol homeostatic genes transcription HMG-CoA reductase (HMGR) and LDLR, which mediate *de novo* cholesterol biosynthesis and also uptake of native low density lipoprotein, respectively.

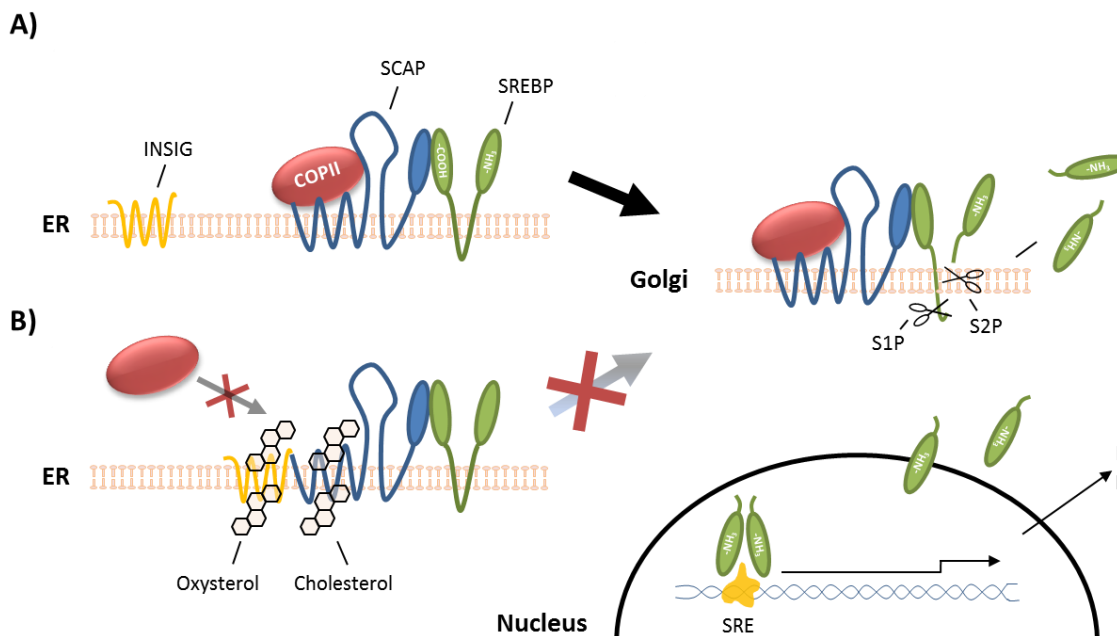


Figure 1.06 : Regulation of SREBP transcription factor for the up-regulation of cholesterologenic genes. When sterol levels are depleted the SCAP Insig interaction is disrupted enabling SCAP mediated transport of SREBP/SCAP complex into a COPII vesicle (A). The protein complex translocates from the ER to the Golgi apparatus in the COPII vesicle where the transcriptionally active portion of SREBP (nSREBP) is cleaved from the protein complex by S1P and S2P proteases (A). nSREBP then translocates to the nucleus where it binds with the necessary SRE sequence in the promoter of the target gene for transcription (A). When intracellular cytosolic sterol/cholesterol levels are high SCAP interacts with Insig which sequesters the SREBP/SCAP protein complex deeper within the ER membrane (B)

### 1.6.2 3-hydroxy-3-methylglutaryl coenzyme A reductase (HMGR)

HMGR is a transmembrane glycoprotein enzyme located on the ER. When activated HMGR catalyses the four-electron reduction of 3-hydroxy-3-methylglutaryl coenzyme A (HMG-CoA) to mevalonate, which undergoes many subsequent transformations to form sterol precursors and ultimately cholesterol (Burg & Espenshade 2011). As intracellular sterol levels fluctuate HMGR is tightly regulated at the transcriptional (SREBP/SCAP) and post-translational (phosphorylation and ubiquitination) levels (Burg & Espenshade 2011).

All cells require cholesterol, and lipoproteins normally function to package this insoluble molecule in a form readily transported in the blood. However, as previously discussed, factors such as unhealthy diet and genetic predisposition overload this essential lipid transport pathway and contribute to the dyslipidaemia that promotes atherosclerotic disease. The management of cholesterol begins in the liver where high LDL levels can result from excessive production of triglyceride-rich very low density lipoprotein (VLDL) as well as inadequate uptake of LDL by liver and peripheral cells due to low number of or genetic defects in LDLR. *De novo* synthesis of cholesterol takes place in the cytosol, where

three molecules of acetyl-coenzyme A interact to form hydroxymethylglutaryl-coenzyme A (HMG-CoA). HMG-CoA then reacts with HMG-CoA reductase (HMGR), an enzyme that resides in the membrane of the smooth ER (Burg & Espenshade 2011). HMGR is a tetrameric macromolecule with binding pockets for HMG-CoA deep within each monomer, with neighbouring monomers contributing additional binding interactions. In total, the tetramer has four pockets, one within each monomer. HMGR uses one molecule of NADPH to catalyses the reduction of HMG-CoA to mevalonate (Burg & Espenshade 2011). After leaving the enzyme, mevalonate undergoes many subsequent transformations to form other sterol precursors in the pathway to cholesterol. Statins competitively bind to the active site of HMGR blocking the binding site for HMG-CoA to inhibit its reduction to mevalonate and therefore the pathway to cholesterol.

#### 1.5.2.3.1 HMGR in atherosclerosis

Lee et al. (2011), demonstrated significant localised expression of *HMGR* in macrophage-rich areas of unstable plaque compared to plaques from patients with stable angina when using anti-HMGR and anti-CD31. These findings suggest that local HMGR is functionally active within the atherosclerotic plaque tissue, and lesion macrophages in plaque from patients with unstable angina more actively produce HMGR than in patients with stable angina. Tuomisto et al. (2003) specifically isolated macrophage-rich shoulder regions of AP tissue using laser microdissection and reported a high up-regulation of HMGR compared to disease-free tissue of the same artery. It was proposed the relatively high expression of HMGR may in fact be due to proliferation and/or differentiation of macrophages because similar expression was observed with THP-1 cells when cultured with phorbol 12-myristate 13-acetate (PMA); a chemical used to differentiate THP-1 monocytes to macrophages *in vitro*. Conversely when THP-1 cells were incubated with ox-LDL, which closer resembles atherogenic conditions, down-regulation of HMGR was observed, which suggests that lipid-loaded THP-1 macrophages may not be an accurate model of macrophages present in shoulder. Thus, HMGR may be expressed as a requirement of macrophage proliferation and/or differentiation rather than dysregulated by inflammatory/lipid stimuli.

### 1.5.3 ATP-binding cassette, sub-family A 1 (ABCA1)

When intracellular cholesterol levels are too high, macrophages activate a compensatory pathway for cholesterol efflux, mediated by the transcription factor Liver-X-Receptor (LXR) and its target gene expression of ABCA1 transporter. However, in the face of systemic hypercholesterolemia the homeostatic mechanism is overwhelmed, causing abundant accumulation of intracytoplasmic cholesteryl esters (CE) that leads to cholesterol homeostatic dysregulation and subsequent endoplasmic reticulum (ER)-mediated apoptosis.

Internalised CE undergoes hydrolysis by acid cholesterol ester hydrolase (ACEH) and is released from lysosomes as unesterified cholesterol (UC) or “free cholesterol” (FC). The fate of FC is determined by two enzymatic processes; first, the re-esterification of UC by the ER-resident enzyme, Acyl-CoA cholesterol acyltransferase 1 (ACAT1) for storage of CE in cytosolic lipid droplets. Some CE remains terminally stored in lipid droplets while others undergo re-hydrolysis to UC by neutral cholesterol ester hydrolase 1 (NCEH1), which provides cholesterol for cell membranes and permits efflux to plasma membrane transporters, such as ABCA1. Macrophages rely on oxysterol activation of LXR and its transcription of ABCA1 for the transport and presentation of cholesterol to extracellular acceptor, apo-A1, thereby initiating the preliminary step in reducing net cholesterol content via reverse cholesterol transport (RCT). However, RCT can be negatively affected by the presence of excess cholesterol, causing a dysregulation of the pathways controlling the fate of FC, which can remain in a ‘futile cycle’ of re-esterification-hydrolysis by ER-resident hydrolases. Thus, imbalance in the pathway favouring cholesterol storage potentiates macrophage lipid-loading and the development of foam cell that collectively form the atherosclerotic lesion.

### 1.5.4 Tumour necrosis factor (TNF) $\alpha$

TNF $\alpha$  is a major cytokine that leads to activation of multiple arms of the innate immune system with potent pro-inflammatory effects on vascular endothelium. TNF- $\alpha$  binds its ligand receptor TNFR1 causing a conformational change in the receptor leading to dissociation of the inhibitor protein SODD from the intracellular death domain (Locksley et al. 2001). The dissociation permits the first intracellular adapter protein (TRADD) to bind to the death domain enabling one of several intracellular protein cascades to occur that result in transcription factor translocation (NF- $\kappa$ B or AP-1) to the nucleus to mediate

the transcription of a vast array of proteins involved in cell survival and proliferation, inflammatory response, and anti-apoptotic factors. The role of TNF death signalling through TNFR1 is only weak compared to its pro-inflammatory functions and often inhibited by the anti-apoptotic effect of NF- $\kappa$ B. Nevertheless, TNFR1 death signalling is activated through the binding of TRADD with FADD in a protein cascade leading to recruitment of the cysteine protease, caspase-8, which can then activate Bid for the permeability of mitochondria membrane resulting in apoptosis through mitochondrial cytochrome C.

TNF- $\alpha$  is predominantly expressed by macrophages, which perpetuates numerous inflammatory reactions associated with atherosclerosis, such as induction of vascular endothelium CAMs and recruitment and proliferation of monocyte/macrophages. In studies using TNF-deficient apoE<sup>-/-</sup> mice, the influence that TNF- $\alpha$  has on plaque development was illustrated by the significant reduction of atherosclerotic lesion size in the aortic sinus of TNF<sup>-/-</sup>/apoE<sup>-/-</sup> mice compared to that of the wild-type apoE<sup>-/-</sup> littermates (Ohta et al. 2005; Xiao et al. 2009). The reduction in plaque mass was significantly associated with the down-regulation of *ICAM-1*, *VCAM-1* and *CCL2* (Ohta et al. 2005; Xiao et al. 2009). Alternatively, ApoE<sup>-/-</sup> mice injected with TNF- $\alpha$  develop a 5-fold-higher mean aortic plaque area compared with control mice that received saline injection (Zhang et al. 2014). During ischemic stroke, TNF- $\alpha$  mediates both intraplaque and systemic inflammation (Montecucco et al. 2010). Plasma levels of TNF- $\alpha$  have been shown to be associated with plasma VLDL, LDL and LDL particle size in men with early carotid atherosclerotic lesions (Skoog & Dichl 2002). These studies demonstrate that TNF $\alpha$  influences plaque development directly through endothelium activation resulting in cell adhesion during recruitment

TNF $\alpha$  has been detected in AP since the early 90's (Barath et al. 1990). Since then numerous investigators have provided further evidence in support of *TNF $\alpha$*  expression in human AP and arterial disease (Rus et al. 1991; P. Tipping & Hancock 1993; Kishikawa et al. 1993; Clausell et al. 1995; Tanaka & Swanson 1995; Kaartinen et al. 1996; DeGraba 1997; Ridker et al. 2000).

### 1.5.5 Interleukin 1 (IL-1) $\beta$

Inflammation plays a pivotal role in all phases of atherogenesis, from the initial endothelial recruitment of immune cells, to the more complex relationship with atherothrombotic events (Libby 2002). Pro-inflammatory cytokines and chemokines secreted from local immune cells facilitate the inflammatory response that functions to sustain the development of the atherosclerotic lesion (Ait-Oufella et al. 2011). Among those responsible, the interleukin-1 family has received particular attention (Dinarello 2009). IL-1 $\beta$  acts on endothelial cells by up-regulating CAMs that mediate the recruitment and ensuing extravasation of immune cells, such as monocytes into the intimal space (Shrikant et al. 1994; Wang et al. 1995; Merhi-Soussi 2005). In turn, macrophages induce EC and SMC secretion of chemokines and cytokines such as IL-6, IL-8 and CCL2, which further promote chemotaxis and sustain local inflammation (Blake & Ridker 2001). These effects are largely influenced by IL-1 $\beta$ , which is produced in high concentrations by lesion-dwelling macrophages through activation of the NOD-like receptor family, pyrin domain containing 3 NLRP3 inflammasome. NLRP3 is triggered in response to PAMPs and atherogenic stimuli, such as bacterial virulence factors and cholesterol crystals, respectively (Rajamäki et al. 2010; Duewell et al. 2010). When TLR activates transcription of pro-IL-1 $\beta$  via NF- $\kappa$ B, NLRP3 is ultimately responsible for the maturation of pro-IL-1 $\beta$  to the active, secreted form of IL-1 $\beta$  via a caspase-1-mediated cleavage (Franchi et al. 2009). IL-1 $\beta$  also impedes cholesterol trafficking through inhibiting ABCA1, thus encouraging foam cell formation by delaying RCT (Yin et al. 2010). Studies with animal models generally show reduced plaque burden in atherosclerosis-prone mice deficient in *IL1 $\beta$*  and increased plaque in mice when *IL1 $\beta$*  is over-expressed (Kirii et al. 2003; Isoda et al. 2004; Merhi-Soussi 2005; Chamberlain et al. 2006). Transcriptomic assessment of surgically-induced carotid stenosis in wistar-kyoto rats by microarray, demonstrates that *IL-1 $\beta$*  expression induces *MMP9*, *MMP12* and *MMP13* mRNA (Forte et al. 2008); thereby potentiating, SMC migration, vascular remodelling, plaque instability and eventual rupture (Newby 2005).

As already discussed, IL-1 $\beta$  mediates numerous pro-inflammatory roles, which potentiate atherosclerotic plaque development. IL-1 $\beta$  expression can promote apoptosis in endothelial cells and SMC; an effect shown to be impeded by overexpression of the interleukin 1 receptor agonist (IL1-ra) *in vitro* (Dewberry et al. 2000). In contrast, increased expression of anti-apoptotic proteins, such as BCL-XL and BCL-2, interact with NALP1, one of the central proteins in the inflammasome complex, by suppressing caspase-

1 activation and IL-1 $\beta$  production (Bruey et al. 2007; Escandell et al. 2010). In addition, caspase-1 activation and IL-1 $\beta$  production increase following prolonged inhibition of NF- $\kappa$ B by chemical and genetic attenuation of I $\kappa$ B kinase- $\beta$  (IKK $\beta$ ); a protein responsible for NF- $\kappa$ B activation (Zong et al. 1999; Greten et al. 2007). Therefore, like BCL-2, NF- $\kappa$ B acts as a negative regulator of IL-1 $\beta$ , which emphasises the complex and intertwined relationship between apoptosis and inflammation (Greten et al. 2007; Escandell et al. 2010).

#### 1.5.6 B Cell Lymphoma-2 protein A1

The B Cell Lymphoma-2 proteins are a family of proteins that form as hetero- or homodimers to function as anti- and pro-apoptotic regulators that mediate an extensive variety of cellular activities including embryonic development, homeostasis and tumorigenesis. The B Cell Lymphoma-2 related protein A1 (*BCL2A1*) gene that encodes the protein of the same name functions as an anti-apoptotic member of the BCL-2 family through its role in reducing the release of pro-apoptotic cytochrome c from mitochondria and subsequent blockage of caspase activation (Vogler 2012). As a direct transcription target gene of NF- $\kappa$ B, *BCL2A1* is expressed in response to pro-inflammatory mediators and thereby induced during a variety of extracellular signalling from GM-CSF, CD40, TNF- $\alpha$  and IL-1, which suggests a cytoprotective function that is essential for lymphocyte activation as well as cell survival.

##### 1.5.6.1 Apoptosis and *BCL2A1*

Apoptosis is firmly associated as a hallmark of atherogenesis by promoting plaque instability, and thrombosis (Kockx 2000). Apoptosis occurs through a diverse combination of stimuli including inflammatory processes mediated through cell-cell interaction, cytokine secretion and oxidised lipid accumulation (Harada-Shiba 1998; Janes et al. 2005; Lu et al. 2014). (Gerber et al. 1998). The efferocytic system for phagocytosis of apoptotic cell debris, becomes defective in advance lesions, leading to post apoptotic necrosis (Tabas 2005). Two broad pathways regulate cell death, namely, “intrinsic” and “extrinsic” governed by intracellular and extracellular environmental conditions, respectively. Both intrinsic and extrinsic routes activate a caspase signalling leading to cellular destruction via cysteine proteolysis. Mitochondrial-stimulated apoptosis is a well-characterised

intrinsic signalling pathway, involving the BCL-2 family of protein family, which comprise pro- and anti-apoptotic regulators (Kutuk & Basaga 2006).

Pro-apoptotic protein, BCL-2 homologous antagonist killer (Bak) and BCL-2-associated X protein (Bax) oligomerise to proteolytically disrupt the mitochondrial membrane, forming pores for the release of pro-apoptotic factors, cytochrome c and Smac, which induce caspase signalling (Westphal et al. 2014). This pathway is inhibited by BCL-2 protein BCL2A1 (also known as BFL-1/A1), which blocks cell death signalling by preventing oligomerisation of Bak and Bax (Letai et al. 2002). BCL2A1 also binds pro-apoptotic activator protein, BH3-interacting-domain death agonist (Bid), preventing its association with Bak and Bax, thereby preventing permeabilisation of the mitochondria outer membrane (Werner et al. 2002). However, BCL2A1 can also promote apoptosis through proteolysis or deletion of its N-terminus (Ko et al. 2007). Also, endothelial cells apoptosis activated by  $\text{TNF}\alpha$ , induces BCL2A1 as part of the activation process, which promotes endothelial cell survival by limiting activation through inhibition of the transcription factor  $\text{NF-}\kappa\text{B}$  (Stroka et al. 1999). BCL2A1 is an  $\text{NF-}\kappa\text{B}$ -target gene and would therefore down-regulate not only the expression of pro-inflammatory proteins, but also its own expression (Zong et al. 1999). This negative feedback loop is thought to bring the cells back to their original quiescent phenotype (Stroka et al. 1999).

#### 1.5.6.2 BCL2A1 and atherosclerosis

One of the earliest investigations of pro and anti-apoptotic expression in advanced human carotid atherosclerotic plaque was performed using IHC (Konstadoulakis et al. 1998). The overall expression profile was one of pro-apoptosis comprising elevated Bax expression that correlated with macrophages by dual-staining, though no detectable expression of protective anti-apoptotic BCL-2-related genes for cellular survival (Konstadoulakis et al. 1998). Woodside et al. (2003), assessed the differential expression of numerous apoptosis-related genes in primary and re-stenotic (>70% stenosis) carotid plaques tissue using microarray cDNA hybridisation. BCL2A1, and other anti-apoptotic genes were decreased in the re-stenotic plaque tissue compared to a “transition zone” (immediately adjacent to the stenotic area) and a “proximal zone” (tissue furthest from stenotic region). However, Woodside et al. (2003) used only one re-stenotic lesion for comparative testing. While it is interesting to establish the extent to which apoptosis presents as an etiological factor in

vascular stenosis, the significance of these particular observations carry no statistical weight.

Silbiger et al. (2013) identified potential candidate genes involved in atherosclerosis when investigation potential predictive markers in patients during the first 48 hours of acute coronary syndrome (ACS) using microarray techniques. ACS is often a result of coronary stenosis caused by atherosclerotic plaque, thus Silbiger et al. (2013) measured expression at the systemic level during symptomatic atherosclerotic disease. A complex network of 549 genes, including anti-apoptotic BCL2A1 and BCL2L1 were found to be significantly expressed in whole blood cells of ACS patients. Expression was reported to be significant, but low, which was suggested to be due to the low expression of ALOX15, a gene previously shown to be active in atherosclerotic plaque and known to influence BCL-2 expression, (Middleton et al. 2006). In addition, Silbiger et al. (2013) showed further significant up-regulation of pro-apoptotic pathway genes, including cytochrome c oxidase (COX)-7B and amphiregulin (AREG), presenting a complex picture of pro- and anti-apoptotic expression during acutely active atherosclerotic disease. Other microarray studies have also demonstrated up-regulation of a whole host of “atherogenic” genes, including BCL2A1 in different vascular beds (Puig et al. 2011). These studies demonstrate the over-expression of BCL2A1 in carotid plaque tissue, which may prolong the life of foam cells within the lesion and thereby progressing the development of the atherosclerotic lesion.

#### 1.5.6.3 BCL2A1, infection and foam cell formation

Both macrophages and SMC are prone to apoptosis in the atherosclerotic lesion and therefore operate this cell survival machinery (Kockx 2000). BCL2A1 expression can increase LDL uptake by human macrophages by inhibiting ox-LDL-induced cell death, a process shown to be greatly enhanced by another anti-apoptotic mediator, IL-10 (Halvorsen et al. 2005). Because mitochondrial cytotoxicity is inhibited by BCL2A1, it is hypothesised to be able to promote cell survival during lipid-loading, thereby enabling lipid-laden macrophages to endure extreme levels of cholesterol retention. This has been shown preliminarily with *in vitro* studies where THP-1 macrophages were challenged with *P. gingivalis* LPS causing an increase in the rate of foam cell formation. The lipid loaded THP-1 cells were shown to significantly up-regulate BCL2A1 both during and after foam cells developed (Li et al. 2010). In a similar *in vitro* investigation, Lei et al. (2011) co-

cultured THP-1 cells with ox-LDL and *P. gingivalis* LPS or ox-LDL alone and reported up-regulation of BCL2A1 that was 2-fold greater when challenged with *P. gingivalis* and ox-LDL compared to ox-LDL alone. Similarly, *P. gingivalis* has also been shown to up-regulate numerous anti-apoptotic genes including BCL2A1 in endothelial cell lines, which are also capable of lipid loading and foam cell development. These studies suggest that infection may exacerbate lipid loading in cells capable of developing into foam cells. Moreover, bacteria-mediate activation or exacerbation of BCL2A1 expression during and after foam cell formation may have a cytoprotective effect on these cells, prolonging their lifespan and allowing them to internalise additional cholesterol. This could potentially have negative implications for plaque development by increasing plaque mass and increasing stenosis. When considering this it is plausible to suggest the presence of bacteria and their virulence factors actively raise the pro-inflammatory milieu within the plaque tissue, which in turn directly affect anti-apoptotic expression in both the lesion and lipid-loading macrophages (Zong et al. 1999).

## 1.6 Inflammation and cholesterol homeostasis

There is mounting evidence to suggest that inflammation may influence lipid retention in cells that are present in the atherosclerotic lesion. Early studies showing an association between inflammation and LDL retention indicate that by accelerating the effects of pro-inflammatory cytokines on various peripheral cells such as human mesangial cells (HMC), SMC and macrophages *in vitro*, this leads to massive lipid retention and foam cell formation (Ruan et al. 2001; Ruan et al. 2006; Ye et al. 2009). Under normal conditions the monocyte cell line, THP-1 cells, show significant down-regulation of SREBP2 and subsequently LDLR when excess medium concentration of LDL is present *in vitro* (Ye et al. 2014). Interestingly, when THP-1 cells were incubated with bacterial LPS in the presence of elevated medium LDL, both SREBP2 and subsequently LDLR were over-expressed despite increased cytosolic LDL levels. Moreover, translocation of SREBP2/SCAP suggests this is not just mRNA expression, but also protein activation in response to bacterial LPS stimulus (Ye et al. 2014). These data suggest that inflammatory stress induced bacterial endotoxin can disrupt LDL receptor negative feedback regulation mediated by intracellular cholesterol and infection. Recently, Zhou et al. (2013) demonstrated that pro-inflammatory cytokine increased the half-life of SCAP glycolysation in THP-1 cells. SCAP glycolysation is a critical post-translational protein regulation step in the activation of LDLR and HMGR by SREBP2 (Eberlé et al. 2004).

The study demonstrated that exposure to inflammatory cytokines increased lipid accumulation in THP-1 macrophages, in a process that directly impacting SCAP protein activation and recycling, even in the presence of a high concentration of LDL. Similarly, a degree of cross-talk has been shown to exist between the Toll-like receptor (TLR)-4-MyD88-NF- $\kappa$ B pathway and SREBP2/SCAP, evidence by MyD88 siRNA silencing experiments (Li et al. 2013). MyD88 is an adapter protein required for most TLR pathway activation in a protein cascade leading to NF- $\kappa$ B transcription of pro-inflammatory cytokines (Bonnert et al. 1997). Through using small interfering RNA (siRNA) oligonucleotide probes that attenuate protein activation by binding active protein sites, Li et al. (2013) demonstrated that MyD88 knockdown significantly attenuated SREBP2/SCAP translocation. This study suggests that Gram-negative LPS, which is the ligand for TLR4 can physically affect lipid loading via activation of this pathway. Macrophages infected with *Chlamydia pneumoniae*; a primary pathogen in the respiratory disease pneumonia, show large accumulation of cytosolic lipid droplets and foam cell formation when co-cultured with LDL and the secretion of IL-1 $\beta$  was significantly higher than when cultured with LDL alone (Tumurkhuu et al. 2013). Foam cell formation was found to be highly dependant on the inflammasome NLRP3, which is responsible for IL-1 $\beta$  maturation in a pathway involving caspase-1 cleavage of pro-IL-1 $\beta$  to IL-1 $\beta$ . This would suggest that IL-1 $\beta$  is involved in the foam cell formation process by promoting lipid loading. Interestingly, these observations have also been demonstrated in athero-prone vessels where SREBP2 has been shown to be active due to disturbed blood flow dynamics and able to activate atherogenic factors in the vessels, such as NADPH oxidase 2, a major producer of ROS, and NLRP3, (Xiao et al. 2013). These findings demonstrate that in addition to inflammatory factors influencing sterol homeostatic pathways, the latter study suggests that the reverse is also possible, as SREBP2 mediates expression of inflammatory genes.

Taken together, these studies demonstrate a degree of cross-talk between cholesterol homeostatic pathways and inflammation. It may be particularly helpful that future studies examining these interactions would focus on inflammatory stimulus mediated by bacteria species that are known to frequent the atherosclerotic plaques tissue. In doing so a greater understanding of how bacterial infection may dysregulate cholesterol homeostasis in common cells of the atherosclerotic plaque may be more representative.

## 1.7 *Propionibacterium acnes*

*P. acnes*, (previously known as *Bacillus acnes*, *Corynebacterium acnes* and in studies describing its role as an adjuvant in tumour therapy, *Corynebacterium parvum*) is a non-motile, Gram-positive, aerotolerant anaerobe that inhabits numerous bodily niches (Cummins & Johnson 1974). *P. acnes* resides in the pilosebaceous follicles of the human skin where it stimulates the secretion of a complex mix of lipids known as sebum (Zouboulis 2009). Two distinct phylotypes of *P. acnes* Type I and Type II were originally identified based on previous antibody testing and phylogenetic evaluation of the *recA* gene and hemolysin/cytotoxin gene (*tly*) (McDowell et al. 2005). A third phylotype was identified more recently (Type III) that shares ~99.8% similarity at the genomic level with Type I strains (McDowell et al. 2008). Type I strains are predominantly isolated from patients with acne or dental (periodontitis, pericoronitis, and endodontic) infections (McDowell et al. 2005).

### 1.7.1 *P. acnes* virulence

In recent years, 82 strains of *P. acnes* have been completely sequenced and extensive comparative and pan-genomic analyses performed for all known lineages; highlighting genetic elements specific to each lineage that illustrates the differences of *P. acnes* in functioning as a commensal of the skin and as a pathogen in the aetiology of diseases (Hunyadkürti et al. 2011; Horváth et al. 2012; Tomida et al. 2013). The pathogenic potential of *P. acnes* is recognised by the organism's encoding of >2300 open reading frames (ORF) for production of several host degrading proteins, including; hemolysins (hemolysin III), cytotoxins (cAMP factor), adhesins (dermatan-sulphate adhesins) and host tissue degrading enzymes (GehA lipases, hyaluronidase, sialidases, endoglycoceramidase, etc) (Valanne et al. 2005; Falcocchio et al. 2006; Holland et al. 2010; Mak et al. 2013). These putative virulence factors of *P. acnes* induce tissue damage through haemolysis, pore-formation, adhesion to multiple surfaces for biofilm formation and cell aggregation, as well as induction of chemotactic and inflammatory pathways (Brüggemann 2005; Tucker et al. 2005).

### 1.7.2 *P. acnes* role in disease and detection in atherosclerotic plaque

*P. acnes* is most noted for being the primary pathogen in the pathogenesis of acne vulgaris where it plays an inflammatory role (Beylot et al. 2014). As an opportunistic pathogen, *P. acnes* is implicated in several inflammatory conditions through chronic and reoccurring infection, such as sarcoidosis, sciatica, arthritis, prostate cancer and infective and aggressive endocarditis, as well as a range of post-operative and clinical device related infections (Gunthard et al. 1994; Stirling et al. 2001; Hiramatsu et al. 2003; Cohen et al. 2005; Berthelot et al. 2006). The detection and isolation of this opportunistic pathogen highlights its ability to systemically infect its host and cause serious infections at sites distant from the primary infection.

*P. acnes* has also been detected in vascular tissue, mostly aortic aneurysm (Silva et al. 2006; Armingohar et al. 2014), but also isolated in a viable state from carotid tissue (Rafferty, Jönsson, et al. 2011). Recently, it was shown that a *P. acnes* strain isolated from carotid atherosclerotic plaque could form a biofilm when cultured *in vitro* (Lanter & Davies 2015). Moreover, *P. acnes* biofilms were susceptible to induction of a biofilm dispersion response when challenged with therapeutic levels of the major stress hormone, norepinephrine (Lanter & Davies 2015). Sometimes when an individual has underlying CVD and experiences great stress an acute cardiovascular event may arise. This latter study potentially demonstrates how stress hormones may act on biofilms that have formed within the atherosclerotic lesion. If the biofilm was formed at a critically vulnerable region of the lesion such as a thin fibrous cap, a rise in serum norepinephrine may cause biofilm dispersion resulting in plaque rupture.

*P. acnes* localises and preferentially proliferates in lipid-rich environments and is a TLR receptor ligand complicit in secretion of chemotactic factors, such as IL-6, IL-8, IL-12 and IL-18 and pro-inflammatory cytokines TNF- $\alpha$  and IL-1 in numerous cell lines *in vitro* (Kim et al. 2002; Jugeau et al. 2005; Nagy et al. 2005; Fathy et al. 2009; Shibata et al. 2009). By evading digestion when phagocytised by macrophages, *P. acnes* has been shown to survive intracellularly for up to two weeks (Fischer et al. 2013). In addition *P. acnes* further contributes to the inflammatory response by triggering the activation of the NLRP3-inflammasome for the secretion of caspase-1 activation-dependent cytokines, particularly IL-1 $\beta$ , both *in vitro* and *in vivo* (Qin et al. 2014; Thiboutot 2014; Kistowska et al. 2014; Contassot & French 2014).

## **Materials & Methods**

## 2.1 Human tissue procurement

### 2.1.1 Ethical clearance & study cohort

This study was ethically approved by the National Research Ethics Service (NRES) and the University of Central Lancashire Ethics Committee (NRES study number 10/H1015/78). Patients agreed to donate their surplus tissue by giving informed consent. Human atherosclerotic plaque tissue was removed during routine carotid endarterectomy surgery and human left internal thoracic artery (LITA) tissue was recovered during coronary artery bypass graft or valve replacement surgery at the Lancashire Cardiac Centre, Blackpool, England. Forty tissue specimens were procured from 36 male and 4 female patients with a combined mean age of  $68.8 \pm 9.4$  years. Of the 40 tissue specimens, 21 specimens were carotid atherosclerotic plaque (CAP) tissue (17 male, 4 female with mean age  $69.9 \pm 8.7$  years) and 19 specimens were LITA tissue (19 male with mean age  $67.5 \pm 10.2$ ).

### 2.1.2 Tissue collection & sample processing

Prior to tissue collection, a reduced transport medium (RTM) comprising tryptone (1%, w/v), yeast extract (0.5%, w/v), glucose (0.1%, w/v), cysteine hydrochloride (0.1%, w/v), sodium hydroxide (50 mM) and horse serum (2%, v/v), was sterilized using a 0.2  $\mu\text{m}$  filter, as previously described by (Hooper et al. 2007). For RNA analysis, samples were placed in vials containing *RNAlater*<sup>®</sup>. Specimens were aseptically transferred from patient to RTM or *RNAlater*<sup>®</sup> (Ambion, UK) by a member of the surgical team. Specimens were transported to the laboratory on ice. Once in the laboratory, specimens were handled under aseptic conditions inside a UV irradiated class II biosafety cabinet. CAP specimens were washed with sterile PBS by gentle vortexing, before transferring the tissue to fresh PBS. Washes were repeated until the solution appeared clear (figure 2.01). Because tissue was to be assessed for the presence of viable organisms, washing specimens with Povidone-Iodine solutions such as Betadine<sup>®</sup> was avoided. Thus, sterile PBS was sufficient to remove contaminating blood from the surface and microvasculature of the specimens. LITA specimens were carefully dissected from surrounding connective tissue to recover the vessel tissue proper. Recovered vessels were washed with sterile PBS as

described for CAP tissue (figure 2.01). Following wash steps, specimens were evenly divided by successions of transverse dissections for the following downstream analyses:-

1. Histopathological examination.
2. Bacterial culturing.
3. DNA extraction for 16S rDNA PCR analysis.
4. RNA extraction for gene expression analysis.

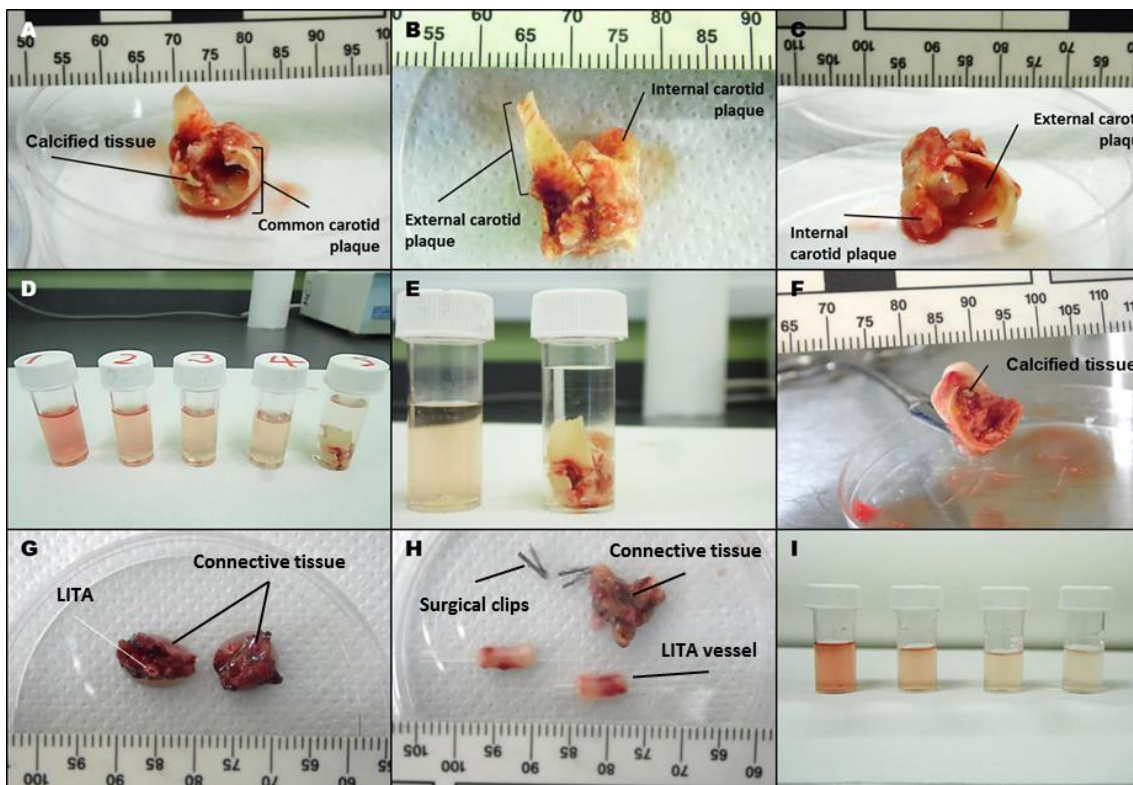


Figure 2.01: CAP and LITA tissue processing. CAP tissue was examined (A – C), rinsed several times with a gentle vortex in sterile PBS until solution appeared clear (D – E) and transversely dissected for downstream analysis (F). LITA tissue comprising connective tissue (G) and surgical ligature clips was dissected to recover the vessel tissue proper (H). To surface decontaminate, LITA tissue was rinsed several times then dissected for downstream analysis.

## 2.2 Histological & immunological examination of atherosclerotic plaque & left internal thoracic artery tissue

### 2.2.1 Tissue fixation, demineralisation and paraffin embedding

CAP and LITA specimens were fixed in 10% formaldehyde solution (Sigma-Aldrich, UK) at a ratio of 20:1 (solution to tissue); at room temperature for 24 h. Occasionally, older, larger and more complex CAP lesions presented with extracellular calcium deposits (figure 2.01a and f); Calcified CAP specimens were demineralised in 5% formic acid solution at a ratio of 20:1 over 3 days. Formic acid solution was changed each day. Specimens were dehydrated in 3 changes of 50% EtOH for 15 min each. This process was repeated for solutions of 70%, 80%, and 90% EtOH. Samples were further dehydrated in 2 changes of absolute EtOH (15 min each), followed by an overnight immersion in absolute EtOH. Dehydrated tissue specimens were cleared in 3 changes of xylene for 5 min each.

Specimens were placed into molten paraffin wax at 70°C for 3 h. Samples were then incubated for 3 h in fresh molten paraffin (Thermo Scientific, UK), followed by a final incubation in fresh molten paraffin for 4 h. Tissues specimens were then ready to be mounted. Each specimen was transferred to the well of a pre-heated plastic mould positioned on a hot plate at 60°C and orientated to a suitable position for setting. Molten paraffin was carefully poured into each mould and a microtome attachment guard placed over the well before adding more paraffin. Moulds containing molten paraffin and specimens were then incubated on ice until the paraffin set. Sections were cut at 5 µm thickness using a microtome and mounted onto gelatine coated slides (0.5% (w/v) gelatine 0.05% (w/v) chromium potassium sulphate).

### 2.2.2 Hematoxylin & eosin staining (HE)

Prior to staining, mounted tissue sections were deparaffinised and rehydrated. Slides were twice submerged in xylene for 5 min each. Slides were then taken through decreasing concentrations of EtOH. Slides were submerged in 3 changes of 90% EtOH for 15 min each. This was repeated with 70% and 50% EtOH. Slides were washed in dH<sub>2</sub>O for 15 min. Sections were submerged in Mayer's haematoxylin (Fisher Scientific, UK) for 5 min, placed into cold running water for 5 min, then placed into hot water for 30 sec. Sections were stained in eosin (Fisher Scientific, UK) for 30 sec. Excess eosin was removed and

sections were submerged in 2 changes of absolute EtOH. Sections were then submerged in 2 changes of xylene for for 3 min. Excess xylene was removed and the sections were mounted with distyrene plasticiser xylene (DPX) mounting medium (Singma-Aldrich, UK).

### 2.2.3 Masson's Trichrome Staining (MTC)

Sections were deparaffinised and rehydrated as already described. Sections were submerged in Weigert's Hematoxylin (equal parts solution A: 1% (v/v) absolute EtOH; solution B: 30% (w/v) ferric chloride in 1% (v/v) hydrochloric acid) for 15 min. Sections were then covered with ponceau red (1% (w/v) ponceau red in 15% (v/v) acetic acid) for 5 min then quickly rinsed with distilled water (dH<sub>2</sub>O) followed by a further 5 min stain with 1% (v/v) phosphomolybdic acid (PA). Excess PA was removed and slides were stained with light green stain (2% (w/v) light green in 2 % (v/v) acetic acid). Slides were immediately dehydrated through a series of increasing EtOH solutions and mounted in DPX.

### 2.2.4 Bacterial peptidoglycan monoclonal antibody staining

Tissue sections were deparaffinised and rehydrated as described previously. The procedure was carried out at room temperature. Sections were incubated for 15 min with 10% (w/v) sodium dodecyl sulphate to expose cellular epitopes then rinsed three times with wash buffer (PBS containing 0.5% Tween-20). Sections were then incubated for 10 min in hydrogen peroxide block solution (Abcam, UK) and rinsed twice with wash buffer. Protein block (Abcam, UK) was applied and sections were incubated for 10 min to block nonspecific background staining. Sections were rinsed with wash buffer then incubated with mouse anti-bacterial peptidoglycan (PGN) monoclonal antibody (Millipore, UK) at a 1:500 dilution in protein block solution for 1 h. A negative control slide was included in each analysis by replacing the primary antibody with protein block solution. Negative control tissue sections were taken in succession to antibody-treated tissue sections and therefore contain the same features. Following the primary antibody incubation step, sections were rinsed four times with wash buffer then incubated with a pre-diluted concentration of biotinylated goat anti-mouse secondary antibody (Abcam, UK) for 10 min. Sections were rinsed four times with wash buffer and incubated for 10 min with a pre-diluted concentration of streptavidin peroxidase. Sections were then rinsed four times with wash buffer. Diaminobenzidine (DAB) chromogen (Abcam, UK) was mixed with

DAB substrate (Abcam, UK) at a ratio 1:50 and 10 µl applied to each section for 2 min. Sections were rinsed four times with wash buffer and counterstained with Mayer's haematoxylin for 5 min. Sections were briefly immersed in absolute EtOH followed by xylene and mounted with DPX.

### 2.2.5 Antibody and chromagen optimisation

Slides containing *P. gingivalis* were used as a positive control to determine staining efficacy and to provide information regarding bacterial morphology in tissue sections. Briefly, a bacterial suspension was prepared using a fresh culture of *P. gingivalis* that had been grown for 72 h. The culture was centrifuged to form a pellet, spent media was discarded and the pellet was re-suspended in 1 ml sterile dH<sub>2</sub>O. A slide was prepared by applying 20 µl bacterial suspension to the surface and heat dried at 70°C on a hot plate, heat killing and partially fixing the bacteria to the slide. A titration of primary antibody was performed using antibody dilutions of 1:100, 1:200, 1:300, 1:400, 1:500, 1:600, 1:700, 1:800, 1:900 and 1:1000. Each dilution was prepared in triplicate and further optimised to determine the optimal exposure time to DAB chromogen. Exposure times to DAB chromogen were set at 2, 4, 6, 8 and 10 min. Each group included a negative control slides (protein block without antibody) stained with DAB chromogen for the maximum exposure time of 10 min.

## 2.3 Anaerobic Bacterial cultures

### 2.3.1 Maintenance of periodontal red complex bacteria

Red complex bacteria (RCB), *Porphyromonas gingivalis*, *Tannerella forsythia* and *Treponema denticola* were utilised as test species for the development of a bacteriologic growth medium to facilitate the isolation of viable bacteria present in CAP tissue. *P. gingivalis* (a kind gift from Dr Graham Stafford, University of Sheffield) was maintained in brain heart infusion (BHI) broth (Oxoid, UK) supplemented with 5 µg/ml hemin (Sigma-Aldrich, UK), 1 µg/ml menadione (Sigma-Aldrich, UK), 1 µg/ml L-cysteine-HCL (Sigma-Aldrich, UK), 0.4% (w/v) yeast extract (Oxoid, UK) as detailed in appendix A. Solid agar medium for growth of *P. gingivalis* comprised fastidious anaerobic agar (FAA) (Lab M, UK) supplemented with 10% defibrinated horse blood (Becton Dickinson, UK) (Suwannakul et al. 2010). *T. forsythia* (a second kind gift from Dr Graham Stafford) was

maintained in tryptic soy broth (TSB) (Oxoid, UK) and was supplemented as for *P. gingivalis* with the addition of 10 µg/ml *N*-acetyl muramic acid (NAM) (Sigma-Aldrich, UK) (appendix B) (Roy et al. 2010). A solid medium for the growth of *T. forsythia* comprised the same agar and supplementation as *P. gingivalis* with the addition of 10 µg/ml NAM supplementation (Roy et al. 2010). *T. denticola* (a kind gift from Dr David Dymock, University of Bristol) was maintained in Tryptone-Yeast extract-Gelatine-Volatile fatty acid-Serum (TYGVVS) medium (appendix C) (Ohta et al. 1986; J. C. Fenno 2005). *T. denticola* colonies were grown within a semi-solid medium consisting of brain heart infusion broth; supplemented with all TYGVVS medium reagents (appendix C) with the addition of 6.25 g/L agar and gelatin.

Pre-reduced, pre-warmed complete growth media or agar equivalents, were inoculated then incubated in an anaerobic atmosphere of 5% H<sub>2</sub>, 5% CO<sub>2</sub>, 90% N<sub>2</sub> at 37°C inside a Bactron I anaerobic chamber (Shel Lab, USA) for 7 and 10 days, respectively. Cultures were archived using a Cryobank™ storage system (Copan Diagnostics Inc, USA) (section 2.2.3) and revived when needed via the addition of a single Cryobank™ bead to liquid or solid media. These systems were used to stock and maintain healthy cultures prior to the development and optimisation of an experimental bacterial growth media for screening CAP specimens for viable isolates.

Prior to experimentations with the RCB strains, 1 ml of 5-day-old culture from each was transferred to sterile microcentrifuge tube for DNA extraction and sequence identification. Molecular identification was performed as described in later sections, “DNA extraction from bacterial cultures” (section 2.4.2), “Polymerase Chain Reaction” (section 2.4.3) and “sequencing using BigDye termination” (section 2.4.8). The generated sequences were cross-referenced using BLAST reference database. All bacterial strains were confirmed as correct at the time of the study

#### 2.3.1.1 Growth characteristics of RCB in liquid media

The identity of each target organism strains (*P. gingivalis*, *T. forsythia* and *T. denticola*) was confirmed prior to their use in testing. All strain sequences matched with 100% max identity when cross-referenced with National Center for Biotechnology Information (NCBI) Basic Local Alignment Search Tool (BLAST) database.

To maintain a consistent amount of inoculum of *P. gingivalis*, *T. forsythia* and *T. denticola* for each medium; bacteria from starter cultures were counted using a hemocytometer (Fisher Scientific, UK). Briefly, serial log dilutions were prepared from 500 µl fresh liquid cultures that had an  $OD_{600} \leq 0.5$ . Twenty microliters of diluted bacterial solution was loaded onto a hemocytometer and discrete cells within the four corner grids and the center grid were counted using a Motic® AE2000 inverted microscope (Motic®, Germany) at x40 magnification with partial phase-contrast optic setting. Counts were multiplied by the relevant dilution factors to establish the final total amount of bacteria within each liquid culture. Approximately  $1 \times 10^5$  bacteria cells of each species/strain were used to inoculate 20 ml of each respective medium. Inoculated cultures ( $T_0$ ) were then incubated for 8 days in an anaerobic environment as previously described (section 2.3.1).

Liquid culture turbidity was measured daily by optical density at 600 nm wave length ( $OD_{600}$ ), over 8 days using a Biochrom WPA Lightwave II Spectrophotometer (Fisher Scientific, UK). Briefly, 1 ml of each fresh liquid media was used to “blank” the spectrophotometer (reference sample), against which, liquid culture samples were compared. Liquid cultures were gently agitated and 1 ml culture transferred to a sterile capped cuvette for  $OD_{600}$  measurement (VWR, UK). When  $OD_{600}$  readings were  $\geq 0.5$ , cultures were diluted 1:4 and the  $OD_{600}$  values of diluted samples were then multiplied by the relevant dilution factors to establish a more accurate measure of culture turbidity. Spectrophotometry measurements were recorded to plot standard growth curves of ‘ $OD_{600}$  vs time’ for each bacteria species as line graphs using Microsoft Office Excel.

#### 2.3.1.2 Growth characteristics of RCB on solid/semi-solid media

For the purposes of counting bacterial colony forming units (cfu) numbers, cultures removed for optical density measurement within sterile capped cuvettes were further utilised to inoculate solid/semi-solid agar plates (media described previously in section 2.3.1) Briefly, 7-fold serial log-dilutions were prepared daily from 1 ml liquid culture of each bacteria species/strain and repeated in technical replicates of three. Two hundred microliters of each diluted culture was spread on the respective solid media. Plates were then sealed and incubated for 10 days, as previously described (section 2.3.1). Solid media plates that yielded between 30 – 300 colonies were counted using a touch-sensitive bench-top colony counter (Stuart, UK). The sum total of colonies counted was multiplied by the relevant dilution factors to establish the number of colony forming units (cfu)/ml. The

recorded cfu numbers were used to produce a linear regression line graphs ‘cfu/ml vs OD<sub>600</sub>’ using Microsoft Office Excel.

### 2.3.2 Development and optimisation of a bacteriological liquid growth medium

The development of a single liquid growth medium that could be used to culture any viable bacteria present in CAP and LITA tissue was investigated. While the ultimate aim was to isolate and identify any viable bacteria species present in atherosclerotic plaque tissue, particular emphasis was placed on developing a liquid medium with the ability to support the growth of RCB. Thus, *P. gingivalis* 11834/W50, *T. forsythia* & *T. denticola* were employed as test species to assess media development at every stage in the process. Firstly, media known to support the individual growth of each RCB test species (BHI, TSB and TYGVS) were assessed to establish whether each medium could support the growth of all or more than one RCB species. Testing how readily each RCB species was supported in each alternative medium provided a foundation “base medium” from which the most efficacious medium could be further developed to include the growth of all RCB test species/strains. Therefore, media development was performed in two distinct stages.

- Stage 1. Test the efficacy of BHI, TSB and TYGVS media (appendices A, B & C) to support the growth of all or more than one RCB species and establish a “base medium” that may be further developed.
- Stage 2. Further development of the “base medium” through a stepwise supplementation of specific growth reagents known to support the growth of any RCB species not satisfied in stage 1 assessment.

#### 2.3.2.1 Stage 1 - Establishment of a base medium that supports the growth of RCB

*P. gingivalis* is typically grown in BHI broth (appendix A), while *T. forsythia* and *T. denticola* are commonly grown in TS broth (appendix B) and TYGVS (appendix C), respectively. To determine which media was most supportive, each medium was inoculated individually with a single RCB species per medium replicate for the growth of pure cultures only (table 2.01). Prior to inoculation, bacteria numbers present in a starter culture (OD<sub>600</sub> 0.4 – 0.6) were counted as described in section 2.3.1.1. Twenty milliliters of pre-reduced, pre-warmed media were each inoculated with  $\sim 1 \times 10^5$  bacteria. Cultures were incubated anaerobically for 8 days within a previously described anaerobic system (section 2.3.1). Cultures were repeated by performing three technical replicates for each

RCB species and alternative medium combination (table 2.01). Liquid culture turbidity was assessed by daily measurement of OD<sub>600</sub> values, as previously detailed (section 2.3.1.1). Finally, the recorded OD<sub>600</sub> values were used to plot line graphs to show standard growth curves of each test species in each of the liquid media.

The most supportive “base medium” was selected based on three general criteria:-

1. The number of RCB species/strain supported by the medium.
2. The consistency of growth in the medium based on three technical replicates.
3. Final yield of each bacterium in each alternative medium, taken as a mean of three technical replicate OD<sub>600</sub> values.

<i>P. gingivalis</i>				
Media	W50	11834	<i>T. forsythia</i>	<i>T. denticola</i>
<i>Alternative</i>	TSB	TSB	BHI	BHI
	TYGVS	TYGVS	TYGVS	TSB
<i>Typical</i>	BHI	BHI	TSB	TYGVS

**Table 2.01:** Alternative growth media used in stage 1 to culture test bacteria species/strains. Each “alternative medium” was used to culture each bacteria species in technical replicates of three. Bottom row shows the “typical media” that have previously been shown support the growth of each test species/strain (Abaibou et al. 2001; Roy et al. 2010).

### 2.3.2.2 Stage 2 - Supplementation of a base medium with specific growth reagents

The second stage of medium development involved building upon the “base medium” established in stage 1, (TSB; appendix A). Since *T. denticola* failed to grow within the stage 1-established medium, particular emphasis was placed on incorporating growth reagent supplements known to support the growth of *T. denticola* (Fenno 2005). Such reagents were selected by considering several complex broth media formulations in common use for growth of *T. denticola* (Wyss 1992; J. Fenno 2005). These media share common features including sources of trace elements, peptides, amino acids, and trace nutrients, as well as reducing agent(s), volatile fatty acids (VFA), and heat-inactivated animal sera, typically rabbit.

All selected growth reagents except volatile fatty acid (VFA) solution were tested as single compounds. VFA solution comprised seven VFA's and was tested in media as an overall percentage of the final medium volume (table 2.02). Briefly, a stock solution of VFA was prepared comprising, 1.42 % glacial acetic acid (v/v), 0.5% propionic acid (v/v), 0.34% butyric acid (v/v), 0.084% valeric acid (v/v), 0.084% isobutyric acid (v/v), 0.084% isovaleric acid (v/v) and 0.084% methylbutyric acid (v/v). Table 2.02 details the final volume ( $\mu\text{l/ml}$ , v/v) of each acid when used at 4, 6, 8 and 10% of the final medium volume.

For the purpose of testing the impact on bacterial growth in the presence of different growth reagents, base media were prepared, each containing an increasing concentration of a single growth reagent supplement, which were compared to bacterial growth in a negative control media (without tested reagent) as detailed in table 2.03. Each varying test medium was inoculated with only pure cultures for separate growth of one RCB species or strain per medium at a density of  $\sim 1 \times 10^5$  bacteria cells and incubated for 8 days in a previously described anaerobic environment (section 2.3.1).

The impact of each reagent concentration on bacterial growth was assessed daily by measuring  $\text{OD}_{600}$  values, as detailed earlier in section 2.3.1.1. When maximum  $\text{OD}_{600}$  values were observed, approximately 108 – 120 h post inoculation, bacterial numbers were considered to be at their greatest density i.e. during late-log/early-plateau growth phase. These maximum  $\text{OD}_{600}$  values were compared between test reagent media and negative control media. A reagent concentration was considered to be optimum when the lowest possible reagent concentration provided the greatest increase in bacterial growth compared to control medium. When an optimum concentration was established for one reagent, that reagent was incorporated as part of the complete growth medium prior to the next round of reagent testing. Table 2.04 lists the reagents in order of assessment and shows the progressive development of each supplemented medium as the optimum concentration of each growth reagent was established.

Final volume of VFA in 1 L medium (v/v) based on percentage used								
Volatile fatty acids	4%	mM	6%	mM	8%	mM	10%	mM
Glacial acetic acid ( $\mu\text{l/ml}$ )	0.57	9.92	0.85	14.9	1.14	19.8	1.42	24.8
Propionic acid ( $\text{nl/ml}$ )	200	2.67	300	4.00	400	5.33	500	6.67
Butyric acid ( $\text{nl/ml}$ )	104	1.47	156	2.21	208	2.94	340	3.68
Valeric acid ( $\text{nl/ml}$ )	33.6	0.31	50.4	0.46	67.2	0.61	84	0.76
Isobutyric acid ( $\text{nl/ml}$ )	33.6	0.37	50.4	0.55	67.2	0.74	84	0.92
Isovaleric acid ( $\text{nl/ml}$ )	33.6	0.30	50.4	0.46	67.2	0.61	84	0.76
Methylbutyric acid ( $\text{nl/ml}$ )	33.6	0.31	50.4	0.46	67.2	0.62	84	0.77

**Table 2.02:** Individual VFA concentrations used as part of a solution to test bacteria growth in culture medium. Stock solutions used for media containing 7 VFAs. Table shows the volume and molarity of each VFA in 100 ml medium (v/v) based on the percentage of the VFA stock solution in the final media volume.

Media supplements	Concentration gradient				
	#1	#2	#3	#4	#5
$(\text{NH}_4)_2\text{SO}_4$ (mg/ml)	NC	0.25	0.5	0.75	1
$\text{K}_2\text{HPO}_4$ (mg/ml)	NC	1	1.25	1.5	1.75
$\text{NaCl}_2$ (mg/ml)	NC	0.5	0.75	1	1.25
VFA solution (%)	NC	4	6	8	10
Thiamine pyrophosphate ( $\mu\text{g/ml}$ )	NC	12.5	13	13.5	14
Sodium pyruvate ( $\mu\text{g/ml}$ )	NC	275	300	325	350
Rabbit serum (%)	NC	5	10	15	-

**Table 2.03:** Media supplements selected for stage 2 of bacterial growth medium development. Media supplements are listed in the left-hand column in order of assessment. A concentration gradient of each reagent was tested to establish the optimum concentration of each reagent required for bacterial growth (columns #2 – #5). Bacterial growth in media containing each reagent concentration was compared to bacterial growth in a negative control medium (NC; column #1). Negative control medium comprised optimum concentrations of all previously tested reagents, minus the reagent being tested or subsequently untested reagents.

Finally, data were presented by plotting bar graphs of  $\text{OD}_{600}$  values for each test species cultured in media containing concentration gradients of growth reagents. Statistical testing was conducted by performing ANOVA, Levene's test and Student's t-test and the significance of each test result was indicated on bar graphs as one, two or three asterisks dependent on test result probabilities of  $\leq 0.05$ ,  $\leq 0.01$  or  $\leq 0.001$ , respectively (section 2.7.1). Moreover, to present data for the growth of RCB species in media containing only established optimum reagent concentrations,  $\text{OD}_{600}$  values were plotted as line graphs to show standard growth curves of 'OD<sub>600</sub> vs time' in each medium.

		Stage 2 medium reagents						
		A	B	C	D	E	F	G
Medium composition	(NH <sub>4</sub> ) <sub>2</sub> SO <sub>4</sub>							
	-	K <sub>2</sub> HPO <sub>4</sub>						
	-	-	NaCl <sub>2</sub>					
	-	-	-	VFA	VFA	VFA	VFA	VFA
	-	-	-	-	TPP	TPP	TPP	TPP
	-	-	-	-	-	SP	SP	SP
	-	-	-	-	-	-	-	RS

Table 2.04: Progressive development of bacterial growth medium. Lists of each individual growth reagent supplement in order of assessment. Each column shows the progressive development of the medium through the incorporation individual reagents (A – G). Reagents were tested individually as a concentration gradient by measuring their impact on bacterial growth to identify the optimum medium concentration required to support the growth of each red complex bacteria species. As an optimum concentration was established for one reagent, that reagent was then incorporated as part of the complete growth medium prior to the next round of reagent testing. (NH<sub>4</sub>)<sub>2</sub>SO<sub>4</sub> (Ammonium Sulphate), K<sub>2</sub>HPO<sub>4</sub> (Potassium Phosphate), NaCl (Sodium Chloride), VFA (volatile fatty acid), TPP (thiamine pyrophosphate), SP (sodium pyruvate) and RS (rabbit serum).

### 2.3.3 Isolating viable anaerobic bacteria from human CAP tissue

Fresh CAP and LITA tissue specimens were macerated on a sterile glass Petri dish with a sterile blade inside a Bactron<sup>®</sup> I Anaerobic Chamber with an anaerobic atmosphere of 5% H<sub>2</sub>, 5% CO<sub>2</sub>, and 90% N<sub>2</sub>. Macerated tissue samples were submerged in 20 ml pre-reduced, pre-warmed (37°C) growth medium. The finalised medium for culture of bacteria present in CAP and LITA tissue specimens is described in appendix D. As discussed in section 2.1.2, prior to tissue maceration, CAP and/or LITA specimens were rinsed with a series of sterile PBS washes and the final wash retained. In parallel with test tissue cultures, 1 ml of final tissue wash was added to growth medium to culture any contaminating microbes that may have remained on the surface of the tissue during procurement. In addition to the final wash control, an environmental control was prepared consisting of 10 ml growth medium inside an open-lid 50 ml falcon tube. Hence, each batch of tissue cultures consisted of 1 x test tissue (CAP or LITA), 1 x final tissue wash control and 1 x open-lid environmental control. Cultures were incubated for 7 days and bacterial growth was assessed by observation. If no visible growth had occurred after 7 days, specimens were incubated for a further 7 days. When positive cultures were observed in liquid medium 0.5 ml of viable culture was spread across blood agar plates comprising fastidious anaerobic agar (FAA) (Lab M, UK) supplemented with 10% defibrinated horse blood (Becton

Dickinson, UK) and 10 µg/ml NAM. Spread plates were incubated for 7 days at 37°C in an anaerobic atmosphere of 5% H<sub>2</sub>, 5% CO<sub>2</sub>, 90% N<sub>2</sub>. In an attempt to isolate pure bacterial strains, single colonies were picked from mixed colony plates and streaked over fresh FAA plates. Plates were incubated anaerobically for another 7 days or colonies formed. Ten individual colonies were picked from single colony plates and re-inoculated back into fresh liquid both (previously described) for 7 days to expand culture stocks.

#### 2.3.4 Archiving viable isolates

Liquid cultures containing single bacterial species were gram stained then separated for Cryobank™ storage (Copan Diagnostics Inc, USA) and DNA extraction. Briefly, cultures were centrifuged at 200 x g for 5 min and the supernatant removed. Pelleted bacteria were gently re-suspended in sterile pre-reduced PBS and centrifuged a second time at 200 x g for 5 min. Supernatant was removed and 500 µl sterile pre-reduced PBS added to re-suspend the bacterial pellet into a highly concentrated liquid culture. Four hundred microliters of the concentrated culture was aseptically transferred to a sterile anaerobically sealed Cryobank™ vial containing glycerol stock and ~20 individual plastic beads. Cultures were mixed with the glycerol by inverting followed by removal of excess glycerol. Cryobank™ vials were then stored at -20°C until needed. The remaining 100 µl concentrated culture were heat-killed at 72°C for 5 min and DNA extracted from this for PCR analysis.

DNA extraction from anaerobic cultures was performed as in section 2.3.1 with an additional pre-incubation step for gram-positive bacteria. Bacterial cultures were centrifuged at 5,000 x g for 5 min and supernatant removed. Bacteria were suspended in 180 µl enzymatic buffer (20 mg/ml lysozyme; 20 mM Tris-HCL, pH 8; 2 mM EDTA; 1.2% (v/v) Triton®) and incubated at 37°C for 5 h. Twenty microliters Proteinase K and 200 µl AL buffer (QIAGEN, UK) were added and mixed by vortexing. Samples were incubated overnight at 56°C, followed by a further 15 min at 95°C. DNA was isolated using equal volumes phenol chloroform isoamyl-alcohol (25:24:1).

## 2.4 Identification of bacterial DNA extracted directly from CAP tissue and cultured anaerobic bacteria

### 2.4.1 DNA extraction from CAP and LITA tissue

Tissue sections ~100 mg were snap-frozen in liquid nitrogen. Frozen specimens were ground to a fine powder in a pestle and mortar in the presence of liquid nitrogen. Ground specimens were then transferred to a microcentrifuge tube and lysed in animal tissue lysis (ATL) buffer (Qiagen, UK) containing 2 mg/ml proteinase K (Qiagen, UK) overnight at 56°C. Lysed tissues specimens were mixed with an equal volume of phenol chloroform isoamyl-alcohol (25:24:1) (Sigma-Aldrich, UK) by vortexing at high speed for 20 sec. Samples were then incubated at room temperature for 5 min to allow partial separation of aqueous and non-aqueous phases then centrifuged at 16,000 x g for 10 min. Approximately 200 µl aqueous phase was transferred to a clean microcentrifuge tube and placed on ice. To encourage DNA precipitation, a final concentration of 0.1 µg/µl glycogen and 3.75 mol/µl ammonium acetate were mixed with the aqueous phase, followed by ice-cold absolute EtOH (2.5 x sample volume). Samples were inverted 10 times then incubated at -80°C for 2 h. Samples were centrifuged at 16,000 x g for 15 min at 4°C to pellet DNA precipitate. Supernatant was removed, 200 µl 75% (v/v) ice-cold EtOH was added. Samples were vortexed at a medium speed for 10 sec to re-suspend the DNA pellet. Samples were centrifuged at 16,000 x g for 30 min at 4°C. Supernatant was removed, 200 µl 75% EtOH was added and samples were centrifuged at 16,000 x g for 10 min at 4°C. Supernatant was removed and samples were centrifuged at 8,000 x g for 3 min to collect residual EtOH for removal. Clean DNA pellets were air dried for 15 min then re-hydrated 100 µl AE Buffer. Finally, DNA absorbance was assessed at 260/280 nm ratio to measure concentration and purify of the DNA stocks. DNA stock with a 260/280 ratio of 1.8 – 2.0 were considered pure. DNA stocks were stored at -20°C until needed.

### 2.4.2 DNA extraction from bacterial cultures

DNA extraction from anaerobic cultures was performed with an additional pre-incubation step for gram-positive bacteria. Bacterial cultures were centrifuged at 5,000 x g for 5 min and supernatant removed. Bacteria were suspended in 180 µl enzymatic buffer (20 mg/ml lysozyme; 20 mM Tris-HCL, pH 8; 2 mM EDTA; 1.2% (v/v) Triton<sup>®</sup>) and incubated at 37°C for 5 h. Twenty microliters Proteinase K and 200 µl AL buffer (Qiagen, UK) were added and mixed by vortexing. Samples were incubated overnight at 56°C, followed by a

further 15 min at 95°C. DNA was isolated using equal volumes phenol chloroform isoamyl-alcohol (25:24:1).

### 2.4.3 Polymerase Chain Reaction

PCR was performed to assess the presence of bacterial DNA (bDNA) in CAP and LITA specimens. In the first phase of the bDNA investigation, specific oligonucleotide primers were used to identify the domain “Bacteria”, and also the Phyla “Bacteroidetes” and “Spirochaetes” (Paster et al. 2001). The PCR primers targeted the highly conserved 16S rRNA (16S rDNA) gene. Primers were synthesised by Applied Biosystems at 25 nM concentration and desalted to purity. PCR detection of Bacteria, Bacteroidetes and Spirochaetes used the same forward primer D88 and a distinct reverse primer which was specific for the 3 bacterial groups (table 2.05). The specific reverse primers used were: C90, specific for Spirochaetes; F01, specific for Bacteroidetes; and E94, specific for the Bacteria (table 2.01). Each PCR reaction comprised 0.2 µM forward/reverse primer, 200 µM each dNTP, 2.5 mM MgCl<sub>2</sub>, 1.25 U AmpliTaq Gold® DNA polymerase (Applied Biosystems, UK) and 0.5 µg DNA template. Reactions were brought to a final volume of 50 µl with molecular grade dH<sub>2</sub>O. *T. forsythia* (Bacteroidetes) or *T. denticola* (Spirochete) DNA was used as a template for positive control reactions. Negative control reactions were prepared by replacing DNA template with molecular grade dH<sub>2</sub>O. An additional positive internal control was include though amplification of the human β-globin to assess the quality, integrity and successful amplification human genomic DNA in each sample. Thermal cycling conditions were as follows; 5 min initial denaturation at 96°C, followed by 30 cycles of denaturation at 96°C for 45 sec, annealing at 60°C for 45 sec and extension at 72°C 60 sec and a final extension step at 72°C for 15 min.

A second group of primers were utilised to identify specific oral bacterial species, including, *P. gingivalis*, *T. forsythia*, *T. denticola*, *P. acnes* and oral Streptococci and Lactobacilli (Nakagawa et al. 1994; Slots et al. 1995; Asai et al. 2002; Eishi et al. 2002; Dubernet et al. 2002; Picard et al. 2004). Oligonucleotide primer sequences and product sizes are listed in table 2.01. Reactions were prepared the same as previously described as 50 µl. Stock DNA from each species was used as template for positive control reactions. Thermal cycler conditions for *P. gingivalis* and *T. denticola* were as follows: an initial denaturation 98°C for 5 min, followed by 30 cycles of denaturation at 98°C for 45 sec, annealing at 55°C for 30 sec and extension at 72°C for 30 sec and a final extension set at

72°C for 15 min. For *T. forsythia*, *P. acnes*, Streptococci and Lactobacilli, thermal cycler conditions were the same except for increased annealing temperatures of 60°C (table 2.06).

#### 2.4.4 Agarose gel electrophoresis

To view amplified 16S rDNA, PCR product was mixed with loading dye (30% (v/v) glycerol, 0.25% (w/v) bromophenol blue and 0.25% (w/v) xylene cyanol FF 6:1 then placed in the wells of a 1.5% agarose gels close to the anode. Positive and negative control PCR products were loaded in agarose wells along with 10 µl exACTGene 10 kb or 1kb DNA ladder (Fisher Scientific, UK) depending on product size 1.5 kb or <1000 bp, respectively. A 100 V current was applied across the gel for ~ 40 min to encourage product migration through the agarose gel towards the cathode. Agarose gels were stained in a 0.5µg/ml solution of ethidium bromide (EtBr) for 30 min then de-stained in dH<sub>2</sub>O for 15 min. EtBr stained gels were visualised under UV light using a BioDoc-It imaging system (UVP, UK).

Species	Primer sequence	Size (bp)	References
Forward (D88)	F: 5'-GAGAGTTTGATYMTGGCTCAG-3'*		
Bacteria (E94)	R: 5'-GAAGGAGGTGWTCCARCCGCA-3'*	1,500	(Paster et al. 2001)
Bacteroidetes (F01)	R: 5'-CCTTGTTACGACTTAGCCC-3'	1,500	
Spirochete (C90)	R: 5'-GTTACGACTTCACCCTCCT-3'	1,500	
<i>P. gingivalis</i>	F: 5'-AGGCAGCTTGCCATACTGCG-3' R: 5'-ACTGTTAGCAACTACCGATGT-3'	404	(Slots et al. 1995)
<i>T. forsythia</i>	F: 5'-GCGTATGTAACCTGCCCGCA-3' R: 5'-TGCTTCAGTGTGAGTTATACCT-3'	641	(Slots et al. 1995)
<i>T. denticola</i>	F: 5'-TAATACCGAATGTGCTCATTACAT-3' R: 5'-CTGCCATATCTCTATGTCATTGCTCTT-3'	860	(Asai et al. 2002)
<i>P. acnes</i>	F: 5'-GCGTGAGTGACGGTAATGGGTA-3' R: 5'-TTCCGACGCGATCAACCA-3'	131	(Eishi et al. 2002)
<i>Strep spp.</i>	F: 5'-GTACAGTTGCTTCAGGACGTATC-3' R: 5'-ACGTTTCGATTTTCATCACGTTG-3'	200	(Picard et al. 2004)
<i>Lacto spp.</i>	F: 5'-CTCAAACTAAACAAAGTTTC-3' R: 5'-CTTGTACACACCGCCCGTCA-3'	250	(Dubernet et al. 2002)
M13	F: 5'-GTAAAACGACGGCCAG-3' R: 5'-CAGGAAACAGCTATGAC-3'	1,700	
HBG	F: 5'-GAAGAGCCAAGGACAGGTAC-3' R: 5'-GGAAAATAGACCAATAGGCAG-3'	408	

Table 2.05 Primer sequences for 16S rDNA amplification. Species name, oligonucleotide sequence and product size are listed. D88 (shaded) was used as the forward primer for the three reverse primers, E94, F01 and C90. (\*) D88 and E94 are degenerate primer sequences. According to the International Union of Pure and Applied Chemistry (IUPAC) nomenclature, degenerate bases are classified as follows, Y (C or T), M (A or C), W (A or T) and R (A or G). Thus, D88 and E94 each have four alternative sequences, giving a total of 8 possible primer binding sites when used together. Alternatively, when D88 is incorporated with either F01 or C90, up to four potential primer binding sites are possible.

Cycle	Stage	Bacteria Bacteroidetes Spirochetes		B-globin		<i>P. gingivalis</i> <i>T. denticola</i>		<i>T. forsythia</i> <i>P. acnes</i> Streptococci spp. Lactobacilli spp.	
		Temp °C	Time (min)	Temp	Time	Temp	Time	Temp	Time
	1	96	5:00	95	5:00	98	5:00	98	5:00
X 30	2	96	0:45	94	0:30	98	0:45	98	0:45
	3	60	0:45	55	0:30	55	0:30	60	0:30
	4	72	1:00	72	0:30	72	0:30	72	0:30
	5	75	15:00	72	15:00	72	15:00	72	15:00

Table 2.06 Thermo cycling conditions for 16S rDNA primer sets and  $\beta$ -globin internal control to amplify 0.5  $\mu$ g DNA template using 1.25U Amplitaq Gold<sup>®</sup> DNA polymerase, 2.5 mM MgCl<sub>2</sub>, 200  $\mu$ M each dNTPs and 0.2  $\mu$ M oligonucleotide. Each group of PCR reactions were subjected to specific temporal heating protocol over 5 general stages of rapid heating and cooling. Heating stages consisted of, Stage 1: Initial denaturation, Stage 2: Denaturation, Stage 3: Oligonucleotide annealing, Stage 4: DNA extension and Stage 5: Final extension.

#### 2.4.5 TOPO<sup>®</sup> 16S rDNA Cloning

PCR samples yielding positive discrete bands of ~ 1.5 Kb on agarose gels were used for molecular cloning. Purification of the PCR product was achieved by performing EtOH precipitation of the PCR product. One microliter glycogen (20 mg/ml), 1  $\mu$ l EDTA (125 mM), 1  $\mu$ l NaOAc (3 M) and 30  $\mu$ l of ice-cold absolute EtOH were added to 40  $\mu$ l PCR product. Samples were inverted 5 times and placed at 4 °C overnight. Samples were centrifuged at 16,000 x g, 4 °C for 40 min to form a pellet. DNA pellets were washed twice with ice-cold 70% EtOH, centrifuging at 16,000 x g for 15 min between each wash step. After the final spin, open tubes were heated at 60 °C for 15 min to dry DNA pellets. Pellets were rehydrated in a sterile AE buffer. Twenty nanograms of purified product was mixed with 1X ligation buffer, 50 ng/ $\mu$ l pCR2.1 vector, 1.0 U T4 DNA ligase and sterile water to a final volume 10  $\mu$ l. Ligation reactions were incubated at 14 °C overnight. Two microliters of ligation reaction was transformed into chemically competent *E. coli* (DH5- $\alpha$ ) and incubated on ice for 30 min. The reaction was then heat-shocked at 42 °C for 30 sec. Two hundred and fifty microlitres of SOC medium was added to transformed cells and then incubated at 37 °C in a shaker at 225 rpm for 1 h. Selective LB agar plates containing kanamycin (50  $\mu$ g/ml) were spread with 40  $\mu$ l (40 mg/ml) X-Gal and pre-heated at 37 °C for 30 min. Two plates were spread with 50  $\mu$ l and 100  $\mu$ l of transformed DH5- $\alpha$  cells. LB agar plates containing transformed DH5- $\alpha$  cells were incubated at 37 °C overnight for colony development.

#### 2.4.6 Colony screening

A colony screen was performed to isolate clones which had successfully taken up the PCR product. pCR2.1 TOPO vector contains a 115 bp polylinker that comprises a small segment of DNA containing the coding information for the first 146 amino acids of  $\beta$ -galactosidase (LacZ). The polypeptide encoded by this region of LacZ is known as the  $\alpha$ -subunit of  $\beta$ -galactosidase and is the basis for determining whether a foreign DNA fragment has been inserted into the polylinker. When a DNA sequence is inserted into the polylinker the extra DNA causes a disruption of the plasmid-encoded  $\alpha$ -subunit blocking  $\beta$ -galactosidase expression. Thus, in the presence of chromogen X-Gal (5-bromo-4-chloro-3-indolyl  $\beta$ -D-galactopyranoside), bacterial colonies with inactivated  $\beta$ -galactosidase (inserted PCR product) are white, while colonies expressing  $\beta$ -galactosidase are blue (no inserted PCR product).

Each cloning reaction produced ~ 200 colonies of which 10% of the white colonies were picked for screening. White colonies were mixed with 20  $\mu$ l sterile water in separate microcentrifuge tubes. To determine the presence of the positive clones, with sequence insert, a PCR reaction was carried out. A PCR master mix was prepared; each reaction comprised 0.2  $\mu$ M of each M13 forward primers (table 2.01) (Applied Biosystems, UK), 200  $\mu$ M of each dNTP, 2.5 mM MgCl<sub>2</sub>, 1.0 U *Taq* ploymease and 10  $\mu$ l of crude suspension of the DH5 $\alpha$  colonies. All reactions were performed with 10 min of denaturation at 94°C, followed by 25 cycles of denaturation at 94°C for 60 sec, annealing at 55 °C for 60 sec and extension at 72°C for 105 sec and a final 72°C extension step for 7 min.

Agarose gel electrophoresis was carried out as described in section 2.3.4. Bands that indicated product size of ~ 1.7 Kb were considered positive results. If the amplified products deviated from 1.7 Kb, they were assumed to be the result of the formation of chimeric molecules or unsuccessful insert ligation and were not analysis further.

#### 2.4.7 Mini-prep isolation of plasmid DNA

Samples that contained inserts (1.7 Kb band) were cultured to generate a greater yields of bacterial clones for plasmid DNA isolation. Positive clones were used to inoculate 10 ml Luria-Bertani (LB) broth containing kanamycin (50  $\mu$ g/ml). Cultures were incubated at 37 °C in a heated shaker at 200 rpm for 18 h. Cultures were then subjected to plasmid mini-prep to isolate plasmid DNA using a QIAprep Kit (Qiagen, UK). Bacteria clone cultures

were centrifuged at 5,000 x g for 10 min at 4 °C. The spent LB broth was removed from the culture and DH5- $\alpha$  cells were re-suspended in 250  $\mu$ l P1 buffer and transferred to a microcentrifuge tube. An equal volume of P2 buffer was added and samples were mixed by inverting the tube 6 times. Next, 350  $\mu$ l N3 buffer was added and immediately mixed by inverting 6 times. Samples were then centrifuged at 16,000 x g for 10 min. Supernatant was decanted into a QIAamp spin column and samples were centrifuged at 16,000 x g for 40 sec and flow through was discarded. The spin columns were washed with 0.5 ml PB buffer by centrifuging at 16,000 x g for 40 sec. Flow through was discarded and a second wash with 0.75 ml PE buffer was performed by centrifuging at 16,000 xg for 40 sec. Flow through was discarded and a second centrifugation step at 16,000 x g was performed to remove residual wash from the column. Plasmid DNA was eluted from the column with 50  $\mu$ l molecular grade water and stored at -20°C until needed. Concentrations of plasmid DNA were measured using a Nanodrop spectrophotometer. Samples with a ratio of 260/280 nm between 1.80 and 2.0 were considered pure.

#### 2.4.8 Sequencing of the vector insert

The cloned DNA insert was first amplified by PCR using M13 primers recognising flanking sequences within the plasmid (table 20.1). PCR reactions comprised 0.2  $\mu$ M of either M13 forward or M13 reverse, 200  $\mu$ M of each dNTP (Fisher Scientific, UK), 2.5 mM MgCl<sub>2</sub>, 1U *Taq* polymerase (Acros Organics, UK) and 200 ng plasmid DNA template. All reactions were performed with a 10 min denaturation step at 94°C, followed by 25 cycles of denaturation at 94°C for 60 sec, annealing at 55°C for 15 sec, extension at 72°C for 105 sec and a final 72°C extension step for 15 min. The resulting ~ 1.7 kb products were purified with EtOH precipitation, as described in section 2.3.4. Pellets were rehydrated in sterile dH<sub>2</sub>O and the concentration and purity of the product was assessed as previously described (section 2.3.1)

The sequence of the amplified plasmid DNA insert was analysed using a dye terminator sequencing PCR reaction. Using BigDye® Terminator v3.1 Cycle Sequencing kit (Lifetechnologies, UK ) a PCR master mix was prepared at reduced volumes comprising 0.16  $\mu$ M of each M13 forward and reverse primers (table 20.1), 0.4  $\mu$ l sequencing premix, 3.6  $\mu$ l sequencing buffer and 40 ng amplified plasmid insert to a final volume of 10  $\mu$ l. All sequencing reactions were performed with 1 minute denaturation at 96°C, followed by 30 cycles of denaturation at 96°C for 10 sec, annealing at 50°C for 5 sec and extension at 60°C

for 4 min. Samples were purified by EtOH precipitation, as previously described (2.3.5). Purified samples were rehydrated with 13  $\mu$ l HiDi (formamide solution). Sequence reactions were loaded onto a 96-well plate and analysed using an automated ABI 3500 genetic analyser with 50 cm capillary array (Applied Biosystems, UK).

Capillary electrophoresis was performed using run module stdseq50\_POP7 with dye set Z (FAM, VIC, NED and size standard ROX) and POP7 sequencing polymer. Default run parameters were as follows: a sample injection voltage of 1.6kV for 8 sec, with a run voltage 8.5 kV at 60°C for 96 min. Sequence reads of >800 nucleotides were searched against GenBank DNA reference sequences using National Centre for Biotechnology Information-Basic Local Alignment Search Tool (NCBI-BLAST) to identify bacterial strains (see <http://blast.ncbi.nlm.nih.gov/Blast.cgi>).

## 2.5 Gene expression analysis of atherosclerotic plaque tissue

### 2.5.1 Oligonucleotide primer design & optimisation

A total of 22 primer sets were designed to evaluate the expression of 19 target genes and 3 endogenous control genes (table 2.04). Target sequences were chosen to measure the expression of genes involved in inflammation and cholesterol metabolism. Target genes were identified by searching within the NCBI database. Target gene accession numbers were used to generate specific oligonucleotide primer sequences with NCBI primer design software. Search parameters were set so that oligonucleotide primers had the following features:-

- Cross an exon-exon boundary.
- Be <25 bp long.
- Amplify products  $\leq$ 150 bp.
- Have GC content between 40% - 60%.
- Have <4 consecutive base repeats.
- Have an annealing temperature  $\sim$  60°C (5°C lower than melting temperature).
- Where possible, have a GC-clamp located at the 3' end of both sense and anti-sense primers.
- Oligonucleotide sequences that met these criteria were only selected when self and intra-primer complementarity was low (NCBI score  $\leq$ 3).

To establish primer specificity, oligonucleotide sequences were cross-referenced against the NCBI-BLAST ref\_seq database. When multiple transcript variants existed for a single target gene, sequences were aligned using DNA sequence alignment tool Bioedit. This allowed primers to be designed across exon-exon boundaries, which were conserved across different transcript variants of a specific gene. Oligonucleotides were synthesised by Life Technologies, UK custom oligonucleotide synthesis service to a 25 nM scale and desalted to purity. All primers were received as lyophilised stocks and were reconstituted to a 100  $\mu$ M stock solution and stored at  $-20^{\circ}\text{C}$ . Table 2.03 lists target genes, accession numbers, oligonucleotide primer sequences, and product sizes. Primers that resulted in successful target genes expression were sequenced using Bigdye<sup>®</sup> Terminator v3.1 as previously described (section 2.4.8) to confirm specificity of the expressed gene. Table 2 lists genes, NCBI accession numbers, oligonucleotide primer sequences and product sizes.

Amplification efficiency of each primer set was determined by generating triplicate  $C_T$  values for a gradient of increasing cDNA template concentrations. Semi-log regression line charts were plotted as “Log cDNA input vs.  $C_T$  value”. A standard curve slope of  $-3.32$  (s) indicated a PCR reaction with 100% efficiency (E) using the formula  $E = (10^{-1/s} - 1) \times 100$ . A reaction with 100% efficiency would yield a 10-fold increase in product every 3.32 cycles during exponential amplification, i.e.  $\log_2 10 = 3.3219$ . For optimum results, SYBR<sup>®</sup> Select chemistry recommends that oligonucleotide primer concentration should be  $\leq 0.2$   $\mu$ M per primer per reaction. Thus, primer concentrations, 0.2  $\mu$ M, 0.1  $\mu$ M or 0.05  $\mu$ M were tested to evaluate the most efficient amplification efficiency for each gene.

### 2.5.2 RNA extraction from atherosclerotic plaque tissue

A portion of human CAP and LITA tissue from the carotid artery were transferred directly from patient to RNAlater<sup>®</sup> to maximise RNA preservation. RNAlater<sup>®</sup> saturated specimens were stored at  $-20^{\circ}\text{C}$  until treated for total RNA extraction. Specimens in RNAlater<sup>®</sup> were incubated on ice until RNAlater<sup>®</sup> thawed. Prior to RNA extraction, RNAlater<sup>®</sup> was removed and specimens were immediately snap-frozen in liquid nitrogen. Frozen specimens were ground to a fine powder with a pestle and mortar in the presence of liquid nitrogen. Ground tissue was carefully transferred to a clean microcentrifuge tube containing 1 ml Tri Reagent<sup>®</sup> solution (Invitrogen, UK) (100 mg tissue to 1 ml Tri Reagent<sup>®</sup> solution). Samples were homogenised in Tri Reagent<sup>®</sup> solution and incubated at room temperature for 30 min in a  $360^{\circ}$  inverting mixer at 10 rpm. Samples were

centrifuged at 12,000 x g for 10 min to separate the high lipid content from the tissue homogenate. The top layer containing insoluble lipid was carefully bypassed and the clear supernatant was collected and transferred to a clean microcentrifuge tube.

Total RNA was extracted by following the manufacturer's guidelines. Briefly, 100  $\mu$ l 1-bromo-3-chloropropane (BCP) was added to the 1 ml lysate and samples were shaken vigorously for 15 sec. The lysate/BCP mix was then incubated at room temperature for 15 min then centrifuged at 12,000 x g for 15 min at 4°C. The aqueous BCP layer containing RNA was transferred to a clean microcentrifuge tube. Isolated RNA was purified by addition 1  $\mu$ l glycogen solution (20  $\mu$ g/ $\mu$ l) to the aqueous lysate followed by 500  $\mu$ l ice-cold absolute isopropanol. Samples were vortexed for 10 seconds and quickly transferred to -80°C overnight. Samples were centrifuged at 12,000 x g for 10 min at 4°C. The supernatant was discarded and the resulting RNA pellet was washed by addition of 1 ml ice cold 75% ethanol and centrifugation at 7,500 x g for 5 min at 4°C. The ethanol supernatant was discarded and a second was performed with fresh ice cold 75% ethanol followed by centrifugation as previously described. Ethanol supernatant was discarded and microcentrifuge tubes were inverted over clean lab tissue and air dried at room temperature for 15 min. Dried samples were then rehydrated with 60  $\mu$ l pre-warmed nuclease-free distilled H<sub>2</sub>O (dH<sub>2</sub>O) and incubated at 55°C for 1 – 2 min or until the RNA pellet dispersed. Total RNA stock solutions were then immediately placed on ice and their purity and concentration were calculated with a nanodrop spectrophotometer. RNA samples that had a 260/280 ratio of 1.8 – 2.0 and a 230/280 ratio of 2.0 – 2.2 were considered pure and were stored at -80°C until required.

### 2.5.3 Optimisation of Reverse-transcription Polymerase Chain Reaction (RT-PCR) reagents

Three concentrations of reverse transcriptase (0.5, 1, 1.5 U) and four MgCl<sub>2</sub> (1.5, 2.5, 3.5 and 4.5 mM) were tested to establish optimum reagent composition for RT-PCR reactions. Reagent mixes were prepared as triplicate and resulting cDNA templates were serially diluted 1<sup>10</sup> over 7 orders of magnitude. The gradients of increasing cDNA templates were real-time PCR amplified generating triplicate C<sub>T</sub> values. Semi-log regression line charts were plotted as “Log cDNA input vs. C<sub>T</sub> value”. The optimal ratio of enzyme and salt was chosen and used for all gene expression analysis.

#### 2.5.4 RT-PCR of CAP and LITA specimens

Prior to reverse transcription RNA samples were treated with DNase I (Sigma-Aldrich, UK). One unit of amplification grade DNase I, completely digests 1 µg DNA. Briefly, 1 µl DNase I (1 unit/µl in a buffer comprising 50% glycerol, 10 mM Tris-HCL, pH 7.5, 10 mM CaCl<sub>2</sub>, 10 mM MgCl<sub>2</sub>) and 1 µl reaction buffer (200 mM Tris-HCL, PH 8.3, 20 mM EDTA) were added to 10 µl RNA stock. Solution was mixed gently and incubated for 15 min at room temperature. One microliter of EDTA (50mM) was added to inactivate DNase I. The solution was then heated to 70°C for 10 min to denature the DNase I, and the RNA was cooled on ice. 0.5 µg of DNase-treated RNA was used as a template to generate first-strand complementary DNA (cDNA). The GoScript™ Reverse Transcription System (Promega, UK) was utilised for reverse transcription of RNA to cDNA. The protocol was performed in two phases: initial anchoring of a 15-mer poly-T tailed oligo(dt) primer followed by first-strand synthesis of the cDNA sequence complementary to the RNA template. Briefly, 0.5 µg Total RNA was mixed with 50 µg (10.1 µM) oligo(dt)<sub>15</sub> primer, and brought to a total volume of 5 µl with nuclease-free dH<sub>2</sub>O. The reaction was incubated at 70°C for 5 min and then reactions were placed on ice for 5 min. Samples were briefly centrifuged to collect the condensate. A master mix was prepared comprising GoScript™ reaction buffer, MgCl<sub>2</sub> (3.5 mM), dNTP mix (0.5 mM each dNTP), 20 U recombinant RNasin® ribonuclease inhibitor, 1 U GoScript® reverse transcriptase. The reaction mix was brought to a final volume of 15 µl with nuclease-free dH<sub>2</sub>O. Fifteen microliters of master mix was gently mixed with 5 µl oligo(dt)-anchored template. A negative control reaction was prepared by omitting GoScript® transcriptase enzyme. Thermal cycling conditions for all reverse transcription reaction were as follows: one annealing cycle at 25°C for 5 min, one extension cycle at 42°C for 60 min followed by one transcriptase inactivation cycle at 70°C for 15 min. The synthesised cDNA was utilised as template for quantitative real-time PCR immediately or stored at -20°C until required.

### 2.5.5 Quantitative real-time PCR (qPCR)

SYBR<sup>®</sup> Select master mix (Lifetechnologies, UK) comprising SYBR<sup>®</sup> GreenER<sup>™</sup> Dye, Ultra-purified AmpliTaq<sup>®</sup> DNA polymerase, ROX<sup>™</sup> passive reference dye, dNTP mix (dUTP/dTTP), was mixed with either 0.2  $\mu$ M, 0.1  $\mu$ M or 0.05  $\mu$ M oligonucleotide primer (table 2.07), dependant on optimal amplification efficiency of each primer set, and brought to a total final volume of 10  $\mu$ l with nuclease-free dH<sub>2</sub>O. Fifty nanograms cDNA template was used for each reaction. Reactions were added to a 96-well optical PCR plate (Lifetechnologies, UK), each plate comprising test (treated) reactions, reference gene reactions (ACTB or RPL27A), a no-template control (PCR negative) and a no-reverse transcriptase control (RT-negative). The plate was sealed with optical adhesive film and centrifuged at 1000 x g for 1 min. Reactions were performed on an ABI 7500 Real-Time PCR Thermal Cycler (Applied Biosystems<sup>®</sup>). Thermal cycling conditions were as follows: 1 cycle of 95°C for 10 min, 40 cycles of 95°C for 15 sec, 60°C for 60 sec, followed by final 1 cycle of 95°C for 15 sec, 60°C for 60 sec, 95°C for 15 sec and 60°C for 15 sec (table 2.08).

<i>HMGR</i>	NM_000859.2	F: 5'-AATTACTCCTTGGTGATGGGAGC-3' R: 5'-ATCTAAGCAAAGGGTCCTGC-3'	90 bp
<i>SCAP</i>	NM_012235.2	F: 5'-ACCCATCACAGCCCTGAAAG-3' R: 5'-CCTCCAGACGGAACACTCTC-3'	83 bp
<i>SREBP2</i>	NM_004599.2	F: 5'-GCTGGCTTCTCTCCCTACTC-3'-3' R: 5'-CTGGCTCATCTTTGACCTTTGC	79 bp
<i>LDLR</i>	Gene ID: 3949	F: 5'-AGAGGAAATGAGAAGAAGCCCAG-3' R: 5'-AAGGAAGACGAGGAGCACGATG-3'	75 bp
<i>ABCA1</i>	NM_005502.3	F: 5'-GAGGCAACAAACGCAAGC-3' R: 5'-GTTTCATCCAGAAACACCACAGG-3'	72 bp
<i>CCL3</i>	Gene ID:6348	F: 5'-GGCTCTCTGCAACCAGTTCT-3' R: 5'-TAGGAAGATGACACCGGGCT-3'	151 bp
<i>CCL2</i>	NM_002982.3	F: 5'-CAGCCAGATGCAATCAATGCC-3' R: 5'-CTTCTTTGGGACACTTGCTGC-3'	118 bp
<i>ICAM1</i>	NM_000201.2	F: 5'-GGAGCTTCGTGTCTGTATGG-3' R: 5'-GCACATTGGAGTCTGCTGGG-3'	94 bp
<i>VCAM1</i>	NM_001078.3	F: 5'-TTGATGAAATGGATTCTGTGCC-3' R: 5'-ATTCTTGGGTGATATGTAGACTTGC-3'	74 bp
<i>CSF2</i>	NM_000758.3	F: 5'-CCTGGGAGCATGTGAATGCC-3' R: 5'-TACTGTTTCATTCATCTCAGCAGC-3'	86 bp
<i>TLR-2</i>	XM_005263194.2	F: 5'-TCGGAGTTCTCCAGTGTGG-3' R: 5'-GCACAATGAGCCCACAGGT-3'	109 bp
<i>TLR-4</i>	NM_138554.4	F: 5'-CCTGCGTGGAGGTGGTTCTAA-3' R: 5'-TGTCTCCACAGCCACCAGCTTC-3'	326 bp
<i>TNF-<math>\alpha</math></i>	NM_000594.3	F: 5'-GTAGCCCATGTTGTAGCAAACC-3' R: 5'-GGTTATCTCTCAGCTCCACGC-3'	103 bp
<i>IL1<math>\beta</math></i>	NM_000576.2	F: 5'-AGATGAAGTGCTCCTTCCAGG-3' R: 5'-GGTCGGAGATTTCGTAGCTGG-3'	72 bp
<i>IL6</i>	NM_000600.3	F: 5'-GTGTGAAAGCAGCAAAGAGGC-3' R: 5'-AGGCAAGTCTCCTCATTGAATCC-3'	105 bp
<i>IL10</i>	NM_000572.2	F: 5'-TGGAGGACTTTAAGGGTTACCTGG-3' R: 5'-ACATGCGCCTTGATGTCTGG-3'	115 bp
<i>NFKB</i>	Gene ID: 4790	F: 5'-TGGACAACATGAGGTCTCTGG-3' R: 5'-CTGAGAGGTGGTCTTCACTGG-3'	125 bp
<i>MyD88</i>	NM_001172567.1	F: 5'-GCTCATCGAAAAGAGGTTGGC-3' R: 5'-ATGGGCACCTGGAGAGAGG-3'	139 bp
<i>BCL2A1</i>	NM_004049.3	F: 5'-AACGGAGGCTGGGAAAATGG-3' R: 5'-TGGAGTGTCTTTCTGGTCAA-3'	137 bp
<i>ACTB</i>	NM_001101.3	F: 5'-TCCTTCCTGGGCATGGAGTC-3' R: 5'-CGATCCACACGGAGTACTTG-3'	323 bp
<i>RPL27A</i>	NM_000990.4	F: 5'-GGAAGACCCGAAACTTAGGG-3' R: 5'-TAGCCTGGGTGGTATTTGTCG-3'	139 bp
<i>GAPDH</i>	NM_002046.5	R: 5'-TGGAGAAGGCTGGGGCTCAT-3' F: 5'-CATGCCAGTGAGCTTCCCGT-3'	308 bp

**Table 2.07:** Oligonucleotide primers designed for real-time PCR assays are listed as follows. Cholesterol biosynthesis: HMG-CoA reductase (*HMGR*), sterol regulatory element-binding protein cleavage-activating protein (*SCAP*), sterol regulatory element-binding protein-2 (*SREBP2*) ATP-binding cassette transporter sub-family member-1 (*ABCA1*) and low density lipoprotein receptor (*LDLR*). Adhesion molecules: intercellular adhesion molecule-1 (*ICAM1*) and vascular cellular adhesion molecule-1 (*VCAM1*). Cytokines and inflammatory: interleukin-1-beta, (*IL1 $\beta$* ), interleukin-6 (*IL6*), interleukin-10 (*IL10*), tumour necrosis factor alpha (*TNF $\alpha$* ), chemokine (C-C motif) ligand-3 (*CCL3*), chemokine (C-C motif) ligand-2 (*CCL2*) and colony stimulating factor-2 (granulocyte-macrophage) (*CSF2*), nuclear factor kappa-light-chain-enhancer of activated B cells (*NFKB*) myeloid differentiation primary response gene-88 (*MYD88*). Apoptosis inhibitor: BCL-2-related protein A1 (*BCL2A1*). Endogenous control genes: Glyceraldehyde 3-phosphate dehydrogenase (*GAPDH*),  $\beta$ -actin (*ACTB*) and 60S ribosomal protein L27a (*RPL27A*) were designed. Oligonucleotide sequences in bold were designed by second supervisor.

Hot-Start Denaturation	Data collection			Dissociation		
1 Repeat	40 Cycles			1 Repeat		
95°C	95°C	60°C	95°C	60°C	95°C	60°C
10 min	0:15 min	1 min	15 sec	20 sec	15 sec	15 sec

**Table 2.08:** Thermal-cycler parameters for gene expression assays using SYBR® Select. Table from left to right – Initial 95°C denaturation step for AmpliTaq® polymerase activation and cDNA denaturation, data collection step (40 cycles 95°C to 60°C) and a final dissociation curves analysis step.

### 2.5.6 Gene expression data analysis for atherosclerotic plaque tissue - $\Delta\Delta C_T$

Analysis of qPCR data were performed in accordance with the Livak and Schmittgen (2001)  $\Delta\Delta C_T$  method for relative gene expression. Real-time PCR was performed on cDNA from AP and LIMA specimens. The data were analysed using Eq (i), where  $\Delta\Delta C_T = \Delta C_T(\text{Sample}_{CAP} - \text{Reference}_{CAP}) - \Delta C_T(\text{Sample}_{LITA} - \text{Reference}_{LITA})$ . The endogenous reference gene, RPL27A, was utilised for tissue gene expression normalisation. A mean of endogenous control  $C_T$  values for each reaction were calculated and utilised for calibrator (LITA) and target (CAP) normalisation. Calculating  $\Delta C_T$  for each tissue established the level of normalised gene expression of the gene of interest (GOI) by subtracting the mean  $C_T$  values of the stable and constantly expressed endogenous control genes. The normalised  $\Delta C_T$  LITA tissue expression was subtracted from the normalised  $\Delta C_T$  CAP tissue expression, thus generating the final normalised  $\Delta\Delta C_T$  value for GOI expression in AP tissue. The  $\Delta\Delta C_T$  value was therefore the difference of GOI expression in AP tissue compared to LIMA tissue and relative to the geometric mean of two stably expressed reference genes. The ratio of target gene expression in AP tissue relative to LIMA tissue was determined by calculating the inverse log  $\Delta\Delta C_T$ , using Eq (i).

Using this method, negative  $\Delta\Delta C_T$  values represented an up-regulated GOI, whereas positive  $\Delta\Delta C_T$  values represented down-regulation of the GOI. Positive  $\Delta\Delta C_T$  values generated fold changes that were less than one. For example,  $\Delta\Delta C_T = 1.23$  generated a fold change of 0.426. Calculating the reciprocal of the fold change gives 2.35 (e.g.  $1/0.426 = 2.35$ ). Therefore, the expression level in the experimental condition would be 2.35fold less than the expression of the control gene.

Final mean fold changes for a given GOI were plotted as excel spreadsheet bar charts.

$$(i) \quad \text{Fold change} = 2^{-\Delta\Delta C_T}$$

Standard deviation (SD) was determined from the level of variation in target gene expression  $\Delta\Delta C_T$  values. Initially SD was calculated for target and reference  $C_T$  values using Eq (ii). The SD for  $\Delta C_T$  could then be calculated using Eq (iii).

$$(ii) \quad \sigma = \sqrt{\frac{\sum(x - \bar{x})^2}{n}}$$

Where, the standard deviation ( $\sigma$ ) is the square root of the sum of ( $\Sigma$ ) each value in the data set ( $x$ ) minus the mean of all values in the data set ( $\bar{x}$ ) divided by the sample size ( $n$ ).

$$(iii) \quad \sigma = \sqrt{(s_1^2 + s_2^2)}$$

Where, the standard deviation is the square root of the squared standard deviation for the target ( $s_1^2$ ) plus the squared standard deviation for the reference ( $s_2^2$ ). SD was incorporated into bar charts as the level of variation between sample replicates.

## 2.6 Infection of a human monocyte cell line with *P. acnes*, *in-vitro*

### 2.6.1 THP-1 cell culture

The human monocytic cell line ATCC THP-1 (a kind gift from Dr Jelena Gavrilovic, School of Biological Sciences, University of East Anglia), derived from acute monocytic leukaemia, was thawed at 37°C with gentle agitation. Nine millilitres fresh pre-warmed complete growth medium comprising RPMI 1640 medium (Lonza, UK) supplemented with 10% heat-inactivated fetal bovine serum (FBS), 0.05 mM  $\beta$ -mercaptoethanol and 2 mM L-glutamine was slowly added to the thawed cell suspension. Cells were gently dispersed then centrifuged at 100 x g for 5 min. Supernatant was discarded and cells were suspended in 10 ml pre-warmed complete growth medium. Cells were counted using a trypan blue stain and haemocytometer to determine percentage viability. Briefly, cells were mixed with medium 1:10 then further diluted 1:1 with trypan blue. Cells were applied to the haemocytometer and counted in the four large corner squares and the centre square. Following cell count, the entire cell suspension was transferred to a T<sub>25</sub> flask and incubated in an upright position in an atmosphere comprising 5% CO<sub>2</sub> and 95% air, for 72 h. Following this, 8 ml spent media was carefully removed and replaced with 8 ml fresh pre-

warmed complete growth media. Cells were then incubated for a further 48 – 72 h, at which point, a second cell count was performed. Cells were subcultured and incubated for a final 72 h, harvested and counted. THP-1 cells were deemed fit for experimental use when counts showed ~100% viability.

Cells were routinely seeded at a density of  $2 - 4 \times 10^5$  cell/ml and subcultured every 72 h or when cells reached a density between  $8 \times 10^5 - 1 \times 10^6$  cell/ml. Prior to experimental use, cells at 72 h of culture were harvested and washed with PBS, then resuspended in serum-free medium (complete growth medium minus FBS) and seeded in 24-well plates at a density of  $3 \times 10^5$  cell/well over night. All experimental assays involving THP-1 cells were performed in a class II biosafety cabinet employing aseptic handling and sterile techniques.

#### 2.6.2 Normal growth characteristics for THP-1 cell line

Normal growth conditions were established for THP-1 cells cultured for 120 h using method previously described (section 2.5.2). Cells were counted every 12 h by haemocytometer to calculate growth characteristics using Eq (iv –vii). It is crucial to establish a record of growth characteristics any cell line before starting experimentation to be able to identify alterations in cell growth, which can signify potential problems with the cells or conditions adopted for growth. If undetected, these potential problems may have detrimental effect on experimental data. The results from these experiments were used to formulate excel charts relating to the aforementioned equations.

$$(iv) \quad N_d = \frac{\log(q_2 - q_1)}{\log(2)}$$

- $N_d$      Number of doublings in time interval  
 $q_1$      Cell count at start of exponential phase  
 $q_2$      Cell count at the end of exponential phase

$$(v) \quad r_g = \frac{N_d}{(t_2 - t_1)}$$

- $r_g$  Growth rate  
 $t_1$  Time when cell count commenced  
 $t_2$  Time when cell count ended

$$(vi) \quad T_d = (t_2 - t_1) \frac{\log(2)}{\log \frac{q_2}{q_1}} \approx \frac{1}{r_g}$$

- $T_d$  Population doubling time  
 $t_1$  Time when cell count commenced  
 $t_2$  Time when cell count ended  
 $q_1$  Cell count at start of exponential phase  
 $q_2$  Cell count at the end of exponential phase  
 $r\%$  Growth rate

$$(vii) \quad r_{\%} = \frac{q_2 - q_1}{q_1}$$

- $r_{\%}$  Percentage cell growth  
 $q_1$  Cell count at start of exponential phase  
 $q_2$  Cell count at the end of exponential phase

### 2.6.3 THP-1 challenge with *Escherichia coli* LPS

To assess whether THP-1 cells respond to bacterial stimuli, cells were incubated with different *E. coli* LPS concentrations (0.5 µg, 1 µg and 2.5 µg) over 20 h. All experiments were carried-out in triplicate. LPS-infected THP-1 cells were harvested at 0.5, 1, 1.5, 2 and 20 h for RNA extraction. Briefly, infected cells were transferred to a microcentrifuge tube and centrifuged at 100 x g for 5 min. Supernatant was removed and cells were gently re-suspended in 1 ml Tri Reagent<sup>®</sup> Solution for isolation of total RNA. Cells were incubated in Tri Reagent<sup>®</sup> Solution at room temperature for 5 min then RNA extracted following manufacturer's guidelines, as previously described (section 2.4.2). mRNA was reverse transcribed to cDNA (section 2.4.4) and utilised as template for qPCR analysis (section 2.4.5) to measure the expression of 10 target GOI. This developmental assay was necessary to evaluate the efficacy of THP-1 as a suitable model cell line for investigating bacterial infection/inflammation. In addition, mRNA derived from LPS-infected THP-1 cells provided an activated tissue that enabled optimisation of the primer sets used in this study.

### 2.6.4 THP-1 challenge with *P. acnes*

Fresh cultures of *P. acnes* were harvested in log phase (OD 0.545) and centrifuged at 1000 x g for 10 min. The bacterial pellet was re-suspended in 10 ml sterile PBS and centrifuged at 1000 x g for 10 min. Supernatant was discarded and bacteria were suspended in 10 ml sterile PBS. *P. acnes* cells were counted using a haemocytometer. THP-1 cell cultures were infected with *P. acnes* at a multiplicity of infection of 100 (i.e. 100 bacteria for every 1 THP-1 cells). The duration of *P. acnes* infection of THP-1 cell cultures was investigated at three time points: 2 h, 6 h and 24 h. For negative controls, 30 µl of the same PBS stock utilised to suspend *P. acnes* culture was applied to cells. All experiments were carried-out in triplicate. For analysis, infected cells were transferred to a microcentrifuge tube and centrifuged at 100 x g for 5 min. Supernatant was removed and cells were gently re-suspended in 1 ml Tri Reagent<sup>®</sup> Solution for isolation of total RNA. Briefly, cells were incubated in Tri Reagent<sup>®</sup> Solution at room temperature for 5 min then RNA extracted following manufacturer's guidelines, as previously described in section 2.4.2. Finally, *P. acne*-stimulated THP-1 mRNA was reverse transcribed (section 2.4.4) and relative gene expression was measured by qPCR (section 2.4.5).

## 2.6.5 Gene expression data analysis for *P. acnes*-infected THP-1

The data were analysed as previously described (section 2.4.6) using equation (i), where  $\Delta\Delta C_T = \Delta C_T(C_{t \text{ Target}} - C_{t \text{ Actin}})_{\text{Time } x} - \Delta C_T(C_{t \text{ Target}} - C_{t \text{ Actin}})_{\text{Time } 0}$ . Time x is any time point and Time 0 represents the untreated calibrator expression of the target gene normalised to  $\beta$ -actin. The calibrator sample Ct values for target gene expression was subtracted from the calibrator Ct values for the reference gene, and a mean was calculated, giving a final normalised calibrator value (Time 0). Therefore, individual fold change values for each target gene (time x), normalised to a stable and constantly expressed reference gene and relative to a mean normalised calibrator value (time 0), was calculated for each gene using Eq (i). The mean fold change at time x was calculated and used to represent overall fold induction of target gene expression at time x. SD was calculated as previously described in section 2.4.5 using Eq (ii and iii).

## 2.7 Statistical testing

### 2.7.1 Power calculations for population sample size

Statistical power is a fundamental consideration when designing experiments. Sample size is a key variable that greatly impacts the validity of the calculated significance. Too few subjects in a population study sample can result in committing type I or II errors. Prior to performing the investigation it was necessary to establish the minimum sample population number ( $n$ ) required to provide acceptable statistical power when calculating the probability of outcomes.

Power calculations for  $n$  were performed using the equation (iv)

$$ME = \bar{x} \pm z_{\alpha/2} \frac{S}{\sqrt{n}} \quad [\text{viii}]$$

Where,

$ME$  = margin of error.

$\bar{x}$  = Sample mean.

$S$  = standard deviation of sample set (“ $\sigma$ ” when using population standard deviation).

$Z_{\alpha/2}$  = boundary of internal probability (1-95%/2 = 1.96).

$\sqrt{n}$  = square root of  $n = 20$

Equation viii was algebraically rearranged to solve for  $n$ .

$$ME = Z_{\alpha/2} \frac{S}{\sqrt{n}} \rightarrow \sqrt{n} = \frac{Z_{\alpha/2} S}{ME} \rightarrow n = \frac{(Z_{\alpha/2})^2 S^2}{ME^2}$$

Therefore, equation iv can be used to establish the size of the sample population needed to provide acceptable margin of error rates.

$$n = \left( \frac{Z_{\alpha/2} S}{ME} \right)^2 \quad [\text{iv}]$$

### 2.7.2 Statistical analysis of bacterial growth in media supplemented with different concentrations of growth reagent supplements

To establish the significance of the bacterial growth ( $OD_{600}$ ) for media containing different concentrations of growth reagent supplements compared to control medium, an analysis of variance (ANOVA) was performed. Data sets comprised  $OD_{600}$  values of bacterial cultures grown in media containing a concentration gradient of growth reagent compared with  $OD_{600}$  values of cultures grown in media without the growth reagent (table 2.02). Cultures were repeated with three technical replicates for each bacteria and reagent concentration. The  $OD_{600}$  data were assessed using Excel 2010 statistical toolpak by testing the hypothesis that there were no significant differences between  $OD_{600}$  values. The null hypothesis was rejected at the significance level  $p = 0.05$  since the value of the ANOVA test was less than the critical value. If the ANOVA test indicated significant differences between  $OD_{600}$  values, data were tested further by performing a Levene’s test to assess the equality of sample variances between data sets with the hypothesis that the group variances are equal. We fail to reject the null hypothesis at the significance  $p = 0.05$  level, since the value of the Levene test statistic is less than the critical values. Finally, dependent on variance equality between  $OD_{600}$  data values a Student’s t-test was

performed to determine which reagent concentration groups provided OD<sub>600</sub> values significantly greater than OD<sub>600</sub> values for the control medium (without reagent).

### 2.7.3 Statistical analysis of gene expression in atherosclerotic plaque tissue

To establish whether target gene expression was significantly different between CAP and LITA tissue (section 2.4), significance testing was performed using statistical package R v3.1.0 [URL <http://www.R-project.org/>] and Excel Analysis Toolpak 2010. Fold change data were formatted in Excel spreadsheet columns and imported to R as text (tab delimited) files. Before any significance testing was performed a Shapiro-Wilk test was carried out to establish normal distribution of each data set. Data were considered normal if  $p > 0.05$ . In the rare instance when data were did not fit a normal distribution, data were log-transformed. Levene's F-tests were performed on normal data to determine variance equality between the tested groups. Data that satisfied parametric conditions were tested with a two-tailed independent student's t-test. Data that did not satisfy parametric conditions were tested with the non-parametric Mann-Whitney U test (MWU). The MWU test tested whether the values of the two sets of non-normal data were significantly different based upon their medians. Both analyses were carried out as two-tailed tests.

### 2.7.4 Statistical analysis of *P. acnes*-infected THP-1 gene expression

Fold change values for both LPS-induced and *P. acnes*-induced gene expression were tested by an analysis of variance (ANOVA) test. Data comprised triplicate fold change values for infected THP-1 target gene expression at a given time point compared to untreated THP-1 expression of the same gene and time point. Data were prepared in excel as stated above and normality was tested. ANOVA were performed on normal log transformed data and overall combined ANOVA scores among all tested conditions were reported. If overall combined ANOVA scores indicated a significant difference ( $p < 0.05$ ), the data were tested further to establish which pairs were significantly different by performing a Tukey's post hoc test for pairwise comparisons.

Where data did not fit the assumption of normal distribution required for ANOVA test a non-parametric alternative to ANOVA, the Kruskal-Wallis test was used. If a significant difference was observed indicated by  $p < .05$ , the Kruskal Wallis test was followed with a Wilcoxon pairwise comparison test to establish which pairs were significantly different.

**EXAMINATION OF CAROTID ATHEROSCLEROTIC  
PLAQUE & LEFT INTERNAL THORACIC ARTERY  
TISSUE THROUGH HISTOPATHOLOGICAL &  
IMMUNOHISTOCHEMICAL ANALYSIS**

### 3.1 Introduction

The atherosclerotic plaque is a highly dynamic and complex mass of accumulating cells that undergoes constant remodelling within the intimal layer of large elastic arteries. As an atherosclerotic plaque progresses through several well-defined stages of development it may take several decades from initiation until plaque symptomatology becomes apparent. Figure 3.01, reconstructed from (George & Johnson 2010) shows the pathogenesis of atherosclerosis and details the common plaques phenotypes in the natural progression of the disease from normal artery through to symptomatic atherosclerotic artery; the figure is adapted to include an additional final ruptured plaque phenotype.

During each stage of progression, the plaque develops common histopathological features typical of its developmental stage that provide information relating to the overall vulnerability and relative symptomatology of the lesion. At present the most detailed histological findings are presented retrospectively from autopsy specimens usually comprising thrombosed coronary arteries. Examination of these culprit lesions detailed in the American Heart Association (AHA) classification criteria of human atherosclerotic histological specimens, which is the most cited system (Stary et al. 1994). Reviewed in 1995 and then 2000, the criteria were simplified and expanded to include a number of previously unconsidered characteristics of advanced plaques (Stary et al. 1995; Virmani et al. 2000). The AHA recommendations are often used to describe the natural evolution of atherosclerotic lesions begins with non-atherosclerotic lesions (1) intimal thickening; a normal accumulation of vascular smooth muscle cells (VSMC) in the absence of macrophage and foam cells. (2) xanthoma (fatty streak) shows accumulation of foam cells in the absence of a necrotic core and fibrous cap. Progressive lesions comprises: (3) pathological intimal thickening, containing a proteoglycan-rich matrix with areas of extracellular lipid accumulation, but lacking necrosis. (4) Same as 2 with addition of a rarely occlusive luminal thrombosis, mostly mural. (5) Fibrous cap atheroma containing a well formed necrotic core with overlaying fibrous cap. (6) Thin fibrous cap atheroma comprising a thin fibrous cap infiltrated by macrophages and leukocyte infiltration, rare SMC and a well-defined necrotic core; these lesions may also show signs of IPH (IPH). (7) Rupturing, as 6 with fibrous cap disruption and luminal thrombosis communicating with necrotic core. (8) Calcified nodule, eruptive nodular calcification with underlying fibrocalcific plaque. Finally, (9) fibrocalcific plaque is a collagen-rich plaque with significant stenosis and large areas of calcification and fewer inflammatory cells.

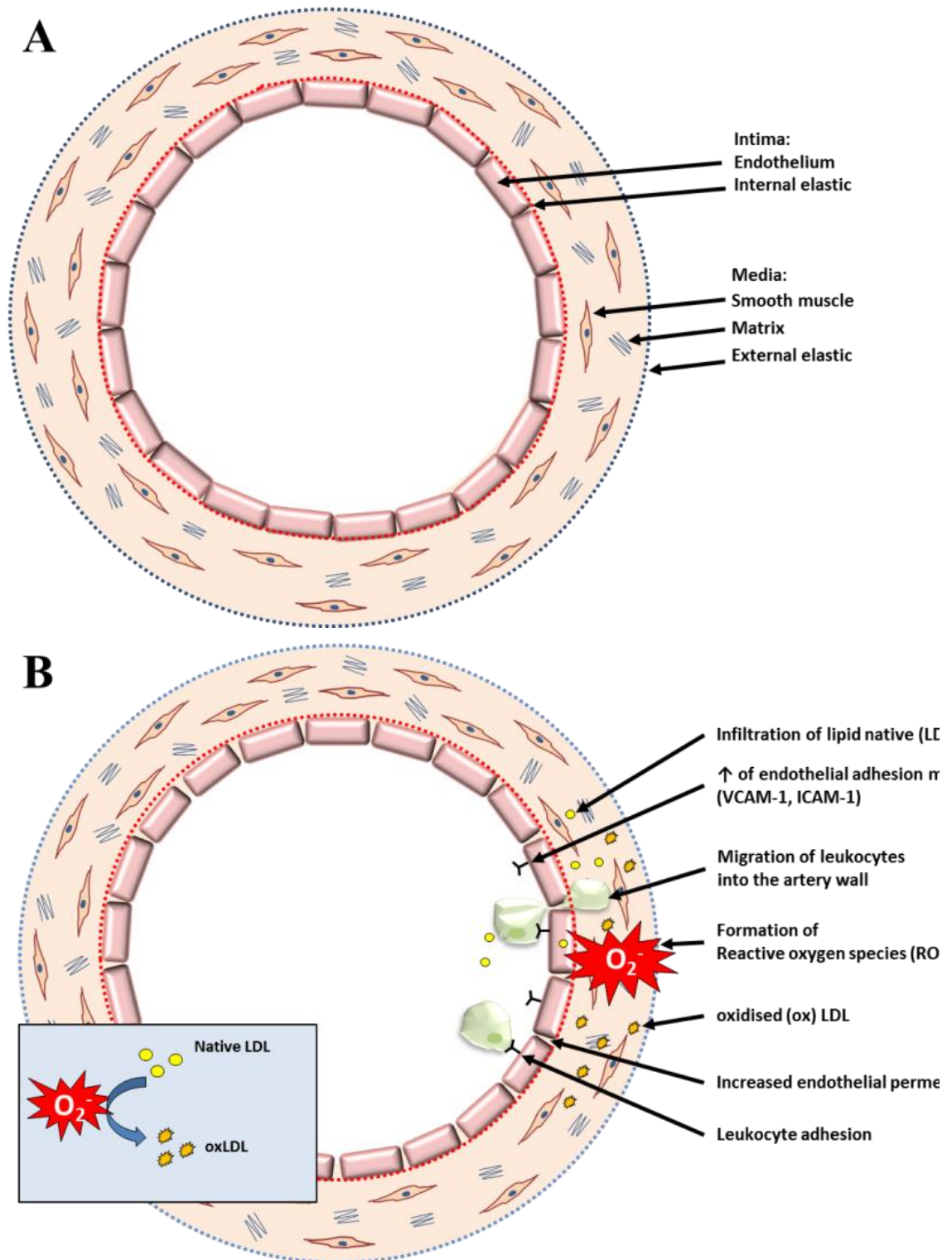
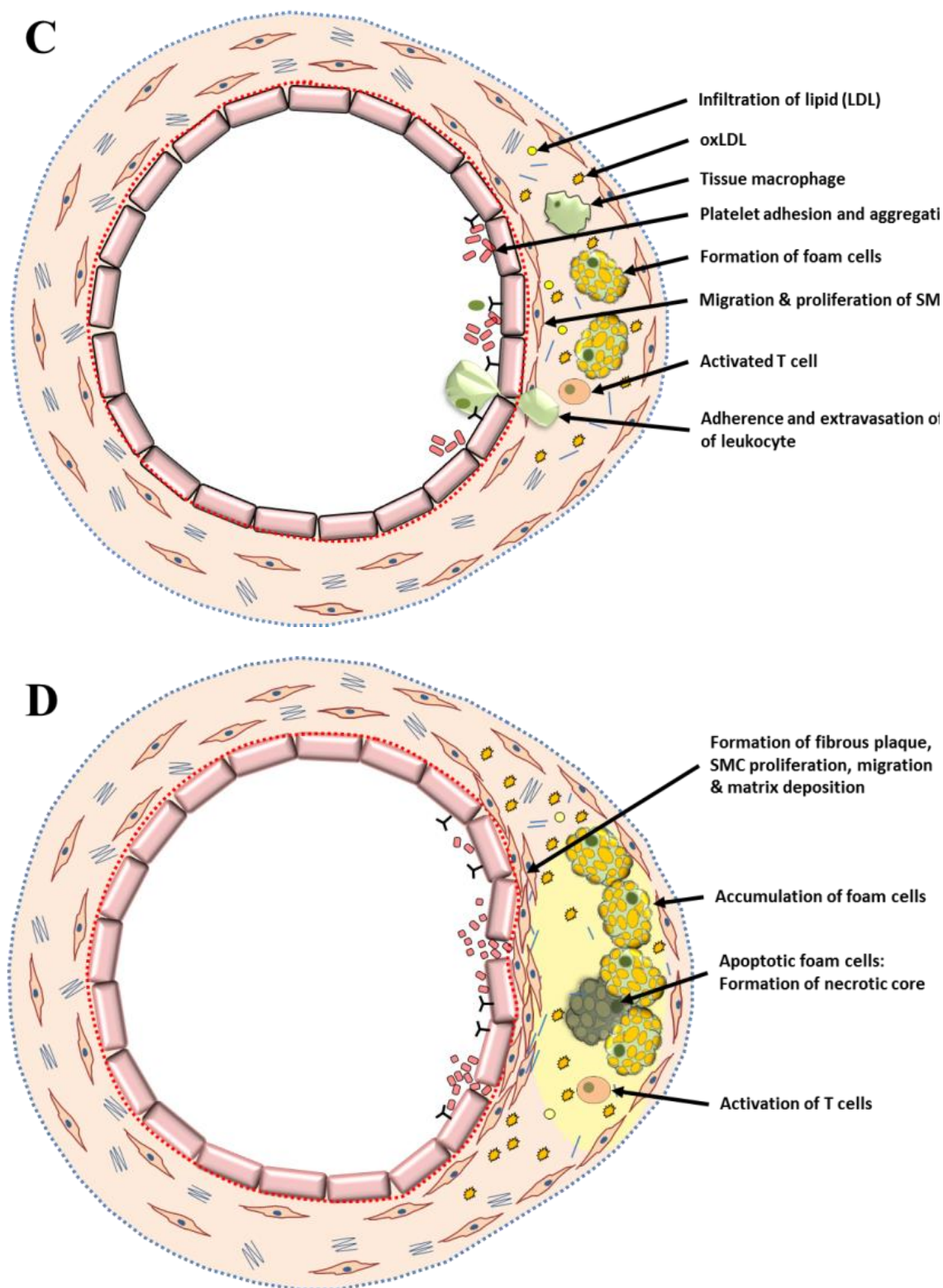
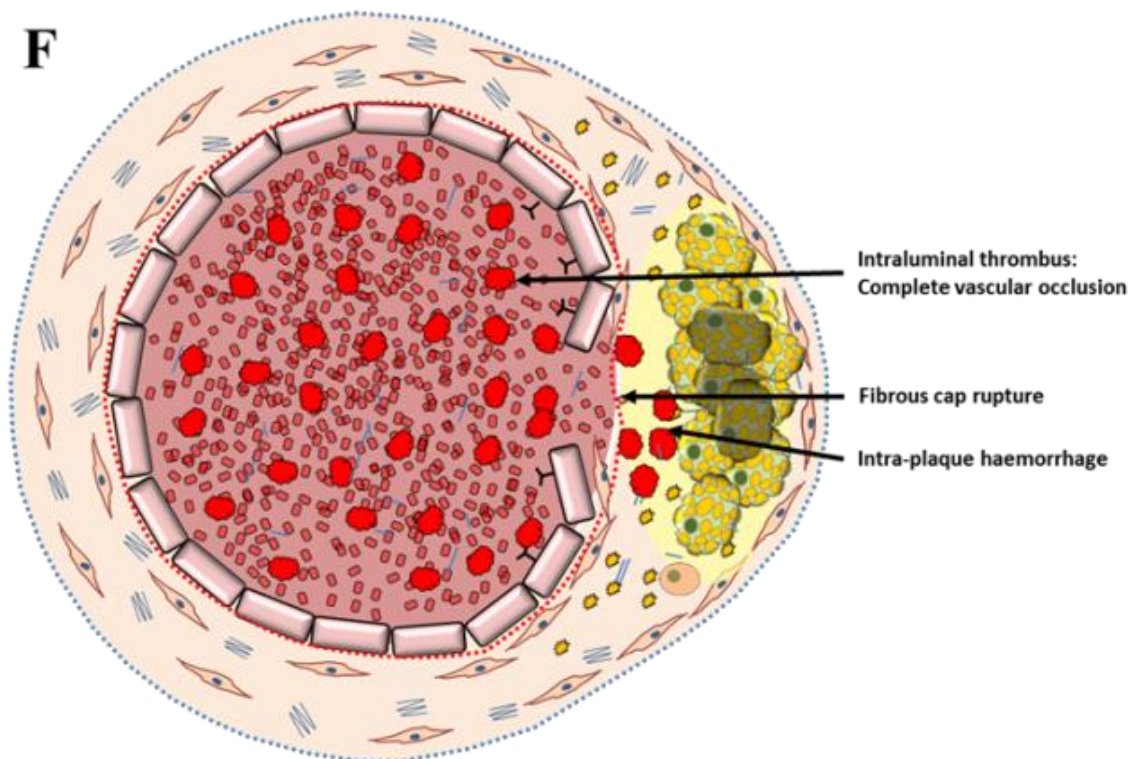
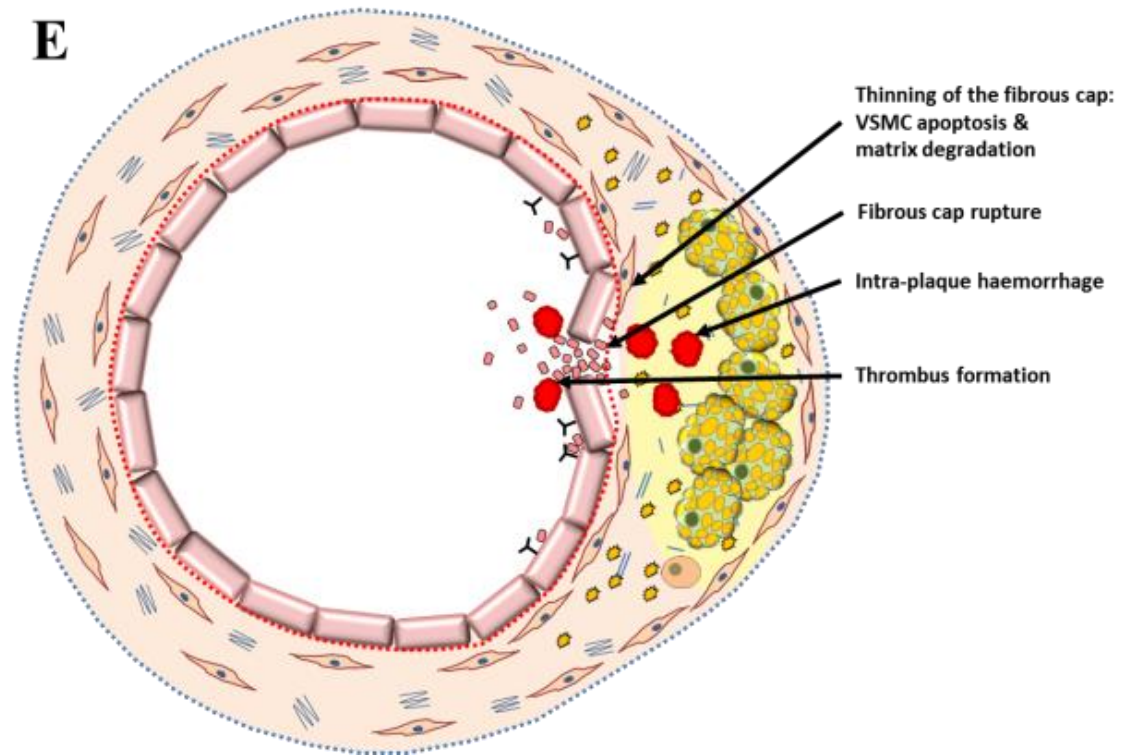
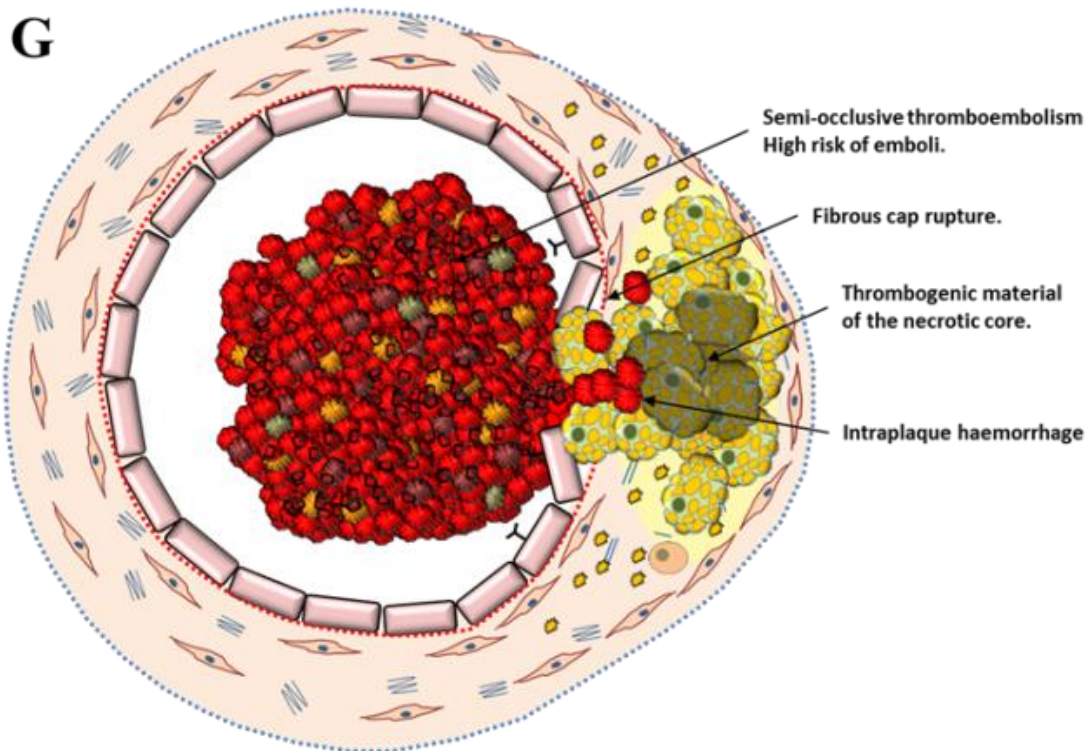


Figure 3.01: Atherosclerotic plaque formation. A: Normal artery is composed of the intima – a layer of endothelial cells seated on the internal elastic lamina – and the media, comprising vascular smooth muscle cells (VSMCs) are embedded in extracellular matrix and surrounded by the external elastic lamina. B Endothelial dysfunction. Damage to the endothelium results from exposure to risk factors and leads to presence of reactive oxygen species (ROS). Adhesion molecules are upregulated and vascular permeability increases. Consequently, leukocytes adhere to the artery wall and migrate to the intima. Low density lipoprotein (LDL) infiltrate the artery wall and are converted to oxidised LDL (oxLDL). Figure adapted and expanded from (George & Johnson 2010).



**Figure 3.01:** *Continued C:* Fatty streak formation. Platelets adhere to the surface of the endothelium and degranulate. ROS continues to convert LDL to oxLDL, which is readily targeted and taken up by macrophages. Macrophages develop into foam cells. Release chemokines and growth factors that lead to further recruitment of inflammatory cells. Activation of T cells and VSMC migration and proliferation. *D:* Stable atherosclerotic plaque formation. VSMCs migration and proliferation lead to the formation of a fibrous cap. Apoptosis of foam cells causes the formation of a necrotic core. Further accumulation of activated T cells and macrophages continues the cycle of influx. Figure adapted and expanded from (George & Johnson 2010).





**Figure 3.01:** *Continued* E: Unstable atherosclerotic plaque formation. Thinning of the fibrous cap occurs as a result of VSMC apoptosis and matrix degradation. IPH occurs. Both these factors render the plaque more unstable and likely to rupture. F: Atherosclerotic plaque rupture #1. Rupture of the fibrous cap or erosion of the luminal surface precipitates thrombus formation, which can be completely occlusive or G: Atherosclerotic plaque rupture #2. As with ruptured plaque #1, but Semi-occlusive thromboembolism forms that may restrict blood flow locally or fragment as emboli and travel with the circulating blood to a vessel with smaller diameter, where it may occlude the flow of blood to the vital organ(s). Figure adapted and expanded from (George & Johnson 2010).

Clinical outcomes caused by the most advanced atherosclerotic plaques are ultimately dictated by the presence of the aforementioned features of plaque vulnerability that collectively weaken the structures of plaque, most critically the thinning of the fibrous cap. Eventually, when the necrotic content of the core exceeds the capacity of the surrounding structure, the thin fibrous cap finally relents, suddenly rupturing its thrombogenic material into the lumen, causing acute irreversible changes in plaque pathology. This catastrophic event results in varying degrees of vascular occlusion and associated ischemic pathologies, such as cerebral or myocardial infarction.

Ischemic outcomes and the resulting tissue infarction in such events depend largely on the location of the affected vessel. Atherosclerosis affecting the carotid artery is beset with its own particular complication, specifically, acute occlusion of the carotid artery due to the propagation of a localised thrombus or occlusion of the cerebral vasculature distant from the atherosclerotic artery that results from embolization of plaque or the resulting thrombus (thromboembolism). Both are critically serious conditions that may be preceded by

transient ischemic attacks (TIA); a small occluding embolism that only temporarily impedes the flow of blood. However, plaque rupture may cause an immediate stroke, in which a permanently occluded vessel results in complete occlusion of circulating blood to the cerebra, causing lengthy ischemia and cerebral infarction.

Many investigations have been conducted to examine the histopathological features of atherosclerotic plaque tissue from the carotid artery (Van Damme et al.; Persson 1983; Ammar et al. 1984; Lennihan et al. 1987; Aburahma et al. 1989; Leen et al. 1990; Avril et al. 1991; Seeger et al. 1995; Park et al. 1998). Other studies focus on the occurrence of features commonly encountered in carotid plaques harvested from asymptomatic and symptomatic patients (McCarthy et al. 1999; Dunmore et al. 2007; Xiong et al. 2009). In these experiments the frequency of histological features and their relative occurrence in symptomatic plaques could provide information relating to each feature and its involvement in plaque symptomatology and destabilisation. More recently, the efficacy of clinical techniques such as magnetic resonance imaging (MRI) (Hatsukami et al. 2000; Yuan et al. 2002; Kerwin 2003; Chu et al. 2004; Cai et al. 2005; Kerwin et al. 2008), computed tomographic (CT) scans (Feinstein 2006; Mofidi et al. 2008; Teng et al. 2014) and ultrasound scans (Feinstein 2006; Shah et al. 2007; Giannoni et al. 2009) have been investigated in identifying histological features of vulnerable plaques *in vivo*. The resulting images from these powerful techniques are then compared to the histopathological features found in gross atherosclerotic plaques harvested from surgical procedures to assess their suitability for detecting vulnerable plaque phenotypes.

There are, in-effect, eight hypotheses proposed for the initiation and pathogenesis of atherosclerosis, each covering a particular major atherogenic pathway; though only two are universally acknowledged; namely, the “lipid or oxidative modification” hypothesis (Witztum 1994) and the “response to injury” hypothesis (Ross et al. 1977). The “lipid or oxidative modification hypothesis” proposes that a link between elevated oxidised and/or modified plasma lipoprotein and atherosclerosis, while the “response to injury” hypothesis suggests that endothelial dysfunction may be the initiation mechanism of plaque formation. Although these hypotheses cover fundamentally different mechanisms they are in no way mutually exclusive as both play critical roles in the development of atherosclerotic plaque, which, to some extent work in unison to fulfil this goal. For example, when a vessel is injured, endothelial cells activate by enhancing vascular adhesiveness for leukocyte and platelet recruitment, increased procoagulant milieu and

permeability factors. Thus, vascular regions affected by endothelium dysfunction are highly permeable for the chemotaxis of leukocytes to the site of injury; this provides the perfect environment to aid transport of native and oxidised LDL (oxLDL) from the circulation to the intima, thereby further progressing plaque development.

Although lipid modification and deposition are thought to be a major source of the continuous inflammatory stimulus, a large body of evidence suggests that infectious agents may contribute to atherosclerotic processes (Campbell & Rosenfeld 2015). This could occur by either local infection of vascular cells and/or through systemic effects by induction of cytokine and acute phase reactant proteins by infection at other sites (Pussinen et al. 2007; Loos 2005). Multiple viral and bacterial pathogens have been associated to atherosclerosis through serological, molecular detection of species within the atherosclerotic plaque and by demonstrating accelerated development of atherosclerosis following infection with putative strains in hyperlipidaemic animal model.

Significant similarities in the pathogenesis of atherosclerosis and chronic infections such as periodontitis have suggested a common underlying biological mechanism for the two conditions. Based on this paradigm, numerous studies have examined the relationship between periodontitis and cardiovascular disease (Meurman et al. 2004; Tonetti & Dyke 2013; Tabeta et al. 2014). Gingival inflammation may influence atherosclerosis in three distinct pathways. Periodontal pathogens cause the development of subgingival plaque which leads to inflammation of the periodontal tissues. Chronic gingival inflammation leads to receding gingival tissues and the formation of periodontal pockets, which act as reservoirs for accumulation of bacteria and food debris. The ensuing local inflammatory response produces micro-ulcerations through the pocket epithelium, promoting distant-site infection via transient bacteraemia (Brodala & Merricks 2005; Forner et al. 2006; Iwai 2009; Raber-Durlacher et al. 2013). Moreover, bacteria release numerous biologically active surface membrane proteins including lipopolysaccharides (LPS), endotoxins, chemotactic peptides, proteins, and organic acids that may then enter the systemic circulation (Pussinen et al. 2007). These products can then initiate the host inflammatory response that can elevate serum concentrations of acute-phase proteins and proinflammatory cytokines (C-reactive protein, fibrinogen, IL-6 and IL-8) (Loos et al. 2000; Ebersole 2003; Loos 2005). Increase of these inflammatory mediators is thought to be a major contributing factor in the pathogenesis of atherosclerosis (Lockhart et al. 2012; Lund Håheim 2014).

This first chapter of work involves two specific phases of investigation. The first of which will involve establishing the frequency and density of histopathological features within H&E and MTC stained sections of atherosclerotic plaque tissue from the carotid artery. Performing these examinations will provide an overall better understanding of the general cellular composition and structural architecture of the plaque tissue being studied, as well as provide an insight into the plaque vulnerability based on the observed features.

One of the main areas of focus for this thesis will be the targeted detection and identification of specific species of bacteria present within atherosclerotic plaque tissue. However, as the opening chapter of work for this thesis, it seems more plausible to first establish the presence of a broad-reaching bacterial marker that can determine the frequency of most bacteria residing within atherosclerotic plaque tissue. Peptidoglycan (PGN) is perfectly suited to this task, as a highly conserved polymer that forms a large portion of the plasma membrane of most bacteria. In Gram-positive bacteria PGN accounts for 35 – 70% of the total bacterial cell wall mass, approximately 10 – 70 layers (Snowden & Perkins 1990), whereas, Gram-negative bacteria have only 1 or 2 layers of PGN, accounting for only 10% of bacterial cell wall mass (Labischinski et al. 1991). Nevertheless, its epitope is available at the cell surface of both Gram-cell types, which negates the need for digestion of tissue sections when performing immunohistochemistry (IHC). Thus, the second phase of work for this chapter will be carried out by using a single antibody for the IHC detection of PGN in FFPE tissue section of atherosclerotic plaque from the carotid artery

### 3.2 Chapter aims

This chapter of work will involve the examination of sections of human atherosclerotic plaque tissue from the carotid artery for the purpose of

- A) Examining FFPE sections of atherosclerotic plaque tissue from the carotid artery stained with H&E & MTC for identification of particular microscopic characteristic features that form the cellular composition and architecture of plaque tissue.
  - i. Determine the frequency and/or percentage spread of observed features.
  - ii. Establish any correlative relationships between histological features and between histological features and patients' data.
- B) Examine FFPE section of atherosclerotic plaque tissue from the carotid artery for the frequency and density of anti-PGN localisation.
  - i. Determine any trends of localisation and establish any correlative relationships between the frequency of PGN staining and any reoccurring histopathological features of atherosclerotic plaque.
- C) Compare findings from section A & B with finding observed with LITA healthy human artery tissue control tissue
  - i. Compare histopathological findings from section A with H&E stained healthy LITA control tissue.
  - ii. Compare histopathological findings from section B with the frequency and density of anti-PGN stained healthy LITA control tissue.

### 3.3 Method overview

Twenty CAP and LITA tissue samples were collected from theatre and transported to the laboratory in RTM and RNAlater<sup>®</sup> (section 2.1.2). Portions of the tissue were fixed, demineralised, dehydrated and paraffin embedded using standard histological methods (section 2.2.1). Tissue section from all CAP and LITA samples were stained with H&E (section 2.2.2) and MTC (section 2.2.3) to assess histological features and cellular architecture of the tissue. An avidin-biotin complex (ABC) method was adopted using primary antibody with secondary antibody anti-bacterial peptidoglycan (anti-PGN) in conjunction with a DAB chromagen (red/brown stain) to determine the localisation of bacterial cell wall components in CAP and/or LITA tissue (section 2.2.4).

### 3.4 Results

#### 3.4.1 Power calculations for population sample size

Data generated here from a small sample population ( $n = 20$ ) for observation of PGN localisation were used to establish the population sample number required to give a margin of error ( $ME$ ) of 3 and below (table 3.01). The actual marginal error calculated with  $n = 20$  subjects was high ( $ME = 4.26$ ) and therefore the sample mean ( $\bar{x} = 17.45$ ) could have been in a range from 13.19 – 21.71. To reduce marginal error observed within this study to an acceptable level, a greater sample size would be needed. An  $n = 91$  or  $n = 363$  would have decreased the margin of error to 2 or 1, respectively (table 3.01). While it was important to establish the population sample size needed prior to this investigation, it was not possible to obtain more than 20. The selection of eligible candidates for tissue donation was considered by the cardiothoracic consultant and research nurse involved in this study. All patients that were eligible for the study and were scheduled for the necessary surgery during the study were recruited.

$n$	20			
Mean ( $\bar{x}$ )	17.45		17.45	17.45
Standard error	2.17		2.17	2.17
Confidence interval (CI)	95%		95%	95%
$Z_{\alpha/2}$	0.025		0.025	0.025
z score	1.96		1.96	1.96
Standard deviation	9.71		9.71	9.71
Marginal error	4.26		3	2
				1
Actual (n)	20	Required (n)	41	91
				363

**Table 3.01:** Power calculations to establish require population number ( $n$ ) to minimise margin of error. Left column shows the formulae calculated to determine the power of the sample size. Left two columns relate to the actual sample size tested in this study, while the remaining columns detail the necessary sample sizes needed to limit marginal error to 3, 2 and 1.

Given the amount of error observed when testing hypotheses with a small population size ( $n = 20$ ), it cannot be said with certainty that type I or type II errors were avoided. Therefore, any statistical testing performed in this chapter for correlation or association are tentative.

### 3.4.2 Histopathology of plaques from the carotid artery

Several notable features were observed when CAP and LITA samples were assessed by hematoxylin and eosin (HE) staining. One plaque specimen, taken from the left internal carotid artery of a 72-year-old-male, showed advanced atherosclerotic disease affecting the whole circumference of the artery (Figure 3.02). The plaque displayed a large necrotic core ~30% of the plaques mass and covered by a thick fibrous cap. The large mass of the atheroma and thick fibrous cap resulted in a marked luminal stenosis. The plaque also displayed regions of increased inflammation, evidenced by a density of dark blue/purple particularly situated around necrotic cores. It must be noted however, to determine the presence of leukocytes; one would need to use antibodies to establish the presence of leukocyte common antigen or an antibody specific to a particular leukocyte cell type.

Seventy percent of plaque samples contained at least one lipid core each showing a varied extent of necrosis at their core. The necrotic core was characterised by cholesterol clefts (Figure 3.03), with areas containing necrotic cell debris that is highly eosinophilic tissue without the presence of nuclei and often surrounded by accumulating foam cell structures (Figure 3.04a-c) and the nuclei of infiltrating immune cells. Foam-cell structures were present in most lesion, the degree of accumulation varied dependant on the size of lipid lesions with large necrotic cores (30 – 50% of the lesion mass) were often protected from the lumen space by a dense layer of fibrous collagen/smooth muscle cell, characterised by a grey-green stain with Masson's trichrome (MTC) stain (Figure 3.03b-d).

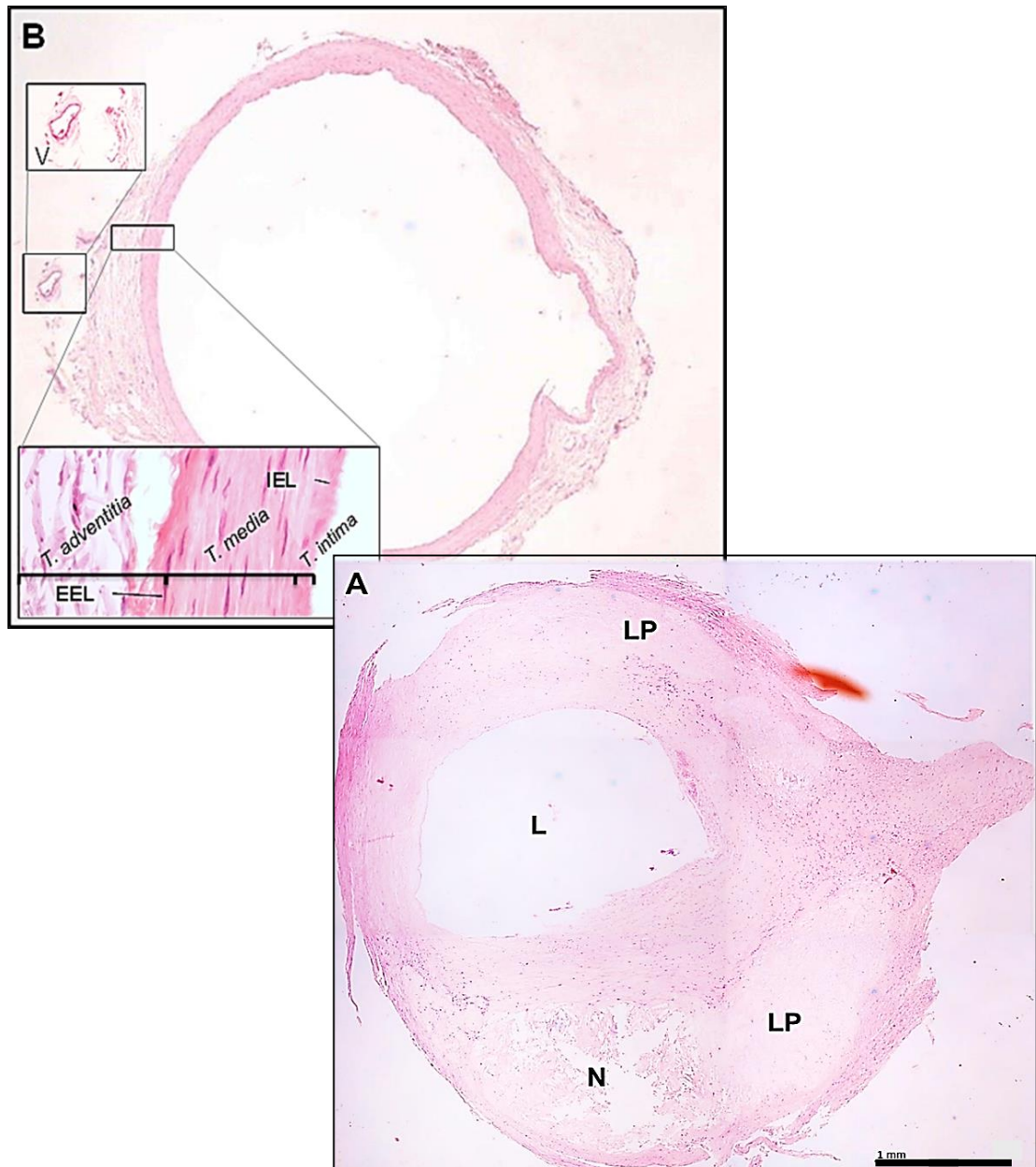


**Figure 3.02:** A six-piece stitched image of atherosclerotic plaque tissue from the internal carotid artery from a 72 year old male (A). Section stained with hematoxylin & eosin and six images captured at X4 magnification then post-manually stitched together (A). The section displays common features of advanced atherosclerotic disease, such as, two lipid pools (LP), one of which covers ~30% of the lesion with a large necrotic core (N) within the lipid pool (A). A marked reduction in lumen space (~60 – 70%) is evident; made more apparent when compared to the lumen space of a similar sized elastic artery, the left internal thoracic artery (LITA) (B). The LITA control tissue had good structure and displayed three discrete layers of cells; 1 layers of endothelial cells and the internal elastic laminae (*tunica intima*) followed by 15 – 16 layers of smooth muscle cells (*tunica media*) and the external elastic laminae and 18 – 20 layers of collagen fibres (*tunica adventitia*). In the outer layers of collagen fibres *vasa vasorum* can be observed (top left box, A).

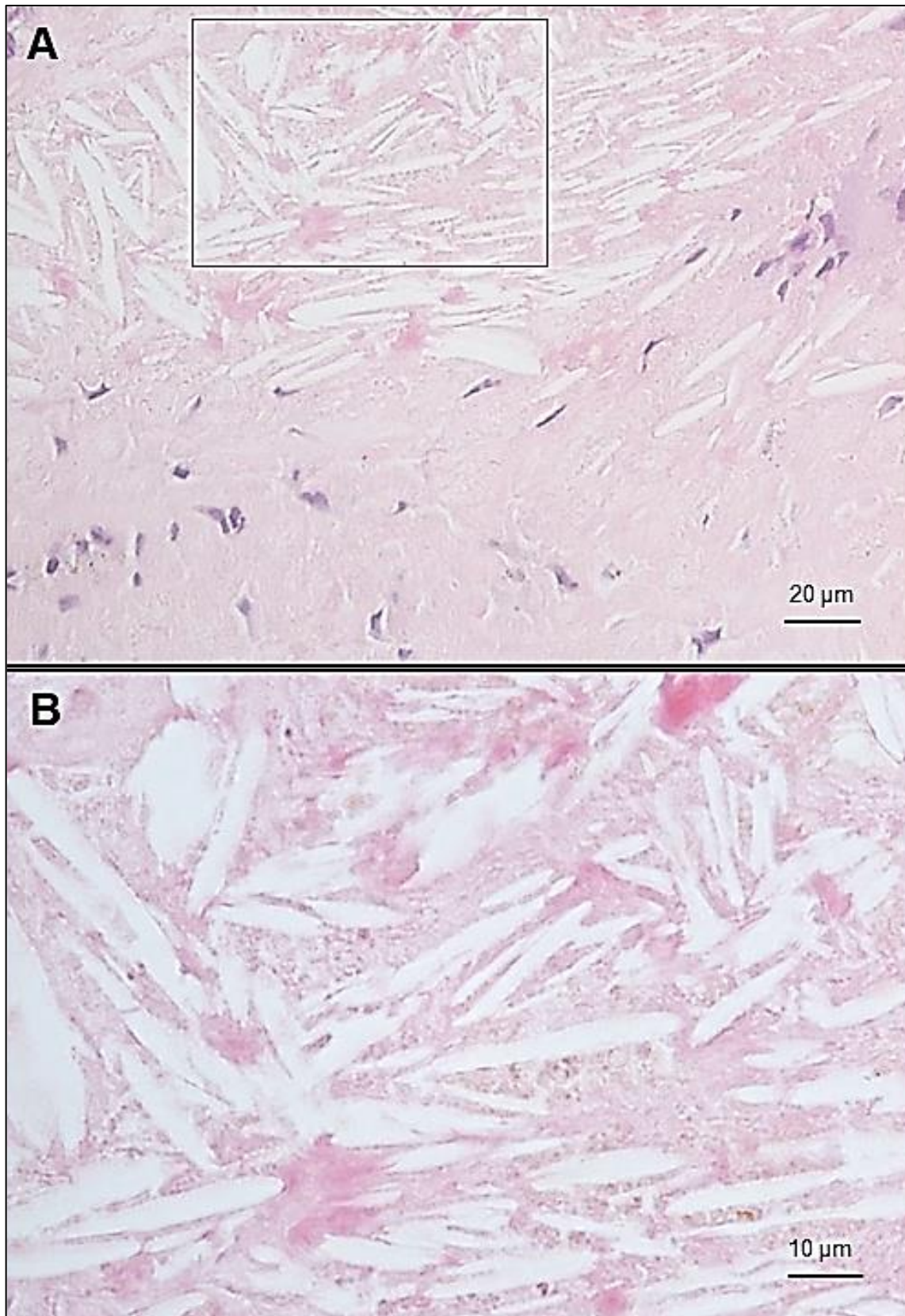


**Figure 3.03:** Cholesterol clefts formation in atherosclerotic plaque tissue stained with H&E. Images A show a region of cholesterol clefts surrounded by immune cell infiltration (purple nuclei) at X40 magnification. Cholesterol crystals form when cholesterol crystals dissolve away during the tissue processing, leaving distinctive needle like voids in the tissue. Clefts occur in and around the lipid core, an area associated with necrosis. Immune cells are often found close to cholesterol clefts though typically no nuclei are observed among clefts. Image B shows a X100 magnification of the original tissue within the rectangle of B.

Collagen takes up Weigert's haematoxylin to produce a vivid green colour of varying depth depending on exposure time, whereas smooth muscle tissue produced a grey-green due to dull red nuclei staining. All plaques showed extensive fibrous collagen composition, particularly throughout fibrous cap regions (Figure 3.04b-d). In combination with HE, MTC provided extra definition to tissue structure such as foam cell (figure 3.04d-f) and IPH (Figure 3.05h-j). IPH tissue was evident in 30% of plaque specimens and was often localised to the fibrous cap, in close proximity to lipid pool regions or intraplaque vessels (IPV). Erythrocytes stained filled IPV and haemorrhagic regions appeared more indistinct in tissue stained with MTC. IPV (Figure 3.06a-e) were observed in 50% of plaque samples and formed at regions nearest the lumen; however, intraplaque vessels were also sporadically distributed throughout the plaque tissue and formed either regular or highly irregular shape (Figure 3.06a-e).

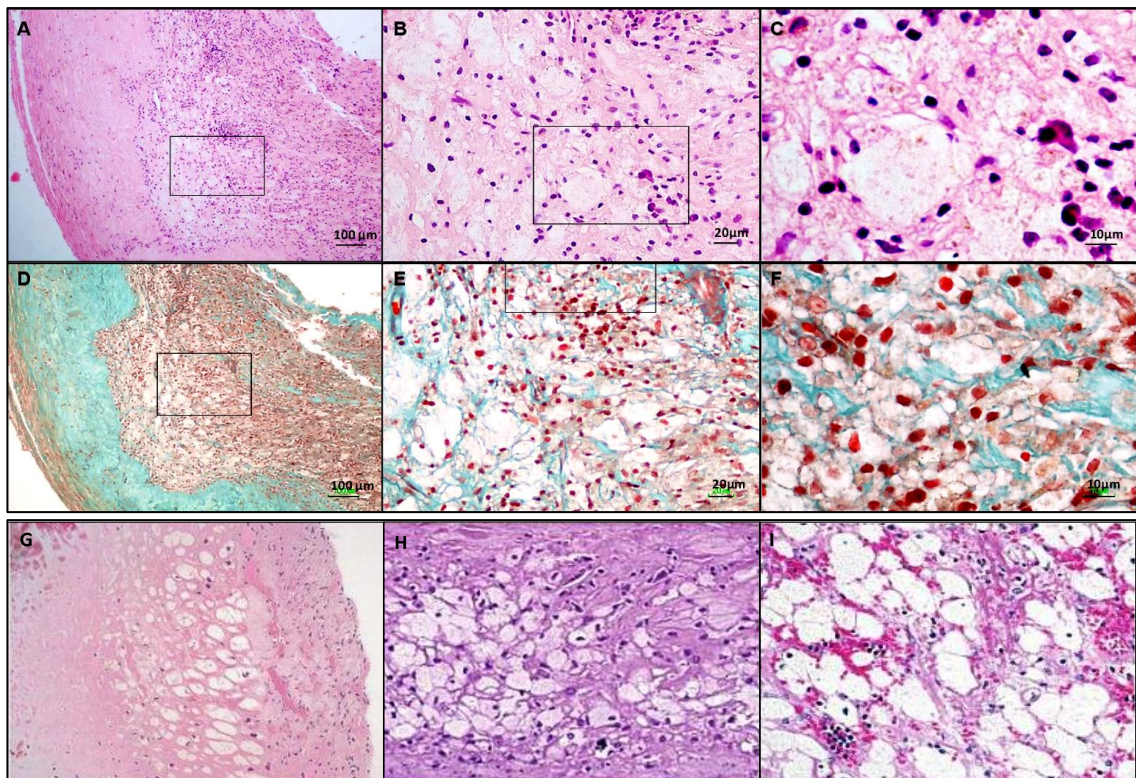


**Figure 3.04:** Shows a large accumulation of foam cell-like structures within and around a sizable lipid pool. The top panel shows CAP tissue stained with H&E and captured at X10 (A), X40 (B) and X100 (C). Accumulated foam cells form a highly distinctive structure that have the appearance of bubbles (foam). Around the perimeter of the lipid pool is a wall of infiltrated immune cell (dark purple nuclei) (A). Dense groups of immune cells are visible within the lipid pool (A). The lower panel of images are of a consecutive section of CAP tissue stained with MTC captured at the same magnifications (D, E & F). Image D shows the larger accumulate of foam cells is encased in a thick wall of collagen (bottom left, D) and a thin fibrous cap (top right corner, D). Greater definition is achieved with MTC staining, giving finer detail to the foam cell-like structures (E & F). MTC stains cytoplasm, muscle and erythrocytes different shades of red and nuclei from grey to black; thus the cytoplasm of numerous cell types can be observed among the foam cell structures (F). The bottom panel shows textbook images of foamed cells that are contained within coronary (G) carotid (H) and femoral (I) arteries sections when stained only with H&E (Sheppard 2011).

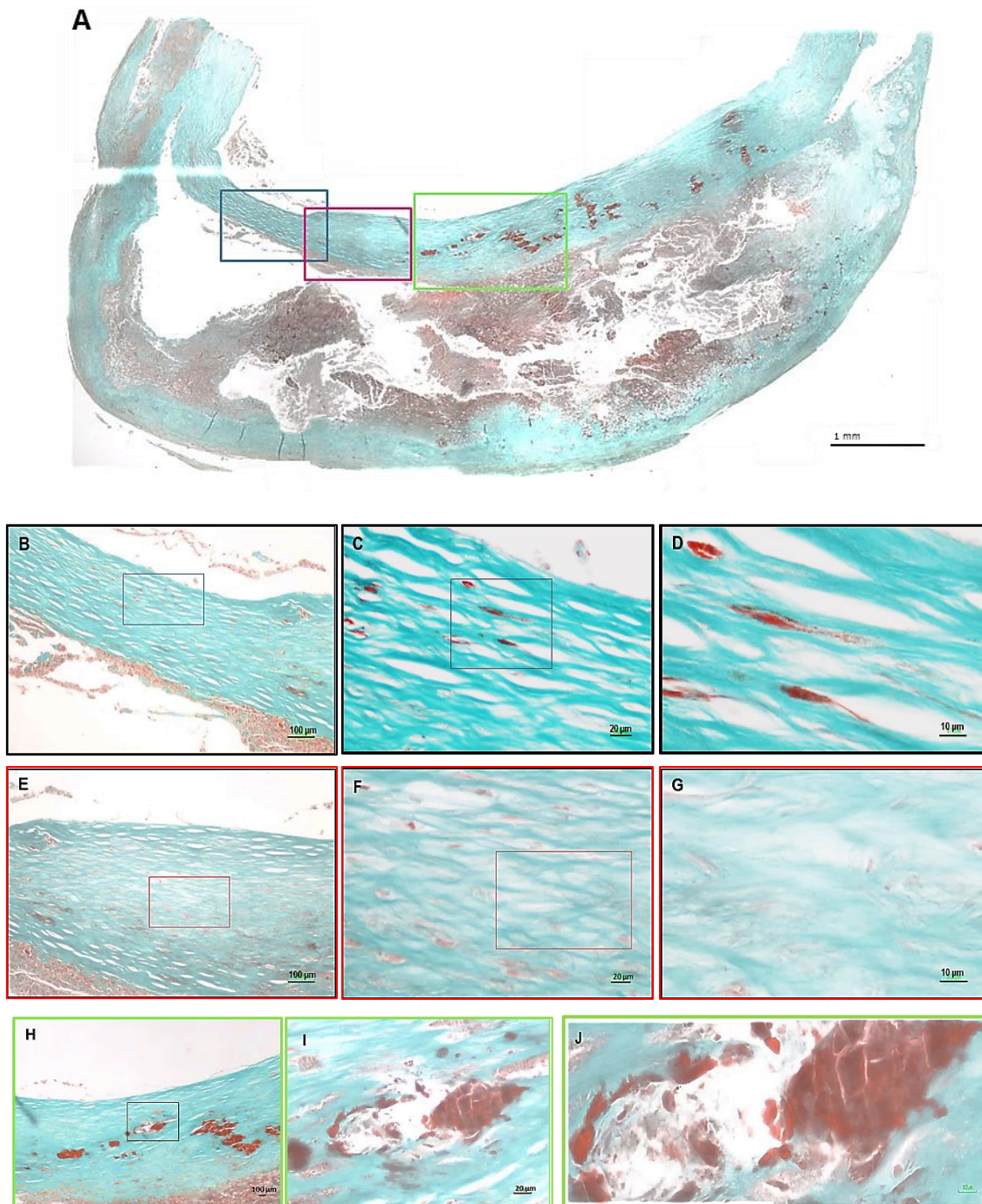


**Figure 3.05:** Large CAP tissue sections stained with MTC and captured at X4 magnification then manually stitched together (A). Abundant collagen composition located around the perimeter of the atheroma conceals a large necrotic core with sporadic haemorrhagic tissue (A). The centre of the plaque shows the formation of a large lipid pool/necrotic core. The boxes on image A relate to the image below with the same colour border. Black box within image A is magnified X20 (B), X40 (C) and X100 (D) revealing the thinnest section of fibrous cap comprising mostly collagen with the presence of elongated (dull red) smooth muscle cells. Middle panel (E, F & G) shows a section of collagen that appears more grey as a result of increasing smooth muscle cell content. The bottom panel (H, I & J) show the formation of large intraplaque vessel with superimposed IPH. Intraplaque haemorrhaging is most prominent throughout the fibrous cap area (H). A mass of haemorrhagic blood with discrete erythrocytes are apparent.

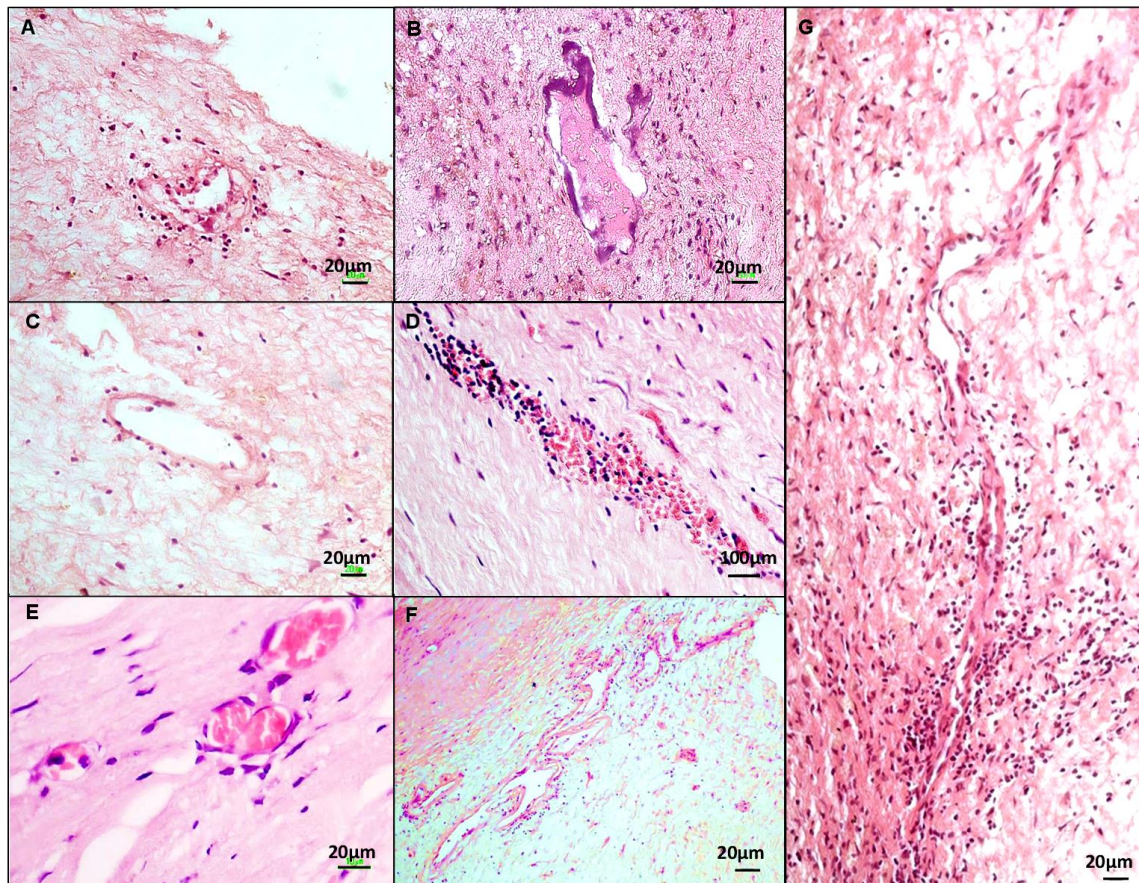


**Figure 3.06:** Shows the varied formation of IPV. The left column (A, C & E) show normal oval vessel structure, whereas the remaining two columns show vessel walls that appear highly irregular (B, D, F & G). A vessel wall can be observed by the appearance of denser darker tissue compared to the lighter surrounding eosinophilic tissue (A, C, F and G). IPV provide a portal into the plaque for migratory leukocytes and other inflammatory mediators. The nuclei of infiltrating immune cells can be observed surrounding the vessels; particularly visible for A, E & G. Some vessels were easily identified when filled with erythrocytes (D & E). Image D shows the presence of both erythrocytes and the nuclei of migratory immune cells within the lumen space of the neovessel

Calcified nodules were rarely observed (15%) but were detected within very fibrous, complicated plaques specimens (Figure 3.07). However, no specific staining method was performed for the detection of calcium, (i.e. Von Kossa). All plaque specimens displayed localised immune cell infiltration that appeared more prevalent around IPV (Figure 3.06). Heavy immune cell infiltration was also observed at the shoulder regions of three plaque specimens (Figure 3.08). High concentrations of nuclei were present at regions around the perimeters of lipid cores where foam cells accumulated (Figure 3.03a), though a distinct lack of nuclei were observed within the necrotic cores or at regions occupied by cholesterol clefts (Figure 3.03a & b).

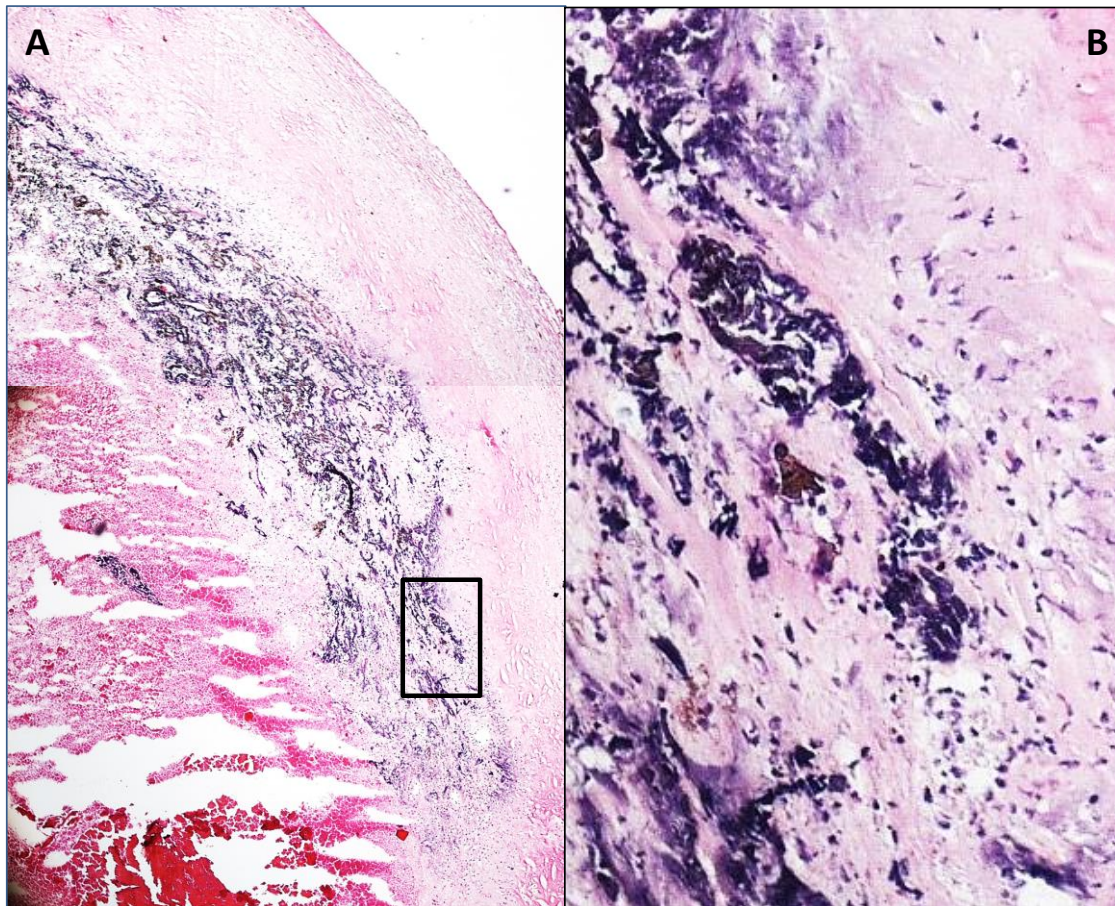


**Figure 3.07:** Large region is characteristic of calcium mineralisation. Typically calcification occurs in the area between the artery wall and the atherosclerotic plaque where the flow of calcium and other minerals is affected; as a result smooth muscle cells die and a long process of osteoblastogenesis and osteoclastogenesis dictate the ensuing mineralisation. Calcium can form where old cholesterol and necrotic cell debris has accumulated in the core of an atheroma. Characteristics of old cholesterol such as clefts remained in sections of the mineralised plaque that would indicate the calcified area may have formed from a lipid core. Thrombus tissue is visible to the bottom of the image (A).

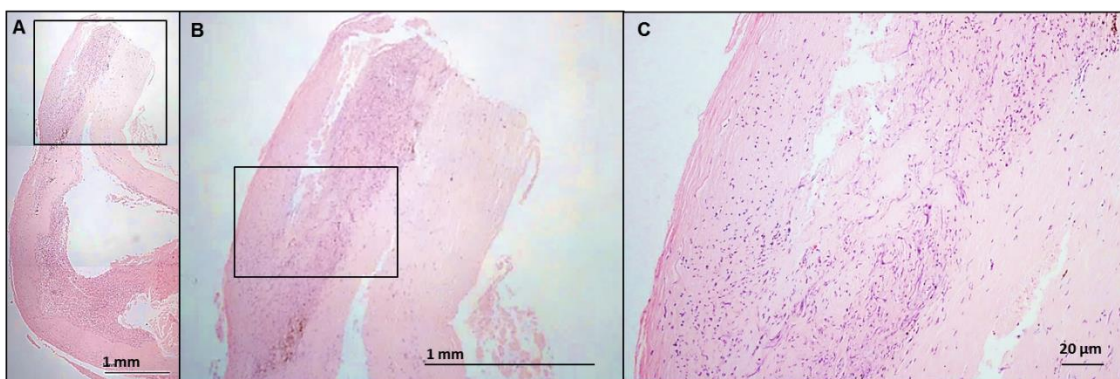


**Figure 3.08:** Shows the immune cell activity at the shoulders of the plaque tissue. Images were captured at X4 (A), X20 (B) and X40 (C) magnifications. A sharp contrast can be observed between the shoulder area highly active with immune cell infiltration and the inactive region of plaque adjacent (B). Image C clearly shows hundreds of active immune cells that have likely gained entry to the plaque near the shoulder region. The plaque shoulders are the farthest extremities of the lesion; at the point where the plaque is least dense. At the shoulder region there is a border where healthy endothelium becomes affected by disease. Leukocytes and other immune cells can therefore easily extravasate through the healthy endothelium and transmigrate to the sub-endothelial layers of the artery affected by atherosclerosis. The shoulder regions of plaque therefore have a dense traffic of migrating leukocytes and other inflammatory mediators as shown above

A Spearman's product-moment correlation coefficient for non-parametric testing of ordinal data was performed to assess the relationship between the frequencies of histological features. Relationships were observed between four of the histological features. The frequency of foam cells was correlated with the frequency of immune cell infiltrations [ $r = 0.494$ ,  $n = 20$ ,  $p = <0.05$ ]. The relationship between the number of observed immune cell infiltrations and the presence of a lipid core(s) was analysed, though no correlation was established [ $r = 0.405$ ,  $n = 20$ ,  $p = <0.069$ ]. The presence of a lipid core(s) did however correlate positively with the presence of foam cell structures [ $r = 0.773$ ,  $n = 20$ ,  $p = <0.0001$ ]. Finally, the presence of intra-plaque vessels was shown to be significantly correlated to the occurrence of intraplaque haemorrhages (IPH) [ $r = 0.6723$ ,  $n = 20$ ,  $p = <0.001$ ]. Figure 3.09 displays the overall frequency of features in histogram form..

<b>Histological features</b>	<b>Number observed</b>	<b>Overall (%)</b>
Foam cells structures	20	100
Inflammatory cells	20	100
Lipid core	14	70
IPH	6	30
IPV	10	50
Fibrous cap	13	65

**Table 3.02:** Histological features observed within formalin fixed paraffin embedded CAP specimens. Left column lists the histological feature followed by the number of observations of that feature. The right column highlights the percentage of the observed feature relative to the total number of samples tested ( $n = 20$ ).

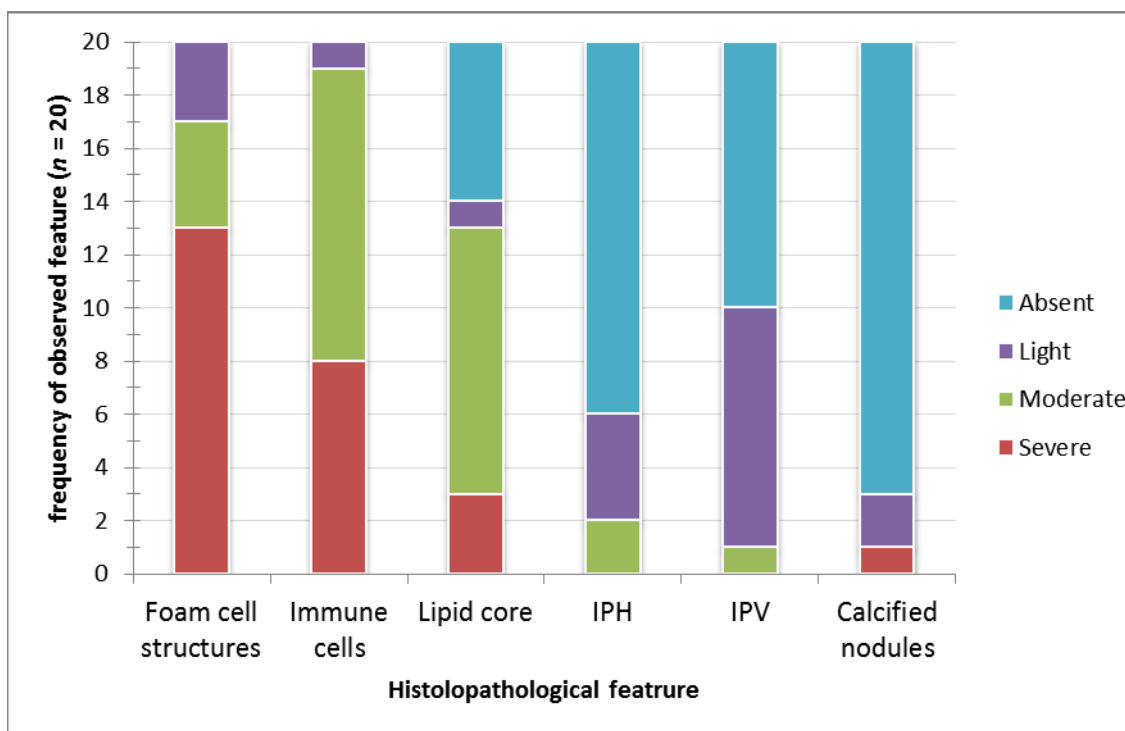


**Figure 3.09:** Frequency of plaques ( $n = 20$ ) that contained common histopathological features of atherosclerotic disease. Foam cell structures were the most commonly detected characteristic, with 13 showing severe foam cell-like structures. Immune cell infiltration was also a commonly detected feature observed throughout the different plaques. Less commonly observed were IPH and IPV. Calcified plaque tissue was the least detected feature among plaques.

### 3.4.3 Localisation of bacterial PGN

PGN was detected in 18/20 (90%) CAP specimens. None of the LITA or negative control specimens showed PGN staining (Figure 3.10). The degree of positive staining was semi-quantitatively measured by observing the amount of PGN localisation under a light microscope. Positive PGN staining was scored as absent (in no fields of view), light (sporadically observed on few fields of view), moderate (in most fields of view), heavy (diffuse staining throughout tissue) and expressed as a percentage of total number of samples. Heavy staining was most frequently observed in 45% of samples, followed by moderate (35%), light (10%) and no stain (10%) (Figure 3.1.1). Positive PGN staining appeared to localise to areas of foam cell accumulation (Figure 3.12) particularly in foam cells that accumulated round a necrotic core (image 2.13). Other areas of localisation observed were between folds of collagen (Figure 3.14) and around cholesterol clefts (Figure 3.15).

A Spearman's product-moment correlation coefficient for non-parametric testing of ordinal data was performed to assess the relationship between intensity of PGN staining and prevalence of foam cell-like structures. There was a significant correlation between

severity of PGN localisation and foam cell like structure presence within plaque tissue [ $r = 0.813$ ,  $n = 20$ ,  $p = <0.0001$ ]. A similar correlation existed between the severity of PGN staining and immune cell infiltration [ $r = 0.703$ ,  $n = 20$ ,  $p = <0.001$ ]. When the relationship between intensity of PGN staining and presence of a lipid core was tested, no significant correlation was observed [ $r = 0.274$ ,  $n = 20$ ,  $p = 0.236$ ]. No further correlations were observed between PGN staining or patient age and the remaining histological features. It must be noted that no antibody treatment was performed to assess foam cell or immune cell localisation. Furthermore, the sample population size tested for this investigation was small, so the possibility of committing type I or II errors is greater. Therefore, it is difficult to conclude true correlation of severity of PGN stain and any histological feature present in the plaque tissue tested here.

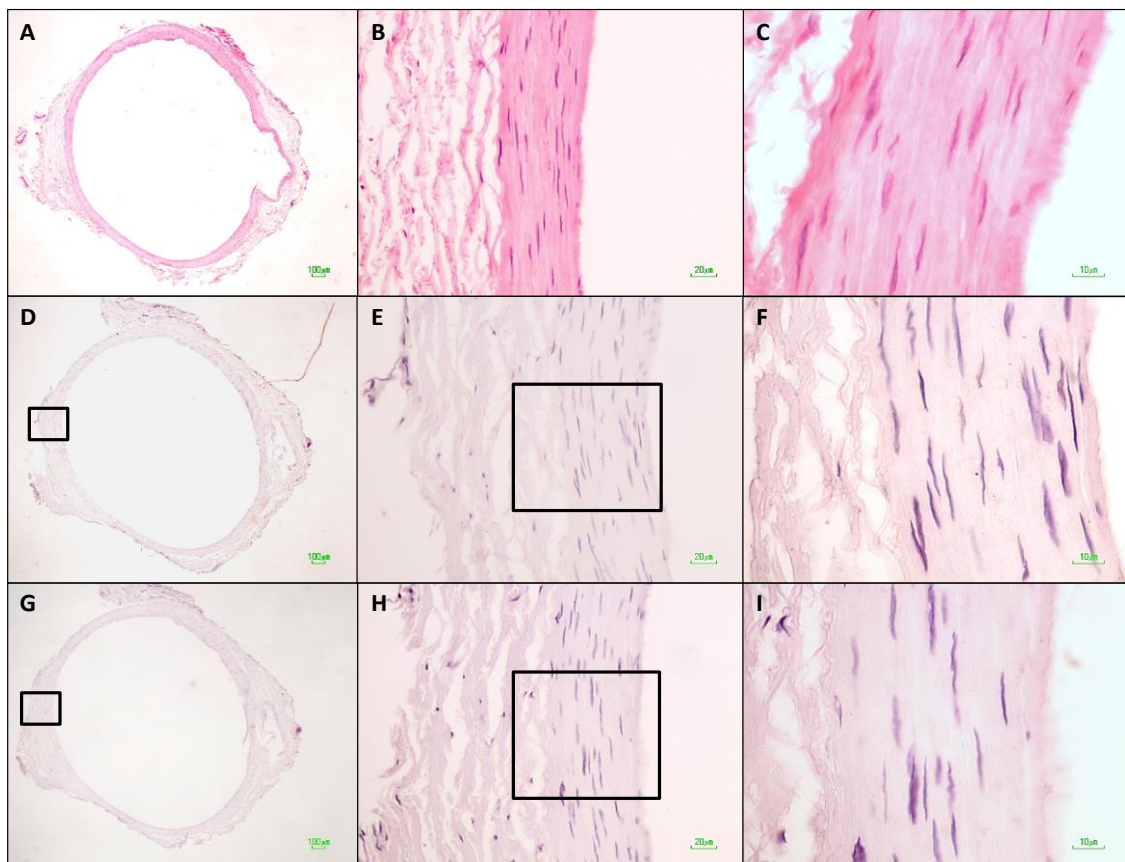


**Figure 3.10:** Representative sections of LITA tissue stained with H&E (A – C), anti-PGN (D – F) and negative control sections (primary antibody omitted) (G – H). As the control tissue for atherosclerotic plaque samples used in this study, all LITA tissue sections were negative for PGN.

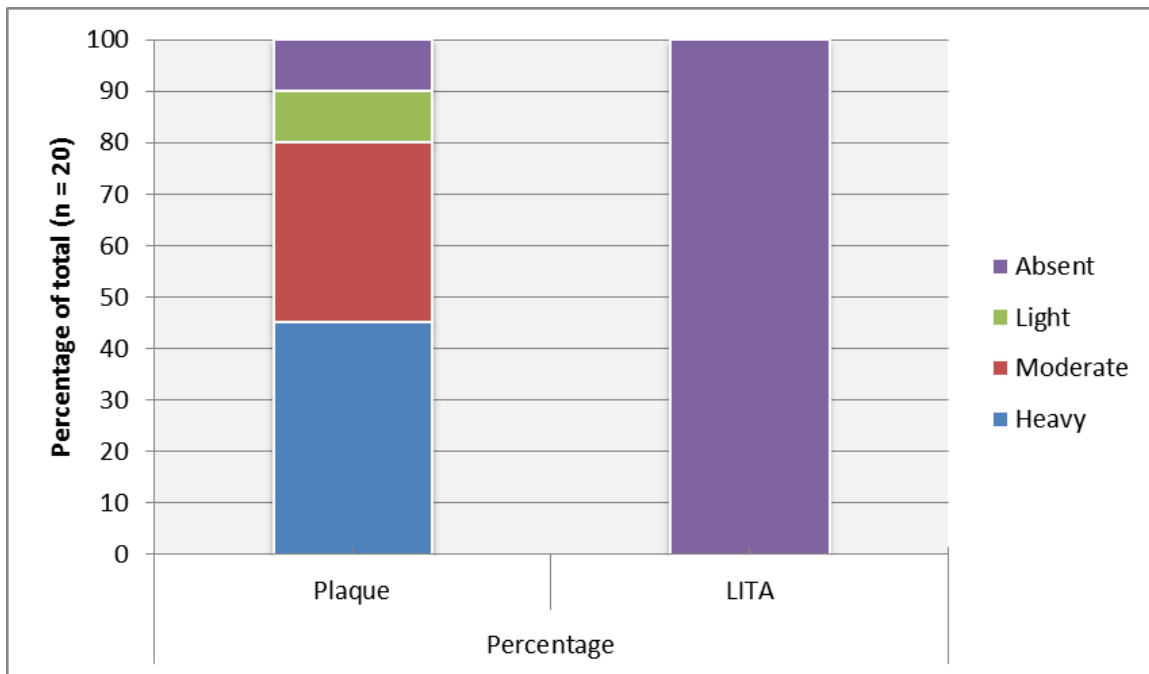


**Figure 3.11:** Bar graph to show the presence and degree of PGN localisation in CAP specimens was expressed as a percentage of total number of samples (n = 20).

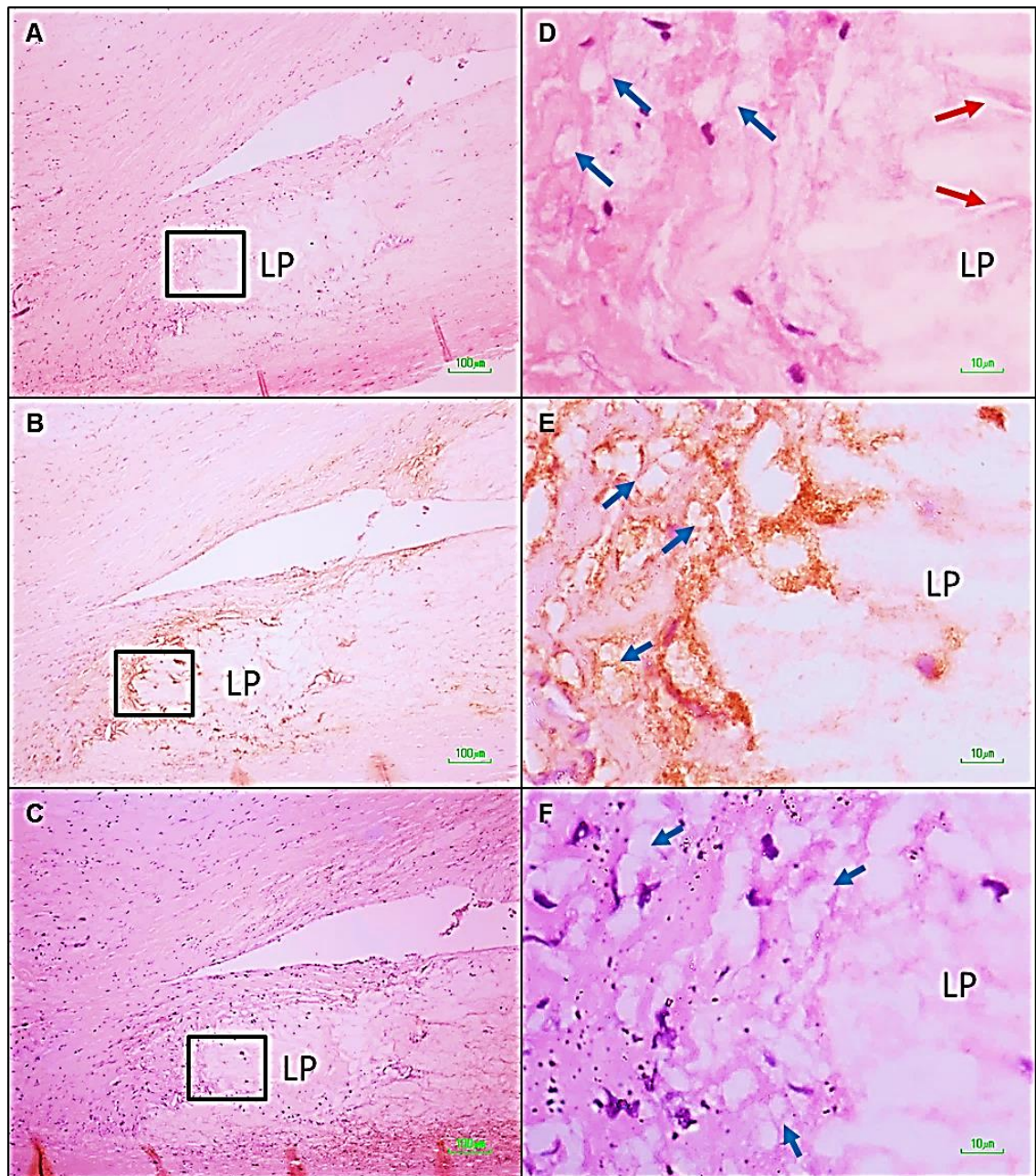


**Figure 3.12:** Anti-PGN staining around a large lipid pool. Top row shows carotid atherosclerotic plaque tissue stained with haematoxylin and eosin at x10 and x100 magnification, respectively (A & D). A large lipid pool was observed as an area of light pink with a necrotic core displaying several cholesterol cleft structures (red arrows) and foam cell structures (blue arrows). Heavy anti-PGN localisation (red/brown stain) can clearly be seen around the perimeter of the lipid pool (B & D). Right row (D, E and F) shows representative tissue section inside black box.. Bottom row (C & F) shows negative control tissue (protein block incubation without PGN IgG) for PGN.

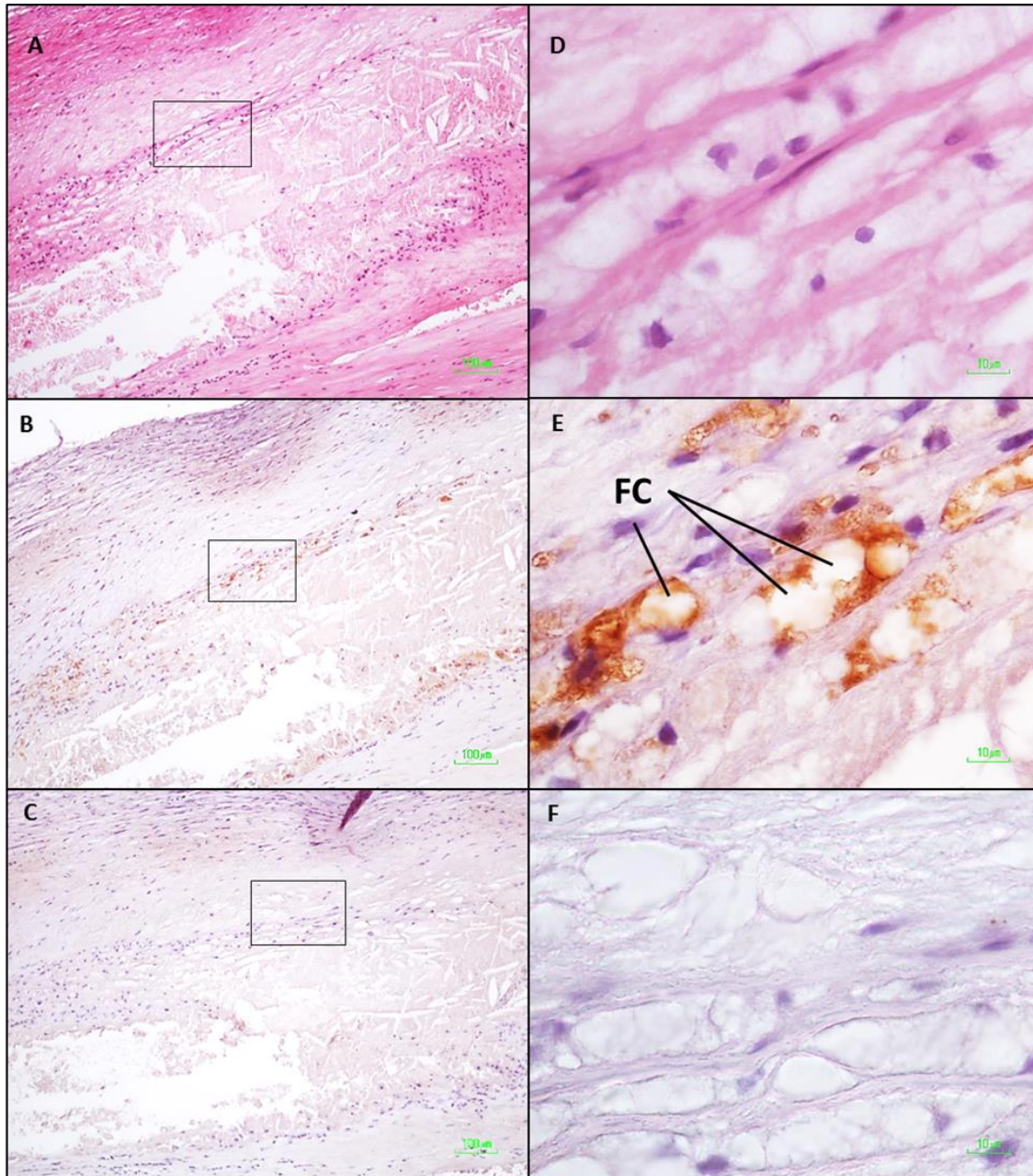


**Figure 3.13: Anti-PGN staining shows PGN localisation between fibrous tissue around a large lipid pool with necrotic core.** Top panel (A & D) shows carotid atherosclerotic plaque tissue stained with haematoxylin and eosin at magnification X10 and X100 respectively. A large lipid pool was observed as an area of light pink with a necrotic core (N) displaying several cholesterol cleft structures (A). A layers of collagen was visible around the perimeter of the lipid pool (D). Middle row (E) shows representative tissue section inside the black box of imabe B, which shows heavy anti-PGN localisation. Anti-PGN can clearly be seen within the collagen layers forming the perimeter of the lipid pool (E). The localisation of anti-PGN has revealed voids in the tissue that appear cirverical and have the characteristic shape and size of foam cells (FC) (E). Bottom panel (C & I) shows negative control tissue (protein block incubation without PGN IgG) for PGN.

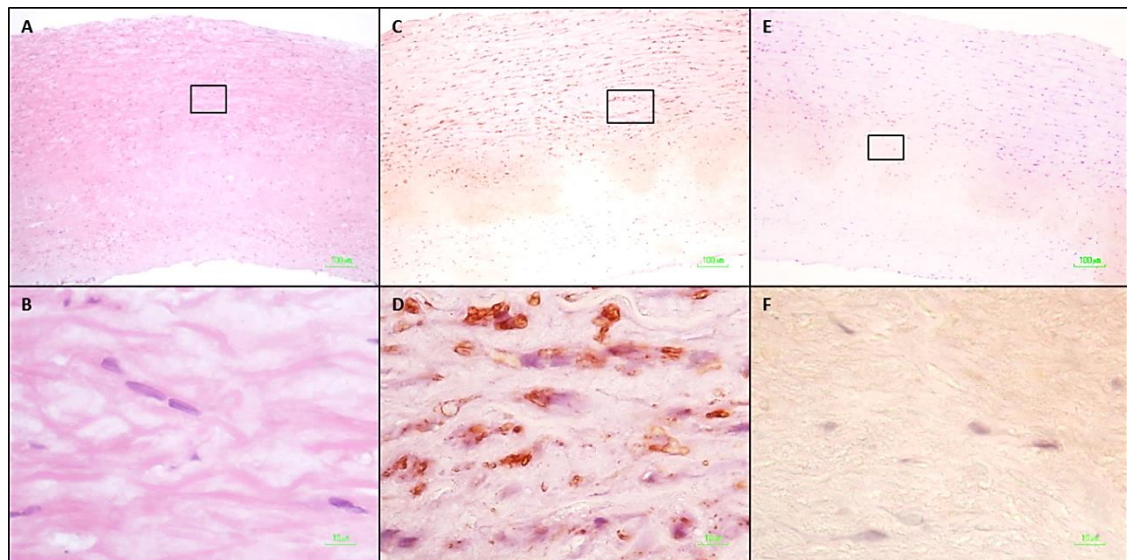


**Figure 3.14: anti-PGN staining in fibrous collagen-like tissue.** Highly fibrous plaque tissue stained with H&E had no lipid pool and few areas of accumulated foam cells observed sporadically throughout the tissue (A & B). Diffuse anti-PGN staining was observed, localised mostly within the folds of collagenous tissue layer (C & D). Negative control tissue was clear of any PGN localisation (E & F).

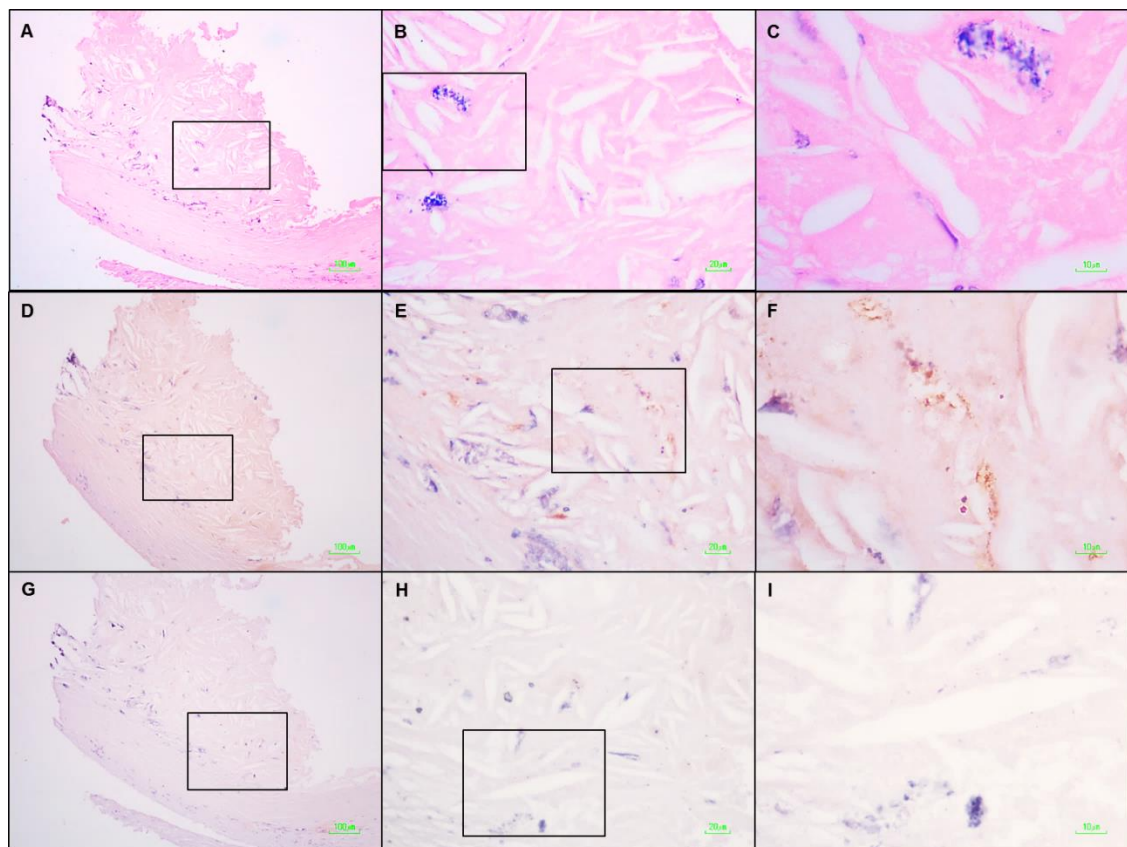


**Figure 2.15: anti-PGN staining within cholesterol region of plaque accompanied by cholesterol clefts.** Atherosclerotic plaque tissue showing a partial section of a lipid pool, evidenced by numerous region cholesterol clefts (black arrows) (A, B & C). Representative sections show PGN localisation within the region of cholesterol (D, E & F). A small area of cholesterol mineralisation is apparent at the margin between collagen and cholesterol pool (H). At X100 PGN does not appear to be directly localised within cholesterol clefts, but resides within the tissue gaps between the clefts (F). The negative control sample prepared to assess the validity of the PGN staining method shows no sign of PGN localisation.

### 3.5 Discussion

The aims of this chapter were two-fold. To first examine the morphological characteristics of carotid atherosclerotic plaque (CAP) tissue by employing routine histological methods. Features common to atherosclerotic plaque tissue provide information relating to the stage of plaque development, relative vulnerability and symptomatology. Second aim was to screen both CAP and LITA tissues for the presence and localisation of the bacterial cell wall component, PGN, using immunohistochemistry. Findings presented in this chapter identified key histopathological characteristics frequently observed in atherosclerotic plaque tissue from the carotid artery and highlighted some of the features synonymous with plaque destabilisation and possible symptomatology. Furthermore, the data obtained in this chapter provides evidence for the presence of bacterial PGN within CAP tissue; a potential indication of historical or recent bacteria/PGN infiltration from bodily sites distant from the carotid artery. Finally, relationships were observed between PGN localisation within CAP tissue and particular reoccurring histopathological features, (i.e. a necrotic core, ghost structures of foam cells and/or elevated infiltrating immune cells); though observations were only correlative and did not imply causality.

In the present investigation, microscopic assessment of FFPE tissue sections were carried out using routine histology stains, haematoxylin and eosin and Masson's trichrome to provide an initial observation of tissue composition and the representative structures of atherosclerotic plaque.

#### 3.5.1 Immune cell infiltration

Immune cells such as T cells, dendritic cells, macrophages, and mast cells are recruited from the bloodstream into atherosclerotic lesions, and they are responsible for the progression and destabilisation of atherosclerotic plaques. Specific immune-staining for these cell types was not conducted when examining the CAP and LITA tissue sections for this chapter. However, collectively, immune cells infiltrates were easily identified as dark nuclei against the predominantly eosinophilic background of atherosclerotic plaque. Immune cell infiltrates were observed in all sections of CAP tissue specimens (40% high, 55% moderate and 5% weak; figure 3.09). Small infiltrates were observed sporadically throughout the tissue, though as infiltrates became more organised they also appeared denser, particularly within the plaque shoulders, around lipid pools and within the fibrous cap. These observations are consistent with a number of investigations where IHC staining

for specific leukocytes show significant localisation within fibrous cap and plaque shoulder regions (Yilmaz et al. 2007; Ionita et al. 2010; de Jager et al. 2013a). Immune cell infiltrates, particularly containing macrophages that localise at the shoulders and cap, weaken the supportive structure of the fibrous plaque by secretion of metalloproteinase (Shah et al. 1995). These patterns of immune cell infiltrates are considered a feature of plaque vulnerability and a primary cause of intimal thickening and ultimately plaque rupture when associated with intra-plaque vessels endothelial chemokines (MCP-1) expression (Newby 2005; Yilmaz et al. 2007).

### 3.5.2 Intra-plaque vessels

Intra-plaque vessel formation was recorded within 50% of the atherosclerotic plaque samples studied for this chapter. Intra-plaque vessels (IPV) were dysmorphic, thin-walled vessels, often surrounded by dense infiltrates of nucleated cells and typically still containing red blood cells within the lumen space. Previous studies show positive anti-intracellular adhesion molecule-1 (ICAM-1) localisation of IPV, which indicates active leukocyte recruitment signalling on the endothelium of these vessels (Mazzone et al. 2006). This may explain the dense populations of nucleated cells observed in areas surrounding vessels; identified as T-lymphocytes and monocytes/macrophages by Mazzone et al. (2006).

Based on the morphological appearance of observed IPV, vessels were classified into three distinct groups; namely “oval or regular”, “elongated” and “highly irregular” vessel. Oval and elongated vessels had varying vessel wall thickness and were frequently observed in clusters, whereas irregular vessels, while still retaining a vessel wall, had a jagged, “lightning bolt” morphology and were typically much larger but rarely formed in clusters. Neovascularisation within the fibrous cap was a common occurrence and a histological feature that has been proven to be a destabilising factor associated with acute thromboembolic events (McCarthy et al. 1999).

The relationship between histological aspects of carotid plaque neovascularisation and cerebral symptoms has been previously described by McCarthy et al. (1999) who recorded neovessel morphologies synonymous with those presented in this chapter. McCarthy et al. (1999) established that 85% of symptomatic lesions contained vessels with an irregular morphology. These findings were in agreement with reports by Dunmore et al. (2007) who identified similar vessel morphologies when CAP tissue sections were immunostained for

endothelial cells, vascular smooth muscle cells macrophages and vascular endothelial growth factor. A significant correlative relationship between clinically-established ipsilateral cerebral symptoms and plaques comprising highly irregular vessel morphology; observed almost exclusively in symptomatic carotid plaques (Dunmore et al. 2007). Others have observed significantly higher neovessel densities in patients with clinical evidence of cerebral infarction (Faggioli et al. 2011). Furthermore, recent studies employing imaging systems such as optical coherence topography and contrast-enhanced ultrasound provide further weight to histological findings through direct comparison with IHC stains; confirming neovascularisation as a major vulnerability factor in plaques symptomology (Xiong, Y. Deng, et al. 2009; Tian et al. 2012)

In light of this evidence, it is clear neovascularisation, in particular thin-walled irregular vessel morphology, is a prominent feature synonymous with plaque vulnerability and destabilisation. Presentation of such vessels within atherosclerotic plaques of the carotid artery can result in cerebral symptomatology, such as TIA and stroke (Park et al. 1998; Mofdi et al. 2001; Dunmore et al. 2007). Thus, when considering this feature alone, it could be proposed that 20% of the carotid plaques examined for this study were likely symptomatic. However, it must be noted, even though neovesels were easily identifiable; histopathological features identified in this chapter were only semi-quantitative. Without staining the CAP tissue for endothelial specific markers (e.g. CD31 or CD34), there is possibly a number of vessels within plaque specimens that may have escaped detection.

### 3.5.3 Intraplaque haemorrhage

As previously discussed intraplaque haemorrhage (IPV) are believed to facilitate entry of inflammatory and red blood cells (RBC) directly into the plaque, which can contribute to lipid deposition, plaque mass and inflammation (Jeney et al. 2014). Tissue matrix is limited within atherosclerotic plaque tissue and due to the lack of SMC structure within the walls of IPV, these vessels are inherently fragile (Dunmore et al. 2007). Subsequently, IPV are considered by some to be the cause of intra-plaque haemorrhaging (IPH) (Virmani et al. 2005; Moreno et al. 2006; Herrmann et al. 2006; Teng et al. 2012). Recent studies strengthen this concept that intra-plaque neovascularisation and haemorrhaging are events that could play a major role in plaque progression and leucocyte infiltration, and may also serve as a prognostic marker of for the development of future thromboembolic events

(Kolodgie et al. 2003; Takaya et al. 2005; Michel et al. 2011; Teng et al. 2014; Kurata et al. 2014).

In the present study, IPH was detected in 30% of plaque samples, particularly within the fibrous tissues of lipid-rich plaques. In addition, a significant positive correlation was observed between IPH and IPV ( $p < 0.001$ ). Mofdi et al. (2001) also established a strong correlation between IPV density, frequency of IPH and symptomatic carotid occlusive disease within 49% of advanced unstable plaques compared to 4.6% early plaques from the carotid artery. Moreno et al. (2004) used multiple antibodies to document increased neovessel density in lipid-rich and ruptured plaques when compared with fibro-calcific lesions. Multiple regression analysis identified microvessels at the base of the plaque as an independent correlate of plaque rupture, along with established variables such as a thin cap, inflammation, lipid area, and rupture of the internal elastic lamina (Moreno et al. 2004). Other investigators have recently expanded on these findings showing a higher density of IPV located within particularly unstable features of haemorrhagic plaques compared to non-haemorrhagic plaques; typically, shoulder, fibrous cap, and necrotic core (Kurata et al. 2014). Furthermore, positive correlations between neovessel density and macrophages were established at each of the additional aforementioned sites (Kurata et al. 2014).

Although density of IPV positively correlated with IPH, the haemorrhagic tissue was rarely observed to be in close proximity to vessels (5%). This particular observation has been seen previously by, Leen et al. (1990) who detected IPV in 87% of symptomatic plaques, yet only 18% of vessels were in close proximity to haemorrhages. Leen et al. (1990) established no difference in the frequency of haemorrhaging between symptomatic and asymptomatic plaques suggesting that haemorrhaging is not necessarily always a feature of plaque instability. This however, is in contrast with recent findings presented by other investigators who show clear physical interaction between IPV and haemorrhagic tissues (Le Dall et al. 2010; Michel et al. 2011).

An important factor in establishing a correlative relationship between neovascularisation and IPHs would be to determine the relative age of the IPHs. Previous studies have been conducted, in which IPH are aged based on histological characteristics such as, fresh: (<1 week) intact erythrocytes, infiltrating polymorph nuclear and macrophage activity; recent: (1 – 6 weeks) haemorrhagic debris and macrophage engulfment of hemosiderin, and old: (>6 weeks) amorphous material surrounded by fibrous tissue

(Lusby et al. 1982; Chu et al. 2004; Takaya et al. 2005). In the present investigation H&E staining allowed for the detection of intact erythrocytes and congealed haemorrhagic masses, while extra definition and fibrous collagen was observed by MTC stain. However, to fully elucidate the relationship between neovascularisation and IPH, a well-considered histological investigation for future analysis may employ additional stains specifically for hemosiderin, such as, Prussian-blue. One could also employ traditional vessel stain, van Gieson, or adopt a more specific IHC approach with antibodies CD105 (abundant in angiogenic endothelial cells) and CD14 (macrophage LPS binding).

#### 3.5.4 Calcified plaques

Calcified nodules were detected in 30% of plaques examined for this chapter. Of the 4 plaques displaying calcified nodules, 50% comprised a large lipid core (>20% plaque mass) with fibrous caps. Only one of the calcified plaques displayed a weak density of IPV that were accompanied by IPH. All calcified plaques showed high density of foam cell ghost structures as well as moderate to high densities of infiltrating nucleated immune cells. These observations are consistent with the notion that calcification is a pathological features associated with advanced atherosclerotic lesions (Mody et al. 2003; Abedin et al. 2004; Doherty et al. 2004). Due to the fact that calcified plaques were rarely detected, no correlative relationships were found between calcium and any other histological features; though, a near significant correlation was calculated with presence of fibrous cap ( $p = 0.053$ ).

These observations are comparable with findings published by Vasuri et al. (2015) who observed a similar histopathology of calcified plaques. In contrast, calcified plaques examined by Vasuri et al. (2015) had less inflammatory infiltrate but the same incidence of IPH as non-calcified lesions; the opposite was observed here. In addition, the authors demonstrated that calcification, as a histological complication, was not correlated with clinical plaque instability; in fact, the incidence of TIA/stroke in patients with calcified plaques was lower than patients with non-calcified plaques, particularly for female patients, despite the same incidence of histological features. This latter observation is consistent with previously published findings that show patients with calcified plaques were 21 times less likely to be symptomatic than non-calcified plaques (Nandalur et al. 2005).

These findings therefore, highlight a possible protective role for calcium deposition, even in the presence of multiple histological features of carotid plaque vulnerability. On the other hand, carotid artery calcification has also been shown to predict mortality and cardiovascular outcomes in certain older patients, independent of traditional CVD risk factors (T. Thompson et al. 2015). Moreover, calcium deposition in the coronary artery can also be used as a prognostic marker for the identification of those at an increased risk for death or MI in symptomatic patients with non-obstructive disease. Thus, calcium deposition is an ambivalent indicator of cardiovascular outcome that is highly dependent on the particular artery being assessed and patient age, while the severity of additional histological features seems to play less of a role.

### 3.5.5 PGN localisation

PGN was chosen as a marker for detection because it is a major component in the cell wall of most bacteria and therefore an abundant and easily targeted antigen. A chromogenic immunohistochemical (IHC) method was adopted for detection of PGN because it has several advantages over fluorescent reporters when examining atherosclerotic plaque. Most importantly, atherosclerotic plaque can be highly auto-fluorescent, which would require lengthy optimisation to establish optimal 'antigen to auto-fluorescence' signal ratio. The efficacy of any selected background quencher can only be assessed at the endpoint of an assay, which can make optimisation timely and costly. Fluorescent in-situ hybridisation (FISH) was considered, however aside from auto-fluorescence, FISH has additional challenges, such as long incubation times at elevated temperatures (>60°C). At high temperature, specimens can detach from the slide causing loss of valuable sample or the buffer containing the probe can evaporate causing specimens to dry out. By adopting a chromogenic IHC procedure, minimal optimisation was required e.g. a simple limit of detection assay to establish optimal antibody concentration. The assay could then be performed at room temperature in <2 h and results could be observed with a readily available light microscope.

PGN was detected in 90% of the CAP tissue specimens examined here. Dense localisation of PGN was predominantly observed in regions containing large accumulations of structures resembling foam cells. These findings are comparable with observations by Laman et al. (2002) who showed PGN localisation in 93.3%, 61.2% and 83.3% in carotid, coronary and femoral atherosclerotic plaque specimens, respectively. Laman et al. (2002)

examined atherosclerotic carotid and femoral arteries; from adventitia to intima using antibodies for PGN, collagen and macrophages. PGN was detected mainly intracellular and localised within the adventitia, media and atherosclerotic plaque tissue. Consistent with the finding of this chapter, Laman et al. (2002) reported frequent localisation of PGN in areas of plaque tissue occupied by macrophage foam cells (CD14). In the present investigation, the frequency of PGN localisation was positively correlated with the presences of the ghost structures of foam cells. PGN localised around the foam cell shape, but not within the void left by the cell, which often provided extra definition to the ghost structure of accumulated foam cells that would not ordinarily be seen.

Frequent localisation with foam cell structures could possibly represent interaction between PGN and macrophages, possibly even clearance via PGN phagocytosis. However, this observation is beyond the limitations of the assay performed and the scope of this chapter. In order to establish the identification of cells frequently localised by PGN a more specific selection IHC markers would need to be incorporated. Though it must be noted, many of the features encountered in the plaques, including ghost structures of macrophage foam cells, have distinctive histopathology and were often identifiable. Many investigators have previously identified such features using routine H&E and MTC staining (Cai 2002; Salem et al. 2014). Moreover, where necessary and for clarity, textbook images were included alongside any results figures in this chapter to highlight similarities.

Laman et al. (2002) also characterised the vulnerability of lesions in relation to the PGN presence and determined that lesions with significantly higher presence of PGN also displayed certain histological features of a vulnerable plaque phenotype. It was further established that the presence of a lipid core and patient age were positively correlated with intensity of PGN staining; though only deemed significant after the exclusion of two patients negative for PGN. These observations support the notion that atherosclerotic disease may be exacerbated by the presence of bacteria or their cell wall components.

Through employing western blot analysis Laman et al. (2002) established upregulation of toll-like receptor-2 (TLR-2) in PGN positive coronary artery tissue suggesting PGN may represent an inflammatory stimulus causing intracellular signalling for the transcription of proinflammatory genes. Further to this, Nijhuis et al. (2007) demonstrated the ability of PGN to upregulate monocyte expression of L-selectin (CD62L) and  $\beta_2$ -integrin-dependent binding to ICAM-1 under flow cytometry conditions. Monocyte L-selectin expression is a critical step for monocyte tethering and rolling on activated endothelial cells and is the

precursor to ICAM-1 attachment and chemotaxis. As upregulation of these membrane proteins can assist monocyte transmigration to the subendothelium, these findings further indicate that PGN localisation in the atherosclerotic lesion may stimulate proinflammatory cytokines for leukocyte recruitment and chemotaxis into the artery/lesion.

Nijhuis et al. (2004) utilised enzyme linked immunosorbent assays (ELISA) to measure immunoglobulin levels against PGN in patients with atherosclerosis. The author established that patients hospitalised with atherosclerosis had lower IgM levels directed against PGN compared to control patients without clinically manifest cardiovascular disease. Interestingly, IgM levels against PGN decreased with increasing mean common carotid intimal thickening. The authors provide several explanations for this observation, most fitting of which proposes the decrease in IgM levels are the consequence of effective binding and removal of PGN from the lesion. This explanation does not seem plausible when considering the extensive localisation and frequency of PGN detection in the plaques examined for this chapter. In addition, PGN is located ubiquitously within all bodily mucosa, hence, it seems unlikely that a decrease in IgM level would be due to the effective clearance of PGN, even just from the lesion alone.

Intimal-medial thickening (IMT) and pathological-IMT are features of early to intermediate atherosclerotic plaque development occurring via lipid deposition and associated inflammatory milieu within the intimal layer of the atherosclerotic vessel; as the plaque matures, IMT becomes more apparent (Finn et al. 2010). With this in mind, there is a possibility that as intimal thickening becomes more pronounced, access to the intimal layers becomes more restricted, thus, PGN located within the plaque becomes less accessible, therefore decreasing the overall IgM levels to PGN. However, this also fails to account for the ubiquitous nature of PGN, to which we are continuously exposed at all mucosa.

### 3.6 Conclusion

The aims of this chapter were two-fold. First, for identification of particular microscopic characteristic features that form the cellular composition and architecture of plaque tissue. The second aim of this chapter was to stain atherosclerotic plaque tissue sections with an antibody to detect the presence and localisation of PGN. With the exception of tissue thrombosis, all major histopathological features of atherosclerotic plaque were detected and presented in this chapter. Staining CAP tissue with H&E and MTC revealed a host of

plaque features such as cholesterol clefts that were typically observed in or around highly lipidous areas of the plaque. Areas of plaque not occupied by lipid features, were diffuse with fibrous collagen, which was most dense at regions of the plaque closest to the lumen. This region of the plaque is typically more fibrous due to a dynamic change in plaque structure to form a fibrous cap, especially when a large lipid pool was evident. Lesions became increasingly more saturated with lipid towards the inner core of lesions where lipid pools and cholesterol clefts formed.

Although positive correlative relationships were established between frequencies of “foam cells and immune cell infiltrates”, “foam cells and lipid core” and “IPV and IPH”, these features were identified based only on their morphology within a simple H&E and MTC. Furthermore, power calculations for  $n$  revealed that at the very least, 41 samples would have needed to be tested to provide acceptable margin of error. It is therefore necessary to reserve judgement on the strength of these relationships until further studies have been conducted that target these features specifically. Nevertheless, Several features were consistently encountered that are consistent with plaque destabilisation and symptomatology, such as presence of IPV and occurrence of IPH and more infrequently, calcified nodules. The most variable plaque feature was IPV; observed either as typical oval shaped vessels or with a highly irregular jagged, lightning bolt-like morphology. Fifty percent of lesions displayed both forms of IPV. When these findings are taken together, many of the plaques examined for this chapter comprised histological features commonly found in intermediate to advanced atherosclerotic lesion.

The findings produced for the second part of this chapter demonstrate that the bacterial cell wall component, PGN, is present in atherosclerotic plaque of the carotid artery. Mostly moderate to high localisation of PGN was detected within almost all of the CAP tissue specimens examined here. Localisation was predominantly detected around structures that had the appearance of macrophage-derived foam cells, though additional plaque features were localised when staining was diffuse, such as between collagen fibrils, around lipid pools and around cholesterol clefts. The intensity PGN localisation was positively correlated with patient ages. This suggests either PGN clearance is less effective in elderly patients or that influx of PGN occurs temporally, possibly at a rate that cannot be efficiently cleared, consequently, PGN levels increase over time with increasing patient age. The latter hypothesis is consistent with the histopathological features observed within these plaques, which show features characteristic of intermediate to advanced

atherosclerotic plaque development. No localisation of PGN was observed in any of the healthy LITA control tissue specimens, which is consistent with the notion that only athero-prone vasculature is invaded by infective agents.

**DETECTION OF PERIODONTAL BACTERIAL  
DNA IN HUMAN INTERNAL CAROTID  
ATHEROSCLEROTIC PLAQUES USING 16S rDNA  
PCR & IDENTIFICATION OF STRAINS THROUGH  
BIGDYE TERMINATOR SEQUENCING**

## 4.1 Introduction

There is currently a clear understanding that atherosclerosis is perpetuated by a chronic inflammatory response. However, the etiological factors of chronic inflammation within atherosclerotic plaque have not yet been fully elucidated. Bacterial and viral infections have been hypothesised to contribute to the inflammation of the vasculature, which leads to endothelial dysfunction, an early stage in the pathogenesis of atherosclerosis. Chronic infectious diseases, such as those affecting the oral cavity, are considered risk factors for the development of cardiovascular and cerebrovascular disease. Only a few species of pathogenic bacteria, predominantly Gram-negative bacteria, have an etiologic role in the pathogenesis of periodontitis. Three major pathogens mainly found in subgingival plaque that are responsible for the pathogenesis of periodontitis are the red complex bacteria (RCB), namely *Porphyromonas gingivalis*, *Tannerella forsythia* and *Treponema denticola*. This trio of “periodontopathogens” act synergistically to potentiate local and systemic host inflammatory mediators that lead to systematic breakdown of gingival tissue and alveolar bone resorption that characterises periodontitis (Kesavalu et al. 2007).

There are two potential mechanisms that may explain the effect of periodontal disease on atherosclerosis. Firstly, in addition to a chronic localised immune response, periodontitis may actually raise inflammatory markers at a systemic level that could cause vascular inflammation. Secondly, oral infections may provide a major source of disseminating periodontal bacteria into the bloodstream that can initiate secondary infections within atherosclerosis-prone vessels (Elkaïm et al. 2008; Sonbol et al. 2009; Marcelino 2010; Mahendra & Mahendra 2013; Armingohar et al. 2014; S. Morita et al. 2014). The latter mechanism of hematogenous spreading of periodontal bacteria and their invasion of endothelial and smooth muscle cells is considered to be the primary model for the association between periodontal disease and cardiovascular disease (Giacona & Papapanou 2004; Chou et al. 2005; Roth et al. 2007; Sonbol et al. 2009). In order to provide evidence for this paradigm, it is first necessary to demonstrate the presence of periodontal bacteria within the atherosclerotic lesion.

To establish identity of the taxa present in atherosclerotic plaques specimens it is necessary to utilise a phylogenetically informative marker that is able to differentiate between bacterial species at the genetic level (Paster et al. 2001). The 16S ribosomal RNA (rRNA) gene is one such marker employed to differentiate between inter and intraspecies variation at the genetic level. Containing nine “hypervariable regions”,

the 16S rRNA gene comprises considerable DNA sequence diversity between different species of bacteria (Van de Peer et al. 1996). The hypervariable regions are flanked by conserved sequences among most bacteria, permitting PCR amplification of target sequences using universal primers (Ghyselinck et al. 2013; Mori et al. 2014). A major advantage for using a phylogenetic marker for investigating plaque microbiota directly is the non-dependence on the targeted species to be of a viable status. Therefore, through targeting bacterial 16S rDNA directly in tissue, a broader and more sensitive detection and identification is achievable (Sarookhani et al. 2010). This is particularly advantageous for identification of uncultivable species as the technique negates the need for culturing. Sequence analysis of the 16S rRNA gene has therefore been widely used as a tool for assessing bacterial diversity in a range of different tissues (Friedrich et al. 1999; Tunney & Patrick 1999; Hold & Pryde 2002; Kuklinsky-Sobral 2004).

In the previous chapter immunohistochemical staining was performed to demonstrate the localisation of bacterial wall component peptidoglycan within atherosclerotic plaque tissue. Many of the tissue sections showed diffuse staining for peptidoglycan with areas of dense co-localisation with sites of tissue inflammation. As a ubiquitous component of most bacteria the presence of peptidoglycan provides evidence that bacterial wall components are present within atherosclerotic tissue, though it cannot differentiate between particular species. Therefore, the main aim of the present investigation is to identify the microbial taxa present in CAP tissue using a combination of species-specific, genus-specific and universal DNA primer sets for amplification of the 16S rRNA gene.

Many investigations to identify periodontal bacterial 16S rDNA in carotid plaque tissue have failed, despite demonstrating a high detection rate in periodontal pockets of the same patients (Cairo et al. 2004; Romano et al. 2007; Aimetti et al. 2007; Aquino et al. 2011). The probable cause for this is very likely experimental design, e.g. DNA extraction and/or detection method (i.e. nested or traditional PCR), as evidenced by multicentre trials (Apfalter et al. 2001). Nevertheless, despite numerous failures to detect periodontal bacteria in CAP tissue; many investigators that have successfully identified periodontal bacterial DNA in atherosclerotic plaque tissue (Farsak, Yildirim, Akyön, Pinar & Öç 2000; Ford et al. 2006; Kozarov et al. 2006; Armingohar et al. 2014; Fernandes et al. 2014; Morita et al. 2014). *Aggregatibacter*

*actinomycescomitans* is the most commonly detected periodontal 16S rDNA sequence in CAP tissue, with detection rate varying from 17 – 50% of carotid specimens (Ford et al. 2006; Kozarov et al. 2006; Morita et al. 2014) Similarly, when encountered, *P. gingivalis* and *T. forsythia* are often detected at a high percentage rate compared to other bacterial sequences; between 52 – 62.5% and 34 – 43.8%, respectively (Ford et al. 2006; Morita et al. 2014). In a recent study by Armingohar et al. 2014, a very high load and mean diversity of previously undetected bacterial 16S rDNA sequences were shown to be present in CAP tissue. Interestingly though, while 70% of subgingival plaque specimens from patients with chronic periodontitis showed presence of red complex bacteria, only *P. gingivalis* was detected in one vascular biopsy (Armingohar et al. 2014). Moreover, the authors showed a large number of oral and non-orally derived bacterial 16S rDNA sequences in carotid atherosclerotic tissue that were not detected in subgingival plaque tissue. Therefore, species that are typically considered to have a commensal relationship with the host, can act as opportunistic pathogens by gaining entry to the blood stream and invading plaque tissue where they may contribute the induction of inflammatory milieu. The detection of commensal species in atherosclerotic tissue has become more frequent in recent years, possibly because previous investigators would dismiss their detection as contamination (Renko et al. 2008; Renko et al. 2013).

When studying any inflammatory tissue for the purpose of identifying the latent bacterial species that may be present, it would be informative to understand the viability of the organisms present. Traditional nucleic acid methods such as standard endpoint PCR or qPCR are unable to provide such information. Conventional methods for detecting and isolating bacterial pathogens involve culturing the organism, which is then identified through microbiological metabolic testing or downstream molecular testing. The turnover of mRNA in living bacterial cells is rapid, with most of mRNA species having a half-life of only minutes. Studies measuring cell viability by calculating the number of copies of 16S rRNA, as determined by reverse-transcription followed by qPCR during bacterial growth and antibiotic-induced cell death of *Streptococcus* spp. (Aellen et al. 2006). The authors demonstrated amplification of 16S rRNA that paralleled both bacterial growth and drug-induced killing compared with 16 rRNA gene amplification that showed an increase in product during cell growth but no decrease during drug-induced killing (Aellen et al. 2006).

Another molecular method that can be employed to assess bacterial cell viability is to measure the expression bacterial housekeeping genes. Housekeeping genes encode for various constant cellular functions concerned with metabolism, enzyme activity and ribosomal trafficking, which are essential for cell viability and would not be regulated in dead cells. Previous studies using RT-PCR to measure the expression of housekeeping genes *rpoH*, *rpoD*, *groEL*, *tufa*, *yjeE*, *yeaZ* and *ygiD* (Sheridan et al. 1998; Handford et al. 2009; Narusaka et al. 2011). The major shortfall in using mRNA copy number to assess cell viability is that it is not possible to determine the difference between dead vs viable bacteria present within the same tissue. This is even more important when tissue such as the atherosclerotic plaque or subgingival tissues are thought to contain bacteria in a viable but nonculturable (VBNC) state as well as dead. Propidium Mono Azide (PMA) is a photoreactive DNA-binding dye that preferentially binds to dsDNA and can be used to differentiate live from dead cells (Nocker et al. 2006). Dead cells lose their ability to maintain their plasma membranes; this provides an entry point for PMA to access to the “naked” dsDNA within the cytosol. When cells are then dosed with visible light inside a thermally stable environment, PMA covalently binds to the naked DNA rendering it unamplifiable. Live cells do not react to PMA due to having intact cell membranes, which prevents PMA-DNA contact. DNA is then extracted from the PMA-treated cells to provide template DNA for qPCR. The resulting qPCR signal from PMA-treated cell DNA shows a significant shift to a higher Ct value for dead cell DNA, thereby providing a clear distinction between live and dead cells (Nocker et al. 2006).

Polonyi et al. (2013) assessed three molecular methods, qPCR, PMA-qPCR and RT-qPCR for detection of periodontal pathogens in the subgingival plaque from patients at different antibiotic treatment stages. The bacterial load was remarkably stable over prolonged periods when assessed by conventional qPCR, while both PMA intercalation as well as cDNA quantitation showed a decline according to decreasing numbers of viable bacteria after antibiotic treatment. PMA-qPCR has also been used to for selective detection of viable bacteria in periapical lesion necrotic pulp tissue (Kim et al. 2013). A significant difference in mean Ct between the before and after dental tooth canal treatment tissue with 80% live cell and 20% dead cell of *E. faecalis* (Kim et al. 2013). The same molecular methodology was used to establish the viable bacterial populations involved in progression of dental caries by Klein et al. (2012), who infected the mouths of 20-day-old rat pups from 3 litters with actively growing in vitro biofilms of *S. mutans* and collected the in vivo subgingival plaque samples 3 weeks later. Biofilms were treated with PMA at the in vitro and in vivo

stages prior to DNA isolation/qPCR analysis and the same samples were analysed for CFU. The viable population of both *S. mutans* and total bacteria assessed by qPCR were positively correlated with the CFU data ( $p < 0.001$ ;  $r > 0.8$ ). However, the qPCR data showed higher bacterial cell counts, particularly for total bacteria (vs. CFU). Moreover, *S. mutans* proportion in the plaque-biofilm determined by qPCR analysis showed strong correlation with incidence of smooth-surface caries ( $p = 0.0022$ ,  $r = 0.71$ ). In parallel Klein et al. (2012) measure gene expression of *S. mutans* virulence genes, which demonstrates that measurements viable microbes and gene expression can be analysed simultaneously, providing a more inclusive assessment of the pathology of dental disease. Similar studies have been conducted pertaining to the cultivation and cocultivation of all inhabitant of subgingival biofilm (H. Thompson et al. 2015).

Sánchez et al. (2014) used qPCR combined with PMA to selectively quantify the viable portion of *P. gingivalis*, *A. actinomycetemcomitans*, *F. nucleatum* and total bacteria in an in vitro biofilm model after antimicrobial treatment. Biofilms were exposed to isopropyl alcohol immersion over set time points to determine the optimal exposure time antimicrobial treatment. Bacterial cells were then treated with PMA prior to DNA isolation and qPCR analysis using specific primers and probes to target bacteria and determine cell viability. PMA-treated cells resulted in a significant total reduction of qPCR amplification of 4 log<sub>10</sub>. *A. actinomycetemcomitans* and *F. nucleatum* showed a viability reduction in the biofilm of 2 log<sub>10</sub>, while *P. gingivalis* viability reduced by 3 log<sub>10</sub>. No significant change in Ct values were observed for PMA-treated viable control cells (Sánchez et al. 2014). These results demonstrate the efficacy of PMA for differentiating viable and dead periodontal bacteria cells in an in vitro model post antimicrobial exposure.

PMA treatment prior to DNA extraction for 16S rRNA gene analysis has previously been conducted on porcine heart valve replacement tissue expected of infective endocarditis (IE) (Bouchiat et al. 2015). The blood-culture-negative cardiac samples were suspected of IE with non-tuberculous mycobacteria (NTM). Bouchiat et al. (2015) found that Gram staining and conventional cultures remained negative, whereas Ziehl-Neelsen staining showed acid-fast bacilli in all samples. PCR using a pre-treatment with PMA provided evidence for the presence and viability of both *Mycobacterium chelonae* and *Mycobacterium lentiflavum*. While both species are rare infective agents of heart valve replacement tissue, this study highlights the advantage of using the highly

sensitive PMA PCR method for identification of viable strains in clinical tissue where traditional methodology has failed (Bouchiat et al. 2015).

Given the diverse variety of bacterial 16S rDNA sequences previously detected in atherosclerotic plaque tissue, it is hypothesised here that additional previously undetected species will be identified in the CAP tissue samples examined for this investigation. Using direct PCR analysis of CAP tissue a unique profile of bacterial 16S rDNA sequences may be identified relating to pathogenic and commensal species. Through the identification of a unique profile of microbial inhabitants of carotid atherosclerotic tissue, a deeper understanding of how infection may contribute to the development of atherosclerosis may be acquire that can advance the field. Therefore, the present chapter of work is concerned with detection of bacterial 16S rDNA directly in CAP tissue samples. While oligonucleotide primers for universal amplification of most bacterial DNA were employed for detection, an emphasis was also placed on detecting RCB and other oral bacterial DNA, by using oligonucleotide primers for the detection of Bacteroidetes, Spirochetes, *Streptococcus* spp., *Lactobacillus* spp. and *P. acnes*.

#### 4.2 Aims

- A. To gain a better understanding of the wider bacterial taxa present in human atherosclerotic plaque tissue.
- B. Qualitatively determine the extent of latent 16S rDNA sequences of typically oral, periodontal and extra oral-dwelling bacteria species present in human carotid plaque and healthy LITA control tissue.
  - i. Using universal, phylum specific and species specific primer sets to target amplification of the 16S rRNA gene.
  - ii. To isolate the different DNA sequences amplified using the universal and phyla specific PCR by molecular cloning.
  - iii. To establish the identity of cloned sequences using a BigDye Terminator Sanger's sequencing technique.

### 4.3 Methods overview

Portions of CAP and LITA tissue were lysed in ALT buffer in the presence of proteinase K. DNA was then extracted from the lysate using chloroform isoamyl-alcohol (25:24:1) and the crude extract was purified using a standard EtOH/acetate precipitation method (section 2.4.1). To determine the presence of latent bacterial DNA in CAP tissue Purified nucleic acid was used as template for endpoint PCR (section 2.4.3). Oligonucleotide primers that target the 16S rRNA gene were utilised to amplify DNA from the domain “Bacteria”, (D88/E94), the phyla “Bacteroidetes” (D88/ F01) and “Spirochetes” (D88/C90) and the genera, *Streptococcus* spp. and *Lactobacillus* spp. (section 2.4.3). Species specific primer sets for *P. gingivalis*, *T. forsythia*, *T. denticola* and *P. acnes* were also used (section 2.4.3). Template DNA for positive PCR reactions consisted of pure stock DNA extracted from one or more of the target organisms. Negative PCR reactions contained all PCR reagents with template substituted for water (section 2.4.3). In separate PCR reactions HBG primers were used to amplify DNA from the human component of the tissue samples, which acted as an internal control sample for all samples (section 2.4.3). All PCR reactions were separated in 1.5% agarose gels and visualised following staining with EtBr (section 2.4.4). All PCR reactions for CAP and LITA were performed the same.

Positive amplification using universal and phylum specific primers were further analysed using TOPO<sup>®</sup> TA cloning (section 2.4.5). Positive clones were confirmed by blue/white screening and PCR colony screens (section 2.4.6). Positive clones containing the correct insert were cultured overnight for miniprep vector DNA extraction the following day (section 2.4.7). The purified vector DNA was used as template for PCR using M13 primers that anneal up and downstream of the vector insert sequences. The resulting amplicon containing the 16S rDNA sequences were then purified and used as template for BigDye terminator sequencing PCR (section 2.4.8). Finally, the sequences were analysed using a genetic analyser and the resulting sequences were identified by comparing the sequence reads with sequences within the taxID:2 NCBI BLAST reference database (section 2.4.8).

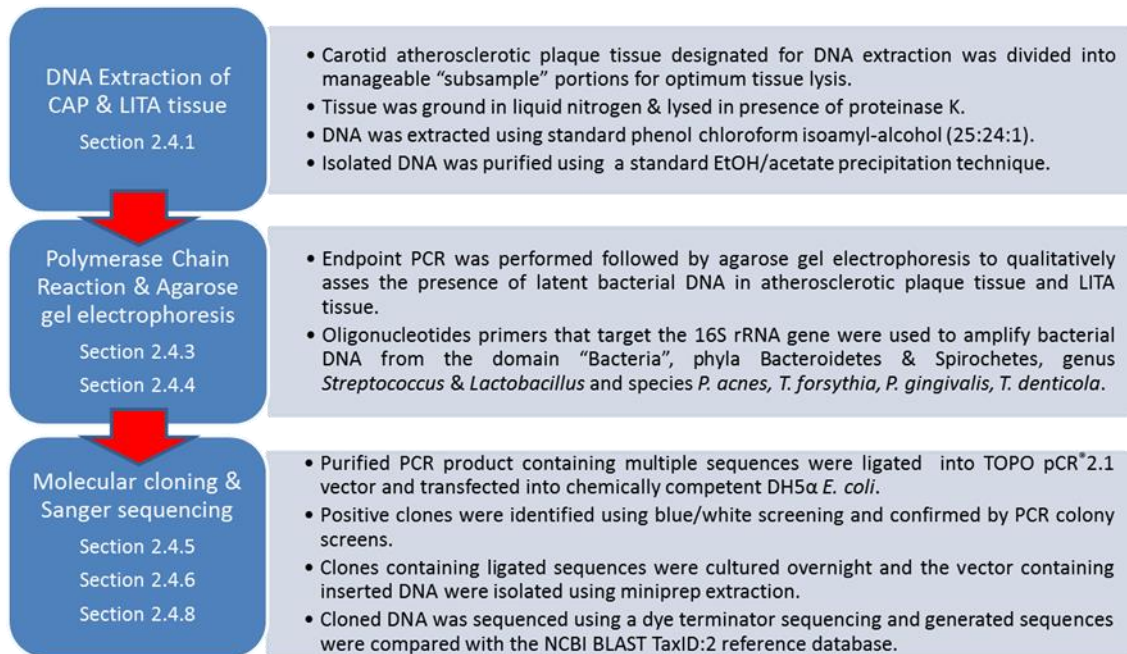


**Figure 4.01:** Flow diagram that details the materials & methods (including section numbers) used in this chapter of work to identify bacterial 16S rDNA sequences present in human internal atherosclerotic plaques.

#### 4.4 Results

In the present study, human atherosclerotic plaque tissue from the carotid artery was investigated for the presence of bacterial 16S rDNA signatures using oligonucleotide primer sets that target the 16S rDNA gene. The following data relates to bacterial 16S rDNA amplified using species-specific, genus-specific primers or a universal degenerate primer set for amplification of most species in the domain bacteria. Overall, a total of 13 of 21 (61.9%) CAP specimens contained bacterial 16S rDNA. No bacterial DNA (bDNA) was detected in any LITA control tissue samples for the primer sets used. Positive PCR controls consisted of 0.5 µg DNA of pure stock bDNA of the species or genus being detected (e.g. Bacteroidetes primer set = *P. gingivalis* or *T. forsythia* pure stock DNA for positive PCR control). Alongside routine positive and negative (template omitted for dH<sub>2</sub>O) PCR control reactions, an additional positive internal control was included, namely human β-globin gene (HBG). This enabled one to assess the quality and adequacy of the tissue and DNA extraction procedure, as well as the consistency of human genomic DNA amplification of each sample. HBG amplification was observed in all CAP (n = 21) tissue samples (figure 4.02).

## 4.4.1 Bacterial DNA amplification using species-specific primer sets

For this section of the study, DNA was extracted from 21 CAP specimens and 18 LITA control specimens and used to detect the presence of bacterial 16S rDNA by conventional PCR. Four sets of published species-specific primers, designed to target 16S rDNA permitted for amplification of *P. gingivalis*, *T. forsythia*, *T. denticola* and *P. acnes* were used. Prior to DNA extraction tissue samples were divided into smaller manageable portions for more efficient tissue lysis. Therefore, a number of subsamples were generated that belong to one patient but were tested individually. When testing these subsamples, internal control gene HBG was consistently amplified in at least one or more of the subsamples from each patient, providing a strong PCR amplification band of approximately 408 bp (Figure 4.02). Of the 21 plaque specimens examined, 9 (42.9%) showed positive amplification of bacterial 16S rDNA with species-specific primers. *P. acnes* DNA was the most frequently amplified DNA, appearing in 7 (33.3%) of 21 CAP samples (Figure 4.03). *P. gingivalis* was detected in 5 (23.8%) of 21 CAP samples (Figure 4.04). *T. forsythia* DNA was detected in 3 (14.3%) of plaque samples (Figure 4.05), whereas none of the plaques showed amplification of *T. denticola* DNA (Figure 4.06). Likewise, all LITA control tissue samples showed no presence of amplifiable bacterial 16S rDNA for any of the species-specific primers used in this study. It is notable that when species-specific primers were used, 5 (23.8%) of 21 CAP samples amplified DNA from more than one species and one of these samples contained three 16S rDNA signatures (Table 4.01). All CAP samples that showed 16S rDNA signatures also amplified HBG in separate reactions.

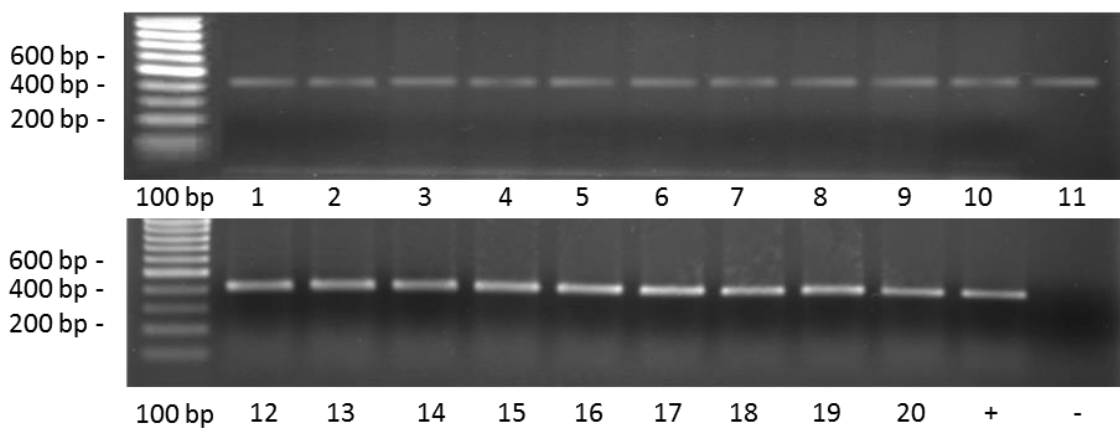


**Figure 4.02:** Gel electropherogram shows amplification of the internal control, HBG. By inclusion of a positive internal control reaction that targets a ubiquitously present human component of the test tissue, one can control for the quality and adequacy of the test tissue, the efficiency of the DNA extraction and the reliability of the PCR assay. Left lane comprises a 1 Kb molecular weight marker showing increments of 100 bp. Samples 1 – 20 represent the 408 bp PCR product for human  $\beta$ -globin amplification. Included is a PCR positive THP-1 cell DNA (+) and negative PCR control (-).

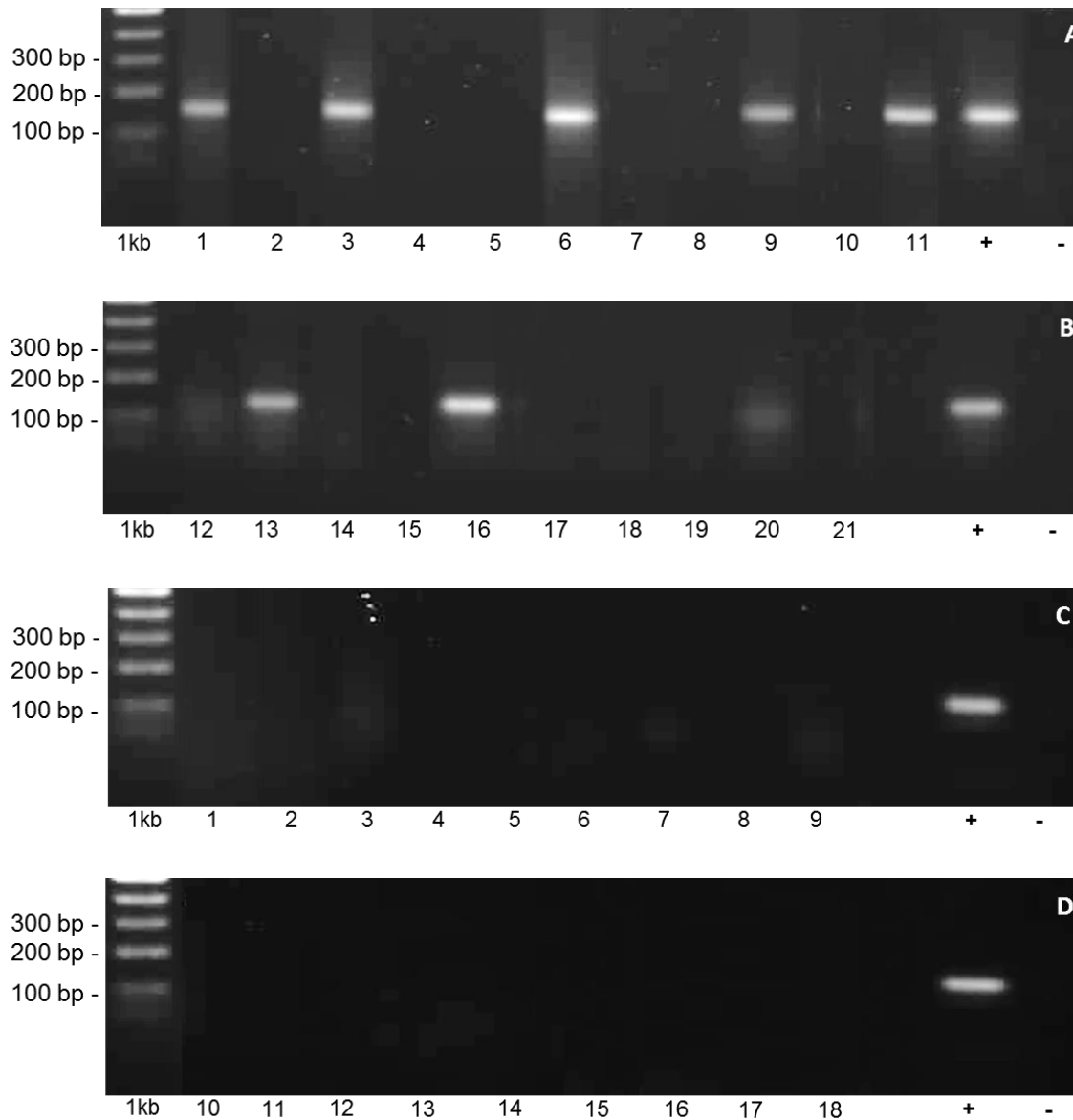


**Figure 4.03:** Agarose gel electropherograms (2%) for the detection of *P. acnes* 16S rDNA in CAP tissue. Positive amplification of *P. acnes* 16S rDNA (~131 bp) was observed for samples 1, 3, 6, 9, 11, 13 & 16 (A & B). The remaining CAP samples 2, 4, 5, 7, 8, 10, 12, 14, 15 & 17 – 21 (A & B) showed no positive amplification of bacterial DNA. None of the LITA control tissue samples 1 – 18 showed positive *P. acnes* 16 rDNA (C & D). Farthest left lanes contain a 1Kb molecular weight marker. The farthest right lanes contain PCR positive (+) and PCR negative (-) reactions.

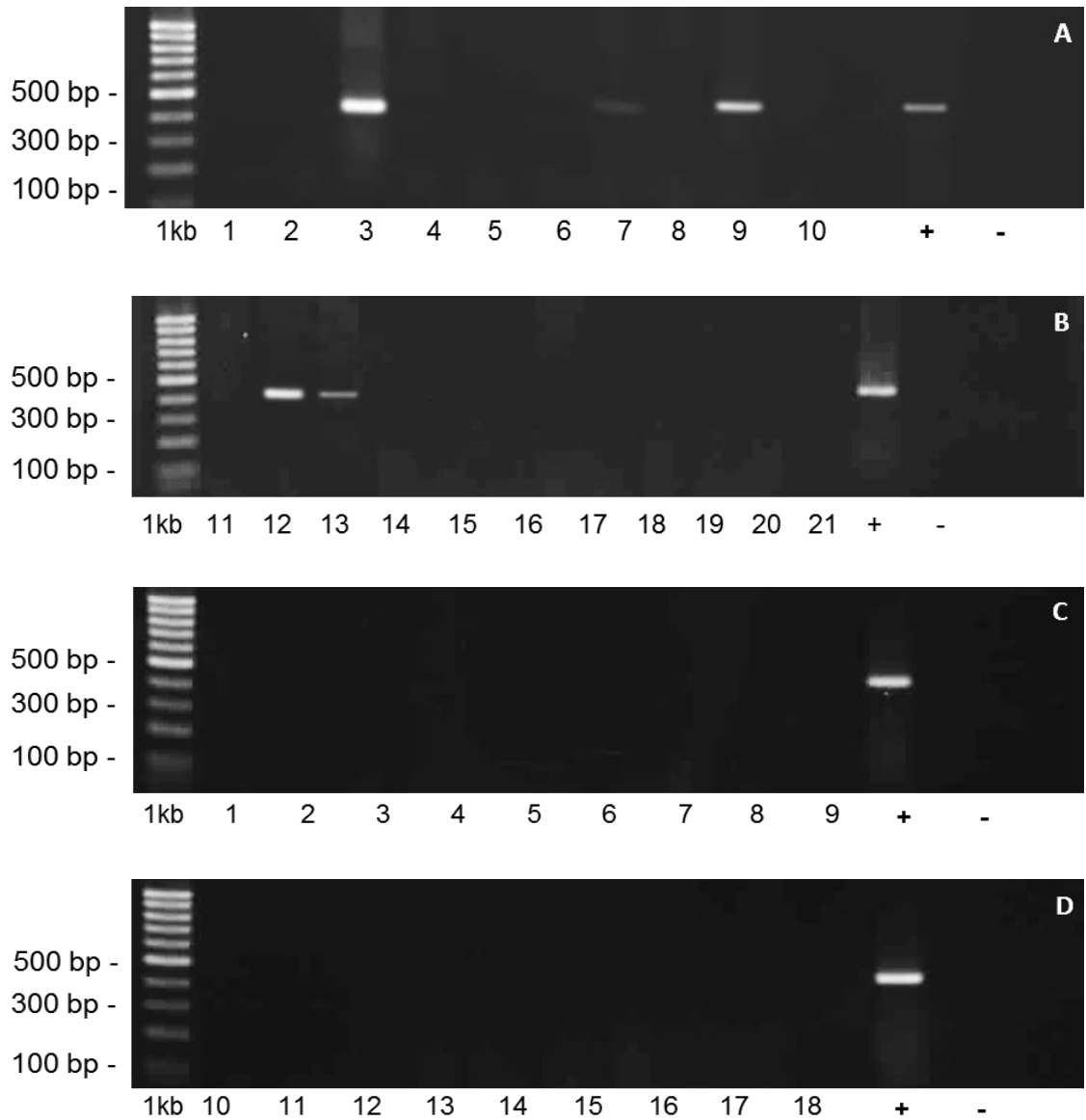


**Figure 4.04:** Agarose gel electropherograms (2%) for the detection of *P. gingivalis* 16S rDNA in CAP tissue and LITA tissue specimens (C & D). Positive amplification of *P. gingivalis* 16S rDNA (404 bp product size) was observed in CAP tissue samples 3, 7, 9, 12 & 13 (A & B). No bacterial DNA was detected in the remaining CAP samples 1, 2, 4 -7, 9, 10, 11 and 14-21 (A & B). LITA control tissue DNA samples 1 – 18 were negative for *P. gingivalis* 16S rDNA amplification. Lane 1 (left) of each gel contains a 1 Kb molecular weight marker with increments of 100 bp. Farthest right lanes contain PCR positive (+) comprising 0.5  $\mu$ g *P. gingivalis* stock DNA and negative (-) reactions.

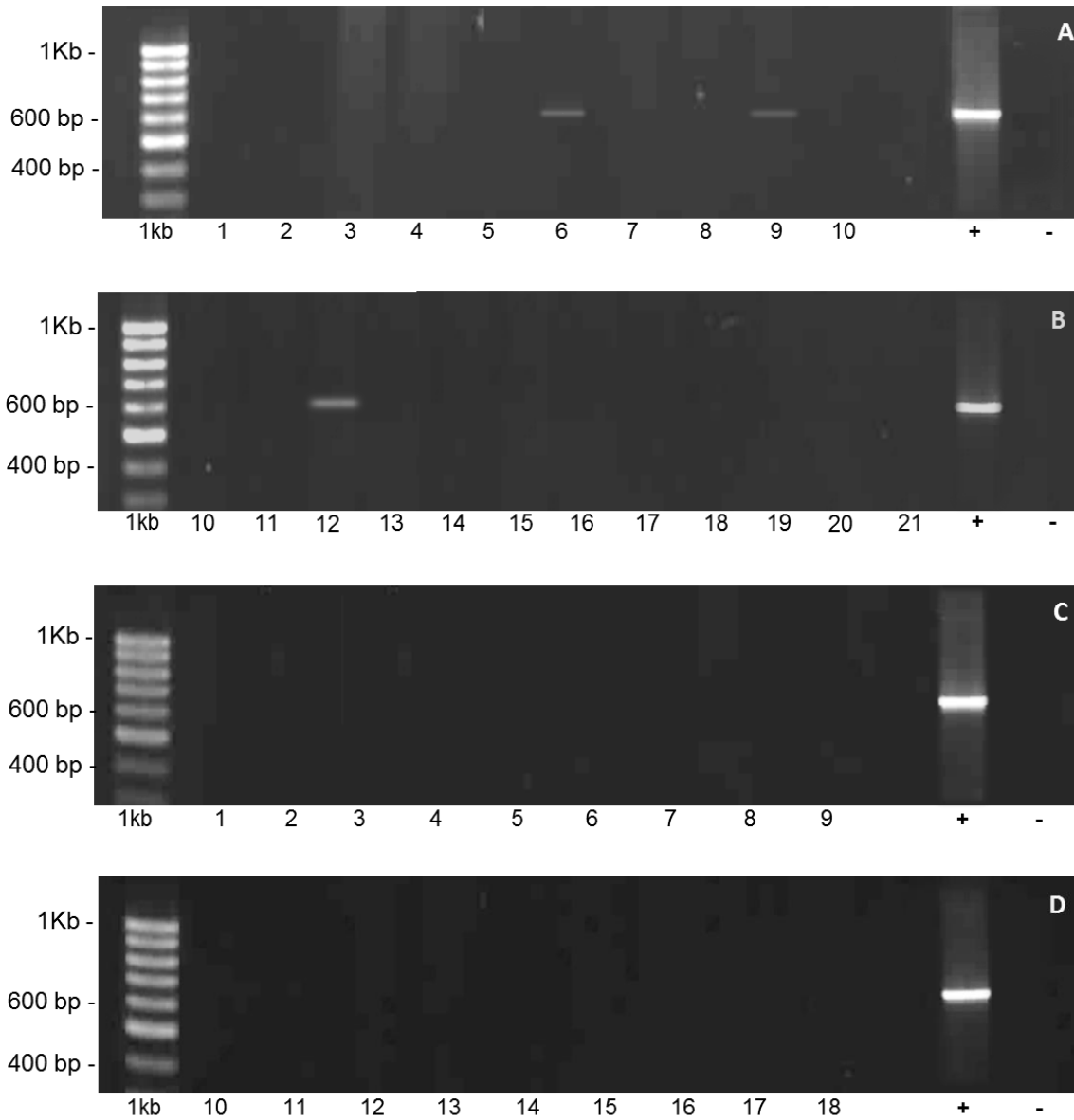


**Figure 4.05:** Agarose gel electropherograms (2%) for the detection of *T. forsythia* 16S rDNA in CAP tissue (A & B) and LITA tissue specimens (C & D). Positive amplification of *T. forsythia* 16S rDNA (~640 bp product size) in CAP samples 6, 9 and 12 (A & B). The remaining CAP samples 1 – 5, 7, 8, 10 – 11, 13 – 21 showed no positive amplification of bacterial DNA (A & B). Left lanes contain a 1Kb molecular weight marker with increments of 100 bp. The farthest right lanes comprise PCR positive (+) and negative (-) reactions.

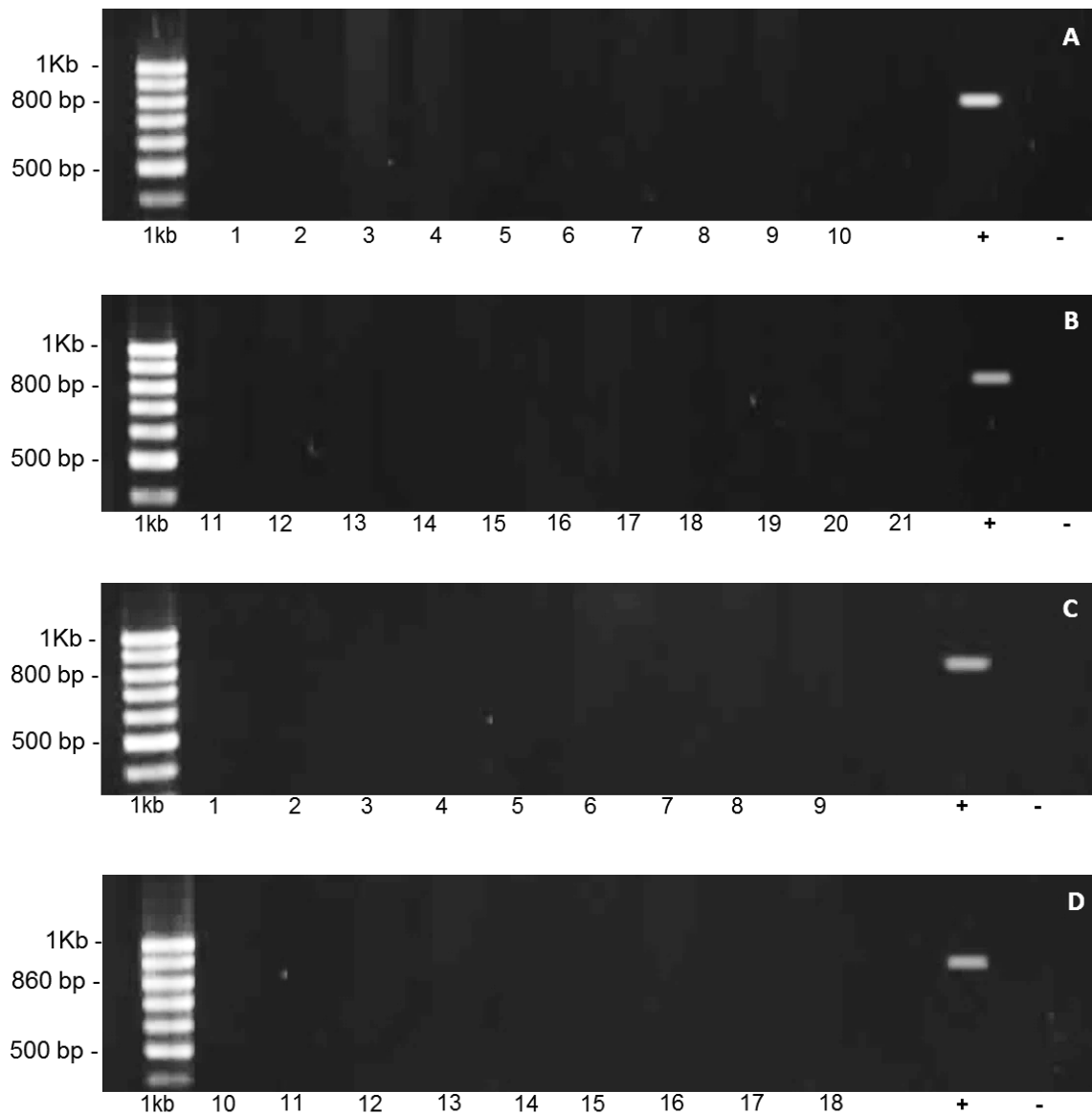


**Figure 4.06:** Agarose gel electropherograms (2%) for the detection of *T. denticola* 16S rDNA. *T. denticola* 16S rDNA was not amplified in any of the CAP samples 1 – 21 (A & B) or LITA samples 1 – 18 (C & D). The left lanes of each gel contain a 1Kb molecular weight marker with increments of 100 bp. The farthest right lanes contain a PCR positive (+) and negative (-) reaction.

#### 4.4.2 Bacterial DNA amplification using genus-specific primer sets

To broaden the scope of analysis, a universal primer set for the detection of most bacteria was included in the investigation; along with two genus-specific and two phylum-specific primers sets, namely, *Streptococcus spp.*, *Lactobacillus spp.*, Bacteroidetes and Spirochetes. *Streptococcus spp.* DNA was detected in just one plaque sample and amplification was extremely weak (Figure 4.07). None of the plaque samples showed amplification of *Lactobacillus* DNA, yet the positive PCR control reaction was amplified (Figure 4.08). Likewise, there was no amplification of *Spirochete* 16S rDNA for any of

the CAP samples tested. The most frequently detected genus was Bacteroidetes, which was amplified in 5 (23.8%) out of 21 plaque samples (Figure 4.09). Bacterial 16S rDNA was successfully amplified using the universal primer set (D88/E94) for 4 (19%) of 21 CAP samples (figure 4.10). Overall, bacterial 16S rDNA was detected in 9 (42.9%) of plaques samples using the universal and genus specific primer sets. Table 4.01 lists all CAP samples with positive bacterial 16S rDNA amplification for universal, genus-specific and species-specific primers sets.

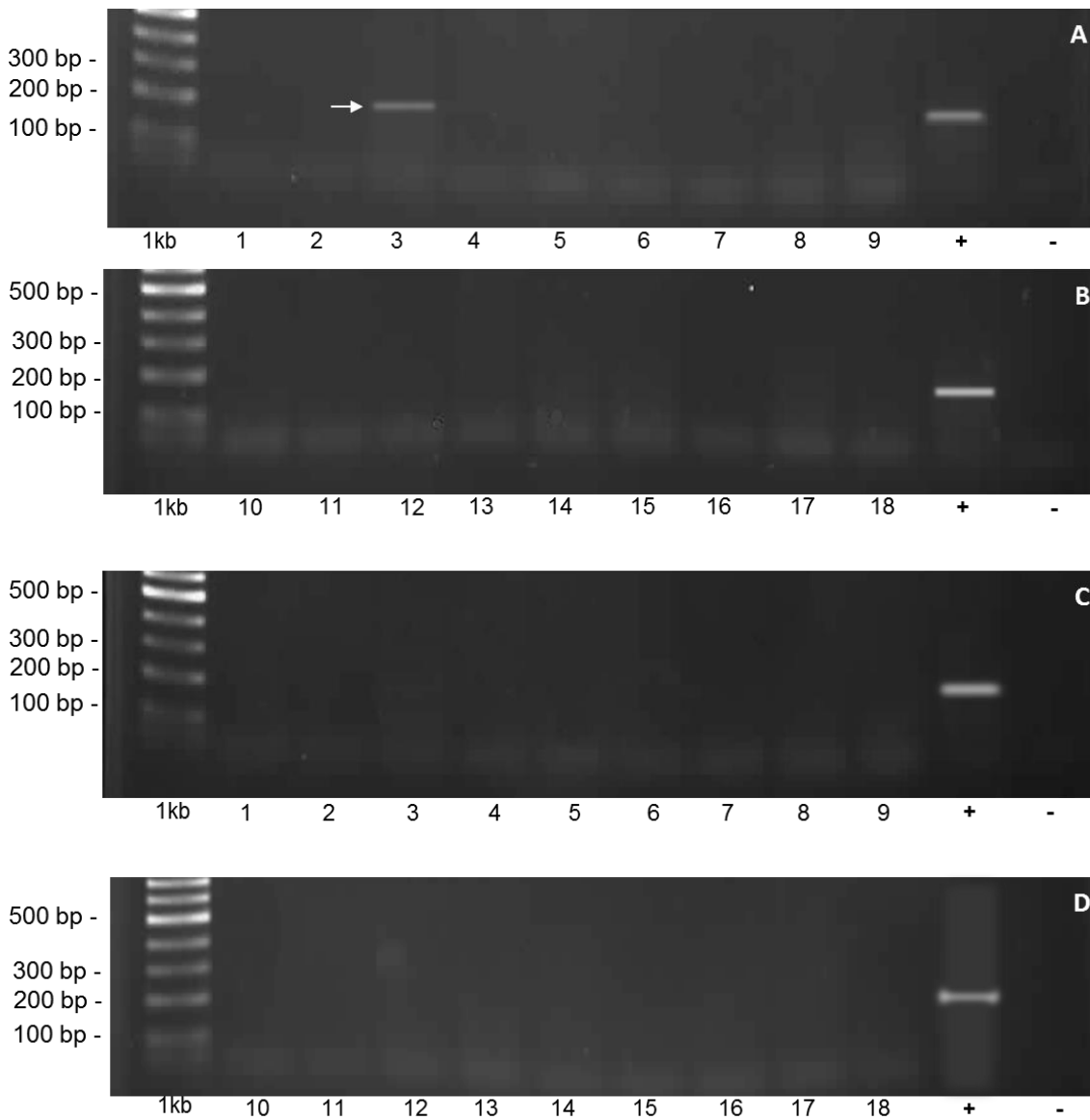


**Figure 4.07:** Agarose gel electropherograms (2%) for the detection of *Streptococcus* spp 16S rDNA in CAP samples (A & B) and LITA control samples (C & D). Each gel comprises a 1Kb molecular weight marker in the farthest left lane and a PCR positive (+) and negative (-) reaction to the farthest right of each gel. A very faint PCR band (white arrow) shows weak amplification of *Streptococcus* spp. for sample 3 (A). The remaining CAP test samples (A & B) 1, & 4 -18 show no positive amplification of *Streptococcus* spp. 16S rDNA. All LITA control samples 1 – 18 (C & D) show no amplification of *Streptococcus* spp. 16S rDNA.

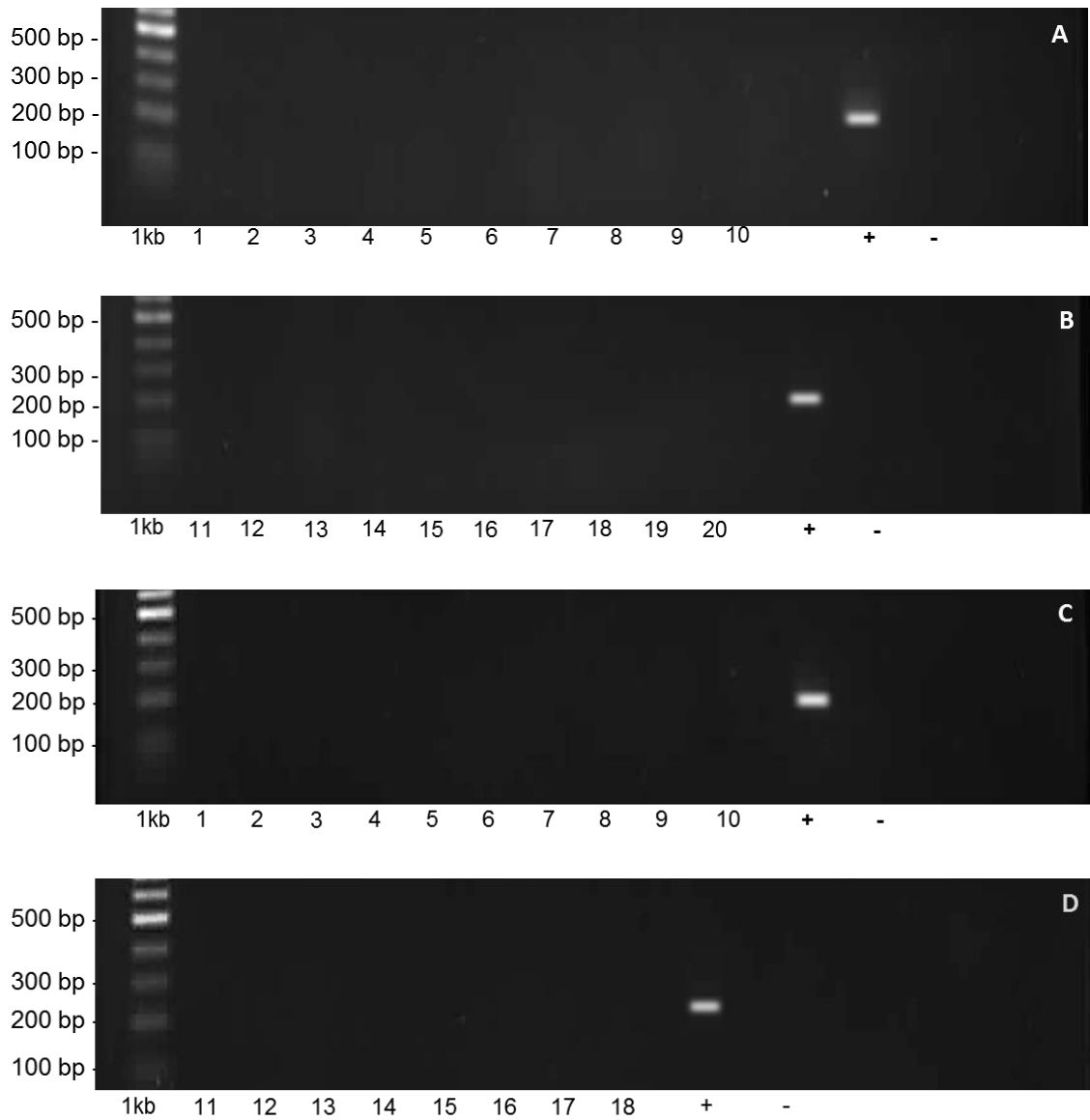


**Figure 4.08:** Agarose gel electropherograms (2%) for the detection of *Lactobacillus spp.* 16S rDNA human CAP DNA samples 1 – 20 (A & B) and LITA control tissue 1 -18 (C & D). None of the test or control samples contained amplifiable *Lactobacillus spp.* 16S rDNA. Each gel comprises a 1Kb molecular weight marker in the farthest left lane. The farthest right lanes contain a PCR positive (+) and negative (-) reaction.

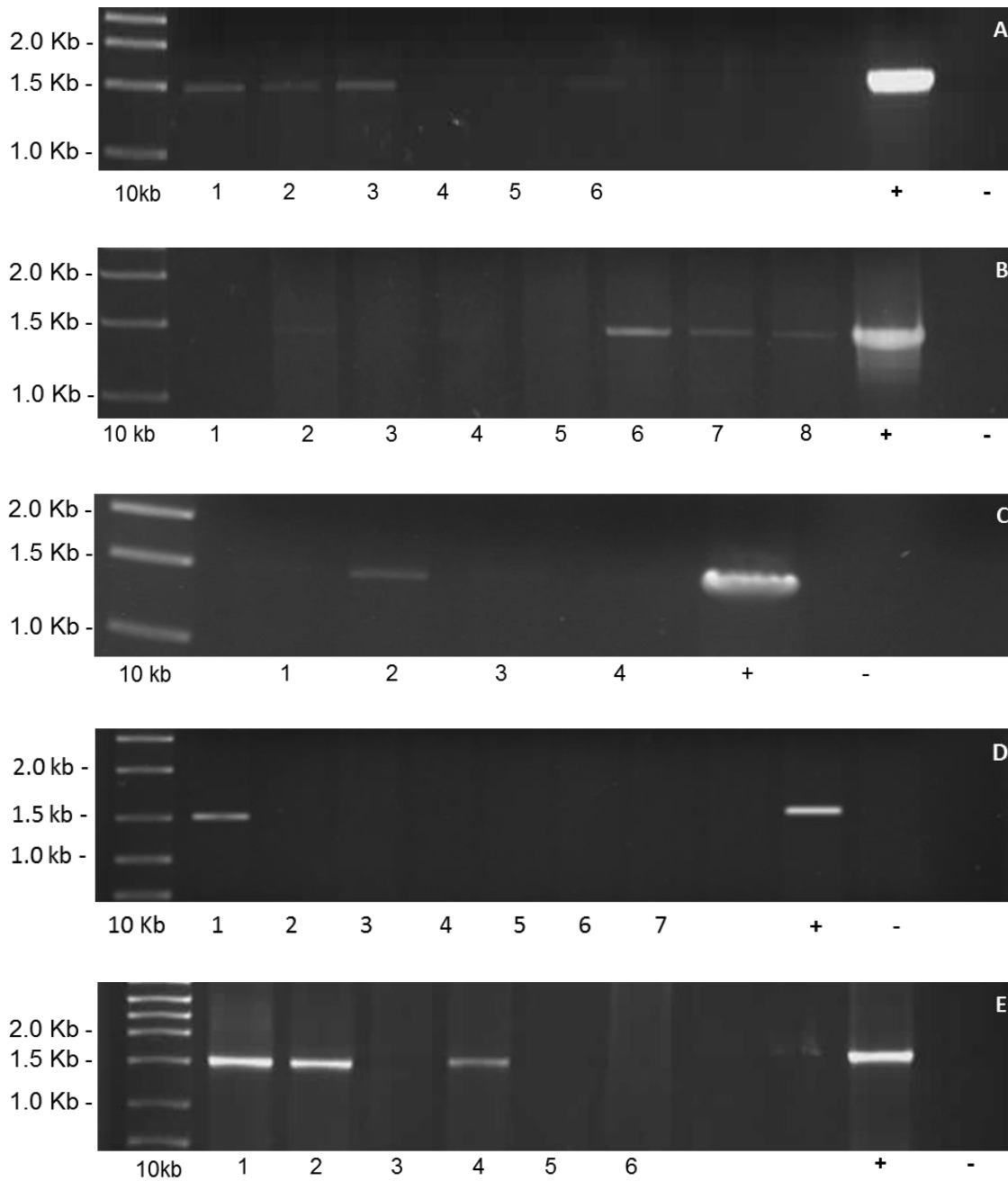


**Figure 4.09:** PCR amplification of Bacteroidetes 16S rDNA. Each gel represents one tissue sample from one patient. CAP specimen was divided into manageable sample sizes for DNA extraction (e.g. 8 subsamples for CAP sample #7 (B)). Positive amplification of Bacteroidetes 16S rDNA was observed in 5 separate CAP samples (A – E) (6, 7, 9, 12 and 13; table 4.01). Positive bacterial DNA amplification occurred for more than one subsample (A - C & E) prior to pooling individual subsample reactions for molecular cloning.

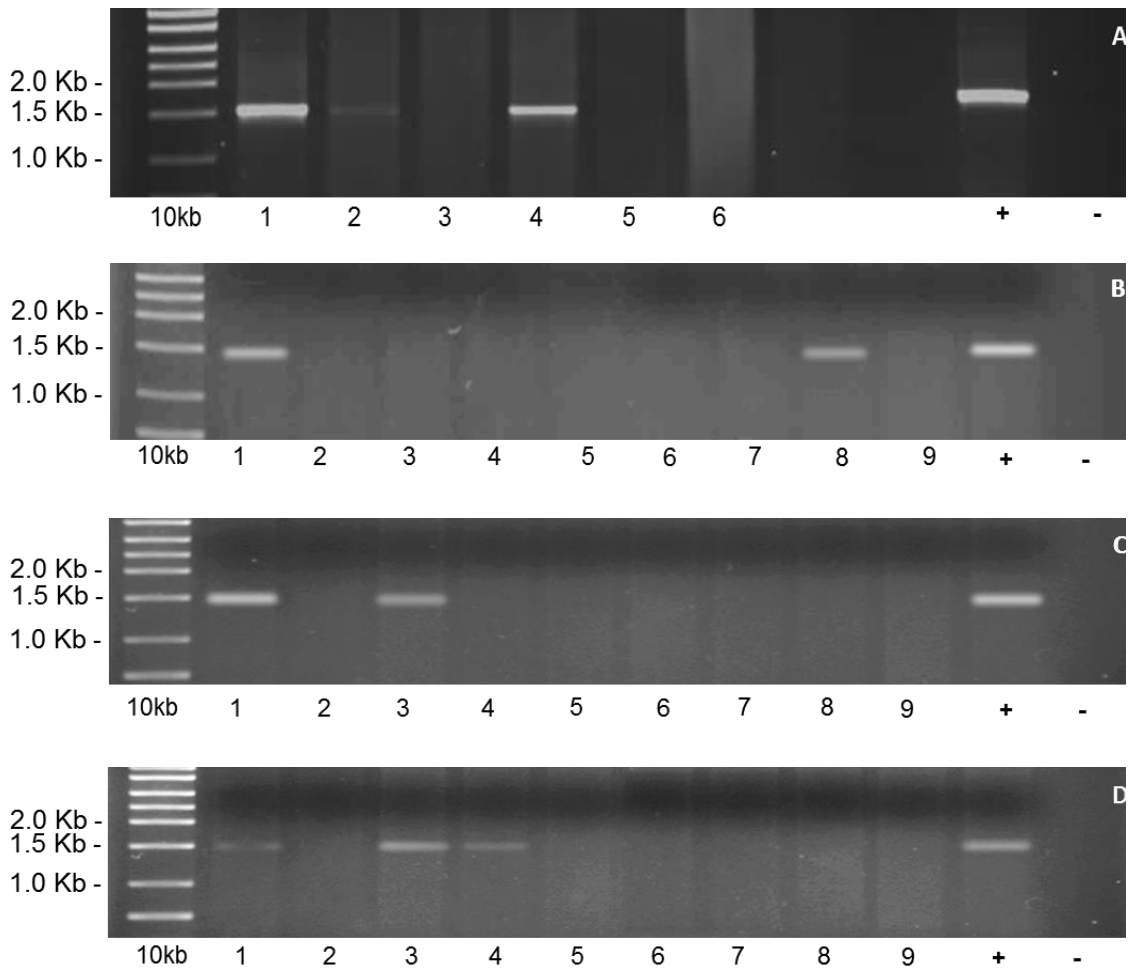


**Figure 4.10:** PCR amplification of 16S rDNA using universal (d88/E94) primers for targeting most bacteria. Each gel represents on tissue sample from one patient. Therefore, positive amplification was observed for 4 separate CAP DNA samples 13 & 17 – 19 (Table 4.01). Each CAP specimen was divided into manageable sample sizes for DNA extraction (e.g. 6 sub-samples for CAP sample #13 (A)). A 10Kb molecular weight marker was included in the first (left) lane. A PCR positive (+) and negative (-) reaction were ran in farthest right lanes. Positive bacterial DNA amplification was observed for more than one subsample. Subsamples were pooled for molecular cloning.

# ID	Patient			Broad scope primers					Species-specific				Cont
	Age	Sex	CAP	Uni	Bac	Spiro	Strep	Lac	Pa	Pg	Tf	Td	
1	65	F	LC						✓				✓
2	53	M	LC										✓
3	75	M	RC				✓		✓				✓
4	71	M	LC										✓
5	70	M	LC										✓
6	72	M	LC		✓				✓		✓		✓
7	84	M	RC		✓					✓			✓
8	63	M	RC										✓
9	70	M	LC		✓				✓	✓			✓
10	83	M	LC										✓
11	72	M	RC						✓	✓			✓
12	62	M	RC		✓					✓			✓
13	79	F	RC	✓	✓				✓	✓			✓
14	77	F	LC										✓
15	70	M	LC										✓
16	68	F	LC						✓				✓
17	62	M	LC	✓									✓
18	81	M	RC	✓									✓
19	71	M	LC	✓									✓
20	51	M	RC										✓
21	68	M	LC										✓

**Table 4.01:** A basic table plot showing the samples that exhibited amplifiable bacterial 16S rDNA. The table is split into four main columns, “patient”, “broad scope primers”, “specific primers” and “control” (Cont) groups. Patient column contains patient information i.e. age, sex and the loci of CAP tissue (LC/RC – left/right carotid artery). Ticked boxes represent positive amplification of bacterial 16S rDNA in relation to each primer set (listed across the second row) **Uni**: Universal primers; **Bac** - Bacteroidetes; **Spiro** - Spirochetes; **Strep** - *Streptococcus*; **Lac** - *Lactobacillus*; **Pa** - *P. acne*; **Pg** - *P. gingivalis*; **Td** - *T. denticola* **Tf** - *T. forsythia*, **HBG** – Human  $\beta$ -globin.

#### 4.4.2.1 Bacteria species identification using molecular cloning & DNA sequencing

Ligation reactions for amplified bacterial 16S rDNA insertion produced hundreds of positive clones in all cases (figure 4.11). Internal positive control reactions consisted of a pure stock of bDNA extracted from species belonging to each genus, which were amplified as PCR positive reactions in the initial detection PCR. These initial positive reactions were carried through the entire cloning workflow in parallel with amplified test samples. Internal positive controls were recovered in all cases and were used as a final positive control to evaluate the colony screening PCR (figure 4.12). HBG was also amplified in all reactions (figure 4.01). The primer set for the phylum Spirochetes (D88/C90) showed no amplification of 16S rDNA in any of the CAP samples tested, though positive controls and HBG reactions were positive. Positive bacterial 16S rDNA sequences were identified

when universal, Bacteroidetes and *Streptococcus* primer sets were used, in 4 (19.0%), 5 (23.8%) and 1 (4.7%) CAP samples, respectively. Of these 10 positive samples using broad scope detection primer, 213 clones were isolated and partial DNA sequences of between 700 – 800 bp were obtained in order to detect the predominant bacteria species present in CAP tissue. In all cases, the sequences reads generated were sufficiently large to establish species identity when compared with the NCBI nucleotide BLAST (BLASTn) reference library, when set to search against reference library bacteria, namely, “taxid:2”. Approximately 78.8% of the 160 clones had 100% sequence homology with NCBI reference strains. For the remaining clones, 30 (~18.8%) and 4 (2.5%) clones showed 99% and 97% sequence homology, respectively (table 4.02). Overall, eleven individual bacteria species were identified belonging to four phyla Actinobacteria, Bacteroidetes, Firmicutes and Proteobacteria. No clones relating to new species were detected in the CAP samples investigated here, however in the unlikely event that chimeric sequences were produced that lead to erroneous identification, sequences were analysed with chimera detection software Pintail v 1.1 (Ashelford et al. 2005). It is estimated that online 16S rDNA reference libraries contain between 1% - 15% chimeric sequences consisting of fused DNA copies generated as an artefact of PCR. In the present study, no chimeric 16S rDNA sequences were amplified. Figure 4.13 illustrates the data output for chimera detection software Pintail v 1.1, which compares evolutionary distances between a query and subject sequence over the length of the 16S rRNA gene.

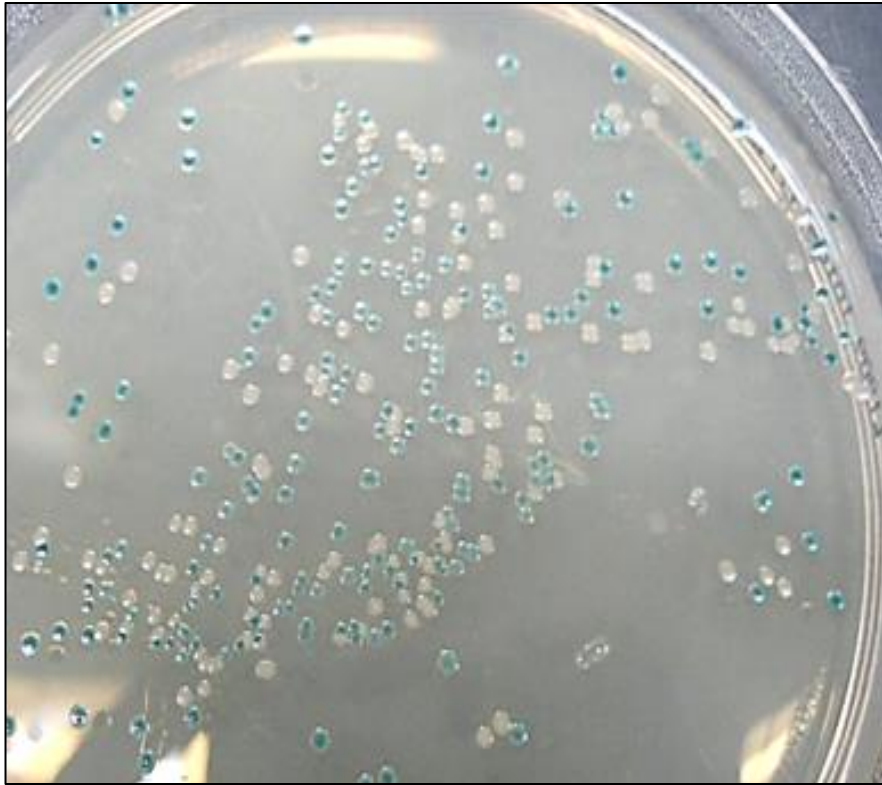


**Figure 4.11:** Chemically competent *E. coli* (DH5 $\alpha$ ) transfected with TOPO<sup>®</sup> pCR<sup>®</sup>2.1 vector on selective LB agar in the presence of (X-gal). Approximately 150 colony clones transfected with a pCR<sup>®</sup>2.1 vector containing a ligated ~1.5 Kb 16S rDNA insert (white colony) or a pCR<sup>®</sup>2.1vector with no insert (blue colonies). Approximately, 15% of white colonies were picked for DNA sequencing.

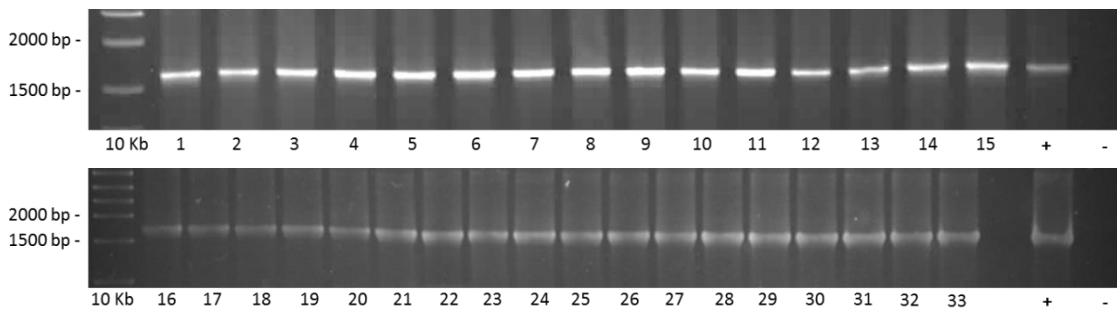


**Figure 4.12:** PCR colony screen analysis of a crude colony cell suspension using M13 primers to confirm the presence of a cloned DNA insert. M13 primers anneal to the vector 100 bp up and downstream of the 1.5 Kb insert PCR insert; therefore observation of an amplified PCR product size of ~1.7 Kb provides confirmation of a successful ligation reaction and positive cloned reproduction of the 1.5 Kb 16S rDNA insert sequence. All 33 picked clones provide confirmation that the 16S rDNA was amplified from CAP tissue (sample #13), successfully ligated, cloned and amplified again. Positive (+) PCR reactions consisted of a pure stock bacterial DNA from each specific genus. These reactions acted as an internal positive control that were carried through the whole cloning workflow in parallel with positively amplified test samples, from the initial detection PCR through to sequence analysis.

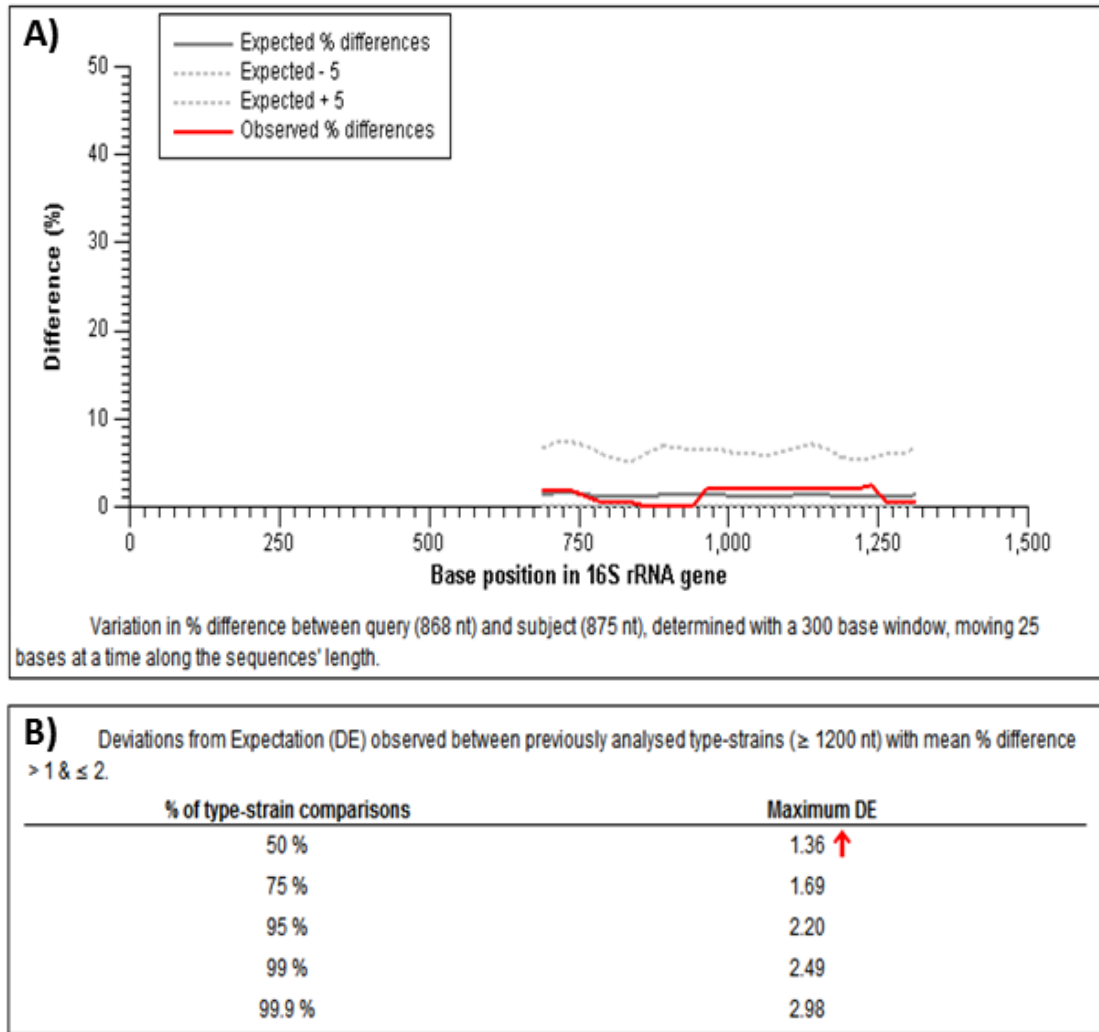


**Figure 4.13:** Data output from chimera detection software Pintail v 1.1. Data relates to a sequence identified as *P. acnes* SK137 using universal primers compared to the reference sequence for the same strain in the NCBI-BLASTn taxID:2 database. The data output shows the mean of the observed % difference (A), which is **1.24%**, and is roughly equivalent to evolutionary distance. The expected % differences (A) are calculated from this mean. The deviation from expected value (DE), summarises the degree of variation between observed and expected values, which is **0.89**. Table (B) summarises the DE values obtained between type-strains for this level of difference. Therefore, based on previous type-strain comparisons, the probability of two non-anomalous sequences producing a DE of **0.89**, when they differ by **1.24%**, is estimated to be  $p > 0.50$ . Thus, there was no sequence anomaly detected, suggesting a true match with neither sequence indicated as chimeric.

Species ID	16S rDNA sequence frequency		Identity (%)	Samples (n)
	Clones (n)	%		
(n=213)				
<u><i>Propionibacterium acnes</i></u> (RM20-2) <sup>†</sup>	51	23.9	100	4
<u><i>Tannerella forsythia</i></u> (RM26-7) <sup>‡</sup>	42	19.7	100	4
<u><i>Staphylococcus epidermidis</i></u> RM38#2-2) <sup>†</sup>	21	9.9	100	3
<u><i>Klebsiella pneumoniae</i></u> (RM20-5) <sup>†</sup>	13	11.5	99	2
<u><i>Mycobacterium tuberculosis</i></u> (RM30-3) <sup>†</sup>	10	6.1	100	1
<u><i>Streptococcus sanguinis</i></u> * (RM10-5) <sup>§</sup>	8	3.8	99	1
<u><i>Streptococcus mitis</i></u> * (RM10-7) <sup>§</sup>	7	3.3	99	1
<u><i>Chryseobacterium haifense</i></u> (RM38#1-8) <sup>†</sup>	4	1.9	97	1
<u><i>Lactobacillus</i></u> spp (RM37-8) <sup>†</sup>	2	0.5	100	1
<u><i>Flavobacterium bacterium</i></u> (RM17-5) <sup>‡</sup>	1	0.5	99	1
<u><i>Chryseobacterium hominis</i></u> (RM34-1) <sup>†</sup>	1	0.5	99	1
<b>Uncultured clones</b>				
<u><i>Streptococcus</i></u> spp. clone (RM10-1) <sup>§</sup>	9	4.2	99	KP294771.1
<u><i>Staphylococcus</i></u> spp. clone (RM38#1-3) <sup>†</sup>	11	5.2	99	KP294710.1
<u><i>Propionibacterium</i></u> spp. clone (RM20-1) <sup>†</sup>	29	13.6	99	KT275137.1
Bacterium clone ET_G_3g01(RM20-8) <sup>†</sup>	4	1.9	84	JF113471.1

**Table 4.02:** List of the bacterial taxa identified using universal, phyla (Bacteroidetes) and genus (*Streptococcus*) specific primer sets. Bacterial taxa underlined are listed among the human oral microbial taxa in Human Oral Microbiome Database (HOMD). Species were identified as the closest match when cross referenced with the nucleotide BLAST NCBI database. If a searches returned more than one species of the same genus with similar identity scores, then only genus was listed (e.g. *Lactobacillus* spp.). Identified NCBI species strain designations are omitted and the identifying numbers designated in this study have been listed in parentheses.

\*Both *S. sanguinis* and *S. mitis* were identified with a score of 100%, though similar scores were also given to uncultured clone sequences of *Streptococcus* spp. in the same search.

<sup>†</sup> Universal primer set

<sup>‡</sup> Bacteroidetes primer set

<sup>§</sup> *Streptococcus* primer set

## 4.5 Discussion

Here we provide further evidence that bDNA representing a unique profile of pathogenic oral and periodontal bacteria species can be detected in atherosclerotic plaque tissue from the carotid artery. Data presented here indicates the occurrence of bacterial 16S rDNA in 57.14% of CAP samples studied. Previous studies show bDNA detection rates from as low as 13% up to 90% of atherosclerotic plaques from patients with periodontal disease (Gaetti-Jardim 2009; Aquino & Lima 2011). A possible reason for such a broad spread of detection, may be due, in part, to the methodology adopted for detection (Figuro et al. 2011). Here we demonstrate the presence of oral bDNA in the CAP tissue of patients with unknown periodontal status. However, studies with similar design as the present investigation have shown that even atherosclerotic plaques taken from patients without periodontal disease; up to 95% of samples contain bacterial 16S rDNA sequences of oral and periodontal origin (Armingohar et al. 2014).

Using species specific primers *P. gingivalis* was the predominant periodontal DNA amplified here (23.8%), followed by *T. forsythia* (14.3%), then 6 bacterial species were identified (table 4.02) that are listed among the human oral microbial taxa in the Human Oral Microbiome Database (HOMD) (Chen et al. 2010). The detection rates for *P. gingivalis* and *T. forsythia* are in agreement with those demonstrated by other investigators, (Figuro et al. 2011; S. Morita et al. 2014). Pucar & Milasin (2007) demonstrated the presence of 16S rDNA for *P. gingivalis* and *T. forsythia* in coronary atherosclerotic plaques. However, detected rates were over twice that observed here in the present investigation. As with the current investigation Pucar & Milasin (2007) also reported no amplification of periodontal DNA in human LITA control samples, although they did report positive amplification of *C. pneumonia* and CMV DNA in LITA samples. Given that the LITA is a vessel that is rarely affected by atherosclerosis, the presence of *C. pneumoniae* and CMV, but absence of periodontal bacterial DNA gives further weight to the hypothesis that periodontal bacteria are associated with the development and progression of atherosclerosis. Several studies performed using species-specific primer sets have reported the presence of *C. pneumoniae* in samples of atherosclerotic plaque (Ramirez 1996; Kuo et al. 1997). In the present study, detection of *C. pneumonia* would only have been possible with the universal primer set. Although the samples examined here were negative for *C. pneumonia*, or other more widely suspected atherogenic species by universal, this does not necessarily mean that the species observed here are more

common inhabitants of atherosclerotic plaque. However, the presence of both commensal and pathogenic bacteria in atherosclerotic plaques suggests that it is unlikely that a single microbe could act as the causative agent behind atherogenesis or plaque rupture.

When evaluating the frequency of 10 periodontal bacteria species in carotid plaques of two groups using qPCR, Kozarov et al. (2006) demonstrated a significantly lower frequency of all 10 species in “young” compared to “elderly” patients. While study designs were different, it is interesting to note that mean age of patients included in the present investigation were ~3 years higher than the “elderly” group studied by Kozarov et al. (2006), yet the detection rates of *P. gingivalis* and *T. forsythia* DNA in the present investigation were closer to group “young” observed by Kozarov et al. (2006). This may be indicative of an overall better oral health of the older patients studied here, especially when considering only one out of nine of the “elderly” patients studied by Kozarov et al. (2006) had full dentition. However, the periodontal status of the patients included in this study was unknown; therefore it is difficult to make this distinction. However, it must be noted that *T. forsythia* DNA was amplified in only one patients sample when using species specific primers, yet *T. forsythia* clones were detected in all four samples amplified with Bacteroidetes primers, which raised the overall detection of *T. forsythia* to 4/21 (19%). This was more comparable with Kozarov et al. (2006) “elderly” group, where *T. forsythia* was observed in 22.2% of samples. Furthermore, 42 out of 213 clones (19.7%) were *T. forsythia* clones (Table 4.02). Therefore, while inter-sample detection of *T. forsythia* was fairly low the frequency of *T. forsythia* within samples was high compared to the frequency of other species.

These findings are in contrast to data presented in a recent study by Fernandes et al. (2014), who recorded high detection rates of putative periodontal bacterial 16S rDNA in oral samples, even in edentulous patients, yet *P. gingivalis* and *T. denticola* were not detected in carotid plaques (Fernandes et al. 2014). These findings are in agreement with a number of previous investigation where patients displaying severe to extensive periodontal disease are completely free from the presence of periodontal bacteria DNA in carotid, coronary and femoral atherosclerotic plaques, despite high prevalence of periodontal bacterial DNA in subgingival plaque and/or periodontal pockets (Cairo et al. 2004; Aimetti et al. 2007; Romano et al. 2007; Aquino & Lima 2011).

*T. denticola* was the only RCB not detected here, however, this observation does not appear to be uncommon. While *T. denticola* DNA has been shown to be present in aortic

and coronary plaque tissue and thrombi, often it is the least detected species in similar investigations (Okuda et al. 2001; Ishihara et al. 2004; Mahendra et al. 2010; Mahendra & Mahendra 2013). *T. denticola* has been detected in carotid plaque using fluorescent in situ hybridization (FISH); however this was only shown for one case study specimen (Cavrini 2005). Furthermore, efforts to amplify *T. denticola* DNA from carotid plaque tissue are often unsuccessful (Fernandes et al. 2014; S. Morita et al. 2014). There are over 50 individual investigations assessing the dissemination of oral bacteria into the blood following various categories of endodontic treatment; however, there has not yet been data describing the dissemination of oral Spirochetes from the mouth in experimental human odontogenic bacteraemias (Parahitiyawa et al. 2009). As treponemes are abundant in the oral cavity (Sutter 1984; Aas et al. 2005), in healthy and diseased oral tissue (Paster et al. 2001), the absence of *T. denticola* DNA in the carotid specimens examined here provides further credence to the notion that *T. denticola* may have poor invasive capability compared to other RCB. Coupled with the fact that no spirochete DNA was amplified at all in this study with specific or genus primers, the aforementioned notion may also be true for other treponemes. These findings would therefore suggest that with regards to the carotid artery, *T. denticola* does not pose the same risk as *P. gingivalis* and *T. forsythia* with regards to the potential inflammatory burden on carotid atherosclerosis.

In the present investigation a universal primer set was used for detection of the domain Bacteria. Three distinct phyla were detected when using the universal primer set, namely, Actinobacteria, Firmicutes and Proteobacteria. In studies where equivalent methodologies were adopted, a high bacterial diversity of over >80 different species were recorded in atherosclerotic plaques from coronary and abdominal aortic aneurysm (Ott et al. 2006; Silva et al. 2006; Calandrini & Ribeiro 2014; Armingohar et al. 2014). In the present investigation a collection of bacterial 16S rDNA sequences previously undetected in carotid atherosclerotic plaque tissue, were amplified in the present study; namely *S. mitis* and *S. sanguinis*, which were detected in 7 (3.3%) and 8 (3.8%) out of 213 clones. However, while the *Streptococcus* primer set sequences showed 99% identity match with BLAST reference sequences for *S. mitis* and *S. sanguinis*, the same identity scores were observed for numerous unculturable *Streptococcus* clone sequences. As there is significant genetic homogeneity within the 16S rRNA gene of Mitis group bacteria (MGB) with only one base pair differentiating *S. mitis* and *S. sanguinis*; the 16S rRNA gene alone is not substantially discriminative to definitively confirm the presence of either species in the CAP samples examined here. To fully differentiate between MGB at the genetic level, a

selection of more discriminative markers are needed, typically enzyme or protein-encoding housekeeping genes such as, manganese-dependent superoxide dismutase gene (*sodA*),  $\beta$ -subunit of RNA polymerase (*rpoB*), histone-like protein A (*hlpA*), glutamate dehydrogenase (*gdh*) or D-alanine:D-alanine ligases (*ddl*) (Garnier et al. 1997; Drancourt et al. 2004; Hoshino et al. 2005; Ferrandiz et al. 2011). PCR-denaturing gradient gel electrophoresis (DGGE) is a common technique used in microbial ecology that can be used to differentiate between DNA sequences of different species that have high genetic homogeneity. The technique is used for separating DNA PCR fragments according to their mobility through agarose gel of increasing denaturing concentration and can theoretically differentiate to a single nucleotide (Buchan et al. 2001).

Ott et al. (2006) demonstrated that *Streptococcus* was predominant genus detected in coronary plaques tissue by excising selected bands from DGGE gels to be reamplified, cloned and sequenced. However, out of seven different *Streptococcus* species identified by the author, none were *S. mitis* or *S. sanguinis*. Armingohar (2014) examined biopsies of femoral and abdominal aortic aneurysms and identified *S. sanguinis*; however, because Armingohar (2014), combined all their vascular samples it is therefore difficult to determine whether *S. sanguinis* was identified in plaque tissue or aortic aneurysms. To the best of our knowledge, this is the first time *S. mitis* has been positively identified in carotid atherosclerotic plaque tissue. *S. sanguinis* has been detected in carotid plaque tissue, though this is the first time this species has been detected by PCR and not IHC. As Viridans Streptococci these species have been implicated in infectious complications including bacteraemia and infective endocarditis and have been shown to evade host detection through expression of surface proteins (C. Morita et al. 2014). More importantly, Viridans are able induce foam cell formation and cell death in macrophage *in vitro* through, production of reactive oxygen species (Okahashi et al. 2011) Therefore, the findings presented here give additional credence to the hypothesis that oral commensal bacteria can exploit opportunities to enter the blood stream and may contribute to the pathogenesis of atherosclerosis, through raising of inflammatory milieu in the affected vessel.

*Mycobacterium tuberculosis* RM30-3 16S rDNA was detected in 10 (6.1%) of the 213 clones from one of the carotid plaque samples amplified with the universal primer set. Although *M. tuberculosis* was only detected in one specimen, the presence of *M. tuberculosis* potentially has very serious implication, particularly for carotid atherosclerosis. In a three-year study, individuals with tuberculosis were found to be at an

elevated risk of having a thromboembolic stroke (Sheu et al. 2010). While *M. tuberculosis* is hitherto undetected in atherosclerotic plaque; this organism has been detected in pericardial fluid of patients with pericardial effusion as a result of pericarditis; thus highlighting the organism ability to invade and infect cardiac tissue (Levy et al. 2006). In addition, high levels of mycobacterial heat shock protein (HSP) 65 and the Mycobacterial cell wall phospholipid, phosphatidylinositol, have been detected in sera of atherosclerotic patients (Rota & Rota 2005). Moreover, Mycobacterial HSP65 and phosphatidylinositol have been studied at length as major atherogenic factors in the progression of atherosclerosis (Rota & Rota 2005). The findings presented here in the present investigation provide the first evidence for the identification of *M. tuberculosis* (H37Rv) in atherosclerotic plaque tissue. These findings therefore highlight the notion that bacteria from other bodily niches, extra to the oral cavity, may also play an equally damaging role in the progression of vascular inflammation and plaque progression. Given the elevated risk of thromboembolic stroke in patients with tuberculosis infection, it would appear *M. tuberculosis* may have particular negative outcome when infecting the carotid artery. It would therefore be informative to establish the extent of to which *M. tuberculosis* may accelerate plaque formation *in vivo* or its ability to induce expression of genes known to play a role in atherogenesis or plaque rupture.

*T. forsythia* was the most frequently detected clone when the Bacteroidetes-specific primers were used. Other bacteroidetes species detected here, included two species from the genus *Chryseobacterium*, namely, *C. haifense* and *C. hominis*. Little is known about these strains from a clinical perspective as they are relatively newly designated members of the genus *Chryseobacterium* (Hantsis-Zacharov & Halpern 2007; Vaneechoutte et al. 2007). *C. haifense* is typically a non-human microbe that has been isolated from raw milk (Hantsis-Zacharov & Halpern 2007). Neither of these species have been identified in atherosclerotic plaque tissue previously. It is difficult to elucidate the origin and therefore the mode of entry for these species took to enter the blood stream and the plaque tissue. It is possible *C. haifense* and *C. hominis* were nosocomial infections, or they may have been present in the intestine or became systemic through the gut bacteraemias. Needless to say, the presence of DNA from these species and the other species identified in the atherosclerotic plaque samples here, demonstrates a diverse microbiota that may cooperate as a collective bacterial load to raise inflammatory milieu within the atherosclerotic lesion contributing to the pathogenesis of atherosclerosis.

Armingohar (2014) identified 16S rDNA sequences from a diverse group of 19 bacterial species in subgingival plaques of patients with chronic periodontitis (CP), including RCB. However, when examining the microbiota of vascular samples from patients with CP, only 3/19 species were synonymous with subgingival plaque. Interestingly, the vascular microbiota identified in patients with CP was more comparable with the species identified in the present investigation and less like the taxa detected in vascular samples from patients without CP. The comparable species (in order of frequency) were *P. acnes*, *S. epidermidis*, *K. pneumonia*, *P. gingivalis*, *S. sanguinis* and *Flavobacterium spp.* This is particularly notable, because even though the species identified here were comparable with the CP group, Armingohar (2014) showed substantial difference between oral and vascular microbiota. This highlights one of two possibilities. First, the species in vascular tissue derive from previous inhabitants of the mouth (i.e. historical oral infections) and have therefore been in the vascular tissue for long periods. Secondly, the species present in vascular samples are derived from more than one niche, including the oral cavity. Both are equally as plausible scenarios for the species identified in the carotid tissue examines here. In order to investigate these paradigms, a study whereby oral microbiota is identified in the months/years leading up to vascular surgery may be helpful. Equally, more studies that include the identification of microbiota from other bodily niches, such as the gut, may provide additional information regarding the source of species identified in atherosclerotic plaque tissue (Koren et al. 2011).

The most abundantly detected DNA was from phylum Actinobacteria, exclusively *Propionibacterium acnes*, which was the most frequently detectable 16S rDNA in CAP tissue when species-specific (33.3%) and universal (19.05%) primers were used. All 4 universally amplified products contained *P. acnes*, which represented 51/160 (31.9%) clones. Unusually, *P. acnes* detection with both universal and species-specific primers sets was observed for the same patient sample only once. A possible cause of inconsistent *P. acnes* amplification between primer sets could be due a reduction in specificity that can be encountered with degenerate primer sets (Jabado et al. 2006). Degenerate primer will have few species that precisely match the template. In early rounds of PCR, the more homologous primers will likely be incorporated into products. The efficiency with which amplification proceeds in subsequent cycles is dependent on the similarity of the remaining primers left in the pool earlier rounds of target amplifications. Hence, primers with the least number of degenerate positions have the greatest likelihood of success (Jabado et al. 2006). When the D88 and E94 primers are combined, they have a moderate degeneracy of

8, which may, in part, explain the disparity in amplifiable *P. acnes* between the degenerate primers compared to species specific primers.

*P. acnes* was detected in all 4 universal amplified products using the universal (D88/E94) primers and was the most frequently detected clone; though, intra-sample detection of *P. acnes* varied from 10% to 80% of clones/plate, which highlights one of the limitations of conventional PCR with species-specific primers as a qualitative assay. *P. acnes* has been shown to be a capable opportunistic pathogen though its inflammatory role in chronic infection, including, orthopaedic and cardiac prostheses, endophthalmitis and infective endocarditis (Aubin et al. 2014). Genetic elements specific to each lineage of *P. acnes* have been established, which highlight the differences of *P. acnes* in functioning as a commensal of the skin and as a pathogen in the aetiology of diseases (Tomida et al. 2013). As a pathogen *P. acnes* has numerous putative virulence factors that can induce tissue damage through haemolysis, pore-formation, adhesion to multiple surfaces for biofilm formation and cell aggregation, as well as induction of chemotactic and inflammatory pathways (Valanne et al. 2005; Falcocchio et al. 2006; Holland et al. 2010; Mak et al. 2013). It would therefore indicate that *P. acnes* is most pathogenic when in tissues distant from its typical commensal niche. Therefore, the predominant presence of *P. acnes* DNA in the carotid plaque samples examined here suggests that *P. acnes* may not simply just be a benign commensal inhabitant of atherosclerotic plaque but may actually be an extremely potent inducer of inflammation that could play a major role in the pathogenesis of atherosclerosis. As the most prevalent species detected here, it is critical to elucidate the potential etiological role *P. acnes* may play in atherogenesis.

The *P. acnes* 16S rDNA sequence detected in the CAP samples examined here was most closely related to the NCBI reference strains SK137 (BLASTn max ID 100%), which based on previous antibody testing and phylogenetic evaluation of the *recA* gene and hemolysin/cytotoxin gene (*tly*), belongs to the lineage type IA (McDowell et al. 2005). Interestingly, this particular lineage of *P. acnes* falls into the subgroup most frequently isolated from dental infections, acne lesions and failed prosthetic implants (McDowell et al. 2005). Up to 9% of the healthy dental microbiome is represented by *P. acnes* strains and studies to identify obligate anaerobes in carious dentin indicated that ~20% of all isolates were *P. acnes* (Hoshino 1985; Ando & Hoshino 1990). Using anaerobic culturing techniques, Fujii et al. (2009) demonstrated that *P. acnes* was the predominant cultivatable species isolated from periapical lesions of patients with chronic periodontal infections following identification using checkerboard DNA-DNA hybridisation. Moreover, *P. acnes*

has been shown to be the major detectable species recovered from root canal and blood samples taken during and after endodontic treatment (Debelian et al. 1992). Heller et al. (2012) examined subgingival plaque of patients with chronic periodontitis (CP) and generalised aggressive periodontitis (GAgP) to assess microbial composition using checkerboard DNA-DNA hybridisation. The author found that while there were no significant differences in *P. acnes* frequency between the two groups, when periodontal sites with a probing depth of  $\geq 4$  mm were examined *P. acnes* was significantly more prevalent in subgingival plaques of patients with GAgP compared to CP.

*P. acnes* has the ability to both systemically invade its host and play a major role as a primary pathogen in several pathologies (Perry & Lambert 2011; Tomida et al. 2013). In light of this evidence and the major presence of a predominantly oral strain of *P. acnes* the carotid atherosclerotic plaque samples examined here, the hypothesis for a potential relationship between oral pathogens and the development atherosclerosis is still maintained.

#### 4.6 Conclusion

The aim of this chapter of work was to establish the presence of latent bDNA signatures present in CAP tissue by targeting the 16S rRNA gene. In this chapter of work a diverse collection of bacterial 16S rDNA sequences were identified in CAP tissue. The species identified here provide a unique profile of commensal and potential pathogenic inhabitants of atherosclerotic plaque tissue. While it was necessary to broaden the scope of this investigation by utilising both universal and phylum specific primer, the main aim was to establish the presence of RCB 16S rDNA in the CAP samples here so an oral origin or of the amplified signatures could be inferred. Both *P. gingivalis* and *T. forsythia* DNA were detected using specific primers and *T. forsythia* clones were detected in 3 further samples amplified using the Bacteroidetes primer set. After *P. acnes*, *T. forsythia* was the most frequently detected clone. However, *T. denticola* failed to amplify with both specific and Spirochetes primers. Although *T. denticola* DNA failed to amplify, it possible it was still present, either below the threshold of detectability or simply absent within the section of tissue that was processed for DNA analysis. Given the varied taxa detected in the plaque samples examined here, no particular source of the DNA signatures can be confirmed. Many of the genera detected, such as *Staphylococcus* spp., *Klebsiella* spp., *Streptococcus* spp., *Lactobacillus* spp. and *Mycobacterium* spp. can thrive in the oral cavity, though some

are also commonly detected in extra-oral niches. Thus, it is probable that the DNA detected in this study originated from multiple sources, such as the gut, lungs and oral cavity.

*P. acnes* was by far the most abundantly detected species amplified with specific primers and also the most frequently detected clone amplified using the universal primers. *P. acnes* is a common skin-dwelling commensal so in previous studies it has often been dismissed as contamination; this notion that cannot absolutely be ignored here either. However, samples were handled with the topmost care to avoid contamination and clean PCR negative control reactions attest to the validity of these findings. While *P. acnes* is a recognised skin commensal, it is also the primary pathogen in numerous pathologies. In addition, particular genotypes of *P. acnes* may play a role in periodontal disease, which, along with the second most specific detected species, *P. gingivalis* cloned sequence and *T. forsythia*, may hint at a periodontal origin for some of the DNA detected in this chapter. These findings are not conclusive to propose a solid argument in support of a relationship between carotid atherosclerotic disease and periodontal disease.

**DEVELOPMENT OF A CULTURE MEDIUM TO  
SUPPORT THE GROWTH OF RED COMPLEX  
BACTERIA**

## 5.1 Introduction

In the preceding chapters, immunological and molecular techniques were implemented to demonstrate the presence of peptidoglycan and 16S rDNA signatures in carotid atherosclerotic plaque specimens. While 16S rDNA analysis is a valuable and rapid molecular tool for bacterial identification, this method tells us little about the viability of the detected organisms. In order to determine whether these previously observed signatures were generated by viable bacteria, it would be necessary to incubate tissue specimens within a bacteriological culture medium that can support the latent microorganisms contained within.

Previous attempts to isolate and identify bacterial species present in atherosclerotic plaque have generally been unsuccessful, possibly due to the presence of unculturable species or through the adoption of a sub-optimal medium (Fiehn & Larsen 2005). To date, only a few viable periodontal bacteria species have been isolated from atherosclerotic plaque, typically *P. gingivalis* and *A. actinomycetemcomitans* (Kozarov et al. 2005; Padilla et al. 2006; Rafferty, Jönsson, et al. 2011). Similarly, pathogenic bacteria originating from other bodily niches have been isolated from AP tissue. For example, *Chlamydia pneumoniae*, a respiratory gram-negative pathogen known to have a strong association with atherosclerotic disease, has frequently been isolated from atherosclerotic plaque tissue by a number of groups (Ramirez 1996; Jackson et al. 1997). Likewise, Gram-negative aerobic pathogens, such as *Enterobacter hormaechei*, found mainly in the microbiome of the small and large intestine, have been cultured from AP tissue from the femoral artery (Rafferty et al. 2011). Other species that are generally considered to have a commensal relationship with its host, such as *Propionibacterium acnes*, can also operate as a capable pathogen, demonstrated by its etiological role as a primary pathogen in multiple pathologies (Brüggemann 2005; Aubin et al. 2014). *P. acnes* is a member of the periodontal microbiota (Paster et al. 2001) and the most prevalent species detected in apical periodontal lesions and generalized aggressive periodontitis (Fujii et al. 2009; Heller et al. 2012). Moreover, *P. acnes* has been shown to be the most abundant species in both root canal and blood of patients undergoing root canal (Debelian et al. 1992). Furthermore, *P. acnes*, along with *P. gingivalis* and *S. epidermidis*, have each been isolated from CAP tissue taken from the same patient (Rafferty et al. 2011; Armingohar et al. 2014).

Given the variability of bacterial inhabitants of atherosclerotic plaque, it is becoming increasingly more unlikely that a single species will be implicated as the major “atherosclerosis bug”. In a recent review by Elkind 2010, it was suggested that if infection does play a primary role in the development of atherosclerosis, it is probably in a more cumulative and continuous fashion. The author proposed the concept that a collective “infectious burden” or “pathogen burden”, better explains the role that infections in aggregate may play in the development of atherosclerosis or clinical cardiovascular events. Thus, until we have identified all the species that may inhabit the atherosclerotic plaque tissue, we cannot truly understand the nature of “infection burden” and the impact it may have on the pathogenesis of atherosclerosis.

When discussing the burden of proof regarding periodontal bacteria as a contributing factor in the development of atherosclerosis, Reyes & Herrera (2013) detailed the 7 ‘proofs’ that need to be met in order to provide a definitive answer for a causal relationship. To fulfil the third proof one must provide, “evidence of live periodontal bacteria in the affected site”. Commercially available culture media for broad species growth do not contain the correct components necessary to support the growth requirements of all species. This becomes problematic when the latent strains being targeted in the plaque tissue have vastly different growth requirements. It would not be good experimental practice to divide ones tissue specimens to culture in different media because there is no certainty one would culture each tissue segment with the correct culture medium. In light of this, the current study is initially concerned with the design of a simplified bacteriological culture medium that supports the growth of, but not limited to, periodontal red complex bacteria (RCB). Thus, the second and main aim of this chapter is to utilise the finalised medium to investigate the microbiota or “pathogen burden” of atherosclerotic plaque by isolating culturable strains for molecular identification. While a plethora of bacterial 16s rDNA signatures have been detected in atherosclerotic plaque tissue over the last 2 decades, only few species have been demonstrated to have the potential to multiply or invade the cells of the atherosclerotic lesion. Because the presence of viable bacteria increases the potential danger, the more we can identify the full range and extent of viable strains present, the greater our understanding of the impact of infection on the pathogenesis atherosclerosis.

## 5.2 Aims and method overview

The development of a single liquid growth medium that could be used to culture viable bacteria present in CAP and LITA tissue was investigated. While the ultimate aim was to isolate and identify any viable bacteria species present in atherosclerotic plaque tissue, particular emphasis was placed on developing a liquid medium with the ability to support the growth of RCB (section 2.3.2). Three media known to support the growth of *P. gingivalis* 11834/W50, *T. forsythia* & *T. denticola* were used, namely BHI, TSB and TYGVS, respectively. Medium development was performed in two stages.

- Stage 1. Test the efficacy of BHI, TSB and TYGVS media (appendices A, B & C) to support the growth of all or more than one RCB species and establish a “base medium” that may be further developed (section 2.3.2.1).
- Stage 2. Further development of the “base medium” through a stepwise supplementation of specific growth reagents known to support the growth of any RCB species not satisfied in stage 1 assessment (section 2.3.2.2).

To establish the significance of the bacterial growth ( $OD_{600}$ ) for media containing different concentrations of growth reagent supplements compared to control medium (stage 2), analysis of variance (ANOVA) was performed (section 2.7.2). If the ANOVA test indicated significant differences between  $OD_{600}$  values, data were tested further by performing a Levene’s test to assess the equality of sample variances between data (section 2.7.2).

The final medium was used for the culture and isolation of latent viable bacteria present in CAP and LITA tissue samples. Tissue was macerated and submerged in medium for 7 – 10 days (section 2.3.3). When positive cultures were observed in liquid medium viable culture was spread across blood agar plates and incubated anaerobically (section 2.3.3). Colonies were picked and re-inoculated in fresh media to expand stock, then archived in Cryobank™ storage vials (section 2.3.4). DNA was extracted from the positive cultures (section 2.4.2) and PCR was performed using D88/E94 universal primer set (section 2.4.3). PCR product was then cloned (section 2.4.5) and sequenced (section 2.4.8) to determine its identity.

## 5.3 Results

### 5.3.1 Growth characteristics of red complex bacteria

Normal growth characteristics of each species in their relative medium were assessed to establish temporal growth patterns of liquid cultures using optical density at a wavelength of 600 nm ( $OD_{600}$ ) to measure liquid culture turbidity (Materials & Methods; section 2.3.1.1). Bacteria were cultured over 192 h (9 days) and liquid cultures were transferred onto solid agar medium daily and incubated to calculate the quantity of colony forming unit (cfu)/ml (Materials & Methods; section 2.3.1.2). The occurrence and duration of each species lag, log, stationary and death phase were plotted on line graphs for  $OD_{600}$ /ml and CFU/ml. Standard deviation was calculated and represented on line graphs as whiskers for each measurement.

#### 5.3.1.1 *T. forsythia* growth characteristics

*T. forsythia* produced tiny off-white colonies that formed a circular and convex form. As colonies aged, they appeared to take on an orange-brown pigmentation from the blood agar and increased slightly in size, but never surpassed 1 mm (figure 5.01a). No haemolysis was observed. Staining showed that *T. forsythia* were gram-negative bacilli and were markedly pleomorphic, with size ranging from 0.5  $\mu\text{m}$  to  $<5 \mu\text{m}$  long (figure 5.01b and c). When incubated in TSB, *T. forsythia* remained in lag phase for the longest time of all test species; taking approximately 3 days to generate exponential growth. *T. forsythia* showed the least, but fastest growth of all test species, with a doubling time ( $t_d$ ) of 9.95 h and growth rate ( $r_g$ ) of  $0.1 \text{ h}^{-1}$ . The final maximum cell number for *T. forsythia* was  $1.3 \times 10^9$  cells/ml which represented a maximum turbidity of  $OD_{600}$  1.381 (figure 5.02).  $OD_{600}$  readings and cfu/ml calculations for *T. forsythia* proliferation were plotted as a semi-log regression plot and the equation for line of best fit showed good linear relationship ( $R^2 = 0.998$ ). In doing so, a chart for the accurate conversion of  $OD_{600}$  readings to cell number (cells/ml) was generated (figure 5.03). From this chart it can be observed that the mean turbidity of a *T. forsythia* culture reaching an absorbance of 1  $OD_{600}$  unit =  $\sim 9.6 \times 10^8$  cells/ml.

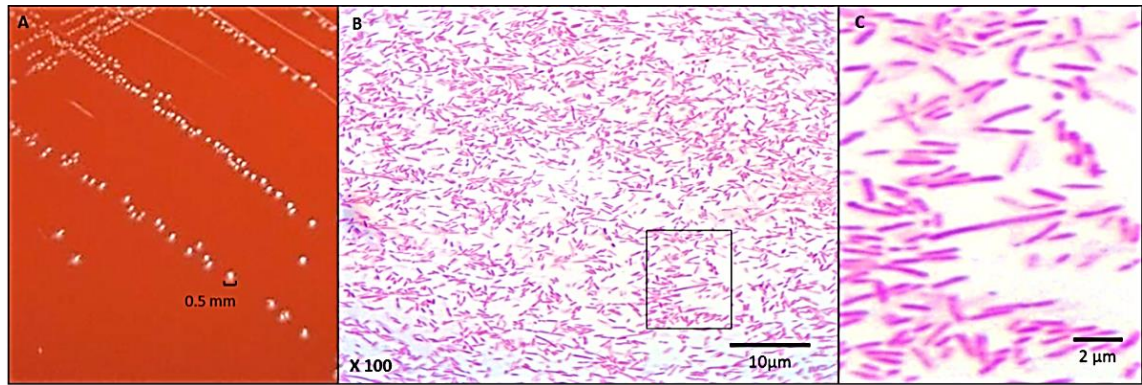


**Figure 5.01:** *T. forsythia* colonies on blood agar. Semi-translucent, dull-white *T. forsythia* colonies of ~0.5 – 1 mm (A) diameter. Gram stain images shows that *T. forsythia* are gram-negative bacilli, which are highly pleomorphic throughout the X100 stain image (A) and x 500 zoomed image (C).

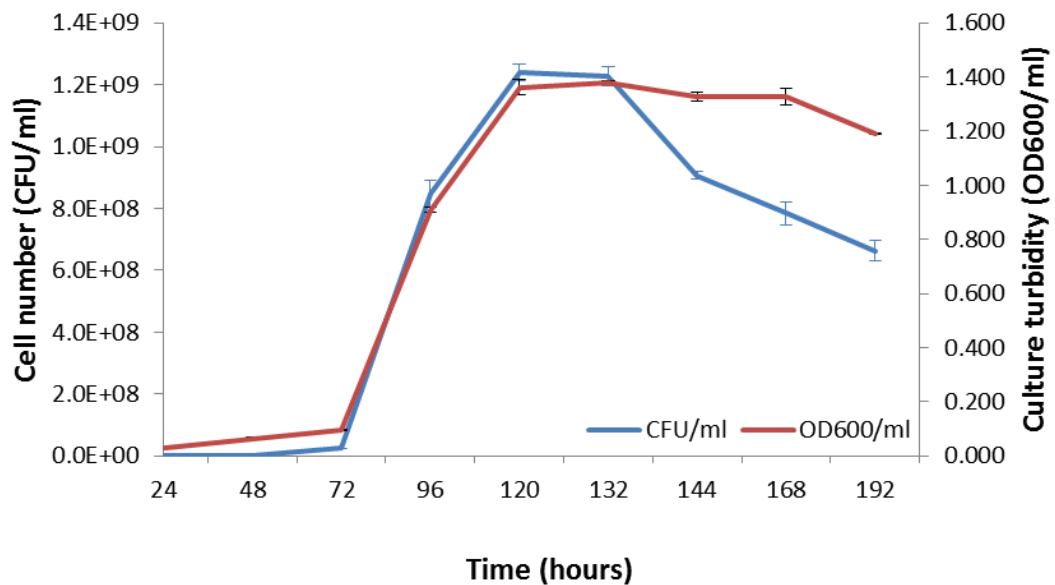


**Figure 5.02:** Growth curve representing the growth of *T. forsythia* in TSB liquid medium over 192 h (9 days). Daily growth of *T. forsythia* was assessed by measuring the absorbance of TSB liquid medium and turbidity of *T. forsythia* cell suspension using OD<sub>600</sub> (right y-axis). At the same time point aliquots of liquid culture were spread on agar medium and grown for the purposes of establishing the number of CFU/ml (left y-axis). The growth curve has a lag, log, stationary and cell death phase. Lag phase lasted approximately 72 h, at which point a rapid exponential growth occurred lasting 48 h. There was a sudden decline in CFU numbers after 132 h. OD<sub>600</sub> measurement showed less decline. Whiskers at each time point represent the standard deviation calculated for three separate cultures per test species measured by OD<sub>600</sub>/ml (blue) and CFU/ml (black).

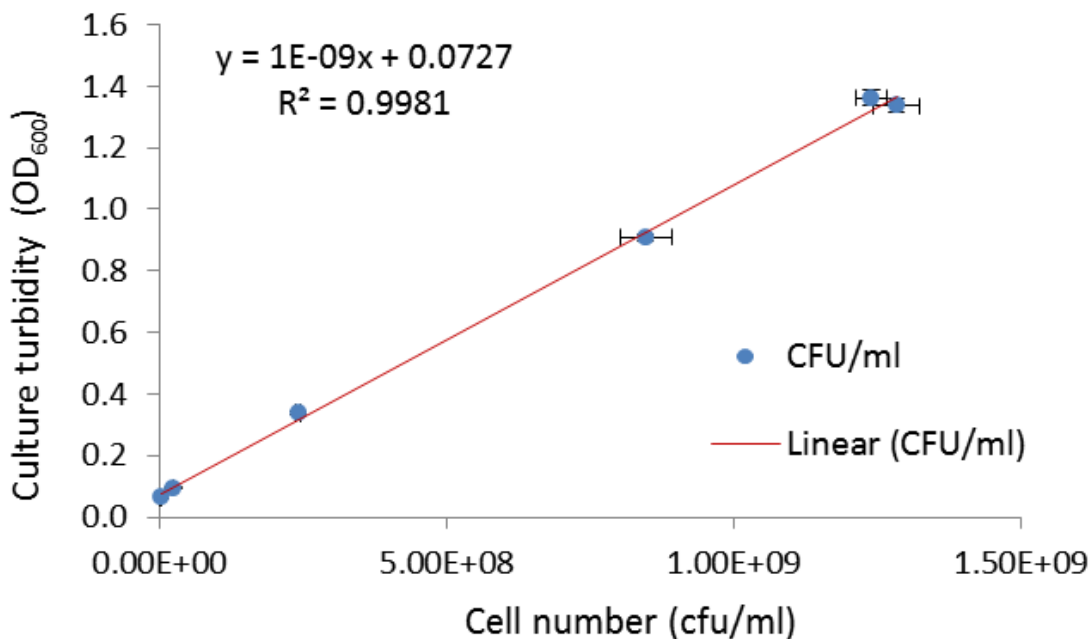


**Figure 5.03:** Shows the linear relationship between number (cfu/ml) vs OD<sub>600</sub> during exponential growth of *T. forsythia*. Whiskers at each time point represent the standard deviation calculated for three separate cultures per test species measured by OD<sub>600</sub>/ml and CFU/ml.

#### 5.3.1.2 *P. gingivalis* (11834 & W50) growth characteristics

Two strains of *P. gingivalis* (11834 and W50) were assessed. Both strains produced large shiny black pigmented colonies that were circular and convex in appearance (figure 5.04a). Colonies from both strains produced  $\beta$ -haemolysis on blood agar plates; however, the haemolysis produced by 11834 colonies was more diffuse compared to W50 colonies. Staining revealed that *P. gingivalis* were extremely small gram-negative coccobacilli (figure 5.04a and b). When inoculated into BHI broth, *P. gingivalis* 11834 showed a very brief lag phase, with exponential growth occurring after 48 h incubation. 11834 showed almost immediate exponential growth and a maximum cell number of  $1.66 \times 10^9$  cells/ml with OD<sub>600</sub> 1.664 (figure 5.05). W50, provided very similar maximum cell numbers  $1.58 \times 10^9$  cells/ml and OD<sub>600</sub> 1.626 (figure 5.08). However, W50 remained in stationary phase for only ~48 h followed by a rapid death phase, whereas 11834 remained in stationary phase for ~12 h followed by moderate cell death. Doubling time for 11834 and W50 were  $t_d = 9.97$  and  $t_d = 10.75$ , with  $r_g = 0.100$  and  $r_g = 0.092$ , respectively. Again, good linear relationships were observed between OD<sub>600</sub> measurements and cfu/ml calculations for both 11834 (figure 5.06) and W50 (figure 5.09), giving lines of best fit equations of  $R^2 0.992$  and  $R^2 0.997$ , respectively. Semi-log regression plots for 11834 and W50 provided

excellent platforms for conversion of OD<sub>600</sub> to cell/ml, where 1 OD<sub>600</sub> unit = 9.5 x 10<sup>8</sup> and 9.0 x 10<sup>8</sup>, respectively.

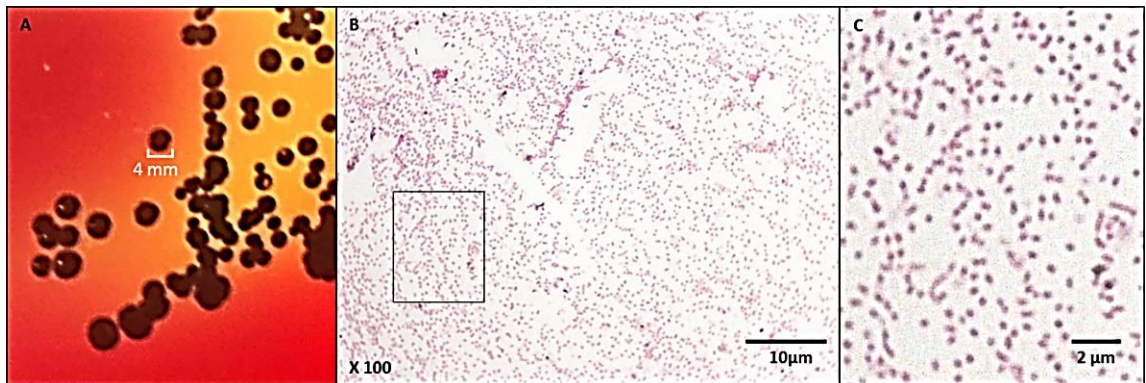


**Figure 5.04:** *P. gingivalis* 11834 grows on blood agar. *P. gingivalis* as black-pigmented colonies on blood agar that showed variation in colony size (A). *P. gingivalis* were Gram-negative small rods (coccobacillus) when viewed at x100 (B) and zoomed to x 500 (C).

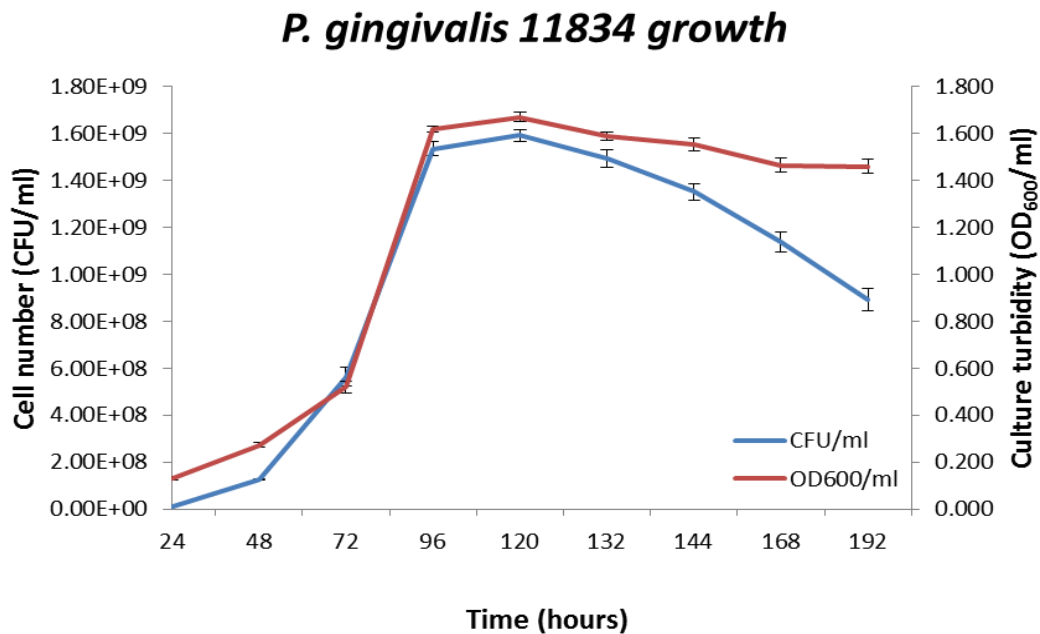


**Figure 5.05:** Growth curve representing the growth of *P. gingivalis* 11834 in BHI liquid medium over 192 h (9 days). Daily growth of 11834 was assessed by measuring the turbidity of 11834 cell suspension using OD<sub>600</sub> (right y-axis). Over the same time course, aliquots of liquid culture were spread on agar medium and grown for the purposes of establishing the number of CFU/ml (left y-axis). The growth curve shows lag, log, stationary and cell death phase for 11834. OD<sub>600</sub> reading shows an almost immediate log growth for 11834, whereas the presence of a lag is more prominent when cfu were counted. Log growth proper, occurs 72 h post inoculation for both modes of measurement. Growth becomes stationary at approximately 96 h of incubation, at which point, cells 11834 begins to die. The maximum growth for 11834 was 2.9 x 10<sup>9</sup> cfu/ml. Whiskers represent standard deviation for OD<sub>600</sub>/ml (blue) and CFU/ml (black). Whiskers at each time point represent the standard deviation calculated for three separate cultures per test species measured by OD<sub>600</sub>/ml (blue) and CFU/ml (black)

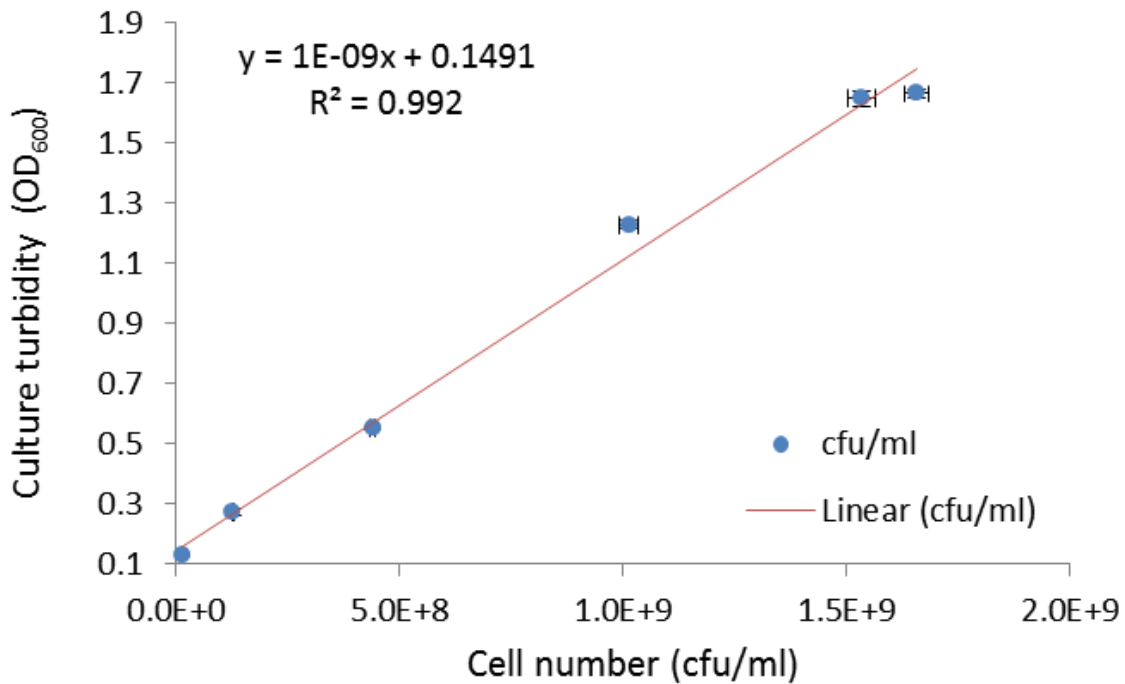


**Figure 5.06:** Shows the linear relationship between bacteria cell number (cfu/ml) vs OD<sub>600</sub> during exponential growth of *P. gingivalis* 11834. Whiskers at each time point represent the standard deviation calculated for three separate cultures per test species measured by OD<sub>600</sub>/ml and CFU/ml.

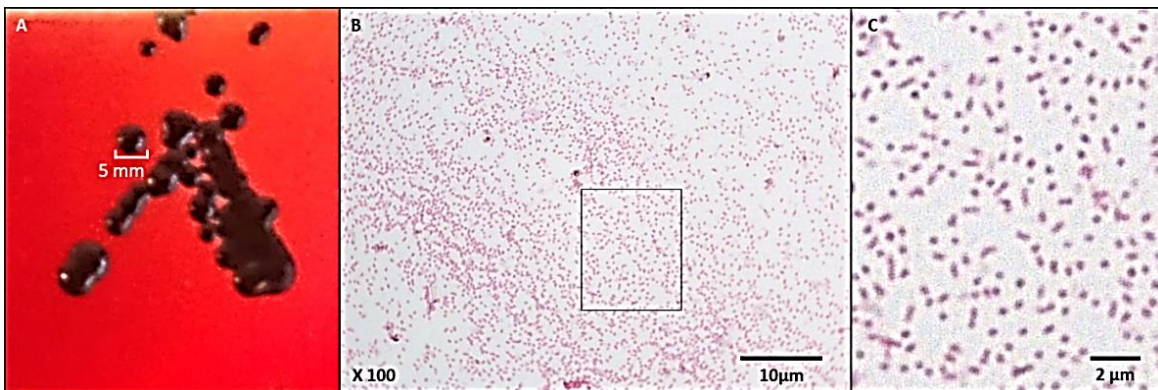


**Figure 5.07:** *P. gingivalis* W50 colonies on blood agar. W50 grows as black-pigmented colonies on blood agar that showed variation in colony size (A). Morphologically, analogous with *P. gingivalis* 11834. *P. gingivalis* W50 were Gram-negative small rods (coccobacillus) when viewed at x100 (B) and zoomed to x 500 (C).

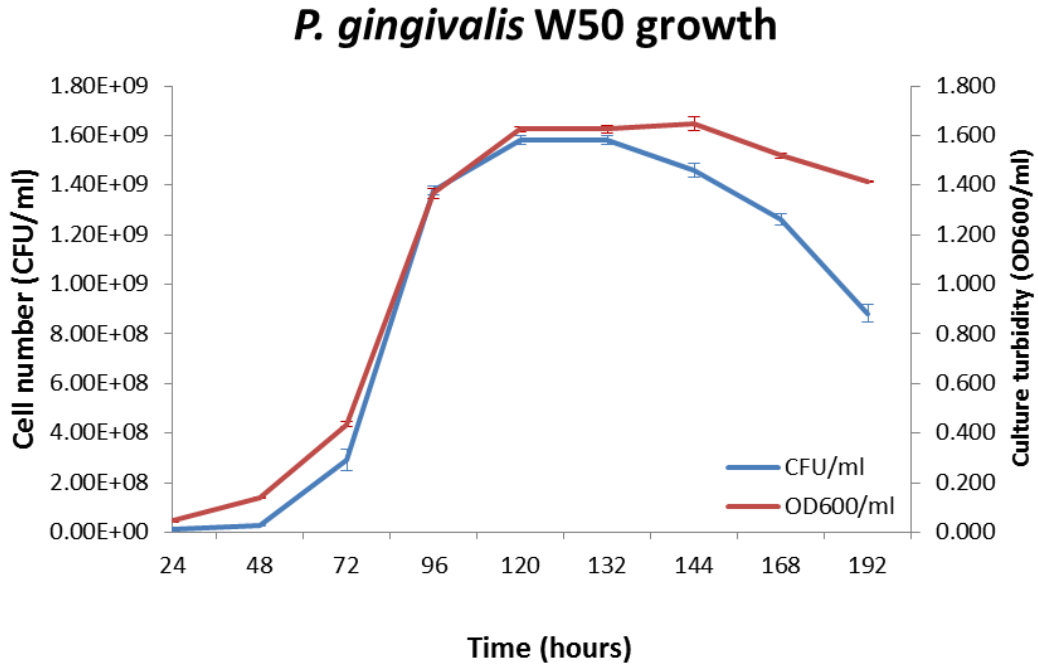


**Figure 5.08:** Growth curve representing the growth of *P. gingivalis* W50 in BHI liquid medium over 192 h (9 days). Daily growth of W50 was assessed by measuring the absorbance of TSB liquid medium and turbidity of W50 cell suspension using OD<sub>600</sub> (right y-axis). Over the same time course, aliquots of liquid culture were spread on agar medium and grown for the purposes of establishing the number of CFU/ml (left y-axis). The growth curve has a lag, log, stationary and cell death phase. Growth of W50 lags for both OD<sub>600</sub> and cfu/ml measurements, lasting 72 h. Exponential growth was short but rapid, lasting 24 h. Growth becomes stationary at approximately 120 h. W50 cells died soon after cell growth plateaued leading to a steep decline in cell numbers, from  $5.8 \times 10^9$  cfu/ml to  $2.8 \times 10^9$  cfu/ml within 24 h. Whiskers represent standard deviation for three separate cultures measured by OD<sub>600</sub>/ml (blue) and CFU/ml (black)

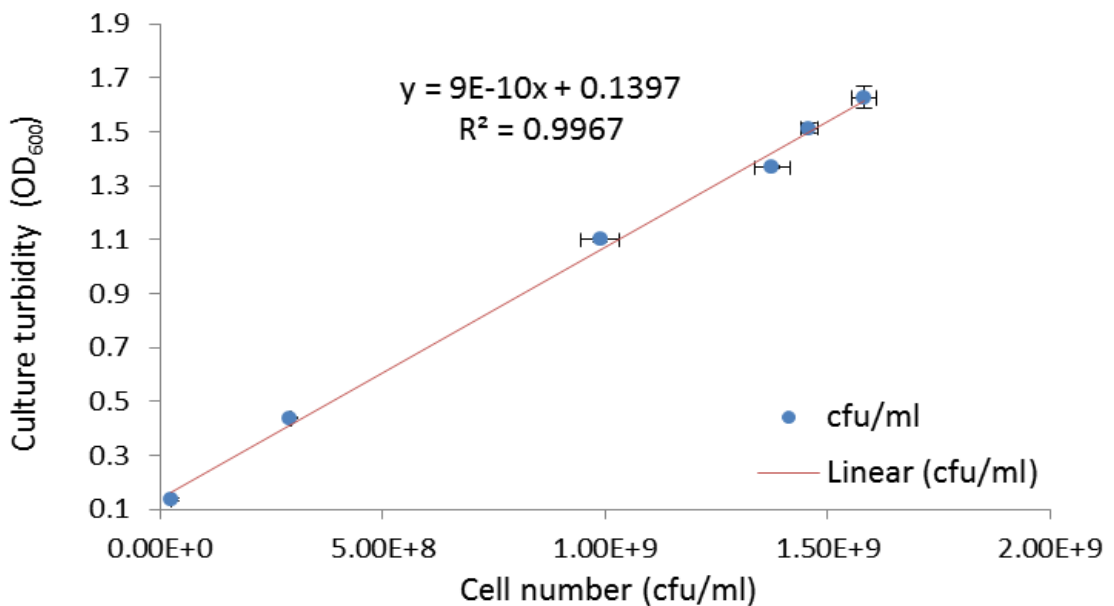


**Figure 5.09:** Shows the linear relationship between number (cfu/ml) vs OD<sub>600</sub> during exponential growth of *P. gingivalis* W50. Whiskers at each time point represent the standard deviation calculated for three separate cultures per test species measured by OD<sub>600</sub>/ml and CFU/ml.

5.3.1.3 *T. denticola* growth characteristics

*T. denticola* produced cream-white hazy colonies, which due to its obligate anaerobic nature grew below the agar surface of semi-solid TYGVS medium (figure 5.10a). Gram-staining revealed the distinctive spirochetes morphology *T. denticola*, which showed gram-negative staining. *T. denticola* cells were pleomorphic, ranging in size from approximately 2  $\mu\text{m}$  to >6  $\mu\text{m}$  (figure 5.10b and c). When incubated in TYGVS medium, growth of *T. denticola* lagged for 72 h before entering log growth, which lasted ~24 h. *T. denticola* had a growth rate of  $r_g = 0.099$  and doubled every  $t_d = 10.05$  h, eventually reaching a maximum cell number of  $1.5 \times 10^9$  cells/ml (figure 5.11). *T. denticola* remained in stationary phase for ~36 h then slowly died over the remaining 48 h. A strong linear relationship between  $\text{OD}_{600}$  measurements and CFU/ml calculations was observed, showing a line of best fit with  $R^2 = 0.99$  (figure 5.11).

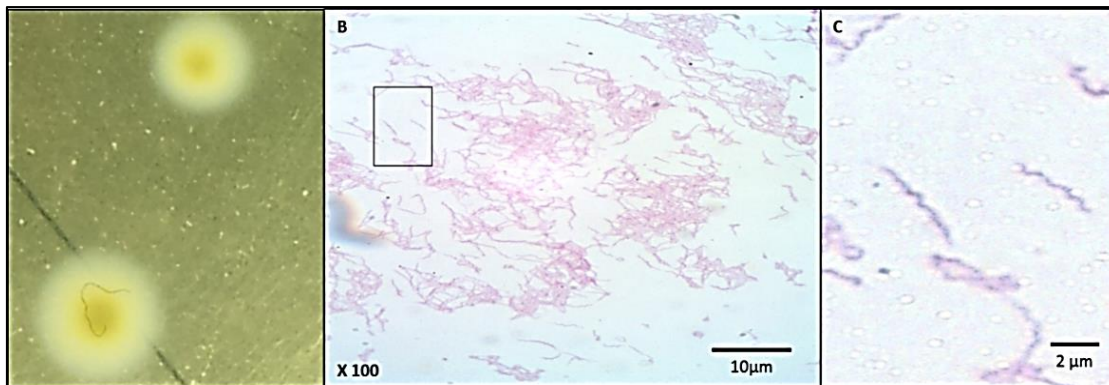


**Figure 5.10:** *T. denticola* colonies on semi-solid TYGVS medium (A). CFU grew below the medium surface rather than on the surface (A). *T. denticola* is a member of the spirochetes phylum, which can be recognised by its helical coil shape (B). The physical length of *T. denticola* ranged from ~2  $\mu\text{m}$  to >6  $\mu\text{m}$  (C).

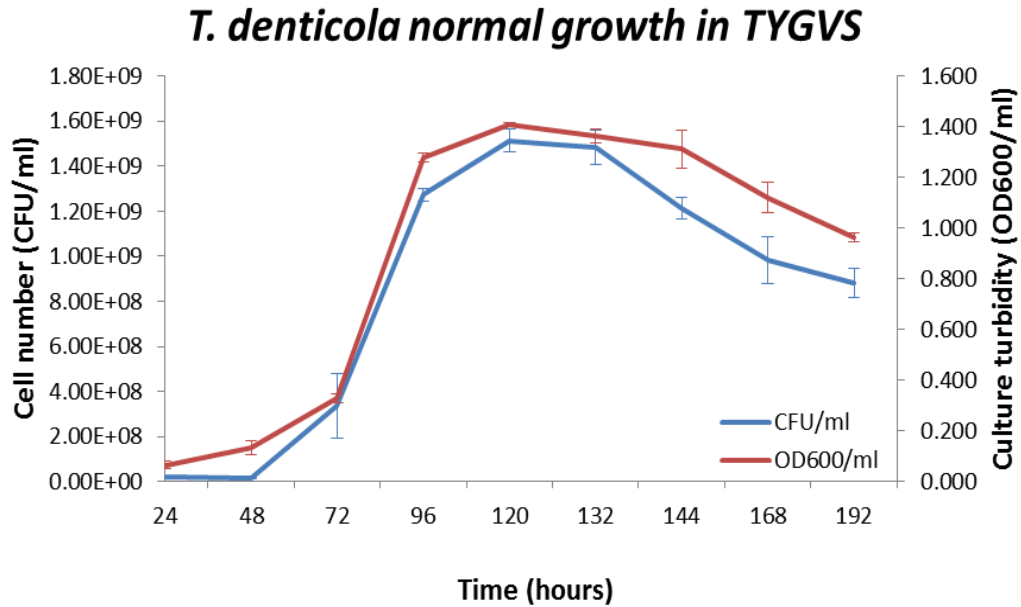


**Figure 5.11:** Growth curve representing the growth of *T. denticola* in TYGVS medium over 192 h (9 days). Daily growth of *T. denticola* was assessed by measuring the culture turbidity of cell suspensions using OD<sub>600</sub> (right y-axis). Over the same time course, aliquots of liquid culture were spread on agar medium and grown for the purposes of establishing the number of CFU/ml (left y-axis). The growth curve for *T. denticola* shows a lag, log, stationary and cell death phase. A growth lag was observed for both OD<sub>600</sub> and cfu/ml measurements, lasting ~72 h. Log growth was short but rapid, lasting 24 h. Growth became stationary at approximately 96 h post-inoculation. *T. denticola* cells died 36 h after cells became stationary (cfu/ml). Stationary phase lasted longer for OD<sub>600</sub> measurements (~72 h), then began to deplete 168 h post-inoculation. Whiskers at each time point represent the standard deviation calculated for three separate cultures per test species measured by OD<sub>600</sub>/ml (blue) and CFU/ml (black)

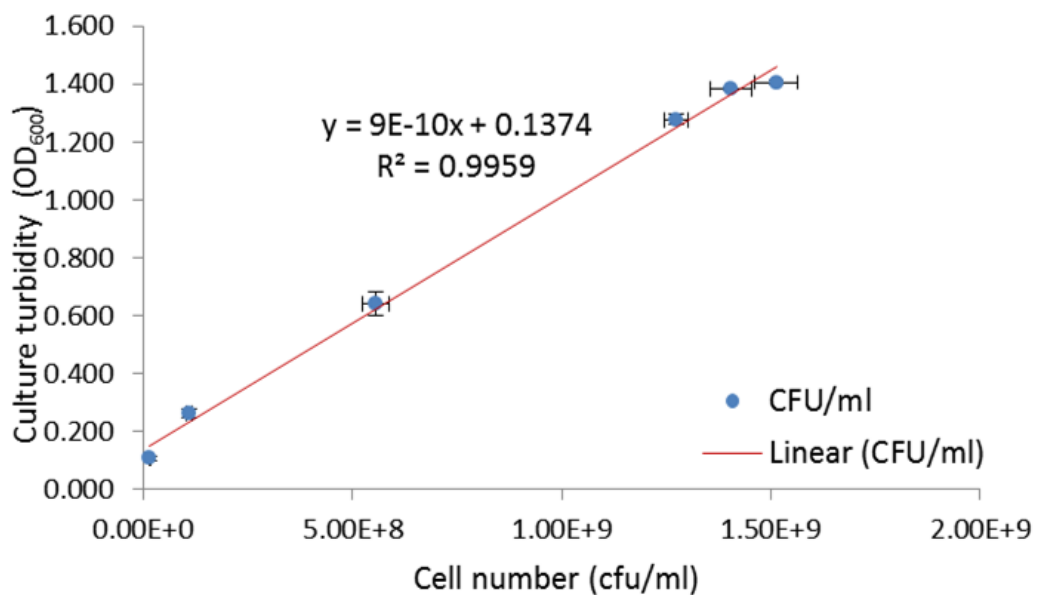


**Figure 5.12:** Shows the linear relationship between number (cfu/ml) vs OD<sub>600</sub> during exponential growth of *T. denticola*. Whiskers represent standard deviation standard deviation for three separate cultures measured by OD<sub>600</sub>/ml and CFU/ml.

	<i>P. gingivalis</i>			
	<i>T. forsythia</i>	11834	W50	<i>T. denticola</i>
# doublings	2.413	1.204	2.231	1.194
Growth rate (h <sup>-1</sup> )	0.101	0.100	0.093	0.099
Doubling time (h)	9.947	9.971	10.760	10.053
1 OD <sub>600</sub> unit (cells/ml)	9.60 x 10 <sup>8</sup>	9.51 x 10 <sup>9</sup>	9.00 x 10 <sup>8</sup>	9.98 x 10 <sup>8</sup>

**Table 5.01:** Shows the number of doublings occurring during the 192 h culture time, growth rate, population doubling time and the cells/ml conversion for 1 optical density unit for *T. forsythia*, *P. gingivalis* (W50 & 11834) and *T. denticola*.

### 5.3.2 Growth of red complex bacteria in alternative media

Medium development was performed in two stages (Materials & Methods; section 2.3.2).

Stage 1. Test the efficacy three media each known to support only pure growth of each test species (*P. gingivalis*, *T. forsythia* and *T. denticola*) for their ability to support all or >1 RCB species; to establish an initial base for further development (Materials & Methods; section 2.3.2.1).

Test species were incubated separately in each complete liquid media, TSB, BHI and TYGVS as three technical replicates cultures for each species in each alternative medium.

TSB medium provided superior support by permitting exponential growth of 3 out of 4 tested species/strains; hence, this medium was selected as the “base medium” for further development. *T. forsythia* showed the greatest growth in TSB (OD<sub>600</sub> 1.322; figure 5.13), followed by *P. gingivalis* W50 (OD<sub>600</sub> 1.199; figure 5.13) and 11834 (OD<sub>600</sub> 0.945; figure 5.13). BHI broth provided support for only *P. gingivalis* 11834 and W50, giving a final maximum OD<sub>600</sub> value of 1.604 and 1.627, respectively (figure 5.14). Finally, TYGVS, provided support for *T. denticola*, (OD<sub>600</sub> 1.461; figure 5.15) and *P. gingivalis* W50 (OD<sub>600</sub> 0.892 figure 5.15).

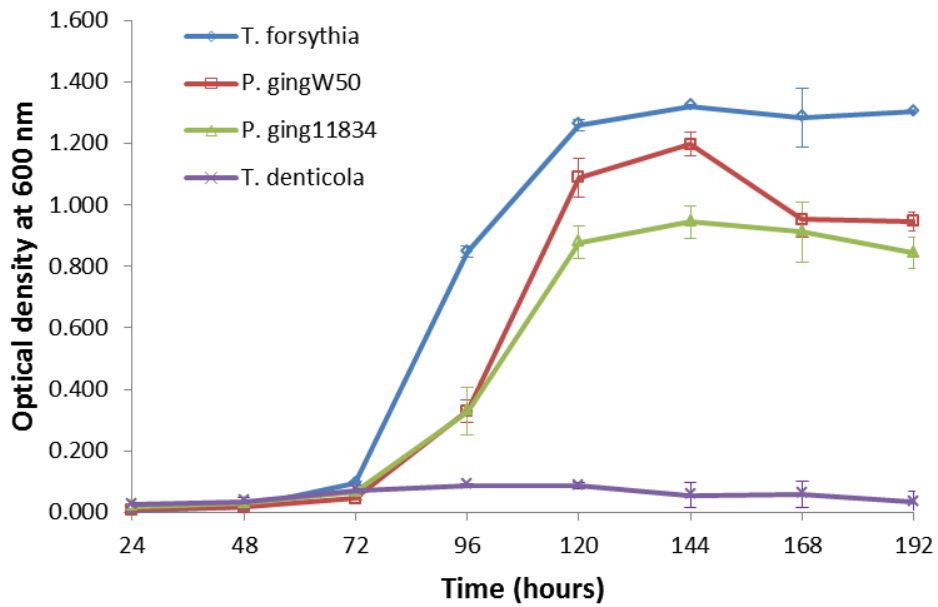


**Figure 5.13:** Shows the mean OD<sub>600</sub> values of RCB cultured in TSB medium for 8 days. Each line represents the mean OD<sub>600</sub> values calculated from three technical replicate cultures of each species. Whiskers at each time point represent the standard deviation calculated for three separate cultures per test species measured by OD<sub>600</sub>/ml

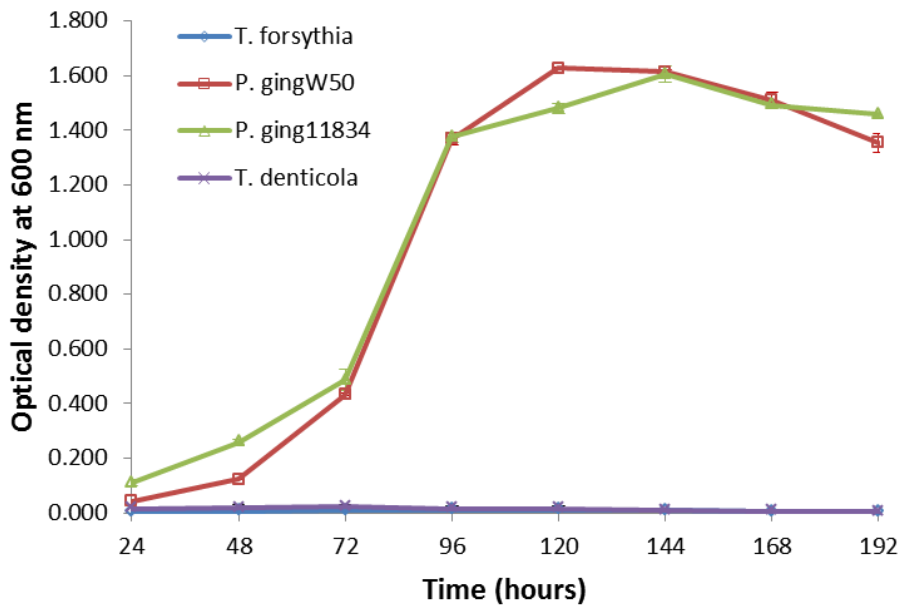


**Figure 5.14:** Shows the mean OD<sub>600</sub> values of RCB cultured in BHI broth for 8 days. Each line represents the mean OD<sub>600</sub> values calculated from three technical replicate cultures of each species. Whiskers at each time point represent the standard deviation calculated for three separate cultures per test species measured by OD<sub>600</sub>/ml

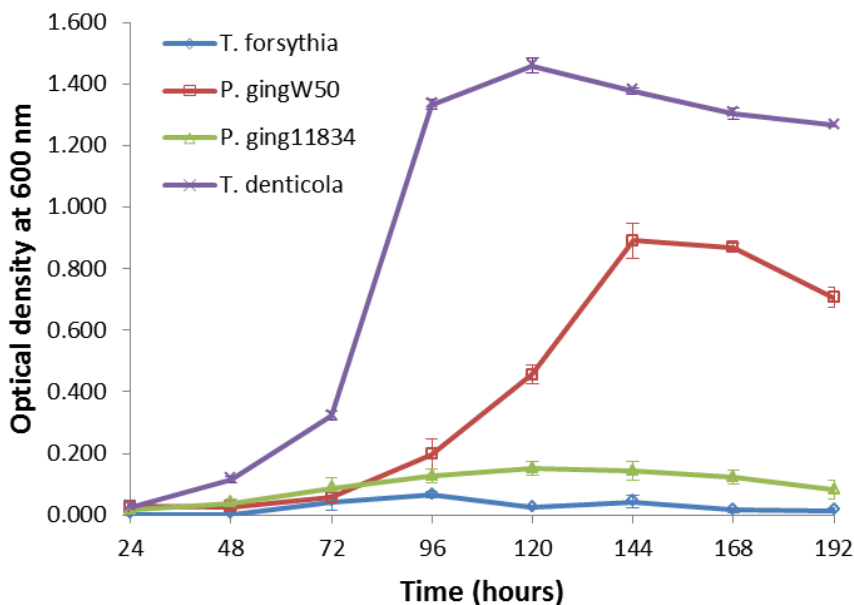


**Figure 5.15:** Shows the mean OD<sub>600</sub> values of RCB cultured in TYGVS medium for 8 days. Each line represents the mean OD<sub>600</sub> values calculated from three technical replicate cultures of each species. Whiskers at each time point represent the standard deviation calculated for three separate cultures per test species measured by OD<sub>600</sub>/ml.

### 5.3.3 Development & optimisation of a Tryptic Soy base medium for the growth of periodontal bacteria

The second stage of medium development involved building upon the most efficacious medium established in stage 1, through the stepwise incorporation of additional media supplements (Materials & Methods; section 2.3.2.2). TSB medium (comprising: 5 µg/ml hemin, 1 µg/ml menadione, 1 µg/ml L-cysteine-HCL, 0.4% (w/v) yeast extract and 10 µg/ml *N*-acetyl muramic acid (NAM)) was established as the most supportive medium in stage 1 (3 of 4 species) and was therefore used as a “base medium” for further development to establish a medium that can support the growth of all test species.

Since, *T. denticola* was the only species that failed to culture in TSB (figure 5.13); emphasis was placed on incorporating growth supplements that are known to support the growth of *T. denticola*. Stage 2 medium design involved the following,

1. Measure growth (OD<sub>600</sub>) of each RCB species in base media prepared with a concentration gradient of each medium supplement being assessed (table 5.02). Presented as bar graphs.

2. Establish the lowest possible supplement concentration that supports significant bacterial growth compared to control medium by ANOVA, Levenes's and Student's t test (bar graphs).
3. Incorporate optimal supplement concentration into medium and measure bacterial growth curves to assess growth as medium constituents increase (line graphs).

In all cases OD<sub>600</sub> values were recorded by calculating the mean of three (n=3) technical replicate cultures for each test species in each medium containing increasing supplement concentrations. Values were obtained during late-log, early-plateau growth phase, when bacterial numbers were at their greatest. As an optimum supplement concentration was identified, that supplement was included as part of the main medium prior to the next round of supplement testing. Table 5.03 details the evolution of TSB medium, listing each optimum media supplement concentration established after each round of gradient testing. There was no particular advantage to testing the different supplements in the order they were tested here.

Medium supplements	Concentration gradient					Prepared in Medium
	#1	#2	#3	#4	#5	
(NH <sub>4</sub> ) <sub>2</sub> SO <sub>4</sub> (mg/ml)	NC	0.25	0.5	0.75	1	TSB base
K <sub>2</sub> HPO <sub>4</sub> (mg/ml)	NC	1	1.25	1.5	1.75	A
NaCl <sub>2</sub> (mg/ml)	NC	0.5	0.75	1	1.25	B
VFA solution (%)	NC	4	6	8	10	C
Thiamine pyrophosphate (µg/ml)	NC	12.5	13	13.5	14	D
Sodium pyruvate (µg/ml)	NC	225	250	275	300	E
Rabbit serum (%)	NC	5	10	15	-	F

**Table 5.02:** Taken from section 2.3.2 materials & method. Medium supplements for stage 2 of the medium development are listed in the left-hand column, in order of assessment. A concentration gradient of each medium supplement (columns #1 – #5) was tested to establish the optimum concentration for bacterial growth. Farthest right column details the medium each concentration gradient was prepared in (A – F). Bacterial growth in media containing each supplement concentration was compared to bacterial growth in a negative control medium (NC; column #1). Negative control medium comprised all preceding optimum supplement concentrations, minus the supplement being tested or subsequently untested supplements.

## Optimal media supplement concentrations

	A	B	C	D	E	F	G
Media composition	(NH <sub>4</sub> ) <sub>2</sub> SO <sub>4</sub> <i>0.5 mg/ml</i>						
	-	<b>K<sub>2</sub>HPO<sub>4</sub></b> <i>2.25 mg/ml</i>					
	-	-	<b>NaCl<sub>2</sub></b> <i>1 mg/ml</i>				
	-	-	-	<b>VFA</b> <b>6%</b>	<b>VFA</b> <b>6%</b>	<b>VFA</b> <b>6%</b>	<b>VFA</b> <b>6%</b>
	-	-	-	-	<b>TPP</b> <i>12.5 µg/ml</i>	<b>TPP</b> <i>12.5 µg/ml</i>	<b>TPP</b> <i>12.5 µg/ml</i>
	-	-	-	-	-	<b>SP</b> <i>250 µg/ml</i>	<b>SP</b> <i>250 µg/ml</i>
	-	-	-	-	-	-	<b>RS</b> <i>10%</i>

**Table 5.03:** Shows the sequential development of experimental TSB medium supplements (media A – G). Optimum supplement concentrations (*italicised*) were established from OD<sub>600</sub> values calculated as the mean of three technical replicate cultures for each test species in each medium containing increasing supplement concentrations. The supplement concentration that provided the greatest mean bacterial growth at the lowest possible concentration was selected. The optimum concentration of each supplement was then included as part of the base medium prior to the next round of gradient testing. (NH<sub>4</sub>)<sub>2</sub>SO<sub>4</sub> (Ammonium Sulphate), K<sub>2</sub>HPO<sub>4</sub> (Potassium Phosphate), NaCl (Sodium Chloride), VFA (volatile fatty acid), TPP (thiamine pyrophosphate), SP (sodium pyruvate) and RS (rabbit serum).

5.3.3.1 Major inorganic salts for *T. denticola* growth

Firstly, all major inorganic salts used in TYGVS medium that are known to support growth of *T. denticola*, were individually omitted from TYGVS in an effort to identify the salts critical for *T. forsythia* growth. The removal of (NH<sub>4</sub>)<sub>2</sub>SO<sub>4</sub>, K<sub>2</sub>HPO<sub>4</sub> and NaCl had visible effect on the growth of *T. denticola*, whereas removal of MgSO<sub>4</sub> did not affect the growth of *T. denticola* (figure 5.16).

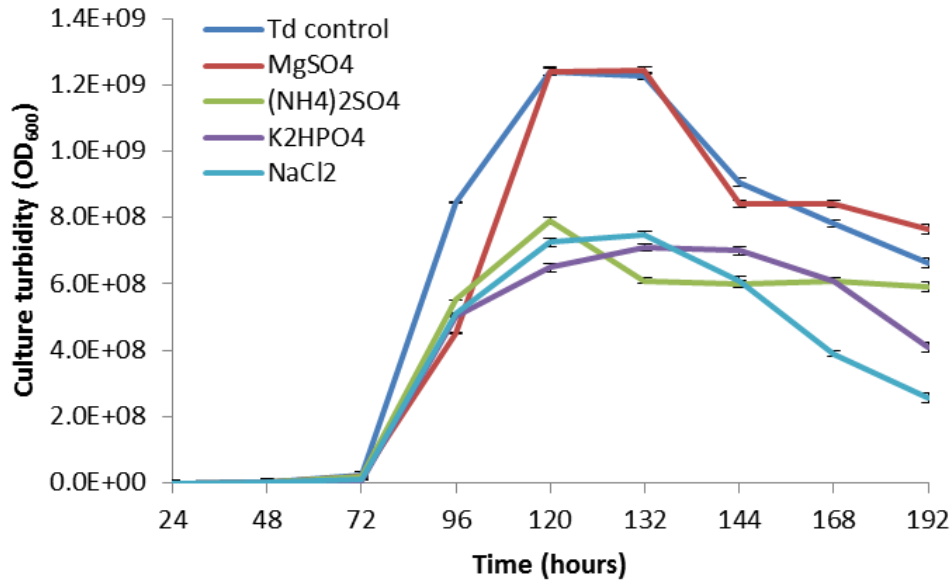


**Figure 5.16:** Growth curves of *T. denticola* in TYGVS medium following the individual removal of each inorganic salt. The removal of  $(\text{NH}_4)_2\text{SO}_4$ ,  $\text{K}_2\text{HPO}_4$  and  $\text{NaCl}$  had an effect on the growth of *T. denticola*, whereas removal of  $\text{MgSO}_4$  does not affect the growth of *T. denticola*. *T. denticola* was cultured in four individual media containing all supplements excluding the salt being assessed. Each line on the chart represents the mean values for three technical replicates which were compared to the normal growth of *T. denticola* (Td control) in TYGVS containing all salts. Whiskers at each time point represent the standard deviation calculated for three separate cultures per test species measured by  $\text{OD}_{600}/\text{ml}$ .

### 5.3.3.2 TSB base medium: concentration gradient of $(\text{NH}_4)_2\text{SO}_4$

Stage 2 began by measuring test species growth when cultured in base media containing a concentration gradient of  $(\text{NH}_4)_2\text{SO}_4$ .  $\text{OD}_{600}$  values for *T. denticola* increased significantly in response to  $(\text{NH}_4)_2\text{SO}_4$  ( $p < 0.05$ ; figure 5.17). *P. gingivalis* 11843 & W50 also showed a significantly increased  $\text{OD}_{600}$  values in TSB comprising  $\geq 0.25$  mg/ml  $(\text{NH}_4)_2\text{SO}_4$  compared to control medium ( $p < 0.001$ ; figure 5.17). Growth plateaued in media containing  $\geq 0.75$  mg/ml  $(\text{NH}_4)_2\text{SO}_4$  for all species except W50, which showed dose-dependant growth ( $p < 0.001$ ; figure 5.17). Because there was only a difference of 0.080 between *T. denticola*  $\text{OD}_{600}$  values in response to 0.5 and 1 mg/ml  $(\text{NH}_4)_2\text{SO}_4$ , the lowest significant result was examined further by growth curve analysis (medium A; figure 5.18)

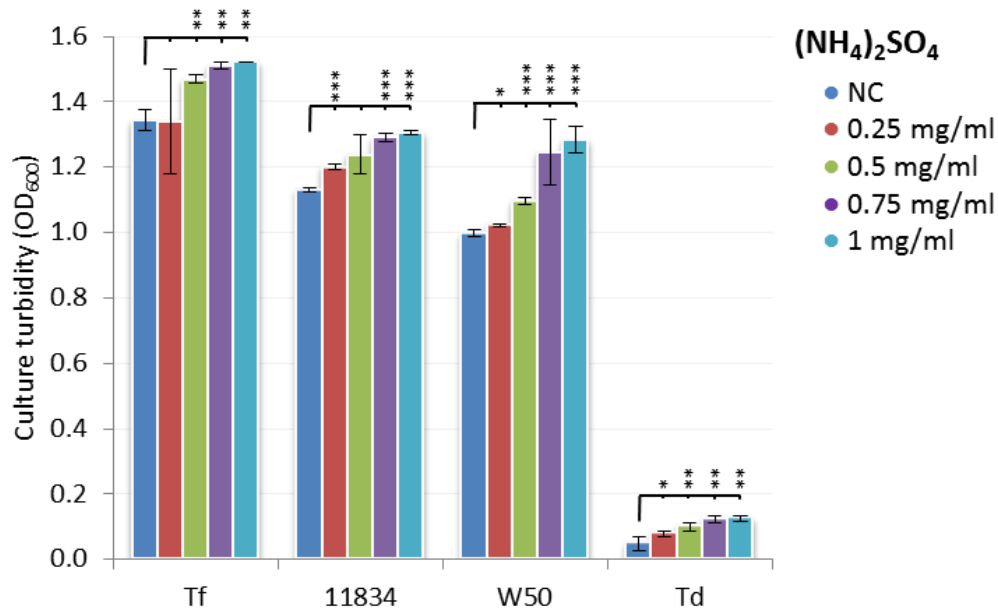


**Figure 5.17:** Bar chart shows the mean (n = 3) culture turbidity readings (OD<sub>600</sub>) for *T. forsythia* (Tf), *P. gingivalis* (11843 & W50) and *T. denticola* (Td) growth incubated in a ‘base’ medium supplemented with 0.25, 0.5, 0.75 or 1 mg/ml (NH<sub>4</sub>)<sub>2</sub>SO<sub>4</sub>. OD<sub>600</sub> measurements were recorded during late-log, early-plateau growth phase when bacteria numbers were at their greatest. OD<sub>600</sub> values for media containing (NH<sub>4</sub>)<sub>2</sub>SO<sub>4</sub> were compared to control medium (without (NH<sub>4</sub>)<sub>2</sub>SO<sub>4</sub>). Significant, dose-dependent increases of OD<sub>600</sub> was observed for all species in media with elevated (NH<sub>4</sub>)<sub>2</sub>SO<sub>4</sub> concentrations compared to a control medium (p < 0.01). OD<sub>600</sub> values plateaued for media containing ≥0.75 mg/ml (NH<sub>4</sub>)<sub>2</sub>SO<sub>4</sub>. Each bar represents the mean OD<sub>600</sub> value of three technical replicate cultures for each species in each medium of increasing supplement concentration

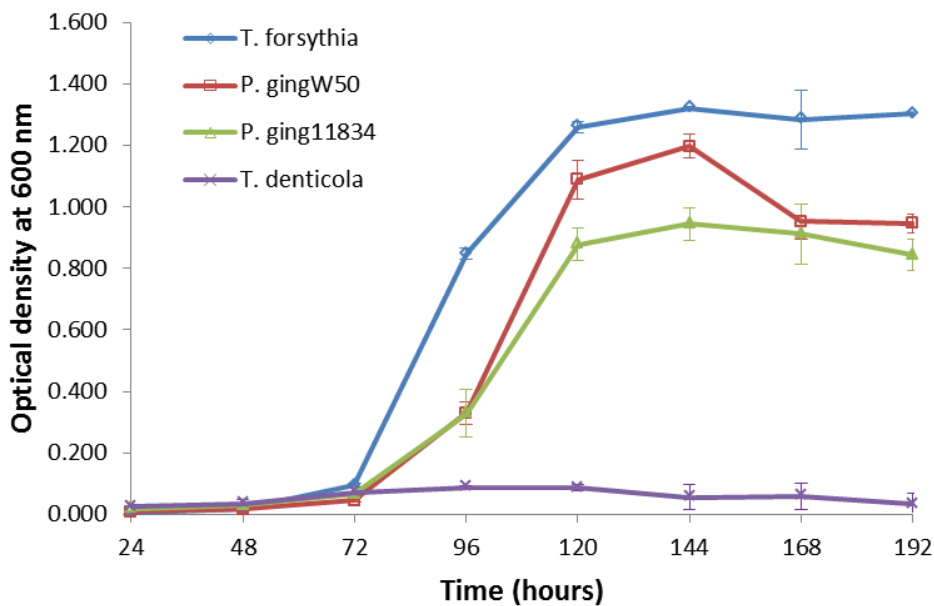


**Figure 5.18:** Growth curve for all species in medium A. Healthy exponential growth was observed for all species, except *T. denticola*, which showed a negligible rise of OD<sub>600</sub> < 0.13. TSB containing 1.25 mg/ml (NH<sub>4</sub>)<sub>2</sub>SO<sub>4</sub> supported maximum growth of *T. forsythia* (OD<sub>600</sub> > 1.5). Growth curves for *P. gingivalis* 11834 & W50 were comparable, with OD<sub>600</sub> 1.318 & 1.363, respectively. Each line represents OD<sub>600</sub> values taken as a mean of three technical replicate cultures of each test species incubated in medium A. Whiskers at each time point represent the standard deviation calculated for three separate cultures per test species measured by OD<sub>600</sub>/ml.

5.3.3.3 Medium A: concentration gradient of K<sub>2</sub>HPO<sub>4</sub>

Medium A containing increasing concentrations of K<sub>2</sub>HPO<sub>4</sub> was assessed. OD<sub>600</sub> values increased significantly in response to  $\geq 2.25$  mg/ml K<sub>2</sub>HPO<sub>4</sub> for *T. forsythia* ( $p < 0.001$ ), 11834 ( $p < 0.05$ ), W50 ( $p < 0.001$ ) and *T. denticola* ( $p < 0.05$ ; figure 5.19) compared to control media. OD<sub>600</sub> values for *T. forsythia* and 11834 or W50 did not show further increases when cultured in media containing  $> 2.25$  mg/ml K<sub>2</sub>HPO<sub>4</sub>. In actuality, *T. forsythia* showed significantly decreased OD<sub>600</sub> values with K<sub>2</sub>HPO<sub>4</sub> concentrations  $> 2.25$  ( $p < 0.01$  figure 5.19). *T. denticola* showed a dose-dependent increase in OD<sub>600</sub> values that plateaued at concentrations of K<sub>2</sub>HPO<sub>4</sub>  $> 2.5$  mg/ml (figure 5.19). Therefore, the lowest possible significant increase was in media containing 2.25 mg/ml and therefore was assessed further by measuring growth curves (medium B; figure 5.20).

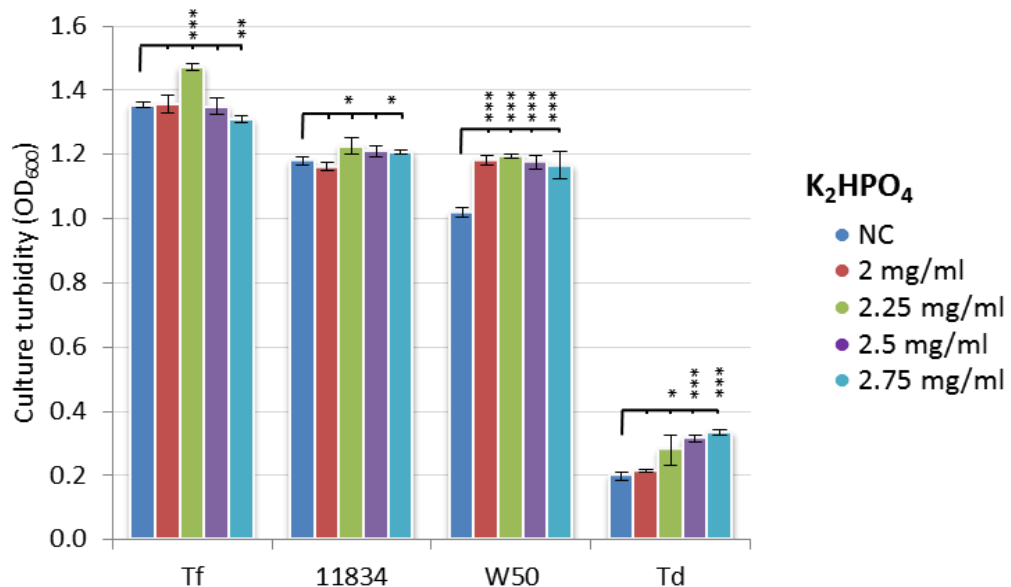


**Figure 5.19:** Bar graph shows the mean culture turbidity readings (OD<sub>600</sub>) for *T. forsythia* (Tf), *P. gingivalis* (11843 & W50) and *T. denticola* (Td) when incubated in base medium supplemented with conc. gradient of K<sub>2</sub>HPO<sub>4</sub> compared to control medium (without K<sub>2</sub>HPO<sub>4</sub>). Significant, dose-dependent increase of OD<sub>600</sub> for Td in medium A containing  $\geq 2.25$  mg/ml K<sub>2</sub>HPO<sub>4</sub> compared to control medium ( $p < 0.05$ ). At  $\geq 2.5$  mg/ml K<sub>2</sub>HPO<sub>4</sub>, Td increased significantly, from OD<sub>600</sub> 0.198 to 0.333 ( $p < 0.001$ ). Tf increased significantly, when incubated with 2.25 mg/ml K<sub>2</sub>HPO<sub>4</sub> (OD<sub>600</sub> 1.354 to 1.473;  $p < 0.001$ ). At doses  $> 3$   $\mu$ g/ml K<sub>2</sub>HPO<sub>4</sub>, Tf suffered mild inhibitory effects ( $p < 0.01$ ). 11834 peaked at 2.25 mg/ml K<sub>2</sub>HPO<sub>4</sub> (OD<sub>600</sub> 1.226;  $p < 0.05$ ), as did W50, which also showed the greatest increase (OD<sub>600</sub> 1.088 to 1.196;  $p < 0.001$ ). Each bar represents the mean OD<sub>600</sub> value of three technical replicate cultures for each species in each medium of increasing supplement concentration.

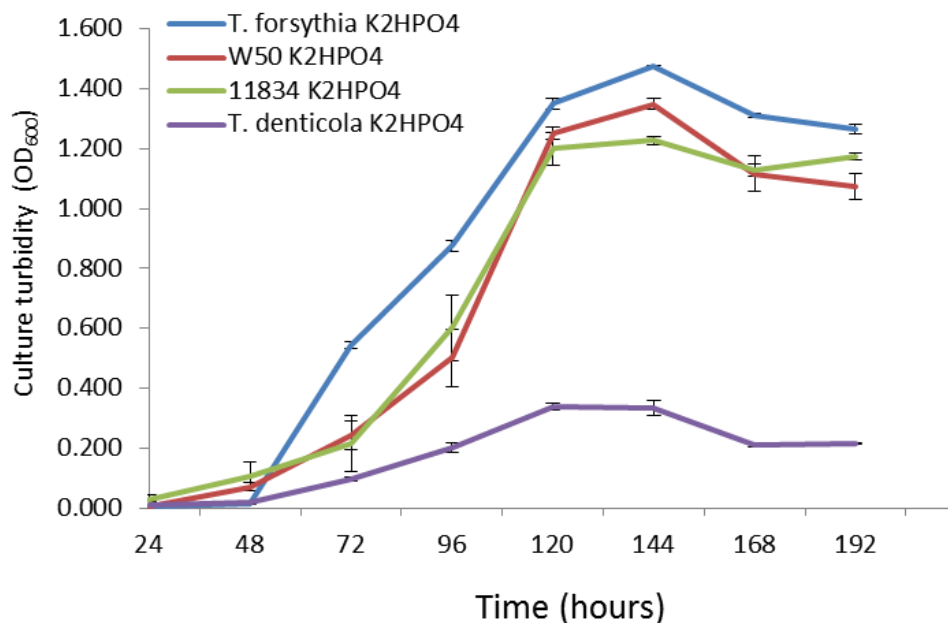


**Figure 5.20:** Shows growth curves for each test species incubated in medium B (containing 0.5 mg/ml  $(\text{NH}_4)_2\text{SO}_4$  and including 2.25 mg/ml  $\text{K}_2\text{HPO}_4$ ; table 5.03). Healthy exponential growth was observed for *T. forsythia* and *P. gingivalis* (11843 & W50), with maximum  $\text{OD}_{600}$  values 1.437, 1.226 and 1.348, respectively. Maximum  $\text{OD}_{600}$  values for *T. denticola* increased compared to medium A; increasing by  $\text{OD}_{600}$  0.207. The subtle outline of typical bacterial growth phases can be observed for *T. denticola* growth in medium B, though *T. denticola* is only partially supported in medium B. Each line represents  $\text{OD}_{600}$  values taken as a mean of three technical replicate cultures of each test species incubated in medium B. Whiskers at each time point represent the standard deviation calculated for three separate cultures per test species measured by  $\text{OD}_{600}/\text{ml}$ .

#### 5.3.3.4 Medium B: concentration gradient of $\text{NaCl}_2$

When media containing a gradient of  $\text{NaCl}_2$  was assessed, all species showed a significant dose-dependent increase of  $\text{OD}_{600}$  values when supplemented with  $\geq 0.75$   $\text{NaCl}_2$  ( $p < 0.05$ ; figure 5.21). When growth curves were plotted for  $\text{OD}_{600}$  values of each species in medium C (table 5.03), good exponential growth was observed for *T. forsythia* and *P. gingivalis* (11834 & W50) (figure 5.22). Growth plateaued in media containing  $> 1$  mg/ml  $\text{NaCl}_2$ , with just and  $\text{OD}_{600}$  of 0.008 between 1 and 1.25 mg/ml. Therefore, 1 mg/ml  $\text{NaCl}_2$  was assessed further by performing growth curve analysis (medium C; figure 5.22)

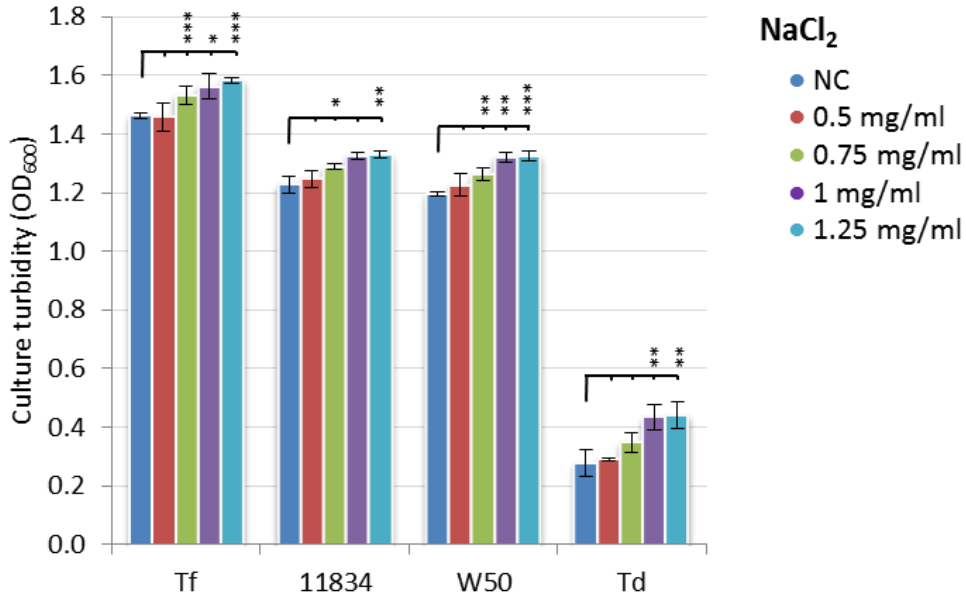


**Figure 5.21:** Bar chart shows the mean (n = 3) culture turbidity readings (OD<sub>600</sub>) for *T. forsythia* (Tf), *P. gingivalis* (11843 & W50) & *T. denticola* (Td) when incubated in medium B supplemented with a conc gradient of NaCl<sub>2</sub> or without NaCl<sub>2</sub> (control). Dose-dependent increases of OD<sub>600</sub> values were observed for all species. OD<sub>600</sub> values for Td, increased significantly compared to control medium when incubated in medium B supplemented with ≥1 mg/ml NaCl (OD<sub>600</sub> 0.279 to 0.441; p. <0.01). OD<sub>600</sub> values for 11834 & W50 were comparable & significantly higher in medium B with ≥0.5 mg/ml NaCl compared to control medium (p <0.05). Tf also had a significantly greater OD<sub>600</sub> values in media containing ≥0.5 mg/ml NaCl compared to control media (p <0.001). Each bar represents the mean OD<sub>600</sub> value of three technical replicate cultures for each species in each medium of increasing supplement concentration.

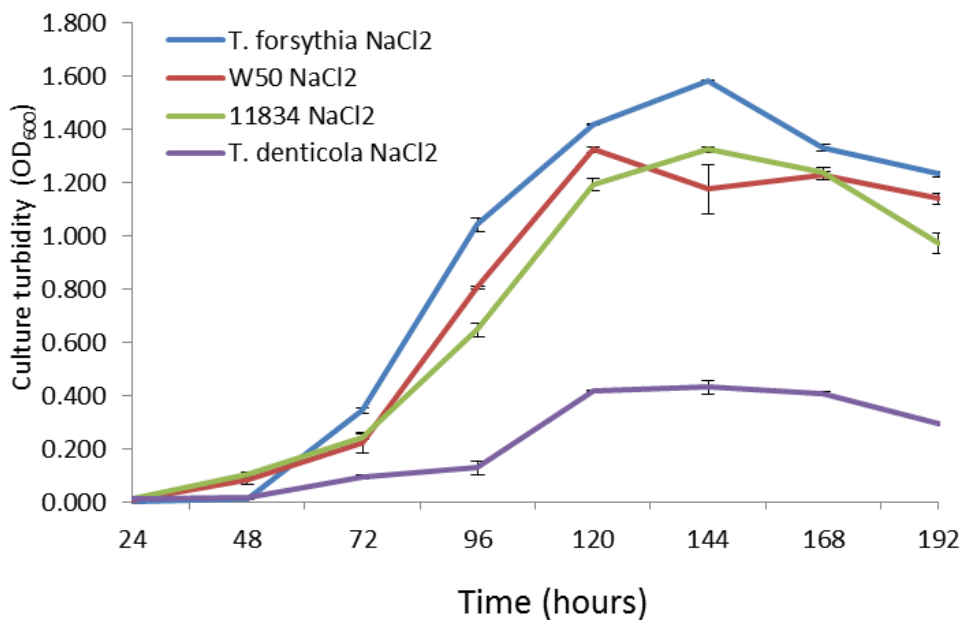


**Figure 5.22:** Shows growth curves for all test species incubated in TSB medium containing all preceding optimum supplement concentrations, including 1 mg/ml NaCl<sub>2</sub>, (medium B; table 5.03). Maximum OD<sub>600</sub> values for *T. forsythia* and *P. gingivalis* (11843 & W50), were increased compared to medium B; rising by 0.273, 0.121 and 0.158, respectively. *T. denticola* also showed an increase of maximum OD<sub>600</sub> values compared to the medium B; from OD<sub>600</sub> 0.333 to 0.441. Each line represents OD<sub>600</sub> values taken as a mean of three technical replicate cultures of each test species incubated in medium C. Whiskers at each time point represent the standard deviation calculated for three separate cultures per test species measured by OD<sub>600</sub>/ml.

## 5.3.3.5 Medium C: concentration gradient of volatile fatty acid solution

VFA solution provided the greatest increase of *T. denticola* growth compared to all other supplements tested here. OD<sub>600</sub> values for *T. denticola* increased significantly in response to all VFA concentrations (figure 5.23). The opposite was observed for *T. forsythia*, 11834 and W50, showing significantly decreased OD<sub>600</sub> values when incubated with  $\geq 4\%$  VFA solution ( $p < 0.001$ ; figure 5.23). Given the conflicting effects of VFA solution on the different species tested, the lowest possible significant increase of *T. denticola* OD<sub>600</sub> (i.e. 6% VFA) was selected for further assessment by growth curve analysis (Medium D; figure 5.24).

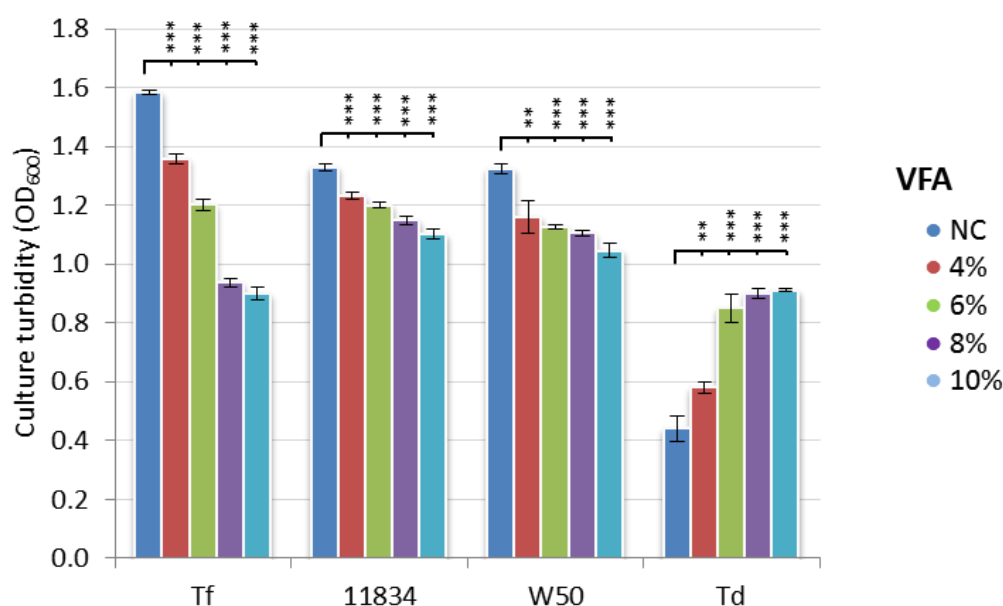


**Figure 5.23:** Bar chart shows the mean ( $n = 3$ ) culture turbidity readings (OD<sub>600</sub> for *T. forsythia* (Tf), *P. gingivalis* (11843 & W50) and *T. denticola* (Td)) in late-log, early-plateau growth phase when incubated in ‘medium C’ supplemented with 4, 6, 8 or 10% volatile fatty acid (VFA) solution or medium without VFA (control). A sharp increase of OD<sub>600</sub> values was observed for Td when incubated in TSB supplemented with 4% VFA (0.432 to 580;  $p < 0.01$ ), 6% (0.849;  $p < 0.001$ ), 8% (0.901;  $p < 0.001$ ) and 10% (0.911;  $p < 0.001$ ). Tf, 11834 and W50 OD<sub>600</sub> values decreased significantly when incubated with  $\geq 4\%$  VFA solution ( $p < 0.001$ ). Tf showed the greatest decrease of OD<sub>600</sub> values from 1.583 (no VFA) to 0.898 (10% VFA;  $p < 0.001$ ). Tf, 11834 and W50 OD<sub>600</sub> values decreased significantly when incubated with  $\geq 4\%$  VFA solution ( $p < 0.001$ ). Each bar represents the mean OD<sub>600</sub> value of three technical replicate cultures for each species in each medium of increasing supplement concentration.

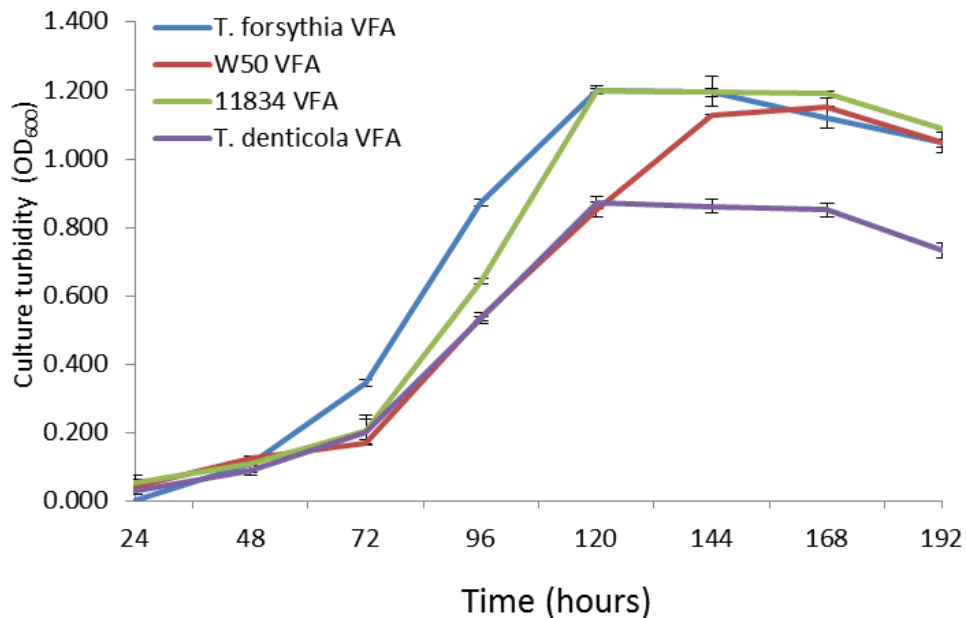


**Figure 5.24:** Shows growth curves for all test species incubated in TSB medium containing all preceding optimum supplement concentrations, including 6% VFA solution, (medium D; table 5.03). A marked reduction of maximum OD<sub>600</sub> values was observed for *T. forsythia* (1.583 to 1.201), 11834 (1.325 to 1.198) and W50 (1.263 to 1.126) when compared to the previous growth curves in ‘medium C’. Maximum OD<sub>600</sub> values doubled for *T. denticola* (OD<sub>600</sub> 0.441 to 0.911) when cultured in ‘medium D’ compared to medium C. Healthy exponential growth was observed for *T. denticola* when incubated in medium D, which showed double the maximum OD<sub>600</sub> values (OD<sub>600</sub> 0.441 to 0.911) compared to medium C. Each line represents OD<sub>600</sub> values taken as a mean of three technical replicate cultures of each test species incubated in medium D. Whiskers at each time point represent the standard deviation calculated for three separate cultures per test species measured by OD<sub>600</sub>/ml.

### 5.3.3.6 Medium D: concentration gradient of thiamine pyrophosphate

In medium D containing increasing concentrations of thiamine pyrophosphate (TPP), *P. W50* OD<sub>600</sub> values were significantly greater in response to 12.5 (figure 5.25). *T. denticola* OD<sub>600</sub> values also increased significantly when cultured in the medium supplemented with 12.5 µg/ml TPP compared to the negative control medium OD<sub>600</sub> values ( $p < 0.05$ ). *T. denticola* growth was similar across all concentrations; 12.5 µg/ml TPP was the only concentration to support a significant increase in *T. denticola* compared to control media and was therefore selected for further assessment by performing growth curve analysis (medium E; figure 5.26).

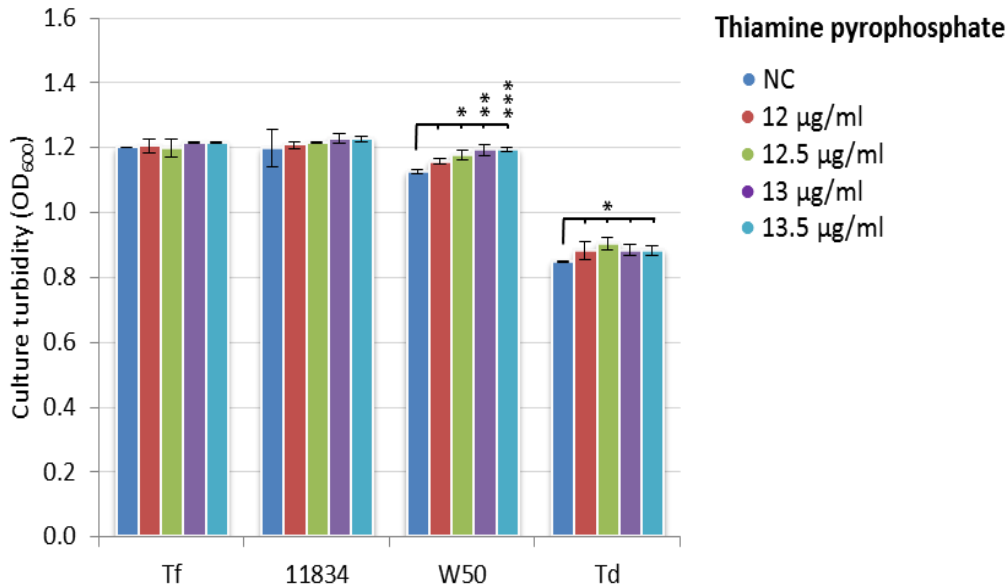


**Figure 5.25:** Bar chart shows the culture turbidity readings ( $OD_{600}$ ) for *T. forsythia* (Tf), *P. gingivalis* (11843 & W50) and *T. denticola* (Td) during late-log, early-plateau growth phase when incubated in medium D supplemented with 12, 12.5, 13 and 13.5  $\mu\text{g/ml}$  thiamine pyrophosphate (TPP) or medium without TPP (control). *P. gingivalis* W50  $OD_{600}$  values were significantly greater in response to 12.5  $\mu\text{g/ml}$  TPP ( $OD_{600}$  1.126 to 1.178;  $p < 0.05$ ), 13  $\mu\text{g/ml}$  ( $OD_{600}$  1.194;  $p < 0.01$ ) and 13.5  $\mu\text{g/ml}$  ( $OD_{600}$  1.196;  $p < 0.001$ ) compared to the control medium. *T. denticola*  $OD_{600}$  values were significantly increased in media containing 12.5  $\mu\text{g/ml}$  ( $OD_{600}$  0.905) compared to negative control medium ( $OD_{600}$  0.840;  $p < 0.05$ ). The remaining species were unchanged for any of the TPP concentration. Each bar represents the mean  $OD_{600}$  value of three technical replicate cultures for each species in each medium of increasing supplement concentration.

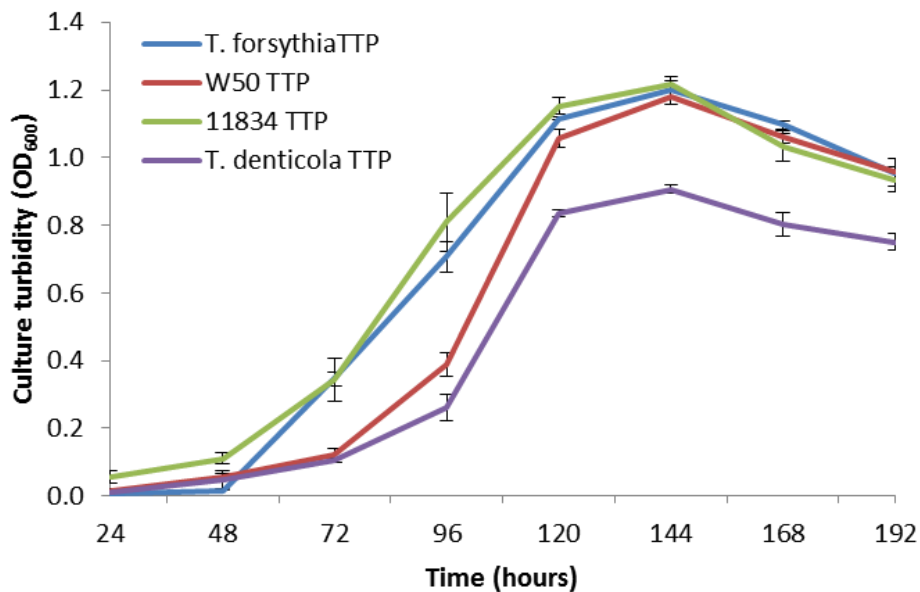


**Figure 5.26:** Growth curves for all test species incubated in TSB medium with all preceding optimum supplement concentrations, including 12.5  $\mu\text{g/ml}$  TPP, (medium E; table 5.03). Line graph shows good exponential growth for all species cultured in medium E, though only a minimal increase in maximum  $OD_{600}$  values were observed compared to medium D. Each line represents  $OD_{600}$  values taken as a mean of three technical replicate cultures of each test species incubated in medium E. Whiskers at each time point represent the standard deviation calculated for three separate cultures per test species measured by  $OD_{600}/\text{ml}$ .

## 5.3.3.7 Medium E: concentration gradient of sodium pyruvate

When species were incubated in medium E containing a concentration gradient of sodium pyruvate (SP), there were no changes in *T. forsythia*, 11834 and W50 OD<sub>600</sub> values for any SP concentration compared to control medium (figure 5.27). However, OD<sub>600</sub> values did increase for *T. denticola* when incubated in medium E supplemented with 250 µg/ml ( $p < 0.05$ ) and 350 µg/ml, ( $p < 0.01$ ; figure 5.27) compared to control media without SP. Thus, 250 µg/ml SP was the lowest possible concentration to induce a significant increase in *T. denticola* OD<sub>600</sub> values and was therefore the only sensible choice to incorporate into the medium for further testing by growth curve analysis (medium F; figure 5.28).

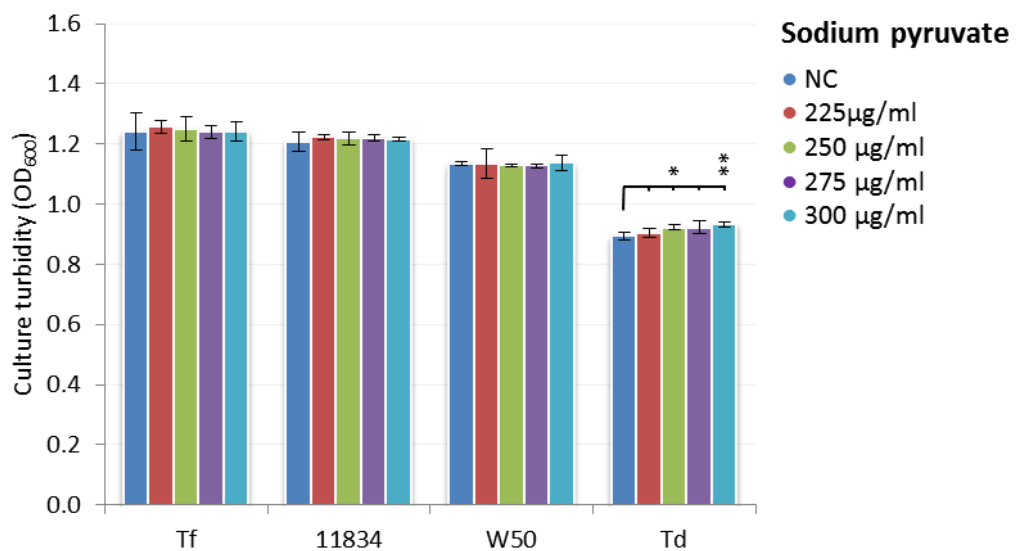


**Figure 5.27:** Bar chart shows the mean ( $n = 3$ ) culture turbidity readings (OD<sub>600</sub>) for *T. forsythia* (Tf), *P. gingivalis* (11834 & W50) and *T. denticola* (Td) in late-log, early-plateau growth phase when incubated in media E supplemented with 225, 250, 275 or 300 µg/ml sodium pyruvate (SP). Media supplemented with  $\geq 225$  µg/ml SP were compared against media containing no SP (control). TSB supplemented with 250 µg/ml SP provided significantly higher OD<sub>600</sub> values for Td compared to control medium. Tf, 11834 and W50 remained unaffected by any of the SP concentrations tested. Each bar represents the mean OD<sub>600</sub> value of three technical replicate cultures for each species in each medium of increasing supplement concentration.

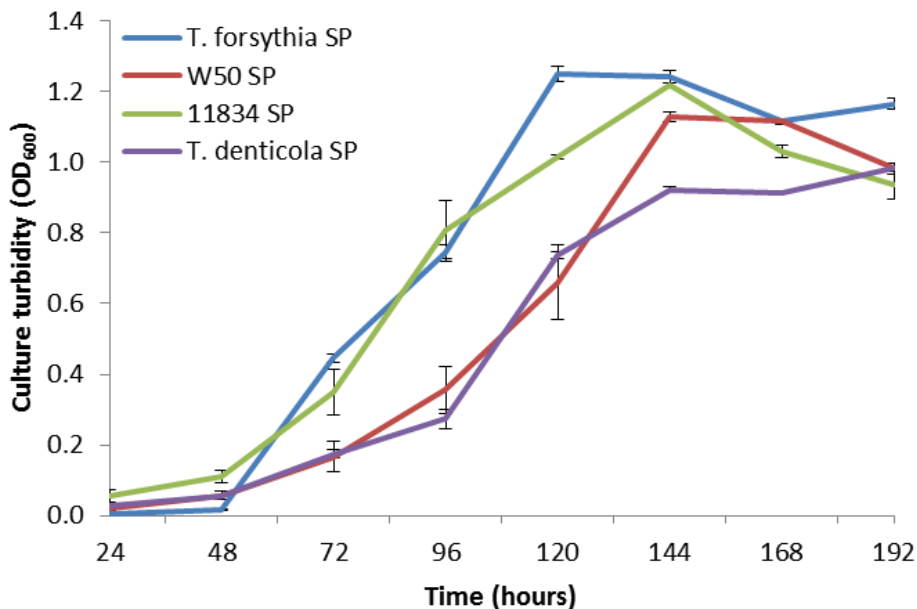


**Figure 5.28:** Growth curves for all test species incubated in TSB medium with all preceding optimum supplement concentrations, including 250 µg/ml SP, (medium F; table 5.03). While health growth was observed in medium F, only a minimal increase of OD<sub>600</sub> was observed compared to media D and E. Each line represents OD<sub>600</sub> values taken as a mean of three technical replicate cultures of each test species incubated in medium F. Whiskers at each time point represent the standard deviation calculated for three separate cultures per test species measured by OD<sub>600</sub>/ml.

#### 5.3.3.8 Medium F: concentration gradient of rabbit serum

Finally, medium F comprising a concentration gradient of rabbit serum (RS) was assessed for its growth-supporting abilities. RS was one of the most influential medium supplements tested, which supported significant increases of OD<sub>600</sub> values for all test species in all media. OD<sub>600</sub> values increased significantly in medium F with elevated concentrations of rabbit serum (RS) compared to values observed for control medium (RS absent) ( $p < 0.05$ ; figure 5.29). *T. denticola* showed the greatest significant increase of OD<sub>600</sub> values in response to RS when compared to negative control medium ( $p < 0.01$ ; figure 5.29). Likewise, values showed significant increases for *T. forsythia*, 11834 and W50 when incubated in medium with elevated RS ( $p < 0.05$ ; figure 5.29). Because OD<sub>600</sub> values showed only negligible further increase at 15% RS compared to 10% in all cases; 10% RS was examined further by performing growth curve analysis (Medium G; figure 5.30)

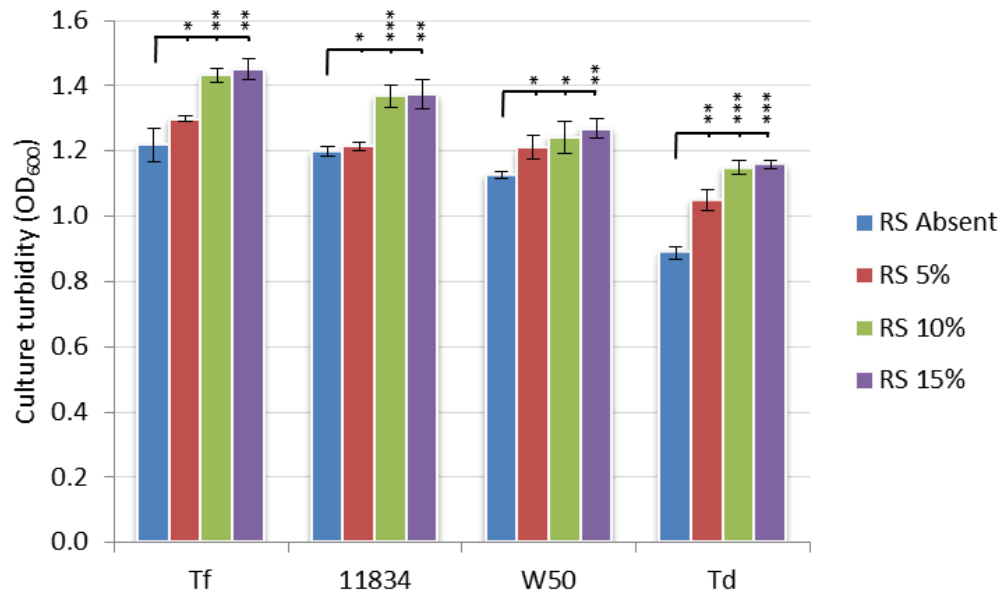


**Figure 5.29:** Bar chart shows the mean ( $n = 3$ ) culture turbidity readings ( $OD_{600}$ ) for *T. forsythia* (Tf), *P. gingivalis* (11834 & W50) and *T. denticola* (Td) when incubated in medium F supplemented with 5, 10 and 15% rabbit serum (RS). Compared to control medium (no RS), significant dose-dependent increases of  $OD_{600}$  values were observed. Td  $OD_{600}$  values increased significantly in TSB with 5% RS (0.882 to 1.049;  $p < 0.01$ ), 10% RS (0.882 to 1.149;  $p < 0.001$ ) and 15% RS (0.882 to 1.160;  $p < 0.001$ ). In all cases  $OD_{600}$  values plateaued at  $\geq 10\%$  ( $p < 0.01$ ). Each bar represents the mean  $OD_{600}$  value of three technical replicate cultures for each species in each medium of increasing supplement concentration.

### 5.3.3.9 Medium G: final fully supplemented and optimised culture medium

The finalised culture medium showed good support for all species tested, including *T. denticola*, which finally showed  $OD_{600}$  values that were comparable with the other RCB species (figure 5.30). The finalised culture medium (per liter) comprised 55g trypticase soy broth supplemented with, 5  $\mu\text{g/ml}$  hemin, 1  $\mu\text{g/ml}$  menadione, 1  $\mu\text{g/ml}$  L-cystiene HCL, 0.4% yeast extract, 10  $\mu\text{g/ml}$  N-acetylmuramic acid, 12.5  $\mu\text{g/ml}$  thiamin pyrophosphate, 250  $\mu\text{g/ml}$  sodium phosphate, 500  $\mu\text{g/ml}$   $(\text{NH}_4)_2\text{SO}_4$ , 2.25 mg/ml  $\text{K}_2\text{HPO}_4$ , 1 mg/ml  $\text{NaCl}_2$ , 6% VFA (comprising 0.29 ml glacial acetic acid, 0.1 ml propionic acid, 0.07 ml butyric acid, 0.0175 ml valeric acid, 0.0175 ml isobutyric acid, 0.0175 ml isovaleric and 0.0175 ml methybutyric acid) and 10% heat inactivated rabbit serum (10%).

Knowing the finalised liquid medium is capable of supporting adequate growth of RCB test species *P. gingivalis* (11834 & W50), *T. forsythia* and *T. denticola* it was further used as a liquid medium to culture any latent species potentially present in CAP and LITA tissue specimens.

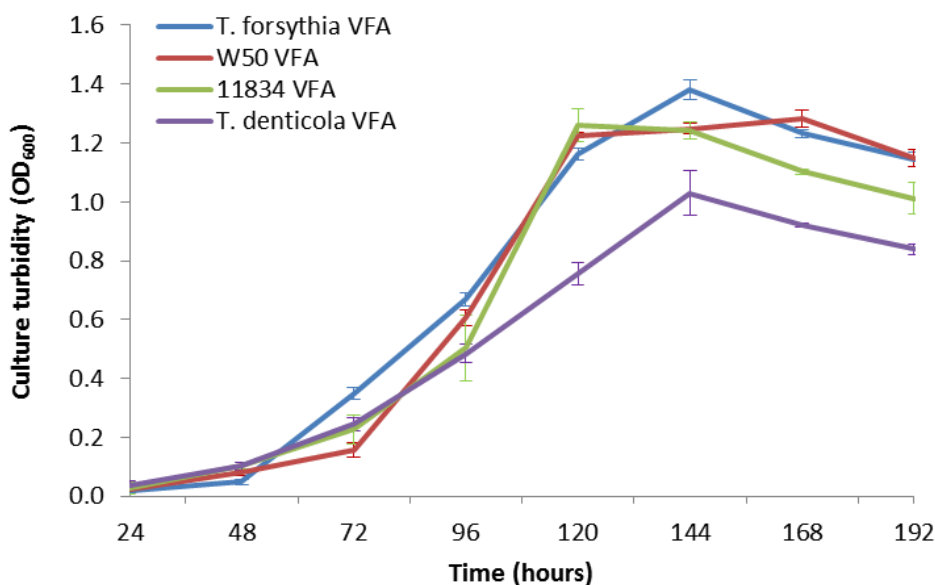


**Figure 5.30:** Line graphs for mean growth curve of all test species, *T. forsythia*, *P. gingivalis* (11843 & W50) and *T. denticola* in TSB medium G containing all optimum media supplements, including 10% RS. Good exponential growth can be observed for all test species, including *T. denticola*, which, although still the lowest growth of all species, is at a level comparable with *P. gingivalis* and *T. forsythia*. Each line represents OD<sub>600</sub> values taken as a mean of three technical replicate cultures of each test species incubated in medium G. Whiskers at each time point represent the standard deviation calculated for three separate cultures per test species measured by OD<sub>600</sub>/ml.

#### 5.3.4 Isolation of viable bacteria species present in CAP tissue.

The complete culture medium (designed and optimised in section 5.2.3 of this chapter and finally described in section 5.2.3.9) was employed to culture latent species present in CAP and LITA tissue samples (Materials & Methods; Section 2.3.3) for isolation and subsequent identification using molecular methods (Materials & Methods; Section 2.4).

Viable cultures were detected in 4/21 (19%) CAP specimens. No bacterial strains were detected in LITA specimens or in environmental and final tissue wash control media (Materials & Methods; Section 2.3.3). The four atherosclerotic plaques that yielded viable cultures were from 2 male and 2 female patients with a mean age of  $74.3 \pm 4.4$  years. Seven-day-old anaerobic liquid cultures grown from CAP tissue were transferred onto fresh blood agar plates and incubated to produce mixed colony plates 200 – 250 colonies/plate (section 2.3.3) (figure 5.31). Ten percent of colonies were picked from each plate and re-inoculated on to fresh blood agar plates to acquire plate containing pure strains for archiving (Materials & Methods; section 2.3.4).

All isolated strains were gram-positive bacilli or cocci (figures 5.32 & 5.33). Isolates were identified using molecular methods (Materials & Methods; (Materials & Methods; Section 2.3.3). Of the total 100 isolated colonies, four separate genera were identified, including *Propionibacterium*, *Staphylococcus*, *Lactobacillus* and *Streptococcus*. The most frequently detected species was *Propionibacterium acnes* (91%), with the most prominent strain being SK137, followed by TypeIA2 P.acn31. The second most encountered species were *Lactobacillus* spp. (3%), along with *Staphylococcus epidermidis*. *Streptococcus mitis* was identified in 2% of isolates and finally *Streptococcus sanguinis* was detected only once out of the 100 isolates. However, as previously described it was not possible to definitively determine the species of MGB using only 16S rRNA gene analysis as more discriminative markers are needed. Therefore, it must be noted that *Streptococcus* spp. were detected only. One plaque specimen contained all of the identified sequences, whereas the remaining three specimens contained only *P. acnes*. The identified sequences had >98% maximum identity when compared to reference sequence of the BLAST database. None of the target RCB species were culture using this method.

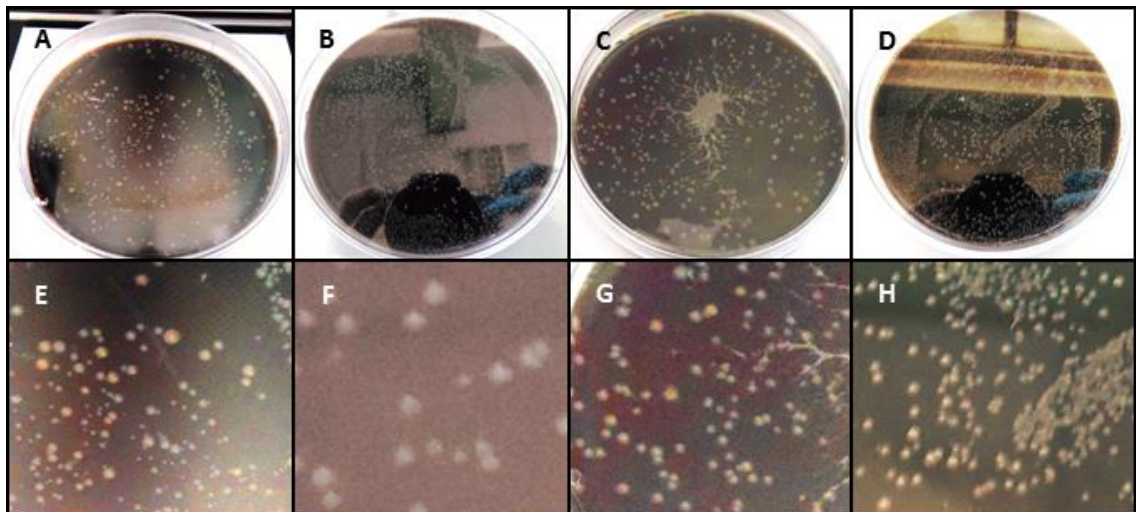


**Figure 5.31:** Multiple colonies incubated on blood agar anaerobically (A, B, C & D) using liquid cultures derived from human CAP tissue homogenates. Each blood agar plate comprised ~200-250 mixed bacteria colonies (E, F, G & H). Each blood agar plate represented an atherosclerotic plaque specimen from four separate patients.

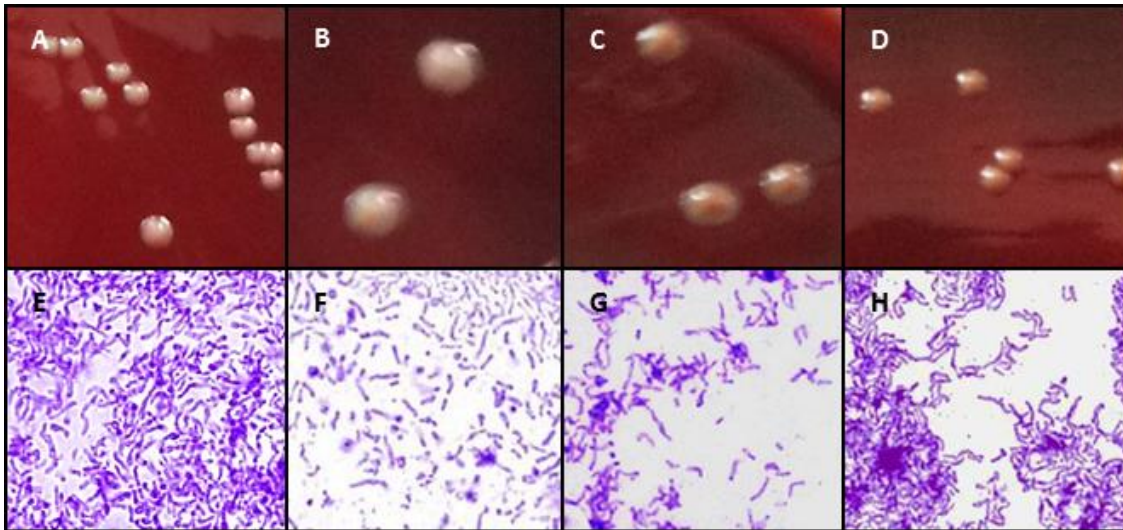


**Figure 5.32:** Fresh colonies of *Propionibacterium acnes* picked from mixed blood agar plates derived from atherosclerotic plaque. Top row (A, B, C & D) shows the different colony morphologies of *P. acnes* at different stages of maturity. *P. acnes* were gram-positive bacillus (E, F, G & H). Colonies were off-white to orange colour, with a circular and convex shape and a shiny appearance. Colonies ranged in size (1-5 mm) dependant on age. Older colonies (C) developed umbonate elevation and had a much deeper colour.

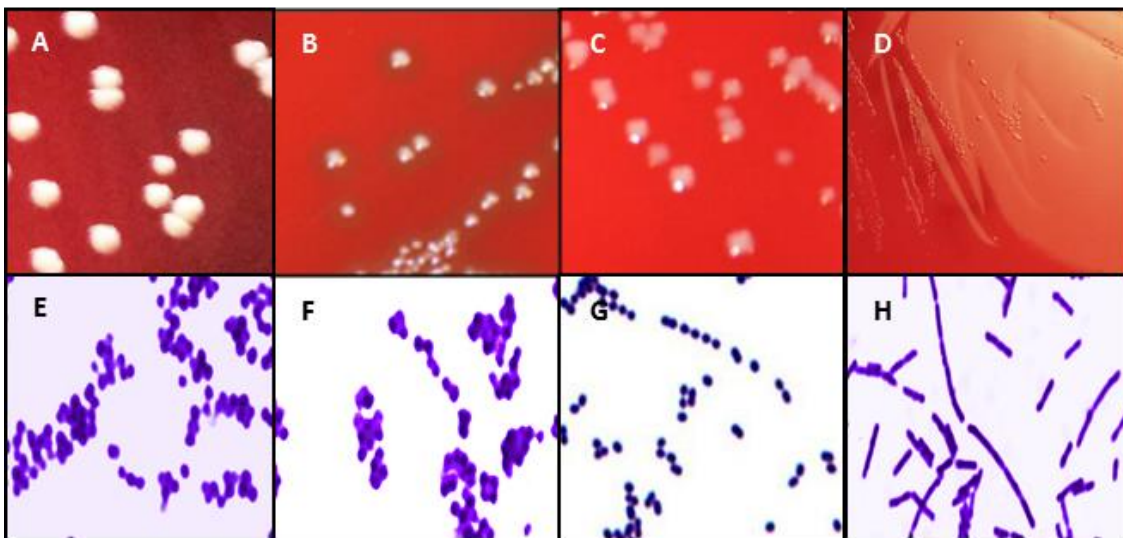


**Figure 5.33:** Fresh blood agar plates containing pure colonies picked and inoculated from mixed plates containing atherosclerotic cultures. *Staphylococcus epidermidis* colonies were white, circular, convex morphology, approximately 3-4 mm and had a mucoid texture (A). *S. epidermidis* were gram-positive chain-forming cocci (E). *Streptococcus mitis* were small (<1-1.5 mm) off-white colonies with a circular, convex shape and prominent  $\alpha$ -hemolysis (B). *S. mitis* was gram-positive chains and bunches forming cocci (F). *Streptococcus sanguinis* were gram-positive cocci (G) that formed small (1-2 mm), translucent gray-white colonies that had a circular convex shape with some  $\alpha$ -hemolysis evident around mature colonies (C). *S. sanguinis*. *Lactobacillus casei* were gram-positive bacilli (H) that formed punctate (<0.8 mm) translucent colonies (D). For illustrative purposes, gram-stain images were enlarged x5 and the original magnification x100 oil-immersion image and cropped.

## 5.4 Discussion

The main concerns of this chapter were firstly; to develop a culture medium designed to encourage the proliferation of oral bacteria, with particular emphasis on supporting the growth of red complex bacteria. The simple and effective medium developed and optimised in this chapter of work has the versatility to cultivate a broad spectrum of bacterial species. Secondly, to implement the developed medium to culture and isolate viable strains present in atherosclerotic plaque specimens from the carotid artery. The evidence obtained in the present study demonstrates the presence of multiple viable bacterial species in human atherosclerotic plaque tissue.

In the present investigation, it was established that TSB medium provided the greatest level of support for 2 of the 3 test species (*T. forsythia*, *P. gingivalis* 11834 and W50), but not *T. denticola*. This was likely due to the fastidious growth requirements of *T. denticola*, which requires a complex environment to support proliferation (J. Fenno 2005; Orth et al. 2010). Because atheroma specimens were to be submerged in the finalised medium, it was essential that the medium would support, if present, all three target organisms. Hence, the enumeration of *T. denticola* became the main focus of the medium development. The most direct way to achieve this was to supplement TSB medium, with the necessary medium supplements known to aid *T. denticola* proliferation. It was critical however, this be carried out in a stepwise fashion so not to sacrifice the support of *P. gingivalis* and *T. forsythia*.

As part of assessing the normal growth conditions, regression line analyses revealed good linear relationships between OD<sub>600</sub> vs cfu/ml for *T. forsythia*, *P. gingivalis* and *T. denticola* in their respective medium (R<sup>2</sup> 0.992, 0.996, 0.998 and 0.996, respectively). Thus, OD<sub>600</sub> values were considered sufficiently representative of cell number values during the exponential growth phase. However, using optical density has its limitation. This method, though not a true representation of viable bacterial cell number, has been widely adopted often without confirmation of cell densities by any other method (Grenier et al. 1990; Edwards et al. 2003; J. Fenno 2005; Roy et al. 2010). The rationale for selecting optical density as a method for enumerating bacterial growth was three-fold. Firstly, it is a rapid method for measuring bacterial growth. Secondly, it was not necessary to generate extremely accurate cell number values for the purposes of this analysis; hence, a method that provided visual confirmation of growth was satisfactory. Thirdly, numerous difficulties were encountered when growing *T. denticola* on semi-solid media. Preparation of the molten semi-solid TYGVS medium for *T. forsythia* inoculations gave inconsistent

results, which has also been highlighted by other investigators (Orth et al. 2010). Colonies that do grow from surface tended to grow down into the agar, making colony counts intricate and often inaccurate (J. Fenno 2005).

Concentration gradients of inorganic salts were supplemented into TSB first, which provide a number of co-factors and energy sources derived from minerals such as ammonia, nitrogen and phosphorus. When determining which inorganic salts were absolutely necessary for proliferation of *T. denticola*, each salts ( $\text{MgSO}_4 \cdot 7\text{H}_2\text{O}$ ,  $(\text{NH}_4)_2\text{SO}_4$ ,  $\text{K}_2\text{HPO}_4$  and  $\text{NaCl}$ ) were systematically omitted from TYGVS medium before culturing *T. denticola*. The absence of  $\text{MgSO}_4 \cdot 7\text{H}_2\text{O}$  had no visible impact on *T. denticola*  $\text{OD}_{600}$  values and was therefore omitted (figure 5.15). The exclusion of  $\text{MgSO}_4 \cdot 7\text{H}_2\text{O}$  from the medium was in contrast to previous media development studies (Caldwell & Bryant 1966; Laughon et al. 1982; Salvador et al. 1987; Wyss 1992). However, spirochete media exist that do not contain  $\text{MgSO}_4 \cdot 7\text{H}_2\text{O}$  such as oral treponeme isolation (OTI) medium (Moore et al. 1982) and new oral spirochete (NOS) medium (Cheng & Chan 1983). Many studies developed media supplemented with excess salts that were not included here, particularly that designed by Wyss (1992), who developed a chemically defined medium with over 150 supplements. In contrast, when  $(\text{NH}_4)_2\text{SO}_4$ ,  $\text{K}_2\text{HPO}_4$  and  $\text{NaCl}$ , were omitted from TYGVS medium a marked decline of  $\text{OD}_{600}$  values were observed, particularly when  $\text{NaCl}$  was removed, and therefore were included.

The stepwise supplementation of  $(\text{NH}_4)_2\text{SO}_4$  into TSB prompted a significant increase in *T. denticola*  $\text{OD}_{600}$  values at concentrations between 0.75-1.25 mg/ml. The higher side of this concentration range was marginally higher than is found in spirochete media developed by other investigators (Laughon et al. 1982; Moore et al. 1982; Salvador et al. 1987). The concentration requirement of *T. denticola* for  $(\text{NH}_4)_2\text{SO}_4$  established here, was comparable with previously designed chemically-defined medium OMIZ-W1, which has been used by several investigators (Wyss 1992). However, even though addition of  $(\text{NH}_4)_2\text{SO}_4$  potentiated significant growth of *T. denticola* compared to the control medium, actual physical growth compared to *P. gingivalis* and *T. forsythia* in TSB was negligible. Similar growth levels were observed following supplementation with  $\text{K}_2\text{HPO}_4$  and  $\text{NaCl}$ , which stimulated significant increases of  $\text{OD}_{600}$  at concentrations of 1 mg/ml and 1.25 mg/ml, respectively. Again, the most efficacious concentrations of  $\text{K}_2\text{HPO}_4$  and  $\text{NaCl}$  were in line with previously developed spirochete media (J. Fenno 2005).

Only when TSB was supplemented with volatile fatty acids (VFA) solution did *T. denticola* OD<sub>600</sub> values increase to a comparable level with *P. gingivalis* and *T. forsythia*. VFA's are incorporated in a number of spirochete media, including M10 (Caldwell & Bryant 1966), GM-1 (Blakemore & Canale Parola 1976), New Oral Spirochete (NOS) medium (Cheng & Chan 1983) and TYGVS (Salvador et al. 1987). VFAs are used as the major energy source by *T. denticola*, thus, recovery rates of *T. denticola* are typically denser and growth faster when media are supplemented with VFA (J. Fenno 2005). Unexpectedly, VFA caused a marked inhibition of *T. forsythia* and *P. gingivalis*, which was dose dependant. Studies have shown significantly more *T. denticola* compared to *P. gingivalis* in short-chain fatty acids-rich gingival cervical fluid of patients with generalized aggressive periodontitis (Lu et al. 2013). This could be reflective of the inhibitory effect observed here, although VFA's, particularly butyric acid, are major by-products of periodontal pathogens, even in the absence of *T. denticola* (Kurita-Ochiai et al. 1995). Therefore, this reduction of *T. forsythia* and *P. gingivalis* is puzzling. At a concentration of 10% VFA the inhibitory effect on *T. forsythia* was too severe. Because OD<sub>600</sub> values for *T. denticola* plateaued at VFA concentration >6%, the inhibitory effect on *T. forsythia* was limited.

Supplementation with TPP made little observable difference to the overall growth of all test species. TPP is the biologically active form of thiamine (vitamin B<sub>1</sub>) which acts as an essential cofactor in all living systems. Surprisingly, there was little to no increase in *T. denticola* OD<sub>600</sub> values following TPP supplementation. Microorganisms can either synthesise TPP via de novo synthesis or uptake exogenous TPP via ATP-binding cassette transporters. (Begley et al. 1999) *T. denticola* lacks this de novo TPP synthesis pathway and so requires exogenous TPP supplementation (De Ciccio et al. 1999; Seshadri et al. 2004). However, yeast extract is rich in B complex vitamins including TPP (vitamin B<sub>1</sub>), which may have provided the necessary requirement. Because TPP supplementation did not produce increased growth, it was not included. The absence of TPP is consistent with the developed media NOS and Laughon media (Laughon et al. 1982; Cheng & Chan 1983).

In the present investigation, rabbit serum provided a significant dose-dependent increase in OD<sub>600</sub> values for each test species, which plateaued at concentrations  $\geq 10\%$ . These findings are consistent with most media designed to support the growth of Treponemes, which supplement between 5-10% rabbit serum or rumen fluid (Laughon et al. 1982;

Moore et al. 1982; Cheng & Chan 1983; Salvador et al. 1987; J. Fenno 2005; Fiehn & Larsen 2005). After VFAs, animal sera provided the greatest support for bacterial proliferation by providing a complex source of growth factors, proteins, vitamins, minerals, hormones, carbohydrate, lipids amino acids and trace elements. *T. denticola* has a rabbit albumin-binding polypeptide and will therefore preferentially migrates toward rabbit serum *in vitro* (Umemoto et al. 2001). Rabbit serum is typically used in spirochete medium because some Treponemes will only grow in its presence, however for *T. denticola* the serum source is not critical (Fenno 2005).

In the present investigation 19% of CAP specimens provided viable cultures, from which *P. acnes* was the most frequently isolated species (91%). The predominant isolation of *P. acnes* from carotid plaques is consistent with findings by other investigators (Rafferty et al. 2011; Kędzia et al. 2012). Applying plaque homogenates to blood agar plates, Kędzia et al. (2012) claimed to have isolated viable periodontal bacteria from 67% of CAP specimens, which included *P. gingivalis* (20%) and *P. acnes* (18%). However, unlike the present investigation where molecular methods were utilized to identify isolates, Kędzia et al. (2012) used Analytical Profile Index (API<sup>®</sup>) to identify the isolates, which has been documented to have between a 3 - 10% misidentification rate (Kidd et al. 2009). Furthermore, the adoption of blood agar plates as the sole medium for isolating viable strains from tissue was used in the initial phase of this investigation with no success. A possible reason for this was the suboptimal tissue to agar surface area contact compared to a planktonic growth system. This method would therefore have reduced the likelihood of isolating organisms from the tissue surfaces not in contact with the agar medium; hence the evolution to a planktonic growth system. Rafferty et al. (2011) expanded on an *in vitro* detection method first published by Kozarov et al. (2005), in which carotid plaque homogenates were co-incubated with human monocyte cell line, THP-1, prior to agar inoculation. The rationale for this distinct approach was based on the premise that pathogenic bacteria may remain unculturable by residing in the monocyte/macrophages of the atherosclerotic plaque. Through implementing this novel approach, Rafferty et al. (2011) recovered 872 isolates, including *P. acnes*, *S. epidermidis* and *P. gingivalis* at a 5.6-fold greater recovery rate with the THP-1 cell co-incubation strategy than without THP-1. This is particularly noteworthy when considering the intracellular evasiveness of *P. acnes in-vitro*, which has been demonstrated to remain viable in macrophages for 2 weeks post infection (Fischer et al. 2013). A similar *in-vitro* methodology was developed by Kozarov

et al. (2005), who utilised endothelial cell line ECV-304 to highlight the invasiveness and therefore viability of *P. gingivalis* and *A. actinomycetemcomitans* in a carotid plaque specimen (Kozarov et al. 2005). However, as a case study analysing only one specimen, only weak associating between periodontal and vascular disease could be drawn. *A. actinomycetemcomitans* has also been shown to be present in both the periodontal pockets and carotid atherosclerotic plaques of the same patients when isolated using solid agar medium (Padilla et al. 2006).

In agreement with the present investigation da Silva et al. (2003) identified *P. acnes* as the most frequently isolated species from abdominal aortic plaques. Moreover, the authors reported that pure *P. acnes* cultures were isolated from two patients' specimens, which is consistent with the 3 of the 4 specimens examined here. Interestingly, two of the plaques with pure *P. acnes* cultures were also showed to contain *P. acnes* when specimen tissue was assessed by direct PCR analysis; providing further confirmation of its presence. Early investigators who cultured *P. acnes* from abdominal plaques have dismissed its presence as a contaminate (Eriksson et al. 1983). While *P. acnes* is known to be indigenous to the skin, it can also act as a primary pathogen and should therefore not just simply be dismissed as contaminate. As previously discussed in the main introduction (Chapter 1), *P. acnes* has been isolated from and identified as an etiological agent in several pathologies, such as prostate cancer (Cohen et al. 2005), sciatica (Stirling et al. 2001) aortic valve endocarditis (Gunthard et al. 1994), sarcoidosis (Hiramatsu et al. 2003) and arthritis (Berthelot et al. 2006). *P. acnes* is a member of the periodontal microbiota (Paster et al. 2001) and is more prevalent in apical periodontal lesions and generalized aggressive periodontitis compared to chronic periodontitis (Fujii et al. 2009; Heller et al. 2012). Debelian et al. (1992) assessed transient bacteraemia in 26 patients undergoing root canal treatment and found *P. acnes* to be the most abundant species in both root canal and blood 10 minutes post dental treatment. The time frame used to assess bacteraemia may have been too short making it possible that *P. acnes* was eventually cleared, possibly even transported to the atherosclerotic vessel within phagocytic cells. It is therefore, biologically plausible that the high frequency of *P. acnes* in the carotid plaques examined here is a symptom of its etiological role in oral infection disease. It is also possible however, that *P. acnes* may have originated from other bodily sites, such as the lymph nodes or the lungs (Ishige et al. 2005)

In addition to *P. acnes*, *S. epidermidis*, *Lactobacillus* spp. and *Streptococcus* spp. were isolated from the tissue examined here, though percentage detections rates were markedly less. *S. epidermidis* has been isolated from abdominal aortic plaque and carotid plaque tissue (da Silva et al. 2003; Rafferty et al. 2011). As an opportunistic pathogen *S. epidermidis* is often co-isolated from periodontal infections with *P. acnes* (Niazi et al. 2010). Similarly, infections distant from the oral cavity, such as those affecting prosthetic implants and intravenous catheters, implicate *S. epidermidis* and *P. acnes* as the primary pathogens (Martín-Rabadán et al. 2008; Portillo et al. 2013). Therefore, as nosocomial species, the possibility these strains originated from a hospital acquired infection cannot be dismissed. Nevertheless, whether the origin of *P. acnes* and/or *S. epidermidis* derives from oral infection or other, the potential for these organisms to potentiate inflammatory milieu at atherosclerosis-prone vascular sites remains the same. In order to elucidate the origin of bacteria isolated from atherosclerotic plaque it would be necessary to thoroughly screen the tissue of suspected sources e.g. periodontal tissue. Unfortunately, the periodontal status of the patients examined in the present investigation was not provided; hence, in the present investigation the potential source of the species isolated cannot fully elucidated.

When trying to identify the specific *Lactobacillus* spp. isolated from atherosclerotic plaque tissue, it was not possible to differentiate between species *L. casei*, *L. paracasei* or *L. rhamnosus*. All provided a 100% maximum identity between the ~600 bp sequence and reference sequences of the NCBI database. These species form a closely related taxonomic group within the heterofermentative group II. In the present investigation, universal primer set D88/E94 was used to amplify 16S rDNA from the clinical isolates prior to sequencing PCR with the D88 primer. While this method can readily differentiate this group of *Lactobacillus* spp. from other members of the *Lactobacillus* genus, it is not possible to unequivocally distinguish between these three species on this basis. To differentiate these isolated species it would be necessary to design PCR primers that are specific for each of these species based on differences in the hypervariable regions of the 16S rRNA gene (Ward & Timmins 1999; Walter et al. 2000). However, even though the precise species/strain cannot be elucidated, to the best of our knowledge there are no data published hitherto that details the isolation of viable *Lactobacillus* spp. (*L. casei*, *L. paracaei* or *L. rhamnosus*) from atherosclerotic plaque tissue.

*Lactobacillus* spp. are primarily oral microbes that play a divisive role in oral health and disease (Badet & Thebaud 2008). Thus, a possible periodontal origin for the *Lactobacilli* spp. cannot be ruled out. *L. casei*, *L. paracasei* or *L. rhamnosus* are moderately cariogenic through their ability to convert lactose and other sugars to lactic acid, which demineralises the hard tissues of the teeth, (i.e. dentin, cementum and to a lesser extent enamel). The initial breakdown of the tooth barrier leaves the tooth open to infections that if left untreated may progress into the deeper tissues of the periodontium, which can eventually lead to systemic infection (Li et al. 2000). Transient bacteraemias resulting from chronic oral infection and the breakdown of periodontal and gingival tissue are a major factor contributing to secondary infections at sites distant from the oral cavity. Interestingly, *ApoE*<sup>-/-</sup> and *Ldlr*<sup>-/-</sup> mice injected with *L. casei* cell wall components, have been shown to develop atherosclerosis with abundant collagen, and both extracellular and intracellular lipid and foam cells, compared to lesions in control mice (Chen et al. 2012).

In the present study, *Streptococcus* spp., most closely related species, *S. mitis* (2%) and *S. sanguinis* (1%) were isolated from the atherosclerotic plaque tissue. However, as with the three *Lactobacillus* spp. detected in this investigation, Mitis Group bacteria (MGB) are also difficult to differentiate between using only 16S rDNA PCR and thus, it is not possible to confirm their presence within the scope of this study. To the best of our understanding there have been no data published hitherto, which demonstrates the isolation of viable *S. mitis* or *S. sanguinis* from atherosclerotic plaque tissue. Both species are members of the viridans streptococcus group that inhabit the mouth and have an abundance of putative surface proteins that permit primary colonisation of dental plaque (Xu et al. 2007; Denapaitte et al. 2010). Viridans group bacteria, including *S. mitis* and *S. sanguinis* have been shown to be opportunistic pathogens, evidenced by their isolation from blood and as the primary pathogens in osteomyelitis and native-valve infective endocarditis (Mylonakis & Calderwood 2001; Presterl et al. 2005; Choudhury et al. 2009; Nomura et al. 2011; Raber-Durlacher et al. 2013). To confirm the presence of viable *S. mitis* and *S. sanguinis* further investigation is required. As discussed in the previous chapter, molecular techniques such as, DGGE or to employ the use of more discriminative markers, typically enzyme or protein-encoding housekeeping genes such as, *sodA*, *rpoB*, *hlpA*, *gdh* and/or *gdh* in addition to the 16S rRNA gene. However, if the species detected in this chapter of work were a true representation of the viable microbiome, then isolation of *S. mitis* and *S. sanguinis* would provide further evidence for an association of oral bacteria and

atherosclerosis by confirming the presence of viable oral bacteria within atherosclerotic plaque.

## 5.5 Conclusion

While a case can be made that supports the hypothesis that opportunistic pathogens, such as the strains isolated here, originate from the oral cavity (periodontium), where they are the predominant strains; it must be done with caution. Although the predominant species detected here was *P. acnes*, also present were *Streptococcus* spp. and *Lactobacillus* spp. While it is not possible to confirm the species of *Streptococcus* or *Lactobacillus*, both genera are commonly found within the oral cavity. It is plausible to propose these strains may have gained entry to the blood stream via dental bacteraemia, however this cannot be proposed with certainty as other bodily niches exist that may also be the source e.g. trachea, gut or lungs (Salminen et al. 2004; Valdés et al. 2008; Dickson et al. 2015). The design and scope of this project cannot conclusively pinpoint the origin of the strains isolated. The large majority of genera isolated here were potentially nosocomial; however, at the time of surgery, no patients were being treated for nosocomial septicaemia. Nevertheless, any suggestion of their source must be done with caution. It is however clear from the literature and from the data presented here that *P. acnes* in particular, should not simply be dismissed as a contaminant, especially when considering its pathogenicity as a primary pathogen in numerous pathologies.

**A STUDY OF GENE EXPRESSION IN HUMAN  
INTERNAL CAROTID ATHEROSCLEROTIC  
PLAQUES**

## 6.1 Introduction

The initiation and progression of atherosclerotic plaque encompasses a series of highly specific cellular and molecular responses that are mediated at every stage by cytokines, chemokines and growth factors. The continual subendothelial accumulation of reactive lipoprotein and the responding influx of inflammatory cells, actively contribute to lesion growth. A critical set of processes that can radically affect the development of atherosclerotic plaque are those that regulate cholesterol homeostasis within cells.

Cholesterol homeostasis is strictly regulated by a sterol sensing feedback pathway that is controlled by endoplasmic reticulum (ER)-residing transcription factor, namely sterol regulatory element binding protein (SREBP)2 and its chaperone protein, SREBP cleavage activating protein (SCAP) (Yang et al. 2002) (cholesterol biosynthesis; figure 6.01). The SREBP2/SCAP protein complex tightly regulates the transcription of genes controlling LDL uptake (e.g. low density lipoprotein receptor (LDLR)) and cholesterol biosynthesis, i.e. 3-hydroxy-3-methylglutaryl-coenzyme A reductase (HMG-CoA reductase) which also controls the synthesis a multitude of isoprenoids and steroids necessary for healthy cellular functions (Burg & Espenshade 2011).

In a lipid-rich environment, such as an atherosclerotic lesion, it would be anticipated that SREBP2/SCAP would remain down-regulated, anchored to INSIG sequestered in the ER (Yang et al. 2002). The uncontrolled uptake of ox-LDL mediated by scavenger receptors rather than native LDL uptake is considered the primary cause of macrophage foam cell formation. However, dysregulation of SCAP feedback in response to pro-inflammatory stimuli (IL-1 $\beta$  and TNF- $\alpha$ ), has been observed *in vitro*; culminating in enhanced SREBP2 translocation and redundant LDLR expression. The extent to which inflammatory mediators affect cholesterol biosynthesis is not yet fully elucidated, therefore understanding cholesterol homeostasis and how it may be affected by inflammation may provide information relating to the development of foam cells or plaque development.

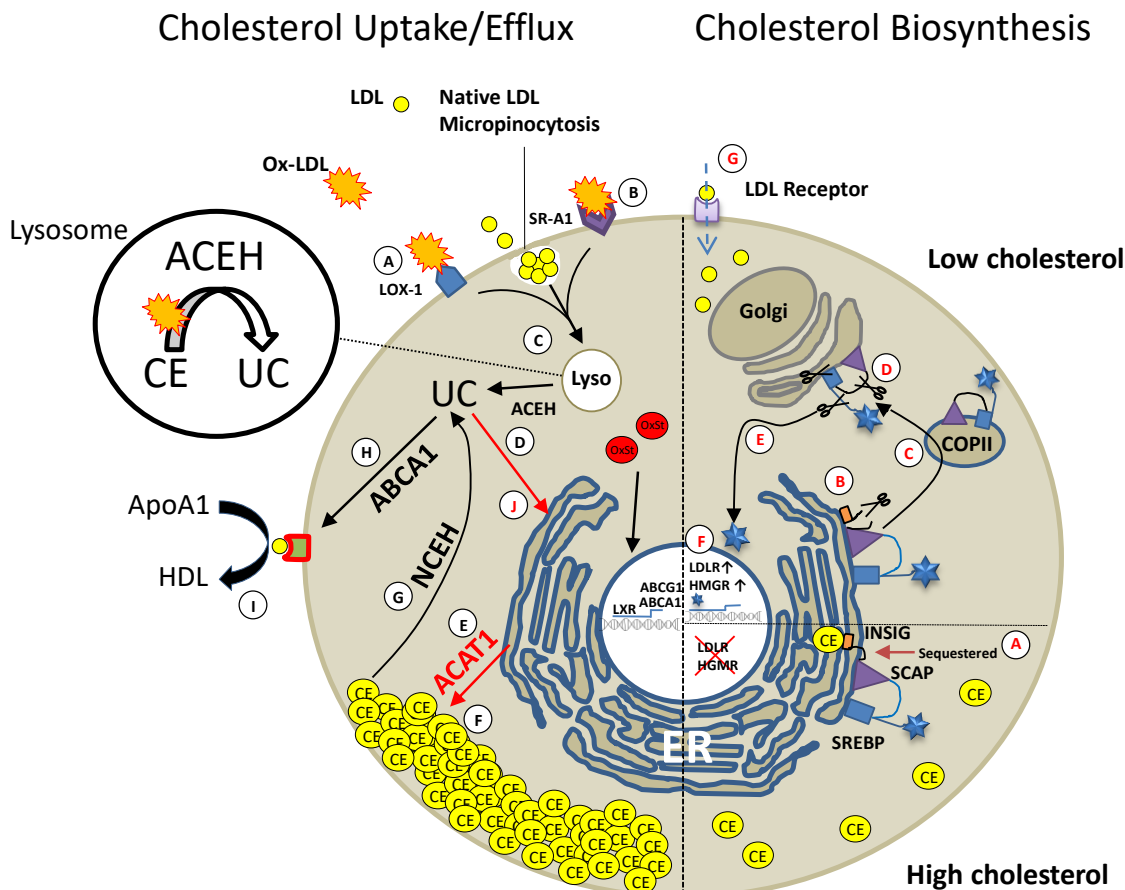


**Figure 6.01: Cholesterol Uptake/Efflux.** Macrophage scavenger receptors expressed on the surface of the macrophage, such as LOX-1 (A), SR-A1 (B) and CD36 relentlessly target oxLDL for internalisation. Ox-LDL is rich in cholesteryl esters (CE), which upon internalisation, are hydrolysed by acid cholesterol ester hydrolase (ACEH) to unesterified cholesterol (UC) and subsequently released from lysosomes as free cholesterol (C). Two critical pathways control the fate of free cholesterol; firstly, the re-esterification of UC to CE by the ER-resident enzyme, Acyl-CoA cholesterol acyltransferase 1 (ACAT1) (E) for its storage in intracellular CE lipid droplets (F). The second pathway, which is critical for macrophage survival, relies on cleavage of CE back to cholesterol by neutral cholesterol ester hydrolase 1 (NCEH1) (G). The latter hydrolysis reaction permits efflux of UC to the plasma membrane by transporters such as ABCA1 (H) for lipidation of lipid-poor ApoA1 (I). However, UC targeted for efflux can undergo a ‘futile cycle’ of esterification hydrolysis by ER-resident hydrolases (J). When an imbalance in these pathways favours cholesterol storage, macrophages become laden with CE and oxysterols and develop into foam cell. **Cholesterol Biosynthesis.** When intracellular cholesterol is abundant, the SREBP2/SCAP protein complex is sequestered in the ER through SCAP sterol sensing domain (SSD)-induced binding of insulin induced gene (INSIG) (A). Alternatively, when cellular cholesterol is deplete, SREBP2/SCAP complex dissociates from INSIG (B) and buds off from the ER as a COPII vesicle (C), which translocates to the Golgi Apparatus (D). A transcriptionally active portion of SREBP is then proteolytically cleaved from the protein complex and translocates to the nucleus (E) where it finally binds the promoter sequences for up-regulation of cholesterologenic genes such as HMGCR and LDLR (F) for de novo synthesis of cholesterol or uptake of LDL, respectively (G). Adapted and expanded from (Moore et al. 2013).

A widely accepted paradigm for much of the last two decades has been the oxidative modification hypothesis proposed by Steinberg and colleagues, in which elevated oxidative stress in the vascular wall gives rise to oxidised LDL (oxLDL) that is preferentially targeted over native LDL and taken up by macrophages. Macrophage internalisation of atherogenic lipoproteins is presumed to be the over-riding cause of

macrophage foam cell formation, a major hallmark of atherosclerotic plaque (*cholesterol uptake/efflux*; figure 6.01). Present on the surface of ox-LDL are biologically active oxidation epitopes that bind with high affinity to pattern recognition receptors, such as macrophage scavenger receptors (CD36, SR-A1 and LOX-1) (Peiser et al. 2002). Ox-LDL is rich in cholesteryl esters (CE), which upon internalisation can undergo numerous cycles of hydrolysis and re-esterification before it is stored as CE lipid droplets in the cytosol of the macrophage (figure 6.01) (Brown et al. 1980). Unlike the LDL receptor, scavenger receptors are not down-regulated in response elevated cholesterol levels and so massive amounts of CE can be internalised resulting in the development of macrophage foam cells, a classic hallmark of the atheroma (Maxfield & Tabas 2005).

In addition to lipoprotein uptake pathways, macrophages are also modulated by pathways that promote the removal of excess cellular cholesterol. The transport mechanisms that promote efflux of excess cholesterol from macrophages to extracellular acceptors (the first step in reverse cholesterol transport (RCT)) are of critical importance in protecting against lipid accumulation and ultimately, foam cell formation (Rosenson et al. 2012). HDL and lipid-poor apolipoprotein play a central role in the RCT pathway by serving as the primary acceptors for macrophage cholesterol efflux. A major advance in our understanding of macrophage cholesterol efflux pathways has come with the identification of ABC transporters that facilitate the transport of unesterified FC to extracellular acceptors. ATP-binding cassette transporter A1 (ABCA1) (figure 6.01) plays a critical role in preventing the excess cholesterol accumulation in macrophages (Schmitz et al. 1999) (figure 6.01). However, UC targeted for efflux can undergo a ‘futile cycle’ of esterification hydrolysis by ER-resident hydrolases (Ouimet & Marcel 2012). When an imbalance in these pathways favours cholesterol storage, macrophages become laden with CE and oxysterols and develop into foam cell. In becoming loaded with lipid, foam cells appear trapped in the vessel wall, where they readily secrete pro-inflammatory cytokines (i.e. IL-1 $\beta$ , TNF- $\alpha$ ), chemokines (CCL2) and ROS, recruiting additional inflammatory cell and ultimately leading to the demise of the surrounding healthy tissue (Figure 1.05 main introduction section 1.2.4 ) (McLaren et al. 2011).

Apoptosis of foam cells contributes to necrotic core formation, a hallmark of plaque severity (Thorp & Tabas 2009). Several cysteine proteases have been described to participate in the apoptotic process (Miller 1997). There are many routes that result in activation of apoptosis though all are broadly categorised under the two main pathways of

action, either intrinsic or extrinsic. A major pathway in foam cells is activated by prolonged stimulation of the ER with excess FC that triggers ER stress resulting in the induction of an ER-activated protein cascade beginning with protein kinase RNA-like ER kinase (PERK) and the release of ROS. PERK activates CCAAT-enhancer-binding protein homologous protein (CHOP), a transcription factor that down-regulates anti-apoptotic members of the BCL-2 family, such as BCL2A1, thereby promoting apoptosis (Feng et al. 2003; Colgan et al. 2011; Scull & Tabas 2011). Apoptosis is activated by Bak/Bim and pro-apoptotic BCL-2 family member proteins that translocate to the mitochondrial outer membrane where they induce the release of apoptotic factors such as, cytochrome C and other proteins involved in the cleavage of caspases (Czabotar et al. 2013; Westphal et al. 2014). The up-regulation of BCL2A1 can interact with and inhibit other pro-apoptotic BCL2 proteins and several BH3-only protein at the mitochondria which is suggested to play a role in survival of foam cells, permitting massive lipid loading (Vogler 2012).

3-hydroxy-3-methyl-glutaryl reductase (HMGR) is a transmembrane glycoprotein enzyme located on the ER. When activated HMGR catalyses the four-electron reduction of 3-hydroxy-3-methylglutaryl coenzyme A (HMG-CoA) to mevalonate, which undergoes many subsequent transformations to form sterol precursors and ultimately cholesterol (figure 6.02; recreated from (Buhaescu & Izzedine 2007)). As intracellular sterol levels fluctuate HMGR is tightly regulated at the transcriptional (SREBP/SCAP) and post-translational (phosphorylation and ubiquitination) levels (Burg & Espenshade 2011). An environment abundant with cholesterol, such as atherosclerotic plaque, should inhibit expression of SREBP2/SCAP, thereby preventing transport of the SREBP/SCAP complex from ER to Golgi apparatus, which would in turn limit end-product expression of genes such as HMGR (Eberlé et al. 2004; Xiaoping & Fajun 2012).

This pathway may be somewhat complicated by the possibility of HMGR inhibitor therapy, namely, statins, which are competitive antagonists of HMGR that occupy a portion of the binding site of HMG-CoA, thus blocking access of this substrate to the active site (Istvan & Deisenhofer 2001). However, one of the main design objectives of statins design is the selective inhibition of hepatic HMGR, while the same mechanism of action should not affect non-hepatic cells; thus, *de novo* cholesterol synthesis in non-hepatic cells should remain uninhibited by statin therapy (Hamelin 1998). Blocking hepatic HMGR reduces the production of mevalonate, which inhibits cholesterol synthesis in the liver (figure 6.02; (Buhaescu & Izzedine 2007)). Reduced hepatocyte cholesterol

production triggers SREBP2 activation, leading to transcription of hepatic-LDLR, increasing LDL clearance from the circulation, thus, improving the lipid profile (Vaughan & Gotto 2004; Dong et al. 2010).

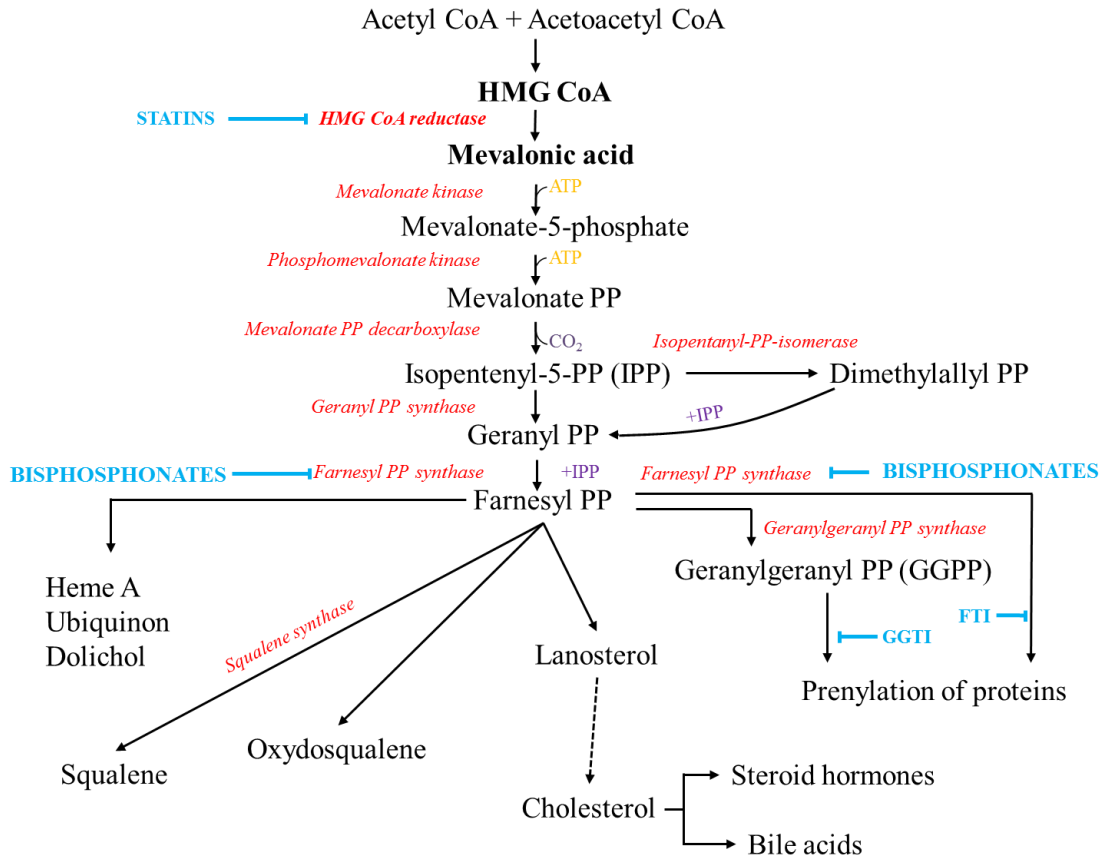


**Figure 6.02:** Mevalonate pathway and isoprenoid synthesis. Shows the rate limiting step in the reduction of HMG CoA to Mevalonic acid (bold). Enzymes (red italics), intervention therapies (blue). PP = pyrophosphate; FTIs = farnesyl transferase inhibitors; GGTI = geranylgeranyl transferase inhibitors; IPP = isopentenyl pyrophosphate. (Buhaescu & Izzedine 2007)

There are also many pleiotropic effects of statin therapy that have a direct effect not just on cholesterol homeostasis but also improving endothelial function, enhancing the stability of atherosclerotic plaques, decreasing oxidative stress and inflammation, and inhibiting the thrombogenic response (Liao & Laufs 2005). Thus, statin therapy has been shown to inhibit expression of numerous facets of the innate immune response such as pro-inflammatory cytokines, TNF- $\alpha$  and IL-1 $\beta$ , adhesion molecules ICAM-1 and VCAM-1 as well as chemokines CCL2, IL-8 and RANTES (Schönbeck & Libby 2004). However, significant up-regulation of IL-1 $\beta$  in simvastatin-treated T cells has also been reported, so the issue becomes complicated further (Jameel et al. 2013). In the present study it was not

known whether patients who donated their plaque tissue were receiving statin therapy. Therefore any attempt at interpreting the results must be done with caution.

The theory supporting that this process occurs as a ‘response to injury’ proposes that endothelial denudation (ED) is the earliest stage of atherogenesis. ED occurs at arterial sites where vascular bifurcation or curvature disrupts blood flow dynamics, creating shear stress that affects homeostatic properties of the endothelium. At regions susceptible to ED, circulating LDL permeates the damaged endothelium and accumulates within the intima where they become oxidised by reactive oxygen species (ROS) (Singh et al. 2002). ox-LDL is pro-inflammatory and chemotactic for leukocytes by stimulating secretion of IL-1 $\beta$  and TNF- $\alpha$ ; both potent stimulators of endothelial selectins (P and E) and cell adhesion molecules (CAMs), ICAM-1 and VCAM-1. Leukocyte P-selectin glycoprotein ligand 1 (PGSL-1) and E-selectin ligand 1 (ESL-1), which are constitutively expressed by circulating monocytes, tethers their respective endothelium selectin (P- and E-selectin, respectively) with low affinity, initiating monocyte “rolling” through detachment and reattachment of selectin interactions (Figure 1.05 main introduction section 1.3.4) (Steidl et al. 2000; Ley 2003). Simultaneously, ox-LDL-induced chemokines such as, monocyte chemoattractant protein-1 (CCL2), binds to the extracellular domain of G-protein coupled membrane receptor CCR2 (Dzenko et al. 2005). Binding causes a conformational change in the cytosolic portion of CCR2 triggering a cascade of intracellular protein activation leading to the up-regulation of monocyte integrin, LFA-1. Selectin interactions decrease monocyte velocity, enabling LFA-1 to bind its ligand, ICAM-1; immobilising the monocyte at the site of ox-LDL-induced inflammation (Marlin & Springer 1987). The monocyte then undergoes complete reorganisation of its cytoskeleton and extravasates to the subendothelial space (Middleton et al. 2002).

Up to now the focus of this thesis has been to establish the presence of bacteria or their cell wall components in atherosclerotic plaque tissue either through immunohistochemical, 16S rDNA or a viable presence via culturing tissue specimens. In the following chapter the focus is shifted to investigate some of the aforementioned pathways that play prominent roles in the initiation and progression of atherosclerotic plaque tissue. Specifically, this chapter investigates the real-time quantitative real time PCR (RT-qPCR) gene expression of 10 genes. The genes are broadly categorised as cholesterol homeostatic genes (*SREBP2*, *SCAP*, *HMGR*, *LDLR* and *ABCA1*), inflammation (*TNF $\alpha$* , *IL1 $\beta$* , *CCL2* and *CCL3*) and apoptotic (*BCL2A1*).

## 6.2 Chapter aims

The aims of this chapter were two-fold.

1. To measure the expression of a panel of genes that are thought to play a role in the development of atherosclerosis such as.
  - a. Inflammation (*TNF $\alpha$* , *IL1 $\beta$* , *CCL2* and *CCL3*).
  - b. Cholesterol mediation (*SREBP2*, *SCAP*, *HMGR*, *LDLR* and *ABCA1*).
  - c. Apoptosis (*BCL2A1*).
2. To generate a unique profile of gene expression from atherosclerotic plaque tissue that can be used to compare with the expression of the same genes regulated in monocytes when challenged with one of the most frequently detected bacteria species present in the plaque tissues examined in earlier chapters, namely *Propionibacterium acnes*.

## 6.3 Method overview

A panel of oligonucleotide primers were designed to target the expression of 19 genes (section 2.5.1). Primers were optimised to ensure they met requirements of amplification efficiency and were sequenced to establish gene specificity (section 2.5.1). CAP ( $n = 15$ ) and LITA ( $n = 7$ ) tissue specimens for RNA analysis had been preserved in RNAlater<sup>®</sup> since collection from theatre. Specimens were ground in liquid nitrogen and RNA extracted using Tri Reagent<sup>®</sup> (section 2.5.2). mRNA was reverse transcribed using a RT-PCR protocol that was performed in two phases: initial anchoring of a 15-mer poly-T tailed oligo(dt) primer followed by first-strand synthesis of the cDNA sequence complementary to the RNA template (section 2.5.4). A negative control reaction was prepared by omitting GoScript<sup>®</sup> transcriptase enzyme. The cDNA generated was used as template for qPCR using SYBR<sup>®</sup> Select mastermix protocol (section 2.5.5). Each plate of qPCR reactions comprised test reactions (CAP cDNA), calibrator reactions (LITA cDNA) a RT-negative and a PCR negative (omitted template for dH<sub>2</sub>O) (section 2.5.5). Analysis of qPCR data were performed in accordance with the Livak and Schmittgen (2001)  $\Delta\Delta C_T$  method for relative gene expression (section 2.5.6).

## 6.4 Results

All reverse-transcription quantitative PCR results were generated to provide technical replicates  $C_t$  values for CAP ( $n = 15$ ) and LITA ( $n = 7$ ). However, not all plaques provided

a qPCR signal and therefore n numbers for both tissues are detailed in table 6.01. All  $C_t$  values were normalised to a stably expressed reference gene *RPL27A*

*HMGR* was highly expressed in plaque tissue ( $23.52 \pm 4.4$ ) compared to LITA ( $1.0 \pm 3.8$ ). Both fold change data sets were normally distributed and so fit the criteria for parametric significance testing with a Student's t-test. A two-tailed t-test revealed that *HMGR* expression in AP tissue was significantly different to *HMGR* expression observed in the healthy control tissue LITA [ $t(19) = 2.196, p = 0.02$ ].

Similarly, *SCAP* showed a comparable up-regulation in AP tissue ( $18.64 \pm 4.4$ ) compared to the level of *SCAP* expression observed in LITA tissue ( $1.07 \pm 4.5$ ). Fold change values for plaque tissue were not normally distributed and could not be made normal by transforming the data. A Shapiro-Wilk test for normal distribution was performed with a null hypothesis, "the population from which the sample set originates are normally distributed" and rejected when  $p < 0.00001$ . The data set remained non-normal following data transformation giving  $p < 0.05$ . Hence, data were analysed using a non-parametric Mann-Whitney *U* (MWU) test. A two-tailed MWU test revealed that *SCAP* expression in AP tissue was significantly different compared to LITA tissue expression of *SCAP* [MWU = 18,  $n_1 = 15, n_2 = 6, p = 0.04$ ]. Had a student's t-test been performed, the test would have revealed that expression of *SCAP* in AP tissue was not different relative to *SCAP* expression in LITA tissue [ $t(19) = 1.64, p = 0.117$ ].

*SREBP2* was up-regulated in AP ( $11.42 \pm 4.17$ ) compared to LITA ( $1.03 \pm 4.7$ ). However, the expression of *SREBP2* in AP was not significantly different to that of the control tissue expression [ $t(18) = 0.76, p = 0.457$ ]. Likewise, *LDLR* expression in AP tissue ( $-1.45 \pm 4.44$ ) was not different to the expression observed in LITA control tissue ( $1.64 \pm 4.8$ ) and so was not statistically significant [ $t(9) = -0.27, p = 0.796$ ]. There was a noticeable reduction in samples showing detectable expression of *LDLR*; only one third of the specimens produced a qPCR signal. Because of this, mean expression fold change was skewed.

In contrast to *SREBP2* and *LDLR*, up-regulated *ABCA1* expression was markedly greater in plaque tissue ( $285.59 \pm 4.5$ ) than it was LITA tissue ( $1.61 \pm 4.9$ ). Indeed, a two-tailed Student's t-test confirmed that fold change difference of *ABCA1* in AP tissue relative to LITA control tissue was highly significant [ $t(18) = 2.76, p = 0.013$ ]. In fact plaque tissue expression of *ABCA1* was by far the most highly expressed gene of all target genes examined here.

Both *CCL3* and *CCL2* were similarly expressed in AP tissue ( $13.43 \pm 4.2$  and  $9.89 \pm 4.7$ , respectively) relative to LITA ( $1.02 \pm 4.2$  and  $1.13 \pm 3.7$ , respectively). After performing a two-tailed Student's t-tests both AP tissue expression *CCL3* and *CCL2* showed fold changes that were significantly different when compared to LITA control tissue, [ $t(12) = 3.23, p = 0.032$ ] and [ $t(18) = 3.50, p = 0.003$ ], respectively.

*ICAM1* ( $2.563 \pm 4.4$ ) showed remarkably low expression in AP tissue compared to the fold change levels of other target genes. Yet, *ICAM1* expression was shown to have changed significantly in AP relative to LITA control expression [ $t(15) = 2.37, p = 0.032$ ]. Surprisingly, the mean expression values for *TNF $\alpha$*  ( $4.327 \pm 4.4$ ), *IL1 $\beta$*  ( $6.05 \pm 4.6$ ) and *NF $\kappa$ B* ( $1.35 \pm 4.8$ ), were also low in AP tissue. Subsequently, their expression in AP tissue did not differ significantly from the level of expression observed in the LITA control tissue *TNF $\alpha$*  [ $t(11) = 1.85, p = 0.091$ ], *IL1 $\beta$*  [ $t(14) = 0.79, p = 0.439$ ] and *NF $\kappa$ B* [ $t(18) = 0.093, p = 0.927$ ]. In contrast, *BCL2A1* expression was the second most highly expressed gene, after *ABCA1*. The level of *BCL2A1* expression in plaque tissue ( $50.59 \pm 4.8$ ) was shown to be significantly different to the expression of *BCL2A1* in LITA tissue ( $1.12 \pm 4.3$ ) giving a probability [ $t(17) = 5.79, p < .0001$ ].

Gene	$p$	$t$ -stat	DF	Plaque	LITA		
				Mean fold	$n$	Mean fold	$n$
HMGR	0.041	2.196	19	23.516±4.45	15	1.003±3.85	6
SREBP2	0.457	0.761	18	11.424±4.17	14	1.033±4.67	6
LDLR	0.796	-0.266	9	-1.449±4.18	6	1.642±4.82	5
ABCA1	0.013	2.758	18	285.593±4.44	15	1.611±4.90	5
CCL3	0.032	3.229	12	13.430±4.49	9	1.021±4.21	5
CCL2	0.003	3.498	18	9.887±4.66	14	1.132±3.73	6
ICAM1	0.032	2.368	15	2.563±4.44	12	1.043±4.33	5
TNF $\alpha$	0.091	1.854	11	4.327±4.45	8	1.103±5.10	5
IL1 $\beta$	0.439	0.797	14	6.058±4.61	12	1.182±5.13	4
BCL2A1	0.00002	5.792	17	50.586±4.80	14	1.115±4.39	5
$U_{\text{test}}/U_{\text{crit}}$							
SCAP*	0.036	18/19	19	18.643±4.44	15	1.072±4.50	6

**Table 6.01:** Gene expression results for CAP expression relative to LITA and normalised to RPL27A. Statistical results for two-tailed, independent Student's  $t$ -test of gene expression  $C_T$  values in plaque tissue vs healthy LITA control tissue and normalised to reference gene RPL27A. Significance testing was performed with the statistical package R v 3.0.3 and probability ( $p$ ),  $t$ -stat score, degrees of freedom (DF), mean fold change and number of observations for AP and LITA are presented.

\* Non-parametric testing for SCAP: AP fold change expression data were not normally distributed and therefore tested using a MWU test. The column  $U_{\text{test}}/U_{\text{crit}}$  denotes the lowest computed  $U(U_{\text{test}})$  value for AP vs LITA, 18. From a table of two-tailed critical  $U(U_{\text{crit}})$  values, comparing sample sizes  $n_1$  15 vs  $n_2$  6,  $U_{\text{crit}} = 19$  for a  $p < 0.05$ . As  $U_{\text{test}} < U_{\text{crit}}$  ( $18 < 19$ ) MWU = 18,  $n_1 = 15$ ,  $n_2 = 6$ ,  $p$  0.036 (two-tailed)

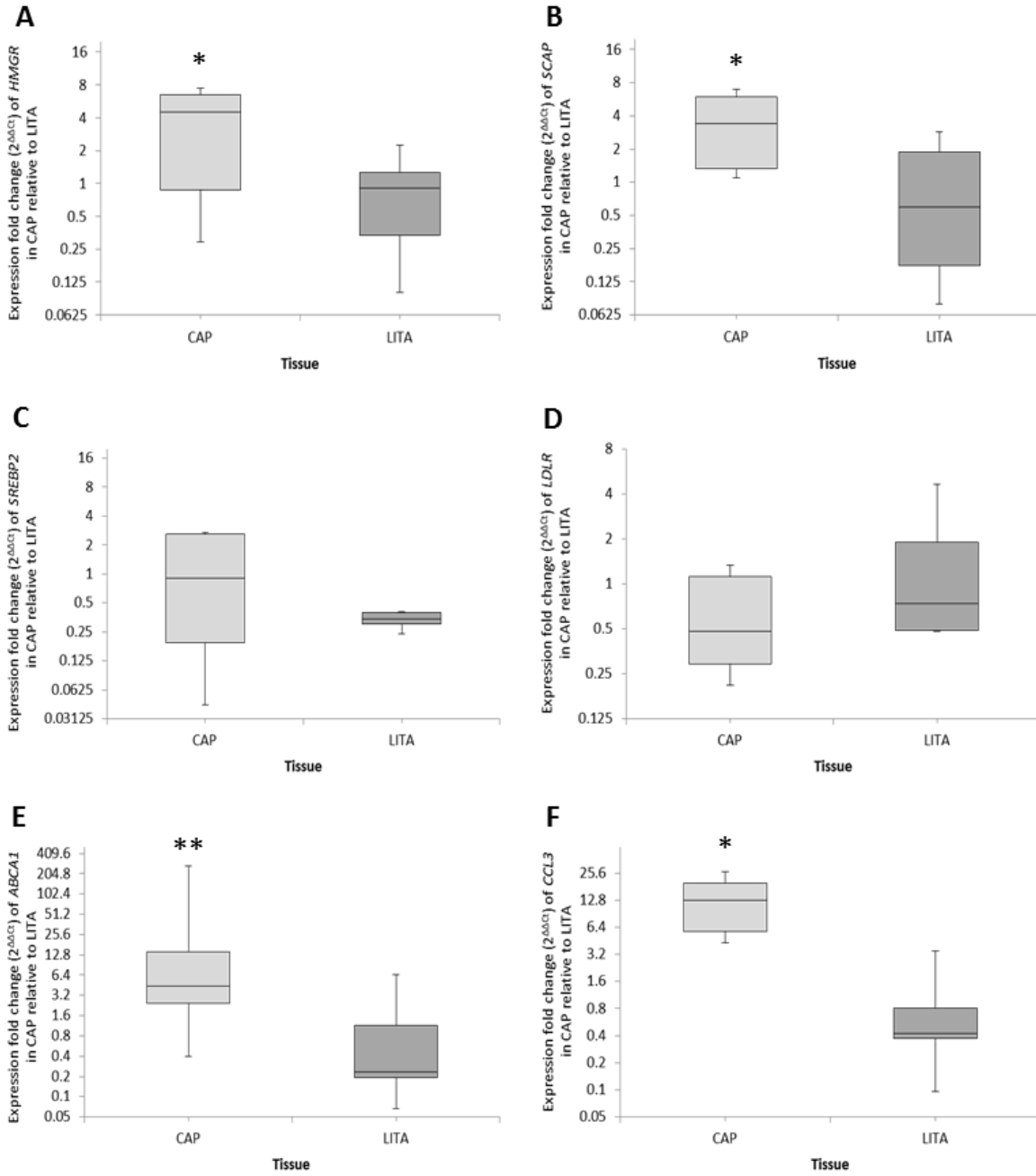


**Figure 6.03:** Shows boxplot graphs for fold change expression of *HMGR* (A), *SCAP* (B), *SREBP2* (C), *ABCA1* (D) and *CCL3* (E) in plaque (n = 15) vs LITA (n = 7) tissue. Gene expression data was calculated using  $C_T$  values for each target gene that were normalised to a stably expressed reference gene *RPL27A*. Boxplots show data for 25%-75%; \* <0.05; \*\* <0.01; \*\*\*<0.001

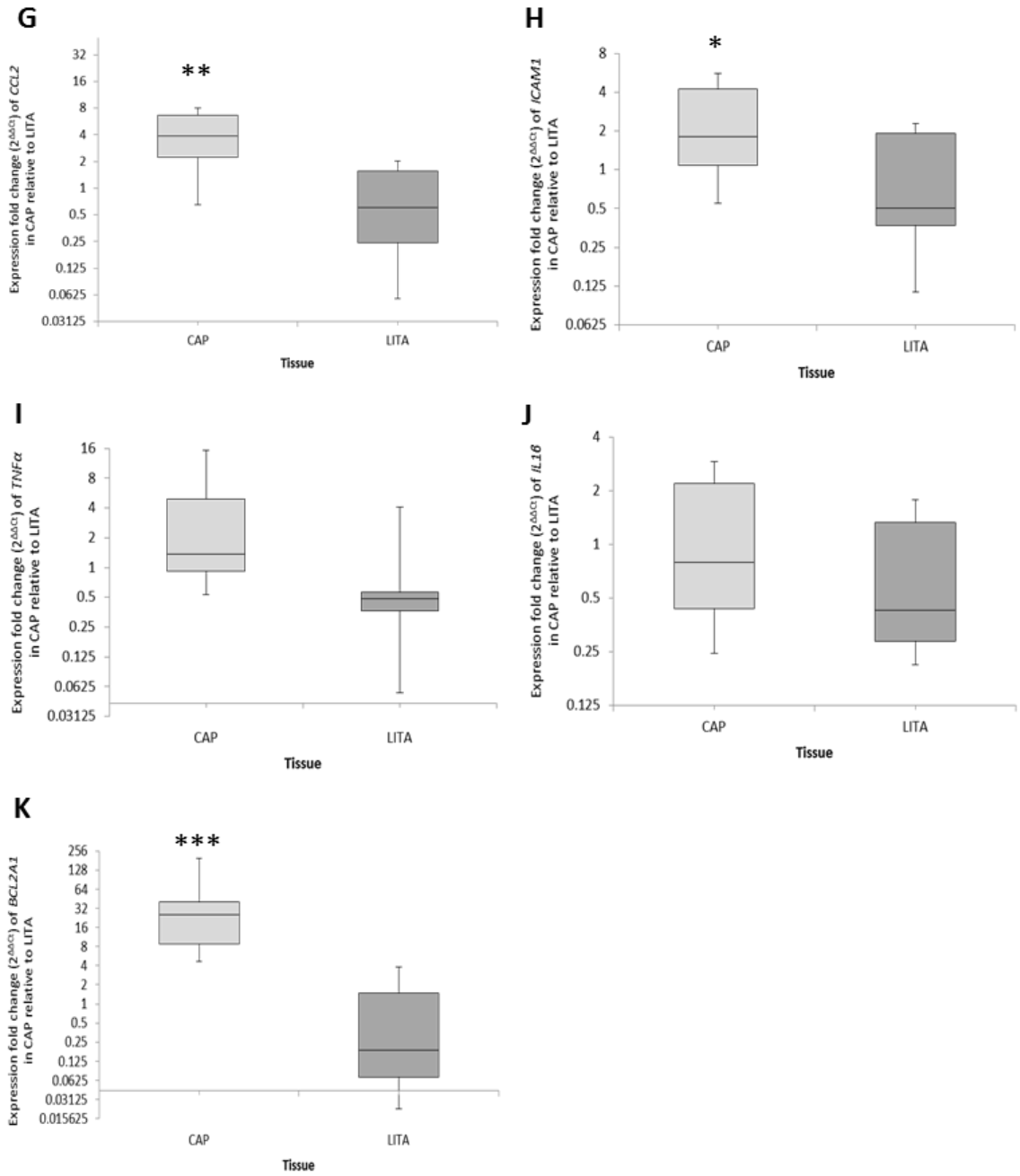


**Figure 6.03:** *Continued.* Shows boxplot graphs for the gene expression fold change of *CCL2* (G), *ICAM1* (H), *TNF $\alpha$*  (I), *IL1 $\beta$*  (J) and *BCL2A1* (K) in plaque (n = 15) vs LITA (n = 7) tissue. Gene expression data was calculated using  $C_T$  values for each target gene that were normalised to a stably expressed reference gene *RPL27A*. Boxplots show data for 25%-75%; \* < 0.05; \*\* < 0.01; \*\*\* < 0.001

## 6.5 Discussion

### 6.5.1 Sterol Regulatory Binding Protein

In the present investigation expression of SREBP2 was mostly the result of a significantly large expression (>144-fold) from just one CAP sample, whereas the remaining plaque samples showed only small increases (<5-fold) or downregulation. Hence, collective expression of SREBP2 was not significantly elevated. These observations suggest the CAP samples examined here were possibly at drastically different stages in their development. These data contrast findings presented by Fan et al. (2008), who performed whole genome sequencing to investigate the expression of SREBP2 and SCAP in human atherosclerotic tissues (type IV – V) and compared them in different arterial beds, i.e. the carotid, aorta and femoral region and normal artery tissue. A significant down-regulation of SREBP2 in atherosclerotic carotid plaques but not in the aorta or femoral arteries compared with non-atherosclerotic tissues. SCAP showed a similar pattern of expression, though levels were not statistically significant. The pattern of expression demonstrated by Fan et al. (2008) completely contrast the findings presented in this chapter, in which both SREBP2 (>11-fold) and SCAP (>18-fold) showed marked upregulation, though only SCAP was significantly expressed in CAP samples compared to healthy LITA controls. Shchelkunova et al. (2013) measured mRNA levels at different stages of aortic atherosclerosis using qPCR and recorded a progressive upregulation of SREBP2 in fatty streaks and fibro-lipid plaques. Interestingly, although different arterial beds were examined data presented by Shchelkunova et al. (2013) are more comparable with finding presented here, which may indicate a certain amount of uniformity between expression of plaques from different bodily sites.

Interestingly, the findings presented here, particularly for expression of SREBP2 in CAP specimens are more aligned with those representing aortic expression. For example, Shchelkunova et al. (2013) measured mRNA levels at different stages of aortic atherosclerosis using qPCR and recorded a progressive upregulation of SREBP2 in fatty streaks and fibro-lipid plaques. Given that genetic mutations of SREBP2 1784G>C and the SCAP 2386A>G have been shown to put men at an increased risk of sudden cardiac death it is likely different genotypes affect the development of atherosclerosis differently, which may partially account the different patterns of expression observed between these studies (Fan et al. 2008).

In simple terms, the role of SCAP as a cholesterol sensing protein activates SREBP2 when intracellular cholesterol levels are depleted. Through a succession of proteolytic cleavages to release SREBP2/SCAP from the ER, SREBP2/SCAP translocate to the Golgi apparatus. From there, the transcriptionally active portion of the SREBP2 is proteolytically cleaved and translocates to the nucleus where it functions as a transcription factor in the transcription of genes needed for uptake and synthesis of cholesterol genes including HMGCR and LDLR. One can make certain inferences based on the pattern of expression observed here. Firstly, the pattern of expression indicates the cells within the plaque tissue are in a cholesterol-depleted state, evidenced by SCAP up-regulation. Secondly, given the lack of significant SREBP2 expression, but significant up-regulation of SCAP, the process was captured at the earliest point in the pathway. Given the high lipid cholesterol composition of an atherosclerotic plaque, it would be more intuitive to expect to see down-regulation or no regulation of SREBP2 and SCAP, particularly for macrophages that have access to or are loaded with cholesterol in excess.

Interestingly, expression of SREBP2 in plaque have been partially reproduced in cultured macrophages upon lipid loading, which suggests the involvement of macrophage foam cells in the expression profiles observed here (Shchelkunova et al. 2013). However, both SCAP and SREBP2 are upregulated in foam cells in response to pro-inflammatory cytokines, such as TNF- $\alpha$  and IL-1 $\beta$ , which suggests more complex mechanisms are at play, other than just sterol sensing (Ruan et al. 2001). Although, while mRNA levels for both TNF $\alpha$  and IL1 $\beta$  were raised in the CAP samples examined here, mRNA levels were not significantly greater than those observed for the LITA control tissue. Nevertheless, monitoring the expression of these genes is a good way of gauging cholesterol mediation in atherosclerotic plaque tissue and it would be informative to replicate these findings in an in vitro model of infection.

### 6.5.2 3-hydroxy-3-methylglutaryl coenzyme A reductase (HMGCR)

As previously mentioned *HMGCR* is another SREBP2/SCAP transcript coding for the enzyme HMG-coA reductase that controls the rate limiting step in the mevalonate pathway for *de novo* synthesis of cholesterol. In the present study, despite no change in the levels of *SREBP2* mRNA, significant up-regulation of *HMGCR* was observed. Given that the expression of HMGCR controlled by SREBP2, this would suggest a very recent up-regulation of SREBP2 in response to low cellular cholesterol cues. The significant expression of SCAP would certainly indicate this. *HMGCR* expression observed in this

study supports earlier findings by Lee et al. (2011), who demonstrated significant localised expression of *HMGR* in macrophage-rich areas of unstable plaque compared to plaques from patients with stable angina when using anti-HMGR and anti-CD31. These findings suggest that local HMG-CoA reductase is functionally active, and lesion macrophages in unstable angina more actively produce HMG-CoA reductase than in stable angina. Tuomisto et al. (2003) specifically isolated macrophage-rich shoulder regions of AP tissue using laser microdissection and reported a high up-regulation of HMGR compared to disease-free tissue of the same artery. It was proposed by that the relatively high expression of HMGR may be due to proliferation and/or differentiation of macrophages because similar expression was observed with THP-1 cells cultured with phorbol 12-myristate 13-acetate (PMA). Conversely when THP-1 cells were incubated with ox-LDL, which closer resembles atherogenic conditions, down-regulation of HMGR was observed, which suggests that lipid-loaded THP-1 macrophages may not be an accurate model of macrophages present in shoulder. Thus, HMGR may be expressed as a requirement of macrophage proliferation and/or differentiation rather than dysregulated by inflammatory/lipid stimuli.

In the present study no specific region of AP tissue or accumulation of particular cell types was isolated for analysis, yet notably, HMGR expression fold change was 30% greater than observed by Tuomisto et al. (2003). This may be the result of large accumulations of lipid-loaded macrophages as observed by Tuomisto et al. (2003); however all other cell types present within the atherosclerotic plaque tissue have the capacity for *de novo* cholesterol synthesis and therefore could be equally as responsible. To elucidate the specific cells responsible for the overexpression of HMGR within the atherosclerotic plaques examined here, it would be necessary to perform IHC by targeting HMGR expression as well as specific cell types present atherosclerotic plaque tissue section. Alternatively, regions of tissue containing accumulations of individual cell types can be microdissected and analysed for expression of HMGR via qPCR. Nevertheless, HMGR has been shown here to be highly expressed in atherosclerotic plaque tissue, which if expressed by tissue macrophages has the potential to influence lipid loading.

### 6.5.3 ATP-binding cassette, sub-family A (ABC1), member 1

In the present study, expression of ABCA1 mRNA was by far the most highly expressed gene of all genes tested, showing a fold increase in CAP tissue that was >285 times higher than ABCA1 expression in healthy LITA control. A previous report of ABCA1 localization in human atherosclerotic tissue using in situ hybridization demonstrated that ABCA1 mRNA was predominantly localized to macrophages in both early fatty streaks and in the shoulders regions of advanced aortic atheromas, but not in LITA (Lawn et al. 2001). Since then, a number of related studies have also recorded increased expression of ABCA1 in various vessels affected by atherosclerosis (Albrecht et al. 2004; Forcheron et al. 2005; Soumian et al. 2005; Isoviita et al. 2010; Liu et al. 2012).

Albrecht et al. (2004) reported significantly increased ABCA1 mRNA in advanced plaque specimens compared to inferior mesenteric arteries (IMA) using qPCR standard curve method. In addition, Albrecht et al. (2004) revealed that ABCA1 activity was localised, rather than systemic up-regulation of ABCA1, evidenced by a lack elevated *ABCA1* expression in circulating leukocytes. Interestingly, *ABCA1* mRNA and protein expression were comparable for IMAs; whereas protein expression was significantly reduced in atheroma, less than IMA, despite significant up-regulation of *ABCA1* mRNA. Liu et al. (2012) showed similar divergence between ABCA1 mRNA and protein levels when investigating expression of carotid endarterectomy specimens at various stages of development (AHA histological features of type I to III) compared to IMA healthy controls. Type II and III *ABCA1* mRNA levels were significantly higher than that of type I. Though, in contrast to mRNA levels, protein levels for type II and III were significantly lower than type I. The same disparity between ABCA1 mRNA and protein levels were observed by Forcheron et al. (2005) who recorded no change of ABCA1 mRNA expression in carotid plaques vs microscopically intact tissue (MIT), though a significantly decreased ABCA1 protein levels was observed.

Taken together these findings provide evidence that *ABCA1* mRNA expression levels are up-regulated throughout early to advanced lesion development, which is consistent with the expression of ABCA1 observed here. Eventually though, expression in advanced lesions leads to a loss of function characterised by a decrease of protein, despite significant up-regulation of mRNA. Clearly, mRNA levels do not always accurately reflect protein expression, particularly it appears for *ABCA1*, where relative mRNA distribution in tissue show marked discordance with protein expression patterns signifying that post-

translational regulation of ABCA1 is critical cholesterol homeostasis (Wellington et al. 2002)

Consequently, when considering these findings, it becomes difficult to elucidate the true meaning of the *ABCA1* expression observed here without evidence of protein induction. However, to our knowledge, the level of ABCA1 mRNA expression presented in this study far exceeds any ABCA1 mRNA levels in atherosclerotic plaque published so far. Ordinarily, this may indicate elevated ABCA1 protein; however, protein levels cannot be hypothesised given the large discourse between mRNA and protein levels observed by other investigators. It can however be suggested, that the population of carotid endarterectomy specimens analysed here produced a pattern of *ABCA1* expression more typically encountered with moderate to advanced lesions.

#### 6.5.4 Low density Lipoprotein Receptor

A non-significant down-regulation of LDLR was noted in the present investigation. As a transcript of SREBP2, LDLR is expressed when intracellular levels are depleted. The LDLR is responsible for receptor-mediate endocytosis of extracellular cholesterol in the form of circulating LDL that can be used by the cell for various intracellular requirements; e.g. for incorporation into the lipid bilayer. Alternatively, hepatic LDLR plays a major role in RCT responsible by uptake LDL into the liver, which is the organ responsible for removing most excess cholesterol from the body. The number of expressed LDLRs on the surface of the liver determines how quick LDL is removed from the bloodstream. Given the susceptibility for development of atherosclerosis in patients with certain genotypes of the LDLR known to be the cause of hypercholesterolemia, the LDLR is a well studied receptor. Surprisingly though, there have been no reports that demonstrate direct expression of LDLR in human atherosclerotic plaque tissue. Unfortunately, this remains the case with the data obtained here.

#### 6.5.5 Chemokine (C-C motif) Ligand 3 (CCL3)

In the present study significant upregulation of *CCL3* was demonstrated in CAP specimens compared to expression levels in a healthy LITA control tissue. Levula et al. (2012) evaluated 256 genes in femoral, aortic and carotid vessels. Numerous significantly up-regulated genes were recorded in carotid specimens, including *CCL3*, which showed a fold change value comparable with the present investigation. Earlier IHC investigations report

similar expression patterns for CCL3 & CCL2, which were often found associated with macrophages and/or T cells within inflammatory zones of human atherosclerotic plaques, e.g. plaque shoulders (Wilcox et al. 1993). Similarly, Hayes et al. (1998) reported qPCR expression of CCL3 and CCL2 in human CAP tissue. In a second experiment, Hayes et al. (1998) characterize the expression of known chemokine receptors by treating primary human VSMC vascular smooth muscle cells with CCL3 and CCL2. With the addition of the finding presented in the current investigation that confirms earlier reports of CCL3 expression in various forms of atherosclerotic disease, it is clear both CCL3 and CCL2 are potently expressed in plaque tissue along with their receptor ligands. This chapter was prepared as a work to establish a gene expression profile that can be compared with the following chapter of work to investigate an in vitro model of infection. Based on the significance of CCL3 expression observed here, it would be interesting to compare the expression of CCL3 within a simple model of bacterial infection to better understand the role infection plays in one of the major cells present in atherosclerotic plaque tissue, monocyte/macrophage.

#### 6.5.6 Chemokine (C-C motif) Ligand 2 (CCL2)

In the present investigation, *CCL2* was found to be significantly up-regulated in AP tissue from the carotid artery relative to expression level observed in a healthy LITA control tissue. Findings presented here are in agreement with Kusano et al. (2004) who showed expression of *CCL2* in the carotid arteries of patients chronic haemodialysis (HD) (a group with ~30% increased risk of cardiovascular mortality). In addition, Kusano et al. (2004) demonstrated that serum concentration of *CCL2* was an independent factor influencing intimal-medial thickening (IMT). Moreover, tissue immunostaining showed that *CCL2* was expressed in both endothelial and smooth muscle cells and that its level of expression correlates with the serum concentration of *CCL2*. These findings suggest *CCL2* is involved in the very earliest intimal thickening stages of atherosclerosis. When taken together with the expression of *CCL2* shown here, in more complicated lesion, this indicates *CCL2* is involved at many stages of plaque development.

Earlier investigations have also reported *CCL2* expression in CAP tissue that is most predominantly expressed in macrophage-rich shoulder tissue bordering the lipid core of CAP and atherosclerotic aorta specimens, though less so in fibrous cap or the lipid core itself (Ylä-Herttuala 1991; Nelken et al. 1991). These findings suggest a predominant pro-inflammatory role of tissue macrophages within plaque tissue, and highlight particular

regions of plaque as more chemotactic than others. Others have reported the immunohistochemical expression of *CCL2* in different stages of atherosclerotic disease revealing *CCL2* was most expressed by endothelial cells and macrophages of the early fatty streaks, rather than advanced plaques (Takeya et al. 1993). Data presented by Takeya et al. (1993) contrasts the findings presented here, in which we show *CCL2* expression occurring in more advanced plaque specimens. Again, this highlights the consistent role of *CCL2* throughout many stages of plaque development. However, this publication pre-dates the AHA classification system used to grade atherosclerotic plaque tissue by histological features, hence, there may be some inconsistency regarding the tissue classification system used.

The findings presented here therefore support findings from early investigations where northern blotting, *in-situ* hybridisation and immunocytochemistry evidence was presented. It would be interesting to see the level of *CCL2* in an in vitro model of atherosclerosis with particular emphasis on infection.

#### 6.5.7 Intracellular Adhesion Molecule 1 (ICAM-1)

In the current investigation a small but significant upregulation of ICAM-1 was observed in CAP tissue compared to healthy LITA control expression. Over the last 20 years there have been numerous investigations to evaluate the expression of adhesion molecules in different atherosclerotic diseased tissues. These are consistent with many investigations that have been performed over the last 20 years evaluating femoral arteries (Poston et al. 1992; Jones et al. 1998) aortic arteries (van der Wal et al. 1992; Poston et al. 1992; Printseva OYu et al. 1992; Parums 1995; Jones et al. 1998; de Vries et al. 2000) and coronary arteries (van der Wal et al. 1992; O'Brien et al. 1993; Davies et al. 1993; O'Brien et al. 1996). Similarly, carotid arteries with various forms of atherosclerotic disease has been investigated and shown to express ICAM-1 (Hwang et al. 1997; Jones et al. 1998) Hwang et al. (1997) performed ELIZA to determine the extent of soluble circulating adhesion molecules, including selectin, VCAM-1 & ICAM-1 in the blood of patients with CHD and carotid artery atherosclerosis (CAA) compared with control subjects. Levels of VCAM-1 were not significantly different among all groups; however, significantly higher levels of E-selectin and ICAM-1 were observed for the patients with CHD and those with CAA compared with the control subjects. Nevertheless, plasma ICAM-1 levels have been shown to not be predictive of symptomatic disease and there is no correlative relationship between risk of stroke and endothelial ICAM-1 expression (DeGraba 1997; DeGraba et al.

1998) In contrast, ICAM-1 expression on the endothelium of the carotid artery is predominantly associated with symptomatic atherosclerotic disease (DeGraba 1997; DeGraba et al. 1998). This elevation in ICAM-1 expression in symptomatic plaque suggests that ICAM-1 is involved in the conversion of carotid plaque to a symptomatic state.

In the present investigation carotid endarterectomy tissue was examined that consists predominantly of plaque, though the endothelium of the carotid artery is removed with the plaque in the process. It is therefore highly likely the large layer of endothelium removed during the surgical procedure is responsible for the ICAM-1 expression observed here (Jones et al. 1998). However, neovessel channels develop in atherosclerotic plaque tissue as it develops more advanced features. Approximately 50% of the plaques examined in this investigation comprised neovessels, which, although immature in structure have been shown to be in an almost permanent state of activation, which may account for expression of ICAM-1 observed here (Mazzone et al. 2006).

Hitherto, investigations targeting adhesion molecules in atherosclerotic plaque tissue have involved IHC or hybridisation techniques. This is the first report showing ICAM-1 expression in CAP tissue specimens using qPCR analysis. While PCR target is mRNA as opposed to the protein target of immunohistochemical testing, PCR is more sensitive and non-subjective. Therefore, the data presented here provided solid conclusive evidence that cell adhesion molecule ICAM-1 is expressed in human CAP tissue. As such, suggests that leukocyte recruitment, an important process central to the development of atherosclerotic plaque, was induced in tissue specimens examined here. However, these results do not tell us what is happening at the protein level. To elucidate protein expression, a future experiment may include both qPCR with IHC or western blotting.

#### 6.5.8 Tumor Necrosis Factor-alpha (TNF- $\alpha$ )

In the present investigation TNF $\alpha$  was not shown to be expressed significantly in CAP samples compared to LITA. This contrasts earlier observations by other investigators examining carotid tissue (P. Tipping & Hancock 1993; DeGraba 1997; Skoog & Dichtl 2002). Expression of TNF $\alpha$  has been detected in plaque tissue mostly by IHC (Barath et al. 1990; Rus et al. 1991; Kishikawa et al. 1993) and expression is associated with symptomatology (DeGraba 1997). In a study by Tipping & Hancock (1993) carotid, aortic and femoral atherosclerotic plaque tissue were analysed by isolating atheromatous macrophages for primary in vitro culture as well as performing IHC directly on sections

of tissue to determine the expression of *TNF $\alpha$*  and *IL1 $\beta$*  in both techniques. The authors reveal *TNF $\alpha$*  was secreted by isolated macrophages to a greater extent than monocytes extracted from the blood of the same patients. Furthermore, *TNF $\alpha$*  expression was shown to be more prominent in carotid tissue than in aortic or femoral lesions when IHC was performed, whereas, *IL1 $\beta$*  was only expressed infrequently and at low intensity. While no significant change was observed for *TNF $\alpha$*  in the CAP samples examined here, expression was up-regulated 4-fold compared to LITA healthy control expression. However, a small sample set was examined in this study, which may, in part, explain the lack of a significant result. To evaluate the expression of *TNF $\alpha$*  in the future a greater population of plaque samples should be investigated.

#### 6.5.9 Interleukin 1-beta (IL-1 $\beta$ )

A detectable, but not significant change of *IL1 $\beta$*  mRNA was observed in the carotid AP tissue compared to control tissue expression. These findings are in agreement with Tipping & Hancock (1993), who reported a distinct lack of *IL1 $\beta$*  expression both within whole-blood monocytes and within plaque macrophages (Tipping & Hancock 1993). Similarly, Frostegård et al. (1999), using immunohistochemical staining, reported limited *IL1 $\beta$*  expression (3/10 carotid plaques), whereas *IL-1 $\alpha$*  expression was significantly expressed. Unlike IL-1 $\beta$ , IL-1 $\alpha$  is constitutively active in its precursor form and cleaved to maturity by calpain proteases rather than caspase-1. IL-1,  $\alpha$  and  $\beta$  facilitate recruitment of diverse endothelial-activated myeloid subsets, thereby sustaining the inflammatory response through discrete activation pathways (Rider et al. 2011). Furthermore, IL-1 $\alpha$  is reported to be a damage-associated molecular pattern (DAMP), released in excess from necrotic cells as a signal to the innate immune system during tissue injury (Kono & Rock 2008). In contrast, earlier studies using IHC staining have reported significant up-regulation of *IL1 $\beta$*  in human AP tissue. For example, Galea & Armstrong (1996) reported increased *IL1 $\beta$*  mRNA levels in ischemic atherosclerotic vessels compared to non-ischemic cardiomyopathic vessels. *IL1 $\beta$*  expression correlated with disease severity and was predominantly expressed by endothelial cells and macrophages of the adventitia (Galea & Armstrong 1996). Similarly Dewberry & Holden (2000), also reported overall localised expression of *IL1 $\beta$*  associated with endothelial cells and macrophages of coronary atherosclerotic tissue, but absent in cardiomyopathic vessel tissue. However, expression of *IL1 $\beta$*  has previously been reported in cardiomyopathic coronary vessels have previously (Wilkinson et al. 1999; Dewberry et al. 2000).

As already discussed, IL-1 $\beta$  mediates numerous pro-inflammatory roles, which potentiate atherosclerotic plaque development. Yet surprisingly, the level of *IL1 $\beta$*  mRNA observed in the present study was not significant. *IL1 $\beta$*  expression can promote apoptosis in EC and SMC; an effect shown to be impeded by overexpression of the interleukin 1 receptor agonist (IL1-ra) *in vitro* (Dewberry et al. 2000). In contrast, increased expression of anti-apoptotic proteins, such as BCL-XL and BCL-2, interact with NALP1, one of the central proteins in the inflammasome complex, by suppressing caspase-1 activation and IL-1 $\beta$  production (Bruey et al. 2007; Escandell et al. 2010). In addition, caspase-1 activation and IL-1 $\beta$  production increase following prolonged inhibition of NF- $\kappa$ B by chemical and genetic attenuation of I $\kappa$ B kinase- $\beta$  (IKK $\beta$ ); a protein responsible for NF- $\kappa$ B activation (Zong et al. 1999; Greten et al. 2007). Therefore, like BCL-2, NF- $\kappa$ B acts as a negative regulator of IL-1 $\beta$ , which emphasises the complex and intertwined relationship between apoptosis and inflammation (Greten et al. 2007; Escandell et al. 2010). When considering the inhibitory action anti-apoptotic genes have on *IL1 $\beta$*  expression; it is plausible to suggest the lack of *IL1 $\beta$*  expression observed in the present investigation may partially be due to the inhibitory influence of *BCL2A1*, which showed significant expression in the AP specimens examined here. However, this cannot be confirmed using relative gene expression alone but rather a more focused analysis of *BCL2A1* expression either by silencing *BCL2A1* or gene knockout experiments.

#### 6.5.9.1 BCL2-related protein A1 (BCL2A1)

One of the earliest investigations of pro and anti-apoptotic expression in advanced human carotid atherosclerotic plaque was performed using IHC (Konstadoulakis et al. 1998). The overall expression profile was one of pro-apoptosis comprising elevated Bax expression that correlated with macrophages by dual-staining, though no detectable expression of protective anti-apoptotic BCL-2-related genes for cellular survival (Konstadoulakis et al. 1998). In agreement, Woodside et al. (2003), assessed the differential expression of numerous apoptosis-related genes in primary and re-stenotic (>70% stenosis) carotid plaques tissue using microarray cDNA hybridisation. *BCL2A1*, and other anti-apoptotic genes were decreased in the restenotic plaque tissue compared to a “transition zone” (immediately adjacent to the stenotic area) and a “proximal zone” (tissue furthest from stenotic region). Microarray technology can be extremely powerful on account of the number of genes that can be examined in a single analysis, yet Woodside et al. (2003) used only one re-stenotic lesion for comparative testing. While it is interesting to establish the

extent to which apoptosis presents as an etiological factor in vascular stenosis, the significance of these particular observations carry no statistical weight. Moreover, these findings greatly contrast our observations, where the up-regulation of BCL2A1 mRNA (50-fold) highly significant in 20 carotid AP specimens compared to health LITA control tissue. The data presented here is comparable with Martinet et al. (2002), who used qPCR to measure the expression of 205 apoptosis-related genes in human carotid endarterectomy specimens. BCL2A1 was up-regulated in plaque tissue compared to LITA control specimens, however, while a significant up-regulation was observed, the fold-change reported by Martinet et al. (2002) was markedly lower than that observed here. Also in agreements with the present study was Silbiger et al. (2013) who identified potential candidate genes as predictive markers in patients during the first 48 hours of acute coronary syndrome (ACS) using microarray techniques. ACS is often a result of coronary stenosis caused by atherosclerotic plaque, thus Silbiger et al. (2013) measured expression at the systemic level during symptomatic atherosclerotic disease. A complex network of 549 genes, including anti-apoptotic BCL2A1 and BCL2L1 were found to be significantly expressed in whole blood cells of ACS patients. Again, although significant, gene expression fold change was a fraction of the level presented here. The authors suggested the low expression could be due to the low expression of ALOX15, a pro and anti-atherosclerotic gene shown to influence BCL-2 gene family expression, (Middleton et al. 2006). In contrast, Silbiger et al. (2013) showed significant up-regulation of pro-apoptotic pathway genes, including cytochrome c oxidase (COX)-7B and amphiregulin (AREG), presenting a complex picture of pro- and anti-apoptotic expression during acutely active atherosclerotic disease.

In the present study it is not possible to determine the exact cell types responsible for BCL2A1 expression. Both macrophages and SMC are controlled by apoptosis in the atherosclerotic lesion and therefore operate this cell survival machinery during active stages of disease (Kockx 2000). Therefore, as a follow up to the expression observed here and in keeping with the focus of this thesis, it would be informative to understand the expression status of macrophage BCL2A1 cells in response to bacterial infection.

## 6.6 Conclusion

The aims of this chapter of work were two-fold. To present a unique gene expression profile of CAP tissue. The generation of said expression profile could then be used to compare with an *in vitro* model of infection in the following chapter. The genes expressed

here highlight pathways that demonstrate the cholesterol homeostatic and inflammatory processes within the plaque tissue. There was a somewhat complicated picture regarding Cholesterol homeostasis. Although SREBP2 was not upregulated in the plaque tissue examined here, the significant expression of *HMGR* would suggest recent upregulation of *SREBP2*. *HMGR* is fundamental for *de novo* synthesis of cholesterol and as a *SREBP2* transcript gene, is activated only when SCAP senses depleted levels of intercellular cholesterol by initiating cleavage of *SREBP2* to release it from the ER. This profile is somewhat confused by the significant upregulation of SCAP and *HMGR* but not *SREBP*. This is confused further by the lack of *LDLR* expression because it would be expected that in lipid-depleted environment the LDL receptor would be upregulated to bolster LDL levels within the cell. These observations do not paint a very clear picture of the hyper lipidous environment of the atherosclerotic plaque. As discussed through this chapter, it is possible that this cholesterol homeostasis machinery is defective in the atherosclerotic vessels. However there are other possible explanations. For example, it has been shown that cholesterol levels are bolstered in reaction to bacterial infection; an antimicrobial measure by activation of *HMGR* to protect the cell wall from pore forming microbes (Kistowska et al. 2008). The latter scenario would go some way to explain why only *de novo* synthesis gene *HMGR* was observed rather than receptor mediated-cholesterol uptake but does not explain the expression of SCAP without *SREBP2*. It is noteworthy to highlight the fact that the lesion is a multicellular dynamic mass of tissue that would be in multiple phases of development and cellular activity. Thus, a slightly different region of plaque tissue may provide a completely different profile of expression. Furthermore, it must be noted that although a significant increase in *HMGR* mRNA was observed, this does not suggest an increase in *HMGR* protein, as there is a potential for post-transcriptional regulation.

The significant expression of *ABCA1* observed here goes counter to *HMGR* expression by suggesting a cholesterol rich environment within the cells of the atherosclerotic plaque tissue examined here. Monocyte –derived macrophages and SMC make up a large proportion of an atherosclerotic lesion, both of which are incapable of regulating scavenger receptor mediate internalisation of modified or oxidised LDL. Because these cells are in a constant “futile cycle” of cholesterol storage and efflux, it is not surprising to observe the extremely high expression of *ABCA1* measured in this investigation.

While preservation of the vessel is important during the surgical removal of the plaque, it is likely that endothelial cells and SMC were recovered with the CAP lesion during the endarterectomy procedure. An increase in chemokine genes CCL2 and CCL3 mRNA was observed, which would suggest active leukocyte recruitment by endothelial cells that are present in the atherosclerotic plaque. Leukocyte recruitment to endothelium is one of the initial processes that perpetuate the growth of an atherosclerotic plaque. The expression of ICAM-1 adds further credence to the activation of endothelial cells in the process of capturing rolling leukocytes for transmigration into the intimal layer of the artery. Interestingly, both TNF $\alpha$  and IL-1 $\beta$  were not expressed in the plaque tissue analysed here. As a major inflammatory cytokines TNF $\alpha$  initiates monocyte differentiation to macrophage and is also involved in signalling and activating the endothelium for leukocyte recruitment. IL1 $\beta$  also plays a major role in inflammation including cell proliferation, differentiation and apoptosis.

BCL2A1 was significantly expressed in the plaques examined here. BCL2A1 is activated as a pathway to cell survival by attenuating the release of pro-apoptotic cytochrome c from mitochondria and thereby blocks caspase activation (Vogler 2012). A primary source of BCL2A1 expression in atherosclerotic plaque is as a cell survival strategy in lipid-loaded macrophages that switch to a protective anti-apoptotic profile of gene expression (Martinet et al. 2002; Kutuk & Basaga 2006).

This chapter of work presents a unique gene expression profile that could be investigated further by generating protein expression profiles. Within the scope of this investigation it would be informative to measure the same panel of genes within a model of bacterial infection using a strain isolated from atherosclerotic plaque tissue.

**THE EFFECT OF PROPIONIBACTERIUM ACNES  
ON A HUMAN MONOCYTIC CELL LINE *IN VITRO***

## 7.1 Introduction

The predominant and foremost identifiable hallmark of atherosclerotic disease is the formation and retention of monocyte-derived macrophage foam cells in the intimal layer of the artery wall, particularly within early ‘fatty streak’ lesions. Foam cells are lipid-loaded macrophages that are generated through massive uptake of modified low density lipoprotein (McLaren et al. 2011). Lipoprotein deposition and retention in the artery wall is susceptible to oxidation and enzymatic modification, which is believed to potentiate endothelial dysfunction, triggering monocyte/macrophages recruitment to the site of inflammation through pro-inflammatory cytokine/chemokine signalling (Valente et al. 2014). Recruited monocytes extravasate the endothelium and undergo phenotypic differentiation to macrophages within the intimal layer, finally targeting modified lipoprotein for endocytosis via scavenger receptor-mediated recognition. Unlike the LDL receptor, which is regulated depending on cellular lipid requirement, scavenger receptor LDL uptake is unregulated; hence a large internalisation of oxLDL is permitted. In response to lipid-loading, macrophages activate a compensatory pathway for cholesterol efflux, mediated by transcription factor Liver-X-Receptor (LXR) and its target gene expression of transporter ABCA1. However, when systemic hypercholesterolemia is manifest, the homeostatic mechanism can be overwhelmed, causing an abundant accumulation of intracytoplasmic cholesteryl esters (CE) that leads to dysregulation of cholesterol homeostatic mechanisms and subsequent endoplasmic reticulum (ER)-mediated apoptosis.

Internalised CE undergoes hydrolysis and is released from lysosomes as unesterified cholesterol (UC) or “free cholesterol” (FC). The fate of FC is determined by enzymatic pathways where FC can undergo numerous cycles of esterification and hydrolysis by ER-resident hydrolases before reaching its final destination. When esterified, cholesterol is either terminally stored in lipid droplets or undergoes re-hydrolysis (UC) to provide cholesterol for cell membranes or to be effluxed to plasma membrane transporters, such as ABCA1. Oxysterol-mediated LXR for the transcription of ABCA1, provides transport and presentation of cholesterol to extracellular acceptor, apo-A1, thereby initiating the preliminary step in reverse cholesterol transport (RCT). Expression of ABCA1 therefore indicates the presence of excess intracellular cholesterol. However, RCT can be negatively affected by the presence of excess cholesterol, causing a dysregulation of the pathways controlling the fate of FC, which can remain in a ‘futile cycle’ of re-esterification-

hydrolysis. Thus, any imbalance in the pathways favouring cholesterol storage potentiates macrophage lipid-loading and the development of foam cell that collectively form the atherosclerotic lesion.

An increase in systemic LDL can be observed during infection as an immune defence mechanism facilitated by lipoproteins that bind endotoxin, rendering them inactive (Cavaillon et al. 1990). In previous *in vitro* investigations, numerous bacterial species that are frequently detected in human atherosclerotic plaque have demonstrated an ability to promote lipid retention in human and murine macrophage cell lines following co-culture with LDL (Kalayoglu & Byrne 1998; Qi et al. 2003; Giacona & Papapanou 2004; Lei et al. 2011; Okahashi et al. 2011; Nicolaou et al. 2012). Microbial-induced dysregulation of cholesterol homeostasis is believed to result through toll-like receptor (TLR) ligand activation of the IRF3 pathway, which in turn has been shown to have an inhibitory effect on LXR target gene expression (ABCA1) in cultured macrophages and *in vivo* (Castrillo et al. 2003; Cao et al. 2007; Chen et al. 2008; Higashimori & Tatro 2011). Consequently, macrophage pathogen recognition can attenuate cholesterol efflux from infected macrophages in addition to initiating an inflammatory response.

In chapters 4 and 5 of this thesis, *P. acnes* was the most frequently detected bacterial species in human carotid atherosclerotic plaque tissue. *P. acnes*, (previously known as *Corynebacterium parvum* (Cummins & Johnson 1974)) is a non-motile, gram-positive, aerotolerant anaerobe that inhabits numerous bodily niches. The strain SK137 is commonly isolated from the oral cavity and detected in failed prosthetic implants, among other bodily sites. The detection and isolation of this opportunistic pathogen highlights its ability to systemically infect its host and survive within its host for long periods of time. As an opportunistic pathogen, *P. acnes* is implicated in several inflammatory conditions through chronic and reoccurring infection, such as sarcoidosis, sciatica, arthritis, prostate cancer and infective and aggressive endocarditis, as well as a range of post-operative and clinical device related infections (Gunthard et al. 1994; Stirling et al. 2001; Hiramatsu et al. 2003; Cohen et al. 2005; Berthelot et al. 2006). In recent years, 82 strains of *P. acnes* have been completely sequenced and extensive comparative and pan-genomic analyses performed for all known lineages; highlighting genetic elements specific to each lineage that illustrates the differences of *P. acnes* in functioning as a commensal of the skin and as a pathogen in the aetiology of diseases (Hunyadkürti et al. 2011; Horváth et al. 2012; Tomida et al. 2013). The pathogenic potential of *P. acnes* is recognised by the organism's

encoding of >2300 open reading frames (ORF) for production of several host degrading proteins, including; hemolysins, cytotoxins, adhesins and host tissue degrading enzymes (Valanne et al. 2005; Falcocchio et al. 2006; Holland et al. 2010; Mak et al. 2013). These putative virulence factors of *P. acnes* can induce tissue damage through haemolysis, pore-formation, adhesion to multiple surfaces for biofilm formation and cell aggregation, as well as induction of chemotactic and inflammatory pathways (Brüggemann 2005; Tucker et al. 2005).

In the current chapter, we investigate the pro-inflammatory and cholesterol regulatory potential of the isolated *P. acnes* strain. *P. acnes* localises and preferentially proliferates in lipid-rich environments and is a TLR receptor ligand complicit in secretion of chemotactic factors, such as IL6, IL8, IL12 and IL18 and pro-inflammatory cytokines TNF- $\alpha$  and IL1 in numerous cell lines *in vitro* (Kim et al. 2002; Jugeau et al. 2005; Nagy et al. 2005; Fathy et al. 2009; Shibata et al. 2009). In addition *P. acnes* further contributes to the inflammatory response by triggering the activation of the NLRP3-inflammasome for the secretion of caspase-1 activation-dependent cytokines, particularly IL1 $\beta$ , both *in vitro* and *in vivo* (Qin et al. 2014; Thiboutot 2014; Kistowska et al. 2014; Contassot & French 2014).

Here we investigate the potential pro-inflammatory and cholesterol regulatory characteristics of *P. acnes* strain SK137 isolated from human atherosclerotic plaque. The quantitative and temporal expression of cytokine genes, *IL1B*, *TNF $\alpha$* , and *CCL2 CCL3* and cellular adhesion molecule *ICAM1* were measured during following *in vitro* challenge of THP-1 monocytes with SK137. Also, evidence is mounting that demonstrates cross-talk between pro-inflammatory and cholesterol homeostasis pathways such as SCAP-SREBP-regulated transcription of HMG-CoA reductase (*HMGR*) and low density lipoprotein receptor (*LDLR*) (Castrillo et al. 2003; Li et al. 2013; Zhang et al. 2014). It has been suggested that bacterial infections dysregulate the mevalonate pathway, through inducing *HMGR* up-regulation. This mechanism of immediate antimicrobial immunity serves to meet the demand for increased cholesterol, which is directed to the plasma membrane to bolster the defence against bacterial pore-forming toxins (Kistowska et al. 2008). Moreover, increased HMGR causes a reduction of LDLR expression and therefore an increase in serum LDL, which are known to bind and inactivate bacterial lipopolysaccharide (Cavaillon et al. 1990; Weinstock et al. 1992) This mechanism in response to bacterial infection, may potentiate foam cell formation (Qi et al. 2003; Giacona

& Papapanou 2004; Okahashi et al. 2011). In relation to this we provide novel evidence that *P. acnes*-infection mediates the expression of genes involved with cholesterol biosynthesis (*SREBP2*, *LDLR* and *HMGR*) and efflux (*ABCA1*).

## 7.2 Aims

The aims of this chapter of work were to,

1. Design a selection 21 oligonucleotide primer sets for genes involved in three broad areas of cellular functions that may contribute to the pathogenesis of atherosclerosis
  - a. Cholesterol mediation (*HMGR*, *SCAP*, *SREBP2*, *LDLR* & *ABCA1*).
  - b. Inflammation (*CCL2* *CCL3*, *ICAM1*, *TNF $\alpha$* , *IL1 $\beta$*  & *NF $\kappa$ B*).
  - c. Apoptosis (*BCL2A1*).
2. Optimise primer sets by measuring relative mRNA levels in the human monocytic cell line; THP-1 cells challenged with *E. coli* LPS.
  - a. Establish optimum amplification efficiency of primer sets.
  - b. Test the THP-1 cell line as a medium for suitable *in vitro* model of infection using clinical isolated strain *P. acnes*.
3. Challenge THP-1 cells with isolated strain *P. acnes* for the purpose of measuring relative expression of optimised genes (aim 1a-c) using quantitative real-time PCR.
  - a. Investigate the extent to which *P. acnes* may regulate genes known to be involved in the pathogenesis of atherosclerosis.

## 7.3 Method

To assess whether human monocyte cell line THP-1 responds to bacterial stimulus, cells were incubated with *E. coli* LPS (section 2.6.3) and RNA was extracted from the cell at 30 min, 1 h, 1.5 h, 2 h and 20 h, following manufacturer's guidelines, as previously described (section 2.4.2). The mRNA was reverse transcribed to cDNA (section 2.4.4) and utilised as template for qPCR analysis (section 2.4.5) to measure the expression of 21 target GOI relative to endogenous control gene *ACTB*. THP-1 cell incubation with *E. coli* LPS provided a platform for establishing primer specificity/amplification efficiency and to test the efficacy of THP-1 cells was a suitable cell line for a model of inflammation, cholesterol metabolism/transport and apoptosis. Serial dilutions of cDNA for 6 orders of magnitude were utilised as qPCR template.  $C_T$  values were used to plot a chart for  $C_T$  value vs. log cDNA input to generate a standard curve with regression line of best fit. The slope

of the regression line of best fit was optimal at  $-3.32 \pm 0.332$  ( $E=2.00 \pm 0.14$ ). Any primer sets that fell below the optimal amplification efficiency were omitted (section 2.5.4). THP-1 cells were then challenged with whole heat-killed *P. acnes* (section 2.6.4) isolated from CAP tissue in chapter 5, (section 5.2.4). mRNA was extracted from *P. acnes*-stimulated THP-1 cells at 2 h, 6 h and 24 h along with THP-1 negative vehicle control cells treated with a PBS (section 2.4.2). *P. acne*-stimulated THP-1 mRNA was reverse transcribed (section 2.4.4) and relative gene expression was measured by qPCR using the final optimal primer sets (section 2.4.5). Analysis of qPCR data were performed in accordance with the Livak and Schmittgen (2001)  $\Delta\Delta C_T$  method to calculate gene expression fold change relative to PCS control cells and normalised by endogenous control gene *ACTB* (section 2.5.6). The significance of observed fold change values for both LPS-induced and *P. acnes*-induced gene expression were calculated by analysis of variance (ANOVA) test. The difference in expression fold change between test and control gene expression was deemed significant when  $p = <0.05$ .

## 7.2 Results

### 7.2.1 THP-1 growth characteristics

Normal growth conditions were measured for THP-1 by determining growth characteristics such as, number of population doublings ( $n_d$ ), growth rate ( $r_g$ ), population doubling time ( $t_d$ ) and percentage growth ( $r_0$ ), thus providing an optimal baseline growth profile of unchallenged cells. A clear lag, log and stationary phase were recorded. The exponential growth occurring between 48 – 72 h, during which time THP-1 cell doubled once with a population doubling time of approximately  $24.5 \pm 3.4$  h and showed a growth rate of  $0.04 T_d/h$ . The percentage growth during this time was 98.86% ( $r_0$ ). When cells reached stationary growth phase at ~72 h, cell viability decreased; as determined by manual counting the ratio of cells that did or didn't stain with trypan blue dye. At 120 h after  $T_0$ , mean percentage cell viability decreased 34.62%. Figure 7.01 shows the normal growth characteristics for THP-1 cells over 120 h.

THP-1 cells challenged with three separate concentrations of *Escherichia coli* lipopolysaccharide (LPS) (0.5  $\mu$ g, 1  $\mu$ g and 2.5  $\mu$ g) were assessed during exponential growth (24 – 72 h) to measure cell number, population doubling time, percentage growth. All cells treated with LPS showed an apparent decrease in doubling time during exponential growth phase compared to control cells (PBS vehicle control). THP-1 cells

inoculated with 2.5 µg LPS doubled every  $18.1 \pm 2.7$  h and had a growth rate of  $0.06 T_d/h$  compared to control cells, which doubled every 26.5 h with a growth rate of 0.03 (figure 7.02). Cells stimulated with 0.5 µg and 1 µg LPS had similar doubling times of  $19.6 \pm 3.4$  h and  $19.9 \pm 2.3$  h, respectively.

To assess whether a significant proliferative response had occurred in cells challenged with LPS; cells challenged with LPS for each concentration group and time point were counted and compared to control cells.

A one-way ANOVA with Tukey's post hoc pairwise comparison test revealed a significant increase of THP-1 cell proliferation at 72 h following challenge with 2.5 µg LPS compared to PBS vehicle control cell numbers for the same time point ( $p < 0.001$ ; figure 7.03). Also at 72 h, a significant increase of THP-1 cell numbers was observed in response to 0.5 and 1 µg LPS, ( $p < 0.01$  and  $p < 0.05$ , respectively). No significant increases in cell numbers were observed prior to 72 h (figure 7.02).

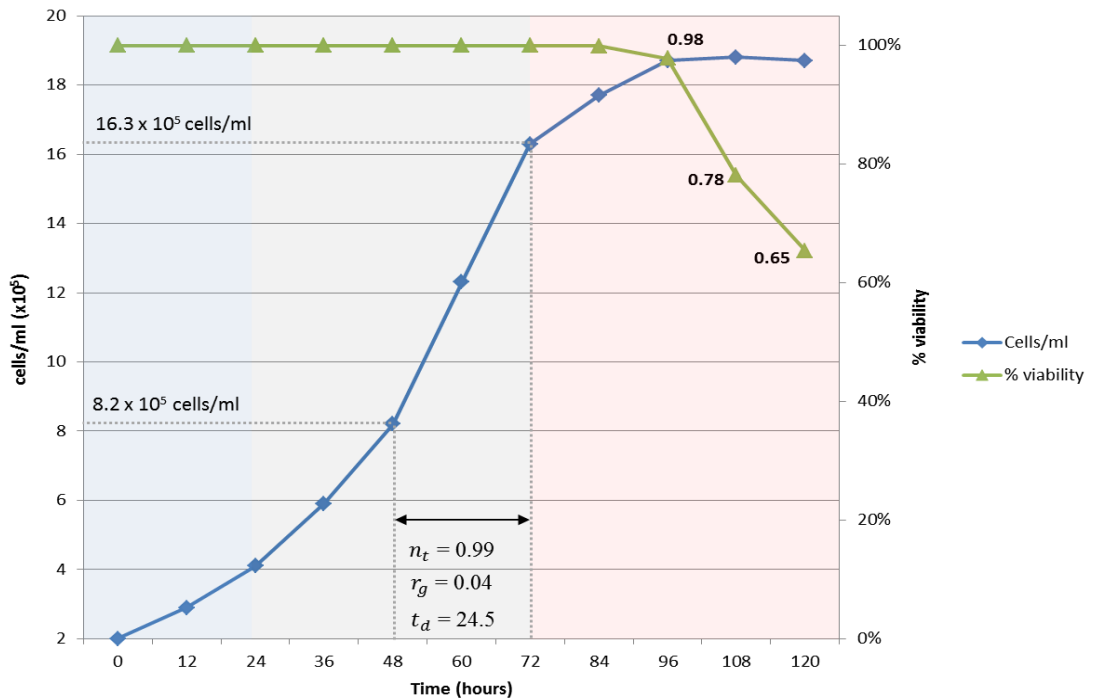


**Figure 7.01:** Basal growth curve and population doubling calculations for THP-1 cells. Mean growth curve (blue line) displays proliferation of THP-1 cells over 120 h. Lag (blue shade), log (grey shade) and stationary phase (red back) can be observed. The number of population doublings ( $n_d$ ), growth rate ( $r_g$ ), and population doubling times ( $t_d$ ) were calculated during log growth 48 and 72 hours (black lines). THP-1 cells took ~24 hours to double under normal conditions. Green line indicates THP-1 cell viability over 120 h. At  $T_0 2 \times 10^5$  cells/ml were seeded and cells counts were performed, measuring cell numbers and percentage viability at each 12 h count. Viability remained at 100% until cells reached the stationary growth phase (~72 h), then percentage viability rapidly decreased.

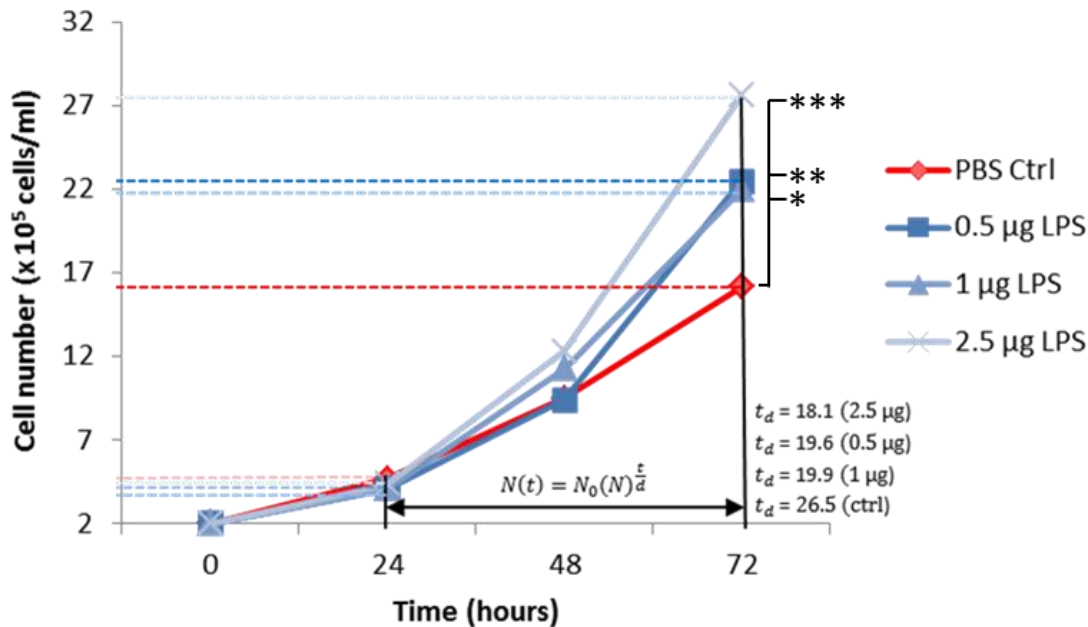


**Figure 7.02:** Line graph of mean THP-1 cell exponential growth (24-72 h). Population doubling times for THP-1 cells infected with *E. coli* LPS (0.5, 1 & 2.5 µg) compared with control cells (PBS treatment). Decreased doubling times were observed for all cells challenged with LPS compared to cells treated with PBS alone. Cells were maintained in exponential growth over three 72 h subcultures. Data represents three biological replicates that each comprised three technical replicates for each LPS group and control.

## 7.2.2 Oligonucleotide optimisation

Twenty one primer sets were designed to measure gene expression of 21 target genes and were optimised with 3 commercially sourced endogenous control genes to confirm optimum amplification efficiency with THP-1 cells.  $C_T$  values generated from five-fold log serial dilutions of cDNA from LPS infected THP-1 cells were plotted to evaluate PCR efficiencies ( $C_T$  values vs. log template input). Fourteen of 21 primer sets amplified their target genes within 10% of the optimum amplification efficiency (slope  $-3.32 \pm 0.332 \approx E = 2.00 \pm 0.14$ ; table 7.01). Two of the three endogenous control genes (*ACTB* and *RPL27A*) provided highly accurate amplification efficiencies ( $E = 2.0$ ; 100%; table 7.03). Amplification efficiency and dynamic range for endogenous control gene *GAPDH* was poor across all primer concentrations and was therefore omitted from the study. Similarly, primers for *MYD88* provided poor amplification and so were also omitted. A further six genes were omitted from the study due to being consistently undetected (complete lack of PCR signal). These genes failed to amplify when genomic DNA extracted from THP-1 cell was used as template; therefore the sub-optimal design of the oligonucleotide sequences is the likely cause for failure (table 7.01). Thirteen of the 14 successfully amplified genes had amplification efficiencies within 5% of the optimum amplification efficiency (i.e. slope  $-3.32 \pm 0.166 \approx E = 2.0 \pm 0.07$ ; table 7.01).

PCR efficiencies were tested further by calculating the difference between  $C_T$  values for target and reference genes amplification of cDNA serial log dilutions. The difference between target and reference genes  $C_T$  values was plotted vs the logarithm of the template cDNA amount as regression line graphs. All amplification efficiencies between target and reference genes were highly comparable, providing almost horizontal regression lines ( $r^2 = <0.1$ ). Figure 7.04 demonstrates a regression line graph of the difference in  $C_T$  values of *HMGR* and *ACTB* vs log cDNA input; amplification efficiencies were highly comparable ( $r^2 = 0.0089$ ).

When designing primer sequences for *LDLR*, *CCL3* and *NFKB*, multiple transcript variants were available that showed little variation of DNA sequence when aligned using BioEdit v 7.2.5. Because the correct transcript variant was unknown, oligonucleotides were designed to target a single conserved region across multiple transcript variants. Because of this, there was a possibility for amplification of more than one transcript variant during PCR. To assess this possibility, melt-curve analysis was performed to monitor the specificity of each PCR reaction and revealed no indication of secondary amplification for these three genes (figure 7.05a-c). Secondary products or primer artefacts were easily differentiated from specific target gene amplification using melt-curve analysis (figure 7.06). Primers targeting *MYD88* displayed poor amplification efficiencies ( $E = 2.20 - 2.70 \approx 120.02\% - 169.79\%$ ) and poor target specificity (figure 7.06d). When *MYD88* PCR product was run on 2.5% agarose gel, two discrete PCR products were found to be amplified (figure 7.06)

cDNA PCR products of successfully amplified target genes were sequenced and target gene amplification confirmed by comparing DNA sequences with NCBI nucleotide reference database. DNA sequences for each of the target genes investigated here matched the correct reference sequences with 100% identity.

Genes	PCR Efficiencies		Primer conc.
	Slope ( $E = 10^{-1/s}$ )	Percentage efficiency % $E = (E - 1) \times 100$	( $\mu\text{M}$ )
<i>HMGR</i>	-3.35 (1.99)	98.84	0.05
<i>SCAP</i>	-3.27 (2.02)	102.21	0.2
<i>SREBP2</i>	-3.35 (1.99)	98.84	0.2
<i>LDLR</i>	-3.23 (2.04)	103.98	0.2
<i>ABCA1</i>	-3.16 (2.07)	107.23	0.1
<i>CCL2</i>	-3.49 (1.93)	93.43	0.05
<i>CCL3</i>	-3.47 (1.94)	94.17	0.1
<i>ICAM1</i>	-3.19 (2.06)	105.81	0.05
<i>TLR2</i>	-3.17 (2.07)	106.76	0.1
<i>TLR4</i>	-3.41 (1.96)	96.45	0.2
IL- $\beta$	-3.39 (1.97)	97.23	0.05
<i>TNF<math>\alpha</math></i>	-3.42 (1.96)	96.06	0.05
NF- $\kappa$ B	-3.17 (2.07)	106.75	0.05
<i>BCL2A1</i>	-3.38 (1.98)	97.63	0.2
<i>ACTB</i>	-3.30 (2.00)	100.92	0.2
<i>RPL27A</i>	-3.31 (2.00)	100.50	0.05
Failed genes			
<i>VCAM1</i>	n/a	-	-
<i>n/a</i>			
<i>GM-CSF</i>	n/a	-	-
<i>IL6</i>	n/a	-	-
<i>IL8</i>	n/a	-	-
<i>IL10</i>	n/a	-	-
<i>TLR4</i>	n/a	-	-
Poor efficiency			
	-2.32 (2.70)	169.79	0.2
<i>MYD88</i>	-2.76 (2.30)	130.31	0.1
	-2.92 (2.20)	120.02	0.05
	-3.72 (1.85)	85.70	0.2
<i>GAPDH</i>	-3.76 (1.84)	84.48	0.1
	-4.59 (1.65)	65.11	0.05

**Table 7.01:** Primer optimisation to amplification efficiency of primer over three primer concentrations 0.2  $\mu\text{M}$ , 0.1  $\mu\text{M}$  and 0.05  $\mu\text{M}$ . Serial dilutions of cDNA for 6 orders of magnitude were utilised as qPCR template.  $C_T$  values were used to plot a chart for  $C_T$  value vs. log cDNA input to generate a standard curve with regression line of best fit. The slope of the regression line of best fit was optimal at  $-3.32 \pm 0.332$  ( $E = 2.00 \pm 0.14$ ). Efficiencies are listed with the optimal primer concentration for each score. Reference genes *ACTB* and *RPL27A* provided good PCR efficiency (light grey) compared to *GAPDH* (dark grey).

- n/a no amplification

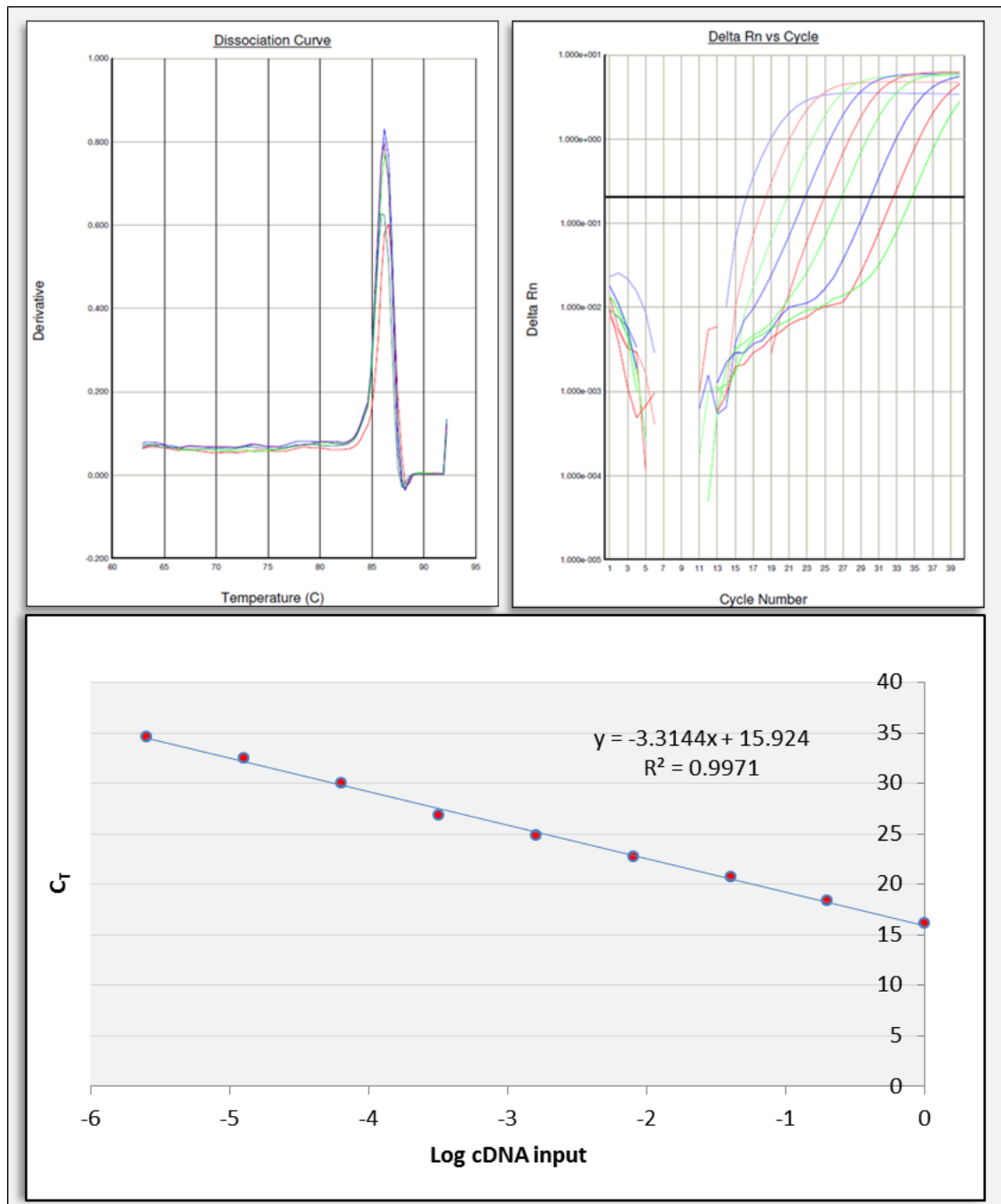


**Figure 7.03:** Optimum amplification efficiency for the endogenous control gene *RPL27A*. Top left panel shows sharp overlaid peaks at ~86°C suggesting high annealing specificity for amplification of a discrete product. A flat line before melting peak indicating no self-complementarity between the primer pair. The top left panel shows nine evenly spaced amplification curves indicating consistent amplification with a good dynamic range of detection. Bottom panel shows a semi-log regression line plot (C<sub>T</sub> value vs. log cDNA input) method used to assess amplification efficiencies of all genes. The regression line slope -3.31 is equal to an amplification efficiency of  $E = 2.01$  (~100%) determined using the formula  $E = 10^{-1/\text{slope}-1}$ . An amplification efficiency of 2.01 provides assurance that PCR product is doubling every 3.31 cycles during the exponential amplification phase.

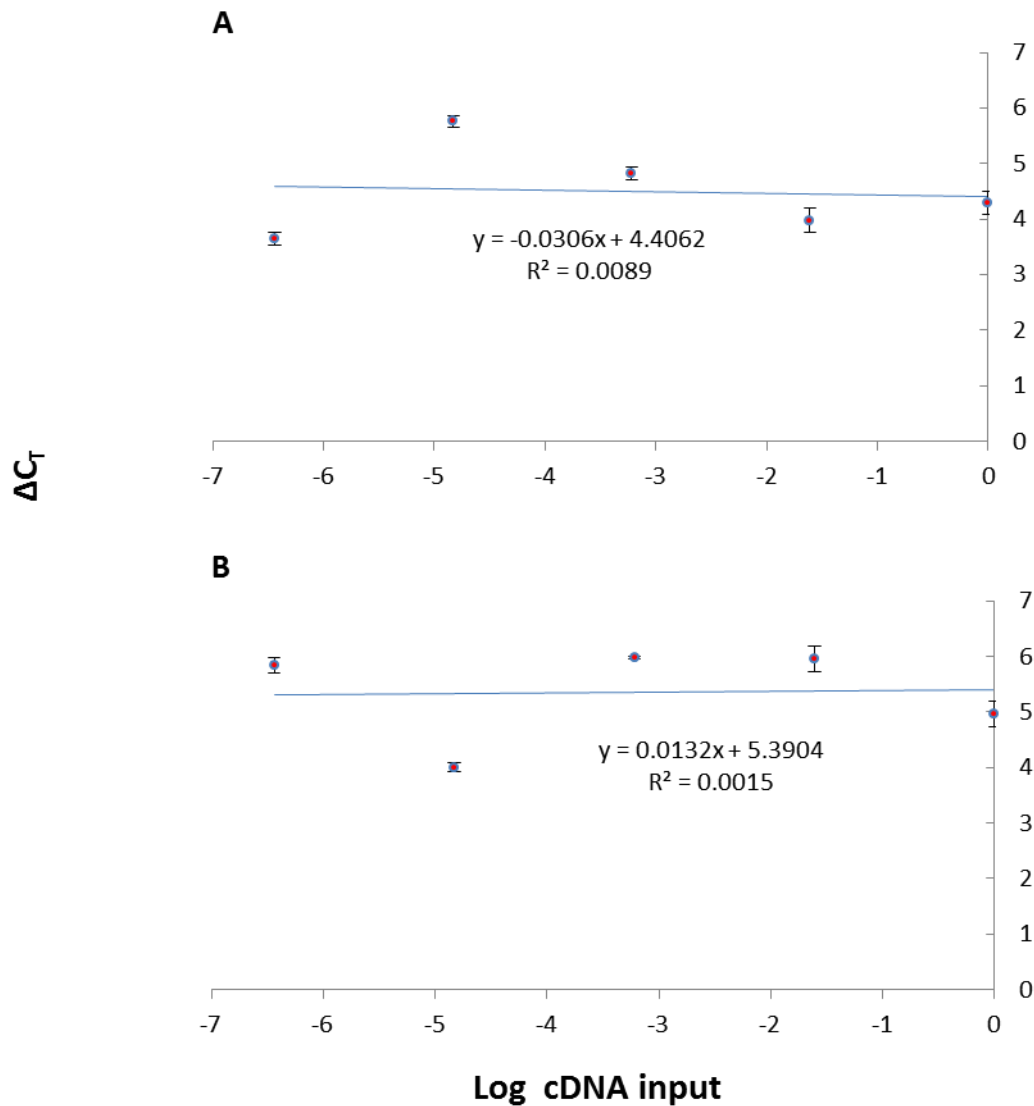


**Figure 7.04:** Efficiency comparison example.  $C_T$  values were determined for HMGR and housekeeping gene *ACTB* (A) and *RPL27A* (B) using cDNA extracted and reverse transcribed from LPS infected THP-1 cells. The difference in  $C_T$  values was plotted against log template input. The difference in PCR efficiency was determined by calculating the slope of the line. The slope of the resulting straight line was  $<0.1$ ; amplification efficiencies are therefore highly comparable for HMGR and *ACTB* (A) and *RPL27A* (B).

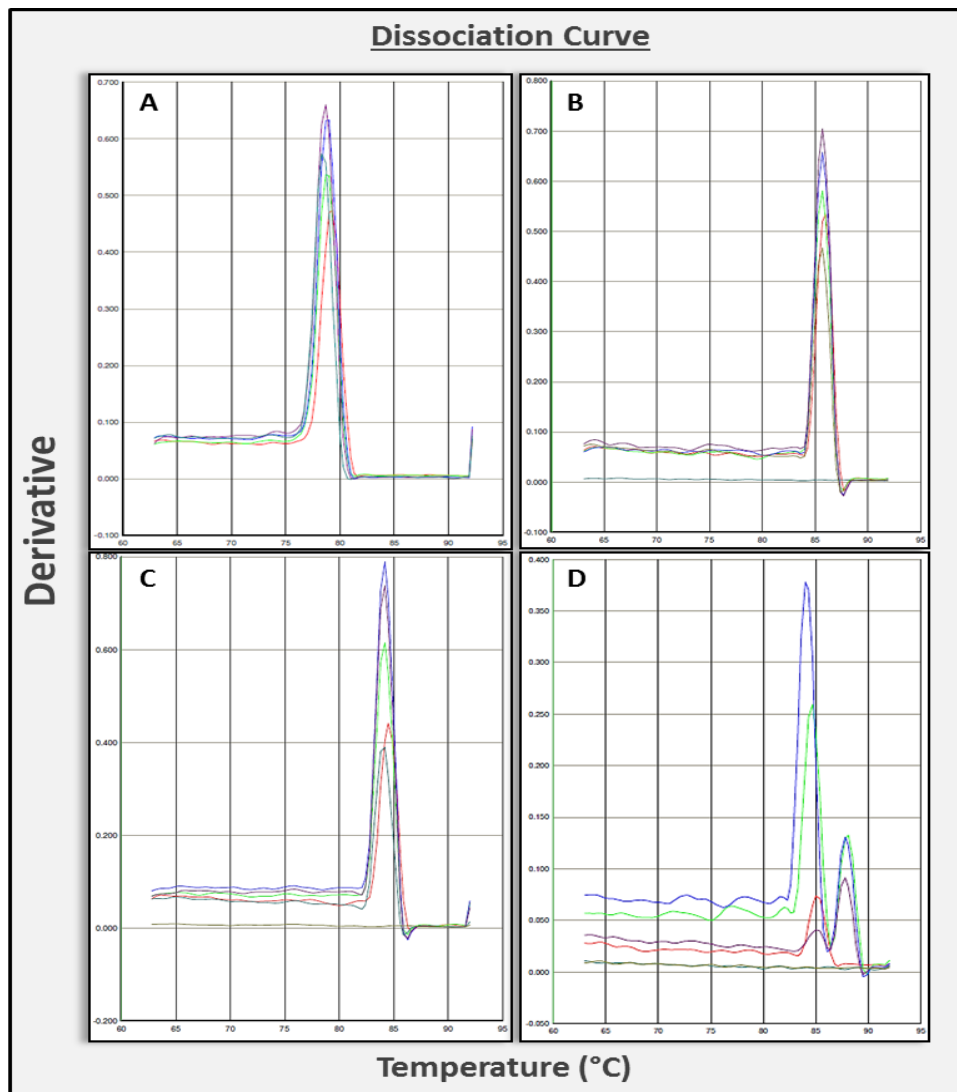


**Figure 7.05:** Dissociation curves from melt curve analysis. This diagnostic tool was utilised to establish primer specificity during the amplification reaction. Panel A, B and C (*LDLR*, *CCL3* and *NF-κB*, respectively) represent primer pairs that have potential to amplify more than one transcript variant. A, B and C all have sharp single melting peaks at 80 – 85°C indicating high specificity for a single target amplicon. Panel D shows a dissociation curve for *MYD88* with poor amplification efficiency ( $E = 2.20 - 2.70 \approx 120.02\% - 169.79\%$ ) and target specificity. Multiple peaks are observed for *MYD88*; an indication that more than one product was primed and successfully amplified during the reaction.

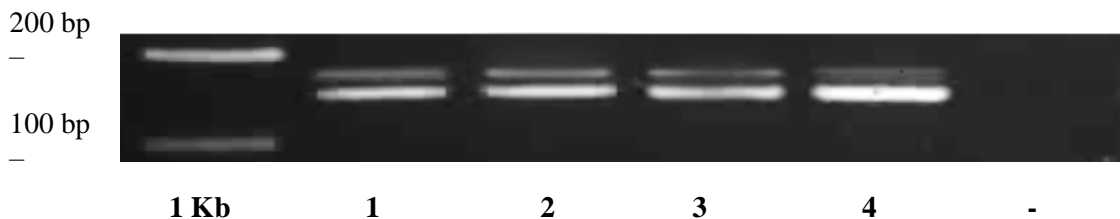


**Figure 7.06:** Agarose gel electropherogram for PCR amplification of *MYD88* cDNA shows the amplification of two discrete PCR products (~140 bp) in the same reaction with *MYD88* primers. LPS infected THP-1 cell cDNA was amplified and migrated through a 2.5% agarose gel. A 1Kb DNA ladder was loaded in the left lane. Lanes 1 – 4 represent individual PCR amplifications of four biological replicates.

## 7.2.3 RT-PCR reagent optimisation

Optimisation of the reverse-transcription (RT) step in RT-PCR is critical to assure the assay is performed with the highest of accuracy and efficiency. It is vital that the RNA template is reverse-transcribed efficiently to limit the introduction of error in this initial stage, which would affect downstream calculations. The two most adjustable components in the kit that can impact RT efficiency are reverse transcriptase and MgCl<sub>2</sub>. To optimise the RT reaction three concentrations of reverse transcriptase (0.5, 1, 1.5 U) and four MgCl<sub>2</sub> (1.5, 2.5, 3.5 and 4.5 mM) were tested. C<sub>T</sub> values were generated from five-fold log serial dilutions of cDNA from LPS infected THP-1 cells. Reactions containing 0.5 U reverse transcriptase enzyme combined with 1.5 mM MgCl<sub>2</sub> concentrations showed low efficiency and dynamic range (table 7.02; figure). Whereas amplification efficiencies for 1.5 U reverse transcriptase and 3.5 mM MgCl<sub>2</sub> had the greatest dynamic range to the 8th dilution; i.e down 4 orders of magnitude to ~60 pg concentrations. All MgCl<sub>2</sub> dilutions combined with 1.5 U reverse transcriptase were within an optimal range (-3.32±0.332). Reactions using 1 U reverse transcriptase and a MgCl<sub>2</sub> concentration of 2.5 mM or 3.5 mM showed the best amplification efficiency and ample detection range (table 7.02). Table 7.02 lists observations from reverse transcriptase and MgCl<sub>2</sub> combinations showing regression line slopes, efficiencies and dynamic ranges for all combinations. Altering oligo(dt) primer concentration or increasing RT-PCR annealing or extension times had no beneficial effect on the resulting PCR efficiency of subsequent qPCR assays. No great advantage was observed by increasing reverse transcriptase input to 1.5 U; thus, the optimum and chosen reagent composition for RT-PCR was 1 U reverse transcriptase with 3.5 mM MgCl (table 7.02).

			MgCl <sub>2</sub> conc. (mM)			
			1.5	2.5	3.5	4.5
Reverse transcriptase (Units)	0.5	<i>Slope</i>	-4.44	-3.81	-	-
		<i>Efficiencies</i>	67.96%	83.00%	-	-
		<i>Range</i>	4	5	-	-
	1	<i>Slope</i>	-	-3.32	-3.27	-3.81
		<i>Efficiencies</i>	-	100.08%	102.21%	83.00%
		<i>Range</i>	-	6	7	6
	1.5	<i>Slope</i>	-3.56	-3.35	-3.44	-3.20
		<i>Efficiencies</i>	90.94%	98.84	95.29%	105.35%
		<i>Range</i>	4	7	8	6

**Table 7.02:** Amplification efficiencies and dynamic ranges for different combinations of reverse transcriptase and MgCl<sub>2</sub>. Grey shaded area indicates the reagents composition chosen for reverse transcription that provided the optimum reaction efficiency and range.

#### 7.2.4 THP-1 gene expression response to *Escherichia coli* lipopolysaccharide

To assess whether THP-1 cells respond to bacterial stimuli, THP-1 cells were incubated with different *E. coli* LPS concentrations (0.5 µg, 1 µg and 2.5 µg). This developmental assay was necessary to investigate whether THP-1 cells are responsive to bacterial stimulation. In addition, mRNA derived from LPS-challenged THP-1 cells provided a positive control, thus helping to optimise PCR primer set used in this study. Box plot charts displaying target gene fold changes at each time point are displayed in figures 7.09– 7.20. Table 6.03 shows all gene expression fold changes for each LPS-infected THP-1 cells for each concentration and each time point compared to PBS vehicle control cell expression at the same time point.

##### 7.2.4.1 Cholesterol mediating genes

HMGR was mainly unaffected by LPS, as evidenced by few significant changes in *HMGR* target gene expression compared to the vehicle control. A significant down-regulation of *HMGR* was observed at 1 h (1 µg LPS,  $p < 0.05$ ; figure 7.07). A sharp shift to an up-regulated response of THP-1 cell *HMGR* mRNA expression occurred at 20 hours following exposure to 0.5 µg LPS ( $p < 0.01$ ; figure 7.07). Overall, *HMGR* expression remained unregulated in response to LPS across the 20 h time course; however a subtle tread from down to up-regulation was observed.

*SCAP* was sporadically down-regulated during the 20 h LPS-exposure time. Significant down regulation of *SCAP* mRNA was observed following 30 min and 2 h exposure to 2.5 µg LPS, ( $p < 0.05$ ). A final significant down-regulation of *SCAP* was observed following 20 h exposure to 0.5 µg LPS ( $p < 0.01$ ; figure 7.08) Overall, *SCAP* was mostly unregulated, though did showed significant down-regulation, both early and late in the time course and mainly in response to 2.5 µg LPS.

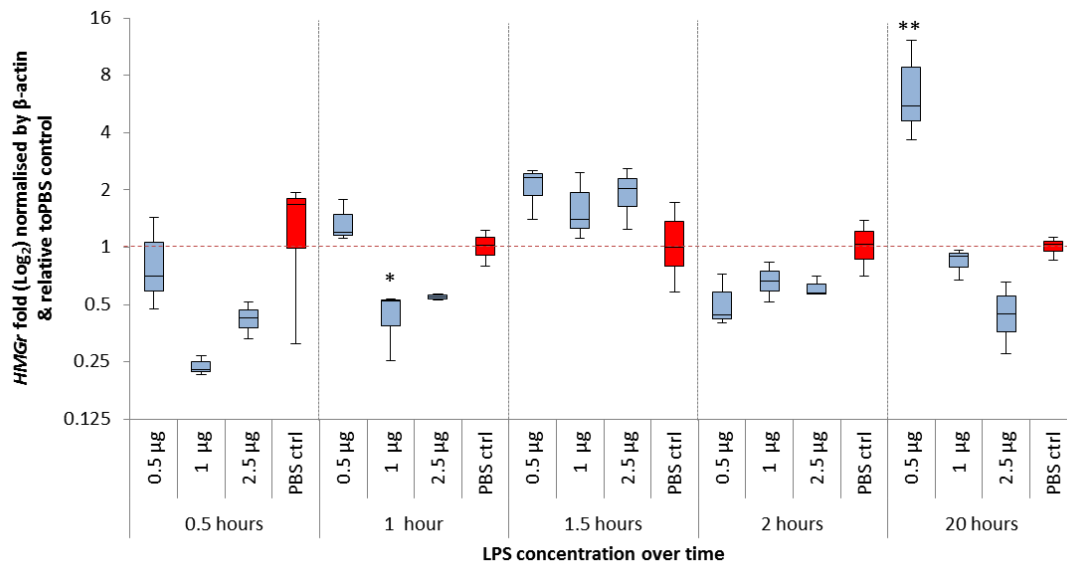


**Figure 7.07:** Temporal expression of THP-1 gene *HMGR* in response to *E. coli* LPS. Target gene expression was measured by calculating the fold difference (blue) relative to the expression of a PBS vehicle control (red) and  $C_t$  values were normalised by stably expressing housekeeping gene *ACTB*. Expression was evaluated for three discrete LPS concentrations at different time points from 30 min to 20 h. Data represents  $n = 3$  biological replicate samples for each concentration at each time point.

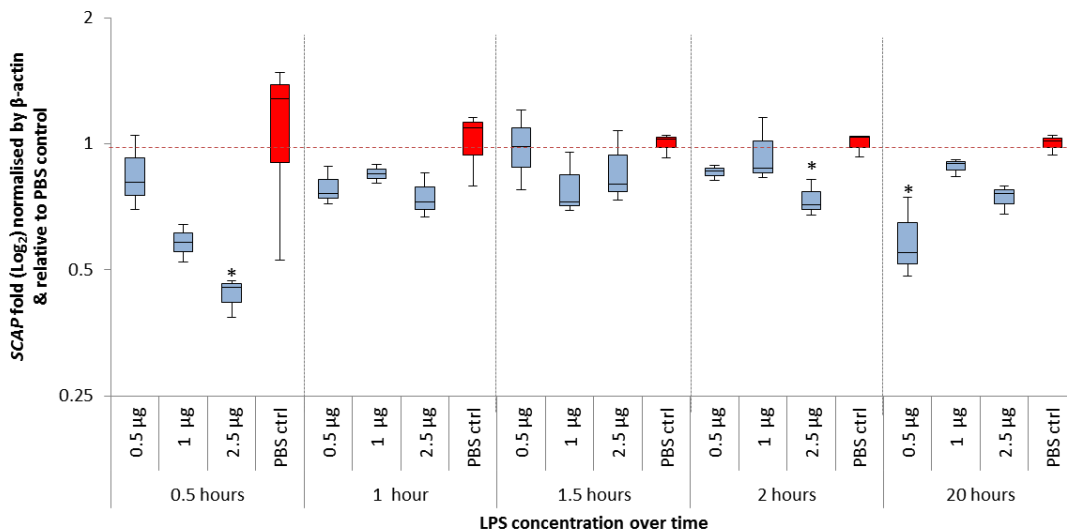


**Figure 7.08:** Temporal expression of THP-1 gene *SCAP* in response to *E. coli* LPS. Target gene expression was measured by calculating the fold difference (blue) relative to the expression of a PBS vehicle control (red) and  $C_t$  values were normalised by stably expressing housekeeping gene *ACTB*. Expression was evaluated for three discrete LPS concentrations at different time points from 30 min to 20 h. Data represents  $n = 3$  biological replicate samples for each concentration at each time point.

*SREBP2* mRNA was mainly down-regulated over 20 h, with significant down-regulated responses observed at 30 min (1 and 2.5 µg LPS,  $p < 0.01$ ), 1.5 h (2.5 µg LPS,  $p < 0.05$ ) and 2 h (0.5 and 2.5 µg LPS,  $p < 0.001$  and  $p < 0.01$ , respectively). Finally, at 20 h up-regulated expression of *SREBP2* was observed for THP-1 cells exposed to 0.5 µg LPS compared to vehicle control cell expression ( $p < 0.001$ ; figure 7.19). *SREBP2* mRNA was predominantly down-regulated over the 20 h time course, though a temporal shift from down to up-regulation was observed.

*LDLR* mRNA was predominantly up-regulated over the 20 h time course. Up-regulated responses were observed at 1 h (0.5 µg LPS,  $p < 0.01$ ), 2 h (0.5 µg LPS,  $p < 0.0001$ ) and 20 h (1 µg LPS,  $p < 0.05$ ; figure 7.10) time points. However, a shift to down-regulation of *LDLR* was observed at 1.5 h (0.5 µg LPS;  $p < 0.01$ ). Overall, *LDLR* was regulated in response to 0.5 µg LPS.

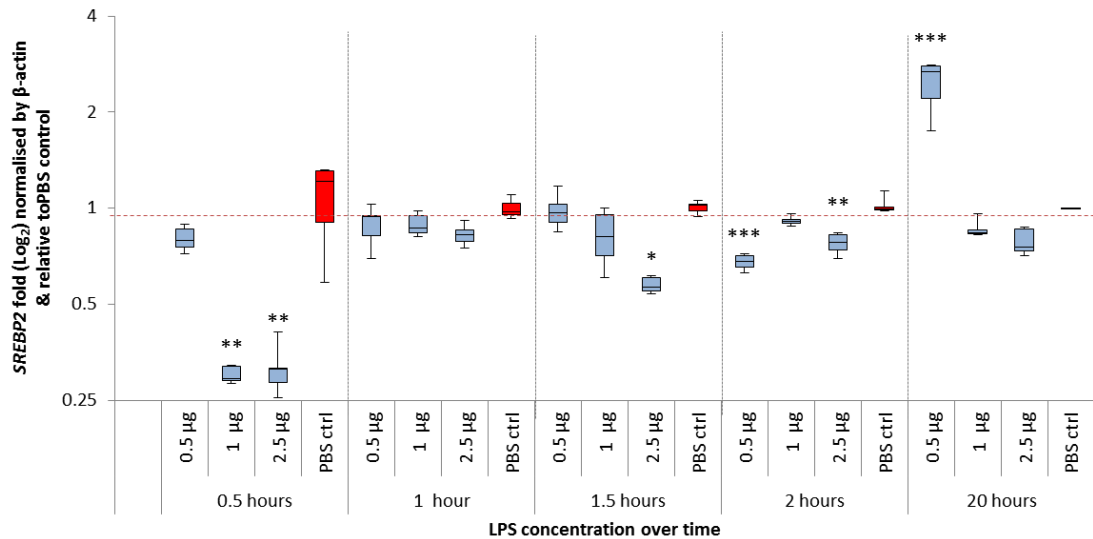


**Figure 7.09:** Temporal expression of THP-1 gene *SREBP2* in response to *E. coli* LPS. Target gene expression was measured by calculating the fold difference (blue) relative to the expression of a PBS vehicle control (red) and Ct values were normalised by stably expressing housekeeping gene *ACTB*. Expression was evaluated for three discrete LPS concentrations at different time points from 30 min to 20 h. Data represents  $n = 3$  biological replicate samples for each concentration at each time point.

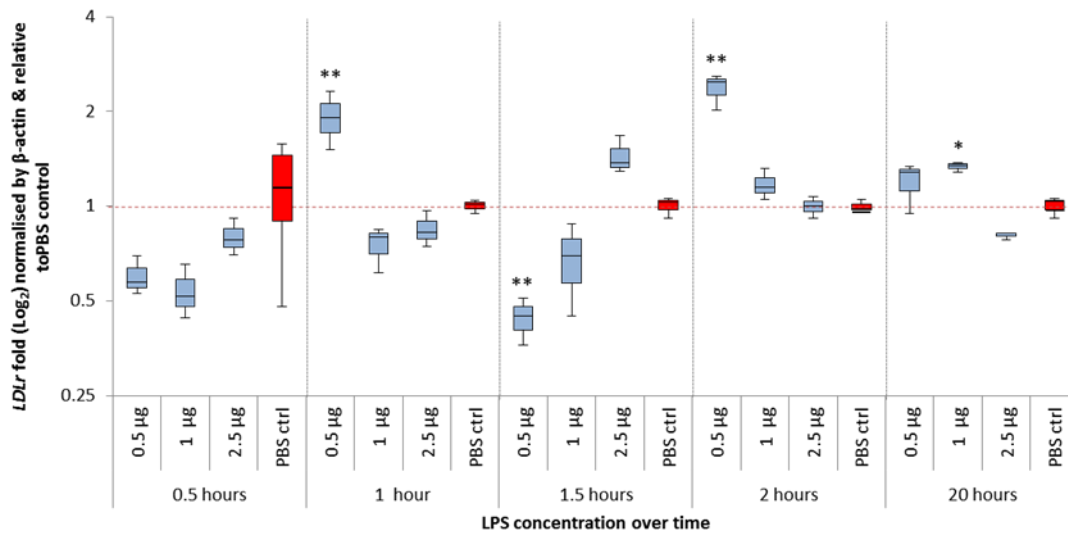


**Figure 7.10:** Temporal expression of THP-1 gene *LDLR* in response to *E. coli* LPS. Target gene expression was measured by calculating the fold difference (blue) relative to the expression of a PBS vehicle control (red) and Ct values were normalised by stably expressing housekeeping gene *ACTB*. Expression was evaluated for three discrete LPS concentrations at different time points from 30 min to 20 h. Data represents  $n = 3$  biological replicate samples for each concentration at each time point.

#### 7.2.4.2 Pro-Inflammatory cytokines genes

*CCL3* expression was significantly up-regulated and showed a temporal increase over the 20 h period. *CCL3* mRNA expression was induced between 1 h (2.5 µg LPS,  $p < 0.05$ ) and 1.5 h (2.5 µg LPS,  $p < 0.001$ ; figure 7.11). *CCL3* expression remained significantly regulated at 2 h for THP-1 cells challenged with 0.5 µg ( $p < 0.01$ ), 1 µg ( $p < 0.001$ ) and 2.5 µg LPS ( $p < 0.00001$ ). Up-regulated *CCL3* mRNA expression continued to increase following 20 h exposure to each of the LPS concentrations, 0.5 µg LPS ( $p < 0.005$ ), 1 µg LPS ( $p < 0.002$ ) and 2.5 µg LPS ( $p < 0.002$ ; figure 7.11). In summary, significant *CCL3* up-regulation was observed that showed temporal increase over the 20 hours exposure time.

Similarly, *CCL2* showed a temporal increase in expression over the 20 h exposure time course. The initial significant up-regulation of *CCL2* compared to PBS control cells was observed at 1 h (0.5 µg LPS,  $p < 0.01$ ; figure 7.12). At 1.5 h and 2 h exposure time *CCL2* expression remained significantly up-regulated when challenged with 1 and 2.5 µg LPS ( $p < 0.01$  and  $p < 0.001$ , respectively). Finally, a significant increase in *CCL2* mRNA expression was observed following 20 h exposure to each of the LPS concentrations relative to the PBS vehicle control cell expression ( $p < 0.000001$ ; figure 7.12). Overall, while *CCL2* expression remained up-regulated over the 20 hours LPS-exposure time, a very sharp increase in *CCL2* expression was observed later in the time course. The

temporal increase in *CCL2* expression may indicate an increase in inflammatory response to LPS. It is also possible the increasing expression is a result of a proliferative response.

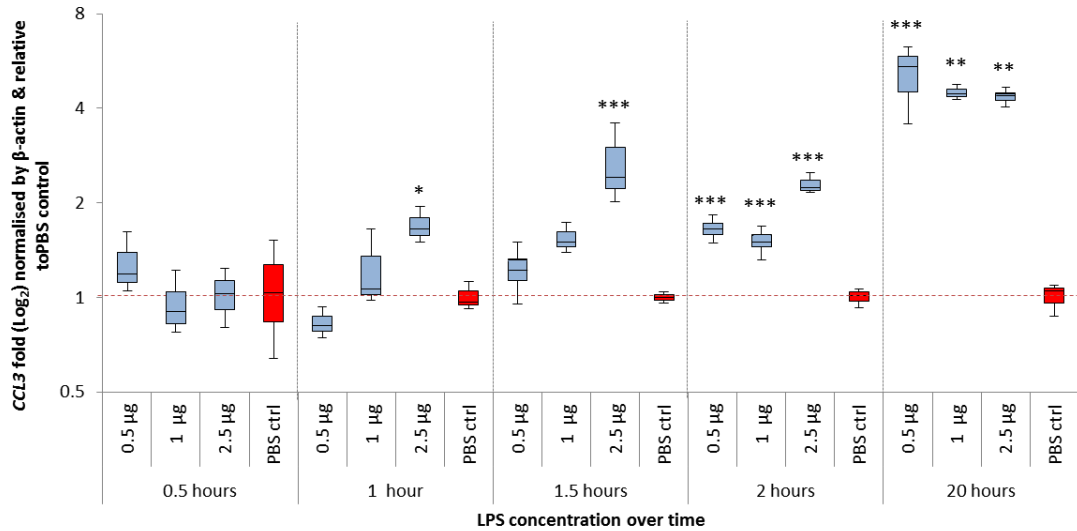


**Figure 7.11:** Temporal expression of THP-1 gene *CCL3* in response to *E. coli* LPS. Target gene expression was measured by calculating the fold difference (blue) relative to the expression of a PBS vehicle control (red) and  $C_t$  values were normalised by stably expressing housekeeping gene *ACTB*. Expression was evaluated for three discrete LPS concentrations at different time points from 30 min to 20 h. Data represents  $n = 3$  biological replicate samples for each concentration at each time point.

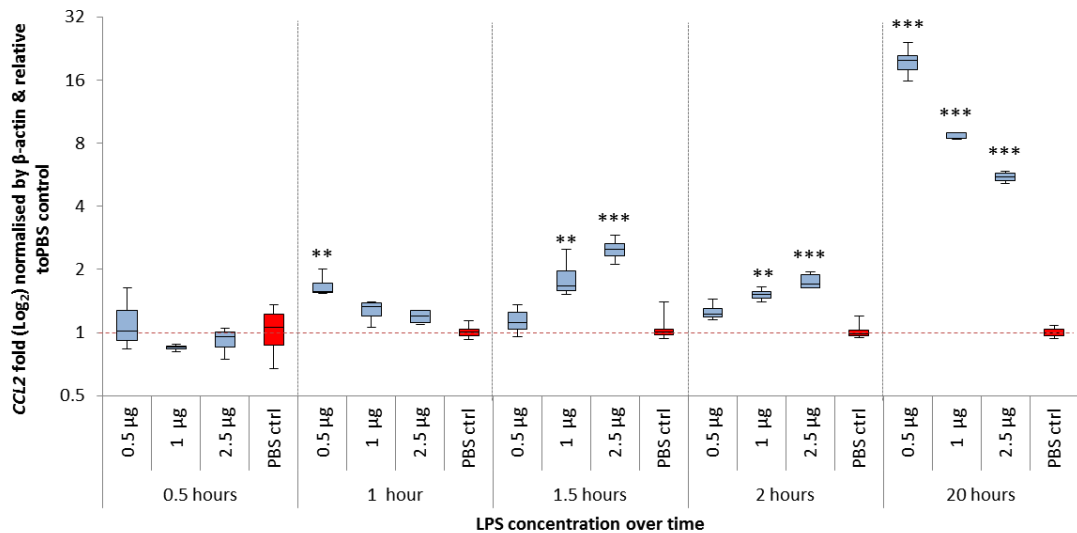


**Figure 7.12:** Temporal expression of THP-1 gene *CCL2* in response to *E. coli* LPS. Target gene expression was measured by calculating the fold difference (blue) relative to the expression of a PBS vehicle control (red) and  $C_t$  values were normalised by stably expressing housekeeping gene *ACTB*. Expression was evaluated for three discrete LPS concentrations at different time points from 30 min to 20 h. Data represents  $n = 3$  biological replicate samples for each concentration at each time point.

*ICAM1* was consistently up-regulated in response to all LPS concentrations starting at 1.5 h when cells were challenged with 0.5  $\mu\text{g}$  LPS ( $p < 0.01$ ), 1  $\mu\text{g}$  LPS ( $p < 0.01$ ) and 2.5  $\mu\text{g}$  LPS ( $p < 0.001$ ). *ICAM1* expression increased further at 2 h showing highly significant up-regulation of *ICAM1* for cells infected with 0.5  $\mu\text{g}$  LPS ( $p < 0.001$ ), 1  $\mu\text{g}$  LPS ( $p < 0.000001$ ) and 2.5  $\mu\text{g}$  LPS ( $< 0.000001$ ). A final significant up-regulation of *ICAM1* was observed at 20 h in response to 1  $\mu\text{g}$  and 2.5  $\mu\text{g}$  LPS, both at  $p < 0.05$ . For LPS concentrations 0.5  $\mu\text{g}$  and 1  $\mu\text{g}$  expression fold change levels were similar between 1.5 h, 2 h and 20 h time points. However, fold change levels for samples exposed to 2.5  $\mu\text{g}$  LPS fell by almost two thirds for 2h and 20 h. Expression prior to 1.5 h were not statistically significant; 30 min [ $F(3,8) = 1.805$ ,  $p = 0.224$ ] and 1 h [ $F(3,8) = 3.328$ ,  $p = .0772$ ] (figure 7.13).

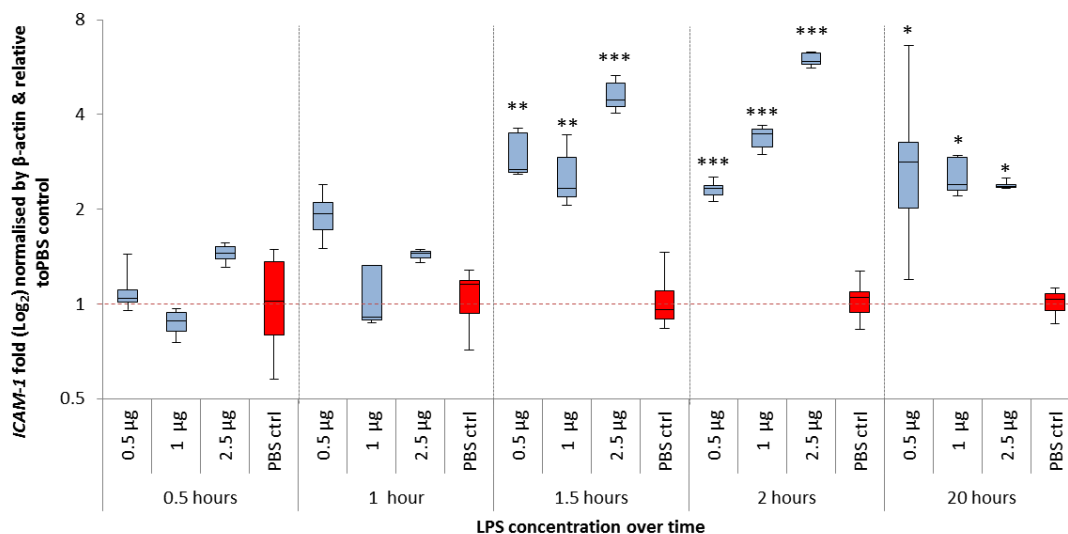


**Figure 7.13:** Temporal expression of THP-1 gene *ICAM-1* in response to *E. coli* LPS. Target gene expression was measured by calculating the fold difference (blue) relative to the expression of a PBS vehicle control (red) and Ct values were normalised by stably expressing housekeeping gene *ACTB*. Expression was evaluated for three discrete LPS concentrations at different time points from 30 min to 20 h. Data represents  $n = 3$  biological replicate samples for each concentration at each time point.

*TNF $\alpha$*  mRNA was up-regulated early, within the first 30 minutes in response to 2.5  $\mu\text{g}$  LPS ( $p < 0.01$ ). At 1 h there was a significant shift to down-regulated *TNF $\alpha$*  expression that was due to the addition of 1  $\mu\text{g}$  ( $p < 0.01$ ; figure 7.14). All LPS concentrations induced significant up-regulation of *TNF $\alpha$*  from 1.5 h to 20 h with prominent up-regulation observed at 1.5 h [ $F(3,8) = 19.4$ ,  $p = 0.0001$ ], 2 h [ $F(3,8) = 27.33$ ,  $p = 0.0001$ ] and 20 h [ $F(3,8) = 14.51$ ,  $p = 0.001$ ].

*IL-1 $\beta$*  showed the greatest increase in in gene expression relative to a PBS vehicle control compared with other genes analysed. Up-regulated expression of *IL-1 $\beta$*  peaked ( $p < 0.00001$ ), followed by a second highly significant up-regulation at 20 h ( $p < 0.0001$ ). Prior to the first major *IL-1 $\beta$*  up-regulation at 1.5 h *IL-1 $\beta$*  was unregulated excluding one significant down-regulated response at 30 min for cells infected with 0.5  $\mu\text{g}$  LPS ( $P < 0.05$ ; figure 7.15).

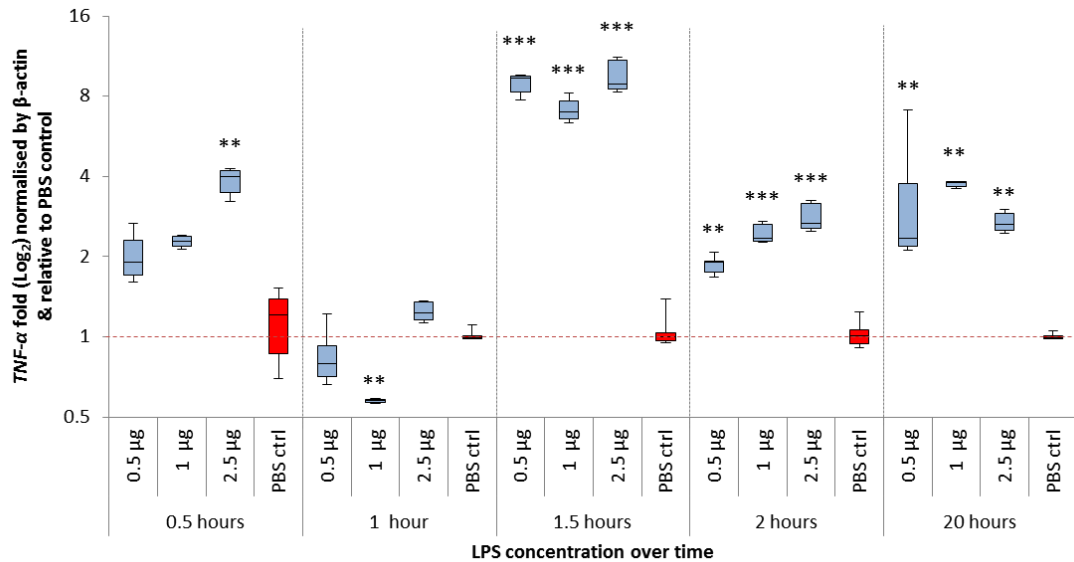


**Figure 7.14:** Temporal expression of THP-1 gene *TNF $\alpha$*  in response to *E. coli* LPS. Target gene expression was measured by calculating the fold difference (blue) relative to the expression of a PBS vehicle control (red) and  $C_t$  values were normalised by stably expressing housekeeping gene *ACTB*. Expression was evaluated for three discrete LPS concentrations at different time points from 30 min to 20 h. Data represents  $n = 3$  biological replicate samples for each concentration at each time point.

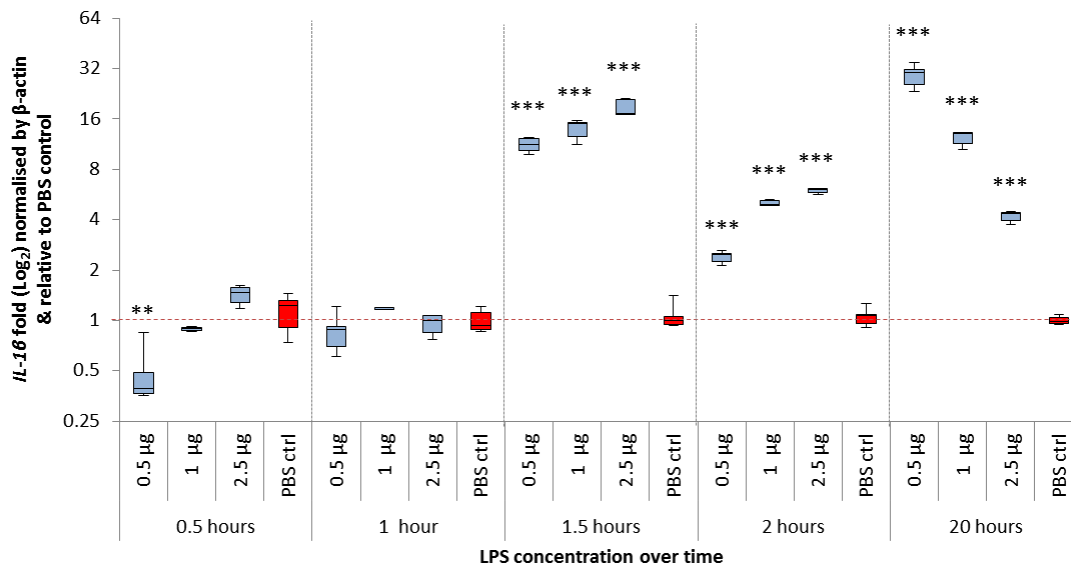


**Figure 7.15:** Temporal expression of THP-1 gene *IL-1 $\beta$*  in response to *E. coli* LPS. Target gene expression was measured by calculating the fold difference (blue) relative to the expression of a PBS vehicle control (red) and Ct values were normalised by stably expressing housekeeping gene *ACTB*. Expression was evaluated for three discrete LPS concentrations at different time points from 30 min to 20 h. Data represents  $n = 3$  biological replicate samples for each concentration at each time point.

#### 7.2.4.3 Toll-like receptor (TLR)-2

TLR-2 remained down-regulated until 1.5 h exposure, at which point TLR-2 was consistently up-regulated, though at no point was expression of TLR2 significantly different in LPS infected THP-1 cells compared to PBS vehicle control cells; 30 min [F(3,8) = 4.324,  $p$  0.434], 1 h [F(3,8) = 2.155,  $p$  0.171], 1.5 h [F(3,8) = 1.734,  $p$  0.237], 2 h [F(3,8) = 1.625,  $p$  0.259]. ANOVA revealed a significant difference in between TLR-2 expression at 20 h [F(3,8) = 4.37,  $p$  = 0.0423] however, these data were due to significant differences between LPS concentration groups and not difference between LPS-challenged cells vs PBS control cells. There were sizable variances between  $C_T$  values for PBS control replicates at each time point for TLR-2, which affected the  $\Delta\Delta C_T$  values and ultimately impacted statistical analyses (figure 7.16).

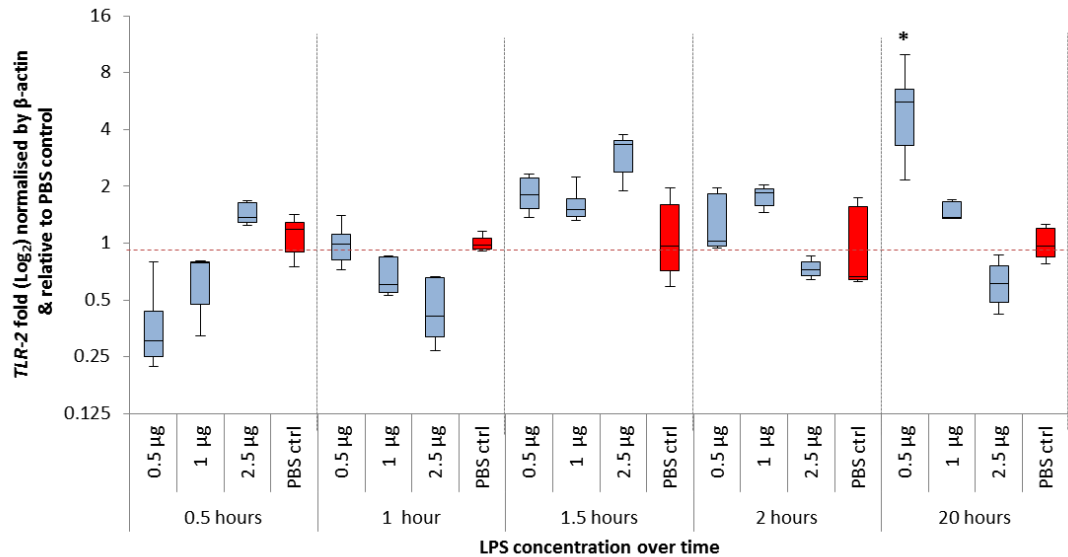


**Figure 7.16:** Temporal expression of THP-1 gene *TLR2* in response to *E. coli* LPS. Target gene expression was measured by calculating the fold difference (blue) relative to the expression of a PBS vehicle control (red) and  $C_t$  values were normalised by stably expressing housekeeping gene *ACTB*. Expression was evaluated for three discrete LPS concentrations at different time points from 30 min to 20 h. Data represents  $n = 3$  biological replicate samples for each concentration at each time point.

#### 7.2.4.4 Transcription factors

Expression of *NF-κB* remained evenly down-regulated after the first 30 min for all LPS concentrations compared to the untreated control ( $p < 0.05$ ). There was no significant changes in *NF-κB* expression at 1 h for any of the LPS concentrations compared to control cells [ $F(3,8) = 2.737$ ,  $p = 0.113$ ]. Expression shifted to an up-regulation of *NF-κB* at 1.5 h for all LPS concentrations relative to PBS control cells ( $p < 0.01$ ). A final up-regulation of *NF-κB* at 2 h for cell treated with 2.5 μg LPS ( $p < 0.05$ ; figure 7.17).

#### 7.2.4.5 Pro-apoptosis inhibitors

*BCL2A1* was initially down-regulated at 30 min across all LPS concentrations 0.5 μg ( $p < 0.05$ ) 1 μg LPS ( $p < 0.05$ ) and 2.5 μg LPS ( $p < 0.01$ ). *BCL2A1* remained down-regulated at 1 h with cells infected with 0.5 μg LPS showing the strongest down-regulation ( $p < 0.001$ ). At 1.5 h a shift to up-regulation was observed but expression was not significant, which continued until 20 h exposure. *BCL2A1* was up-regulated at 20 h for all LPS concentrations resulting in highly significant changes in *BCL2A1* expression for cells infected with 0.5 μg LPS ( $p < 0.05$ ), 1 μg LPS ( $p < 0.001$ ) and 2.5 μg LPS ( $p < 0.0001$ ) compared to PBS control cells (figure 7.18).

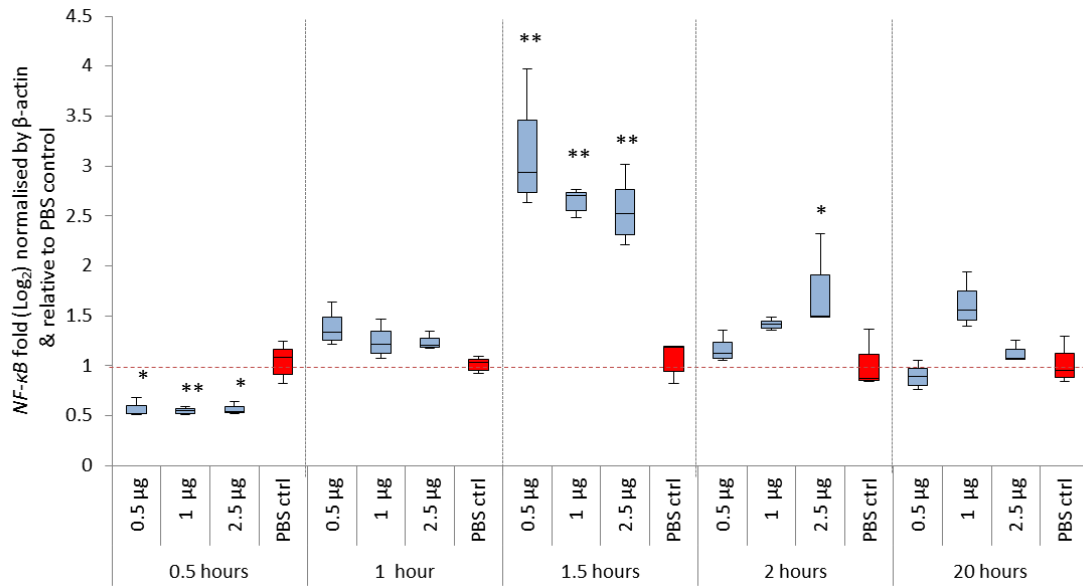


**Figure 7.17:** Temporal expression of THP-1 gene *NF-κB* in response to *E. coli* LPS. Target gene expression was measured by calculating the fold difference (blue) relative to the expression of a PBS vehicle control (red) and  $C_t$  values were normalised by stably expressing housekeeping gene *ACTB*. Expression was evaluated for three discrete LPS concentrations at different time points from 30 min to 20 h. Data represents  $n = 3$  biological replicate samples for each concentration at each time point.

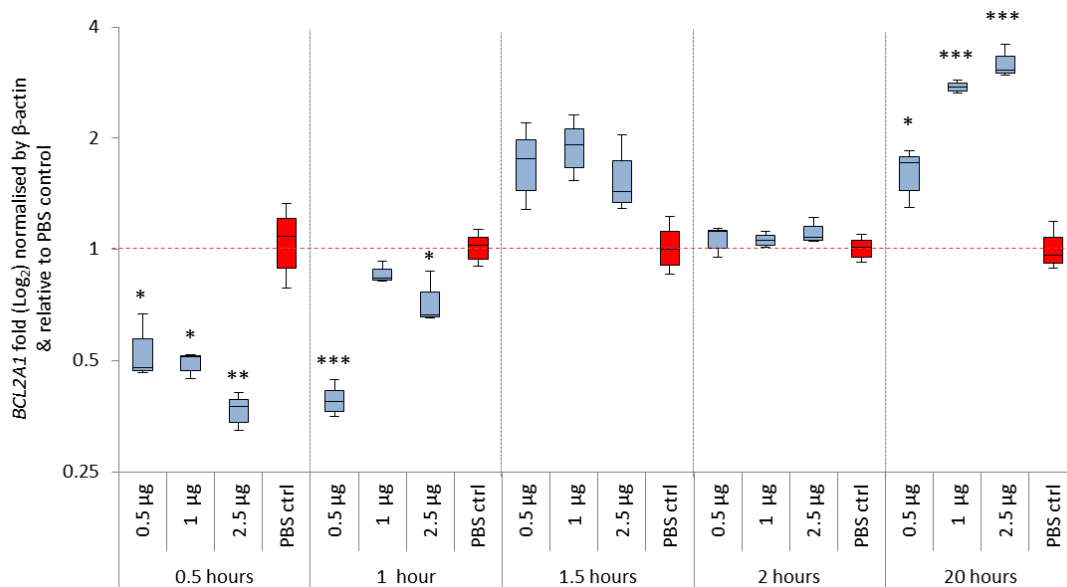


**Figure 7.18:** Temporal expression of THP-1 gene *BCL2A1* in response to *E. coli* LPS. Target gene expression was measured by calculating the fold difference (blue) relative to the expression of a PBS vehicle control (red) and  $C_t$  values were normalised by stably expressing housekeeping gene *ACTB*. Expression was evaluated for three discrete LPS concentrations at different time points from 30 min to 20 h. Data represents  $n = 3$  biological replicate samples for each concentration at each time point.

		Concentrations ( $\mu\text{g}$ )					Concentrations ( $\mu\text{g}$ )		
		Time (h)	0.5	1	2.5	Time (h)	0.5	1	2.5
HMGR	SCAP	0.5	1.15±0.61	4.21±0.19	2.36±0.25	0.5	1.17±0.38	1.71±0.31	2.29±0.16
		1	1.36±0.27	2.29±0.53	1.82±0.52	1	1.26±0.13	1.17±0.12	1.33±0.13
		1.5	2.09±0.36	1.66±0.75	1.94±0.43	1.5	1.01±0.32	1.26±0.41	1.15±0.27
		2	1.92±0.41	1.49±0.31	1.63±0.20	2	1.17±0.05	1.04±0.21	1.35±0.13
		20	7.14±0.73	1.18±0.30	2.17±0.55	20	1.68±0.31	1.13±0.06	1.34±0.12
SREBP2	LDLR	0.5	1.22±0.40	3.24±0.15	3.39±0.32	0.5	1.67±0.39	1.85±0.22	1.25±0.19
		1	1.16±0.23	1.10±0.14	1.22±0.12	1	1.91±0.23	1.33±0.28	1.18±0.14
		1.5	1.03±0.31	1.19±0.31	1.71±0.30	1.5	2.27±0.25	1.48±0.36	1.44±0.30
		2	1.46±0.16	1.10±0.12	1.27±0.15	2	2.36±0.16	1.17±0.19	1.00±0.11
		20	2.44±0.38	1.18±0.07	1.23±0.23	20	1.34±0.36	1.34±0.08	1.23±0.14
CCL3	CCL2	0.5	1.30±0.45	1.02±0.30	1.02±0.21	0.5	1.15±0.59	1.18±1.34	1.09±0.52
		1	1.20±0.23	1.23±0.67	1.69±0.12	1	1.65±0.44	1.28±0.52	1.21±1.09
		1.5	1.19±0.36	1.54±0.37	2.67±0.28	1.5	1.15±0.72	1.81±0.36	2.53±0.65
		2	1.68±0.13	1.49±0.22	2.29±0.14	2	1.25±0.80	1.50±0.32	1.80±0.32
		20	5.09±0.96	4.48±0.32	4.31±0.15	20	19.14±0.31	8.72±0.32	5.53±0.56
ICAM1	TLR-2	0.5	1.05±0.39	1.13±0.11	1.47±0.22	0.5	2.81±0.36	1.72±0.11	1.49±0.24
		1	1.90±0.29	1.17±0.17	1.43±0.16	1	1.05±0.41	1.36±0.14	1.95±0.50
		1.5	3.19±0.27	2.63±0.25	4.71±0.31	1.5	1.88±0.25	1.55±0.31	2.80±0.28
		2	2.29±0.16	3.46±0.16	6.04±0.25	2	1.52±0.15	1.73±0.07	1.36±0.08
		20	2.57±0.52	2.68±0.06	2.37±0.28	20	4.70±0.42	1.55±0.26	1.60±0.13
TNF- $\alpha$	IL-1 $\beta$	0.5	2.03±0.37	2.28±0.11	3.80±0.20	0.5	2.26±0.36	1.13±0.12	1.40±0.18
		1	1.21±0.21	1.75±0.24	1.26±0.10	1	1.28±0.15	1.18±0.12	1.06±0.31
		1.5	8.74±0.28	7.15±0.30	9.98±0.59	1.5	11.32±0.35	13.40±0.28	19.67±0.29
		2	1.81±0.17	2.50±0.08	2.92±0.32	2	2.32±0.24	5.08±0.12	5.90±0.09
		20	3.17±0.32	3.70±0.26	2.73±0.19	20	27.94±0.42	12.04±0.26	4.10±0.13
NF-KB	BCL2AI	0.5	1.74±0.37	1.83±0.11	1.75±0.20	0.5	1.86±0.36	2.056±0.12	2.74±0.18
		1	1.38±0.21	1.23±0.24	1.23±0.10	1	2.55±0.15	1.16±0.12	1.37±0.31
		1.5	3.14±0.28	2.62±0.30	2.55±0.59	1.5	1.69±0.35	1.88±0.28	1.57±0.29
		2	1.16±0.17	1.41±0.08	1.77±0.32	2	1.05±0.24	1.05±0.12	1.11±0.09
		20	1.12±0.32	1.61±0.26	1.13±0.19	20	1.57±0.42	2.7±0.09	3.19±0.22

**Table 7.03:** Gene expression fold change values for THP-1 cells exposed to three concentrations of *E. coli* LPS over 20 hours.

	Up-regulation of target gene expression relative to calibrator expression.
	Down-regulation of target gene expression relative to calibrator expression.

### 7.2.5 Measuring optimal multiplicity of infection (MOI) for monocyte cell line infection with *Propionibacterium acnes*

To establish the lowest possible bacterial load needed to stimulate gene expression in THP-1 cells, a panel of 6 genes were challenged with a series of 3 *P. acnes* MOI (100, 50 and 25). Genes were chosen to represent a spread of both cholesterol biosynthesis and inflammatory actions to gauge how bacterial load may affect THP-1 gene expression. mRNA was extracted from *P. acnes*-infected THP-1 cells after 2 h of exposure and qPCR performed. All of the six genes tested were regulated in response to the different MOI of *P. acnes*. *IL-1 $\beta$*  was the most potently expressed gene followed by *HMGR* and *TNF- $\alpha$* . Both *SREBP2* and *LDLR* showed down-regulation for each MOI group; the down-regulation became more noticeable as the MOI increased. Figure 7.21a – c displays the fold changes of the six THP-1 genes when exposed to *P. acnes* MOI 25, 50 and 100. A one-way ANOVA with Tukey's pairwise comparison showed there was no significant difference in the expression of these six genes between groups of THP-1 cells exposed to different MOI (MOI 25 vs MOI 50  $p = 0.956$ ; MOI 50 vs MOI 100  $p = 0.972$  and MOI 25 vs MOI 100  $p = 0.998$ ). A boxplot of ANOVA test results are presented in figure 7.21d. Based on these results it was established that MOI 25 was sufficient enough ratio of bacteria to THP-1 cell, hence an MOI of 25 was used for all further THP-1 infections with *P. acnes*.

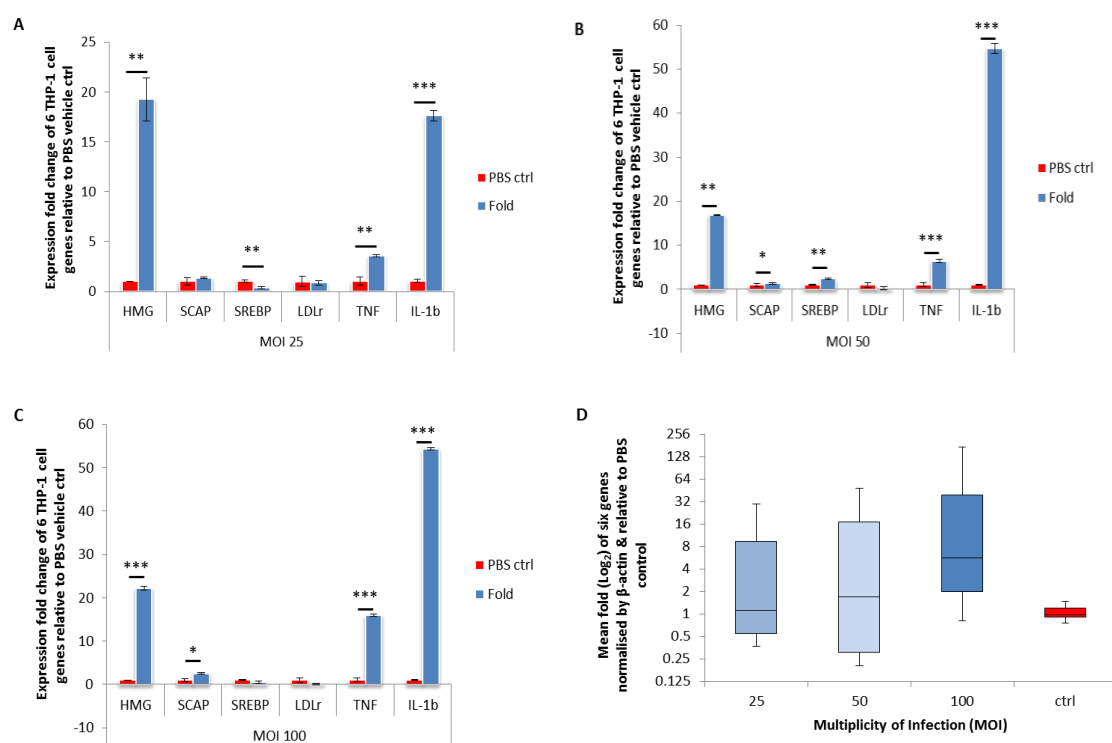


**Figure 7.19:** Fold change gene expression of 6 THP-1 cell target genes when exposed to three different MOI of *P. acnes* (MOI 25, 50 & 100; figures A-C, respectively). Expression was calculated by normalisation to reference gene *ACTB* and relative to a PBS treatment control for each gene in each MOI concentration group. Significance of expression was tested using  $\Delta C_T$  values for target gene expression vs. PBS control and fold values plotted. There were no significant differences in combined mean expression of the six genes for each MOI concentration group (D).

### 7.2.6 THP-1 cells challenged with *Propionibacterium acnes*: an *in vitro* model of infection

While the following finding of *P. acnes*-induced gene expression in THP-1 cells provides potentially interesting evidence that *P. acnes* may activate key genes in the atherosclerotic process, no LPS control was used directly within the *P. acnes* model of infection. It therefore cannot be said with absolute certainty that the profile of expression observed with *P. acnes*-challenged THP-1 cells could not be similar or the same as the expression observed if THP-1 cells were challenged with other bacteria. Four out of five lipid regulatory genes were up-regulated in response to *P. acnes*. *HMGR* was not regulated at 2 and 6 hour time points when challenged with *P. acnes*; however, after 24 h infection, a significant up-regulation of *HMGR* was observed in challenged cells relative to PBS-treatment control cells ( $p < 0.05$ ; figure 7.20). In contrast, *SCAP* was not regulated when exposed to *P. acnes* at any of the time points examined here, though a slight increase in fold change from 1.4 at 2 h to 4.4 at 24 h was observed for infected cells compared to PBS control cell expression [ $F(3,8) = 2.159$ ,  $p = 0.181$ ; figure 7.21]. *P. acnes*-infected THP-1

cells showed a significant up-regulation of *SREBP2* mRNA compared to control cell expression at each of the time points tested here [ $F(3,8) = 33.19$ ,  $p < 0.001$ ]. Expression increased steadily at 2 and 6 hour time points ( $p < 0.05$ ) followed by a marked increase from  $4.12 \pm 0.85$ -fold at 6 h to  $40.03 \pm 1.13$ -fold at 24 h compared to the PBS control cell expression of *SREBP2* ( $p < 0.001$ ; figure 7.22). *SREBP2* mRNA levels did not change after 2 h exposure to *P. acnes* relative to the control cell expression ( $p = 0.289$ ). Similarly, *LDLR* remained unregulated over earlier time points until a significant *LDLR* up-regulation in response to 24 h exposure to *P. acnes* ( $p < 0.05$ ; figure 7.23). The same pattern of expression was observed for *ABCA1*, which remained unregulated at 2 and 6 hours; only after THP-1 cells were challenged with *P. acnes* for 24 h did a significant increase in *ABCA1* (121-fold) occur relative to the PBS-treated control cell expression ( $p < 0.001$ ; figure 7.24)

Four out of six THP-1 inflammatory genes were up-regulated in response to *P. acnes* challenge. THP-1 cells showed a pattern of increasing *CCL3* expression over the 24 h time course when infected with *P. acnes*. A significant up-regulation of *CCL3* was observed after 6 h exposure ( $p < 0.05$ ), followed by a further significant increase of *CCL3* at 24 h ( $p < 0.001$ ) relative to the PBS control cell expression (figure 7.25). In contrast, THP-1 *CCL2* was not regulated by *P. acnes* infection, despite a  $5.8 \pm 2.92$ -fold increase of *CCL2* expression over the 24 h time course; however, the changes relative to the PBS control expression were deemed not significant [ $F(3,8) = 0.886$ ,  $p = 0.441$ ; figure 7.26]. This was likely due to the particularly high variance of  $C_T$  value for *P. acnes*-infected and PBS control cell expression.

*ICAM-1* also remained unregulated at 2 h and 6 h time points when exposed to *P. acnes*, whereas a significantly high up-regulation of *ICAM-1* was observed following 24 h challenge with *P. acnes* ( $p < 0.05$ ; figure 7.27). Similarly, *TNF $\alpha$*  was not regulated at the earlier time points examined here, followed by a significant up-regulation of *TNF- $\alpha$*  in cells exposed to *P. acnes* at 24 h ( $p < 0.01$ ; figure 7.28). The same pattern of expression was also observed for THP-1 expression of *IL-1 $\beta$* ; whereby only after 24 h *P. acnes* challenge was a significant increase in *IL-1 $\beta$*  expression observed relative to PBS-treated cell expression ( $p < 0.05$ ; figure 7.29). There were no significant changes in *P. acnes*-infected THP-1 cell expression of *NF- $\kappa$ B* relative to the expression of *NF- $\kappa$ B* in the PBS-treated control cells [ $F(3,8) = 0.871$ ,  $p = 0.495$ ; figure 7.30]. In contrast, *BCL2A1* was the most potently expressed of all genes tested in response to *P. acnes* [ $F(3,8) = 76.85$ ,  $p < 0.0001$ ]. Expression of *BCL2A1* was up-regulated at each time point and showed an

extremely sharp increase in fold change between 6 h ( $23.08 \pm 1.13$ ,  $p < 0.001$ ) and 24 h ( $560.08 \pm 1.14$ ,  $p < 0.00001$ ) relative to control cell expression. The up-regulation of *BCL2A1* after 2 h exposure to *P. acnes* did not change relative to the expression of *BCL2A1* in the PBS control reaction (figure 7.31).

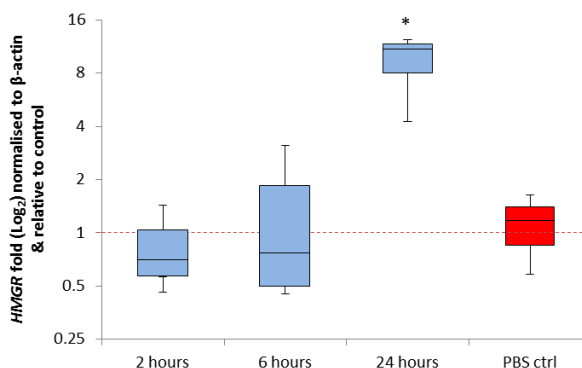


**Figure 7.20:** Gene expression fold change for *HMGR* following challenge of THP-1 monocyte cell line with *P. acnes* at an MOI OF 25 (blue boxes). Target gene expression was calculated at 2, 6 and 24 h intervals. Expression was normalised by *ACTB* and calculated relative to *HMGR* expression for THP-1 cells treated with a PBS vehicle (red box). Data represents the mean target gene expression fold change from three technical replicates of *P. acnes*-challenged THP-1 cells. PBS control expression represents the mean of 9 technical replicates PBS treated cells (3 technical replicate samples at each time point).

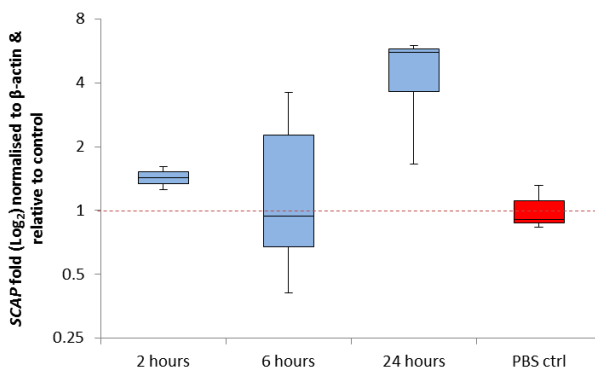


**Figure 7.21:** Gene expression fold change for *SCAP* following challenge of THP-1 monocyte cell line with *P. acnes* at an MOI of 25 (blue boxes). Target gene expression was calculated at 2, 6 and 24 h intervals. Expression was normalised by *ACTB* and calculated relative to *SCAP* expression for THP-1 cells treated with a PBS vehicle (red box). Data represents the mean target gene expression fold change from three technical replicates of *P. acnes*-challenged THP-1 cells. PBS control expression represents the mean of 9 technical replicates PBS treated cells (3 technical replicate samples at each time point).

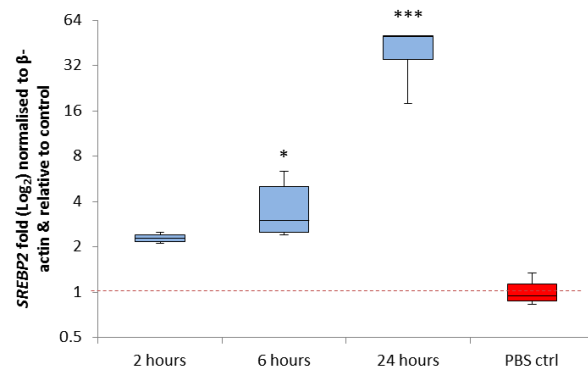


**Figure 7.22:** Gene expression fold change for *SREBP2* following challenge of THP-1 monocyte cell line with *P. acnes* at an MOI of 25 (blue boxes). Target gene expression was calculated at 2, 6 and 24 h intervals. Expression was normalised by *ACTB* and calculated relative to *SREBP2* expression for THP-1 cells treated with a PBS vehicle (red box). Data represents the mean target gene expression fold change from three technical replicates of *P. acnes*-challenged THP-1 cells. PBS control expression represents the mean of 9 technical replicates PBS treated cells (3 technical replicate samples at each time point).

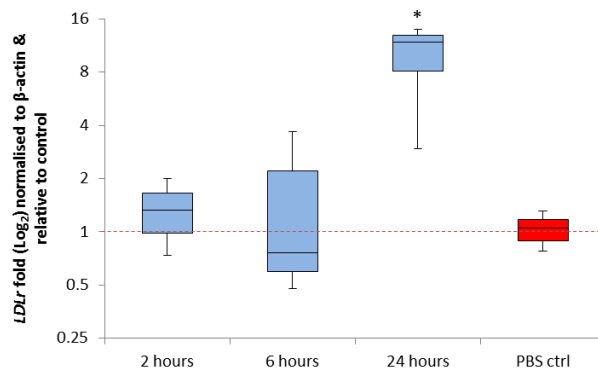


**Figure 7.23:** Gene expression fold change for *LDLr* following challenge of THP-1 monocyte cell line with *P. acnes* at an MOI of 25 (blue boxes). Target gene expression was calculated at 2, 6 and 24 h intervals. Expression was normalised by *ACTB* and calculated relative to *LDLr* expression for THP-1 cells treated with a PBS vehicle (red box). Data represents the mean target gene expression fold change from three technical replicates of *P. acnes*-challenged THP-1 cells. PBS control expression represents the mean of 9 technical replicates PBS treated cells (3 technical replicate samples at each time point).

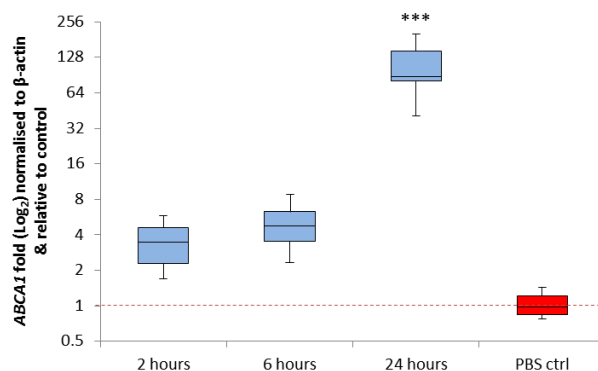


**Figure 7.24:** Gene expression fold change for *ABCA1* following challenge of THP-1 monocyte cell line with *P. acnes* at an MOI of 25 (blue boxes). Target gene expression was calculated at 2, 6 and 24 h intervals. Expression was normalised by *ACTB* and calculated relative to *ABCA1* expression for THP-1 cells treated with a PBS vehicle (red box). Data represents the mean target gene expression fold change from three technical replicates of *P. acnes*-challenged THP-1 cells. PBS control expression represents the mean of 9 technical replicates PBS treated cells (3 technical replicate samples at each time point).

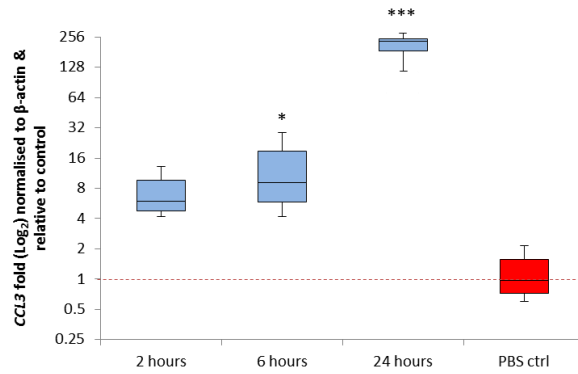


**Figure 7.25:** Gene expression fold change for *CCL3* following challenge of THP-1 monocyte cell line with *P. acnes* at an MOI of 25 (blue boxes). Target gene expression was calculated at 2, 6 and 24 h intervals. Expression was normalised by *ACTB* and calculated relative to *CCL3* expression for THP-1 cells treated with a PBS vehicle (red box). Data represents the mean target gene expression fold change from three technical replicates of *P. acnes*-challenged THP-1 cells. PBS control expression represents the mean of 9 technical replicates PBS treated cells (3 technical replicate samples at each time point).

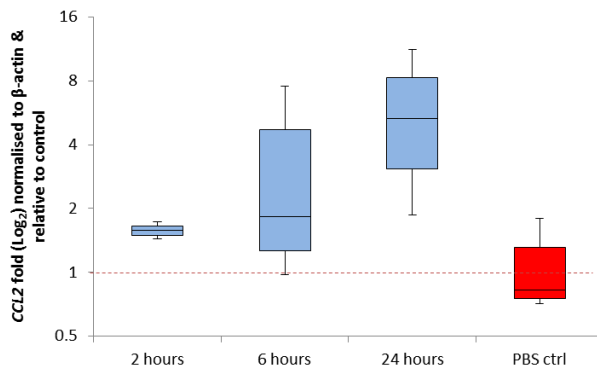


**Figure 7.26:** Gene expression fold change for *CCL2* following challenge of THP-1 monocyte cell line with *P. acnes* at an MOI of 25 (blue boxes). Target gene expression was calculated at 2, 6 and 24 h intervals. Expression was normalised by *ACTB* and calculated relative to *CCL2* expression for THP-1 cells treated with a PBS vehicle (red box). Data represents the mean target gene expression fold change from three technical replicates of *P. acnes*-challenged THP-1 cells. PBS control expression represents the mean of 9 technical replicates PBS treated cells (3 technical replicate samples at each time point).

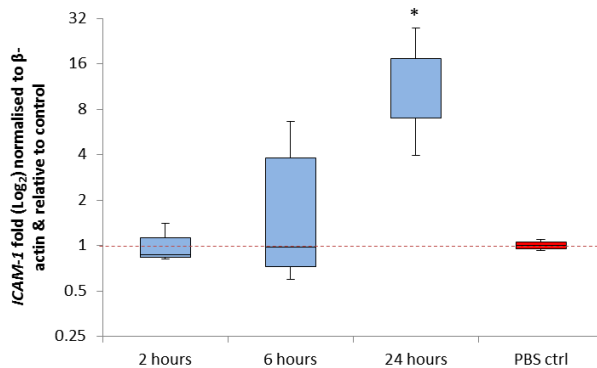


**Figure 7.27:** Gene expression fold change for *ICAM-1* following challenge of THP-1 monocyte cell line with *P. acnes* at an MOI of 25 (blue boxes). Target gene expression was calculated at 2, 6 and 24 h intervals. Expression was normalised by *ACTB* and calculated relative to *ICAM-1* expression for THP-1 cells treated with a PBS vehicle (red box). Data represents the mean target gene expression fold change from three technical replicates of *P. acnes*-challenged THP-1 cells. PBS control expression represents the mean of 9 technical replicates PBS treated cells (3 technical replicate samples at each time point).

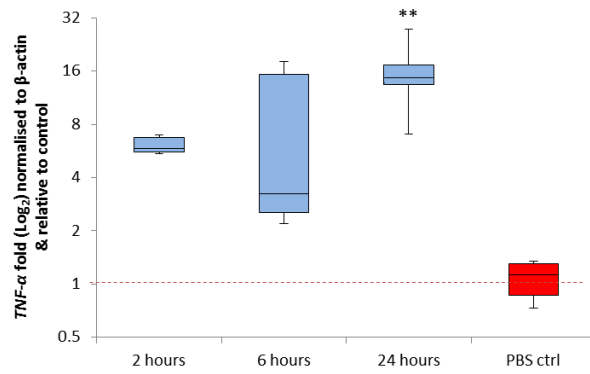


**Figure 7.28:** Gene expression fold change for *TNF $\alpha$*  following challenge of THP-1 monocyte cell line with *P. acnes* at an MOI of 25 (blue boxes). Target gene expression was calculated at 2, 6 and 24 h intervals. Expression was normalised by *ACTB* and calculated relative to *TNF $\alpha$*  expression for THP-1 cells treated with a PBS vehicle (red box). Data represents the mean target gene expression fold change from three technical replicates of *P. acnes*-challenged THP-1 cells. PBS control expression represents the mean of 9 technical replicates PBS treated cells (3 technical replicate samples at each time point).

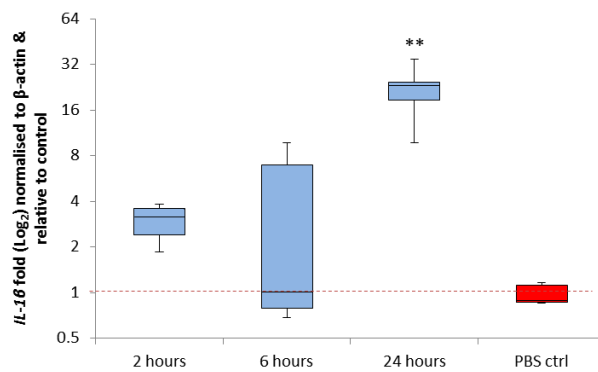


**Figure 7.29:** Gene expression fold change for *IL1 $\beta$*  following challenge of THP-1 monocyte cell line with *P. acnes* at an MOI of 25 (blue boxes). Target gene expression was calculated at 2, 6 and 24 h intervals. Expression was normalised by *ACTB* and calculated relative to *IL1 $\beta$*  expression for THP-1 cells treated with a PBS vehicle (red box). Data represents the mean target gene expression fold change from three technical replicates of *P. acnes*-challenged THP-1 cells. PBS control expression represents the mean of 9 technical replicates PBS treated cells (3 technical replicate samples at each time point).

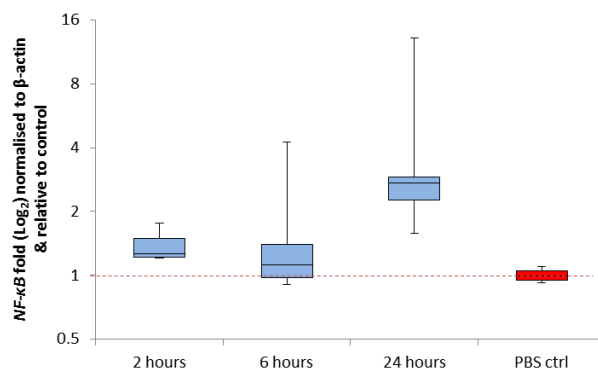


**Figure 7.30:** Gene expression fold change for *NF- $\kappa$ B* following challenge of THP-1 monocyte cell line with *P. acnes* at an MOI of 25 (blue boxes). Target gene expression was calculated at 2, 6 and 24 h intervals. Expression was normalised by *ACTB* and calculated relative to *NF- $\kappa$ B* expression for THP-1 cells treated with a PBS vehicle (red box). Data represents the mean target gene expression fold change from three technical replicates of *P. acnes*-challenged THP-1 cells. PBS control expression represents the mean of 9 technical replicates PBS treated cells (3 technical replicate samples at each time point).

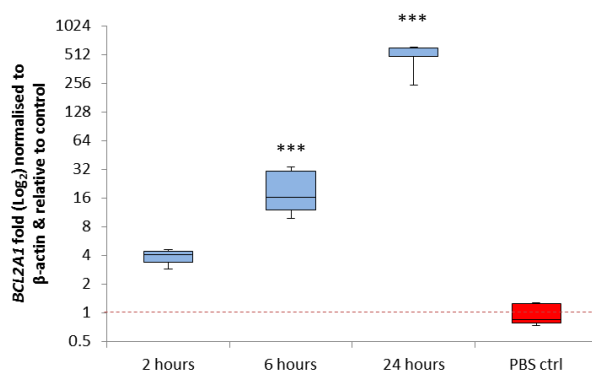


**Figure 7.31:** THP-1 monocyte expression fold change of *BCL2A1* following challenge with *P. acnes* at an MOI of 25 (blue boxes). Target gene expression was calculated at 2, 6 and 24 h intervals. Expression was normalised by *ACTB* and calculated relative to *BCL2A1* expression for THP-1 cells treated with a PBS vehicle (red box). Data represents the mean target gene expression fold change from three technical replicates of *P. acnes*-challenged THP-1 cells. PBS control expression represents the mean of 9 technical replicates PBS treated cells (3 technical replicate samples at each time point).

Gene	Time (hours)	Fold Change	Gene	Time (hours)	Fold Change
<i>HMGR</i>	2	0.75±0.74	<i>SCAP</i>	2	1.43±0.34
	6	1.37±0.42		6	1.65±0.53
	24	9.46±0.56**		24	4.40±0.94
<i>SREBP2</i>	2	2.29±0.29	<i>LDLR</i>	2	1.32±0.24
	6	4.12±0.73*		6	1.62±0.54
	24	40.03±0.66***		24	10.03±0.81*
<i>ABCA1</i>	2	3.44±0.75	<i>CCL3</i>	2	7.56±0.45
	6	4.45±0.70		6	13.46±0.79*
	24	120.76±0.17***		24	205.63±0.38***
<i>CCL2</i>	2	1.57±0.87	<i>ICAM1</i>	2	1.02±0.51
	6	3.35±1.79		6	2.701±0.76
	24	5.76±2.77		24	13.84±1.63*
<i>TNF-α</i>	2	6.26±0.25	<i>IL-1β</i>	2	2.81±0.67
	6	10.83±0.95		6	4.83±0.27
	24	15.87±1.1*		24	20.87±0.61*
<i>NF-KB</i>	2	1.39±1.40	<i>BCL2A1</i>	2	3.74±0.51
	6	1.21±0.52		6	23.09±1.32***
	24	2.17±2.28		24	560.08±1.03***

**Table 7.04:** Gene expression fold change values for THP-1 cells challenged with a *P. acnes* MOI of 20. Fold change was calculated using the comparative  $C_T$  ( $\Delta\Delta C_T$ ) method. Target gene expression fold change values were calculated for *P. acnes*-infected cells relative, normalised to *ACTB* and relative to target gene expression of cells treated with a vehicle control (PBS) at 2 h, 6 h and 24 h exposure to *P. acnes*. Target gene expression in *P. acnes*-infected cells was significantly different to control cell expression when p values were  $p < 0.05$ ; \*,  $p < 0.01$ ; \*\*, or  $p < 0.001$ ; \*\*\*.

### 7.3 Discussion

The aim of this chapter was to investigate *P. acnes* infection and evaluate host cell inflammatory and metabolic responses by analysing relative mRNA levels within *P. acnes*-infected THP-1 cells. The data above provides novel information regarding real-time mRNA expression of pro-inflammatory cytokines, cholesterol biosynthesis and efflux, and host cell survival responses to *P. acnes* infection, which hitherto has received little attention.

qPCR was employed to detect transcript expression levels from THP-1 cells infected with a *P. acnes* strain isolated from human atherosclerotic plaque tissue. qPCR is a powerful analytical tool that allows the detection of minute changes in gene expression from trace amounts of template mRNA/cDNA. Using qPCR has distinct advantages over endpoint PCR because the kinetics of transcript amplification are examined in the early stages of the PCR reaction, opposed to monitoring relative transcript levels at the end of the PCR reaction. The accuracy of qPCR is a consequence of measuring reaction kinetics during the exponential amplification phase, where, assuming 100% amplification efficiency ( $E = 2$ ), an exact doubling of transcription product occurs at each cycle, resulting in a more precise assessment of the initial transcript copy number.

THP-1 cells were employed in this investigation to evaluate a basic *in vitro* model of inflammation arising from bacteria and host interaction. Some investigators believe the differentiated THP-1 phenotype provides a more activated response to infective challenge, and as such, can be more informative (Takashiba et al. 1999; Park et al. 2007). Differentiation occurs when THP-1 monocytes are exposed to phorbol esters, such as phorbol-12-myristate-13-acetate (PMA), resulting in a phenotypic shift from monocyte to cells that closely mimic native monocyte-derived macrophages. PMA exposure also promotes phagocyte activation, characterised by alterations in cellular metabolism and plasma membrane composition (Todd and Liu 1986). Therefore, THP-1 macrophages provide an extremely useful *in vitro* model cell line for investigating phagocytosis and destruction or evasion mechanisms of host/pathogen interactions. Crucially however, both THP-1 phenotypes can potentiate powerful inflammatory responses to bacterial stimulus through the release of hundreds of cytokines via a NF- $\kappa$ B-dependant or independent pathways (Cohen 2000; Pollard et al. 2004; Carayol et al. 2006; Nahid et al. 2011). It was never the aim of this investigation to establish the fate of phagocytosed *P. acnes*, so no clear advantages would have been gained from differentiating cells to THP-1 macrophages

prior to infection. Hence, undifferentiated THP-1 monocytes were employed for measuring target gene expression of a host cell line in response to *P. acnes* infection. Until now, previous investigations involving *P. acnes*-infected THP-1 cells have concentrated on the responses from the differentiated phenotype. Unconventionally, the findings presented here provide information on how the undifferentiated THP-1 monocyte responds to *P. acnes* infection, giving insight into one of the first immune responses to infection at the transcription level.

This study shows that human monocytic cell line, THP-1, can induce an inflammatory response when exposed to clinical isolates of *P. acnes*. A total of twelve genes were investigated by measuring their regulation in response to *P. acnes* infection. All target genes showed a temporal increase of mRNA over the 24 h time course. Only one down-regulated response was observed for *HMGr* at 2 h; though the down-regulation of *HMGr* in response to *P. acnes* was not significantly different from the control condition. Nine of the tested genes were significantly up-regulated in response to *P. acnes* infection. *SCAP*, *CCL2* and *NF- $\kappa$ B* all showed a steady increase in expression over 24 h but the regulated response was not significantly different to that of the PBS treated control cells. The aforementioned genes had a particularly high level of variation of  $C_T$  value for replicate samples compared to the highly analogous  $C_T$  values of other tested genes. In certain instances, mean fold change of *P. acnes*-challenged cells was nearly 5 times that of the PBS-treated control cells (*CCL2*, table 6.04), however, the level of deviation in expression between technical replicate for these genes was excessive, and thus, the mean fold change values are unreliable.

The genes significantly up-regulated in response *P. acnes* can be broadly categorised into three main groups; inflammation (*TNF- $\alpha$* , *IL-1 $\beta$* , *CCL3* and *ICAM-1*), cholesterol biosynthesis and efflux (*HMGr*, *SREBP2*, *LDLr* and *ABCA1*), and anti-apoptosis (*BCL2A1*). The *P. acnes* strain employed in this study was isolated from atherosclerotic tissue specimens that were surgically removed from the carotid artery. Because atherosclerosis is an inflammatory condition, when selecting genes for this study, emphasis was placed on genes that have known involvement in the pathogenesis of atherosclerosis. During the initial phases of atherogenesis, circulating monocytes adhere to and transmigrate activated endothelium, extravasate to the sub-intimal space then finally differentiate into monocyte-derived macrophage. The release of pro-inflammatory cytokines by monocytes and monocyte-derived macrophages is the dominant force that

drives leukocyte recruitment, trans-endothelial migration and monocyte differentiation. Here it is shown that some of the pro-inflammatory cytokines, TNF- $\alpha$ , IL-1 $\beta$ , CCL3 and cell adhesion molecule ICAM1, which are fundamental to these inflammatory processes, are similarly up-regulated by THP-1 monocytes in response to *P. acnes* infection.

*P. acnes* stimulation of pro-inflammatory cytokines TNF- $\alpha$  and IL-1 $\beta$  in THP-1 cells has been reported by other investigators. Vowels et al. (1995) demonstrated abundant dose dependant release of IL-8, IL-1 $\beta$  and TNF- $\alpha$  from THP-1 cells infected with various concentrations of whole, heat killed (HK) *P. acnes*. Similarly, but to a lesser extent, the authors demonstrated that different concentrations of 3-day *P. acnes* culture supernatants (CS) were found to stimulate release of the same three cytokines, indicating that *P. acnes* also releases factors capable of stimulating production of pro-inflammatory cytokines in THP-1 cells. By separating the active factor present in the *P. acnes* supernatant by fractionation, the authors sequentially inhibited potential active factors by heat and enzyme treatments, followed by incubating THP-1 cells with the modified CS. Vowels et al. (1995) identified that factors between 3 – 30 kDa, a molecular weight range fitting that of peptidoglycan-polysaccharide, lipoteichoic acid (LTA), were the most potent inducers of cytokine release. Finally, through selective blockage of the major LPS/LTA and peptidoglycan receptor, CD14, resulted in a significant reduction in the cytokine secretion in THP-1 cells exposed to supernatant; suggesting a major virulence factors of *P. acnes* was a form of peptidoglycan-polysaccharide.

Here, whole HK *P. acnes* was utilised as the stimulating component, and as such, it cannot be suggested that *P. acnes* LTA was the sole virulence factor responsible for mediating the observed inflammatory response. Vowels et al. (1995) reported that whole HK *P. acnes* infection resulted in the most abundant release of IL-1 $\beta$  and TNF- $\alpha$ ; even when infection with whole *P. acnes* was reduced 10 and 100-fold, cytokines release was greater than the most potent response from the most concentrated supernatant infection. These findings suggest a possible synergistic action between more than one *P. acnes* virulent factor could be responsible for pro-inflammatory cytokine activation in THP-1 cells infected with whole *P. acnes*.

CCL3, also known as macrophage inflammatory protein-1 alpha (MIP-1 $\alpha$ ) is a cytokine of the C-C chemokine family secreted by monocytes, macrophages and lymphocytes during acute inflammation (Wolpe et al. 1988). CCL3 protein, which acts via G-protein-coupled cell surface receptors, is a potent mediator of leukocyte chemotaxis and

proliferation during inflammation. Thus, CCL3 plays a prominent role in the pathogenesis of many inflammatory conditions, including periodontal disease and atherosclerosis. MIP-1 proteins have also been shown to promote homeostasis. In the study carried out here, a temporal expression of CCL3 in response to *P. acnes* was observed. Expression of CCL3 began at 2 h; but did not change significantly compared to the control until 6 h (13.5-fold, <.05) followed by a large increase in expression at 24 h (205-fold, <.001; figure 6.25a and b). To our knowledge, no previous investigations have shown CCL3 expression in THP-1 or human monocytes in response to *P. acnes*. However, in vitro studies have shown that human peripheral blood monocytes infected with LTA from other gram-positive bacteria result in both time- and dose-dependent expression of CCL3 mRNA and protein after 24 h co-culture (Danforth et al. 1995; Yam et al. 2008). Interestingly, Yam et al. (2008) showed that even at MOI 10,000, *E. coli* and *Lactococcus lactis* evoked expression of CCL3 in macrophages that was nearly 200-fold lower than the expression observed here with an MOI 25 of *P. acnes*.

In the study carried out here, *E. coli* LPS was utilised to evaluate THP-1 gene expression. Significant expression of CCL3 in THP-1 was induced by *E. coli* LPS from as early as 1 h, yet expression induced by *E. coli* was markedly weaker than the expression induced by *P. acnes* infection (figure 6.10). As a mediator of acute and chronic inflammation, CCL3 interacts with chemokine receptors CCR4, CCR1 and CCR5, of which the latter two have been implicated in atherogenesis (Kuziel et al. 2003; Potteaux et al. 2005; Potteaux et al. 2006; Braunersreuther et al. 2007). CCL3 is able to augment neutrophil chemotaxis induced by the proinflammatory cytokine TNF $\alpha$  in a CCR5-dependent manner (de Jager et al. 2013a). Moreover, CCL3 itself significantly up-regulated during atherosclerotic lesion formation (Moos et al. 2005; de Jager et al. 2010). *P. acnes* was shown here to induce strong up-regulation of CCL3. Given the origin of the *P. acnes* isolate utilised here, and its capacity for prompting potent chemotactic activity, it could be proposed that atherosclerotic vessels infected with *P. acnes* expose the vessel to increased inflammatory burden. To our knowledge a comprehensive analysis of monocytic cell chemokines, including CCL3 gene and protein expression deriving from *P. acnes*-infection has not been undertaken. Therefore, studies investigating chemotactic activity in vascular inflammation with particular emphasis on *P. acnes*-infection may provide information on the extent to which *P. acnes* sustains chronic inflammation.

Recognition of microbial pathogens by the cells of the immune system triggers host defence mechanisms to combat infection and prevent disease. A group of highly conserved transmembrane pattern recognition receptors (PRRs), known as Toll-like receptors (TLRs) are fundamental in the coordinated innate and adaptive immune responses to invading microbes. TLRs recognise conserved membrane bound proteins known as 'pathogen associated molecular patterns' (PAMPs) that are critical to the pathogen function. *P. acnes* produce bioactive exocellular products that interact with the host immune system. Several genes in the *P. acnes* genome have been identified that encode different virulence factors such as, hemolysins, proteases and lipases, CAMP factors, surface associated proteins with immunoreactivity, such as peptidoglycan and LTA (Holland et al. 2010; Horváth et al. 2012; Tomida et al. 2013). LTA is a major ligand of TLR-2, which activate intercellular signalling pathways leading to the transcription of numerous cytokine genes via transcription factors NF- $\kappa$ B and AP-1. TLR-2 activation to *P. acnes* was demonstrated by Kim et al. (2002) who transfected TLR-2 into a naturally LPS and LTA-unresponsive cell line. In transfectants with functional TLR-2 and CD14, *P. acnes* induced IL-12, IL-6 IL-18 and TNF- $\alpha$  via TLR-2/NF- $\kappa$ B dependant pathway. In contrast, *P. acnes* could not activate NF- $\kappa$ B in cells expression TLR-4. In addition *P. acnes*-infected primary human monocytes secrete IL-8 and IL-18, which are successfully attenuated via anti-TLR-2 blocking antibodies (Kim et al. 2002). Likewise, Chen et al. (2002) reported the same TLR-2 activation pathway resulting in the secretion of IL-8 and IL-18 in response to *P. acnes* via NF- $\kappa$ B activation in THP-1 cells. Moreover, in animal studies peritoneal macrophages from *Tlr2* knockout mice fail to produce IL-6 in response to *P. acnes*, whereas IL-6 production was not diminished in wild-type, *Tlr6* knockout, and *Tlr1* knockout mice (Kim et al. 2002).

*P. acnes*-induced activation of TLR-2 and subsequent intercellular signalling leading to transcription of pro-inflammatory cytokines demonstrates a highly effective and targeted host immune response mechanism. Recognition of microbial pathogens by the cells of the immune system triggers host defence mechanisms to combat infection and prevent disease. However, the same activated pathways can also be destructive exacerbating inflammation at the site of disease resulting in tissue injury. Chen et al. (2002) investigated IL-8 and IL-18, which were not considered in the study carried out here. However, when taken together with findings by Kim et al. (2002) and reports of the same TLR-2 response to *P. acnes* in keratinocytes (Nagy et al. 2005; Jugeau et al. 2005; Lee et al. 2008; Shibata et al. 2009), sebocytes (Nagy et al. 2006) and prostate epithelial cells (Fassi Fehri et al. 2011)

strong evidence for *P. acnes*-induced activation of TLR-2/ NF- $\kappa$ B-dependant pathway exists. TLR-2 consistently failed in this investigation and so was not investigated further. However, based on the aforementioned studies it could be hypothesised that the genes activated here in response to *P. acnes*-infection did so via TLR2 in an NF- $\kappa$ B, CD14 and MYD88 dependant manner.

The innate response activation of pro-inflammatory cytokines such as IL-1 $\beta$  is not solely controlled through TLR signalling pathways. NOD-like receptors (NLRs) initiate signalling through recognition of microbial PAMPs as well as host-mediated Danger Associated Molecular Patterns, (DAMPs). As previously discussed, TLR-2 has been proposed as a key receptor in response to *P. acnes* through recognition of bacteria wall components such as muramyl dipeptide or LTA and lipoprotein. Unlike TLRs, NLRs are entirely cytoplasmic, and as such provide intercellular sensing of microbial agents. Upon ligand sensing, NLRs form caspase-1-activating multi-protein complex known as an inflammasome. Most characterised is NLR family pyrin domain-containing 3 (NLRP3) inflammasome. Pro-IL-1 $\beta$  is not constitutively expressed and requires transcriptional induction via TLR stimulus. *P. acnes* is a potent trigger of THP-1 cell NLRP3-inflammasome activation, IL- $\beta$  processing and secretion (Sahdo et al. 2013; Kistowska et al. 2014; Qin et al. 2014; Thiboutot 2014). The mechanism of *P. acnes* induced-NLRP3 activation is dependent on lysosomal destabilisation, reactive oxygen species and cellular potassium ion (K<sup>+</sup>) efflux (Kistowska et al. 2014). As well as IL-1 $\beta$ , *P. acnes* induced secretion of IL-6, TNF- $\alpha$ , and IL-8 by at an MOI 25. Qin et al. (2014) and subsequent IL-1 $\beta$  secretion involved K<sup>+</sup> efflux. Also, caspase-1 and caspase-2 gene expression is up-regulated in monocytes when stimulated with live *P. acnes*, however, IL-1 $\beta$  requires only caspase-1 activity (Franchi et al. 2009; Sahdo et al. 2013; Qin et al. 2014; Contassot & French 2014). What is more, inhibition of NLRP3 is sufficient to result in attenuated IL-1 $\beta$  expression, preventing inflammation; the same inhibitory action on NLRP1 does not have the same effect (Qin et al. 2014).

In the study carried out here IL-1 $\beta$  was significantly up-regulated by THP-1 cells in response to both LPS and *P. acnes*. For LPS-infected THP-1, there was a significantly greater expression in the early stages of the time course (figure 6.15; 1.5 h) that was comparable to later expression levels observed with *P. acnes* exposure (figure 6.29; 24 h), however IL-1 $\beta$  was expressed to a similar final maximum level.

Phagocytosis of *P. acnes* is necessary for NLRP3-inflammasome activation and subsequent IL-1 $\beta$  production in THP-1, (Sahoo et al. 2011). Interestingly, Fischer et al. (2013) describes a study into the intracellular fate of *P. acnes* in macrophages. In this important study, *P. acne* was observed to have an ability to survive in prostate macrophages of mice at 2 weeks after *P. acnes* inoculation, and not just survive but persist in THP-1. This has great implications because the ability to persist in macrophages and other cell types as an intracellular pathogen may be important in the context of *P. acnes*-related diseases and chronic infection. More importantly, this intercellular survival may go some way to explain how the isolate of *P. acnes* used in this *in vitro* model of infection came to be isolated so frequently in the atherosclerotic plaques examined in earlier chapters.

Seven of the genes analysed in this study activate via NF- $\kappa$ B-dependant signalling, i.e. ABCA1 (Gerbod-Giannone et al. 2006), CCL3 (Grove & Plumb 1993), CCL2 (Ueda et al. 1997), ICAM-1 (van de Stolpe et al. 1994), TNF- $\alpha$  (Shakhov et al. 1990), IL-1 $\beta$  (Hiscott et al. 1993) and BCL2A1 (Zong et al. 1999). TLR-2 activation and the intercellular signalling involve many protein interactions before NF- $\kappa$ B is free to translocate through the nuclear membrane to initiate gene transcription. While the entire signal cascade is expansive, including transcription of the NF- $\kappa$ B-target gene, expression completes within 40 min. This was apparent when using *E. coli* LPS to stimulate THP-1 cells, as significant expression of TNF- $\alpha$  was observed at the first 30 minute time point. Unfortunately, NF- $\kappa$ B did not show significant regulation by *P. acnes* infected THP-1 cells, nor was there any NF- $\kappa$ B signalling observed. As NF- $\kappa$ B regulation is necessary for transcription of all the genes investigated here except HMGR, SCAP, SREBP2 and LDLR; NF- $\kappa$ B signalling must have occurred. When explaining this lack of NF- $\kappa$ B induction, one must consider the length of time between RNA isolations; it is entirely plausible expression of NF- $\kappa$ B occurred within the 24 hour incubation. When considering this and the rapid signalling response from stimulation to transcription (30 minutes for TNF- $\alpha$  expression) it's entirely possible that NF- $\kappa$ B was induced several times prior to mRNA isolation.

In addition to the pro-inflammatory cytokine response induced in THP-1, ICAM-1 was also significantly up-regulated in response to *P. acnes* at 24 h (figure 6.04;  $p < .05$ ). To the best of our knowledge, there have been no previous studies that show up-regulated THP-1 ICAM-1 in response to *P. acnes*. Expression occurred steadily over the 24 h time course with the greatest and only significant change occurring at 24 h. Expression of ICAM-1 in

*P. acnes*-infected THP-1 was greater than LPS-induced ICAM-1. ICAM-1 is a cellular adhesion molecule member of the immunoglobulin superfamily that plays a key role in regulating the recruitment and trans-endothelial migration of leukocytes into the vessel wall. Activated by cytokines, leukocytes express L-selectin, ligands for P- and E-selectins expressed on the endothelium membrane (Tedder et al. 1999). A sequence of receptor-ligand interactions commences by initial tethering of L-selectin and P-selectin (PSGL-1). Selectins poses low affinity and therefore the circulating leukocyte tethers the endothelium and begins to roll, breaking selectin ligands and re-ligating while in motion (Ley 2003). Macrophages residing in the tissue release chemokines such as IL-8 and MCP-1 that activate chemokine receptors MAC-1 and LFA-1 on the leukocytes (Mukaida 1998). LFA-1 and MAC-1 are  $\beta$ 2-integrins with high affinity for ICAM-1 and ICAM-2, respectively (Sanchez-Madrid et al. 1983). Due to the high affinity of integrins, leukocyte adhesion to the endothelium is a highly stable. Cytokines such as vascular permeability factor/vascular growth factor, induce vascular dilation and endothelium permeability enabling monocyte diapedesis, aided by platelet endothelial cell adhesion molecule 1 (PCAM-1).

However, this process is only part facilitated by endothelial activation of ICAM-1. It has been shown that monocyte ICAM-1 also plays an equally important role in this process, verified by oligodeoxyribonucleotide (ODN) blocking of monocyte ICAM-1 expression in monocyte-endothelium migration assays (Steidl et al. 2000). Inhibition of monocyte ICAM-1 via transfection of an antisense ODN sequence resulted in a significant reduction (38%) of monocyte adhesion to a HUVEC endothelial monolayer. Furthermore, inhibiting monocyte ICAM-1 also significantly reduces monocyte trans-endothelial migration by 40% compared to a random ODN sequence control (Steidl et al. 2000). This suggests the expression of ICAM-1 on monocytes is a key inflammatory response, controlling in part, adhesion and migration independent of other critical monocyte cell adhesion molecules, P and L-selectin.

This has particular relevance when translating *P. acnes* infection and its observed ability to up-regulate ICAM-1 in vitro. The viable *P. acnes* used in this study was isolated from atherosclerotic tissue surgically removed from the carotid artery. Although it cannot be stated that the particular *P. acnes* isolate utilised as an in vitro stimulus was responsible for the ex vivo ICAM-1 expression observed here; it does provide some insight into *P. acnes* host interaction at a simple innate response level. Steidl et al. (2000) findings suggests that effective leukocyte recruitment and trans-endothelial migration is

determined, in part, by induction of monocytic ICAM-1. Given the origin of *P. acnes* isolation and its ability to significantly up-regulate monocytic ICAM-1, it could be proposed that atherosclerotic lesions comprising *P. acnes* are subjected to additional inflammatory burden through enhanced leukocyte recruitment. Consequently, an increase in leukocytes to the artery wall could lead to an increase in foam cell numbers and a physical increase in lesion mass.

It is not confirmed from the in vitro model of infection carried out here whether monocytic ICAM-1 was directly up-regulated in response to *P. acnes* or indirectly through cytokine signalling. From these data TNF- $\alpha$  or IL-1 $\beta$  cannot be discounted as mediators of ICAM-1 up-regulation as all three genes were up-regulated at 24 h but not at 2 or 6 h. It has long been understood that endothelial ICAM-1 is mediated in response to pro-inflammatory cytokine signalling from TNF- $\alpha$  and IL-1 $\beta$  (Bevilacqua et al. 1985; Pober et al. 1986). This mediating action has been confirmed in several studies in which inhibitory factors targeting TNF- $\alpha$  and IL-1 $\beta$  signalling pathways show marked reductions in endothelial ICAM-1 expression (Zhang et al. 2002; Zhou et al. 2005). TNF- $\alpha$  is a potent stimulator of the cell adhesion molecules ICAM-1 and VCAM-1 which occurs through ligation of TNF receptor 1 subtype and mediated by the NF-KB pathway (Zhou et al. 2007). It is worth noting that although the majority of studies primarily investigate the role of TNF- $\alpha$  and IL-1 as facilitators of endothelial ICAM-1 expression and protein activation, the same effector pathways are responsible for monocytic ICAM-1 induction (Xie & Gu 2008). In addition, endotoxin-stimulated THP-1 expression of ICAM-1 has been reported to induce TNF- $\alpha$  in adjacent naïve cells, a response observed when blocking ICAM-1 on endotoxin-stimulated THP-1 cells resulted in a reduced THP-1 production of TNF- $\alpha$  of approximately 30% (Xie & Gu 2008).

Here we show that *P. acnes* was capable of up-regulating genes involved with cholesterol biosynthesis, trafficking and efflux (HMGR, SREBP2, LDLR and ABCA1) in THP-1 cells. Sterols and fatty acids are common intermediary metabolites that play key roles in many biological pathways involved in inflammatory diseases such as atherosclerosis and chronic heart disease (Lusis, 2000; Makowski & Hotamisligil, 2005; Wood et al., 1984). Significantly, mounting evidence shows a connection between innate immune signaling processes and the regulation of sterol and fatty acid metabolism (Castrillo et al. 2003; Ogawa et al. 2005; Zelcer & Tontonoz 2006; Wang et al. 2009; Li et al. 2013). However it cannot be determined whether *P. acnes* is directly or indirectly responsible for activation

of cholesterol mediating genes. Specifically, cholesterol and its metabolites have been shown to alter inflammatory mediator behavior (Zhu et al. 2008; Bauman et al. 2009; Yvan-Charvet et al. 2010), and conversely, innate immune signalling has been shown to modulate the dynamics of cholesterol transport, storage, and excretion (Eguchi et al. 2008; Maitra et al. 2009; Haas & Mooradian 2010). Here, significant expression was observed in all but one (SCAP) lipid mediating gene. Like NF- $\kappa$ B, SCAP expression showed high deviation between biological replicate expression values, and so was deemed an unreliable target gene. HMGR, although down-regulated in the first two hours showed an increase in expression over the 24 h exposure time, rising to a significant expression at the 24 h. HMG-CoA reductase is the rate-determining enzyme of the cholesterol biosynthetic pathway and, like HMG-CoA synthase, is highly regulated by the availability of free cellular cholesterol (Burg & Espenshade 2011). Hence, up-regulation indicates depletion in free cellular cholesterol or a dysregulation in the mevalonate pathway brought on by *P. acnes* presence. Kistowska et al. (2008) found that both *E. coli* and *Streptococcus aureus*-infected THP-1 cells promoted increased expression of HMGR. The authors suggest this to be an evolved ability to readily respond to bacterial infection by sensing the dysregulation of the mevalonate pathway, thus acting as a mechanism of immediate antimicrobial immunity. However, Kistowska et al. (2008) found dysregulation of mevalonate was characterised by an large increase in HMGR expression within the first hour of bacterial infection. Here, this clearly isn't the case; an initial down-regulation of HMGR was followed by >9-fold expression of HMGR by 24 h. Another explanation then for HMGR up-regulation in response to *P. acnes* could be active porphyrin damage of THP-1 cell plasma membrane. Studies show that *P. acnes* produces various porphyrins that actively assist pore formation in target cell plasma membrane; thus HMGR up-regulation is to synthesise extra cholesterol for cell membrane repair .

The same pattern of increasing expression for HMGR was echoed for LDLR, ABCA1 and SREBP-2. The cholesterol feedback regulation of LDLR and HMGR are mediated by the SCAP-SREBP2 pathway and are key regulatory elements for cholesterol homeostasis in human cells (Bauman et al. 2009; Wang et al. 2009). It is suggested that high serum cholesterol or high LDL has protective effects against infection (Ravnskov 2003). Indeed, during acute infections, cholesterol synthesis, measured as degree of <sup>3</sup>H-mevalonic acid incorporation into free cholesterol, increases, but the disappearance rate of cholesterol from plasma is also increased (Fiser et al. 1971) probably explained by the excessive expression of ABCA1 seen here. ABCA1 expression promotes cholesterol export from

cells to high-density lipoproteins and constitutes an important element of 'reverse cholesterol transport'. ABCA1 was the most highly expressed gene of the cholesterol genes (table 6.04). The large expression of ABCA1 would suggest the efflux of excess cholesterol from *P. acnes*-infected THP-1 cells. However, as the medium was not supplemented with LDL, it is difficult to interpret this result. The expression of ABCA1 is responsive to many cytokines and microbial stimuli (Schmitz & Langmann 2005). Interestingly, LPS-infected ABCA1<sup>-/-</sup> macrophages express enhanced levels of pro-inflammatory cytokines with increased activation of the NF-κB and MAPK pathways. In addition ABCA1<sup>-/-</sup> mice injected with LPS also resulted in a higher pro-inflammatory response in compared with wild type mice (Zhu et al. 2008). This would suggest that a down-regulated ABCA1 promotes a protective innate response by increasing pro-inflammatory cytokine expression. Interestingly this protective response was not at play here.

To our knowledge, this is the first evidence that shows regulation of genes that mediate cholesterol biosynthesis, trafficking and efflux in THP-1 cells exposed to *P. acnes*. Although the present study demonstrates expression of HMGR, SREBP2, LDLR and ABCA1 in *P. acnes*-infected THP-1, which invariably relates cholesterol synthesis, trafficking and efflux during infection, it tells us little about the potential cross-talk between inflammation and cholesterol mediation. For this it would be necessary to silence key inflammatory mediators, such as TLR2 in *P. acnes*-infected THP-1 in the presence of LDL cholesterol (Li et al. 2013). Moreover, these findings relate to mRNA levels only and therefore, any interpretation of cellular pathways can only be done superficially. By investigating *P. acnes* infection and how bacteria may influence cholesterol homeostasis, it may be possible to understand how infection may contribute to the development of foam cells through encouraging lipid-loading in macrophages cells within the atherosclerotic lesion.

#### 7.4 Conclusion

In this chapter of work it has been shown that *P. acnes* was capable of up-regulating THP-1 cell genes involved with cholesterol biosynthesis, trafficking and efflux, inflammation and apoptosis. As a commonly detected species within the atherosclerotic plaque samples examined here, *P. acnes* has the potential to induce several genes that are known to contribute to atherosclerosis. A major hallmark of atherosclerosis is the development of macrophage foam cells as a result of unregulated internalisation of modified and oxidised

LDL. *P. acnes*-induced upregulation of HMGR, SCAP and LDLR could increase intracellular cholesterol levels in monocyte/macrophages through *de novo* synthesis and receptor mediated uptake. This is important because any additional lipid to an already unregulated process of cholesterol uptake could actively contribute to atherosclerotic plaque mass. Genes involved in leukocyte recruitment were also upregulated in response to *P. acnes*. In addition to cholesterol mediation, *P. acnes* was also capable of upregulating cytokine and chemotactic genes. Typically, cytokines and chemokines are regulated by macrophages in response to bacterial stimuli and inflammation. Here we demonstrate that *P. acnes* is capable of inducing expression of monocytes genes that have potential to increase inflammatory milieu that could have a negative effect within an atherosclerotic lesion. However, due to the design of this study it is not possible to suggest that this profile of THP-1 cell gene expression would not be observed if a different species of bacteria was used.

# **GENERAL DISCUSSION**

*The prime objective of this thesis was to begin to uncover the role that infection plays on the development of atherosclerosis through the identification of bacteria species present within CAP tissue. The evidence discussed within this thesis provides novel insight into a unique collection of bacterial 16S rDNA and viable bacteria species residing in CAP tissue. In addition, this thesis also provides potential novel data for the expression of genes affecting inflammation, cholesterol homeostasis and apoptosis, both in tissue and in THP-1 monocyte cells following challenge with commonly encountered plaque-dwelling isolate P. acnes. This chapter brings together those findings to discuss the potential source of the bacterial signatures observed in CAP tissue and attempts to present a role for bacteria within the pathogenesis of atherosclerosis.*

## 8.1 Bacteria present in atherosclerotic plaque tissue

### 8.1.1 Periodontopathic bacteria

The theory that bacteria may be present in atherosclerotic plaque tissue is established with the findings presented within this thesis. While the focus of this thesis has been a to screen for the presence of any latent bacteria present within atherosclerotic plaque tissue a particular emphasis has been placed on the detection of the periodontopathic species of the red complex. Both *P. gingivalis* and *T. forsythia* DNA was readily detected in the CAP samples examined. This is in stark contrast to, *T. denticola*, which was the only RCB not detected. This comes as no surprise, although *T. denticola* DNA has been identified in aortic and coronary plaque tissue, often detection rates are either poor or detection relates to just one case study (Okuda et al. 2001; Ishihara et al. 2004; Mahendra et al. 2010; Mahendra & Mahendra 2013). This observation is difficult to explain and the only stand out feature that differentiates *T. denticola* from its complex counterparts is its large size and anatomical structure. Compared to the much smaller coccobacillus *P. gingivalis* or the pleomorphic *T. forsythia* that both readily disseminate the blood of infected patients, the physical size of *T. denticola* may hinder its systemic dissemination. However, given its previous detection in some vessels but not others suggests its size cannot be the sole factor in its lack of detection. *T. denticola* is also the only motile species of the RCB, consequently then it has more control over its direction and can therefore control its fate to an extent. These features likely directly and indirectly affect the dissemination of *T. denticola* into the bloodstream and its transport from periodontium to vessel. Another possible explanation may be the heterogeneity of bacterial species present in the periodontal pockets and subgingival plaque of patients with periodontitis. An additional examination of patients periodontal status or an assessment of the microbiota present in the periodontal tissues of the patients who donated their plaque may have provided further information for the discrepancy between the prevalence of some but not all RCB in atheromatous tissue.

To the best of our knowledge, twelve previous studies have attempted to detect periodontopathic bacteria in carotid artery plaque samples (Haraszthy & Zambon 2000; Cairo et al. 2004; Fiehn & Larsen 2005; Ford et al. 2006; Padilla et al. 2006; Aimetti et al. 2007; Romano et al. 2007; Aquino et al. 2011; Armingohar et al. 2014; Figuero & Lindahl 2014; S. Morita et al. 2014; Rangé et al. 2014). Of these, eight studies managed to detect periodontopathic bacteria in carotid samples (Haraszthy & Zambon 2000; Fiehn & Larsen

2005; Ford et al. 2006; Padilla et al. 2006; Armingohar et al. 2014; Figuero & Lindahl 2014), but the remaining four did not (Cairo et al. 2004; Aimetti et al. 2007; Romano et al. 2007; Aquino et al. 2011), thus highlighting the lack of consistency in study findings to date. The fact, the majority of these studies used the sensitive method of PCR for the detection of bacterial 16S rDNA suggests the inconsistencies may be partly due to the different DNA extraction methods used. In the present thesis tissue was ground to a fine powder in the presence of liquid nitrogen, which ensured homogeneity followed by treatment with a series of enzymes that permitted lysis of both Gram-negative and the more hardy Gram-positive bacteria; this we feel provided an optimum extraction of DNA from any bacteria present.

In the present investigation, 0.5 µg extracted DNA was used as template for PCR, which would normally be considered too high and would normally inhibit the reaction due to an over-presence of amplifiable target DNA that would exhaust reagents early in the reaction. However, it was predicted that actual amplifiable target bacterial DNA would be considerably less than the genomic component, hence it was unlikely the actual amplifiable bacterial template was excessive. Interestingly, the four studies that failed to detect periodontopathic bacteria, two failed to monitor the PCR template amount used for PCR (Cairo et al. 2004; Aquino et al. 2011). Of the eight studies that detected periodontopathic bacterial DNA in carotid plaque tissue only had success using nested PCR (Fiehn & Larsen 2005; Figuero et al. 2011), which suggests that the presence of very low copy number bacterial DNA. Remarkably, an actual quantitative assessment of periodontal bacteria copy number has never been conducted in carotid atherosclerosis. The best estimate comes from a qPCR assessment of periodontopathic DNA present in the carotid artery, which demonstrated that periodontopathic bacterial DNA represented 47.3% of the total bacterial DNA found in atheromatous samples from patients with periodontitis and 7.2% of the total bacterial DNA detected in atheromas from periodontally healthy subjects (Gaetti-Jardim 2009). Therefore it is clear that patients with periodontal disease has much greater incidence of periodontopathic bacteria in their athero-prone vessels. Nevertheless, while it could not be elucidated in the present thesis whether the DNA extraction method is responsible for the discrepancies in detection of periodontopathic bacteria in carotid artery plaque samples; both the aforementioned literature and the present thesis highlight the necessity for careful DNA extraction when investigating the presence of these species using PCR. Maybe a universal method for bacterial DNA extraction would be useful.

### 8.1.2 *Streptococcus* spp.

In addition to periodontopathic bacteria, DNA from other oral bacteria were detected, specifically *Streptococcus* spp., which gives further credence to the hypothesis that bacteria from the oral cavity are present in the atherosclerotic plaque tissue of the carotid artery. Within the scope of this investigation it was not possible to absolutely differentiate SMG bacteria to a species level or rather it was not possible to differentiate between *S. mitis* and *S. sanguinis*. These two species were the most closely related sequences identified in BLAST reference searches both showing maximum identity of 100%. To the best of our knowledge this is the first ever detection of *S. mitis* in carotid atherosclerotic plaque tissue, which seems surprising given its abundant colonisation with the oral cavity. While, *Streptococcus* spp. are not highly pathogenic relative to RCB, they are involved in dental decay to varying degrees and can in certain situations cause aggressive periodontitis (AG) with streptococcal gingivitis in certain immune susceptible individuals; thus demonstrating this genera's potential to induce a similar pathology in periodontal tissue (Kara et al. 2007). However, AG caused by streptococcal species is rare; it seems far more plausible that if periodontal tissues are compromised due to periodontopathic species infection, the close interaction between RCB and other species in dental biofilms would provide opportunities for *Streptococcus* spp. to gain entry to the bloodstream. As the initial colonisers of the tooth surface for biofilm formation, both *P. gingivalis* and *T. forsythia* require *Streptococcus* spp. for aggregation/colonisation and so have a particularly close relationship during subgingival biofilm formation (Daep et al. 2008; Shimotahira et al. 2013).

The findings presented here demonstrate a viable presence of *Streptococcus* spp., possibly *S. mitis* and *S. sanguinis* in the CAP specimens examined. These findings are particularly interesting as it demonstrates the physical survival of oral bacteria both throughout their systemic translocation and extended survival within the atherosclerotic plaque itself. This has particularly greater negative health implications in that both these species are early colonisers of the tooth surface active in biofilm formation. If *Streptococcus* spp. were able to thrive in atherosclerotic plaque tissue, then, by replicating, could possibly adhere to plaque surfaces and initiate biofilm formation in the atheroma. In answering the question of whether the isolated strains of *Streptococcus* spp. can adhere to the plaque surfaces one may conduct an *in situ* hybridisation or IHC assessment of *Streptococcus* spp. localisation

and measure adhesin protein activation, such as fibronectin binding protein 1 (Nobbs et al. 2009; Yamaguchi et al. 2013).

### 8.1.3 *Propionibacterium acnes*.

*P. acnes* was the most encountered species both in terms of 16S rDNA direct in tissue (33% species specific and 32% cloned sequences) and in the 100 viable isolated colonies 91% were *P. acnes*. The *P. acnes* detected in the CAP samples were closely related to the NCBI reference strains SK137, which based on previous antibody testing and phylogenetic evaluation of the *recA* gene and hemolysin/cytotoxin gene (*tly*), belongs to the lineage type IA (McDowell et al. 2005). This particular lineage of *P. acnes* falls into the subgroup most frequently isolated from dental infections, acne lesions and failed prosthetic implants (McDowell et al. 2005). The patients who donated their plaque tissue for this study had a mean age of  $69.9 \pm 8.69$  years, so the possibility that any of them were suffering with *acne vulgaris* was negligible. Thus, it is far more likely that prosthetic implants or periodontal bacteraemia were the likely source of *P. acnes* infection. It could be proposed that given the presence of strictly oral bacteria in the plaque samples examined here, the likelihood that *P. acnes* was originated from the same source is strong, though this cannot be said for certain. To begin to answer this question of the origin of the *P. acnes* isolates, one could acquire a more detailed medical history of patients who donated their tissue for this study, e.g. previous implant surgery. Furthermore, a more extensive screen for 16S rDNA signatures by incorporating the analysis of other bodily sites frequented by *P. acnes*, such as dental sites, intestines and skin sites may narrow down the potential origin.

Nevertheless, *P. acnes* has been shown here to be a capable opportunistic pathogen, in light of its detection in a viable state. *P. acnes* has previously been discounted as a contaminant on account of its role as a commensal. However, genetic elements specific to each lineage of *P. acnes* have been established, which highlight the differences of *P. acnes* in functioning as a commensal of the skin and as a pathogen in the aetiology of diseases (Tomida et al. 2013). Also an early coloniser of the tooth surface, *P. acnes* carries the same potential aptitude for dental biofilm formation by providing a receptor bridge between *Streptococcus gordonii* (first coloniser) and the periodontopathogen *Fusobacterium nucleatum* (Kolenbrander et al. 2010). The formation of biofilms in atherosclerotic plaque tissue is potentially very hazardous. For example, a phenomenon known as “biofilm dispersion” could have devastating consequences if occurring with vulnerable plaque. Biofilm dispersion is the release of live bacteria from the biofilm as physiologically

regulated response to internal or external stimulus (Kaplan 2010). The induction of a biofilm dispersion response within an atheroma may, therefore, have the potential to induce collateral tissue damage resulting from the localized release of degradative enzymes by the participating bacteria (Lanter et al. 2014). This response, in turn, could influence the integrity of the surrounding arterial tissues, leading to an enhanced risk of plaque rupture and thrombogenesis. Recently it has been demonstrated that *P. acnes* does form as a biofilm in carotid atherosclerotic plaque (Lanter et al. 2014). In addition, *P. acnes* isolated from the carotid artery has the ability to form biofilms *in vitro*, which dispersed when treated with physiologically relevant levels of norepinephrine, a stress hormone responsible for the fight-or-flight response (Lanter & Davies 2015). Given the abilities of *P. acnes* to act as an opportunistic pathogen and its overwhelmingly high presence in a viable state within the atherosclerotic plaques samples examined here, it felt like the necessary bacterium to investigate further.

#### 8.1.4 *Lactobacillus* spp.

*Lactobacillus* spp. DNA was also detected, which not only gives weight to the argument that oral bacteria can infect the atherosclerotic artery but also raises the question, “is it only putative periodontopathic strains of bacteria that play a potential negative role in atherogenesis?” Certain clues come from how *Lactobacilli* operates in the oral cavity where it has an predominantly protective, antimicrobial effect on *P. gingivalis*, *T. forsythia* and certain cariogenic species by limiting the secretion of pro-inflammatory cytokine/chemokines IL-1 $\beta$ , IL-6 and IL-8 by gingival cells (Zhao et al. 2012; Baca-Castañón et al. 2015). However, this anti-inflammatory role is confused somewhat when considering how it operates in the vessel as *L. casei* cell wall components have been shown to accelerate atherosclerosis in hypercholesterolemic mice models, suggesting this particular microbe may operate in a different way within distinct bodily niches (Chen et al. 2012). It is therefore difficult to interpret the extent to which *Lactobacilli* species may impact atherosclerosis in humans.

#### 8.1.5 *Mycobacterium tuberculosis*

In addition to oral species, species from other bodily niches were detected. Two pulmonary infective species were identified, namely *Mycobacterium tuberculosis* (H37Rv) and *Klebsiella pneumoniae* (sub sp. KP5-1). The findings presented in this thesis provide the first evidence for the presence of *M. tuberculosis* DNA in CAP tissue. While the general

experimental design for this and other detection based investigations is the use of a broad range primer set for a wide scale screen of bacterial DNA, previous investigators have specifically targeted *M. tuberculosis*, with no success (Farsak, Yildirim, Akyön, Pinar, Öç, et al. 2000; Rota et al. 2005). There are significant findings for the possible involvement of *M. tuberculosis* in the pathogenesis of atherosclerosis such as high levels of antibodies to mycobacterial heat shock protein 65 (Rota & Rota 2005). Also, a large cohort was studied to estimate the risk of ischemic stroke during a 3-year follow-up period after a tuberculosis diagnosis (Sheu et al. 2010). The authors concluded that patients with a tuberculosis diagnosis are at 1.52-times increased risk for ischemic stroke but not hemorrhagic stroke in the next 3 years. As the relationship was cerebral in nature, suggesting the link may be between carotid atherosclerosis and *M. tuberculosis*. This warrants further investigation to elucidate the atherogenic potential of *M. tuberculosis*.

## 8.2 Potential routes of translocation to the Carotid artery

### 8.2.1 Oral bacteraemia

Successful identification of *P. gingivalis* and *T. forsythia* in CAP tissue demonstrates a relationship between infective agents of periodontal disease and vascular sites affected by atherosclerosis. As previously discussed in the main introduction of this thesis oral cavity is densely colonised by bacteria, which, can enter the bloodstream via transient bacteraemias, following routine daily activities such as mastication, teeth brushing and dental treatment (Forner et al. 2006). However, when chronic periodontal disease is evident, the tissue of the periodontium is compromised providing increased opportunity for systemic challenge of periodontal or oral species that cause secondary infections at sites distant from the oral cavity (Kozarov & Grbic 2012). This is one possibility for the mechanism of systemic entry of *P. gingivalis*, *T. forsythia*, *S. mitis* and *S. sanguinis*. It is possible this route accounts for *P. acnes* and *Lactobacillus* spp, also, although this cannot be said for certain for reasons already discussed. Table 8.01 represent the hypothetical mechanism of bacterial systemic dissemination from source tissue and their translocation to distant vascular sites where they induce vascular inflammation and contribute to atherosclerosis.

### 8.2.2 Macrophage internalisation and translocation

Bacteria may also be transported to vascular sites by macrophages following phagocytosis of pathogens at sites distant from the vessel wall, then, by responding to inflammatory

signals created by injured endothelial cells, the macrophages inadvertently transport the bacterial cargo to the artery wall (figure 8.01). Subsequently, when the macrophage later becomes necrotic from excess lipid loading, releases the bacteria into the artery wall. Interestingly, *P. acnes*, can survive intracellularly for up to 2 weeks in macrophages *in vitro*, thus, this mechanism of transport may be reflective of how *P. acnes* infected the plaques examined here (Fischer et al. 2013).

### 8.2.3 Leaky gut and intestinal bacteraemia

Secretory IgA in the gut can bind to the mucus layer on top of the epithelial cells to form a barrier capable of neutralizing threats before they reach the cell and preventing the passage of bacteria (Mantis et al. 2011). Some species of bacteria *Streptococcus pneumoniae* release protease that degrades IgA and breakdown the normally tight cell-cell junctions between the epithelial cells of the gut providing entry to the submucosa (Proctor & Manning 1990) (figure 8.01). Bacteria can then become systemic through accessing damaged capillaries created by tares in the gut or chronic diseases such as Crohn's disease.

## 8.3 THP-1 gene expression

### 8.3.1 Expression of cholesterol homeostatic gene in *P. acnes*-infected THP-1 cells

#### 8.3.1.1 SREBP2

In the current study SREBP2 mRNA expression in THP-1 cells challenged with *P. acnes* showed significant up-regulation following 24 hours infection compared to PBS-treated control cell expression at the same time point. Evidenced by our understanding of the role of SREBP2, such a significant increase in SREBP2 expression suggests a cell condition with diminishing cytosolic cholesterol levels. To the best of our knowledge this is the first observation of *P. acnes*-induced SREBP2 expression in THP-1 cells, thus such a marked increase in SREBP2 in monocytes challenged with *P. acnes* is difficult to interpret. *P. acnes* is considered to play a etiological role in the pathogenesis of acne vulgaris where it has been proposed to directly influence lipogenesis in the sebaceous gland. It may be possible then to take certain clues from our understanding of *P. acnes* etiological role in disease and the increasing *in vitro* evidence in that field.

In a similar *in vitro* investigation, *P. acnes* infection was found to augment the formation of intracellular lipid droplets in sebocytes (Iinuma et al. 2009). Furthermore, *P. acnes*-infected sebocytes showed significant up-regulated diacylglycerol acyltransferase

(DGAT), the rate-limiting enzyme for triglyceride synthesis, which was found to physically increase the intracellular levels of triglyceride in both undifferentiated and differentiated sebocytes (Iinuma et al. 2009).

Similarly, culture supernatant of *P. acnes* has been shown to induced SREBP-1 expression in sebocytes and system of activation that is dependent on protease-activated receptor-2 (Lee et al. 2015). While direct comparisons cannot be made between the aforementioned studies finding and those presented here; these studies are important in confirming that *P. acnes* can directly influence a lipid pathway, which has certain parallels with findings presented here. Ultimately, the lipid loading effect of *P. acnes* in sebocytes encompasses an isoform of the same gene (SREBP1) shown here to be highly expressed in monocytes (SREBP2). In addition, the up-regulation of DGAT for the *de novo* synthesis of triglyceride in *P. acnes*-infected sebocytes observed by Iinuma et al. (2009) is equivalent to the rate limiting step in the mevalonate pathway, HMGR, shown here to be significantly up-regulated in THP-1 cells. As the master gene for transcription of numerous cholesterol homeostatic genes, *P. acnes*-induced dysregulation of SREBP2 of SREBP2 could have negative implications, although without protein expression data, any interpretation of these findings should be approached with caution. Nevertheless, the findings presented here indicate that *P. acnes* may be involved in up-regulating SREBP2 which warrants further investigation

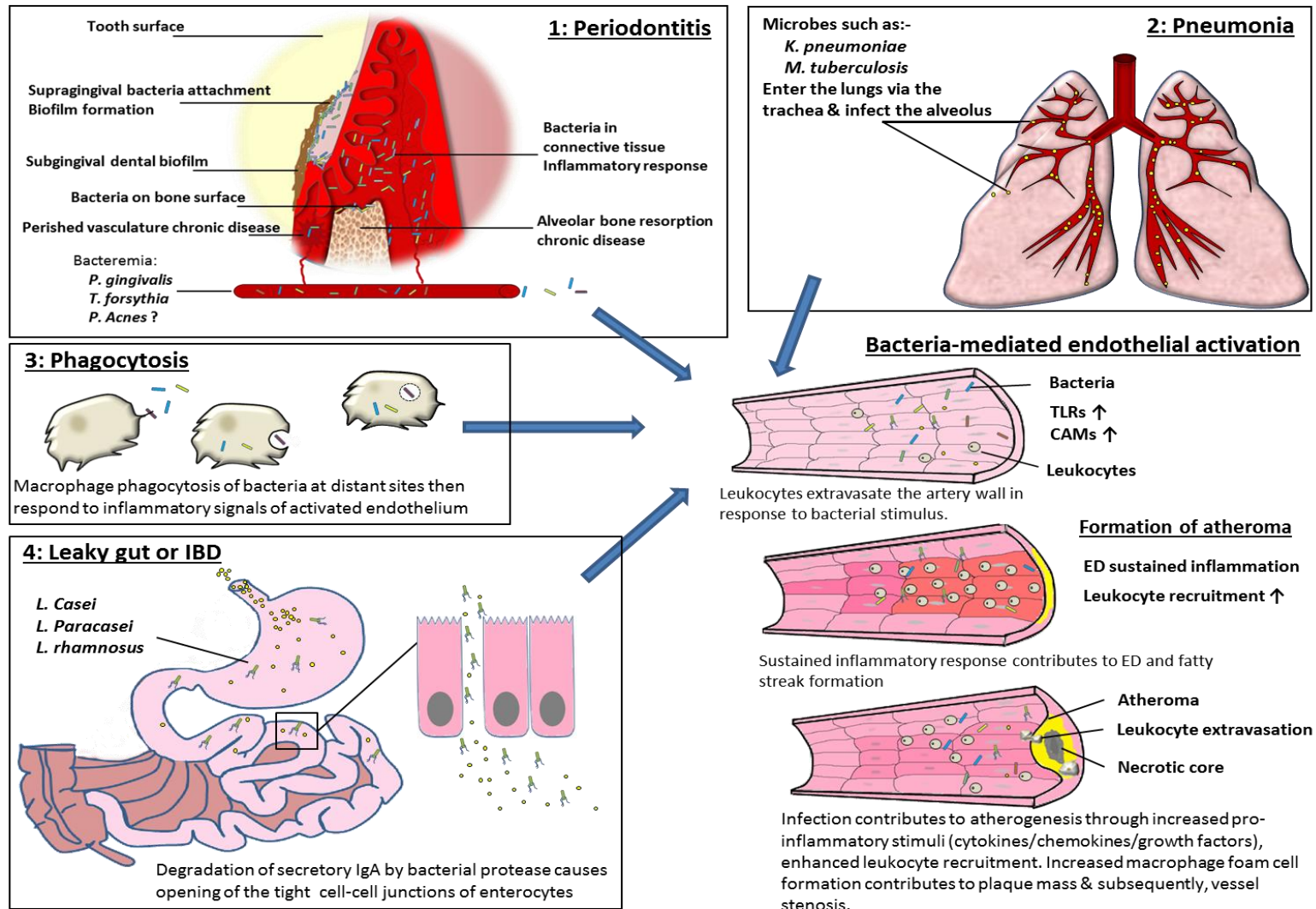


**Figure 8.01:** Flow schematic of the hypothetical mechanisms that may give rise to transient bacteraemia of the species detected in CAP samples studied in the present investigation. The tissue at the primary infection site (e.g. periodontal (1), pulmonary (2) or intestinal (4)) is subject to inflammation & tissue damage that gives rise to transient bacteraemia. Bacteria translocate to the vascular tissue where a secondary infection ensues. Macrophages phagocytose commensal and pathogenic bacteria at each of the primary infection sites and within the blood, which survive intercellularly (3). When macrophages are activated in response to vascular injury, they respond, carrying the internalised bacteria that are subsequently released when the macrophage becomes necrotic due to foam cell development in the intimal layer of atherosclerotic vessels.

### 8.3.1.2 HMGR

The significant up-regulation of HMGR in *P. acnes*-infected THP-1 cells compared to a PBS vehicle control cells is, to the best of our understanding, not been previously observed. Because HMGR is a transcript of SREBP2, the up-regulation of HMGR expression also gives further validity to the expression of SREBP. The expression of HMGR in *P. acnes*-challenged monocytes suggests that *P. acnes* may influence *de novo* cholesterol synthesis in monocyte, which could have negative atherogenic implications, particularly in terms of foam cell development. For example, if *P. acnes* influences of monocyte/macrophage HMGR expression within the atherosclerotic lesion, this could essentially contribute to intracellular net cholesterol content via lipid loading, thus it may be that *P. acnes* actively contributes to foam cell formation. To try and elucidate if this is actually the case, it may be informative to conduct future investigation of monocyte challenge with *P. acnes* by measuring physical intracellular cholesterol levels via oil red O staining.

### 8.3.1.3 LDLR

Another SREBP2 transcript that was significantly expressed in monocytes following challenge with *P. acnes* was LDLR up-regulation. Again, this is a novel observation that has not, to the best of our understanding; been previously observed. The expression of LDLR suggests a cellular signalling in response to depleted cholesterol levels via the SREBP2 pathway for uptake of native LDL. Apart from the substitution of *P. acnes* for PBS, control cells were treated in an identical manner to *P. acnes* challenged cells, which suggests the up-regulated response of LDLR in *P. acnes*-challenged cells is due to the presence of *P. acnes*. It is therefore plausible to suggest that the presence of *P. acnes* in the atherosclerotic plaque may have a negative effect on monocytes/macrophages by exacerbating lipoprotein uptake in that may contribute to excess net cholesterol content and foam cell formation. It is therefore possible that *P. acnes* responsible for inducing lipid loading in these cells a process highly associated with atherosclerotic disease.

### 8.3.1.4 ABCA1

Finally, ABCA1 was the greatest expressed gene of the cholesterol mediating genes studied here, which showed a >120-fold increase in mRNA levels for *P. acnes*-infected THP-1 cells compared to PBS vehicle control cell expression of ABCA1. This significant up-regulation of ABCA1 indicates that THP-1 cells have excess cholesterol levels and presence of intracellular oxysterols that stimulated LXR/RXR transcription of ABCA1 for

cholesterol efflux. However, it cannot be the case that excess cholesterol is present within the THP-1 cells cultured here, based on the absence of LDL in culture medium used. The up-regulation of ABCA1 conflicts with cell behaviour regarding the earlier observed expression of SREBP2 transcript up-regulation of HMGCR, LDLR and SREBP2 itself, which all suggest a cellular condition of diminished cholesterol level, whereas ABCA1 up-regulation would suggest active efflux of excessive intracellular cholesterol.

These results would suggest that either genes concerned with uptake or *de novo* synthesis of cholesterol are dysregulated or *ABCA1*, which should be down-regulated by SREBP2 is overactive in response to *P. acnes*. ABCA1 has been demonstrated to have a supplementary, more antimicrobial role, in which it participates in the removal of the immune-stimulatory bacterial lipid, LPS (Thompson et al. 2010). While this process for monocytes requires an exogenous lipoprotein acceptor it may, in part, begin to explain the mechanism and reason for ABCA1 activation in response to bacterial infection. In addition, ABCA1 can be up-regulated by pro-inflammatory cytokines, such as, TNF- $\alpha$  (Gerbod-Giannone et al. 2006). It must be noted though, that *ABCA1* protein is highly regulated in the transcriptional and post-translation stage at numerous stages, thus, ABCA1 mRNA levels are a poor indicator of protein (Iwamoto et al. 2010; Yokoyama et al. 2012). Hence, it is difficult to decipher the actual cellular status without first understanding the relative amounts of protein activation for each of these cholesterol homeostatic gene expressions. Nevertheless, this is a very interesting observation and one that warrants further investigation.

#### 8.3.1.5 THP-1 response to *P. acnes*: further work

The evidence obtained in this thesis points to SREBP2 as a potential dysregulated mediator of cholesterol levels in the monocytic cell line THP-1. This paradigm suggests that when an infective agent is present, SREBP2 expression is increased as a response. As a major transcriber of cholesterologenic genes, SREBP2 may unnecessarily increase intracellular net cholesterol levels that may eventually play a part in the development of foam cell formation in affected cells. Thus, the main hypothesis arising from the present thesis is that bacterial infection potentially plays a role in atherogenesis via this mechanism.

Typically overexpression of this transcription factor in THP-1 cells would lead to the transcription of other cholesterologenic genes that were measured here, such as LDLR and

HMGR, but also should attenuate the expression of cholesterol efflux genes such as ABCA1. While the elevated levels of SREBP2 mRNA and the subsequent expression of SREBP2 transcripts in THP-1 cells would suggest a response to the infective agent, *P. acnes*, this cannot be said for certain with just a raise in mRNA levels. Could enhanced expression of SREBP2 be responsible for transcription of LDLR and HMGR observed in THP-1 cells in response to *P. acnes*? To begin to address this question Western blotting could be employed to compare the relative amounts of SREBP2 protein between *P. acnes*-infected and PBS vehicle treated THP-1. The same experiment could be performed to measure the relative protein levels of LDLR and HMGR. Although this would indicate the relative abundance of this transcription factor and the other transcripts of SREBP2 within *P. acnes*-infected cells, it would not however prove that an increase in LDLR and HMGR transcription is a consequence of SREBP2 activity or that the activity of SREBP2 was caused by *P. acnes*. A gel-mobility shift assay could in theory demonstrate binding of SREBP2 to the sterol regulatory element (SRE) sequences in the control regions of the genes that encode LDLR and HMGR. Briefly, nuclear protein would be purified from *P. acnes*-infected THP-1 and combined with nuclear extracts from the same challenged cells and from PBS vehicle control cells. Each mixture would be incubated with biotin-labelled cDNA constructs coding for the SRE sequences in the promoter regions of LDLR and HMGR. The protein-cDNA extract could then be separated on a polyacrylamide gel, which would hopefully identify SREBP2 bound to the SRE site of LDLR and/or HMGR.

The gel-mobility shift assay could be done in conjunction with a SREBP2 translocation assay in which *P. acnes*-infected THP-1 cells would be stained with a specific SREBP2 primary antibody to track SREBP2 localisation from ER to the Golgi apparatus using a confocal microscope. A positive control reaction would include cells treated with a cholesterol trafficking inhibitor (U18666A), which would restrict cholesterol egress from the cells, thereby activating SREBP2 translocation into the nuclei that could be used as a reference (Cenedella 2009). *P. acnes*-infected cells would be compared to both the positive and PBS vehicle control cells to determine the effect of *P. acnes* on cholesterologenic gene expression and protein activation.

### 8.3.2 Expression of cytokines/chemokines in *P. acnes*-infected THP-1 cells

#### 8.3.2.1 CCL3 (MIP-1 $\alpha$ )

Of all the cytokines tested CCL3 is the only cytokine that indicates bacterial infection and as expected very large fold increase in CCL3 expression was observed in *P. acnes*-infected THP-1 cells compared to the expression observed in cells treated with vehicle control. To the best of our knowledge, this is the first evidence that demonstrates CCL3 up-regulation in *P. acnes*-infected monocytes. This has particular negative implications inside the setting of an atherosclerotic artery. For example, CCL3 can induce chemotaxis of different leukocyte subsets, including monocytes/macrophages and T-lymphocytes via CC chemokine receptor (CCR)1, CCR4, or CCR5 (Lee et al. 2000). Furthermore, it was shown that CCL3 is a mediator of firm adherence and (subsequent) transmigration of neutrophils, as a result of lipid mediator production, which, in turn, directly activate neutrophils (Reichel et al. 2012). Hence, CCL3 is critical in the recruitment and transmigration process during vascular inflammations. Most importantly, CCL3 deficiency inhibits atherosclerotic plaque formation in LDLR knockout mouse model by reducing leukocytes and neutrophil chemotaxis (de Jager et al. 2013b). Therefore, the findings presented here show that *P. acnes* is capable of inducing particularly high levels of CCL3 mRNA, which if present in the atherosclerotic vessel may actively contribute to lesion development via recruitment and transmigration of different subsets of leukocytes, neutrophils and T cells. Interestingly, CCL3 was also significantly upregulated in the CAP samples examined for this thesis, which provides further evidence for the potential involvement of CCL3 in the atherosclerotic process that may also be associated with bacterial infection.

#### 8.3.2.2 CCL2 (MCP-1)

CCL2 is another potent chemoattractant that was shown here to be induced in THP-1 cells in response to *P. acnes* exposure compared to control cell expression following PBS treatment. Although CCL2 was not significantly up-regulated in THP-1 cells-infected with *P. acnes*, a >5-fold increase was observed in comparison to PBS control treated cells. Expression of CCL2 was significantly up-regulated in plaque tissue and in LPS-infected THP-1. The only obvious observation was that the standard deviation of CCL2 expression in *P. acnes* exposed cells was high due to one sample down-regulated outlier and therefore, considering the relatively low regulation, the statistical significance of the result was

drastically reduced. CCL3 is well recognised as a chemoattractant and plays a significant role in recruitment and transmigration of leukocytes into the artery wall of atherosclerotic vessels (Kusano et al. 2004; Yu et al. 2004). Any additional increase in leukocyte recruitment or transmigration would have potential atherogenic consequences (Packard et al. 2009).

### 8.3.2.3 ICAM-1

To the best of our knowledge, the data presented in this thesis demonstrate the first up-regulated response of THP-1 ICAM-1 in response to *P. acnes* infection. Expression of ICAM-1 in *P. acnes*-infected THP-1 was greater than LPS-induced ICAM-1. Expression occurred steadily over the 24 h time course with the greatest and only significant change occurring at 24h. As the key cellular adhesion molecule ICAM-1 plays a central role in regulating the recruitment and trans-endothelial migration of leukocytes into the vessel wall and has been associated with the development of atherosclerotic plaque (DeGraba et al. 1998; Jones et al. 1998). While, ICAM-1 was also up-regulated in the CAP tissue examined for this thesis, the level of mRNA were markedly less than the levels observed in response to *P. acnes* but similar to those seen in response to *E. coli* LPS. Monocyte ICAM-1 is analogous to ICAM-1 present on the surface of endothelium cells; both are activated during tissue stress/injury and function by forming a strong ligand interaction to bring the monocyte to a stop after rolling along the surface of the endothelium. As *P. acnes* infected cells showed the greatest up-regulation of ICAM-1 compared to *E. coli* LPS and in CAP tissue directly, it could be suggested that *P. acnes* could aggravate plaque formation by inducing leukocyte recruitment, thereby advancing plaque formation. To provide additional assurance that leukocyte recruitment was elevated in response to *P. acnes*, it would be necessary to measure protein levels reflect the mRNA profile observed here.

### 8.3.2.4 TNF $\alpha$

TNF- $\alpha$  was significantly up-regulated in THP-1 cells in response to *P. acnes* infection compared to cells treated with a PBS vehicle control. This reaction was replicated in *E. coli* LPS-infected THP-1 cell, though a significant regulation of TNF- $\alpha$  was not observed in the atherosclerotic plaque samples examined for this project. Although it is not good practice to compare single sample gene expression data, it was observed that every single plaque sample that was previously observed to contain 16S rDNA signatures of *P. acnes*

was either down-regulated or un-regulated, which could suggest that the load of *P. acnes* must have been extremely low copy number levels. The lack of TNF- $\alpha$  expression in the atherosclerotic plaque samples examined here is quite unusual given that this cytokine plays a considerable role in atherogenesis.

#### 8.3.2.5 IL-1 $\beta$

IL-1 $\beta$  was highly expressed in THP-1 cells in response to *P. acnes* compared to PBS treated control cells. Also, a similar level of mRNA expression was observed in THP-1 that were exposed to *E. coli* LPS compared to control cells. Like TNF- $\alpha$ , IL-1 $\beta$  was not significantly expressed directly in atherosclerotic plaque compared to LITA tissue. IL-1 $\beta$  was expressed within 1.5 hours in LPS infected cells, which suggests cytokine gene expression of is extremely rapid, particularly for IL-1 $\beta$ . Also cytokine expression occurs in waves which may account for observation of IL-1 $\beta$  in vitro but not in tissue (Schaue et al. 2012). One of the major pathways that mediates the production of IL-1 $\beta$  is via the NLRP3 inflammasome, in which pro-IL-1 $\beta$  is cleaved by caspase-1 to produce mature IL-1 $\beta$ . Interestingly *P. acnes* has been shown to trigger NLRP3 for the increased IL-1 $\beta$  productions, which indicates intracellular activation/stimulus (Sahdo et al. 2013; Kistowska et al. 2014; Qin et al. 2014; Thiboutot 2014).

Both TNF $\alpha$  and IL-1 $\beta$  have been shown to induce the expression of the cholesterologenic genes such as SREBP2-SCAP (Ruan et al. 2001). As mRNA from both cytokines were elevated significantly in the *P. acnes*-infected THP-1 cells compared to PBS vehicle control cells, it may be that the pro-inflammatory cytokine up-regulation influenced SREBP2 expressed in these cells. To determine whether this is a possibility, one could perform an RNA interference assay to attenuate the expression levels of pro-inflammatory cytokines. Briefly, if *P. acnes*-infected THP-1 was transfected with small interfering (si)RNA oligonucleotide probes for the silencing of MyD88; a universal adapter protein used by almost all TLRs in the protein cascade to activate NF- $\kappa$ B transcription of IL-1 $\beta$  and TNF- $\alpha$ . If SREBP2-SCAP mRNA and protein levels were significantly reduced in the MyD88-silenced THP-1 cells but levels remained elevated in non-silenced cells, it could be suggested that the pro-inflammatory pathway may be influencing the expression of SREBP2.

### 8.3.2.6 B-cell lymphoma 2 protein A1 (BCL2A1)

BCL2A1 was by far the most potently expressed of all genes tested in the present study, with a 560-fold increase of BCL2A1 mRNA observed in *P. acnes*-infected THP-1 compared to PBS vehicle control cells expression. BCL2A1 was also up-regulated in response to LPS, although expression was markedly less in LPS exposed cells than that observed for *P. acnes*. While there is a strong possibility that BCL2A1 expression in *P. acnes* challenged cells is actually the result of bacterial stimulus, there are a number of other possible stimuli in the atherosclerotic plaque tissue that may have led to a rise in expression. BCL2A1 is activated as a pathway to cell survival by reducing the release of pro-apoptotic cytochrome c from mitochondria and thereby blocks caspase activation (Vogler 2012). A primary source of BCL2A1 expression in atherosclerotic plaque is as a cell survival strategy in lipid-loaded macrophages that switch to a protective anti-apoptotic profile of gene expression (Martinet et al. 2002; Kutuk & Basaga 2006). The very large increase in BCL2A1 mRNA expression observed in the current investigation suggests that anti-apoptotic genes are up-regulated in monocytic cells in response to infection, more specifically, *P. acnes*. Given that BCL2A1 plays a role in foam cell survival, expression of BCL2A1 in response to bacterial infection could have serious implications for atherosclerotic plaque progression.

### 8.4 Conclusion

Data in this thesis provides evidence demonstrating the identification and isolation of several different species of bacteria in atherosclerotic plaque tissue from the human carotid artery. The bacterial species identified are representative of various bodily niches such as the gut and skin, but most predominant of which, the oral cavity and periodontal tissue. Two out of the three RCB species specifically targeted, i.e. *P. gingivalis* and *T. forsythia* were present in the CAP samples, though not as viable isolates. The identification of periodontopathic species in carotid atherosclerotic plaque tissue indicates that bacterial infection associated with the chronic breakdown of periodontal soft and hard tissue may possibly be related to further secondary complications in carotid artery tissue which drive atherogenesis. Here we showed this may also be the case the most predominant species of bacteria present in the CAP samples examined here, *P. acnes*; a strain most isolated from diseased tissue, including periodontal disease. The data presented in this thesis provides evidence demonstrating that *P. acnes* infection can mediate the up-regulation of genes that

control *de novo* synthesis and uptake of extracellular cholesterol, leukocyte cell adhesion, inflammation and apoptosis. In almost every case gene expression was analogous between plaque tissue, and THP-1 cells infected with *E. coli* LPS and *P. acnes*, which would suggest that the genes examined here play an atherogenic role. The cholesterol homeostatic and anti-apoptotic gene expression in *P. acnes*-infected cells, which provide particularly novel findings that indicate *P. acnes* may affect foam cell development, a major hallmark of atherosclerotic disease. Overall these observations indicate a possible cholesterol mediating role of bacteria that inhabit the atherosclerotic lesion that may be driven by a perpetual inflammatory response in the CAP lesion. The bacteria species that drive this response originate from the microflora of numerous bodily site, of which the periodontal tissue is a major contributor; disseminating into the bloodstream to cause secondary infections within the atherosclerotic plaque.

## 9.0 References

- Aas J., Paster B. & Stokes L., (2005). Defining the normal bacterial flora of the oral cavity. *J Clin Periodont*, 43(11), pp.5721–32.
- Abaibou H., Chen Z., Olango G.J., Liu Y., Edwards J. & Fletcher H.M., (2001). *vimA* gene downstream of *recA* is involved in virulence modulation in *Porphyromonas gingivalis* W83. *Infect Immun*, 69, pp.325–335.
- Abedin M., Tintut Y. & Demer L.L., (2004). Vascular calcification: mechanisms and clinical ramifications. *Arterio Thromb Vasc Biol*, 24(7), pp.1161–70.
- Aburahma A.F., Robinson P. & Decanio R., (1989). Prospective clinicopathologic study of carotid intraplaque hemorrhage. *Am Surg*, 55(3), pp.169–73.
- Abusleme L., Dupuy A.K., Dutzan N., Silva N., Burleson J.A., Strausbaugh L.D., Gamonal J. & Diaz P.I., (2013). The subgingival microbiome in health and periodontitis and its relationship with community biomass and inflammation. *ISME J*, 7(5), pp.1016–25.
- Aellen S., Que Y.-A., Guignard B., Haenni M. & Moreillon P., (2006). Detection of live and antibiotic-killed bacteria by quantitative real-time PCR of specific fragments of rRNA. *Antimicrob Agents Chemo*, 50(6), pp.1913–20.
- Aimetti M., Romano F. & Nessi F., (2007). Microbiologic analysis of periodontal pockets and carotid atheromatous plaques in advanced chronic periodontitis patients. *J Periodont*, 78(9), p.1718–23.
- Ait-Oufella H., Taleb S., Mallat Z. & Tedgui A., (2011). Recent advances on the role of cytokines in atherosclerosis. *Arterio Thromb Vasc Biol*, 31(5), pp.969–79.
- Albrecht C., Soumian S., Amey J.S., Sardini A., Higgins C.F., Davies A.H. & Gibbs R.G.J., (2004). ABCA1 expression in carotid atherosclerotic plaques. *Stroke*, 35(12), pp.2801–6.
- Allahverdian S., Chehroudi A.C., McManus B.M., Abraham T. & Francis G.A., (2014). Contribution of intimal smooth muscle cells to cholesterol accumulation and macrophage-like cells in human atherosclerosis. *Circulation*, 129(15), pp.1551–9.
- Ammar A.D., Wilson R.L., Travers H., Lin J.J., Farha S.J. & Chang F.C., (1984). Intraplaque hemorrhage: Its significance in cerebrovascular disease. *Am J Surg*, 148(6), pp.840–843.
- Ando N. & Hoshino E., (1990). Predominant obligate anaerobes invading the deep layers of root canal dentine. *Int Endodont J*, 23(1), pp.20–27.
- Anon, (2002). National Cholesterol Education Program (NCEP) Expert Panel on Detection, Evaluation and Treatment of High Blood Cholesterol in Adults (Adult Treatment Panel III). Third Report of the NCEP Expert Panel on Detection, Evaluation and Treatment of High Blood. *Circulation*, 106(25), pp.3143–421.
- Apfalter P., Blasi F., Boman J., Gaydos C.A., Kundi M., Maass M., Makristathis A., Meijer A., Nadrichal R., Persson K., et al., (2001). Multicenter comparison trial of DNA extraction methods and PCR assays for detection of *Chlamydia pneumoniae* in endarterectomy specimens. *J Clin Microbiol*, 39(2), pp.519–24.
- Aquino A. & Lima K., (2011). Molecular survey of atheromatous plaques for the presence of DNA from periodontal bacterial pathogens, archaea and fungi. *J Periodont Res*, 46(3), pp.303–309.
- Aquino A.R.L., Lima K.C., Paiva M.S., Rôças I.N. & Siqueira J.F., (2011). Molecular survey of atheromatous plaques for the presence of DNA from periodontal bacterial pathogens, archaea and fungi. *J Periodont Res*, 46(3), pp.303–9.
- Armingohar Z., Jørgensen J.J., Kristoffersen A.K., Abesha-Belay E. & Olsen I., (2014). Bacteria

- and bacterial DNA in atherosclerotic plaque and aneurysmal wall biopsies from patients with and without periodontitis. *J Oral Microbiol*, 6, pp.23408–23421.
- Aronson D. & Rayfield E., (2002). How hyperglycemia promotes atherosclerosis: molecular mechanisms. *Cardiovascular Diabetology*, 1(1), p.1.
- Asai Y., Jinno T., Igarashi H., Ohyama Y. & Ogawa T., (2002). Detection and quantification of oral treponemes in subgingival plaque by real-time PCR. *J Clin Microbiol*, 40(9), pp.3334–40.
- Ashelford K.E., Chuzhanova N.A., Fry J.C., Jones A.J. & Weightman A.J., (2005). At least 1 in 20 16S rRNA sequence records currently held in public repositories is estimated to contain substantial anomalies. *App Environ Microbiol*, 71(12), pp.7724–36.
- Ashimoto a, Chen C., Bakker I. & Slots J., (1996). Polymerase chain reaction detection of 8 putative periodontal pathogens in subgingival plaque of gingivitis and advanced periodontitis lesions. *Oral Microbiol Immun*, 11, pp.266–273.
- Assmann G., Schulte H., von Eckardstein A. & Huang Y., (1996). High-density lipoprotein cholesterol as a predictor of coronary heart disease risk. The PROCAM experience and pathophysiological implications for reverse cholesterol transport. *Atherosclerosis*, 124 Suppl, pp.S11-20.
- Aubin G.G., Portillo M.E., Trampuz A. & Corvec S., (2014). Propionibacterium acnes, an emerging pathogen: From acne to implant-infections, from phylotype to resistance. *Méd Malad Infect*, 44(6), pp.241–250.
- Autieri M.V., (2012). Pro- and anti-inflammatory cytokine networks in atherosclerosis. *ISRN Vasc Med*, 2012(Ldl), pp.1–17.
- Avril G., Batt M., Guidoin R., Marois M., Hassen-Khodja R., Daune B., Gagliardi J.M. & Le Bas P., (1991). Carotid endarterectomy plaques: correlations of clinical and anatomic findings. *Ann Vasc Surg*, 5(1), pp.50–4.
- Baca-Castañón M.L., De la Garza-Ramos M.A., Alcázar-Pizaña A.G., Grondin Y., Coronado-Mendoza A., Sánchez-Najera R.I., Cárdenas-Estrada E., Medina-De la Garza C.E. & Escamilla-García E., (2015). Antimicrobial Effect of Lactobacillus reuteri on Cariogenic Bacteria Streptococcus gordonii, Streptococcus mutans, and Periodontal Diseases Actinomyces naeslundii and Tannerella forsythia. *Probiot Antimicrob Proteins*, 7(1), pp.1–8.
- Badet C. & Thebaud N.B., (2008). Ecology of lactobacilli in the oral cavity: a review of literature. *Open Microbiol J*, 2, pp.38–48.
- Barath P., Fishbein M. & Cao J., (1990). Detection and localization of tumor necrosis factor in human atheroma. *Am J Path*, 65(5), pp.297–302.
- Bauman D.R., Bitmansour A.D., McDonald J.G., Thompson B.M., Liang G. & Russell D.W., (2009). 25-Hydroxycholesterol secreted by macrophages in response to Toll-like receptor activation suppresses immunoglobulin A production. *Proc. Natl. Acad. Sci. U.S.A*, 106(39), pp.16764–9.
- Begley T.P., Downs D.M., Ealick S.E., McLafferty F.W., Van Loon A.P., Taylor S., Campobasso N., Chiu H.J., Kinsland C., Reddick J.J., et al., (1999). Thiamin biosynthesis in prokaryotes. *Arch Microbiol*, 171(5), pp.293–300.
- Bélanger M., Kozarov E., Song H., Whitlock J. & Progulske-Fox A., (2012). Both the unique and repeat regions of the Porphyromonas gingivalis hemagglutinin A are involved in adhesion and invasion of host cells. *Anaerobe*, 18(1), pp.128–34.
- Beltrán-Aguilar E.D., Eke P.I., Thornton-Evans G. & Petersen P.E., (2012). Recording and surveillance systems for periodontal diseases. *Periodont 2000*, 60(1), pp.40–53.
- Benowitz N.L. & Gourlay S.G., (1997). Cardiovascular Toxicity of Nicotine: Implications for

- Nicotine Replacement Therapy 11 All editorial decisions for this article, including selection of referees, were made by a Guest Editor. This policy applies to all articles with authors from the Universi. *J Am Coll Cardiol*, 29(7), pp.1422–1431.
- Berthelot P., Carricajo A., Aubert G., Akhavan H., Gazielly D. & Lucht F., (2006). Outbreak of postoperative shoulder arthritis due to *Propionibacterium acnes* infection in nondebilitated patients. *Infect control hospit edipemiol*, 27(9), pp.987–90.
- Bevilacqua M.P., Pober J.S., Wheeler M.E., Cotran R.S. & Gimbrone M.A., (1985). Interleukin 1 acts on cultured human vascular endothelium to increase the adhesion of polymorphonuclear leukocytes, monocytes, and related leukocyte cell lines. *J Clin Invest*, 76(5), pp.2003–2011.
- Beylot C., Auffret N., Poli F., Claudel J.-P., Leccia M.-T., Del Giudice P. & Dreno B., (2014). *Propionibacterium acnes*: an update on its role in the pathogenesis of acne. *JEADV*, 28(3), pp.271–8.
- Björkbacka H., Kunjathoor V. V, Moore K.J., Koehn S., Ordija C.M., Lee M.A., Means T., Halmen K., Luster A.D., Golenbock D.T., et al., (2004). Reduced atherosclerosis in MyD88-null mice links elevated serum cholesterol levels to activation of innate immunity signaling pathways. *Nat Med*, 10(4), pp.416–21.
- Blake G.J. & Ridker P.M., (2001). Novel Clinical Markers of Vascular Wall Inflammation. *Clin Res*, 89(9), pp.763–771.
- Blakemore R.P. & Canale Parola E., (1976). Arginine catabolism by *Treponema denticola*. *J Bacteriol*, 128(2), pp.616–622.
- Bonetti P.O., (2002). Endothelial Dysfunction: A Marker of Atherosclerotic Risk. *Arterio Thromb Vasc Biol*, 23(2), pp.168–175.
- Bonnert T.P., Garka K.E., Parnet P., Sonoda G., Testa J.R. & Sims J.E., (1997). The cloning and characterization of human MyD88: a member of an IL-1 receptor related family 1 The nucleotide sequences reported in this paper have been submitted to the Genbank/EMBL Data Bank with accession numbers U84408 and U84409.1. *FEBS Letters*, 402(1), pp.81–84.
- Bouchiat C., Saison J., Boisset S., Flandrois J.-P., Issartel B., Dauwalder O., Benito Y., Jarraud S., Grando J., Boibieux A., et al., (2015). Nontuberculous Mycobacteria: An Underestimated Cause of Bioprosthetic Valve Infective Endocarditis. *Open Forum Infect Dis*, 2(2), p.ofv047.
- Braunersreuther V., Zerneck A., Arnaud C., Liehn E.A., Steffens S., Shagdarsuren E., Bidzhekov K., Burger F., Pelli G., Luckow B., et al., (2007). Ccr5 but not Ccr1 deficiency reduces development of diet-induced atherosclerosis in mice. *Arterio Thromb Vasc Biol*, 27(2), pp.373–9.
- Brodala N. & Merricks E., (2005). *Porphyromonas gingivalis* bacteremia induces coronary and aortic atherosclerosis in normocholesterolemic and hypercholesterolemic pigs. *Arterio Thromb Vasc Biol*, 25(7), pp.1446–51.
- Brown M.S., Ho Y.K. & Goldstein J.L., (1980). The cholesteryl ester cycle in macrophage foam cells. Continual hydrolysis and re-esterification of cytoplasmic cholesteryl esters. *J Biol Chem*, 255(19), pp.9344–52.
- Bruey J.-M., Bruey-Sedano N., Luciano F., Zhai D., Balpai R., Xu C., Kress C.L., Bailly-Maitre B., Li X., Osterman A., et al., (2007). Bcl-2 and Bcl-XL regulate proinflammatory caspase-1 activation by interaction with NALP1. *Cell*, 129(1), pp.45–56.
- Brüggemann H., (2005). Insights in the pathogenic potential of *Propionibacterium acnes* from its complete genome. *Sem Cutan Med Surg*, 24, pp.67–72.
- Buchan A., Alber M. & Hodson R.E., (2001). Strain-specific differentiation of environmental *Escherichia coli* isolates via denaturing gradient gel electrophoresis (DGGE) analysis of the 16S–23S intergenic spacer region. *FEMS Microbiol Ecol*, 35(3), pp.313–321.

- Buhaescu I. & Izzedine H., (2007). Mevalonate pathway: a review of clinical and therapeutical implications. *Clin Biochem*, 40(9–10), pp.575–84.
- Burg J.S. & Espenshade P.J., (2011). Regulation of HMG-CoA reductase in mammals and yeast. *Prog Lipid Res*, 50(4), pp.403–10.
- Cai J., Hatsukami T.S., Ferguson M.S., Kerwin W.S., Saam T., Chu B., Takaya N., Polissar N.L. & Yuan C., (2005). In vivo quantitative measurement of intact fibrous cap and lipid-rich necrotic core size in atherosclerotic carotid plaque: comparison of high-resolution, contrast-enhanced magnetic resonance imaging and histology. *Circulation*, 112(22), pp.3437–44.
- Cai J.-M., (2002). Classification of Human Carotid Atherosclerotic Lesions With In Vivo Multicontrast Magnetic Resonance Imaging. *Circulation*, 106(11), pp.1368–1373.
- Cairo F., Gaeta C., Dorigo W., Oggioni M.R., Patesi C., Pin Prato G.P. & Pozzi G., (2004). Periodontal pathogens in atheromatous plaques. A controlled clinical and laboratory trial. *J Periodont Res*, 39, pp.442–446.
- Calandrini C. & Ribeiro A., (2014). Microbial composition of atherosclerotic plaques. *Oral Dis*, 20, pp.128–134.
- Caldwell D.R. & Bryant M.P., (1966). Medium without rumen fluid for nonselective enumeration and isolation of rumen bacteria. *Appl Microbiol*, 14(5), pp.794–801.
- Campbell L.A. & Rosenfeld M.E., (2015). Infection and Atherosclerosis Development. *Arch Med Res*, 46(5), pp.339–350.
- Cao F., Castrillo A. & Tontonoz P., (2007). Chlamydia pneumoniae-induced macrophage foam cell formation is mediated by Toll-like receptor 2. *Infect Immun*, 75(2), pp.753–9.
- Carayol N., Chen J., Yang F., Jin T., Jin L., States D. & Wang C.-Y., (2006). A dominant function of IKK/NF-kappaB signaling in global lipopolysaccharide-induced gene expression. *J Biol Chem*, 281(41), pp.31142–51.
- Castelli W.P., (1986). Incidence of Coronary Heart Disease and Lipoprotein Cholesterol Levels. *JAMA*, 256(20), p.2835.
- Castrillo A., Joseph S.B., Vaidya S.A., Haberland M., Fogelman A.M., Cheng G. & Tontonoz P., (2003). Crosstalk between LXR and toll-like receptor signaling mediates bacterial and viral antagonism of cholesterol metabolism. *Mol Cell*, 12(4), pp.805–16.
- Cavaillon J.M., Fitting C., Haeffner-Cavaillon N., Kirsch S.J. & Warren H.S., (1990). Cytokine response by monocytes and macrophages to free and lipoprotein-bound lipopolysaccharide. *Infect Immun.*, 58(7), pp.2375–2382.
- Cavrini F., (2005). Molecular detection of *Treponema denticola* and *Porphyromonas gingivalis* in carotid and aortic atheromatous plaques by FISH: report of two cases. *J Med Microbiol*, 54(1), pp.93–96.
- Cekici A., Kantarci A., Hasturk H. & Van Dyke T.E., (2014). Inflammatory and immune pathways in the pathogenesis of periodontal disease. *Periodont 2000*, 64(1), pp.57–80.
- Cenedella R.J., (2009). Cholesterol synthesis inhibitor U18666A and the role of sterol metabolism and trafficking in numerous pathophysiological processes. *Lipids*, 44(6), pp.477–87.
- Chamberlain J., Evans D. & King A., (2006). Interleukin-1 $\beta$  and signaling of interleukin-1 in vascular wall and circulating cells modulates the extent of neointima formation in mice. *Am J Pathol*, 168(4), pp.1396–1403.
- Chatzizisis Y.S., Coskun A.U., Jonas M., Edelman E.R., Feldman C.L. & Stone P.H., (2007). Role of endothelial shear stress in the natural history of coronary atherosclerosis and vascular remodeling: molecular, cellular, and vascular behavior. *J Am Coll Cardiol*, 49(25), pp.2379–93.

- Chen S., Lee Y., Crother T.R., Fishbein M., Zhang W., Yilmaz A., Shimada K., Schulte D.J., Lehman T.J.A., Shah P.K., et al., (2012). Marked acceleration of atherosclerosis after *Lactobacillus casei*-induced coronary arteritis in a mouse model of Kawasaki disease. *Arterio Thromb Vasc Biol*, 32(8), pp.e60-71.
- Chen S., Sorrentino R. & Shimada K., (2008). Chlamydia pneumoniae-induced foam cell formation requires MyD88-dependent and-independent signaling and is reciprocally modulated by liver X receptor. *J Immunol*, 181(10), pp.7186–93.
- Chen T., Yu W.-H., Izard J., Baranova O. V, Lakshmanan A. & Dewhirst F.E., (2010). The Human Oral Microbiome Database: a web accessible resource for investigating oral microbe taxonomic and genomic information. *Database (Oxford)*, 2010, p.baq013.
- Cheng S.-L. & Chan E.C.S., (1983). The routine isolation, growth, and maintenance of the intermediate-size anaerobic oral spirochetes from periodontal pockets. *J Periodont Res*, 18(4), pp.362–368.
- Chiu B., (1999). Multiple infections in carotid atherosclerotic plaques. *Am Heart J*, 138(5), pp.534–536.
- Chou H., Yumoto H., Davey M., Miyamoto T., Iii F.C.G., Genco C. a & Takahashi Y., (2005). Porphyromonas gingivalis Fimbria-Dependent Activation of Inflammatory Genes in Human Aortic Endothelial Cells. *Infect Immun*, 73(9), pp.5367–5378.
- Choudhury M., Patel B.R., Patel M. & Bashir T., (2009). Streptococcus viridans osteomyelitis and endocarditis following dental treatment: a case report. *Cases J*, 2, p.6857.
- Chu B., Kampschulte A., Ferguson M.S., Kerwin W.S., Yarnykh V.L., O'Brien K.D., Polissar N.L., Hatsukami T.S. & Yuan C., (2004). Hemorrhage in the atherosclerotic carotid plaque: a high-resolution MRI study. *Stroke*, 35(5), pp.1079–84.
- De Ciccio A., McLaughlin R. & Chan E.C., (1999). Factors affecting the formation of spherical bodies in the spirochete *Treponema denticola*. *Oral Microbiol Immun*, 14(6), pp.384–6.
- Clausell N., Lima V. de & Molossi S., (1995). Expression of tumour necrosis factor alpha and accumulation of fibronectin in coronary artery restenotic lesions retrieved by atherectomy. *BHF*, 73, pp.534–539.
- Cohen P., (2000). Monitoring Cellular Responses to *Listeria monocytogenes* with Oligonucleotide Arrays. *J Biol Chem*, 275(15), pp.11181–11190.
- Cohen R.J., Shannon B.A., McNeal J.E., Shannon T. & Garrett K.L., (2005). Propionibacterium acnes associated with inflammation in radical prostatectomy specimens: a possible link to cancer evolution? *J Urol*, 173(6), pp.1969–74.
- Colgan S.M., Hashimi A.A. & Austin R.C., (2011). Endoplasmic reticulum stress and lipid dysregulation. *Expert Rev Mol Med*, 13, p.e4.
- Contassot E. & French L.E., (2014). New insights into acne pathogenesis: propionibacterium acnes activates the inflammasome. *J Invest Derm*, 134(2), pp.310–3.
- Cornfield J., (1962). Joint dependence of risk of coronary heart disease on serum cholesterol and systolic blood pressure: a discriminant function analysis. *Fed Poceed*, 21(4), pp.58–61.
- Cummins C.S. & Johnson J.L., (1974). *Corynebacterium parvum*: a Synonym for *Propionibacterium acnes*? *J General Microbiol*, 80(2), pp.433–442.
- Curb J.D., Abbott R.D., Rodriguez B.L., Masaki K., Chen R., Sharp D.S. & Tall A.R., (2004). A prospective study of HDL-C and cholesteryl ester transfer protein gene mutations and the risk of coronary heart disease in the elderly. *J Lipid Res*, 45(5), pp.948–53.
- Czabotar P.E., Lessene G., Strasser A. & Adams J.M., (2013). Control of apoptosis by the BCL-2

- protein family: implications for physiology and therapy. *Nat Rev Mol Cell Biol*, 15(1), pp.49–63.
- Daep C.A., Lamont R.J. & Demuth D.R., (2008). Interaction of *Porphyromonas gingivalis* with oral streptococci requires a motif that resembles the eukaryotic nuclear receptor box protein-protein interaction domain. *Infect Immun*, 76(7), pp.3273–80.
- Le Dall J., Ho-Tin-Noé B., Louedec L., Meilhac O., Roncal C., Carmeliet P., Germain S., Michel J.-B. & Houard X., (2010). Immaturity of microvessels in haemorrhagic plaques is associated with proteolytic degradation of angiogenic factors. *Cardiovasc Res*, 85(1), pp.184–93.
- Van Damme H., Demoulin J.C., Zicot M., Creemers E., Trotteur G. & Limet R., Pathological aspects of carotid plaques. Surgical and clinical significance. *J Cardiovasc S*, 33(1), pp.46–53.
- Danforth J.M., Strieter R.M., Kunkel S.L., Arenberg D.A., VanOtteren G.M. & Standiford T.J., (1995). Macrophage inflammatory protein-1 alpha expression in vivo and in vitro: the role of lipoteichoic acid. *Clin Immunol Immunopathol*, 74(1), pp.77–83.
- Davies M.J., Gordon J.L., Gearing A.J., Pigott R., Woolf N., Katz D. & Kyriakopoulos A., (1993). The expression of the adhesion molecules ICAM-1, VCAM-1, PECAM, and E-selectin in human atherosclerosis. *J Pathol*, 171(3), pp.223–9.
- Debelian G.J., Olsen I. & Tronstad L., (1992). Profiling of *Propionibacterium acnes* recovered from root canal and blood during and after endodontic treatment. *Dent Traumatol*, 8(6), pp.248–254.
- DeGraba T.J., (1997). Expression of inflammatory mediators and adhesion molecules in human atherosclerotic plaque. *Neurology*, 49(5 Suppl 4), pp.S15–S19.
- DeGraba T.J., Siren A.-L., Penix L., McCarron R.M., Hargraves R., Sood S., Pettigrew K.D. & Hallenbeck J.M., (1998). Increased Endothelial Expression of Intercellular Adhesion Molecule-1 in Symptomatic Versus Asymptomatic Human Carotid Atherosclerotic Plaque. *Stroke*, 29(7), pp.1405–1410.
- Denapate D., Brückner R., Nuhn M., Reichmann P., Henrich B., Maurer P., Schähle Y., Selbmann P., Zimmermann W., Wambutt R., et al., (2010). The genome of *Streptococcus mitis* B6--what is a commensal? *PLoS ONE*, 5(2), p.e9426.
- Deshpande R.G., Khan M.B. & Genco C.A., (1998). Invasion of aortic and heart endothelial cells by *Porphyromonas gingivalis*. *Infect Immun*, 66(11), pp.5337–43.
- Dewberry R. & Holden H., (2000). Interleukin-1 receptor antagonist expression in human endothelial cells and atherosclerosis. *Arterio Thrombo Vasc Biol*, 20(11), pp.2394–2400.
- Dewberry R., Holden H., Crossman D. & Francis S., (2000). Interleukin-1 Receptor Antagonist Expression in Human Endothelial Cells and Atherosclerosis. *Arterio Thromb Vasc Biol*, 20(11), pp.2394–2400.
- Dickson R.P., Huffnagle G.B., Horikoshi K., Grant W., Gleeson K., Egli D., Maxwell S., Huxley E., Viroslav J., Gray W., et al., (2015). The Lung Microbiome: New Principles for Respiratory Bacteriology in Health and Disease W. E. Goldman, ed. *PLOS Path*, 11(7), p.e1004923.
- Dinareello C.A., (2009). Immunological and inflammatory functions of the interleukin-1 family. *Ann Rev Immunol*, 27, pp.519–50.
- Doherty T.M., Fitzpatrick L.A., Inoue D., Qiao J.-H., Fishbein M.C., Detrano R.C., Shah P.K. & Rajavashisth T.B., (2004). Molecular, endocrine, and genetic mechanisms of arterial calcification. *Endoc Rev*, 25(4), pp.629–72.
- Dong B., Wu M., Li H., Kraemer F.B., Adeli K., Seidah N.G., Park S.W. & Liu J., (2010). Strong induction of PCSK9 gene expression through HNF1alpha and SREBP2: mechanism for the resistance to LDL-cholesterol lowering effect of statins in dyslipidemic hamsters. *J Lipid Res*, 51(6), pp.1486–95.

- Drancourt M., Roux V., Fournier P.-E. & Raoult D., (2004). *rpoB* gene sequence-based identification of aerobic Gram-positive cocci of the genera *Streptococcus*, *Enterococcus*, *Gemella*, *Abiotrophia*, and *Granulicatella*. *J Clin Microbiol*, 42(2), pp.497–504.
- Dubernet S., Desmasure N. & Guéguen M., (2002). A PCR-based method for identification of lactobacilli at the genus level. *FEMS Microbiol Lett*, 214(2), pp.271–275.
- Duewell P., Kono H., Rayner K. & Sirois C., (2010). NLRP3 inflammasomes are required for atherogenesis and activated by cholesterol crystals. *Nature*, 464, pp.1357–1361.
- Duncan E.A., (1997). Cleavage Site for Sterol-regulated Protease Localized to a Leu-Ser Bond in the Luminal Loop of Sterol Regulatory Element-binding Protein-2. *J Biol Chem*, 272(19), pp.12778–12785.
- Dunmore B.J., McCarthy M.J., Naylor A.R. & Brindle N.P.J., (2007). Carotid plaque instability and ischemic symptoms are linked to immaturity of microvessels within plaques. *J Vasc Surg*, 45(1), pp.155–9.
- Dzenko K.A., Song L., Ge S., Kuziel W.A. & Pachter J.S., (2005). CCR2 expression by brain microvascular endothelial cells is critical for macrophage transendothelial migration in response to CCL2. *Microvasc Res*, 70(1–2), pp.53–64.
- Eberlé D., Hegarty B., Bossard P., Ferré P. & Foufelle F., (2004). SREBP transcription factors: master regulators of lipid homeostasis. *Biochimie*, 86(11), pp.839–48.
- Ebersole J.L., (2003). Humoral immune responses in gingival crevice fluid: local and systemic implications. *Periodont 2000*, 31(1), pp.135–166.
- Edwards A.M., Dymock D. & Jenkinson H.F., (2003). From tooth to hoof: treponemes in tissue-destructive diseases. *J Appl Microbiol*, 94(5), pp.767–780.
- Eguchi J., Yan Q.-W., Schones D.E., Kamal M., Hsu C.-H., Zhang M.Q., Crawford G.E. & Rosen E.D., (2008). Interferon regulatory factors are transcriptional regulators of adipogenesis. *Cell Metab*, 7(1), pp.86–94.
- Eishi Y., Suga M., Ishige I., Kobayashi D., Yamada T., Takemura T., Takizawa T., Koike M., Kudoh S., Costabel U., et al., (2002). Quantitative analysis of mycobacterial and propionibacterial DNA in lymph nodes of Japanese and European patients with sarcoidosis. *J Clin Microbiol*, 40(1), pp.198–204.
- Elkaïm R., Dahan M., Kocgozlu L., Werner S., Kanter D., Kretz J.G. & Tenenbaum H., (2008). Prevalence of periodontal pathogens in subgingival lesions, atherosclerotic plaques and healthy blood vessels: A preliminary study. *J Periodont Res*, 43(2), pp.224–231.
- Elkind M.S. V., (2010). Infectious burden: a new risk factor and treatment target for atherosclerosis. *Infect Disord Drug Targ*, 10(2), pp.84–90.
- Enersen M., Nakano K. & Amano A., (2013). *Porphyromonas gingivalis* fimbriae. *J Oral Microbiol*, 5(20265) pp.1-10.
- Eriksson I., Forsberg O., Lundqvist B. & Schwan A., (1983). Significant of positive bacterial cultures from aortic aneurysms. *Acta Chiru Scand*, 149(1), pp.33–5.
- Escandell J.M., Recio M.C., Giner R.M., Mánuez S. & Ríos J.L., (2010). Bcl-2 is a negative regulator of interleukin-1beta secretion in murine macrophages in pharmacological-induced apoptosis. *Britt J Pharm*, 160(7), pp.1844–56.
- Espenshade P.J., Cheng D., Goldstein J.L. & Brown M.S., (1999). Autocatalytic Processing of Site-1 Protease Removes Propeptide and Permits Cleavage of Sterol Regulatory Element-binding Proteins. *J Biol Chem*, 274(32), pp.22795–22804.
- Faggioli G.L., Pini R., Mauro R., Pasquinelli G., Fittipaldi S., Freyrie A., Serra C. & Stella A.,

- (2011). Identification of carotid “vulnerable plaque” by contrast-enhanced ultrasonography: correlation with plaque histology, symptoms and cerebral computed tomography. *Eur J Vasc Endovasc Surg*, 41(2), pp.238–48.
- Falcochio S., Ruiz C., Pastor F.I.J., Saso L. & Diaz P., (2006). Propionibacterium acnes GehA lipase, an enzyme involved in acne development, can be successfully inhibited by defined natural substances. *Journal of Molecular Catalysis B: Enzymatic*, 40(3–4), pp.132–137.
- Falk E., (2006). Pathogenesis of Atherosclerosis. *J Am Coll Cardiol*, 47(8), pp.C7–C12.
- Fan Y.-M., Karhunen P.J., Levula M., Ilveskoski E., Mikkelsen J., Kajander O.A., Järvinen O., Oksala N., Thusberg J., Vihinen M., et al., (2008). Expression of sterol regulatory element-binding transcription factor (SREBF) 2 and SREBF cleavage-activating protein (SCAP) in human atheroma and the association of their allelic variants with sudden cardiac death. *Throb J*, 6(17), pp.1–8.
- Farsak B., Yildirim A., Akyön Y., Pinar A. & Öç M., (2000). Detection of Chlamydia pneumoniae and Helicobacter pylori DNA in Human Atherosclerotic Plaques by PCR. *J Clin Microbiol*, 38(12), pp.4408–4411.
- Farsak B., Yildirim A., Akyön Y., Pinar A., Öç M., Akyon Y., Pinar A., Oc M., Boke E. & Kes S., (2000). Detection of Chlamydia pneumoniae and Helicobacter pylori DNA in Human Atherosclerotic Plaques by PCR. *J Clin Microbiol*, 38(12), pp.4408–4411.
- Fassi Fehri L., Mak T.N., Laube B., Brinkmann V., Ogilvie L.A., Mollenkopf H., Lein M., Schmidt T., Meyer T.F. & Brüggemann H., (2011). Prevalence of Propionibacterium acnes in diseased prostates and its inflammatory and transforming activity on prostate epithelial cells. *IJMM*, 301(1), pp.69–78.
- Fathy A., Mohamed R.W., Ismael N.A. & El-Akhras M.A., (2009). Expression of toll-like receptor 2 on peripheral blood monocytes of patients with inflammatory and noninflammatory acne vulgaris. *Egypt J Immunol*, 16(1), pp.127–34.
- Feinstein S.B., (2006). Contrast ultrasound imaging of the carotid artery vasa vasorum and atherosclerotic plaque neovascularization. *J Am Coll Cardiol*, 48(2), pp.236–43.
- Feng B., Yao P.M., Li Y., Devlin C.M., Zhang D., Harding H.P., Sweeney M., Rong J.X., Kuriakose G., Fisher E. a, et al., (2003). The endoplasmic reticulum is the site of cholesterol-induced cytotoxicity in macrophages. *Nat Cell Biol*, 5(9), pp.781–92.
- Fenno J., (2005). Laboratory Maintenance of Treponema denticola. *Curr Protocols Microbiol*, 12(1), pp.1–21.
- Fernandes C.P., Oliveira F.A.F., Silva P.G. de B., Alves A.P.N.N., Mota M.R.L., Montenegro R.C., Burbano R.M.R., Seabra A.D., Lobo Filho J.G., Lima D.L.F., et al., (2014). Molecular analysis of oral bacteria in dental biofilm and atherosclerotic plaques of patients with vascular disease. *Int J Cardiol*, 174(3), pp.710–2.
- Ferrandiz M.-J., Ardanuy C., Linares J., Balsalobre L., Garcia M.T. & de la Campa A.G., (2011). New Species Genetic Approach To Identify Strains of Mitis Group Streptococci That Are Donors of Rifampin Resistance to Streptococcus pneumoniae. *Antimicrob Agents Chemo*, 55(1), pp.368–372.
- Ferro J.M. & Fonseca A.C., (2014). Clinical Features of Acute Stroke. In B. Norrving, ed. *Oxford Textbook of Stroke and Cerebrovascular Disease*. Oxford: Oxford University Press, pp. 85–92.
- Fiehn N. & Larsen T., (2005). Identification of periodontal pathogens in atherosclerotic vessels. *J Periodont*, 75(5), pp.731–736.
- Figuro E. & Lindahl C., (2014). Quantification of Periodontal Pathogens in Vascular, Blood and Subgingival Samples from Patients with Peripheral Arterial Disease or Abdominal Aortic

Aneurysms. *J Periodont*, 85(9), pp.1182–1193.

Figuro E., Sánchez-Beltrán M., Cuesta-Frechos S., Tejerina J.M., del Castro J.A., Gutiérrez J.M., Herrera D. & Sanz M., (2011). Detection of Periodontal Bacteria in Atheromatous Plaque by Nested Polymerase Chain Reaction. *J Periodont*, 82(10), pp.1469–1477.

Finn A. V, Kolodgie F.D. & Virmani R., (2010). Correlation between carotid intimal/medial thickness and atherosclerosis: a point of view from pathology. *Arterio Thromb Vasc Biol*, 30(2), pp.177–81.

Fischer N., Mak T.N., Shinohara D.B., Sfanos K.S., Meyer T.F. & Brüggemann H., (2013). Deciphering the intracellular fate of *Propionibacterium acnes* in macrophages. *BioMed Res Int*, 2013(Article ID 603046), p.11 pages.

Fiser R.H., Denniston J.C., Rindsig R.B. & Beisel W.R., (1971). Effects of Acute Infection on Cholesterogenesis in the Rhesus Monkey. *Exp Biol Med*, 138(2), pp.605–609.

Forcheron F., Legedz L., Chinetti G., Feugier P., Letexier D., Bricca G. & Beylot M., (2005). Genes of cholesterol metabolism in human atheroma: overexpression of perilipin and genes promoting cholesterol storage and repression of ABCA1 expression. *Arterio Thromb Vasc Biol*, 25(8), pp.1711–7.

Ford P., Gemmell E. & Chan A., (2006). Inflammation, heat shock proteins and periodontal pathogens in atherosclerosis: an immunohistologic study. *Oral Microbiol Immun*, 21, pp.206–211.

Forner L., Larsen T., Kilian M. & Holmstrup P., (2006). Incidence of bacteremia after chewing, tooth brushing and scaling in individuals with periodontal inflammation. *J Clin Periodont*, 33(6), pp.401–7.

Forte A., Finicelli M., De Luca P., Quarto C., Onorati F., Santè P., Renzulli A., Galderisi U., Berrino L., De Feo M., et al., (2008). Expression profiles in surgically-induced carotid stenosis: a combined transcriptomic and proteomic investigation. *J Cellular Med Mol Med*, 12(5B), pp.1956–73.

Franchi L., Eigenbrod T., Muñoz-Planillo R. & Nuñez G., (2009). The inflammasome: a caspase-1-activation platform that regulates immune responses and disease pathogenesis. *J Immunol*, 10(3), pp.241–7.

Freund K.M., Belanger A.J., D'Agostino R.B. & Kannel W.B., (1993). The health risks of smoking. The Framingham Study: 34 years of follow-up. *Ann Epidem*, 3(4), pp.417–24.

Friedrich A., Merkert H., Fendert T. & Hacker J., (1999). Microbial diversity in the marine sponge *Aplysina cavernicola* (formerly *Verongia cavernicola*) analyzed by fluorescence in situ hybridization (FISH). *Mar Biol*, 134(3), pp.461–70.

Frostegård J., Ulfgrén A.-K., Nyberg P., Hedin U., Swedenborg J., Andersson U. & Hansson G.K., (1999). Cytokine expression in advanced human atherosclerotic plaques: dominance of pro-inflammatory (Th1) and macrophage-stimulating cytokines. *Atherosclerosis*, 145(1), pp.33–43.

Fujii R., Saito Y., Tokura Y., Nakagawa K.-I., Okuda K. & Ishihara K., (2009). Characterization of bacterial flora in persistent apical periodontitis lesions. *Oral Microbiol Immun*, 24(6), pp.502–5.

Gaetti-Jardim E., (2009). Quantitative detection of periodontopathic bacteria in atherosclerotic plaques from coronary arteries. *J Med Microbiol*, 58, pp.1568–75.

Galea J. & Armstrong J., (1996). Interleukin-1 $\beta$  in coronary arteries of patients with ischemic heart disease. *Arterio Thromb Vasc Biol*, 16(8), pp.1000–1006.

Garnier F., Gerbaud G., Courvalin P. & Galimand M., (1997). Identification of clinically relevant viridans group streptococci to the species level by PCR. *J Clin Microbiol*, 35(9), pp.2337–41.

- George S.J. & Johnson J. eds., (2010). *Atherosclerosis: Molecular and Cellular Mechanisms* 1st ed., Wiley.
- Gerber H.P., Dixit V. & Ferrara N., (1998). Vascular endothelial growth factor induces expression of the antiapoptotic proteins Bcl-2 and A1 in vascular endothelial cells. *J Biol Chem*, 273(21), pp.13313–6.
- Gerbod-Giannone M.-C., Li Y., Holleboom A., Han S., Hsu L.-C., Tabas I. & Tall A.R., (2006). TNF $\alpha$  induces ABCA1 through NF-kappaB in macrophages and in phagocytes ingesting apoptotic cells. *Proc. Natl. Acad. Sci. U.S.A*, 103(9), pp.3112–7.
- Ghyselinck J., Pfeiffer S., Heylen K., Sessitsch A. & De Vos P., (2013). The effect of primer choice and short read sequences on the outcome of 16S rRNA gene based diversity studies. *PLoS ONE*, 8(8), p.e71360.
- Giacona M. & Papapanou P., (2004). Porphyromonas gingivalis induces its uptake by human macrophages and promotes foam cell formation in vitro. *FEMS Microbiol Lett*, 241, pp.95–101.
- Giannoni M.F., Vicenzini E., Citone M., Ricciardi M.C., Irace L., Laurito A., Scucchi L.F., Di Piero V., Gossetti B., Mauriello A., et al., (2009). Contrast carotid ultrasound for the detection of unstable plaques with neoangiogenesis: a pilot study. *Eur J Vasc Endovasc Surg*, 37(6), pp.722–7.
- Gibson F.C., Hong C., Chou H.-H., Yumoto H., Chen J., Lien E., Wong J. & Genco C.A., (2004). Innate immune recognition of invasive bacteria accelerates atherosclerosis in apolipoprotein E-deficient mice. *Circulation*, 109(22), pp.2801–6.
- Golledge J., Greenhalgh R.M. & Davies A.H., (2000). The Symptomatic Carotid Plaque. *Stroke*, 31(3), pp.774–781.
- Grenier D., Uitto V.J. & McBride B., (1990). Cellular location of a Treponema denticola chymotrypsinlike protease and importance of the protease in migration through the basement membrane. *Infect Immun*, 58(2), pp.347–351.
- Greten F.R., Arkan M.C., Bollrath J., Hsu L.-C., Goode J., Miething C., Göktuna S.I., Neuenhahn M., Fierer J., Paxian S., et al., (2007). NF-kappaB is a negative regulator of IL-1beta secretion as revealed by genetic and pharmacological inhibition of IKKbeta. *Cell*, 130(5), pp.918–31.
- Griffen A.L., Beall C.J., Campbell J.H., Firestone N.D., Kumar P.S., Yang Z.K., Podar M. & Leys E.J., (2012). Distinct and complex bacterial profiles in human periodontitis and health revealed by 16S pyrosequencing. *ISME J*, 6(6), pp.1176–85.
- Grove M. & Plumb M., (1993). C/EBP, NF-kappa B, and c-Ets family members and transcriptional regulation of the cell-specific and inducible macrophage inflammatory protein 1 alpha immediate-early gene. *Mol Cell Biol*, 13(9), pp.5276–89.
- Grundy S.M., Cleeman J.I., Merz C.N.B., Brewer H.B., Clark L.T., Hunninghake D.B., Pasternak R.C., Smith S.C. & Stone N.J., (2004). Implications of recent clinical trials for the National Cholesterol Education Program Adult Treatment Panel III guidelines. *Circulation*, 110(2), pp.227–39.
- Gunthard H., Hany A., Turina M. & Wust J., (1994). Propionibacterium acnes as a cause of aggressive aortic valve endocarditis and importance of tissue grinding: case report and review. *J Clin Microbiol*, 32(12), pp.3043–3045.
- Haas M.J. & Mooradian A.D., (2010). Regulation of high-density lipoprotein by inflammatory cytokines: establishing links between immune dysfunction and cardiovascular disease. *Diabet Metab Res Rev*, 26(2), pp.90–9.
- Haffajee A.D., Socransky S.S., Patel M.R. & Song X., (2008). Microbial complexes in supragingival plaque. *Oral Microbiol Immun*, 23(3), pp.196–205.

- Halvorsen B., Waehre T., Scholz H., Clausen O.P., von der Thüsen J.H., Müller F., Heimli H., Tonstad S., Hall C., Frøland S.S., et al., (2005). Interleukin-10 enhances the oxidized LDL-induced foam cell formation of macrophages by antiapoptotic mechanisms. *J Lipid Res*, 46(2), pp.211–9.
- Hamelin B., (1998). Hydrophilicity/ lipophilicity: relevance for the pharmacology and clinical effects of HMG-CoA reductase inhibitors. *Trends Pharmacol Sci*, 19(1), pp.26–37.
- Hamilton J.A., (2008). Colony-stimulating factors in inflammation and autoimmunity. *Nat Rev Immunol*, 8(7), pp.533–44.
- Handford J.I., Ize B., Buchanan G., Butland G.P., Greenblatt J., Emili A. & Palmer T., (2009). Conserved network of proteins essential for bacterial viability. *J Bacteriol*, 191(15), pp.4732–49.
- Hantsis-Zacharov E. & Halpern M., (2007). *Chryseobacterium haifense* sp. nov., a psychrotolerant bacterium isolated from raw milk. *Int J System Evol Microbiol*, 57(Pt 10), pp.2344–8.
- Harada-Shiba M., (1998). Oxidized Low Density Lipoprotein Induces Apoptosis in Cultured Human Umbilical Vein Endothelial Cells by Common and Unique Mechanisms. *J Biol Chem*, 273(16), pp.9681–9687.
- Haraszthy V. & Zambon J., (2000). Identification of periodontal pathogens in atheromatous plaques. *J Periodont*, 7(10), pp.1554–1560.
- Hatsukami T.S., Ross R., Polissar N.L. & Yuan C., (2000). Visualization of Fibrous Cap Thickness and Rupture in Human Atherosclerotic Carotid Plaque In Vivo With High-Resolution Magnetic Resonance Imaging. *Circulation*, 102(9), pp.959–964.
- Hayes I.M., Jordan N.J., Towers S., Smith G., Paterson J.R., Earnshaw J.J., Roach a. G., Westwick J. & Williams R.J., (1998). Human Vascular Smooth Muscle Cells Express Receptors for CC Chemokines. *Arterio Thromb Vasc Biol*, 18(3), pp.397–403.
- Hegy L., Skepper J.N., Cary N.R. & Mitchinson M.J., (1996). Foam cell apoptosis and the development of the lipid core of human atherosclerosis. *J Pathol*, 180(4), pp.423–9.
- Heller D., Silva-Boghossian C.M., do Souto R.M. & Colombo A.P.V., (2012). Subgingival microbial profiles of generalized aggressive and chronic periodontal diseases. *Arch Oral Biol*, 57(7), pp.973–80.
- Herrmann J., Lerman L.O., Mukhopadhyay D., Napoli C. & Lerman A., (2006). Angiogenesis in atherogenesis. *Arterio Thromb Vasc Biol*, 26(9), pp.1948–57.
- Higashimori M. & Tatro J., (2011). Role of Toll-Like Receptor 4 in Intimal Foam Cell Accumulation in Apolipoprotein E-Deficient Mice. *Arterio Thromb Vasc Biol*, 31(1), pp.50–7.
- Hiramatsu J., Kataoka M., Nakata Y., Okazaki K., Tada S., Tanimoto M. & Eishi Y., (2003). Propionibacterium acnes DNA detected in bronchoalveolar lavage cells from patients with sarcoidosis. *Sarcoid Vasculit Diffuse Lung Dis*, 20(3), pp.197–203.
- Hiscott J., Marois J., Garoufalos J., D'Addario M., Roulston A., Kwan I., Pepin N., Lacoste J., Nguyen H. & Bensi G., (1993). Characterization of a functional NF-kappa B site in the human interleukin 1 beta promoter: evidence for a positive autoregulatory loop. *Mol Cell Biol*, 13(10), pp.6231–40.
- Hobbs H.H., Brown M.S. & Goldstein J.L., (1992). Molecular genetics of the LDL receptor gene in familial hypercholesterolemia. *Human Mut*, 1(6), pp.445–66.
- Hold G. & Pryde S., (2002). Assessment of microbial diversity in human colonic samples by 16S rDNA sequence analysis. *FEMS Microbiol Lett*, 39(1), pp.33–39.
- Holland C., Mak T.N., Zimny-Arndt U., Schmid M., Meyer T.F., Jungblut P.R. & Brüggemann H., (2010). Proteomic identification of secreted proteins of Propionibacterium acnes. *BMC Microbiol*, 10(1), p.230.

- Holt S. & Kesavalu L., (1999). Virulence factors of *Porphyromonas gingivalis*. *Periodont 2000*.
- Hooper S.J., Crean S.-J., Fardy M.J., Lewis M. a O., Spratt D. a, Wade W.G. & Wilson M.J., (2007). A molecular analysis of the bacteria present within oral squamous cell carcinoma. *J Med Microbiol*, 56(Pt 12), pp.1651–9.
- Horton J.D., Goldstein J.L. & Brown M.S., (2002). SREBPs: activators of the complete program of cholesterol and fatty acid synthesis in the liver. *The J Clin Invest*, 109(9), pp.1125–31.
- Horváth B., Hunyadkúrti J., Vörös A., Fekete C., Urbán E., Kemény L. & Nagy I., (2012). Genome sequence of *Propionibacterium acnes* type II strain ATCC 11828. *J Bacteriol*, 194(1), pp.202–3.
- Hoshino E., (1985). Predominant obligate anaerobes in human carious dentin. *J Dent Res*, 64(10), pp.1195–8.
- Hoshino T., Fujiwara T. & Kilian M., (2005). Use of Phylogenetic and Phenotypic Analyses To Identify Nonhemolytic Streptococci Isolated from Bacteremic Patients. *J Clin Microbiol*, 43(12), pp.6073–6085.
- Howard G., Wagenknecht L.E., Burke G.L., Diez-Roux A., Evans G.W., McGovern P., Nieto F.J. & Tell G.S., (1998). Cigarette smoking and progression of atherosclerosis: The Atherosclerosis Risk in Communities (ARIC) Study. *JAMA*, 279(2), pp.119–24.
- Hua X., Wu J., Goldstein J.L., Brown M.S. & Hobbs H.H., (1995). Structure of the human gene encoding sterol regulatory element binding protein-1 (SREBF1) and localization of SREBF1 and SREBF2 to chromosomes 17p11.2 and 22q13. *Genomics*, 25(3), pp.667–673.
- Hubert H.B., Feinleib M., McNamara P.M. & Castelli W.P., (1983). Obesity as an independent risk factor for cardiovascular disease: a 26-year follow-up of participants in the Framingham Heart Study. *Circulation*, 67(5), pp.968–77.
- Hunyadkúrti J., Feltóti Z., Horváth B., Nagymihály M., Vörös A., McDowell A., Patrick S., Urbán E. & Nagy I., (2011). Complete genome sequence of *Propionibacterium acnes* type IB strain 6609. *J Bacteriol*, 193(17), pp.4561–2.
- Hwang S.-J.S., Ballantyne C.M.C., Sharrett A.R.A., Smith L.C., Davis C.E., Gotto A.M. & Boerwinkle E., (1997). Adhesion molecules VCAM-1, ICAM-1, and E-selectin in carotid atherosclerosis and incident coronary heart disease cases the Atherosclerosis Risk In Communities. *Circulation*, 96(12), pp.4219–4225.
- Iacoviello L., Vischetti M., Zito F. & Benedetta Donati M., (2001). Genes encoding fibrinogen and cardiovascular risk. *Hypertension*, 38(5), pp.1199–203.
- Iinuma K., Sato T., Akimoto N., Noguchi N., Sasatsu M., Nishijima S., Kurokawa I. & Ito A., (2009). Involvement of *Propionibacterium acnes* in the augmentation of lipogenesis in hamster sebaceous glands in vivo and in vitro. *J Invest Derm*, 129(9), pp.2113–9.
- Ionita M.G., van den Borne P., Catanzariti L.M., Moll F.L., de Vries J.-P.P.M., Pasterkamp G., Vink A. & de Kleijn D.P. V., (2010). High neutrophil numbers in human carotid atherosclerotic plaques are associated with characteristics of rupture-prone lesions. *Arterio Thromb Vasc Biol*, 30(9), pp.1842–8.
- Ishige I., Eishi Y., Takemura T., Kobayashi I., Nakata K., Tanaka I., Nagaoka S., Iwai K., Watanabe K., Takizawa T., et al., (2005). *Propionibacterium acnes* is the most common bacterium commensal in peripheral lung tissue and mediastinal lymph nodes from subjects without sarcoidosis. *Sarcoid Vasculit Diffuse Lung Dis*, 22(1), pp.33–42.
- Ishihara K., Nabuchi A. & Ito R., (2004). Correlation between detection rates of periodontopathic bacterial DNA in carotid coronary stenotic artery plaque and in dental plaque samples. *J Clin Microbiol*, 42(3), pp.1313–1315.
- Isoda K., Sawada S. & Ishigami N., (2004). Lack of interleukin-1 receptor antagonist modulates

- plaque composition in apolipoprotein E-deficient mice. *Arterio Thromb Vasc Biol*.
- Isoviita P.M., Nuotio K., Saksi J., Turunen R., Ijäs P., Pitkaniemi J., Soine L., Kaste M., Kovanen P.T. & Lindsberg P.J., (2010). An imbalance between CD36 and ABCA1 protein expression favors lipid accumulation in stroke-prone ulcerated carotid plaques. *Stroke*, 41(2), pp.389–93.
- Istvan E.S. & Deisenhofer J., (2001). Structural mechanism for statin inhibition of HMG-CoA reductase. *Science (New York, N.Y.)*, 292(5519), pp.1160–4.
- Iwai T., (2009). Periodontal bacteremia and various vascular diseases. *J Periodont Res*, 44(6), pp.689–94.
- Iwamoto N., Lu R., Tanaka N., Abe-Dohmae S. & Yokoyama S., (2010). Calmodulin interacts with ATP binding cassette transporter A1 to protect from calpain-mediated degradation and upregulates high-density lipoprotein generation. *Arterio Thromb Vasc Biol*, 30(7), pp.1446–52.
- Jabado O.J., Palacios G., Kapoor V., Hui J., Renwick N., Zhai J., Briese T. & Lipkin W.I., (2006). Greene SCPrimer: A rapid comprehensive tool for designing degenerate primers from multiple sequence alignments. *Nuc Acid Res*, 34(22), pp.6605–6611.
- Jackson L.A., Campbell L.A., Kuo C.-C., Rodriguez D.I., Lee A. & Grayston J.T., (1997). Isolation of Chlamydia pneumoniae from a Carotid Endarterectomy Specimen. *J Infect Dis*, pp.292–295. Available at: <http://jid.oxfordjournals.org/content/176/1/292.full.pdf> [Accessed September 29, 2014].
- de Jager S.C.A., Bot I., Kraaijeveld A.O., Bot M., Westra M.M., van Santbrink P.J., van Berkel T.J.C. & Biessen E.A.L., (2010). Leukocyte specific CCL3 deficiency inhibits atherosclerosis by attenuation of intimal neutrophil accumulation. *Atherosclerosis*, 213(1), pp.e11–e12.
- de Jager S.C.A., Bot I., Kraaijeveld A.O., Korporaal S.J.A., Bot M., van Santbrink P.J., van Berkel T.J.C., Kuiper J. & Biessen E.A.L., (2013a). Leukocyte-specific CCL3 deficiency inhibits atherosclerotic lesion development by affecting neutrophil accumulation. *Arterio Thromb Vasc Biol*, 33(3), pp.e75-83.
- de Jager S.C.A., Bot I., Kraaijeveld A.O., Korporaal S.J.A., Bot M., van Santbrink P.J., van Berkel T.J.C., Kuiper J. & Biessen E.A.L., (2013b). Leukocyte-specific CCL3 deficiency inhibits atherosclerotic lesion development by affecting neutrophil accumulation. *Arterio Thromb Vasc Biol*, 33(3), pp.e75-83.
- Jakubovics D.N., (2010). Oral multispecies biofilm development and the key role of cell-cell distance, *Nat Rev Microbiol*, 8(7), pp.471-80.
- Jameel A., Ooi K.G.J., Jeffs N.R., Galatowicz G., Lightman S.L. & Calder V.L., (2013). Statin modulation of human T-cell proliferation, IL-1?? and IL-17 production, and IFN-?? T cell expression: Synergy with conventional immunosuppressive agents. *Int J Inflam*, 2013.
- Janes K.A., Albeck J.G., Gaudet S., Sorger P.K., Lauffenburger D.A. & Yaffe M.B., (2005). A systems model of signaling identifies a molecular basis set for cytokine-induced apoptosis. *Science*, 310(5754), pp.1646–53.
- Jeney V., Balla G. & Balla J., (2014). Red blood cell, hemoglobin and heme in the progression of atherosclerosis. *Front Physiol*, 5, p.379.
- Jones G.T., van Rij A.M. & Thomson I. a., (1998). Endothelial Cell ICAM-1 Staining in Human Carotid Arteries. *Cardiovasc Path*, 7(5), pp.245–250.
- Jones L.C. & Hingorani A.D., (2005). Genetic regulation of endothelial function. *Heart*, 91(10), pp.1275–7.
- Joshi R., Khandelwal B., Joshi D. & Gupta O.P., (2013). Chlamydia pneumoniae infection and cardiovascular disease. *North Am J Med Sci*, 5(3), pp.169–81.

- Jugeau S., Tenaud I., Knol A.C., Jarrousse V., Quereux G., Khammari A. & Dreno B., (2005). Induction of toll-like receptors by *Propionibacterium acnes*. *Brit J Derm*, 153(6), pp.1105–13.
- Kaartinen M., Penttila A. & Kovanen P., (1996). Mast cells in rupture-prone areas of human coronary atheromas produce and store TNF- $\alpha$ . *Circulation*, 94, pp.2787–2792.
- Kalayoglu M. V & Byrne G.I., (1998). Induction of macrophage foam cell formation by *Chlamydia pneumoniae*. *J Infect Dis*, 177, pp.725–729.
- Kannel W., Dawber T., Kagan A., Revotskie N. & Stokes J., (1961). Factors of risk in the development of coronary heart disease--six year follow-up experience. The Framingham Study. *Ann Intern Med*, 55, pp.33–50.
- Kannel W.B., Dawber T.R., Thomas H.E. & Mcnamara P.M., (1965). Comparison of Serum Lipids IN the Prediction of Coronary Heart Disease. Framingham Study Indicates that Cholesterol Level and Blood Pressure are Major Factors in Ccoronary Heart Disease; Effect of Obesity and Cigarette Smoking also Noted. *Rhode Isl Med J*, 48, pp.243–50.
- Kannel W.B. & McGee D.L., (1979). Diabetes and cardiovascular risk factors: the Framingham study. *Circulation*, 59(1), pp.8–13.
- Kaplan J.B., (2010). Biofilm dispersal: mechanisms, clinical implications, and potential therapeutic uses. *J Dent Res*, 89(3), pp.205–18.
- Kara C., Demir T., Tezel A. & Zihni M., (2007). Aggressive periodontitis with streptococcal gingivitis: a case report. *Eur J Dent*, 1(4), pp.251–5.
- Kathiresan S., Willer C.J., Peloso G.M., Demissie S., Musunuru K., Schadt E.E., Kaplan L., Bennett D., Li Y., Tanaka T., et al., (2009). Common variants at 30 loci contribute to polygenic dyslipidemia. *Nat Gen*, 41(1), pp.56–65.
- Kędzia A., Ciecierski M., Kufel A., Wierzbowska M. & Kwapisz E., (2012). Isolation of anaerobic bacteria from atherosclerotic plaques from carotid arteries. *Acta Angio*, 18(2), pp.59–67.
- Kerwin W., (2003). Quantitative Magnetic Resonance Imaging Analysis of Neovasculature Volume in Carotid Atherosclerotic Plaque. *Circulation*, 107(6), pp.851–856.
- Kerwin W.S., Oikawa M., Yuan C., Jarvik G.P. & Hatsukami T.S., (2008). MR imaging of adventitial vasa vasorum in carotid atherosclerosis. *Magnet Res Med*, 59(3), pp.507–14.
- Kesavalu L., Sathishkumar S., Bakthavatchalu V., Matthews C., Dawson D., Steffen M. & Ebersole J.L., (2007). Rat model of polymicrobial infection, immunity, and alveolar bone resorption in periodontal disease. *Infect Immun*, 75(4), pp.1704–12.
- Khlgatian M., Nassar H., Chou H.-H., Gibson F.C. & Genco C.A., (2002). Fimbria-dependent activation of cell adhesion molecule expression in *Porphyromonas gingivalis*-infected endothelial cells. *Infect Immun*, 70(1), pp.257–67.
- Kidd T.J., Ramsay K.A., Hu H., Bye P.T.P., Elkins M.R., Grimwood K., Harbour C., Marks G.B., Nissen M.D., Robinson P.J., et al., (2009). Low Rates of *Pseudomonas aeruginosa* Misidentification in Isolates from Cystic Fibrosis Patients. *J Clin Microbiol*, 47(5), pp.1503–1509.
- Kim J., Ochoa M.-T.M.-T., Krutzik S.R., Takeuchi O., Uematsu S., Legaspi A.J., Brightbill H.D., Holland D., Cunliffe W.J., Akira S., et al., (2002). Activation of Toll-Like Receptor 2 in Acne Triggers Inflammatory Cytokine Responses. *J Immunol*, 169(3), pp.1535–1541.
- Kim J.B., Spotts G.D., Halvorsen Y.D., Shih H.M., Ellenberger T., Towle H.C. & Spiegelman B.M., (1995). Dual DNA binding specificity of ADD1/SREBP1 controlled by a single amino acid in the basic helix-loop-helix domain. *Mol Cell Biol*, 15(5), pp.2582–2588.
- Kim S.-Y., Shin Y., Lee C.-Y., Jung I.-Y., Sundqvist G., Johansson E., Sjogren U., Chu F.C., Tsang C.S., Chow T.W., et al., (2013). In vivo quantitative evaluation of live and dead bacteria in

- root canal infection by using propidium monoazide with real-time PCR. *J Endood*, 39(11), pp.1359–63.
- Kirii H., Niwa T. & Yamada Y., (2003). Lack of interleukin-1 $\beta$  decreases the severity of atherosclerosis in ApoE-deficient mice. *Arterio Thromb Vasc Biol*, 23(4), pp.656–660.
- Kishikawa H., Shimokama T. & Watanabe T., (1993). Localization of T lymphocytes and macrophages expressing IL-1, IL-2 receptor, IL-6 and TNF in human aortic intima. Role of cell-mediated immunity in human. *Vir Arch A Pathol Anat Histopath*, 423(6), pp.433–42.
- Kistowska M., Gehrke S., Jankovic D., Kerl K., Fettelschoss A., Feldmeyer L., Fenini G., Kolios A., Navarini A., Ganceviciene R., et al., (2014). IL-1 $\beta$  drives inflammatory responses to propionibacterium acnes in vitro and in vivo. *J Invest Derm*, 134(3), pp.677–85.
- Kistowska M., Rossy E., Sansano S., Gober H.-J., Landmann R., Mori L. & De Libero G., (2008). Dysregulation of the host mevalonate pathway during early bacterial infection activates human TCR gamma delta cells. *Eur J Immunol*, 38(8), pp.2200–9.
- Kiyan Y., Tkachuk S., Hilfiker-Kleiner D., Haller H., Fuhrman B. & Dumler I., (2014). oxLDL induces inflammatory responses in vascular smooth muscle cells via urokinase receptor association with CD36 and TLR4. *J Mol Cell Cardiol*, 66, pp.72–82.
- Klein M.I., Scott-Anne K.M., Gregoire S., Rosalen P.L. & Koo H., (2012). Molecular approaches for viable bacterial population and transcriptional analyses in a rodent model of dental caries. *Mol Oral Microbiol*, 27(5), pp.350–61.
- Ko J.-K., Choi K.-H., Pan Z., Lin P., Weisleder N., Kim C.-W. & Ma J., (2007). The tail-anchoring domain of Bfl1 and HCCS1 targets mitochondrial membrane permeability to induce apoptosis. *J Cell Sci*, 120(Pt 16), pp.2912–23.
- Kockx M., (2000). Apoptosis in atherosclerosis: beneficial or detrimental? *Cardiovasc Res*, 45(3), pp.736–746.
- Kolenbrander P.E., Palmer R.J., Periasamy S. & Jakubovics N.S., (2010). Oral multispecies biofilm development and the key role of cell-cell distance. *Nat Rev Microbiol*, 8(7), pp.471–80.
- Kolodgie F.D., Gold H.K., Burke A.P., Fowler D.R., Kruth H.S., Weber D.K., Farb A., Guerrero L.J., Hayase M., Kutys R., et al., (2003). Intraplaque hemorrhage and progression of coronary atheroma. *New Eng J Med*, 349(24), pp.2316–25.
- Kono H. & Rock K.L., (2008). How dying cells alert the immune system to danger. *Nat Rev Immunol*, 8(4), pp.279–89.
- Konstadoulakis M.M., Kymionis G.D., Karagiani M., Katergianakis V., Doundoulakis N., Pararas V., Koutselinis a, Sehas M. & Peveretos P., (1998). Evidence of apoptosis in human carotid atheroma. *J Vasc Surg*, 27(4), pp.733–9.
- Koren O., Spor A., Felin J., Fåk F., Stombaugh J., Tremaroli V., Behre C.J., Knight R., Fagerberg B., Ley R.E., et al., (2011). Human oral, gut, and plaque microbiota in patients with atherosclerosis. *Proc. Natl. Acad. Sci. U.S.A*, 108 Suppl, pp.4592–8.
- Kozarov E. & Grbic J., (2012). Systemic Effects of Periodontal Diseases: Focus on Atherosclerosis. In Jane Manakil, ed. *Periodontal Diseases - A Clinician's Guide*. Croatia: InTech, pp. 165–179.
- Kozarov E., Sweier D., Shelburne C., Pogulske-Fox A. & Lopatin D., (2006). Detection of bacterial DNA in atheromatous plaques by quantitative PCR. *Microb Infect*, 8, pp.687–693.
- Kozarov E. V, Dorn B.R., Shelburne C.E., Dunn W.A. & Progulske-Fox A., (2005). Human atherosclerotic plaque contains viable invasive *Actinobacillus actinomycetemcomitans* and *Porphyromonas gingivalis*. *Arterio Thromb Vasc Biol*, 25(3), pp.e17-8.

- Kuklinsky-Sobral J., (2004). Isolation and characterization of soybean-associated bacteria and their potential for plant growth promotion. *Environ Microbiol*, 6(12), pp.1244–51.
- Kumar P.S., Griffen A.L., Moeschberger M.L. & Leys E.J., (2005). Identification of candidate periodontal pathogens and beneficial species by quantitative 16S clonal analysis. *J Clin Microbiol*, 43(8), pp.3944–55.
- Kuo C., Coulson A.S., Campbell L.A., Cappuccio A.L., Lawrence R.D., Wang S. & Grayston J.T., (1997). Detection of *Chlamydia pneumoniae* in atherosclerotic plaques in the walls of arteries of lower extremities from patients undergoing bypass operation for arterial obstruction. *J Vasc Surg*, 26(1), pp.29–31.
- Kurata M., Nose M., Shimazu Y., Aoba T., Kohada Y., Yorioka S., Suehiro S., Fukuoka E., Matsumoto S., Watanabe H., et al., (2014). Microvasculature of Carotid Atheromatous Plaques: Hemorrhagic Plaques Have Dense Microvessels with Fenestrations to the Arterial Lumen. *J Stroke Cerebrovasc Dis*, 23(6), pp.1440–6.
- Kurita-Ochiai T., Fukushima K. & Ochiai K., (1995). Volatile fatty acids, metabolic by-products of periodontopathic bacteria, inhibit lymphocyte proliferation and cytokine production. *J Dent Res*, 74(7), pp.1367–73.
- Kusano K.F., Nakamura K., Kusano H., Nishii N., Banba K., Ikeda T., Hashimoto K., Yamamoto M., Fujio H., Miura A., et al., (2004). Significance of the level of monocyte chemoattractant protein-1 in human atherosclerosis. *Circulation*, 68(7), pp.671–6.
- Kutuk O. & Basaga H., (2006). Bcl-2 protein family: Implications in vascular apoptosis and atherosclerosis. *Apoptosis*, 11, pp.1661–1675.
- Kuziel W.A., Dawson T.C., Quinones M., Garavito E., Chenuaux G., Ahuja S.S., Reddick R.L. & Maeda N., (2003). CCR5 deficiency is not protective in the early stages of atherogenesis in apoE knockout mice. *Atherosclerosis*, 167(1), pp.25–32.
- Labischinski H., Goodell E.W., Goodell A. & Hochberg M.L., (1991). Direct proof of a “more-than-single-layered” peptidoglycan architecture of *Escherichia coli* W7: a neutron small-angle scattering study. *J. Bacteriol.*, 173(2), pp.751–756.
- Lalla E., Lamster I.B., Hofmann M.A., Bucciarelli L., Jerud A.P., Tucker S., Lu Y., Papananou P.N. & Schmidt A.M., (2003). Oral infection with a periodontal pathogen accelerates early atherosclerosis in apolipoprotein E-null mice. *Arterio Thromb Vasc Biol*, 23(8), pp.1405–11.
- Laman J.D., Schoneveld A.H., Moll F.L., van Meurs M. & Pasterkamp G., (2002). Significance of peptidoglycan, a proinflammatory bacterial antigen in atherosclerotic arteries and its association with vulnerable plaques. *Am J Cardiol*, 90(2), pp.119–123.
- Lamont R.J., Chan A., Belton C.M., Izutsu K.T., Vasel D. & Weinberg A., (1995). *Porphyromonas gingivalis* invasion of gingival epithelial cells. *Infect Immun*, 63(10), pp.3878–85.
- Lanter B.B. & Davies D.G., (2015). *Propionibacterium acnes* recovered from atherosclerotic human carotid arteries undergoes biofilm dispersion and releases lipolytic and proteolytic enzymes in response to norepinephrine challenge in vitro. *Infect Immun*, 83(10).
- Lanter B.B., Sauer K. & Davies D.G., (2014). Bacteria present in carotid arterial plaques are found as biofilm deposits which may contribute to enhanced risk of plaque rupture. *mBio*, 5(3), pp.e01206-14.
- Laughon B.E., Syed S.A., Loesche W.J., Annu A. & Am M., (1982). API ZYM System for Identification of *Bacteroides* spp., *Capnocytophaga* spp., and *Spirochetes* of Oral Origin. *J Clin Microbiol*, 15(1), pp.97–102.
- Lawn R.M., Wade D.P., Couse T.L. & Wilcox J.N., (2001). Localization of Human ATP-Binding Cassette Transporter 1 (ABC1) in Normal and Atherosclerotic Tissues. *Arterio Thromb Vasc Biol*,

21(3), pp.378–385.

Leal J., Luengo-Fernández R., Gray A., Petersen S. & Rayner M., (2006). Economic burden of cardiovascular diseases in the enlarged European Union. *Eur Heart J*, 27(13), pp.1610–9.

Lee C.W., Park C.-S., Hwang I., Kim Y., Park D.-W., Kang S.-J., Lee S.-H., Kim Y.-H., Park S.-W. & Park S.-J., (2011). Expression of HMG-CoA reductase in human coronary atherosclerotic plaques and relationship to plaque destabilisation. *Heart*, 97(9), pp.715–20.

Lee S.C., Brummet M.E., Shahabuddin S., Woodworth T.G., Georas S.N., Leiferman K.M., Gilman S.C., Stellato C., Gladue R.P., Schleimer R.P., et al., (2000). Cutaneous Injection of Human Subjects with Macrophage Inflammatory Protein-1 Induces Significant Recruitment of Neutrophils and Monocytes. *J Immunol*, 164(6), pp.3392–3401.

Lee S.E., Kim J.-M., Jeong S.K., Choi E.H., Zouboulis C.C. & Lee S.H., (2015). Expression of Protease-Activated Receptor-2 in SZ95 Sebocytes and its Role in Sebaceous Lipogenesis, Inflammation, and Innate Immunity. *J Invest Derm*, 135(9), pp.2219–2227.

Lee Y.J., Choi H.J., Kang T.W., Kim H.O., Chung M.J. & Park Y.M., (2008). CBT-SL5, a bacteriocin from *Enterococcus faecalis*, suppresses the expression of interleukin-8 induced by *Propionibacterium acnes* in cultured human keratinocytes. *J Microbiol Biotechnol*, 18(7), pp.1308–16.

Leen E.J., Feeley T.M., Colgan M.P., O'Malley M.K., Moore D.J., Hourihane D.O. & Shanik G.D., (1990). “Haemorrhagic” carotid plaque does not contain haemorrhage. *European J Vasc Surg*, 4(2), pp.123–128.

Lei L., Li H., Yan F., Li Y. & Xiao Y., (2011). Porphyromonas gingivalis lipopolysaccharide alters atherosclerotic-related gene expression in oxidized low-density-lipoprotein-induced macrophages and foam cells. *J Periodont Res*, 46(4), pp.427–37.

Lennihan L., Kupsky W.J., Mohr J.P., Hauser W.A., Correll J.W. & Quest D.O., (1987). Lack of association between carotid plaque hematoma and ischemic cerebral symptoms. *Stroke*, 18(5), pp.879–881.

Letai A., Bassik M.C., Walensky L.D., Sorcinelli M.D., Weiler S. & Korsmeyer S.J., (2002). Distinct BH3 domains either sensitize or activate mitochondrial apoptosis, serving as prototype cancer therapeutics. *Cancer Cell*, 2(3), pp.183–192.

Levula M., Oksala N., Airla N., Zeitlin R., Salenius J.-P., Järvinen O., Venermo M., Partio T., Saarinen J., Somppi T., et al., (2012). Genes involved in systemic and arterial bed dependent atherosclerosis--Tampere Vascular study. *PLoS ONE*, 7(4), p.e33787.

Levy P.-Y., Fournier P.-E., Charrel R., Metras D., Habib G. & Raoult D., (2006). Molecular analysis of pericardial fluid: a 7-year experience. *Eur Heart J*, 27(16), pp.1942–6.

Ley K., (2003). The role of selectins in inflammation and disease. *Trends in Mol Med*, 9(6), pp.263–268.

Li H., Yan F. & Lei L., (2010). Effects of Porphyromonas gingivalis lipopolysaccharide on apoptotic genes in foam cells. *Cin J Stomatol*, 45(5), pp.274–8.

Li L., Messas E., Batista E.L., Levine R.A. & Amar S., (2002). Porphyromonas gingivalis infection accelerates the progression of atherosclerosis in a heterozygous apolipoprotein E-deficient murine model. *Circulation*, 105(7), pp.861–7.

Li L.-C., Varghese Z., Moorhead J.F., Lee C.-T., Chen J.-B. & Ruan X.Z., (2013). Cross-talk between TLR4-MyD88-NF-κB and SCAP-SREBP2 pathways mediates macrophage foam cell formation. *Am J Physiol*, 304(6), pp.H874-84.

Li X., Kolltveit K.M., Tronstad L. & Olsen I., (2000). Systemic Diseases Caused by Oral Infection. *Clin Microbiol Rev*, 13(4), pp.547–558.

- Liao J.K. & Laufs U., (2005). Pleiotropic effects of statins. *Ann Rev Pharm Tox*, 45, pp.89–118.
- Libby P., (2002). Inflammation and Atherosclerosis. *Circulation*, 105(9), pp.1135–1143.
- Liu H.-F.H., Cui K.-F.K., Wang J.-P.J., Zhang M., Guo Y.-P., Li X.-Y. & Jiang C., (2012). Significance of ABCA1 in human carotid atherosclerotic plaques. *Exp Therap Med*, 4(2), pp.297–302.
- Lockhart P.B., Bolger A.F., Papapanou P.N., Osinbowale O., Trevisan M., Levison M.E., Taubert K.A., Newburger J.W., Gornik H.L., Gewitz M.H., et al., (2012). Periodontal disease and atherosclerotic vascular disease: does the evidence support an independent association?: a scientific statement from the American Heart Association. *Circulation*, 125(20), pp.2520–44.
- Locksley R.M., Killeen N. & Lenardo M.J., (2001). The TNF and TNF receptor superfamilies: integrating mammalian biology. *Cell*, 104(4), pp.487–501.
- Loos B.G., (2005). Systemic Markers of Inflammation in Periodontitis. *J Periodont*, 76(11–s), pp.2106–2115.
- Loos B.G., Craandijk J., Hoek F.J., Wertheim-van Dillen P.M. & van der Velden U., (2000). Elevation of systemic markers related to cardiovascular diseases in the peripheral blood of periodontitis patients. *J Periodont*, 71(10), pp.1528–34.
- Lu M., Marsters S., Ye X., Luis E., Gonzalez L. & Ashkenazi A., (2014). E-cadherin couples death receptors to the cytoskeleton to regulate apoptosis. *Mol Cell*, 54(6), pp.987–98.
- Lu R., Feng L., Gao X., Meng H. & Feng X., (2013). Relationship between volatile fatty acids and Porphyromonas gingivalis and Treponema denticola in gingival crevicular fluids of patients with aggressive periodontitis. *J Peking Univ*, 45(1), pp.12–6.
- Luengo-Fernández R., Leal J., Gray A., Petersen S. & Rayner M., (2006). Cost of cardiovascular diseases in the United Kingdom. *Heart*, 92(10), pp.1384–9.
- Lund Håheim L., (2014). The infection hypothesis revisited: Oral infection and cardiovascular disease. *Epidem Res Int*, 2014(735378), pp.1–9.
- Lusby R.J., Ferrell L.D., Ehrenfeld W.K., Stoney R.J. & Wylie E.J., (1982). Carotid plaque hemorrhage. Its role in production of cerebral ischemia. *Arch Surg*, 117(11), pp.1479–88.
- Lusis A.J., (2000). Atherosclerosis. *Nature*, 407(6801), pp.233–41.
- Madjid M., Aboshady I., Awan I., Litovsky S. & Casscells S.W., (2004). Influenza and cardiovascular disease: is there a causal relationship? *Tex Heart Inst J*, 31(1), pp.4–13.
- Mahdy Ali K., Wonnerth A., Huber K. & Wojta J., (2012). Cardiovascular disease risk reduction by raising HDL cholesterol--current therapies and future opportunities. *Britt J Pharm*, 167(6), pp.1177–94.
- Mahendra J. & Mahendra L., (2013). Prevalence of periodontopathogenic bacteria in subgingival biofilm and atherosclerotic plaques of patients undergoing coronary revascularization surgery. *J Indian Soc Periodont*, 17(6), pp.719–724.
- Mahendra J., Mahendra L., Kurian V., M.M., Jaishankar K. & Mythilli R., (2010). 16S rRNA-based detection of oral pathogens in coronary atherosclerotic plaque. *Indian J Dent Res*, 21(2), pp.248–52.
- Maitra U., Parks J.S. & Li L., (2009). An innate immunity signaling process suppresses macrophage ABCA1 expression through IRAK-1-mediated downregulation of retinoic acid receptor alpha and NFATc2. *Mol Cell Biol*, 29(22), pp.5989–97.
- Mak T.N., Schmid M., Brzuszkiewicz E., Zeng G., Meyer R., Sfanos K.S., Brinkmann V., Meyer T.F. & Brüggemann H., (2013). Comparative genomics reveals distinct host-interacting traits of

- three major human-associated propionibacteria. *BMC genomics*, 14, p.640.
- Makowski L. & Hotamisligil G.S., (2005). The role of fatty acid binding proteins in metabolic syndrome and atherosclerosis. *Curr Opin Lipidol*, 16(5), pp.543–8.
- Manjunath C.N., Rawal J.R., Irani P.M. & Madhu K., (2013). Atherogenic dyslipidemia. *Indian J Endocrin Metab*, 17(6), pp.969–76.
- Mann D.L., Zipes D.P., Libby P. & Bonow R.O., (2011). Braunwald's Heart Disease: A Textbook of Cardiovascular Medicine. Single Volume: Expert Consult Premium Edition, 9th ed. R. O. Bonow et al., eds., Philadelphia, USA.
- Mantis N.J., Rol N. & Corthésy B., (2011). Secretory IgA's complex roles in immunity and mucosal homeostasis in the gut. *Mucos Immun*, 4(6), pp.603–11.
- Marcelino S., (2010). Presence of periodontopathic bacteria in coronary arteries from patients with chronic periodontitis. *Anaerobe*, 16, pp.629–632.
- Marlin S.D. & Springer T.A., (1987). Purified intercellular adhesion molecule-1 (ICAM-1) is a ligand for lymphocyte function-associated antigen 1 (LFA-1). *Cell*, 51(5), pp.813–819.
- Marsh P.D., (2006). Dental plaque as a biofilm and a microbial community - implications for health and disease. *BMC Oral Heal*, 6 Suppl 1(Suppl 1), p.S14.
- Martinet W., Schrijvers D., De Meyer G., Thielemans J., Knaapen M., Herman A. & Kockx M., (2002). Gene Expression Profiling of Apoptosis-Related Genes in Human Atherosclerosis: Upregulation of Death-Associated Protein Kinase. *Arterio Thrombo Vasc Biol*, 22(12), pp.2023–2029.
- Martín-Rabadán P., Gijón P., Alcalá L., Rodríguez-Crèixems M., Alvarado N. & Bouza E., (2008). *Propionibacterium acnes* is a common colonizer of intravascular catheters. *J Infect*, 56(4), pp.257–60.
- Maxfield F. & Tabas I., (2005). Role of cholesterol and lipid organization in disease. *Nature*, 438, pp.612–21.
- Mazzone A., Epistolato M.C., Gianetti J., Castagnini M., Sassi C., Ceravolo R., Bevilacqua S., Glauber M., Biagini A. & Tanganelli P., (2006). Biological features (inflammation and neoangiogenesis) and atherosclerotic risk factors in carotid plaques and calcified aortic valve stenosis: two different sites of the same disease? *Am J Clin Path*, 126(4), pp.494–502.
- McCarthy M.J., Loftus I.M., Thompson M.M., Jones L., London N.J., Bell P.R., Naylor a R. & Brindle N.P., (1999). Angiogenesis and the atherosclerotic carotid plaque: an association between symptomatology and plaque morphology. *J Vasc Surg*, 30(2), pp.261–8.
- McDowell A., Perry A.L., Lambert P. a & Patrick S., (2008). A new phylogenetic group of *Propionibacterium acnes*. *J Med Microbiol*, 57(Pt 2), pp.218–24.
- McDowell A., Valanne S., Ramage G., Tunney M.M., Glenn J. V., McLorinan G.C., Bhatia A., Maisonneuve J.-F., Lodes M., Persing D.H., et al., (2005). *Propionibacterium acnes* Types I and II Represent Phylogenetically Distinct Groups. *J Clin Microbiol*, 43(1), pp.326–334.
- McLaren J.E., Michael D.R., Ashlin T.G. & Ramji D.P., (2011). Cytokines, macrophage lipid metabolism and foam cells: implications for cardiovascular disease therapy. *Prog Lipid Res*, 50(4), pp.331–47.
- Merhi-Soussi F., (2005). Interleukin-1 plays a major role in vascular inflammation and atherosclerosis in male apolipoprotein E-knockout mice. *Cardiovasc Res*, 66(3), pp.583–593.
- Mestas J. & Ley K., (2008). Monocyte-Endothelial Cell Interactions in the Development of Atherosclerosis. *Trend Cardiovasc Med*, 18(6), pp.228–232.

- Meurman J.H., Sanz M. & Janket S.-J., (2004). Oral Health, Atherosclerosis, and Cardiovascular Disease. *Crit Rev Oral Biol Med*, 15(6), pp.403–413.
- Michel J.-B., Virmani R., Arbustini E. & Pasterkamp G., (2011). Intraplaque haemorrhages as the trigger of plaque vulnerability. *Eur Heart J*, 32(16), pp.1977–1985.
- Middleton J., Patterson A.M., Gardner L., Schmutz C. & Ashton B.A., (2002). Leukocyte extravasation: chemokine transport and presentation by the endothelium. *Blood*, 100(12), pp.3853–60.
- Middleton M.K., Zukas A.M., Rubinstein T., Jacob M., Zhu P., Zhao L., Blair I. & Puré E., (2006). Identification of 12/15-lipoxygenase as a suppressor of myeloproliferative disease. *J Experim Med*, 203(11), pp.2529–40.
- Miller D.K., (1997). The role of the Caspase family of cysteine proteases in apoptosis. *Semin Immun*, 9(1), pp.35–49.
- Miserez A.R., Cao G., Probst L.C. & Hobbs H.H., (1997). Structure of the human gene encoding sterol regulatory element binding protein 2 (SREBF2). *Genomics*, 40(1), pp.31–40.
- Mody N., Tintut Y., Radcliff K. & Demer L.L., (2003). Vascular calcification and its relation to bone calcification: possible underlying mechanisms. *J Nuc Cardiol*, 10(2), pp.177–83.
- Mofidi R., Powell T.I., Crotty T., Mehigan D., Macerlaine D. & Keaveny T. V., (2008). Angiogenesis in carotid atherosclerotic lesions is associated with timing of ischemic neurological events and presence of computed tomographic cerebral infarction in the ipsilateral cerebral hemisphere. *Ann Vasc Surg*, 22(2), pp.266–72.
- Montecucco F., Lenglet S., Gayet-Ageron A., Bertolotto M., Pelli G., Palombo D., Pane B., Spinella G., Steffens S., Raffaghello L., et al., (2010). Systemic and intraplaque mediators of inflammation are increased in patients symptomatic for ischemic stroke. *Stroke*, 41(7), pp.1394–404.
- Moore K.J., Sheedy F.J. & Fisher E.A., (2013). Macrophages in atherosclerosis: a dynamic balance. *Nat Rev Immunol*, 13(10), pp.709–21.
- Moore W.E.C., Holdeman L. V., Smibert R.M., Good I.J., Burmeister J. a., Palcanis K.G. & Ranney R.R., (1982). Bacteriology of experimental gingivitis in young adult humans. *Infect Immun*, 38(2), pp.651–667.
- Moos M.P.W., John N., Gräbner R., Nossmann S., Günther B., Vollandt R., Funk C.D., Kaiser B. & Habenicht A.J.R., (2005). The lamina adventitia is the major site of immune cell accumulation in standard chow-fed apolipoprotein E-deficient mice. *Arterio Thromb Vasc Biol*, 25(11), pp.2386–91.
- Moreno P.R., Purushothaman K.R., Fuster V., Echeverri D., Truszczyńska H., Sharma S.K., Badimon J.J. & O'Connor W.N., (2004). Plaque neovascularization is increased in ruptured atherosclerotic lesions of human aorta: implications for plaque vulnerability. *Circulation*, 110(14), pp.2032–8.
- Moreno P.R., Purushothaman K.-R., Sirol M., Levy A.P. & Fuster V., (2006). Neovascularization in human atherosclerosis. *Circulation*, 113(18), pp.2245–52.
- Mori H., Maruyama F., Kato H., Toyoda A., Dozono A., Ohtsubo Y., Nagata Y., Fujiyama A., Tsuda M. & Kurokawa K., (2014). Design and experimental application of a novel non-degenerate universal primer set that amplifies prokaryotic 16S rRNA genes with a low possibility to amplify eukaryotic rRNA genes. *DNA research*, 21(2), pp.217–227.
- Morita C., Sumioka R., Nakata M., Okahashi N., Wada S., Yamashiro T., Hayashi M., Hamada S., Sumitomo T. & Kawabata S., (2014). Cell wall-anchored nuclease of *Streptococcus sanguinis* contributes to escape from neutrophil extracellular trap-mediated bacteriocidal activity. *PLoS*

*ONE*, 9(8), p.e103125.

Morita S., Iwasaki K., Maruoka Y., Okada Y. & Ando T., (2014). Identification of periodontal bacteria from carotid artery plaque in chronic periodontitis patients. *J Oral Maxill Surg Med Path*, 26(4), pp.450–455.

Mukaida N., (1998). Interleukin-8 (IL-8) and monocyte chemoattractant and activating factor (MCAF/MCP-1), chemokines essentially involved in inflammatory and immune reactions. *Cytok Growth Fact Rev*, 9(1), pp.9–23.

Mylonakis E. & Calderwood S.B., (2001). Infective endocarditis in adults. *New Eng J Med*, 345(18), pp.1318–30.

Mysak J., Podzimek S., Sommerova P., Lyuya-mi Y., Bartova J., Janatova T., Prochazkova J. & Duskova J., (2014). Review Article Porphyromonas gingivalis : Major Periodontopathic Pathogen Overview. *J Immun Res*, 2014(ID476068), pp.1–8.

Nagy I., Pivarcsi A., Kis K., Koreck A., Bodai L., McDowell A., Seltmann H., Patrick S., Zouboulis C.C. & Kemény L., (2006). Propionibacterium acnes and lipopolysaccharide induce the expression of antimicrobial peptides and proinflammatory cytokines/chemokines in human sebocytes. *Microb Infect*, 8(8), pp.2195–205.

Nagy I., Pivarcsi A., Koreck A., Széll M., Urbán E. & Kemény L., (2005). Distinct strains of Propionibacterium acnes induce selective human beta-defensin-2 and interleukin-8 expression in human keratinocytes through toll-like receptors. *J Invest Derm*, 124(5), pp.931–8.

Nahid M.A., Rivera M., Lucas A., Chan E.K.L. & Kesavalu L., (2011). Polymicrobial infection with periodontal pathogens specifically enhances microRNA miR-146a in ApoE<sup>-/-</sup> mice during experimental periodontal disease. *Infect Immun*, 79(4), pp.1597–605.

Nakagawa T., Shimada M., Mukai H., Asada K., Kato I., Fujino K. & Sato T., (1994). Detection of alcohol-tolerant hiochi bacteria by PCR. *App Environ Microbiol*, 60(2), pp.637–640.

Nakanishi K., Yoshimoto T., Tsutsui H. & Okamura H., (2001). Interleukin-18 regulates both Th1 and Th2 responses. *Ann Rev Immunol*, 19, pp.423–74.

Nakano K., Inaba H. & Nomura R., (2006). Detection of cariogenic Streptococcus mutans in extirpated heart valve and atheromatous plaque specimens. *J Clin Microbiol*, 44(9), pp.3313–3317.

Nakano K., Wada K. & Nomura R., (2011). Characterization of aortic aneurysms in cardiovascular disease patients harboring Porphyromonas gingivalis. *Oral diseases*, 17, pp.370–378.

Nandalur K.R., Baskurt E., Hagspiel K.D., Phillips C.D. & Kramer C.M., (2005). Calcified carotid atherosclerotic plaque is associated less with ischemic symptoms than is noncalcified plaque on MDCT. *AJR*, 184(1), pp.295–8.

Narusaka M., Shiraishi T., Iwabuchi M. & Narusaka Y., (2011). rpoD gene expression as an indicator of bacterial pathogens in host plants. *J General Plant Path*, 77(2), pp.75–80.

Nelken N., Coughlin S., Gordon D. & Willcox J., (1991). Monocyte chemoattractant protein-1 in human atheromatous plaques. *J Clin Invest*, 88(4), p.1121–7.

Newby A.C., (2005). Dual role of matrix metalloproteinases (matrixins) in intimal thickening and atherosclerotic plaque rupture. *Physiol Rev*, 85(1), pp.1–31.

Niazi S. a., Clarke D., Do T., Gilbert S.C., Mannocci F. & Beighton D., (2010). Propionibacterium acnes and Staphylococcus epidermidis isolated from refractory endodontic lesions are opportunistic pathogens. *J Clin Microbiol*, 48(11), pp.3859–3869.

Nichols M., Townsend N., Scarborough P. & Rayner M., (2013). Cardiovascular disease in Europe: epidemiological update. *Eur Heart J*, 34(39), pp.3028–34.

- Nichols M., Townsend N., Scarborough P. & Rayner M., (2014). Cardiovascular disease in Europe 2014: epidemiological update. *Eur Heart J*, 35(42), pp.2950–9.
- Nicolaou G., Goodall A.H. & Erridge C., (2012). Diverse Bacteria Promote Macrophage Foam Cell Formation Via Toll-Like Receptor-Dependent Lipid Body Biosynthesis. *J Athero Thromb*, 19(2), pp.137–148.
- Nijhuis M.M.O., van der Graaf Y., Melief M.-J., Schoneveld A.H., de Kleijn D.P. V, Laman J.D. & Pasterkamp G., (2004). IgM antibody level against proinflammatory bacterial peptidoglycan is inversely correlated with extent of atherosclerotic disease. *Atherosclerosis*, 173(2), pp.245–51.
- Nijhuis M.M.O., Pasterkamp G., Sluis N.I., de Kleijn D.P. V, Laman J.D. & Ulfman L.H., (2007). Peptidoglycan increases firm adhesion of monocytes under flow conditions and primes monocyte chemotaxis. *J Vasc Res*, 44(3), pp.214–22.
- Nobbs A.H., Lamont R.J. & Jenkinson H.F., (2009). Streptococcus adherence and colonization. *MMBR*, 73(3), p.407–50, Table of Contents.
- Nocker A., Cheung C.-Y. & Camper A.K., (2006). Comparison of propidium monoazide with ethidium monoazide for differentiation of live vs. dead bacteria by selective removal of DNA from dead cells. *J Microbiol Meth*, 67(2), pp.310–320.
- Nomikos T., Panagiotakos D., Georgousopoulou E., Metaxa V., Chrysohoou C., Skoumas I., Antonopoulou S., Tousoulis D., Stefanadis C. & Pitsavos C., (2015). Hierarchical modelling of blood lipids' profile and 10-year (2002-2012) all cause mortality and incidence of cardiovascular disease: the ATTICA study. *Lipid Heal Dis*, 14(1), p.108.
- Nomura R., Nakano K., Mäkelä K., Vaara M., Salo E., Alaluusua S. & Ooshima T., (2011). Isolation and characterization of *Streptococcus mitis* from blood of child with osteomyelitis. *Int J Paed Dent*, 21(3), pp.192–9.
- O'Brien K.D., Allen M.D., McDonald T.O., Chait A., Harlan J.M., Fishbein D., McCarty J., Ferguson M., Hudkins K. & Benjamin C.D., (1993). cell adhesion molecule-1 is expressed in human coronary atherosclerotic plaques. Implications for the mode of progression of advanced coronary atherosclerosis. *J Clin Periodont*, 92(2), pp.945–51.
- O'Brien K.D., McDonald T.O., Chait A., Allen M.D. & Alpers C.E., (1996). Neovascular Expression of E-Selectin, Intercellular Adhesion Molecule-1, and Vascular Cell Adhesion Molecule-1 in Human Atherosclerosis and Their Relation to Intimal Leukocyte Content. *Circulation*, 93(4), pp.672–682.
- Ogawa S., Lozach J., Benner C., Pascual G., Tangirala R.K., Westin S., Hoffmann A., Subramaniam S., David M., Rosenfeld M.G., et al., (2005). Molecular determinants of crosstalk between nuclear receptors and toll-like receptors. *Cell*, 122(5), pp.707–21.
- Ohki T., Itabashi Y. & Kohno T., (2012). Detection of periodontal bacteria in thrombi of patients with acute myocardial infarction by polymerase chain reaction. *Am Heart J*, 163, pp.164–167.
- Ohta H., Wada H., Niwa T., Kirii H., Iwamoto N., Fujii H., Saito K., Sekikawa K. & Seishima M., (2005). Disruption of tumor necrosis factor-alpha gene diminishes the development of atherosclerosis in ApoE-deficient mice. *Atherosclerosis*, 180(1), pp.11–7.
- Ohta K., Makinen K.K. & Loesche W.J., (1986). Purification and characterization of an enzyme produced by *Treponema denticola* capable of hydrolyzing synthetic trypsin substrates. *Infect Immun*, 53(1), pp.213–20.
- Okahashi N., Okinaga T., Sakurai A., Terao Y., Nakata M., Nakashima K., Shintani S., Kawabata S., Ooshima T. & Nishihara T., (2011). Streptococcus sanguinis induces foam cell formation and cell death of macrophages in association with production of reactive oxygen species. *FEMS Microbiol Lett*, 323(2), pp.164–70.

- Okuda K., Ishihara K., Nakagawa T., Hiriyama A., Inayama Y. & Okuda K., (2001). Detection of *Treponema denticola* in atherosclerotic lesions. *J Clin Microbiol*, 39(3), pp.1117–1117.
- Orth R., O'Brien-Simpson N., Dashper S., Walsh K. & Reynolds E., (2010). An efficient method for enumerating oral spirochetes using flow cytometry. *J Microbiol Meth*, 80(2), pp.123–8.
- Osler S., (1908). Diseases of the arteries.
- Ott S.J., El Mokhtari N.E., Musfeldt M., Hellmig S., Freitag S., Rehman A., Kühbacher T., Nikolaus S., Namsolleck P., Blaut M., et al., (2006). Detection of diverse bacterial signatures in atherosclerotic lesions of patients with coronary heart disease. *Circulation*, 113(7), pp.929–37.
- Ouimet M. & Marcel Y.L., (2012). Regulation of lipid droplet cholesterol efflux from macrophage foam cells. *Arterio Thromb Vasc Biol*, 32(3), pp.575–81.
- Packard R., Lichtman A. & Libby P., (2009). Innate and adaptive immunity in atherosclerosis. *Semin Immunopath*, 91, pp.281–291.
- Padilla C., Lobos O., Hubert E., González C., Matus S., Pereira M., Hasbun S. & Descouvieres C., (2006). Periodontal pathogens in atheromatous plaques isolated from patients with chronic periodontitis. *J Periodont Res*, 41, pp.350–353.
- Parahitiyawa N.B., Jin L.J., Leung W.K., Yam W.C. & Samaranyake L.P., (2009). Microbiology of odontogenic bacteremia: beyond endocarditis. *Clin Microbiol Rev*, 22(1), p.46–64, Table of Contents.
- Park a E., McCarthy W.J., Pearce W.H., Matsumura J.S. & Yao J.S., (1998). Carotid plaque morphology correlates with presenting symptomatology. *J Vasc Surg*, 27(5), pp.872–878.
- Park E.K., Jung H.S., Yang H.I., Yoo M.C., Kim C. & Kim K.S., (2007). Optimized THP-1 differentiation is required for the detection of responses to weak stimuli. *Inflam Res*, 56(1), pp.45–50.
- Parums D., (1995). *The Distribution of Adhesion Molecules in Normal and Atherosclerotic Arteries and Aortas* L. L. Gallo, ed., London: Plenum Press.
- Paster B.J., Boches S.K., Galvin J.L., Ericson E., Lau C.N., Levanos V.A., Dewhirst F.E., Ericson R.E. & Sahasrabudhe A., (2001). Bacterial Diversity in Human Subgingival Plaque. *J Bacteriol*, 183(12), pp.3770–3783.
- Van de Peer Y., Chapelle S. & De Wachter R., (1996). A quantitative map of nucleotide substitution rates in bacterial rRNA. *Nuc Acid Res*, 24(17), pp.3381–91.
- Peiser L., Mukhopadhyay S. & Gordon S., (2002). Scavenger receptors in innate immunity. *Curr Opin Immun*, 14(1), pp.123–8.
- Perry A. & Lambert P., (2011). Propionibacterium acnes: Infection Beyond the Skin. *Expert Rev Anti- nfect Thera*, 9(12), pp.1149–1156.
- Persson A. V., (1983). The Natural History of Carotid Plaque Development. *Arch Surg*, 118(9), p.1048.
- Picard F.J., Ke D., Boudreau D.K., Boissinot M., Huletsky A., Richard D., Ouellette M., Roy P.H. & Bergeron M.G., (2004). Use of tuf sequences for genus-specific PCR detection and phylogenetic analysis of 28 streptococcal species. *J Clin Microbiol*, 42(8), pp.3686–95.
- Pober J.S., Bevilacqua M.P., Mendrick D.L., Lapierre L.A., Fiers W. & Gimbrone M.A., (1986). Two distinct monokines, interleukin 1 and tumor necrosis factor, each independently induce biosynthesis and transient expression of the same antigen on the surface of cultured human vascular endothelial cells. *J Immun*, 136(5), pp.1680–1687.
- Poirier P., Giles T.D., Bray G.A., Hong Y., Stern J.S., Pi-Sunyer F.X. & Eckel R.H., (2006).

- Obesity and cardiovascular disease: pathophysiology, evaluation, and effect of weight loss: an update of the 1997 American Heart Association Scientific Statement on Obesity and Heart Disease from the Obesity Committee of the Council on Nutrition, Physical. *Circulation*, 113(6), pp.898–918.
- Pollard A.J., Currie A., Rosenberger C.M., Heale J.-P., Finlay B.B. & Speert D.P., (2004). Differential post-transcriptional activation of human phagocytes by different *Pseudomonas aeruginosa* isolates. *Cell Microbiol*, 6(7), pp.639–50.
- Polonyi M., Prenninger N., Arweiler N.B., Haririan H., Winklehner P. & Kierstein S., (2013). Assessment of viable periodontal pathogens by reverse transcription quantitative polymerase chain reaction. *J Periodont Res*, 48(5), pp.671–6.
- Portillo M.E., Corvec S., Borens O. & Trampuz A., (2013). *Propionibacterium acnes*: An underestimated pathogen in implant-associated infections. *BioMed Res Int*, 2013(Article ID: 804391), p.10 pages.
- Poston R.N., Haskard D.O., Coucher J.R., Gall N.P. & Johnson-Tidey R.R., (1992). Expression of intercellular adhesion molecule-1 in atherosclerotic plaques. *Am J Path*, 140(3), pp.665–73.
- Potteaux S., Combadière C., Esposito B., Casanova S., Merval R., Ardouin P., Gao J.-L., Murphy P.M., Tedgui A. & Mallat Z., (2005). Chemokine receptor CCR1 disruption in bone marrow cells enhances atherosclerotic lesion development and inflammation in mice. *Mol Med*, 11(1–12), pp.16–20.
- Potteaux S., Combadière C., Esposito B., Lecureuil C., Ait-Oufella H., Merval R., Ardouin P., Tedgui A. & Mallat Z., (2006). Role of bone marrow-derived CC-chemokine receptor 5 in the development of atherosclerosis of low-density lipoprotein receptor knockout mice. *Arterio Thromb Vasc Biol*, 26(8), pp.1858–63.
- Presterl E., Grisold A.J., Reichmann S., Hirschl A.M., Georgopoulos A. & Graninger W., (2005). Viridans streptococci in endocarditis and neutropenic sepsis: biofilm formation and effects of antibiotics. *J Antimicrob Chemo*, 55(1), pp.45–50.
- Printseva OYu, Pecló M.M., Gown A.M., OYu P., Pecló M.M. & Gown A.M., (1992). Various cell types in human atherosclerotic lesions express ICAM-1. Further immunocytochemical and immunochemical studies employing monoclonal antibody 10F3. *Am J Path*, 140(4), pp.889–96.
- Proctor M. & Manning P.J., (1990). Production of immunoglobulin A protease by *Streptococcus pneumoniae* from animals. *Infect Immun*, 58(9), pp.2733–7.
- Pucar A., Milasin J., Lekovic V., Vukadinovic M., Ristic M., Putnik S. & Kenney B., (2007). Correlation between atherosclerosis and periodontal putative pathogenic bacterial infections in coronary and internal mammary arteries. *J Periodont*, 78(4), pp.677–682.
- Puig O., Yuan J., Stepaniants S., Zieba R., Zycband E., Morris M., Coulter S., Yu X., Menke J., Woods J., et al., (2011). A gene expression signature that classifies human atherosclerotic plaque by relative inflammation status. *Circulation. Cardiovasc Gen*, 4(6), pp.595–604.
- Pussinen P.J., Tuomisto K., Jousilahti P., Havulinna A.S., Sundvall J. & Salomaa V., (2007). Endotoxemia, immune response to periodontal pathogens, and systemic inflammation associate with incident cardiovascular disease events. *Arterio Thromb Vasc Biol*, 27(6), pp.1433–1439.
- Qi M., Miyakawa H. & Kuramitsu H., (2003). *Porphyromonas gingivalis* induces murine macrophage foam cell formation. *Microb Pathog*, 35(6), p.259–67.
- Qin M., Pirouz A., Kim M.-H., Krutzik S.R., Garbán H.J. & Kim J., (2014). *Propionibacterium acnes* Induces IL-1 $\beta$  secretion via the NLRP3 inflammasome in human monocytes. *J Invest Derm*, 134(2), pp.381–8.
- Queiroz-Junior C.M., Silva M.J.B., Corrêa J.D., Madeira M.F.M., Garlet T.P., Garlet G.P., Cunha

- F.Q., Teixeira M.M. & da Silva T.A., (2010). A controversial role for IL-12 in immune response and bone resorption at apical periodontal sites. *Clin Devel Immunol*, 2010, p.327417.
- R. Mofdi, T. B. Crotty, P. McCarthy, S. J. Sheehan D.M. and T.V.K., (2001). Association between plaque instability, angiogenesis and symptomatic carotid occlusive disease. *Brit J Surg*, pp.945–950. Available at: <http://eds.a.ebscohost.com/ehost/pdfviewer/pdfviewer?vid=3&sid=09a9a854-d2f5-4004-9cb86c41efeb0be5@sessionmgr4005&hid=4108> [Accessed March 31, 2014].
- Raber-Durlacher J.E., Laheij A.M.G.A., Epstein J.B., Epstein M., Geerligs G.M., Wolffe G.N., Blijlevens N.M.A. & Donnelly J.P., (2013). Periodontal status and bacteremia with oral viridans streptococci and coagulase negative staphylococci in allogeneic hematopoietic stem cell transplantation recipients: a prospective observational study. *Supportive Care in Cancer*, 21(6), pp.1621–7.
- Rader D.J., Cohen J. & Hobbs H.H., (2003). Monogenic hypercholesterolemia: new insights in pathogenesis and treatment. *The J Clin Invest*, 111(12), pp.1795–803.
- Rafferty B., Dolgilevich S., Kalachikov S., Morozova I., Ju J., Whittier S., Nowygrod R. & Kozarov E., (2011). Cultivation of *Enterobacter Hormaechei* from Human Atherosclerotic Tissue. *J Athero Thromb*, 18(1), pp.72–81.
- Rafferty B., Jönsson D., Kalachikov S., Demmer R.T., Nowygrod R., Elkind M.S. V, Bush H. & Kozarov E., (2011). Impact of monocytic cells on recovery of uncultivable bacteria from atherosclerotic lesions. *J Intern Med*, 270(3), pp.273–80.
- Rajamäki K., Lappalainen J. & Öörni K., (2010). Cholesterol crystals activate the NLRP3 inflammasome in human macrophages: a novel link between cholesterol metabolism and inflammation. *PLoS ONE*, 5(7), pp.1–9.
- Ramirez J.A., (1996). Isolation of *Chlamydia pneumoniae* from the coronary artery of a patient with coronary atherosclerosis. The *Chlamydia pneumoniae/Atherosclerosis Study Group*. *Ann Intern Med*, 125(12), pp.979–82.
- Rangé H., Labreuche J., Louedec L., Rondeau P., Planesse C., Sebbag U., Bourdon E., Michel J.-B., Bouchard P. & Meilhac O., (2014). Periodontal bacteria in human carotid atherothrombosis as a potential trigger for neutrophil activation. *Atherosclerosis*, 236(2), pp.448–55.
- Ravalli S., Szabolcs M., Albala A., Michler R.E. & Cannon P.J., (1996). Increased Immunoreactive Endothelin-1 in Human Transplant Coronary Artery Disease. *Circulation*, 94(9), pp.2096–2102.
- Ravnskov U., (2003). High cholesterol may protect against infections and atherosclerosis. *QJM*, 96(12), pp.927–934.
- Reichel C.A., Pühr-Westerheide D., Zuchtriegel G., Uhl B., Berberich N., Zahler S., Wymann M.P., Luckow B. & Krombach F., (2012). C-C motif chemokine CCL3 and canonical neutrophil attractants promote neutrophil extravasation through common and distinct mechanisms. *Blood*, 120(4), pp.880–90.
- Renko J., Koskela K. & Lepp P., (2013). Bacterial DNA signatures in carotid atherosclerosis represent both commensals and pathogens of skin origin. *Eur J Derm*, 23(1), pp.53–8.
- Renko J., Lepp P., Oksala N., Nikkari S. & Nikkari S., (2008). Bacterial signatures in atherosclerotic lesions represent human commensals and pathogens. *Atherosclerosis*, 201(1), pp.192–197.
- Reyes L. & Herrera D., (2013). Periodontal bacterial invasion and infection: contribution to atherosclerotic pathology. *J Periodont*, 40(14), pp.30–50.
- Rider P., Carmi Y., Guttman O., Braiman A., Cohen I., Voronov E., White M.R., Dinarello C.A. & Apte R.N., (2011). IL-1 $\alpha$  and IL-1 $\beta$  recruit different myeloid cells and promote different stages of sterile inflammation. *J Immun*, 187(9), pp.4835–43.

- Ridker P., Rifai N., Pfeffer M. & Sacks F., (2000). Elevation of tumor necrosis factor- $\alpha$  and increased risk of recurrent coronary events after myocardial infarction. *Circulation*, 101(18), pp.1-6.
- Riemersma R.A., Perkins D., Brown A.J. & Brown J., (1994). Linoleic acid and coronary artery disease. *Am J Clin Nut*, 59(4), pp.949–50.
- Romano F., Barbui A. & Aimetti M., (2007). Periodontal pathogens in periodontal pockets and in carotid atheromatous plaques. *Min Stomatol*, 56(4), p.169–79.
- Rosenfeld M.E., (2013). Inflammation and atherosclerosis: direct versus indirect mechanisms. *Curr Opin Pharm*, 13(2), pp.154–60.
- Rosenfeld M.E. & Campbell L.A., (2011). Pathogens and atherosclerosis: Update on the potential contribution of multiple infectious organisms to the pathogenesis of atherosclerosis. *Thrombo Haemo*, 106(5), pp.858–867.
- Rosenson R.S., Brewer H.B., Davidson W.S., Fayad Z.A., Fuster V., Goldstein J., Hellerstein M., Jiang X.C., Phillips M.C., Rader D.J., et al., (2012). Cholesterol efflux and atheroprotection: Advancing the concept of reverse cholesterol transport. *Circulation*, 125(15), pp.1905–1919.
- Ross R., Glomset J. & Harker L., (1977). Response to injury and atherogenesis. *Am J Path*, 86(3), pp.675–84.
- Rota S. & Rota S., (2005). Mycobacterium tuberculosis complex in atherosclerosis. *Acta Med Okaya*, 59(6), pp.247–251.
- Rota S., Tuncer S., Rota S. & Kanat O., (2005). Mycobacterium tuberculosis complex DNA does not exist in atheromatous plaques. *New Microbiol*, 28(2), pp.165–9.
- Roth G.A., Moser B., Roth-Walter F., Giacona M.B., Harja E., Papapanou P.N., Schmidt A.M. & Lalla E., (2007). Infection with a periodontal pathogen increases mononuclear cell adhesion to human aortic endothelial cells. *Atherosclerosis*, 190(2), pp.271–281.
- Roy S., Douglas C.W.I. & Stafford G.P., (2010). A novel sialic acid utilization and uptake system in the periodontal pathogen *Tannerella forsythia*. *J Bacteriol*, 192(9), pp.2285–2293.
- Ruan X.Z., Moorhead J.F., Tao J.L., Ma K.L., Wheeler D.C., Powis S.H. & Varghese Z., (2006). Mechanisms of dysregulation of low-density lipoprotein receptor expression in vascular smooth muscle cells by inflammatory cytokines. *Arterio Thromb Vasc Biol*, 26(5), pp.1150–5.
- Ruan X.Z., Varghese Z., Powis S.H. & Moorhead J.F., (2001). Dysregulation of LDL receptor under the influence of inflammatory cytokines: a new pathway for foam cell formation. *Kid Int*, 60(5), pp.1716–25.
- Rudijanto A., The role of vascular smooth muscle cells on the pathogenesis of atherosclerosis. *Acta Med Indo*, 39(2), pp.86–93.
- Rus F., Niculescu F. & Vlaicu R., (1991). Tumor necrosis factor-alpha in human arterial wall with atherosclerosis. *Atherosclerosis*, 89(2–3), pp.247–254.
- Sahdo B., Särndahl E., Elgh F. & Söderquist B., (2013). Propionibacterium acnes activates caspase-1 in human neutrophils. *APMIS*, 121(7), pp.652–63.
- Sahoo M., Ceballos-Olvera I., del Barrio L. & Re F., (2011). Role of the inflammasome, IL-1 $\beta$ , and IL-18 in bacterial infections. *Sci World J*, 11, pp.2037–50.
- Sakai J., (1995). Hairpin Orientation of Sterol Regulatory Element-binding Protein-2 in Cell Membranes as Determined by Protease Protection. *J Biol Chem*, 270(49), pp.29422–29427.
- Salem M.K., Bown M.J., Sayers R.D., West K., Moore D., Nicolaidis A., Robinson T.G. & Naylor A.R., (2014). Identification of patients with a histologically unstable carotid plaque using

- ultrasonic plaque image analysis. *Eur J Vasc Endovasc Surg*, 48(2), pp.118–25.
- Salminen M.K., Rautelin H., Tynkkynen S., Poussa T., Saxelin M., Valtonen V. & Jarvinen A., (2004). Lactobacillus Bacteremia, Clinical Significance, and Patient Outcome, with Special Focus on Probiotic *L. Rhamnosus*. *Clin Infect Dis*, 38(1), pp.62–69.
- Salvador S.L., Syed S. a. & Loesche W.J., (1987). Comparison of three dispersion procedures for quantitative recovery of cultivable species of subgingival spirochetes. *J Clin Microbiol*, 25(11), pp.2230–2232.
- Sánchez M.C., Marín M.J., Figuero E., Llama-Palacios A., León R., Blanc V., Herrera D. & Sanz M., (2014). Quantitative real-time PCR combined with propidium monoazide for the selective quantification of viable periodontal pathogens in an in vitro subgingival biofilm model. *J Periodont Res*, 49(1), pp.20–28.
- Sanchez-Madrid F., Nagy J.A., Robbins E., Simon P. & Springer T.A., (1983). A human leukocyte differentiation antigen family with distinct  $\alpha$ -subunits and a common  $\beta$ -subunit: The lymphocyte function-associated antigen (LFA-1), the C3bi complement receptor (OKM1/Mac-1), and the p150,95 molecule. *J Exp Med*, 158(6), pp.1785–1803.
- Sarookhani M.-R., Ayazi P., Alizadeh S., Foroughi F., Sahmani A. & Adineh M., (2010). Comparison of 16S rDNA-PCR Amplification and Culture of Cerebrospinal Fluid for Diagnosis of Bacterial Meningitis. *Iran J Paed*, 20(4), pp.471–5.
- Schaefer E.J., (2002). Lipoproteins, nutrition, and heart disease. *Am J Clin Nutr*, 75(2), pp.191–212.
- Schaue D., Kachikwu E.L. & McBride W.H., (2012). Cytokines in radiobiological responses: a review. *Rad Res*, 178(6), pp.505–23.
- Schmitz G., Bodzioch M., Orsó E., Klucken J., Langmann T., Böttcher A., Diederich W., Drobnik W., Barlage S., Büchler C., et al., (1999). The gene encoding ATP-binding cassette transporter 1 is mutated in Tangier disease. *Nat Gen*, 22(4), pp.347–351.
- Schmitz G. & Langmann T., (2005). Transcriptional regulatory networks in lipid metabolism control ABCA1 expression. *Biochim Biophys Acta*, 1735(1), pp.1–19.
- Schmitz G. & Orsó E., (2015). Lipoprotein(a) hyperlipidemia as cardiovascular risk factor: pathophysiological aspects. *Clin Res Cardiol Suppl*, 10, pp.21–5.
- Schönbeck U. & Libby P., (2004). Inflammation, immunity, and HMG-CoA reductase inhibitors: statins as antiinflammatory agents? *Circulation*, 109(21 Suppl 1), p.II18-26.
- Scull C.M. & Tabas I., (2011). Mechanisms of ER stress-induced apoptosis in atherosclerosis. *Arterio Thromb Vasc Biol*, 31(12), pp.2792–7.
- Seeger J.M., Barratt E., Lawson G.A. & Klingman N., (1995). The relationship between carotid plaque composition, plaque morphology, and neurologic symptoms. *J Surg Res*, 58(3), pp.330–6.
- Seshadri R., Myers G.S.A., Tettelin H., Eisen J.A., Heidelberg J.F., Dodson R.J., Davidsen T.M., DeBoy R.T., Fouts D.E., Haft D.H., et al., (2004). Comparison of the genome of the oral pathogen *Treponema denticola* with other spirochete genomes. *Proceed Nation Acad Sci USA*, 101(15), pp.5646–51.
- Shah F., Balan P., Weinberg M., Reddy V., Neems R., Feinstein M., Dainauskas J., Meyer P., Goldin M. & Feinstein S.B., (2007). Contrast-enhanced ultrasound imaging of atherosclerotic carotid plaque neovascularization: a new surrogate marker of atherosclerosis? *Vascular medicine (London, England)*, 12(4), pp.291–7.
- Shah P.K., (2001). Link Between Infection and Atherosclerosis: Who Are The Culprits: Viruses, Bacteria, Both, or Neither? *Circulation*, 103(1), pp.5–6.

- Shah P.K., Falk E., Badimon J.J., Fernandez-Ortiz A., Mailhac A., Villareal-Levy G., Fallon J.T., Regnstrom J. & Fuster V., (1995). Human monocyte-derived macrophages induce collagen breakdown in fibrous caps of atherosclerotic plaques. Potential role of matrix-degrading metalloproteinases and implications for plaque rupture. *Circulation*, 92(6), pp.1565–9.
- Shakhov A.N., Collart M.A., Vassalli P., Nedospasov S.A. & Jongeneel C. V., (1990). Kappa B-type enhancers are involved in lipopolysaccharide-mediated transcriptional activation of the tumor necrosis factor alpha gene in primary macrophages. *J Experim Med*, 171(1), pp.35–47.
- Sharma V. & Aggarwal A., (2015). Helicobacter pylori: Does it add to risk of coronary artery disease. *World journal of cardiology*, 7(1), pp.19–25.
- Shchelkunova T.A., Morozov I.A., Rubtsov P.M., Bobryshev Y. V, Sobenin I.A., Orekhov A.N., Andrianova I. V & Smirnov A.N., (2013). Lipid regulators during atherogenesis: expression of LXR, PPAR, and SREBP mRNA in the human aorta. E. Aikawa, ed. *PloS one*, 8(5), p.e63374.
- Sheppard M.N. ed., (2011). *Practical Cardiovasc Path, 2nd edition - CRC Press Book* 2nd ed., Boca Raton, FL: CRC Press.
- Sheridan G.E., Masters C.I., Shallcross J.A. & MacKey B.M., (1998). Detection of mRNA by reverse transcription-PCR as an indicator of viability in Escherichia coli cells. *App Environ Microbiol*, 64(4), pp.1313–8.
- Sherman S., D’Agostino R., Cobb J. & Kannel W., (1994). Physical activity and mortality in women in the Framingham Heart Study. *Am Heart J*, 128(5), pp.879–84.
- Sheu J.-J., Chiou H.-Y., Kang J.-H., Chen Y.-H. & Lin H.-C., (2010). Tuberculosis and the risk of ischemic stroke: a 3-year follow-up study. *Stroke*, 41(2), pp.244–9.
- Shi C. & Pamer E.G., (2011). Monocyte recruitment during infection and inflammation. *Nat Rev Immunol*, 11(11), pp.762–74.
- Shibata M., Katsuyama M., Onodera T., Ehama R., Hosoi J. & Tagami H., (2009). Glucocorticoids enhance Toll-like receptor 2 expression in human keratinocytes stimulated with Propionibacterium acnes or proinflammatory cytokines. *J Invest Derm*, 129(2), pp.375–82.
- Shimotahira N., Oogai Y., Kawada-Matsuo M., Yamada S., Fukutsuji K., Nagano K., Yoshimura F., Noguchi K. & Komatsuzawa H., (2013). The surface layer of Tannerella forsythia contributes to serum resistance and oral bacterial coaggregation. *Infect Immun*, 81(4), pp.1198–206.
- Shrikant P., Ballestas M.E. & Benveniste E.N., (1994). Regulation of intercellular adhesion molecule-1 gene expression by tumor necrosis factor- $\alpha$ , interleukin-1 $\beta$ , and interferon- $\gamma$  in astrocytes. *Journal of neuroimmunology*, 51(2), pp.209–220.
- Silbiger V., Luchessi A. & Hirata R., (2013). Novel genes detected by transcriptional profiling from whole-blood cells in patients with early onset of acute coronary syndrome. *Clinica chimica acta*, 421, pp.184–190.
- Silva R.M. da, Caugant D., Eribe E., Aas J., Lingaas P., Geiran O., Tronstad L. & Olsen I., (2006). Bacterial diversity in aortic aneurysms determined by 16S ribosomal RNA gene analysis. *J Vasc Surg*, 44(5), p.1055–1060.
- da Silva R.M., Lingaas P.S., Geiran O., Tronstad L. & Olsen I., (2003). Multiple bacteria in aortic aneurysms. *J Vasc Surg*, 38(6), pp.1384–1389.
- Simanek A.M., Dowd J.B., Pawelec G., Melzer D., Dutta A. & Aiello A.E., (2011). Seropositivity to cytomegalovirus, inflammation, all-cause and cardiovascular disease-related mortality in the United States. *PloS one*, 6(2), p.e16103.
- Singh R.B., Mengi S.A., Xu Y.-J., Arneja A.S. & Dhalla N.S., (2002). Pathogenesis of atherosclerosis: A multifactorial process. *Experimental and clinical cardiology*, 7(1), pp.40–53.

- Siri-Tarino P.W., Sun Q., Hu F.B. & Krauss R.M., (2010). Saturated fatty acids and risk of coronary heart disease: modulation by replacement nutrients. *Current atherosclerosis reports*, 12(6), pp.384–90.
- Skoog T. & Dichtl W., (2002). Plasma tumour necrosis factor- $\alpha$  and early carotid atherosclerosis in healthy middle-aged men. *Eur Heart J*, 23(5), pp.376–83.
- Slots J., Ashimoto A., Flynn M.J., Li G. & Chen C., (1995). Detection of putative periodontal pathogens in subgingival specimens by 16S ribosomal DNA amplification with the polymerase chain reaction. *Clin Infect Dis*, 20 Suppl 2, pp.304–307.
- Snowden M.A. & Perkins H.R., (1990). Peptidoglycan cross-linking in *Staphylococcus aureus*. An apparent random polymerisation process. *European journal of biochemistry*, 191(2), pp.373–377.
- Socransky S.S., Haffajee A.D., Cugini M.A., Smith C. & Kent R.L., (1998). Microbial complexes in subgingival plaque. *J Clin Periodont*, 25(2), pp.134–44.
- Sonbol H., Spratt D., Roberts G.J. & Lucas V.S., (2009). Prevalence, intensity and identity of bacteraemia following conservative dental procedures in children. *Oral Microbiol Immun*, 24(3), pp.177–82.
- Soumian S., Gibbs R., Davies A. & Albrecht C., (2005). mRNA expression of genes involved in lipid efflux and matrix degradation in occlusive and ectatic atherosclerotic disease. *Journal of clinical pathology*, 58(12), pp.1255–60.
- Soutar A.K. & Naoumova R.P., (2007). Mechanisms of disease: genetic causes of familial hypercholesterolemia. *Nature clinical practice. Cardiovascular medicine*, 4(4), pp.214–25.
- Sowers J.R., Epstein M. & Frohlich E.D., (2001). Diabetes, Hypertension, and Cardiovascular Disease : An Update. *Hypertension*, 37(4), pp.1053–1059.
- Strydom H.C., Chandler A.B., Dinsmore R.E., Fuster V., Glagov S., Insull W., Rosenfeld M.E., Schwartz C.J., Wagner W.D. & Wissler R.W., (1995). A Definition of Advanced Types of Atherosclerotic Lesions and a Histological Classification of Atherosclerosis : A Report From the Committee on Vascular Lesions of the Council on Arteriosclerosis, American Heart Association. *Circulation*, 92(5), pp.1355–1374.
- Strydom H.C., Chandler A.B., Glagov S., Guyton J.R., Insull W., Rosenfeld M.E., Schaffer S.A., Schwartz C.J., Wagner W.D. & Wissler R.W., (1994). A definition of initial, fatty streak, and intermediate lesions of atherosclerosis. A report from the Committee on Vascular Lesions of the Council on Arteriosclerosis, American Heart Association. *Circulation*, 89(5), pp.2462–78.
- Steidl U., Haas R. & Kronenwett R., (2000). Intercellular adhesion molecule 1 on monocytes mediates adhesion as well as trans-endothelial migration and can be downregulated using antisense oligonucleotides. *Annals of hematology*, 79(8), pp.414–423.
- Steinberg D., Parthasarathy S., Carew T.E., Khoo J.C. & Witztum J.L., (1989). Beyond cholesterol. Modifications of low-density lipoprotein that increase its atherogenicity. *New Eng J Med*, 320(14), pp.915–24.
- Stirling A., Worthington T., Rafiq M., Lambert P.A. & Elliott T.S., (2001). Association between *Staphylococcus aureus* and *Propionibacterium acnes*. *Lancet*, 357(9273), pp.2024–5.
- van de Stolpe A., Caldenhoven E., Stade B.G., Koenderman L., Raaijmakers J.A., Johnson J.P. & van der Saag P.T., (1994). 12-O-tetradecanoylphorbol-13-acetate- and tumor necrosis factor  $\alpha$ -mediated induction of intercellular adhesion molecule-1 is inhibited by dexamethasone. Functional analysis of the human intercellular adhesion molecular-1 promoter. *J Biol Chem*, 269(8), pp.6185–92.
- Stroka D.M., Badrichani A.Z., Bach F.H. & Ferran C., (1999). Overexpression of A1, an NF- $\kappa$ B-inducible anti-apoptotic bcl gene, inhibits endothelial cell activation. *Blood*, 93(11),

pp.3803–10.

Sun L.-P., Li L., Goldstein J.L. & Brown M.S., (2005). Insig required for sterol-mediated inhibition of Scap/SREBP binding to COPII proteins in vitro. *J Biol Chem*, 280(28), pp.26483–90.

Sutter V.L., (1984). Anaerobes as Normal Oral Flora. *Clin Infect Dis*, 6(Supplement 1), pp.S62–S66.

Suwannakul S., Stafford G.P., Whawell S. a. & Douglas C.W.I., (2010). Identification of bistable populations of Porphyromonas gingivalis that differ in epithelial cell invasion. *Microbiology*, 156(10), pp.3052–3064.

De Syo D., Franjić B.D., Lovricević I., Vukelić M. & Palenkić H., (2005). Carotid bifurcation position and branching angle in patients with atherosclerotic carotid disease. *Collegium antropologicum*, 29(2), pp.627–32.

Szafranski S.P., Wos-Oxley M.L., Vilchez-Vargas R., Jáuregui R., Plumeier I., Klawonn F., Tomasch J., Meisinger C., Kühnisch J., Sztajer H., et al., (2015). High-resolution taxonomic profiling of the subgingival microbiome for biomarker discovery and periodontitis diagnosis. *App Environ Microbiol*, 81(3), pp.1047–58.

Szocs K., (2004). Endothelial dysfunction and reactive oxygen species production in ischemia/reperfusion and nitrate tolerance. *General physiology and biophysics*, 23(3), pp.265–95.

Tabas I., (2005). Consequences and therapeutic implications of macrophage apoptosis in atherosclerosis: the importance of lesion stage and phagocytic efficiency. *Arterio Thromb Vasc Biol*, 25(11), pp.2255–64.

Tabata T., Mine S., Kawahara C., Okada Y. & Tanaka Y., (2003). Monocyte chemoattractant protein-1 induces scavenger receptor expression and monocyte differentiation into foam cells. *Biochemical and biophysical research communications*, 305(2), pp.380–5.

Tabeta K., Yoshie H. & Yamazaki K., (2014). Current evidence and biological plausibility linking periodontitis to atherosclerotic cardiovascular disease. *Japanese dental science review*, 50(3), pp.55–62.

Takashiba S., Van Dyke T.E., Amar S., Murayama Y., Soskolne A.W. & Shapira L., (1999). Differentiation of monocytes to macrophages primes cells for lipopolysaccharide stimulation via accumulation of cytoplasmic nuclear factor kappaB. *Infect Immun*, 67(11), pp.5573–8.

Takaya N., Yuan C., Chu B., Saam T., Polissar N.L., Jarvik G.P., Isaac C., McDonough J., Natiello C., Small R., et al., (2005). Presence of intraplaque hemorrhage stimulates progression of carotid atherosclerotic plaques: a high-resolution magnetic resonance imaging study. *Circulation*, 111(21), pp.2768–75.

Takeya M., Yoshimura T., Leonard E. & Takahashi K., (1993). Detection of monocyte chemoattractant protein-1 in human atherosclerotic lesions by an anti-monocyte chemoattractant protein-1 monoclonal antibody. *Human pathology*, 24(5), pp.534–9.

Tanaka H. & Swanson S., (1995). Smooth muscle cells of the coronary arterial tunica media express tumor necrosis factor-alpha and proliferate during acute rejection of rabbit cardiac allografts. *Am J Path*, 147(3), pp.617–26.

Tedder T.F., Li X. & Steeber D.A., (1999). The Adhesive Interaction of Cells. *Advances in molecular and cell biology*, 28, pp.65–111.

Teng Z., He J., Degnan A.J., Chen S., Sadat U., Bahaei N.S., Rudd J.H.F. & Gillard J.H., (2012). Critical mechanical conditions around neovessels in carotid atherosclerotic plaque may promote intraplaque hemorrhage. *Atherosclerosis*, 223(2), pp.321–6.

Teng Z., Sadat U., Brown A.J. & Gillard J.H., (2014). Plaque hemorrhage in carotid artery disease: Pathogenesis, clinical and biomechanical considerations. *Journal of Biomechanics*, 47(4), pp.847–

58.

- Thiboutot D.M., (2014). Inflammasome activation by *Propionibacterium acnes*: the story of IL-1 in acne continues to unfold. *J Invest Derm*, 134(3), pp.595–7.
- Thompson H., Rybalka A., Moazzez R., Dewhirst F.E. & Wade W.G., (2015). In vitro culture of previously uncultured oral bacterial phylotypes. *App Environ Microbiol*, 81(24), pp.8307–14.
- Thompson P.A., Gauthier K.C., Varley A.W. & Kitchens R.L., (2010). ABCA1 promotes the efflux of bacterial LPS from macrophages and accelerates recovery from LPS-induced tolerance. *J Lipid Res*, 51(9), pp.2672–85.
- Thompson T., Shields K.J., Barinas-Mitchell E., Newman A. & Sutton-Tyrrell K., (2015). Calcified carotid artery plaques predict cardiovascular outcomes in the elderly. *Journal of Hypertension*, 33(4), pp.810–817.
- Thorp E. & Tabas I., (2009). Mechanisms and consequences of efferocytosis in advanced atherosclerosis. *Journal of leukocyte biology*, 86(5), pp.1089–95.
- Tian J., Hou J., Xing L., Kim S.-J., Yonetsu T., Kato K., Lee H., Zhang S., Yu B. & Jang I.-K., (2012). Significance of intraplaque neovascularisation for vulnerability: optical coherence tomography study. *Heart*, 98(20), pp.1504–9.
- Tipping P. & Hancock W., (1993). Production of tumor necrosis factor and interleukin-1 by macrophages from human atheromatous plaques. *Am J Path*, 142(6), pp.1721–8.
- Tipping P.G. & Hancock W.W., (1993). Production of tumor necrosis factor and interleukin-1 by macrophages from human atheromatous plaques. *Am J Path*, 142(6), pp.1721–8.
- Tomida S., Nguyen L., Chiu B.-H., Liu J., Sodergren E., Weinstock G.M. & Li H., (2013). Pan-genome and comparative genome analyses of *propionibacterium acnes* reveal its genomic diversity in the healthy and diseased human skin microbiome. *mBio*, 4(3), pp.e3-13.
- Tonetti M. & Dyke T., (2013). Periodontitis and atherosclerotic cardiovascular disease: consensus report of the Joint EFP/AAP Workshop on Periodontitis and Systemic Diseases. *J Clin Periodont*, 84(Supplement 4), pp.24–9.
- Townsend N., Bhatnagar P., Wickramasinghe K. & Rayner M., (2014). *Cardiovascular Disease Statistics 2014*, London.
- Trevisan M. & Dorn J., (2010). The relationship between periodontal disease (pd) and cardiovascular disease (cvd). *Mediterranean Medjournal of hematology and infectious diseases*, 2(3), p.e2010030.
- Tucker E., Bayston R. & Scammell B.E., (2005). Primary Virulence Factors of *Propionibacterium acnes*. *Journal of Bone & Joint Surgery*, 87–B(Supp III), p.229.
- Tumurkhuu G., Kenichi S., Crother T., Zhang W., Huang G., Arditi M. & Chen S., (2013). Abstract 15214: Chlamydia Pneumoniae-Induced Foam Cell Formation Requires Nlrp3 Inflammasome Activation. *Circulation*, 128(22), p.A15214-.
- Tunney M. & Patrick S., (1999). Detection of prosthetic hip infection at revision arthroplasty by immunofluorescence microscopy and PCR amplification of the bacterial 16S rRNA gene. *Journal of clinical Microbiol*, 37(10), pp.3281–91.
- Tuomisto T.T., Korkeela A., Rutanen J., Viita H., Bräsen J.H., Riekkinen M.S., Rissanen T.T., Karkola K., Kiraly Z., Kölblle K., et al., (2003). Gene expression in macrophage-rich inflammatory cell infiltrates in human atherosclerotic lesions as studied by laser microdissection and DNA array: overexpression of HMG-CoA reductase, colony stimulating factor receptors, CD11A/CD18 integrins, and interl. *Arterio Thromb Vasc Biol*, 23(12), pp.2235–40.
- Ueda A., Ishigatsubo Y., Okubo T. & Yoshimura T., (1997). Transcriptional regulation of the

- human monocyte chemoattractant protein-1 gene. Cooperation of two NF-kappaB sites and NF-kappaB/Rel subunit specificity. *J Biol Chem*, 272(49), pp.31092–9.
- Umemoto T., Jinno T., Taiji Y. & Ogawa T., (2001). Chemotaxis of Oral Treponemes toward Sera and Albumin of Rabbit. *Microbiology and Immunology*, 45(8), pp.571–577.
- Valanne S., McDowell A., Ramage G., Tunney M.M., Einarsson G.G., O'Hagan S., Wisdom G.B., Fairley D., Bhatia A., Maisonneuve J.-F., et al., (2005). CAMP factor homologues in *Propionibacterium acnes*: a new protein family differentially expressed by types I and II. *Microbiology (Reading, England)*, 151(Pt 5), pp.1369–79.
- Valdés C., Tomás I., Alvarez M., Limeres J., Medina J. & Diz P., (2008). The incidence of bacteraemia associated with tracheal intubation. *Anaesthesia*, 63(6), pp.588–92.
- Valente A.J., Irimpen A.M., Siebenlist U. & Chandrasekar B., (2014). OxLDL induces endothelial dysfunction and death via TRAF3IP2: inhibition by HDL3 and AMPK activators. *Free radical biology & medicine*, 70, pp.117–28.
- Vanechoutte M., Kämpfer P., De Baere T., Avesani V., Janssens M. & Wauters G., (2007). *Chryseobacterium hominis* sp. nov., to accommodate clinical isolates biochemically similar to CDC groups II-h and II-c. *Int J System Evol Microbiol*, 57(11), pp.2623–2628.
- Vasuri F., Fittipaldi S., Pini R., Degiovanni A., Mauro R., Errico-grigioni A.D., Faggioli G., Stella A. & Pasquinelli G., (2015). Diffuse Calcifications Protect Carotid Plaques regardless of the Amount of Neoangiogenesis and Related Histological Complications. *Biomedical Research International*, 2015(Article ID 795672), pp.1–9.
- Vaughan C.J. & Gotto A.M., (2004). Update on statins: 2003. *Circulation*, 110(7), pp.886–92.
- Veith P.D., Chen Y.-Y., Gorasia D.G., Chen D., Glew M.D., O'Brien-Simpson N.M., Cecil J.D., Holden J.A. & Reynolds E.C., (2014). *Porphyromonas gingivalis* outer membrane vesicles exclusively contain outer membrane and periplasmic proteins and carry a cargo enriched with virulence factors. *Journal of proteome research*, 13(5), pp.2420–32.
- Virmani R., Kolodgie F.D., Burke A.P., Finn A. V, Gold H.K., Tulenko T.N., Wrenn S.P. & Narula J., (2005). Atherosclerotic plaque progression and vulnerability to rupture: angiogenesis as a source of intraplaque hemorrhage. *Arterio Thromb Vasc Biol*, 25(10), pp.2054–61.
- Virmani R., Kolodgie F.D., Burke a. P., Farb a. & Schwartz S.M., (2000). Lessons From Sudden Coronary Death: A Comprehensive Morphological Classification Scheme for Atherosclerotic Lesions. *Arterio Thromb Vasc Biol*, 20(5), pp.1262–1275.
- Vogler M., (2012). BCL2A1: the underdog in the BCL2 family. *Cell death and differentiation*, 19(1), pp.67–74.
- Vowels B.R., Yang S. & Leyden J.J., (1995). Induction of proinflammatory cytokines by a soluble factor of *Propionibacterium acnes*: implications for chronic inflammatory acne. *Infect Immun*, 63(8), pp.3158–65.
- de Vries C.J., van Achterberg T.A., Horrevoets A.J., ten Cate J.W. & Pannekoek H., (2000). Differential display identification of 40 genes with altered expression in activated human smooth muscle cells. Local expression in atherosclerotic lesions of smags, smooth muscle activation-specific genes. *J Biol Chem*, 275(31), pp.23939–47.
- van der Wal A.C., Das P.K., Tigges A.J., Becker A.E., Wal A. van der & Das P.K., (1992). Adhesion molecules on the endothelium and mononuclear cells in human atherosclerotic lesions. *Am J Path*, 141(6), pp.1427–33.
- Walter J., Tannock G.W., Tilsala-Timisjarvi A., Rodtong S., Loach D.M., Munro K. & Alatosava T., (2000). Detection and identification of gastrointestinal *Lactobacillus* species by using denaturing gradient gel electrophoresis and species-specific PCR primers. *App Environ Microbiol*,

66(1), pp.297–303.

Wang M., Krauss J.L., Domon H., Hosur K.B., Liang S., Magotti P., Triantafilou M., Triantafilou K., Lambris J.D. & Hajishengallis G., (2010). Microbial hijacking of complement-toll-like receptor crosstalk. *Science signaling*, 3(109), p.ra11.

Wang S., Wu D., Lamon-Fava S., Matthan N.R., Honda K.L. & Lichtenstein A.H., (2009). In vitro fatty acid enrichment of macrophages alters inflammatory response and net cholesterol accumulation. *The British journal of nutrition*, 102(4), pp.497–501.

Wang X., Feuerstein G.Z., Gu J.L., Lysko P.G. & Yue T.L., (1995). Interleukin-1 beta induces expression of adhesion molecules in human vascular smooth muscle cells and enhances adhesion of leukocytes to smooth muscle cells. *Atherosclerosis*, 115(1), pp.89–98.

Wara-Aswapati N., Pitiphat W., Chanchaimongkon L., Taweekhaisupapong S., Boch J.A. & Ishikawa I., (2009). Red bacterial complex is associated with the severity of chronic periodontitis in a Thai population. *Oral diseases*, 15(5), pp.354–9.

Ward L.J. & Timmins M.J., (1999). Differentiation of *Lactobacillus casei*, *Lactobacillus paracasei* and *Lactobacillus rhamnosus* by polymerase chain reaction. *Letters in Appl Microbiol*, 29(2), pp.90–2.

Weinstock C., Ullrich H., Hohe R., Berg A., Baumstark M.W., Frey I., Northoff H. & Flegel W.A., (1992). Low density lipoproteins inhibit endotoxin activation of monocytes. *Arteriosclerosis and thrombosis*, 12(3), pp.341–7.

Wellington C.L., Walker E.K.Y., Suarez A., Kwok A., Bissada N., Singaraja R., Yang Y.-Z., Zhang L.-H., James E., Wilson J.E., et al., (2002). ABCA1 mRNA and Protein Distribution Patterns Predict Multiple Different Roles and Levels of Regulation. *Laboratory Investigation*, 82(3), pp.273–283.

Werner A.B., de Vries E., Tait S.W.G., Bontjer I. & Borst J., (2002). Bcl-2 family member Bfl-1/A1 sequesters truncated bid to inhibit its collaboration with pro-apoptotic Bak or Bax. *J Biol Chem*, 277(25), pp.22781–8.

Westphal D., Dewson G., Menard M., Frederick P., Iyer S., Bartolo R., Gibson L., Czabotar P.E., Smith B.J., Adams J.M., et al., (2014). Apoptotic pore formation is associated with in-plane insertion of Bak or Bax central helices into the mitochondrial outer membrane. *Proceedings of the national academy of sciences of the USA*, 111(39), pp.e4076-85.

Wilcox J.N., Nelken N.A., Coughlin S.R., Gordon D. & Schall T.J., (1993). Local expression of inflammatory cytokines in human atherosclerotic plaques. *J Athero Thromb*, 1(1), pp.10–3.

Wilkinson R.J., Patel P., Llewelyn M., Hirsch C.S., Pasvol G., Snounou G., Davidson R.N. & Toossi Z., (1999). Influence of Polymorphism in the Genes for the Interleukin (IL)-1 Receptor Antagonist and IL-1 on Tuberculosis. *J Exp Med*, 189(12), pp.1863–1874.

Williams P.L., Bannister L.H., Berry M.M., Collins P., Dyson M., Dussek J.E. & Ferguson M.W.J., (1995). *Gray's anatomy* Ed., London: Robinson Publishing.

Wilson P.W.F., D'Agostino R.B., Levy D., Belanger A.M., Silbershatz H. & Kannel W.B., (1998). Prediction of Coronary Heart Disease Using Risk Factor Categories. *Circulation*, 97(18), pp.1837–1847.

Witztum J., (1994). The oxidation hypothesis of atherosclerosis. *The Lancet*, 344(8925), pp.793–795.

Wolpe S.D., Davatellis G., Sherry B., Beutler B., Hesse D.G., Nguyen H.T., Moldawer L.L., Nathan C.F., Lowry S.F. & Cerami A., (1988). Macrophages secrete a novel heparin-binding protein with inflammatory and neutrophil chemokinetic properties. *J Experim Med*, 167(2), pp.570–81.

Wood D.A., Butler S., Riemersma R.A., Thomson M., Oliver M.F., Fulton M., Birtwhistle A. &

- Elton R., (1984). Adipose tissue and platelet fatty acids and coronary heart disease in Scottish men. *Lancet*, 2(8395), pp.117–21.
- Woodfin a., Voisin M.-B. & Nourshargh S., (2007). PECAM-1: A Multi-Functional Molecule in Inflammation and Vascular Biology. *Arterio Thromb Vasc Biol*, 27(12), pp.2514–2523.
- Woodside K.J., Hernandez A., Smith F.W., Xue X.Y., Hu M., Daller J.A. & Hunter G.C., (2003). Differential gene expression in primary and recurrent carotid stenosis. *Biochemical and Biophysical Research Communications*, 302(3), pp.509–514.
- Wyss C., (1992). Growth of Porphyromonas gingivalis, Treponema denticol, T. pectinovorum, T. socranskii and T. vincentii in a Chemically Defined Medium. *J Clin Microbiol*, 30(9), pp.2225–2229.
- Xiao H., Lu M., Lin T.Y., Chen Z., Chen G., Wang W.-C., Marin T., Shentu T.-P., Wen L., Gongol B., et al., (2013). Sterol regulatory element binding protein 2 activation of NLRP3 inflammasome in endothelium mediates hemodynamic-induced atherosclerosis susceptibility. *Circulation*, 128(6), pp.632–42.
- Xiao N., Yin M., Zhang L., Qu X. & Du H., (2009). Tumor necrosis factor-alpha deficiency retards early fatty-streak lesion by influencing the expression of inflammatory factors in apoE-null mice. *Molecular genetics and mwtabolism*, 96(4), pp.239–44.
- Xiaoping Z. & Fajun Y., (2012). Regulation of SREBP-Mediated Gene Expression. *Sheng Wu Wu Li Hsueh Bao*, 28(4), pp.287–294.
- Xie H. & Gu X.-X., (2008). Moraxella catarrhalis lipooligosaccharide selectively upregulates ICAM-1 expression on human monocytes and stimulates adjacent naïve monocytes to produce TNF-alpha through cellular cross-talk. *Cell Microbiol*, 10(7), pp.1453–67.
- Xiong L., Deng Y., Zhu Y., Liu Y. & Bi X., (2009). Correlation of Carotid Plaque Neovascularization Detected by Using Contrast-enhanced US with Clinical Symptoms. *Radiology*, 251(2), pp.583–589.
- Xiong L., Deng Y.-B., Zhu Y., Liu Y.-N. & Bi X.-J., (2009). Correlation of Carotid Plaque Neovascularization Detected by Using Contrast-enhanced US with Clinical Symptoms1. *Radiology*.
- Xu P., Alves J.M., Kitten T., Brown A., Chen Z., Ozaki L.S., Manque P., Ge X., Serrano M.G., Puiu D., et al., (2007). Genome of the opportunistic pathogen Streptococcus sanguinis. *J Bacteriol*, 189(8), pp.3166–75.
- Yam K.K., Pouliot P., N'diaye M.M., Fournier S., Olivier M. & Cousineau B., (2008). Innate inflammatory responses to the Gram-positive bacterium Lactococcus lactis. *Vaccine*, 26(22), pp.2689–99.
- Yamaguchi M., Terao Y. & Kawabata S., (2013). Pleiotropic virulence factor - Streptococcus pyogenes fibronectin-binding proteins. *Cell Microbiol*, 15(4), pp.503–11.
- Yang F., Tan H.-M. & Wang H., (2005). Hyperhomocysteinemia and atherosclerosis. *Sheng li xue bao : [Acta physiologica Sinica]*, 57(2), pp.103–14.
- Yang T., Espenshade P.J., Wright M.E., Yabe D., Gong Y., Aebersold R., Goldstein J.L. & Brown M.S., (2002). Crucial Step in Cholesterol Homeostasis. *Cell*, 110(4), pp.489–500.
- Ye Q., Chen Y., Lei H., Liu Q., Moorhead J.F., Varghese Z. & Ruan X.Z., (2009). Inflammatory stress increases unmodified LDL uptake via LDL receptor: an alternative pathway for macrophage foam-cell formation. *Inflam Res*, 58(11), pp.809–818.
- Ye Q., Lei H., Fan Z., Zheng W. & Zheng S., (2014). Difference in LDL receptor feedback regulation in macrophages and vascular smooth muscle cells: foam cell transformation under inflammatory stress. *Inflammation*, 37(2), pp.555–65.

- Yilmaz A., Lipfert B., Cicha I., Schubert K., Klein M., Raithel D., Daniel W.G. & Garlichs C.D., (2007). Accumulation of immune cells and high expression of chemokines/chemokine receptors in the upstream shoulder of atherosclerotic carotid plaques. *Experimental and molecular pathology*, 82(3), pp.245–55.
- Yin K., Liao D. & Tang C., (2010). ATP-binding membrane cassette transporter A1 (ABCA1): a possible link between inflammation and reverse cholesterol transport. *Mol Med*, 16(9–10), pp.438–49.
- Ylä-Herttuala S., (1991). Expression of monocyte chemoattractant protein 1 in macrophage-rich areas of human and rabbit atherosclerotic lesions. *Proceed Nation Acad Sci USA*, 88(12), pp.5252–5256.
- Yokoyama S., Arakawa R., Wu C.-A., Iwamoto N., Lu R., Tsujita M. & Abe-Dohmae S., (2012). Calpain-mediated ABCA1 degradation: post-translational regulation of ABCA1 for HDL biogenesis. *Biochim Biophys Acta*, 1821(3), pp.547–51.
- Yu R., Kim C.-S., Kawada T., Kwon T.-W., Lim T.-H., Kim Y.-W. & Kwon B.-S., (2004). Involvement of leukotactin-1, a novel CC chemokine, in human atherosclerosis. *Atherosclerosis*, 174(1), pp.35–42.
- Yuan C., Kerwin W.S., Ferguson M.S., Polissar N., Zhang S., Cai J. & Hatsukami T.S., (2002). Contrast-enhanced high resolution MRI for atherosclerotic carotid artery tissue characterization. *JMRI*, 15(1), pp.62–7.
- Yvan-Charvet L., Wang N. & Tall A.R., (2010). Role of HDL, ABCA1, and ABCG1 transporters in cholesterol efflux and immune responses. *Arterio Thromb Vasc Biol*, 30(2), pp.139–43.
- Zelcer N. & Tontonoz P., (2006). Liver X receptors as integrators of metabolic and inflammatory signaling. *The J Clin Invest*, 116(3), pp.607–14.
- Zhang F., Yu W., Hargrove J.L., Greenspan P., Dean R.G., Taylor E.W. & Hartle D.K., (2002). Inhibition of TNF- $\alpha$  induced ICAM-1, VCAM-1 and E-selectin expression by selenium. *Atherosclerosis*, 161(2), pp.381–6.
- Zhang Y., Yang X., Bian F., Wu P., Xing S., Xu G., Li W., Chi J., Ouyang C., Zheng T., et al., (2014). TNF- $\alpha$  promotes early atherosclerosis by increasing transcytosis of LDL across endothelial cells: crosstalk between NF- $\kappa$ B and PPAR- $\gamma$ . *J Mol Cell Cardiol*, 72, pp.85–94.
- Zhao J., Feng X., Zhang X. & Le K., (2012). Effect of *Porphyromonas gingivalis* and *Lactobacillus acidophilus* on secretion of IL1B, IL6, and IL8 by gingival epithelial cells. *Inflammation*, 35(4), pp.1330–7.
- Zhou C., Lei H., Chen Y., Liu Q., Li L.-C., Moorhead J.F., Varghese Z. & Ruan X.Z., (2013). Enhanced SCAP glycosylation by inflammation induces macrophage foam cell formation. *PLoS one*, 8(10), p.e75650.
- Zhou Z., Connell M.C. & MacEwan D.J., (2007). TNFR1-induced NF- $\kappa$ B, but not ERK, p38MAPK or JNK activation, mediates TNF-induced ICAM-1 and VCAM-1 expression on endothelial cells. *Cell Sig*, 19(6), pp.1238–48.
- Zhou Z., Liu Y., Miao A.-D. & Wang S.-Q., (2005). Protocatechuic aldehyde suppresses TNF- $\alpha$ -induced ICAM-1 and VCAM-1 expression in human umbilical vein endothelial cells. *Eur J Pharm*, 513(1–2), pp.1–8.
- Zhu X., Lee J.-Y., Timmins J.M., Brown J.M., Boudyguina E., Mulya A., Gebre A.K., Willingham M.C., Hiltbold E.M., Mishra N., et al., (2008). Increased cellular free cholesterol in macrophage-specific Abca1 knock-out mice enhances pro-inflammatory response of macrophages. *J Biol Chem*, 283(34), pp.22930–41.
- Zong W.X., Edelstein L.C., Chen C., Bash J. & Gélinas C., (1999). The prosurvival Bcl-2 homolog

Bfl-1/A1 is a direct transcriptional target of NF-kappaB that blocks TNFalpha-induced apoptosis. *Gen Devel*, 13(4), pp.382–7.

Zouboulis C.C., (2009). Propionibacterium acnes and sebaceous lipogenesis: a love-hate relationship? *J Invest Derm*, 129(9), pp.2093–6.

## 10.0 Appendices

## Appendix A. Brain heart infusion (BHI)

BHI broth was used for the maintenance of *P. gingivalis* W50/11834 and was prepared by mixing the following ingredients.

Component	100 ml	250 ml	500 ml
BHI broth powder <sup>†</sup>	3.7 g	18.5 g	37 g
Hemin (1 mg/ml) <sup>‡</sup>	500 µl	1.25 ml	2.5 ml
Menadione (16 mg/ml) <sup>§</sup>	6.25 µl	15.6 µl	31.25 µl
L-cystiene HCL (1 mg/ml) <sup>¶</sup>	400 mg	250 µl	500 µl
Yeast extract	100 µl	1 g	2 g
dH <sub>2</sub> O	To 100 ml	To 250 ml	To 500 ml

- Mix all ingredients and autoclave immediately.
- Allow to cool at room temperature then store at 4°C until required.

<sup>†</sup> For 1 L medium BHI broth powder provides: 12.5 g brain infusion solids, 5 g beef infusion solids, 10 g protease peptone, 2 g glucose, 5 g NaCl and 2.5 g Na<sub>2</sub>HPO<sub>4</sub>.

<sup>‡</sup> Hemin stock solution was prepared by dissolving in dH<sub>2</sub>O in the presence of 1 M NaOH (100 µl NaOH:1 ml hemin solution).

<sup>§</sup> Menadione (vitamin K<sub>3</sub>) stock solution was prepared in 95% EtOH.

<sup>¶</sup> L-cystiene HCL stock solution was prepared by dissolving in dH<sub>2</sub>O.

## Appendix B. Tryptic Soy Broth (TSB)

TSB was used for the maintenance cultures of *T. forsythia* and was prepared by mixing the following ingredients.

Component	100 ml	250 ml	500 ml
TSB powder <sup>†</sup>	2.75 g	13.75 g	27.5 g
Hemin (1 mg/ml) <sup>‡</sup>	500 µl	1.25 ml	2.5 ml
Menadione (16 mg/ml) <sup>§</sup>	6.25 µl	15.6 µl	31.25 µl
L-cystiene HCL (1 mg/ml) <sup>  </sup>	400 mg	250 µl	500 µl
<i>N</i> -acetylmuramic acid (50 mg/ml) <sup>¶</sup>	10 µl	25 µl	100 µl
Yeast extract	100 µl	1 g	2 g
dH <sub>2</sub> O	To 100 ml	To 250 ml	To 500 ml

- Mix all ingredients and autoclave immediately.
- Allow to cool at room temperature then store at 4°C until required.

<sup>†</sup> For 1 L medium TSB broth powder provides: 17 g Pancreatic digest of casein, 3 g enzymatic digest of soya bean, 2.5 g glucose, 5 g NaCl and 2.5 g Na<sub>2</sub>HPO<sub>4</sub>.

<sup>‡</sup> Hemin stock solution was prepared by dissolving in dH<sub>2</sub>O in the presence of 1 M NaOH (100 µl NaOH:1 ml hemin solution).

<sup>§</sup> Menadione (vitamin K<sub>3</sub>) stock solution was prepared in 95% EtOH.

<sup>||</sup> L-cystiene HCL stock solution was prepared by dissolving in dH<sub>2</sub>O.

<sup>¶</sup> *N*-acetylmuramic acid (NAM) was prepared as a solution in sterile dH<sub>2</sub>O.

## Appendix C. Tryptone-Yeast extract-Gelatine-Volatile Fatty Acid-Serum (TYGVS)

YGVS broth was used for the maintenance of *T. denticola* and was prepared by mixing the following ingredients.

## Solution A:

Component	For 400mL	For 100mL
Tryptone	5 g	1.25 g
Brain Heart Infusion Broth	2.5 g	0.625 g
Yeast Extract	5 g	1.25 g
Gelatine (for non-semi-solid)	5 g	0.5 g
Ammonium Sulphate	0.25 g	0.06 g
Magnesium Sulphate Heptahydrate	0.05 g	0.0125 g
Potassium phosphate, dibasic	1 g	0.25 g
Sodium Chloride	0.5 g	0.125 g
Distilled water	To 400 mL	To 100 mL
For semi-solid		
Agar	2.5 g	0.5 g
Gelatine	2.5 g	

- Mix with gentle heating to dissolve gelatine and/or agar
- Autoclave immediately
- Store at RT (pH should be 7.2 without adjusting)

## VFA Solution: (Use glassware only; avoid plastic, work in fume hood)

Component	For 150mL	For 125mL	To 62.5mL
Glacial acetic acid	8.5 mL	7.1 mL	3.55 mL
Propionic acid	3 mL	2.5 mL	1.25 mL
Butyric acid	2 mL	1.7 mL	0.85 mL
Valeric acid	0.5 mL	0.42 mL	0.21 mL
Isobutyric acid	0.5 mL	0.42 mL	0.21 mL
Isovaleric acid	0.5 mL	0.42 mL	0.21 mL
Methylbutyric acid	0.5 mL	0.42 mL	0.21 mL
Distilled water	To 150 mL	To 125 mL	To 62.5 mL

## Solution B:

Component	For 500 mL	For 250 mL
Glucose (i.e. dextrose)	5 g	2.5 g
L-Cysteine hydrochloride	5 g	2.5 g
Sodium pyruvate	1.25 g	0.625 g
VFA Solution	125 mL	62.5 mL
Thiamine pyrophosphate	62.5 mg	31.25 mg
Distilled water	To 500 mL	To 250 mL

- pH to 7.2 with 7M KOH Filter sterilise and store at 4C

Complete Medium

- 50 uL Solution B
- 400 mL Solution A
- 50 mL Normal Rabbit Serum (heat inactivated at 56C for 30 mins)
-

## Appendix D. Final developed growth medium to support the growth of all RCB

A complex growth medium formula was developed from TSB (appendix A) through the stepwise addition of growth supplements known to support the growth of *T. denticola*. The final medium was shown to support the pure growth of all RCB. The finalised medium was used to culture RCB and other supported strains of bacteria present in CAP and LITA tissues.

Solution A				
Component	For 400 ml	For 100 ml	Stock solution	Final conc.
Tripticase soy broth	27.5 g	2.75 g		
Hemin	2.5 ml	500 $\mu$ l	1 mg/ml stock	5 $\mu$ g/ml
Menadione (Vit K <sub>3</sub> )	31.25 $\mu$ l	6.25 $\mu$ l	16 mg/ml stock	1 $\mu$ g/ml
L-cystiene HCL	500 $\mu$ l	100 $\mu$ l	1 mg/ml stock	1 $\mu$ g/ml
N-acetylmuramic acid	100 $\mu$ l	10 $\mu$ l	50 mg/ml stock	10 $\mu$ g/ml
Yeast extract	2 g	400 mg	-	0.4%
(NH <sub>4</sub> ) <sub>2</sub> SO <sub>4</sub>	250 mg	62.5 mg		
K <sub>2</sub> HPO <sub>4</sub>	625 mg	156.25 mg		
NaCl <sub>2</sub>	500 mg	125 mg		
Distilled water	To 400 ml	To 100 ml		

Autoclave immediately

Store at RT (pH should be 7.2 without adjusting)

VFA Solution: (Use glassware only; avoid plastic, work in fume hood)

Component	For 150 ml	For 125 ml	For 62.5 ml	Final conc. in media
Glacial acetic acid	8.5 ml	7.1 ml	3.55 ml	14.9 mM
Propionic acid	3 ml	2.5 ml	1.25 ml	4.00 mM
Butyric acid	2 ml	1.7 ml	0.85 ml	2.21 mM
Valeric acid	0.5 ml	0.42 ml	0.21 ml	0.46 mM
Isobutyric acid	0.5 ml	0.42 ml	0.21 ml	0.55 mM
Isovaleric acid	0.5 ml	0.42 ml	0.21 ml	0.46 mM
Methylbutyric acid	0.5 ml	0.42 ml	0.21 ml	0.46 mM
Distilled water	To 150 ml	to 125 ml	0.21 ml	

Solution B:

Component	For 500 ml	For 250 ml	Final conc. in media
Thiamine pyrophosphate	104.25 mg	52.125 mg	12.5 ug/ml (27.18 $\mu$ M)
Sodium pyruvate	2.08 g	1.04 g	250 $\mu$ g/ml
VFA solution	125 ml	62.5 ml	
Distilled water	To 500 ml	To 250 ml	

- pH to 7.2 with 7M KOH Filter sterilise and store at 4°C

Complete Medium (500 ml)

- 30 ml Solution B
- 420 ml Solution A
- 50 ml Normal Rabbit Serum (heat inactivated at 56°C for 40 mins)